

The Evolution of Snout Shape in Eudromaeosaurians and its Ecological Significance

By

Mark James Powers

A thesis submitted in partial fulfillment of the requirements for the degree of

Master of Science

In

Systematics and Evolution

Department of Biological Sciences

University of Alberta

© Mark James Powers, 2020

Abstract

Dromaeosaurids were small to medium sized theropod dinosaurs that diversified during the Late Cretaceous, reaching a near cosmopolitan distribution. They were diverse in morphology from the small four-winged gliders of Microraptorinae, to the bear-sized giant ‘raptors’ like *Achillobator* or *Utahraptor* from the Eudromaeosauria. Eudromaeosauria and its constituents that make up the general public’s view of ‘raptor’ dinosaurs. This group comprises the medium to large dromaeosaurids with pronounced teeth and claws to fill their respective predatory niches and were largely restricted to Laurasia. The known diversity of this clade has increased dramatically since the 1990s, new species described almost yearly. Except for a few nearly complete skeletons, eudromaeosaurians are represented by limited material used in diagnosing distinct species. The maxilla has been given a lot of phylogenetic and ecological weight due to its complexity and its relation to feeding behaviour. This creates an image of eudromaeosaurian systematics that is largely based on one element of the skeletal anatomy. It is important then to have the most complete understanding of the morphology of this one element and how it varies among specimens. This can be difficult as individual bones within a species can show ontogenetic, sexual and/or individual variation. Additionally, taphonomic processes can influence our understanding and interpretations of features affected by deformation. Once these factors are assessed, the level of phylogenetic and ecological inference can be better hypothesized.

In this thesis project, I acquired computed tomography data of eudromaeosaurian maxillae to study these elements within this clade. This allowed me to perform a thorough examination of the morphology of internal features and suture patterns and attempt to retro-deform areas that were distorted during the fossilization process. Previous morphological

descriptions were expanded on and modified as needed. Morphological variation of the maxilla was examined with an emphasis on the ingroup variation of Eudromaeosauria. Linear measurements were taken from a wide range of eudromaeosaurian maxillae for bivariate and principal component analyses to test for trends. Maxillary characters that are ratio-based were examined to look for natural breaks in the range of variation observed to assess the validity of character state thresholds. The characters were then either dropped or adjusted to fit the data. Using the same methods, the range of variation within *Velociraptor* was examined, coupled with a description of a previously undescribed specimen, to develop a baseline for intraspecific variation.

Complex morphology of the maxillary sinus system is demonstrated to be shared among North American eudromaeosaurians from the Late Cretaceous. The sinus systems are noticeably different in related Asian taxa. Ratio-based maxillary characters pertaining to the anterior ramus overshadowed phylogenetically informative features previously not coded. Reinterpretation of the maxilla of *Deinonychus* revealed a morphology more in line with other North American dromaeosaurids, and thereby changed its close phylogenetic placement to Asian taxa. PCA analysis of the maxillae across eudromaeosaurian species shows clear distinction between Asian and North American morphologies. Asian taxa are shallow and elongate while North American taxa have either stout maxillary morphologies or intermediate between the extremes. The gradient of maxilla elongation across PC 1 possibly represents adaptations for prey selection. Maxillary variation within specimens previously identified as *Velociraptor mongoliensis* suggests one specimen falls outside a conservative range of variation and should be classified as a new species -- *Velociraptor vadarostrum* sp. nov. Supported by discrete autapomorphies of the frontal and pelvis, *V. vadarostrum* sp. nov. fits well in the trend in maxillary morphology in

Asian velociraptorines, possessing the most elongate form compared to *Linheraptor* and *Tsaagan*, which possess the least elongate maxillae of the Asian velociraptorines. The consistency of elongate snout morphology in derived Asian eudromaeosaurians supports a monophyletic Velociraptorinae. Persistence of this trait may have been driven by environmental pressures of predominantly arid to sub arid environments which define the Djadokhta Formation of Mongolia and equivalent sediments in China. These arid environments would not support a high diversity of large animals and would cause pressure on Asian eudromaeosaurians to specialize in hunting and eating smaller, more abundant prey. The maxilla is an informative element due to its importance in theropods, for interacting with its lifestyle and environment. Therefore, ecological pressures and vicariance were likely driving eudromaeosaurian biodiversity and morphological disparity during the Late Cretaceous of Laurasia.

Preface

Chapter 3 (“Re-examining ratio based premaxillary and maxillary characters in Eudromaeosauria (Dinosauria: Theropoda): divergent trends in snout morphology between Asian and North American taxa”) was published in *Palaeogeography, Palaeoclimatology, Palaeoecology* on March 24, 2020. The manuscript and its contents were originally produced by me, and the co-authors (Drs. Philip Currie and Corwin Sullivan) provided valuable discussion and edits to improve the quality of the manuscript. The content of this chapter – including its tables, figures, and appendices – have only been altered to reflect the data presented in chapter 2 and formatted to fit the thesis document. The introduction of the published manuscript has been modified and included in the introductory chapter of this thesis, and the introduction for Chapter 3 has been abbreviated.

Powers M. J., Sullivan C., and Currie P. J. 2020. Re-examining ratio based premaxillary and maxillary characters in Eudromaeosauria (Dinosauria: Theropoda): divergent trends in snout morphology between Asian and North American taxa. *Palaeogeography, Palaeoclimatology, Palaeoecology* 547:1-20.

Dedication

“Perfection? I don’t want that ... cuz that would mean stopping. Standing in place. I’m always aiming higher.” – Son Goku, Dragon Ball Super manga Ch. 39

“The only constant in life is change. One’s ability to adapt to those changes will determine your success in life” – Benjamin Franklin

To everyone I have met along the way and how they have changed me. I would not be here if it were not for them.

To my mother, Barbara Powers.

You were the fire under my ass mom, and you pushed those around you to do better – be better. Were you still with us today I have no doubts this thesis would have been finished months ago.

Acknowledgements

Funding for Chapter 3 was in part provided by the Natural Science and Engineering Research Council of Canada (NSERC), Canadian Graduate Scholarship – Master’s (CGS-M) award.

I would like to thank the Natural Science and Engineering Research Council of Canada (NSERC), for the Canadian Graduate Scholarship – Master’s (CGS-M) award, which allowed me to have teaching relief for a year while writing this thesis. I like to thank the Dinosaur Research Institute for providing funding to travel to various museums and look through collections to collect data for this study. For collections visits I would like to thank TMP curator Donald Brinkman, collections manager Brandon Strilisky, and collections staff Becky Sanchez, Rhian Russell and Tom Courtenay for access to and assistance with specimens of *Atrociraptor* and *Saurornitholestes* and facilitating the acquisition of CT scanning these specimens for whom I would like to thank the technician Lynn Kostenuk at Mayfair Diagnostics; BYUVP collections manager Rodney Scheetz and graduate student Rebecca Esplin for access to *Utahraptor* material; CEUM curator Kenneth Carpenter and collections staff member Katherine Corneli for access to *Geminiraptor* and *Utahraptor* material; AMNH fossil Fish, Amphibians, Reptiles and Birds collections manager Carl Mehling, and curator Mark Norell, for access to *Bambiraptor*, *Tsaagan*, and *Velociraptor* specimens and allowing access to the *Tsaagan* scans as well as authorizing the scanning MPC-D 100/982; YPM assistant professor and curator Bhart-Anjan Bhullar, and his PhD student Matteo Fabbri, for access to *Deinonychus* material and for scanning *Deinonychus* and *Velociraptor* material, and museum assistant Daniel Brinkman for facilitating the collections visit to the YPM; and ROM collections manager Kevin Seymour, collections technician Brian Iwama, and curator David Evans for access to the *Acheroraptor* and providing scans of the

holotype specimen, and access to various other comparative dromaeosaurid material. I would also like to thank Dr. Gregory Funston and Dr. Philip Currie for providing photos of *Velociraptor* specimens from the MPC, and for discussion their discussions and mentorship. For valuable skills learned and mentorship I would like to thank Dr. Michael Caldwell and Dr. Corwin Sullivan. I thank the committee members for reviewing this behemoth of Appendices and them plus the chair for sitting through the impending defence. For discussion I would also like to thank Gavin Bradley, Meghan Dueck, Aaron Dyer, David Evans, Samantha Hamilton, Michael Hudgins, Aaron LeBlanc, Annie McIntosh, Ilaria Paparella, James Powers, Luke Powers, Matthew Rhodes, Tiago Simões, Catie Strong, Oksana Vernyogora, Rebekah Vice, and Yan-yin Wang. I would like to thank Adam Brozny-Powers for supporting his dad even when it meant spending less time together. Last but by no means in her contributions, I thank Stephanie Poirier for being there for me throughout all the hardships and believing in me when I did not.

Table of Contents

List of Tables	xii
List of Figures	xiii
Institutional Abbreviations.....	xv
Chapter 1. Introduction	1
1.1 Literature Cited	14
1.2 Tables and Figures	26
Chapter 2. Analysis of eudromaeosaurian maxillae using CT data: re-interpretation of morphology and comments on maxilla character construction	33
2.1 Introduction	33
2.2 Materials.....	35
2.2.1 Computed tomography scan data	35
2.3 Methods.....	36
2.4 Description	40
2.4.1 ROM 63777- <i>Acheroraptor temertyorum</i>	40
2.4.2 TMP 1995.166.0001- <i>Atrociraptor marshalli</i>	44
2.4.3 YPM 5232 (557)- <i>Deinonychus antirrhopus</i>	49
2.4.4 Comparative description.....	53
2.5 Discussion	66
2.5.1 Snout morphology interpretations	67
2.5.2 The effects of taphonomic processes on ratio-based characters.....	68
2.5.3 Maxillary sinus system and character construction.....	72
2.5.4 Nasal and lacrimal contacts	83
2.5.5 Tooth characters	86
2.5.6 Tooth replacement	89
2.6 Conclusions.....	90
2.7 Literature Cited	93
2.8 Tables and Figures	101
Chapter 3. Re-examining ratio based premaxillary and maxillary characters in Eudromaeosauria (Dinosauria: Theropoda): divergent trends in snout morphology between Asian and North American taxa	134
3.1. Introduction	134
3.2 Materials and Methods.....	137
3.2.1 Regression analysis	138
3.2.2 Principal component analysis (PCA) and cluster analysis	139

3.2.3 Character assessment.....	142
3.2.4 Phylogenetic analysis	143
3.3 Results	145
3.3.1 Regression analysis	145
3.3.2 Principal component analysis (PCA) and cluster analysis	145
3.3.3 Character assessment.....	149
3.3.4 Phylogenetic analysis	154
3.4 Discussion	156
3.4.1 Maxilla length/height ratio as a proxy for snout shape	156
3.4.2 Maxillary shape variation and clustering.....	157
3.4.3 Character assessment.....	160
3.4.4 Phylogenetic analysis	168
3.4.5 Evolutionary trends	168
3.5 Conclusions	175
3.6 Literature Cited	177
3.7 Tables and Figures	189
Chapter 4. Description of a new species of <i>Velociraptor</i> and new insights into intrageneric variation	210
4.1 Introduction	210
4.2 Materials and Methods	212
4.2.1 Principal component analyses	212
4.2.2 Regression analyses.....	213
4.2.3 Phylogeny	215
4.3 Systematic Palaeontology	217
4.4 Description	219
4.4.1 Cranium	219
4.4.2 Mandible.....	238
4.4.3 Axial skeleton.....	242
4.4.4 Appendicular skeleton	247
4.5 Results	255
4.5.1 Principal component analysis.....	255
4.5.2 Regression analyses.....	257
4.5.3 Phylogeny	261
4.6 Discussion.	264
4.6.1 Variation in <i>Velociraptor</i>	264

4.6.2 Evolution and ecology	272
4.7 Conclusions	279
4.8 Literature Cited	282
4.9 Tables and Figures	293
Chapter 5. Conclusions	338
5.1 Literature Cited	347
5.2 Figures.....	352
References.....	355
Appendix 1	375
A 1.1. Anterior ramus regression analyses data	375
A 1.2. Character revisions	375
Appendix 2.....	383
A 2.1. Raw data.	383
A 2.2. Linear regression analysis.	384
A 2.3. Length corrected measurements for PCA. All	385
A 2.4. Length of the first nine alveoli corrected data.....	387
A 2.5 Ratio-based character analysis.	389
A 2.6 Character-taxon data matrix	399
Appendix 3.....	406
A 3.1. Raw data for PCA and quadrateH/maxillaH RMA	406
A 3.2. Finalized character list including support for ratio-based characters.....	407
A 3.3. Character-taxon matrix.....	433

List of Tables

Table 1.1. Referenced eudromaeosaurian and relevant outgroup taxa with continental locations.	27
Table 2.1. Maxillary ratios, proportions, posterodorsal inclination, and tooth counts of eudromaeosaurian dromaeosaurids.	102
Table 3.1. Specimens and measurement methods for morphometric analysis.	190
Table 3.2. Linear measurements of maxillae and premaxillae in lateral aspect.	193
Table 3.3. Character state changes and additions to Currie and Evans (2019) data matrix.	195
Table 3.4. Character consistency index values for characters added or	198
Table 4.1. List of specimens used for metric comparison with <i>V. vadarostrum</i> n. sp.	294
Table 4.2. Size measurements of <i>V. vadarostrum</i> n. sp.	295
Table 4.3. List of PCA scores for raw linear measurements and log transformed data.	296
Table 4.4. List of PC loadings for raw data linear measurement PCA and log transformed data PCA.	297
Table 4.5. Results of multiple regression analysis of Asian eudromaeosaurian maxillary comparative analyses.	299
Table 4.6. Results of multiple regression analysis of maxillary measurements comparison across <i>Velociraptor</i>	300
Table 4.7. Reduced major axis regression analysis of <i>V. mongoliensis</i> with and without <i>V. vadarostrum</i> n. sp.	301
Table 4.8. Values for parsimony and Bayesian consensus trees.	302
Table 4.9. Comparison of premaxillary and maxillary character CI values among phylogenetic analyses.	303

List of Figures

Figure 1.1. Composition of snout and maxilla morphology in eudromaeosaurians.	29
Figure 1.2. Lateral views of Eudromaeosaurian maxillae that are representative of the taxonomic diversity considered in this study.....	31
Figure 2.1. Angle of ascending ramus	104
Figure 2.2. Maxillary fenestra and sinus system of <i>Acheroraptor temertyorum</i>	105
Figure 2.3. Parasagittal sections of ROM 63777 showing internal maxilla structures.....	107
Figure 2.4. Retro-deformed right maxilla of <i>Acheroraptor temertyorum</i>	109
Figure 2.5. Skull reconstruction of <i>Acheroraptor temertyorum</i>	111
Figure 2.6. Coronal and parasagittal sections of TMP 1994.012.0844, <i>Saurornitholestes langstoni</i> CT data.....	112
Figure 2.7. 3D rendering of <i>Saurornitholestes langstoni</i> (TMP 1994.012.0844) and maxillary teeth.....	114
Figure 2.8. CT data of <i>Tsaagan mangas</i> maxilla with 3D rendering of the right maxilla.....	116
Figure 2.9. Right lateral view of the holotype of <i>Atrociraptor marshalli</i> with coronal CT sections.....	118
Figure 2.10. 3D rendering of the maxilla of <i>Atrociraptor marshalli</i>	120
Figure 2.11. Articulated 3D models of TMP 1995.166.0001.	121
Figure 2.12. CT data of YPM 5232 (557) <i>Deinonychus antirrhopus</i>	123
Figure 2.13. Segmentation of the maxilla of <i>Deinonychus antirrhopus</i> (YPM 5232 [557]).....	125
Figure 2.14. 3D mesh of the maxilla of YPM 5232 (557) <i>Deinonychus antirrhopus</i>	126
Figure 2.15. Skull reconstruction of <i>Deinonychus antirrhopus</i>	127
Figure 2.16. CT data of the skull of a <i>Velociraptor</i> sp. specimen (MPC-D 100/982).....	128
Figure 2.17. Reduced Major Axis regression analysis of eudromaeosaurian anterior ramus and maxillary dimensions.	130
Figure 2.18. Tooth replacement in eudromaeosaurians.	132
Figure 3.1. Maxillary measurements used for PCA and bivariate analyses.	199
Figure 3.2. Simple linear regression of premaxillary length-to-height ratio on maxillary length-to-height ratio in eudromaeosaurian specimens.....	200
Figure 3.3. Results from linear measurement principal component analyses of the maxillae of eudromaeosaurian taxa and closely related outgroups.....	201
Figure 3.4. Classic cluster analysis using UPGMA pairing algorithm and Euclidean similarity index.....	203
Figure 3.5. Ratio-based character distributions with Jenks Natural Breaks Optimization	205
Figure 3.6. Character distributions for new ratio-based characters in dromaeosaurids.....	207

Figure 3.7. 50% majority rule consensus trees generated from a modified taxon-character matrix	208
Figure 4.1. Comparison of <i>Velociraptor</i> skull profiles.....	304
Figure 4.2. Dorsal aspect of the skull of <i>V. vadarostrum</i> n. sp. with comparison to <i>V. mongoliensis</i>	306
Figure 4.3. Lateral aspects of the skull of <i>V. vadarostrum</i> n. sp.	308
Figure 4.4. 3D rendering of the left lacrimal of <i>V. vadarostrum</i> n. sp.	310
Figure 4.5. Frontal comparison between <i>V. vadarostrum</i> n. sp. and <i>V. mongoliensis</i>	311
Figure 4.6. Skull of <i>V. vadarostrum</i> n. sp. in posterior view with comparison to <i>V. mongoliensis</i>	313
Figure 4.7. Ventral aspect of the skull of <i>V. vadarostrum</i> n. sp. with comparison to <i>V. mongoliensis</i>	315
Figure 4.8. Articulated skeleton of the holotype of <i>Velociraptor vadarostrum</i> n. sp. in right lateral view.....	317
Figure 4.9. Articulated skeleton of <i>Velociraptor vadarostrum</i> n. sp. in left lateral aspect.....	319
Figure 4.10. Pectoral girdle of <i>Velociraptor vadarostrum</i> n. sp.....	321
Figure 4.11. Pelvis and upper hindlimb of <i>Velociraptor vadarostrum</i> n. sp.	323
Figure 4.12. Interpretive line drawing of the sternal plate of <i>Velociraptor vadarostrum</i> n. sp..	325
Figure 4.13. Left and right proximal metatarsus of <i>Velociraptor vadarostrum</i> n. sp.....	327
Figure 4.14. PCA analysis of Asian eudromaeosaurians using both raw linear measurements and log transformed data.	329
Figure 4.15. Linear measurement PCA analysis of eudromaeosaurian taxa.	331
Figure 4.16. Ordinary least squares and reduced major axis regression analyses of <i>Velociraptor</i> maxillae.....	332
Figure 4.12. Consensus trees of parsimony and Bayesian analyses of Dromaeosauridae dataset including <i>Velociraptor vadarostrum</i> n. sp.....	334
Figure 4.13. Consensus trees of parsimony and Bayesian analyses of Eudromaeosauria dataset including <i>Velociraptor vadarostrum</i> n. sp.....	336
Figure 5.1. Eudromaeosauria snout dimensions mapped onto Bayesian phylogeny.....	353

Institutional Abbreviations

AMNH FARB American Museum of Natural History, New York City NY, USA;
BYUVP Brigham Young University Museum of Paleontology, Provo UT, USA; **CEUM** College of Eastern Utah Prehistoric Museum, Price UT, USA; **IMM** Inner Mongolian Museum, Hohhot, China; **IVPP** Institute of Vertebrate Paleontology and Paleoanthropology, Beijing, China; **MML** Museo Municipal de Lamarque, Rio Negro, Argentina; **MNUFR** Mongolian National University, Ulaan Baatar, Mongolia; **MPC** Paleontological and Geological Center of the Mongolian Academy of Sciences, Ulaan Baatar, Mongolia; **ROM** Royal Ontario Museum, Toronto ON, Canada; **TMP** Royal Tyrrell Museum of Palaeontology, Drumheller AB, Canada; **UALVP** University of Alberta Laboratory for Vertebrate Palaeontology, Edmonton AB, Canada; **YPM** Yale Peabody Museum of Natural History, New Haven CT, USA

Chapter 1. Introduction

Dromaeosaurids are small to medium sized, carnivorous theropod dinosaurs that were highly diverse in the Late Cretaceous (Longrich and Currie 2009, Turner et al. 2012, Evans et al. 2013). They ranged in size from the diminutive *Microraptor* Xu et al., 2000, to bear-sized taxa such as *Achillobator* Perle et al., 1999, *Austroraptor* Novas et al., 2009, and *Utahraptor* Kirkland et al., 1993 (Kirkland et al. 1993, Perle et al. 1999, Xu et al. 2000, Erickson et al. 2009, Novas et al. 2009). Compared to other large carnivorous dinosaurs of the Cretaceous, even the largest dromaeosaurids would be considered medium sized, whereas the smallest were comparable to modern birds such as the Black Billed Magpie and other small avialans such as *Archaeopteryx* Meyer, 1861 (Elzanowski and Wellnhofer 1996, Xu et al. 2000).

Most members of the family Dromaeosauridae Matthew and Brown, 1922, belong to the clade Eudromaeosauria Longrich and Currie, 2009, which includes Dromaeosaurinae Matthew and Brown, 1922, Saurornitholestinae Longrich and Currie, 2009, and Velociraptorinae Barsbold, 1983 but excludes Halszkaraptorinae Cau et al., 2017, Microraptorinae Senter et al., 2004 and Unenlagiinae Bonaparte, 1999. Eudromaeosauria is predominantly composed of species from Asia and North America (Turner et al. 2012). The first eudromaeosaurian species described was *Dromaeosaurus albertensis* Matthew and Brown, 1922. It was placed in the subfamily Dromaeosaurinae within the Deinodontidae, which is now Tyrannosauridae Osborn, 1906. The description of *Velociraptor mongoliensis* Osborn, 1924 followed shortly after, however, these two taxa were not found to be united in the family Dromaeosauridae until the description of *Deinonychus antirrhopus* Ostrom, 1969, over 40 years later (Ostrom 1969). Ostrom's work on *Deinonychus* championed the idea of swift active predators. These ideas inspired great works of fiction such as *Jurassic Park* (Crichton 1991), which portrayed the new

image of ‘raptor’ dinosaurs in a frighteningly real way. The image of ‘raptor’ dinosaurs in the view of the public has largely been shaped by characteristics of members of Eudromaeosauria. Eudromaeosaurians share many dromaeosaurid characteristics such as generally long arms with recurved manual unguals, well developed hindlimbs with a raised hypertrophied ungual on digit II making them effectively didactyl during locomotion, and a stiffened tail from elongate prezygapophyses (Ostrom 1969, Norell and Makovicky 1997, 1999, Burnham et al. 2000). Eudromaeosaurians are medium to large size for dromaeosaurids and have relatively large and few teeth compared to unenlagiines, which reach comparable sizes. Direct evidence of feathers within Eudromaeosauria has also been found using CT data. Large forearm feathers are inferred for *Velociraptor* based on the presence of knobs along the ulna (Turner et al. 2007b). These knobs have also been found in other larger bodied coelurosaurians such as oviraptorosaurs (Funston and Currie 2016), and large forearm feathers are preserved in the closely related dromaeosaurid *Zhenyuanlong suni* Lü and Brusatte, 2015. While the evidence of feathers and gracile builds are indicative of active animals, they largely pertain to high metabolic activity and thermoregulation. However, these anatomical features have been used as support for the hypothesis of swift and active hunters.

This hypothesis remained relatively unchallenged until more complete specimens were uncovered in recent decades (Norell and Makovicky 1997, 1999, Burnham et al. 2000, Xu et al. 2010a, Currie and Evans 2019). From comparisons of hindlimb anatomy to other theropod groups, however, it was revealed that eudromaeosaurians showed relatively poor adaptations for cursoriality (Gatesy and Middleton 1997, Farlow et al. 2000, Fowler et al. 2011, Persons and Currie 2016). The hindlimb adaptations eudromaeosaurians display, such as their relatively short metatarsi and trenchant unguals of pedal digit II appear more akin to ambush predators that were

efficient at holding and capturing prey (Fowler et al. 2011). These features have also been proposed as useful for climbing and supporting an arboreal life habit (Manning et al. 2006). While it remains unclear the exact purpose of the raptorial claw and short metatarsals, eudromaeosaurians remain a remarkably diverse group with disparate morphology (Turner et al. 2012). While morphological variation can be observed throughout the anatomy of eudromaeosaurians, the skulls hold the most obvious variable characteristics (Currie and Varricchio 2004, Godefroit et al. 2008, Turner et al. 2012).

Whereas many eudromaeosaurian specimens from Asia include articulated postcrania and/or skulls (Osborn 1924, Barsbold 1983, Norell and Makovicky 1997, 1999, Barsbold and Osmólska 1999, Norell et al. 2006, Xu et al. 2010a), specimens from North America typically comprise isolated or at least disarticulated elements (Matthew and Brown 1922, Ostrom 1969, Sues 1976, Currie and Varricchio 2004, Evans et al. 2013). The few known exceptions include a nearly complete, articulated specimen of *Saurornitholestes langstoni* Sues, 1976 (Currie and Evans 2019), a bonebed containing some articulated elements of *Deinonychus antirrhopus* alongside many disarticulated ones (Ostrom 1969), and a nearly complete, associated juvenile skeleton (AMNH FARB 30556) of the dromaeosaurid *Bambiraptor feinbergi* Burnham et al., 2000. Note that the last specimen likely includes parts of at least two individuals (Turner et al. 2012). However, species such as *Acheroraptor temertyorum* Evans et al., 2013, *Achillobator giganticus* Perle et al., 1999, *Atrociraptor marshalli* Currie and Varricchio, 2004, and *Velociraptor osmolskae* Godefroit et al., 2008, have been described on the basis of isolated bones or partial skeletons, and their phylogenetic positions within Dromaeosauridae have largely been inferred from morphological features of their maxillae.

The maxilla is an intricate element in dromaeosaurids and other theropods (Hendrickx and Mateus 2014) (Fig. 1.1B-C), and beyond superficial features the medial surface contains the maxillary sinus system and palatal shelf. The latter makes up part of the palate and contacts the premaxilla, vomer and pterygoids (Witmer 1997, Witmer et al. 2008). Dromaeosaurid maxillae have also provided many characters used in phylogenetic analyses, and have been used for generating palaeoecological inferences (Currie and Varricchio 2004, Godefroit et al. 2008, Evans et al. 2013) based on the strong relationship between snout shape and prey selection (Janis and Ehrhardt 1988). Studies of modern carnivorans, in particular, have shown positive correlations between cranial snout shape (Fig. 1.1) and prey selection (Slater et al. 2009). While most studies on snout shape and dietary preference in dinosaurs have involved herbivorous taxa (Carrano et al. 1999, Whitlock 2011), some functional studies have set out to infer the possible diets of extinct carnivorous archosaurs (Rayfield et al. 2001, Therrien et al. 2005, Sakamoto 2010, Walmsley et al. 2013). However, most such studies have focused on mandibular shape and simple lever models, as opposed to the detailed morphology of the cranium. Direct evidence regarding prey selection in extinct predators is rarely available. The possibility remains, however, that a quantifiable divergence in snout morphology between predators known to have inhabited different areas can be linked to variations in available prey between the two ecosystems.

Eudromaeosaurian taxa have been suggested to show a morphological dichotomy in snout proportions across their geographical range (Barsbold and Osmólska 1999, Longrich and Currie 2009, Evans et al. 2013), with long-snouted species predominantly in Asia and short-snouted species restricted mostly to North America. This comparative framework was first established by Barsbold and Osmólska (1999) who described the skull of *Velociraptor*

mongoliensis in detail. The strikingly long snout of *Velociraptor mongoliensis* was hard to ignore and ratios of various skull elements – particularly ones of the snout – became a standard for comparison of dromaeosaurid taxa. However, some comparisons are based on specimens that only maxillae are known from the snout (Perle et al. 1999, Godefroit et al. 2008, Evans et al. 2013). Like inferences on diet, generalizations about snout shape based only on maxillary morphology depends fundamentally on the assumption that the proportions of the maxilla are reflective of those of the snout as a whole. For example, Evans et al. (2013) hypothesized an elongate snout for *Acheroraptor temertyorum* due to the elongate dimensions of the maxilla, unusual for a North American species. This is a reasonable ad hoc procedure, as the maxilla makes up most of the snout, defined as the part of the skull anterior to the orbital bar of the lacrimal (Fig. 1.1). However, the snout also includes the nasals and premaxilla, which can also vary a great deal in their proportions (Kirkland et al. 1993, Cau et al. 2017). The reliability of maxillary proportions as a proxy for overall snout shape should be carefully tested, particularly given the wide-reaching palaeoecological implications of the latter parameter.

Similarly, maxillae appear quite different across eudromaeosaurian species (Fig. 1.2) and many matrices for phylogenetic analysis of Eudromaeosauria have generated many characters around this tooth bearing element of the cranium along with characters of the teeth themselves (Longrich and Currie 2009, Evans et al. 2013, Currie and Evans 2019). In the most recent phylogenetic analysis of Eudromaeosauria (Currie and Evans 2019), 180 characters were coded, 17 of which are maxillary whereas 13 are constructed from maxillary teeth (either exclusively or partially). This means 30 of the 180 ($\approx 17\%$) of the coded characters pertain, at least in part, to one element of the skeleton. Many of the characters that have been developed for phylogenetic analysis to encode the observed variability of the maxilla require further examination because

they each divide a range of quantitative variation in some aspect of maxillary proportions into discrete character states (Senter et al. 2004, Longrich and Currie 2009, Evans et al. 2013). Despite the complexity of the maxilla, this element may not have the phylogenetic significance accorded it and by an attempt to extract more phylogenetic characters from one element may lead to increased problematic characters that may increase noise in phylogenetic analyses (Simões et al. 2016). Simões et al. (2016) defined numerous types of problematic character, and classified characters for which discrete states had unjustifiably been used to describe variation in a continuous range of data as Type II-B. Where data appear potentially continuous, discrete character states should only be used in a phylogenetic analysis if they can be justified by statistical testing. If significant gaps occur in the distribution of values for a numerical character such as a ratio, it is acceptable to treat the states on either side of the gap as discrete. If no such gap exists, the character should be left continuous, and processed in a phylogenetic analysis using software that can handle this type of input (Goloboff and Mattoni 2006). If such a test is not performed prior to defining discrete states, then the character states are at best a product of intuition. If a matrix accumulates many problematic characters, the results of phylogenetic analysis can be quite different from those that would be obtained from a matrix for the same taxa with carefully constructed characters (Simões et al. 2016). However, the discrete states defined for proportion-based characters in published dromaeosaurid matrices – as well as in many other matrices – have generally not been justified by explicit gap analysis, and instead have been based on arbitrary delineations within ranges of simple ratios (Longrich and Currie 2009, Turner et al. 2012). Because nearly a fifth of our phylogenetic data is derived from one element, it is paramount that we take the utmost care in construction of phylogenetic characters associated

with a single element. To do this, the data must be interpreted as thoroughly as possible through description in a comparative framework.

Description of specimens is the first step to analysing fossil data. Once we have identified patterns of similarity across available specimens, we can construct phylogenetic characters to determine relatedness amongst specimens (Patterson 1982). Taphonomic (post mortality) processes, however, may cause distortion of specimens, which may affect our interpretation of the morphology (White 2003, Arbour and Currie 2012, Baert et al. 2014). To reduce these effects, non-invasive imaging techniques can be used to examine total morphology and retro-deformation may be attempted on distorted specimens (Boyd and Motani 2008, Arbour and Currie 2012). This can be an effective method to restore the proportions of a specimen to better assess similarities to other related specimens.

Proportions of elements – either intrinsically or compared to other elements – can be attractive features for character construction and are frequently used in taxon-character matrices (Evans et al. 2013, Lü and Brusatte 2015, Carr et al. 2017, Cau et al. 2017, Currie and Evans 2019). Evans et al. (2013) relied heavily on ratio-based characters to support the hypothesis of an Asian affinity for their newly described North American dromaeosaurid, *Acheroraptor temertyorum*. Evans et al. (2013) primarily focused on the elongation of the anterior ramus (Fig. 1.1), the anteroposteriorly short and ventrally restricted antorbital fossa, and a low sitting maxillary fenestra, all features the authors suggested linked it with Asian taxa such as *Linheraptor exquisitus* Xu et al., 2010, and *Tsaagan mangas* Norell et al., 2006. Ratio-based characters can be problematic in how they are constructed but may also be susceptible to noise via allometry from ontogenetic variation (Sampson et al. 1997, Currie 2003a, Williamson and Carr 2003, Schott et al. 2011), variation from sexual dimorphism (Butler and Losos 2002), or

intraspecific (individual) variation (Sampson et al. 1997, Ibiricu et al. 2013, Barta et al. 2018, Holmes et al. 2020). Elongation of features of the snout may also be ecomorphological, convergently acquired to overlapping ecological niches (Janis and Ehrhardt 1988, Butler and Losos 2002, van Cakenberghe et al. 2002, Slater et al. 2009). Evans et al. (2013) hypothesised that the elongate maxilla of *Acheroraptor temertyorum* was a proxy for an elongate snout. While the maxilla does make up a large portion of a theropod snout in lateral view it was not clearly demonstrated that this element could be used to infer overall snout morphology. Therefore, it is important to quantify the relationship of elements that together compose a functional unit (Fig. 1.1).

The proposed dichotomy of snout morphology between Asian and North American eudromaeosaurians (Barsbold and Osmólska 1999, Evans et al. 2013) has not been quantified but represents a possible ecomorphological trend in which the Asian forms have evolved in different ecological conditions from North American ones that required the acquisition of long, shallow jaws. The number of eudromaeosaurian species from Asia and North America in which cranial material – including a complete maxilla – is known is five representative species for each (Currie and Evans 2019). This provides an opportunity to examine trends in snout shape between these geographically separate groups. However, to test these biogeographical trends, one needs a sense of their phylogenetic relationships and must account for individual and ontogenetic variation.

North American species of eudromaeosaurians (Table 1.1) have various levels of completeness with specimens like *Bambiraptor feinbergi*, *Deinonychus antirrhopus*, and *Saurornitholestes langstoni* being nearly complete while *Acheroraptor temertyorum*, and *Atrociraptor marshalli* Currie and Varricchio, 2004, are known from limited cranial material.

The initial description of *Atrociraptor* was only of the anteroventral section of the snout in lateral view due to incomplete preparation (Currie and Varricchio 2004). Due to the delicate nature of the specimen, it has not been fully prepared and may remain in its current state. Computed tomography offers a way to examine the entire specimen and better assess its overall morphology. While most of these specimens represent adult or sub-adult individuals, the most complete specimen of *Bambiraptor* (AMNH FARB 30556) is a known juvenile (Burnham et al. 2000, Turner et al. 2012). Whereas an adult maxilla referred to *Bambiraptor feinbergi* was described by Currie and Varricchio (2004), it has been maintained that the similarities between *Bambiraptor feinbergi* and *Saurornitholestes langstoni* may imply that the former is in fact a juvenile morph of the latter (Currie and Varricchio 2004, Turner et al. 2012). Due to the limited number of specimens for each of these species, no definitive connection has been made, and *Bambiraptor feinbergi* has continued to be used in phylogenetic analyses of Dromaeosauridae (Longrich and Currie 2009, Turner et al. 2012, Evans et al. 2013, Currie and Evans 2019). The allometric changes in dromaeosaurids during ontogeny are poorly understood and use of ratio-based characters with a juvenile specimen may affect phylogenetic placement.

The only described maxilla of *Deinonychus antirrhopus* has been the one from the initial description more than 50 years ago (Ostrom 1969). It was interpreted as being nearly complete with the nasals, a partial premaxilla, and vomers wedged on the medial side. In the initial description, the maxilla contained 15 maxillary teeth, three more than in any other known eudromaeosaurian (Currie and Evans 2019). The anterior portion is crushed and houses two teeth, and the ascending ramus is longer than in other dromaeosaurids giving it an elongate triangular appearance (Ostrom 1969). Although this could be the appropriate interpretation, it has not been thoroughly investigated. Computed tomography may allow us to observe suture patterns

and confirm the boundaries of the outline of the maxilla. Reassessments of the specimens could clarify previous morphological interpretations and provide more data in the form of coded phylogenetic characters. While the North American specimens are often partial and disarticulated, the problems of Asian eudromaeosaurian specimens is very different.

Asian eudromaeosaurians (Table 1.1) include numerous articulated specimens. The articulated nature of the specimens is what often obscures internal morphological features and computed tomography has been used to great effect in analysing internal cranial bones and medial surfaces of surficial bones (Norell et al. 2006, 2009). Due to poor stratigraphic correlation between localities (Dashzeveg et al. 2005, Dingus et al. 2008), however, closely related species are more contested in their validity (Turner et al. 2012). Of the Asian eudromaeosaurians, *Linheraptor exquisitus* and *Tsaagan mangas* have been proposed by some authors to be the same species, the former being a junior synonym of the latter (Turner et al. 2012). Turner et al. (2012) also proposed that the differences between these two species were likely due to individual variation, akin to what the authors claimed is observed in *Velociraptor mongoliensis*. Xu et al. (2015) defended the phylogenetic position of *Linheraptor exquisitus* and suggested that some specimens assigned to *V. mongoliensis* may be a distinct species, and that a proper test of intraspecific variation should be conducted. *Velociraptor mongoliensis* currently has more than eight specimens assigned to it (Kielan-Jaworowska and Barsbold 1971, Norell and Makovicky 1997, 1999, Barsbold and Osmólska 1999, Hone et al. 2010, 2012) but no assessment of intraspecific variation has been made. A second species of *Velociraptor*, *V. osmolskae*, was erected based on two partial maxillae and a lacrimal found in China (Godefroit et al. 2008). This species was diagnosed primarily by the maxilla, further emphasizing the importance of this element in eudromaeosaurian systematics.

The current state of dromaeosaurid systematics has relied heavily on maxillary morphology due to the rarity of any other material for some genera. Inferences have been made for phylogeny and ecology based on this limited material and no attempts have been made to quantify what inferences are appropriate to make from this single element within Dromaeosauridae, or even the more exclusive clade, Eudromaeosauria. In this thesis I will re-examine and quantify morphological variation in maxillae across Eudromaeosauria to answer the question: how informative is the morphology of maxillae regarding ecology and taxonomy within Eudromaeosauria?

Are the morphologies of maxillae in North American eudromaeosaurians accurately represented, or has post-mortem deformation of these specimens led to misinterpretations of the data? If the interpretation of morphological variation in North American eudromaeosaurian maxillae is accurate, then retro-deformation, and analysis of suture patterns will result in no changes to our interpretation of maxillary morphology between eudromaeosaurian taxa. The first step of this thesis is to analyse problematic specimens of North American eudromaeosaurians and critically assess the data with the aid of computed tomography and 3-dimensional visualizations. Any changes to morphological interpretations will affect assessments of character construction, character coding, ecological inference, and shape analysis.

Can maxillae of eudromaeosaurians be used to infer snout shape in profile? If the maxilla is a reasonable proxy for snout shape profile in eudromaeosaurians, then the premaxilla should change shape in tandem with the maxilla throughout eudromaeosaurian taxa because that is the only way the shape of one could reasonably predict the other. Using articulated specimens of eudromaeosaurians that represent adult individuals, dimensions of the premaxilla and maxilla will be compared with regression analysis to test the predictive potential of each element. In

lateral view these two elements crudely represent snout shape, and this was chosen to accommodate mediolaterally crushed specimens and because the nasal typically forms the roof of the snout with little influence on the shape in lateral aspect.

Is the shape of the maxilla in eudromaeosaurians representative of phylogenetic diversity? If the shape of the maxilla in eudromaeosaurians is representative of phylogenetic diversity, then comparative analysis of linear measurements of maxillae across various taxa within Eudromaeosauria should plot in distinct clusters representative of described taxa. Highly variable measurements may also indicate which measurement ratios have potential for taxonomic utility. Linear measurement morphometrics and cluster analysis will be used to analyse the morphological disparity, and clustering patterns of eudromaeosaurian maxillae.

Are ratio-based characters constructed from the maxillae of eudromaeosaurian taxa phylogenetically informative? If ratio-based characters of the eudromaeosaurian maxilla are phylogenetically informative then they will show discrete groupings within the available data that can be used to distinguish species (Simões et al. 2016). Ratios will be calculated for all specimens used in this thesis and plotted in histograms to observe data distribution. Natural breaks will be identified using Jenks Optimization method to determine how well binning of ratio data fits the distribution. If there are well supported groupings of data, then the continuous data is justified in being treated as discrete.

Does intraspecific variation in maxillary morphology of eudromaeosaurians overshadow phylogenetic signal? If the maxillae of eudromaeosaurians are phylogenetically informative then there should be low intraspecific variability and there should be discrete characteristics that distinguish members of different species from each other. Using specimens assigned to *Velociraptor mongoliensis* and description of a previously undescribed *Velociraptor* sp. (MPC-D

100/982), variations in morphology, with emphasis on maxillae, will be analysed. Techniques used throughout this thesis will be used to analyse variation within the genus *Velociraptor* and will determine if the variation previously reported is warranted or if there are potentially more species within *Velociraptor* than previously recognized. Homologous structures will be used to analyse variation in a comparative framework and ratios of features will be compared as well. Morphometrics will be used to examine the degree of variation between maxillae of all applicable specimens.

Following the assessments of variation in maxillary morphology within Eudromaeosauria, phylogenetic analyses will be conducted to re-examine interrelationships within the clade. Characters pertaining to the maxilla and snout will be examined for their distributions throughout the clade and closely related outgroups to examine the evolution of this element through time. Biogeographical trends will be compared to recovered tree topologies to observe possible ecological drivers for the evolution of the eudromaeosaurian snout.

1.1 Literature Cited

- Arbour, V.M., and Currie, P.J. 2012. Analyzing taphonomic deformation of ankylosaur skulls using retrodeformation and finite element analysis. *PLoS ONE*, **7**: 1–13.
doi:10.1371/journal.pone.0039323.
- Baert, M., Burns, M.E., and Currie, P.J. 2014. Quantitative diagenetic analyses of *Edmontosaurus regalis* (Dinosauria: Hadrosauridae) postcranial elements from the Danek Bonebed, Upper Cretaceous Horseshoe Canyon Formation, Edmonton, Alberta, Canada: Implications for allometric studies of fossil. *Canadian Journal of Earth Sciences*, **51**: 1007–1016. doi:10.1139/cjes-2014-0060.
- Barsbold, R. 1974. Saurornithoididae, a new family of small theropod dinosaurs from Central Asia and North America. *Palaeontologia Polonica*, **30**: 5–52.
- Barsbold, R. 1983. Carnivorous dinosaurs from the Cretaceous of Mongolia. *The Joint Soviet-Mongolian Palaeontological Expedition*, **19**: 117.
- Barsbold, R., and Osmólska, H. 1999. The skull of *Velociraptor* (Theropoda) from the Late Cretaceous of Mongolia. *Acta Palaeontologica Polonica*, **44**: 189–219.
- Barta, D.E., Nesbitt, S.J., and Norell, M.A. 2018. The evolution of the manus of early theropod dinosaurs is characterized by high inter- and intraspecific variation. *Journal of Anatomy*, **232**: 80–104. doi:10.1111/joa.12719.
- Bonaparte, J. 1999. Tetrapod faunas from South America and India: A palaeobiogeographic interpretation. *PINSA*, **65**: 427–437.
- Boyd, A.A., and Motani, R. 2008. Three-dimensional re-evaluation of the deformation removal technique based on “jigsaw puzzling.” *Palaeontologia Electronica*, **11**.

- Burnham, D.A., Derstler, K.L., Currie, P.J., Bakker, R.T., Zhou, Z., and Ostrom, J.H. 2000. Remarkable new birdlike dinosaur (Theropoda: Maniraptora) from the Upper Cretaceous of Montana. *The University of Kansas Paleontological Contributions*, **13**: 14.
- Butler, M.A., and Losos, J.B. 2002. Multivariate sexual dimorphism, sexual selection, and adaptation in greater antillean anolis lizards. *Ecological Monographs*, **72**: 541–559. doi:10.1890/0012-9615(2002)072[0541:MSDSSA]2.0.CO;2.
- van Cakenberghe, V., Herrel, A., and Aguirre, L.F. 2002. Evolutionary relationships between cranial shape and diet in bats (Mammalia : Chiroptera). *In Topics in Functional and Ecological Vertebrate Morphology. Edited by P. Aerts, K. D'Aour, A. Herrel, and R. Van Damme.* Staker Publishing. pp. 205–236.
- Carr, T.D., Varricchio, D.J., Sedlmayr, J.C., Roberts, E.M., and Moore, J.R. 2017. A new tyrannosaur with evidence for anagenesis and crocodile-like facial sensory system. *Scientific Reports*, **7**: 1–11. doi:10.1038/srep44942.
- Carrano, M.T., Janis, C.M., and Sepkoski, J.J. 1999. Hadrosaurs as ungulate parallels: Lost lifestyles and deficient data. *Acta Palaeontologica Polonica*, **44**: 237–261.
- Cau, A., Beyrand, V., Voeten, D.F.A.E., Fernandez, V., Tafforeau, P., Stein, K., Barsbold, R., Tsogtbaatar, K., Currie, P.J., and Godefroit, P. 2017. Synchrotron scanning reveals amphibious ecomorphology in a new clade of bird-like dinosaurs. *Nature*, **552**: 395–399. Nature Publishing Group. doi:10.1038/nature24679.
- Crichton, M. 1991. Jurassic Park. *In 25th Anniv.* Ballantine Books, New York.
- Currie, P., and Varricchio, D.J. 2004. A new dromaeosaurid from the Horseshoe Canyon

- Formation (Upper Cretaceous) of Alberta, Canada. *In Feathered Dragons. Edited by P.J. Currie, E.B. Koppelhus, M.A. Shugar, and J.L. Wright.* Indiana University Press, Bloomington and Indianapolis. pp. 112–132.
- Currie, P.J. 2003a. Cranial anatomy of tyrannosaurid dinosaurs from the Late Cretaceous of Alberta, Canada. *Acta Palaeontologica Polonica*, **48**: 191–226.
- Currie, P.J., and Evans, D.C. 2019. Cranial anatomy of new specimens of *Saurornitholestes langstoni* (Dinosauria , Theropoda , Dromaeosauridae) from the Dinosaur Park Formation (Campanian) of Alberta. *The Anatomical Record*, **04715**: 1–25. doi:10.1002/ar.24241.
- Dashzeveg, D., Dingus, L., Loope, D.B., Swisher, C.C., Dulam, T., and Sweeney, M.R. 2005. New stratigraphic subdivision, depositional environment, and age estimate for the Upper Cretaceous Djadokhta Formation, southern Ulan Nur Basin, Mongolia. *American Museum Novitates*, **3498**: 31. doi:10.1206/0003-0082(2005)498[0001:nssdea]2.0.co;2.
- Dingus, L., Loope, D.B., Dashzeveg, D., Swisher, C.C., Minjin, C., Novacek, M.J., and Norell, M.A. 2008. The geology of Ukhaa Tolgod (Djadokhta Formation, Upper Cretaceous, Nemegt Basin, Mongolia). *American Museum Novitates*, **3616**: 1. doi:10.1206/442.1.
- Elzanowski, A., and Wellnhofer, P. 1996. Cranial morphology of *Archaeopteryx*: Evidence from the seventh skeleton. *Journal of Vertebrate Paleontology*, **16**: 81–94. doi:10.1080/02724634.1996.10011286.
- Erickson, G.M., Rauhut, O.W.M., Zhou, Z., Turner, A.H., Inouye, B.D., Hu, D., and Norell, M.A. 2009. Was dinosaurian physiology inherited by birds? Reconciling slow growth in *Archaeopteryx*. *PLoS ONE*, **4**. doi:10.1371/journal.pone.0007390.

- Evans, D.C., Larson, D.W., and Currie, P.J. 2013. A new dromaeosaurid (Dinosauria: Theropoda) with Asian affinities from the latest Cretaceous of North America. *Naturwissenschaften*, **100**: 1041–1049. doi:10.1007/s00114-013-1107-5.
- Forster, C.A., Sampson, S.D., Chiappe, L.M., and Krause, D.W. 1998. The theropod ancestry of birds: New evidence from the Late Cretaceous of Madagascar. *Science*, **279**: 1915–1919. doi:10.1126/science.279.5358.1915.
- Fowler, D.W., Freedman, E.A., Scannella, J.B., and Kambic, R.E. 2011. The predatory ecology of *Deinonychus* and the origin of flapping in birds. *PLoS ONE*, **6**. doi:10.1371/journal.pone.0028964.
- Funston, G.F., and Currie, P.J. 2016. A new caenagnathid (Dinosauria: Oviraptorosauria) from the Horseshoe Canyon Formation of Alberta, Canada, and a reevaluation of the relationships of Caenagnathidae. *Journal of Vertebrate Paleontology*, **36**. doi:10.1080/02724634.2016.1160910.
- Gauthier, J. 1986. Saurischian monophyly and the origin of birds. *Memoirs of the California Academy of sciences*, **8**: 55.
- Gilmore, C.W. 1924. On *Troodon validus*, an orthopodus dinosaur from the Belly River Cretaceous of Alberta, Canada. *University of Alberta Bulletin*, **1**: 43.
- Godefroit, P., Currie, P.J., Hong, L., Shang, C.Y., and Dong, Z.M. 2008. A new species of *Velociraptor* (Dinosauria: Dromaeosauridae) from the Upper Cretaceous of northern China. *Journal of Vertebrate Paleontology*, **28**: 432–438. doi:10.1671/0272-4634(2008)28[432:ANSOVD]2.0.CO;2.

- Goloboff, P.A., and Mattoni, C.I. 2006. Continuous characters analyzed as such. *Cladistics*, **22**: 589–601.
- Hendrickx, C., and Mateus, O. 2014. *Torvosaurus gurneyi* n. sp., the largest terrestrial predator from Europe, and a proposed terminology of the maxilla anatomy in nonavian theropods. *PLoS ONE*, **9**. doi:10.1371/journal.pone.0088905.
- Holmes, R.B., Persons, W.S., Rupal, B.S., Qureshi, A.J., and Currie, P.J. 2020. Morphological variation and asymmetrical development in the skull of *Styracosaurus albertensis*. *Cretaceous Research*, **107**: 104308. Elsevier Ltd. doi:10.1016/j.cretres.2019.104308.
- Hone, D., Choiniere, J., Sullivan, C., Xu, X., Pittman, M., and Tan, Q. 2010. New evidence for a trophic relationship between the dinosaurs *Velociraptor* and *Protoceratops*. *Palaeogeography, Palaeoclimatology, Palaeoecology*, **291**: 488–492. doi:10.1016/j.palaeo.2010.03.028.
- Hone, D., Tsuihiji, T., Watabe, M., and Tsogtbaatr, K. 2012. Pterosaurs as a food source for small dromaeosaurs. *Palaeogeography, Palaeoclimatology, Palaeoecology*, **331–332**: 27–30. doi:10.1016/j.palaeo.2012.02.021.
- Ibiricu, L.M., Martínez, R.D., Casal, G.A., and Cerda, I.A. 2013. The behavioral implications of a multi-individual bonebed of a small theropod dinosaur. *PLoS ONE*, **8**: 1–11.
- Janis, C.M., and Ehrhardt, D. 1988. Correlation of relative muzzle width and relative incisor width with dietary preference in ungulates. *Zoological Journal of the Linnean Society*, **92**: 267–284. doi:10.1111/j.1096-3642.1988.tb01513.x.
- Kielan-Jaworowska, Z., and Barsbold, R. 1971. Narrative of the Polish-Mongolian expeditions

- 1967-1971. *Palaeontologia Polonica*, **27**: 13.
- Kirkland, J.I., Burge, D., and Gaston, R. 1993. A large dromaeosaur (Theropoda) from the Lower Cretaceous of eastern Utah. *Hunteria*, **2**: 1–16.
- Longrich, N.R., and Currie, P.J. 2009. A microraptorine (Dinosauria-Dromaeosauridae) from the Late Cretaceous of North America. *Proceedings of the National Academy of Sciences of the United States of America*, **106**: 5002–5007. doi:10.1073/pnas.0811664106.
- Lü, J., and Brusatte, S.L. 2015. A large, short-armed, winged dromaeosaurid (Dinosauria : Theropoda) from the Early Cretaceous of China and its implications for feather evolution. *Scientific Reports*,: 1–11. doi:10.1038/srep11775.
- Makovicky, P.J., Apesteguía, S., and Agnolín, F.L. 2005. The earliest dromaeosaurid theropod from South America. *Nature*, **437**: 1007–1011. doi:10.1038/nature03996.
- Manning, P.L., Payne, D., Pennicott, J., Barrett, P.M., and Ennos, R.A. 2006. Dinosaur killer claws or climbing crampons? *Biology Letters*, **2**: 110–112. doi:10.1098/rsbl.2005.0395.
- Matthew, W.D., and Brown, B. 1922. The family Deinodontidae, with notice of a new genus from the Cretaceous of Alberta. *Bulletin of the American Museum of Natural History*, **46**: 367–385.
- Meyer, H. von. 1861. *Archaeopteryx lithographica* (Vogel-Feder) und *Pterodactylus* von Solnhofen. *Neues Jahrbuch für Mineralogie, Geognosie, Geologie und Petrefakten-Kunde*, **1861**: 678–679.
- Norell, M.A., Clark, J.M., Turner, A.H., Makovicky, P.J., Barsbold, R., and Rowe, T. 2006. A new dromaeosaurid theropod from Ukhaa Tolgod (Ömnögov, Mongolia). *American*

- Museum Novitates, **3545**: 51. doi:10.1206/0003-0082(2006)3545[1:andtfu]2.0.co;2.
- Norell, M.A., and Makovicky, P.J. 1997. Important features of the dromaeosaur skeleton: information from a new specimen. *American Museum Novitates*, **3215**: 1–28.
- Norell, M.A., and Makovicky, P.J. 1999. Important features of the dromaeosaurid skeleton II: Information from newly collected specimens of *Velociraptor mongoliensis*. *American Museum Novitates*, **3282**: 1–45.
- Norell, M.A., Makovicky, P.J., Bever, G.S., Balanoff, A.M., Clark, J.M., Barsbold, R., and Rowe, T. 2009. A review of the Mongolian Cretaceous dinosaur *Saurornithoides* (Troodontidae: Theropoda). *American Museum Novitates*, **3654**: 1–63. doi:10.1206/648.1.
- Norell, M.A., Makovicky, P.J., and Clark, J.M. 2000. A new troodontid theropod from Ukhaa Tolgod, Mongolia. *Journal of Vertebrate Paleontology*, **20**: 7–11.
- Novas, F.E., and Pol, D. 2005. New evidence on deinonychosaurian dinosaurs of the Late Cretaceous of Patagonia. *Nature*, **433**: 858–861.
- Novas, F.E., Pol, D., Canale, J.I., Porfiri, J.D., and Calvo, J.O. 2009. A bizarre Cretaceous theropod dinosaur from Patagonia and the evolution of Gondwanan dromaeosaurids. *Proceedings of the Royal Society B: Biological Sciences*, **276**: 1101–1107. doi:10.1098/rspb.2008.1554.
- Osborn, H.F. 1906. *Tyrannosaurus*, Upper Cretaceous carnivorous dinosaur. (second communication.). *Bulletin of the American Museum of Natural History*, **XXII**: 259–265.
- Osborn, H.F. 1924. Three new Theropoda, *Protoceratops* Zone, central Mongolia. *American Museum Novitates*,: 1–12.

- Ostrom, J.H. 1969. Osteology of *Deinonychus antirrhopus*, an unusual theropod from the Lower Cretaceous of Montana. Peabody Museum of Natural History, **30**: 1–165.
- Patterson, C. 1982. Morphological characters and homology. *In* Problems of Phylogenetic Reconstruction. *Edited by* K.A. Joysey and A.E. Friday. Academic Press, London and New York. pp. 21–74.
- Perle, A., Norell, M.A., and Clark, J.M. 1999. A new maniraptoran theropod - *Achillobator giganticus* (Dromaeosauridae)- from the Upper Cretaceous of Burkhan, Mongolia. National University of Mongolia,: 102.
- Rayfield, E.J., Norman, D.B., Horner, C.C., Horner, J.R., Smith, P.M., Thomason, J.J., and Upchurch, P. 2001. Cranial design and function in a large theropod dinosaur. *Nature*, **409**: 1033–1037. doi:10.1038/35059070.
- Sakamoto, M. 2010. Jaw biomechanics and the evolution of biting performance in theropod dinosaurs. *Proceedings of the Royal Society B: Biological Sciences*, **277**: 3327–3333. doi:10.1098/rspb.2010.0794.
- Sampson, S.D., Ryan, M.J., and Tanke, D.H. 1997. Craniofacial ontogeny in centrosaurine dinosaurs (Ornithischia: Ceratopsidae): Taxonomic and behavioral implications. *Zoological Journal of the Linnean Society*,: 293–337. doi:10.1111/j.1096-3642.1997.tb00340.x.
- Schott, R.K., Evans, D.C., Goodwin, M.B., Horner, J.R., Brown, C.M., and Longrich, N.R. 2011. Cranial ontogeny in *Stegoceras validum* (Dinosauria: Pachycephalosauria): A quantitative model of pachycephalosaur dome growth and variation. *PLoS ONE*, **6**. doi:10.1371/journal.pone.0021092.

- Senter, P., Barsbold, R., Britt, B.B., and Burnham, D.A. 2004. Systematics and evolution of Dromaeosauridae (Dinosauria, Theropoda). *Bulletin of Gunma Museum of Natural History*, **8**: 1–20.
- Senter, P., Kirkland, J.I., Bird, J., and Bartlett, J.A. 2010. A new troodontid theropod dinosaur from the lower cretaceous of Utah. *PLoS ONE*, **5**: 1–5. doi:10.1371/journal.pone.0014329.
- Simões, T.R., Caldwell, M.W., Palci, A., and Nydam, R.L. 2016. Giant taxon-character matrices: Quality of character constructions remains critical regardless of size. *Cladistics*,: 1–22.
- Slater, G.J., Dumont, E.R., and Van Valkenburgh, B. 2009. Implications of predatory specialization for cranial form and function in canids. *Journal of Zoology*, **278**: 181–188. doi:10.1111/j.1469-7998.2009.00567.x.
- Sternberg, C.M. 1932. Two new theropod dinosaurs from the Belly River Formation of Alberta. *Canadian Field-Naturalist*, **46**: 99–105.
- Sues, H.-D. 1976. A new small theropod dinosaur from the Judith River Formation (Campanian) of Alberta. *Zoological Journal of the Linnean Society*, **62**: 381–400.
- Therrien, F., Henderson, D.M., and Ruff, C.B. 2005. Bite me. Biomechanical models of theropod mandibles and implications for feeding behavior. *In The Carnivorous Dinosaurs. Edited by K. Carpenter. Indiana University Press, Bloomington. pp. 179–237.*
- Tsuihiji, T., Barsbold, R., Watabe, M., Tsogtbaatar, K., Chinzorig, T., Fujiyama, Y., and Suzuki, S. 2014. An exquisitely preserved troodontid theropod with new information on the palatal structure from the Upper Cretaceous of Mongolia. *Naturwissenschaften*, **101**: 131–142. doi:10.1007/s00114-014-1143-9.

- Turner, A.H., Hwang, S.H., and Norell, M.A. 2007a. A small derived theropod from Öösh, Early Cretaceous, Baykhangor Mongolia. *American Museum Novitates*, **3557**: 27.
doi:10.1206/0003-0082(2007)3557[1:asdtfs]2.0.co;2.
- Turner, A.H., Makovicky, P.J., and Norell, M.A. 2007b. Feather quill knobs in the dinosaur *Velociraptor*. *Science*, **317**. doi:10.1126/science.1145076.
- Turner, A.H., Makovicky, P.J., and Norell, M.A. 2012. A review of dromaeosaurid systematics and paravian phylogeny. *Bulletin of the American Museum of Natural History*, **371**: 1–206.
doi:10.1206/748.1.
- Turner, A.H., Pol, D., Clarke, J.A., Erickson, G.M., and Norell, M.A. 2007c. A basal dromaeosaurid and size evolution preceding avian flight. *Science*, **317**: 1378–1381.
doi:10.1126/science.1144066.
- Walmsley, C.W., Smits, P.D., Quayle, M.R., McCurry, M.R., Richards, H.S., Oldfield, C.C., Wroe, S., Clausen, P.D., and McHenry, C.R. 2013. Why the long face? The mechanics of mandibular symphysis proportions in crocodiles. *PLoS ONE*, **8**: 34.
doi:10.1371/journal.pone.0053873.
- White, T. 2003. Early hominids - diversity or distortion? *Science*, **299**: 1994–1995.
doi:10.1126/science.1078294.
- Whitlock, J.A. 2011. Inferences of diplodocoid (Sauropoda: Dinosauria) feeding behavior from snout shape and microwear analyses. *PLoS ONE*, **6**. doi:10.1371/journal.pone.0018304.
- Williamson, T.E., and Carr, T.D. 2003. A new genus of derived pachycephalosaurian from western North America. *Journal of Vertebrate Paleontology*, **22**: 779–801.

doi:10.1671/0272-4634(2002)022[0779:ANGODP]2.0.CO;2.

Witmer, L.M. 1997. The evolution of the antorbital cavity of archosaurs: A study in soft-tissue reconstruction in the fossil record with an analysis of the function of Pneumaticity. *Journal of Vertebrate Paleontology*, **17**: 1–76. doi:10.1080/02724634.1997.10011027.

Witmer, L.M., Ridgely, R.C., Dufeu, D.L., and Semones, M.C. 2008. Using CT to Peer into the Past : 3D Visualization of the Brain and Ear Regions of Birds , Crocodiles , and Nonavian Dinosaurs. *Anatomical Imaging*,: 33. doi:10.1007/978-4-431-76933-0.

Xu, X., Choiniere, J.N., Pittman, M., Tan, Q., Xiao, D., Li, Z., Tan, L., Clark, J.M., Norell, M.A., Hone, D.W.E., and Sullivan, C. 2010a. A new dromaeosaurid (Dinosauria: Theropoda) from the Upper Cretaceous Wulansuhai Formation of Inner Mongolia, China. *Zootaxa*, **9**: 1–9.

Xu, X., Norell, M.A., Wang, X.L., Makovicky, P.J., and Wu, X.C. 2002. A basal troodontid from the Early Cretaceous of China. *Nature*, **415**: 780–784. doi:10.1038/415780a.

Xu, X., Pittman, M., Sullivan, C., Choiniere, J.N., Tan, Q.-W., Clark, J.M., Norell, M. a., and Wang, S. 2015. The taxonomic status of the Late Cretaceous dromaeosaurid *Linheraptor exquisitus* and its implications for dromaeosaurid systematics. *Vertebrata Palasiatica*, **53**: 29–62.

Xu, X., Wang, X.L., and Wu, X.C. 1999. A dromaeosaurid dinosaur with a filamentous integument from the Yixian Formation of China. *Nature*, **401**: 262–266. doi:10.1038/45769.

Xu, X., Zhou, Z., and Wang, X. 2000. The smallest known non-avian theropod dinosaur. *Nature*, **408**: 705–708. doi:10.1038/35047056.

Zheng, X., Xu, X., You, H., Zhao, Q., and Dong, Z. 2010. A short-armed dromaeosaurid from the Jehol group of China with implications for early dromaeosaurid evolution. *Proceedings of the Royal Society B: Biological Sciences*, **277**: 211–217. doi:10.1098/rspb.2009.1178.

1.2 Tables and Figures

Table 1.1. Referenced eudromaeosaurian and relevant outgroup taxa with continental locations.

<u>Dromaeosauridae</u> Matthew and Brown, 1922	
<i>Tianyuraptor ostromi</i> Zheng et al., 2009	China, Asia
<i>Zhenyuanlong suni</i> Lu and Brusatte, 2015	China, Asia
Eudromaeosauria Longrich and Currie, 2009	
<i>Acheroraptor temertyorum</i> Evans et al., 2013	USA, North America
<i>Achillobator giganticus</i> Perle et al., 1999	Mongolia, Asia
<i>Adasaurus mongoliensis</i> Barsbold 1983	Mongolia, Asia
<i>Atrociraptor marshalli</i> Currie and Varricchio, 2004	Canada, North America
<i>Bambiraptor feinbergi</i> Burnam et al., 2000	USA, North America
<i>Deinonychus antirrhopus</i> Ostrom, 1969	USA, North America
<i>Dromaeosaurus albertensis</i> Matthew and Brown, 1922	Canada, North America
<i>Linheraptor exquisitus</i> Xu et al., 2010	China, Asia
<i>Saurornitholestes langstoni</i> Sues 1978	Canada, North America
<i>Tsaagan mangas</i> Norell et al., 2006	Mongolia, Asia
<i>Utahraptor ostrommaysi</i> Kirkland et al., 1993	USA, North America
<i>Velociraptor mongoliensis</i> Osborn, 1924	Mongolia, Asia
<i>Velociraptor osmolskae</i> Godefroit et al., 2008	China, Asia
<i>Velociraptor</i> sp. nov.	Mongolia, Asia
Halszkaraptorinae Cau et al., 2017	
<i>Halszkaraptor escuilliei</i> Cau et al., 2017	Mongolia, Asia
<i>Mahakala omnogavae</i> , Turner et al., 2007	Mongolia, Asia
Microraptorinae Senter et al, 2004	
<i>Microraptor zhaoianus</i> Xu et al., 2000	China, Asia

<i>Shanag ashile</i> Turner et al, 2007	China, Asia
<i>Sinornithosaurus millenii</i> Xu et al., 1999	China, Asia
Unenlagiinae Bonaparte, 1999	
<i>Austroraptor cabazai</i> Novas et al., 2009	Argentina, South America
<i>Buitreraptor gonzalezorum</i> , Makovicky et al., 2005	Argentina, South America
<i>Neuquenraptor argentinus</i> , Novas and Pol, 2005	Argentina, South America
<i>Rahonavis ostromi</i> , Forster et al., 1998	Madagascar, Africa
<u>Troodontidae</u> Gilmore, 1924	
<i>Byronosaurus jaffei</i> Norell et al., 2000	Mongolia, Asia
<i>Geminiraptor suarezorum</i> Senter et al., 2010	USA, North America
<i>Gobivenator mongoliensis</i> Tsuihiji et al., 2014	Mongolia, Asia
<i>Saurornithoides mongoliensis</i> Osborn, 1924	Mongolia, Asia
<i>Sinovenator changii</i> Xu et al., 2002	China, Asia
<i>Stenonychosaurus inequalis</i> Sternberg, 1932	Canada, North America
<i>Zanabazar junior</i> (Barsbold, 1974)	Mongolia, Asia

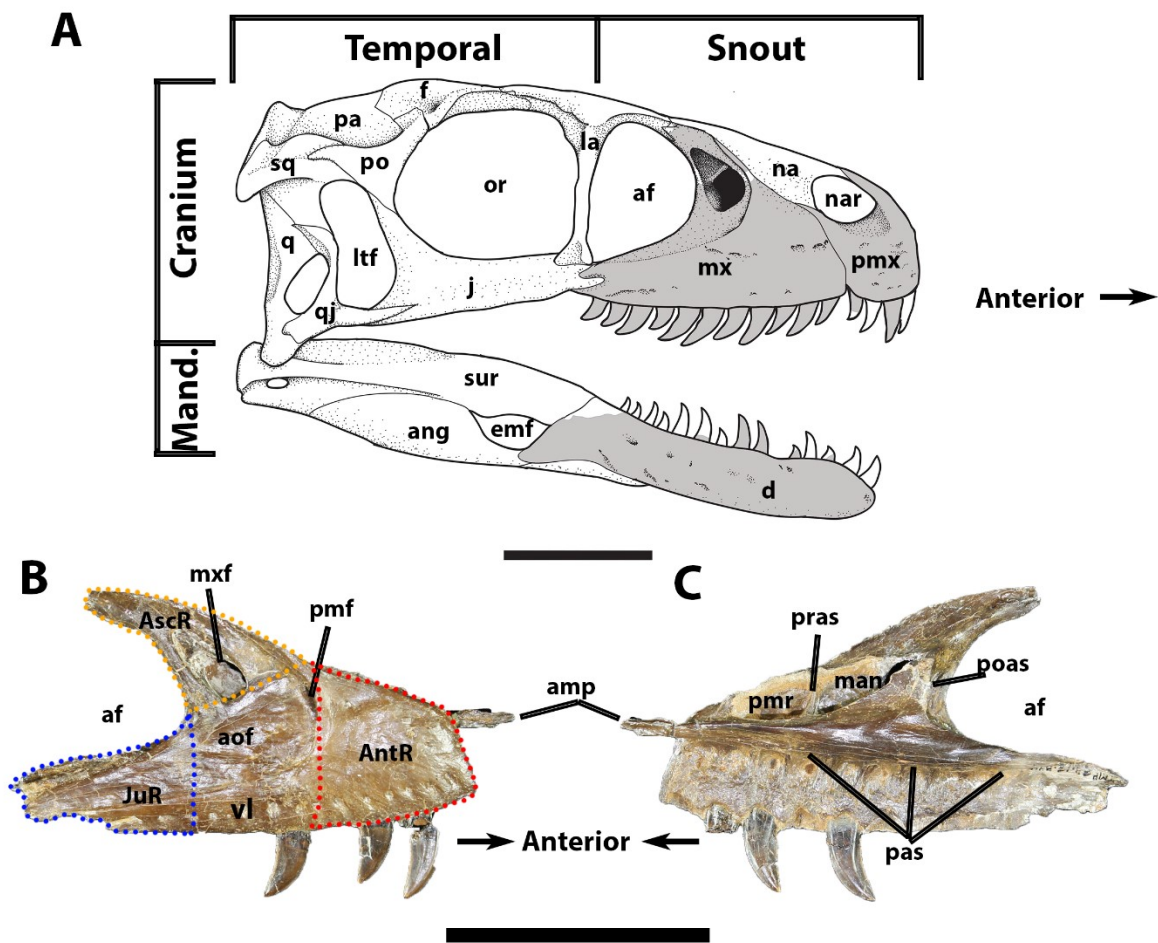


Figure 1.1. Composition of snout and maxilla morphology in eudromaeosaurians. A) skull reconstruction of *Atrociraptor marshalli* (TMP 1995.166.0001) in lateral view with bones and fenestrae labelled, and regions of the skull indicated. The skull was reconstructed using the combination of CT data and the more completely prepared holotype. Greyed areas were illustrated using the holotype specimen as reference while the non-greyed areas were illustrated using specimens of *Saurornitholestes langstoni* (TMP 1974.010.0005, TMP 1988.121.0039, and UALVP 55700) due to the close phylogenetic relationship between these taxa. B) lateral and C) medial views of a *Saurornitholestes langstoni* maxilla (TMP 1994.012.0844) with features and regions labelled. Scale bars = 5 cm. Abbreviations: **af**, antorbital fenestra; **amp**, anteromedial

process; **ang**, angular; **AntR**, anterior ramus; **aof**, antorbital fossa; **AscR**, ascending ramus; **d**, dentary; **emf**, external mandibular fenestra; **f**, frontal; **j**, jugal; **JuR**, jugal ramus; **la**, lacrimal; **ltf**, lateral temporal fenestra; **man**, maxillary antrum; **mx**, maxilla; **mx****f**, maxillary fenestra; **na**, nasal; **nar**, external nares; **or**, orbit; **pa**, parietal; **pas**, palatal shelf; **pmf**, promaxillary fenestra; **pmr**, promaxillary recess; **pmx**, premaxilla; **po**, postorbital; **poas**, postantral strut; **pras**, preantral strut; **q**, quadrate; **qj**, quadratojugal; **sq**, squamosal; **sur**, surangular; **vl**, ventral lamina.

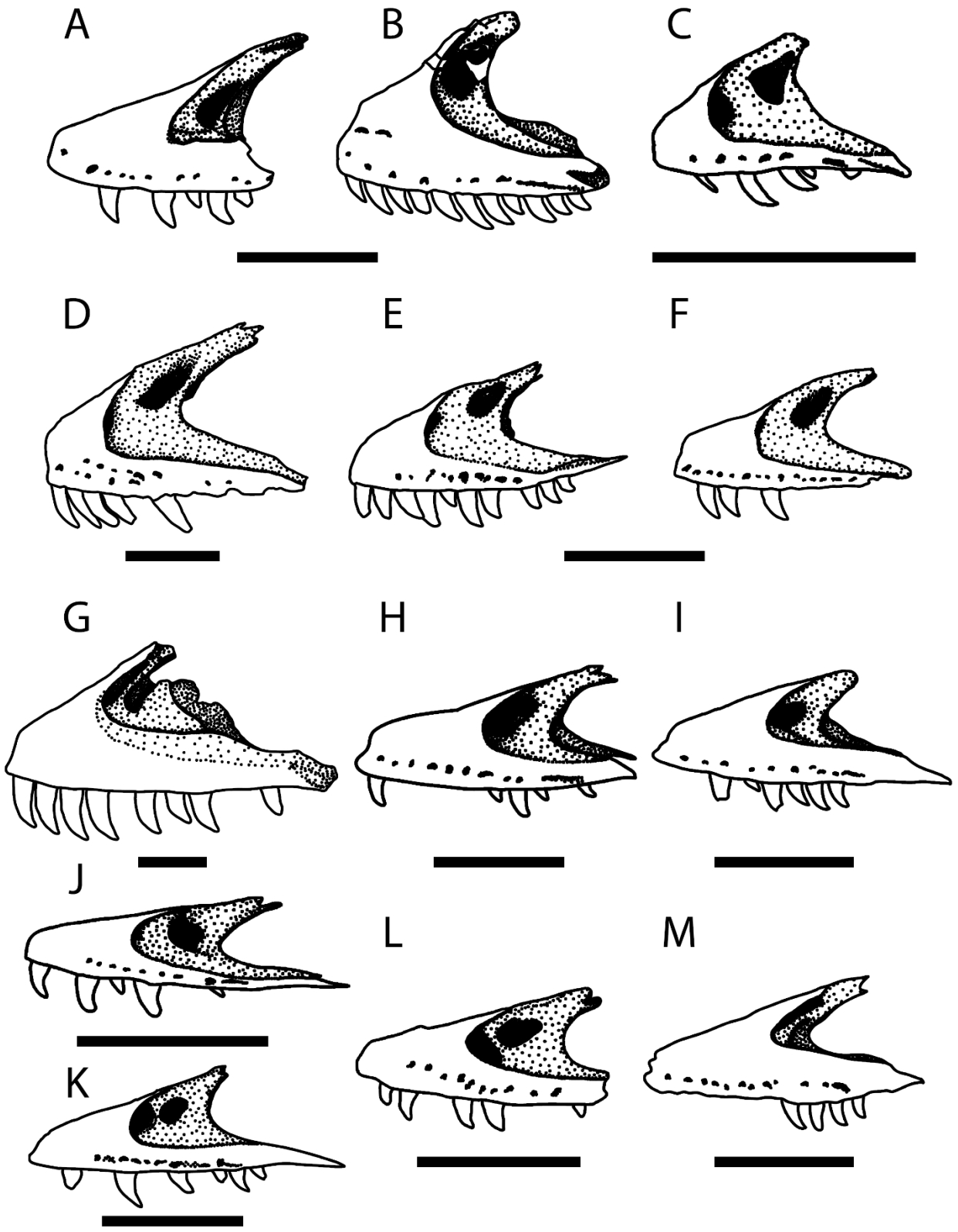


Figure 1.2. Lateral views of Eudromaeosaurian maxillae that are representative of the taxonomic diversity considered in this study. Right maxillae have been reversed so that all specimens appear to be left elements. A) *Acheroraptor temertyorum* (ROM 63777) right maxilla; B) *Atrociraptor marshalli* (TMP 1995.166.0001) right maxilla; C) *Bambiraptor feinbergi* (AMNH FARB 30556) left maxilla; D) *Deinonychus antirrhopus* (YPM 5232 [557]) right maxilla; E) *Saurornitholestes langstoni* (UALVP 55700) right maxilla; F) *Saurornitholestes langstoni* (TMP 1994.012.0844) right maxilla; G) *Achillobator giganticus* (MNUFR 15) left maxilla; H) *Linheraptor exquisitus* (IVPP V16923) right maxilla from Xu et al. 2015 (Fig. 1A); I) *Tsaagan mangas* (IGM 100/1015) right maxilla; J) *Velociraptor mongoliensis* (AMNH 6515 – holotype) left maxilla; K) *Velociraptor mongoliensis* (MPC-D 100/25) right maxilla; L) *Velociraptor osmolskae* (IMM 99NM-BYM-3/3) left maxilla from Godefroit et al. 2008 (Fig. 2A); M) UALVP 49389, right maxilla. Scale bars equal 5 cm.

Chapter 2. Analysis of eudromaeosaurian maxillae using CT data: re-interpretation of morphology and comments on maxilla character construction

2.1 Introduction

Dromaeosaurids are small to medium sized theropod dinosaurs that share recent common ancestry with Avialae Gauthier, 1986, and Troodontidae Gilmore, 1924 (Turner et al. 2012). The most derived members are those classified under Eudromaeosauria Longrich and Currie, 2009. Members of this sub-clade were among the first small theropods discovered (Matthew and Brown 1922, Osborn 1924) and with the additional discovery of *Deinonychus antirrhopus* Ostrom, 1969, dromaeosaurids helped change the way we perceive dinosaurs as a group. Dinosaurs went from lumbering giants that dragged themselves across the landscape to efficient, active animals that would be much more comparable to modern day fauna. The Dinosaur Renaissance was largely incited by these gracile species but our understanding of the diversity of dromaeosaurids would be hampered by the rarity of fossilized remains of these animals.

With the exception of *Deinonychus antirrhopus*, *Velociraptor mongoliensis* Osborn, 1924, and now *Saurornitholestes langstoni* Sues, 1976 (Currie and Evans 2019), each derived dromaeosaurid is largely known from either a single articulated or associated specimen (Matthew and Brown 1922, Perle et al. 1999, Norell et al. 2006, Xu et al. 2010a), or ones that are composed of a very small percentage of a total skeleton (Currie and Varricchio 2004, Godefroit et al. 2008, Evans et al. 2013). One of the most common elements to be used for species description has been the maxilla (Currie and Varricchio 2004, Godefroit et al. 2008, Evans et al. 2013). It was also a major component for the classification of *Achillobator giganticus* Perle et al., 1999, although a number of other diagnostic elements were present for its description. The limited material for dromaeosaurids and other small bodied vertebrates is in part due to certain

preservation environments being biased towards large bodied organisms (Brown et al. 2013). Because of the lack of completeness for a substantial number of eudromaeosaurians, attempts have been made to extract as much taxonomic information from the available specimens as possible. This biases the maxilla taxonomically due to its greater representation in phylogenetic analysis. It has been suggested, however, that the maxilla should have a lot of phylogenetic weight due to the variation observed for this element (Senter et al. 2010, Evans et al. 2013). Because of the inferred phylogenetic weight of the maxilla, it is important to have an accurate view of the morphological diversity for this element. Morphological information can often be obscured, however, by post-mortem distortion and incomplete preparation of specimens.

Several descriptions of eudromaeosaurian maxillae have been incomplete or potentially erroneous due to post-mortem distortion or partial preparation. *Deinonychus antirrhopus* is one such species that has not undergone revisions to its description in 50 years (Ostrom 1969). In the initial description of the maxilla, several elements were described as pressed together against its medial surface. Some fragments were also interpreted as a crushed anterior portion of the maxilla. Contact surfaces with other elements on this specimen are difficult to see because the medial side is distorted and mostly concealed by overlying elements. Distortion can also be from fracture and displacement as is the case in *Acheroraptor temertyorum* Evans et al., 2013. While the description of this specimen is excellent (Evans et al. 2013), some of its proportions could vary substantially with retro-deformation. Interpretations of intercontinental migration of dromaeosaurids during the Late Cretaceous has been postulated based on several ratio-based characters coded for this taxon but retro-deformation may change these interpretations. On the other hand, some specimens were too delicate for complete preparation such as *Atrociraptor marshalli* Currie and Varricchio, 2004. This specimen represents a unique eudromaeosaurian and

is only partially described because most of the specimen was not exposed at the time of its initial description. To better observe the morphology of these specimens, the use of computed tomography would allow all surfaces and contacts to be examined. This level of observation can help to determine the boundaries of a given element, how multiple elements interconnect, and how the medial and lateral morphologies correlate, all without risk to the specimen.

Eudromaeosaurians represent some of the last dromaeosaurids before the K/Pg extinction and their evolutionary trends are important for understanding the complex ecosystems of the Late Cretaceous. Morphological description is vital for phylogenetic analyses. Therefore, the most accurate morphology of a given specimen should be put forth before running any phylogenetic tests.

2.2 Materials

2.2.1 Computed tomography scan data

MPC-D 100/982 – *Velociraptor* sp. (Osborn, 1924) right maxilla; scanned at Yale University, New Haven, USA with a Nikon xt h 225 st scanner, at 100 kV, 90 uA with one second exposure at a resolution of 0.09 mm voxel size. Data housed at the American Museum of Natural History, New York City, USA, Yale University, New Haven, USA, and University of Alberta, Edmonton, Canada

MPC-D 100/1015 – *Tsaagan mangas* Norell et al., 2006, right maxilla; scan details in Norell et al. 2006. Data housed at the American Museum of Natural History, New York City, USA, and University of Alberta, Edmonton, Canada

ROM 63777 – *Acheroraptor temertyorum* Evans et al., 2013, right maxilla; scanned at the Royal Ontario Museum, Toronto, Canada with a SCANNER at 80 kV and 70 mA with a slice

thickness of 0.154 mm. Data housed at the Royal Ontario Museum, Toronto, Canada, and University of Alberta, Edmonton, Canada.

TMP 1994.012.0844 – *Saurornitholestes langstoni* Sues, 1976, left maxilla; Mayfair Diagnostics in Calgary, Alberta, using a GE HD750 64 slice CT. They were scanned at a slice thickness of 0.612 mm. Data housed at the Royal Tyrrell Museum of Palaeontology, Drumheller, Canada, and University of Alberta, Edmonton, Canada.

TMP 1995.166.0001 – *Atrociraptor marshalli* Currie and Varricchio, 2004, right maxilla; Mayfair Diagnostics in Calgary, Alberta, using a GE HD750 64 slice CT. They were scanned at a slice thickness of 0.612 mm voxel size. Data housed at the Royal Tyrrell Museum of Palaeontology, Drumheller, Canada, and University of Alberta, Edmonton, Canada.

YPM 5232 (557) – *Deinonychus antirrhopus* Ostrom, 1969, right maxilla; scanned at Yale University, New Haven, USA with a Nikon xt h 225 st scanner, at 100 kV, 90 uA with one second exposure at a resolution of 0.09 mm voxel size. Data housed at the American Museum of Natural History, New York City, USA, Yale University, New Haven, USA, and University of Alberta, Edmonton, Canada

2.3 Methods

Specimens were examined with the aid of computed tomography to revise previous descriptions of eudromaeosaurians. The specimens for re-examination were ROM 63777, TMP 1995.166.0001, and YPM 5232 (557). Other specimens mentioned in Materials were used for comparative purposes. TMP 1994.012.0844 provided an excellent maxilla of a North American eudromaeosaurian with little to no post-mortem distortion. MPC-D 100/982 and MPC-D

100/1015 were compared to Asian taxa to which ROM 63777 and YPM 5232 (557) were previously compared.

Processes of fossilization can distort fossilized bone extensively. Plastic deformation was determined in this study to be any features that were not associated with large cracks or translocation of broken sections (i.e. depressions along the bone surface not associated with a specific structure, deflection of features out of anatomical position, parasagittal shifts). Mechanical deformation is here used to indicate the transposition of broken sections of the fossil. While plastic deformation is difficult to restore (Arbour and Currie 2012, Baert et al. 2014), mechanical deformation can be easily corrected using CT data and 3D modelling techniques. For ROM 63777, each fragment of the maxilla was segmented in Dragonfly v4.0 and converted to mesh objects. The delicate and highly fragmented bone forming the medial wall (Fig. 1.1C) was excluded from reconstructions to examine comparative topologies with other dromaeosaurids, none of which preserve the medial wall of the maxillary sinus system. Generated meshes were aligned manually using MeshMixer. Some areas were of very thin bone or of such small surface area that they could not be confidently segmented or placed. The small spaces between fragments were assumed to be confluent with the surrounding lamina of bone based on natural borders that were preserved. Reconstruction of the maxilla and hypothetical skull restoration of ROM 63777 were done in Adobe Illustrator CS6 and finalized in Adobe Photoshop CS6. For the skull restoration, missing bones were approximated using the restoration from Evans et al. (2013) as a template with modifications made as needed based on the new interpretations of the data. Dragonfly v4.0 was used for all subsequent segmentation of specimens. Noise from segmentation in the form of highly textured surfaces, or gaps caused by poor contrast between specimen and matrix, were corrected using smoothing and bridging functions in GeoMagic

and/or Zbrush. Adobe Illustrator CS6 and Adobe Photoshop CS6 was used for specimen illustrations.

The CT data for TMP 1995.166.0001 and YPM 5232 (557) were used to examine previously inaccessible topology such as the medial surfaces of these specimens and to complete the description of the maxilla in the former. The maxilla of YPM 5232 is in contact with the nasals, a premaxilla, and the vomers, all of which are pressed against its medial surface. Sutures of YPM 5232 (557) were examined with the CT data and each bone was segmented separately. Segmentations were used to generate meshes for morphological assessment and various slices of the CT data were used for direct comparison of the data.

The maxillary sinus system was compared throughout all specimens used in this study for morphological trends within Eudromaeosauria. Although a thorough description of this system in theropods has been performed (Witmer 1997), a comparison within eudromaeosaurians has not. MPC-D 100/982, MPC-D 100/1015, and TMP 1994.012.0844 are used as comparative specimens for the paranasal sinus system, the nasal and lacrimal sutures, and maxillary proportions. Tooth replacement is also commented on but in a limited capacity.

Following the reassessment of the retro-deformation of ROM 63777 and YPM 5232 (557), a comprehensive description of the previously undescribed sections of the maxilla of TMP 1995.166.0001 was made. This allows for comparisons with a wider range of dromaeosaurid maxillae with new perspectives on topological similarities of the medial surface. Measurements of the maxillae and the features thereof were taken with digital calipers, or the use of the calibrated line tool in the ImageJ software, and various ratios were calculated (Table 2.1). Anterior ramus length and height measurements were compared to maxillary length and height measurements respectively via Reduced Major Axis regression analysis. Measurements were log

transformed to standardize the data (A 1.1) and the analyses were performed using PAST 3 software. A new measurement was used in this study, which consisted of the angle between the maxillary tooth row and the posterodorsal extent of the ascending ramus of the maxilla (Fig. 2.1). To estimate the dimensions of ROM 63777, complete maxillae of other eudromaeosaurians were compared. The anteroposterior length of the anterior ramus to the posterior extent of the ascending ramus in proportion to total maxillary length was taken from *Velociraptor mongoliensis* (AMNH 6515 and MPC-D 100/25) and *Saurornitholestes langstoni* (TMP 1994.012.0844 and UALVP 55700). The average ratio of these specimens (74%) was then used to estimate the maxillary length for *Acheroraptor temertyorum*. These two specimens were selected due to either close phylogenetic relationship as with *Velociraptor mongoliensis* (Currie and Evans 2019), whereas *Saurornitholestes langstoni* has a similar angle of the ascending ramus (Table 2.1). A similar method was used to estimate the maxillary length of *Velociraptor osmolskae* Godefroit et al., 2008, but only the average ratio for *V. mongoliensis* (69%) was used because both taxa belong to the same genus. These ratios and the angle measurement were compared across Eudromaeosauria and previous measurements for *Acheroraptor temertyorum* and *Deinonychus antirrhopus* were revised.

Characters and their states from a recent analysis of Eudromaeosauria phylogenetics by Currie and Evans (2019) were revised as needed based on observation of CT data. The recent analysis by Currie and Evans (2019) has compiled characters from previous phylogenetic analyses that incorporated dromaeosaurid characters, added some new characters, and modified previous characters. This study represents the most extensive ingroup analysis of Eudromaeosauria to date and will be the focal point for character assessment. Maxillary characters were reviewed following the criteria for character construction as laid out by Simões

et al. (2016). Revised characters and characters recommended for removal or future re-analysis are in Appendix A 1.2.

2.4 Description

2.4.1 ROM 63777-*Acheroraptor temertyorum*

For a detailed description of the anatomical features, and species diagnosis of *Acheroraptor temertyorum*, see Evans et al. (2013). Due to a limited field of view, the scans done for this project are missing the posterodorsal extent of the ascending ramus of the maxilla. However, this region is well preserved in the original specimen, and the description by Evans et al. (2013) is referenced for comparison of this region with other specimens in this study.

ROM 63777 is distorted both plastically and by a series of cracks, concentrated in the mid and posterior regions (Fig. 2.2A). On the lateral surface there is a small concave, plastically deformed surface ventral to the ventral margin of the antorbital fossa (Figs. 1.1B, 2.2A-B). This region was not retro deformed for this study, but comments on the effect of morphological interpretation are presented in the description of the antorbital fossa. Further plastic deformation is present at the junction between the anterior ramus and the ascending ramus. In this region, the ascending ramus has been plastically bent medially at its anteroventral base (Figs. 1.1B, 2.2A-B). The promaxillary fenestra and surrounding bone appear undistorted relative to the ascending ramus and were used to approximate the original orientation of the ascending ramus (Figs 2.2, 2.3A). The maxilla is laterally bowed and medially crushed, showing greater distortion along the medial side (Figs 2.3A, 2.4C). The largest cracks are midway through the anterior ramus and through the ascending ramus just dorsal to the maxillary fenestra. Along these cracks the

ascending ramus of the specimen has been displaced and shifted dorsomedially compared to the alveolar region, which is comparatively undistorted.

Once distortion is removed, this element is slightly shallower than previously described (Evans et al. 2013) because the angle of the ascending ramus from maxillary tooth row was accentuated by the distortion from the cracks (length to height ratio 2.18 distorted, or 2.36 undistorted) (Table 2.1, Fig. 2.4B). . This ratio is visualized in the proposed skull reconstruction of *Acheroraptor temertyorum* (Fig. 2.5), which follows the ratio estimated from the reconstructed maxilla.

The anterior ramus of the maxilla was displaced anteriorly due to mechanical deformation (Figs 2.2A, 2.4A-B) and once retro-deformed has a length to height ratio of 1.09 as opposed to a ratio of 1.22 measured on the original specimen (Table 2.1, Fig. 2.4B). In proportion to the estimated maxillary length, the anterior ramus makes up 31% of the total maxillary length, less than the 36% based on the measurements of the distorted specimen (Table 2.1). The ascending ramus is generally straight but bows slightly dorsally proximal from the lacrimal contact. This gives the sutural-sutural facet for the lacrimal a more horizontal orientation rather than the posterodorsal orientation observed in the distorted specimen (Figs. 2.4A, 2.5). The maxillary fenestra extends less posterodorsally than initially described but is still elongate rather than circular. It is housed in a well-defined maxillary fossa with a deep pneumatic excavation posterodorsal to the maxillary fenestra proper (Figs. 2.2D-E, 2.3C-D). The excavation opens ventromedially into a diverticulum that extends anteriorly along the dorsomedial edge of the maxilla (Fig. 2.3B-C). The lateral side of the diverticulum opens into the maxillary sinus system, which is distinctly encapsulated on all other sides throughout its extent along the maxilla (Fig. 2.2C-E). The ventral wall of the diverticulum deflects medioventrally as

the diverticulum opens broadly into the promaxillary recess roughly at mid-length along the anterior ramus (Figs. 1.1C, 2.3C). This feature is not observed in other dromaeosaurids, although due to the delicate nature of the walls of bone in this area, it may not have been preserved in other specimens such as TMP 1994.012.0844 (Figs. 2.6C-D, 2.7A). Instead, TMP 1994.012.0844 shows a supramaxillary recess extending posterodorsal from an excavation posterodorsal to the maxillary fenestra. The shape of the antorbital fossa is essentially the same as previously described (Evans et al. 2013). However, it is noted that the fossa is separated from the ventral lamina by a distinct boundary accompanied by a lateroventral slope that gradually shifts to the sheer vertical face of the lateral lamina (Fig. 2.4B). A slope ventral to the antorbital fossa is also observed in *Achillobator giganticus* Perle et al., 1999 but contrasts with the stark ventral border of the antorbital fossa observed in *Linheraptor exquisitus* and *Tsaagan mangas* (Fig. 2.8A), to which *Acheroraptor temertyorum* was previously compared (Evans et al. 2013).

The thin bones of the dorsal part of the medial surface are badly crushed, and complete restoration could not be done accurately. The coating of crushed bone is supportive of the proposed hypothesis that the area surrounding the maxillary sinus system was housed in a thin walled bony bulla (Witmer 1997, Currie and Varricchio 2004, Evans et al. 2013). Although crushed, the wall of bone can be observed in coronal sections throughout the maxillary sinus region of the specimen (Fig. 2.2C-G). Due to the delicate nature of the bone encapsulating the pneumatic sinus system, this region does not often preserve and the morphology of the sinuses are primarily inferred in specimens like ROM 63777 (Figs. 2.2-2.4) and TMP 1994.012.0844 (Currie and Varricchio 2004) (Fig. 2.7B). The medial wall of the bulla would have attached lateral to the base of the ventral wall of the maxillary diverticulum and become confluent with the postantral strut posteriorly (Figs. 2.2C-E, 2.3C). The medial surface, lateral to the crushed

bullae (Fig. 2.4D) has morphological features of the maxillary sinus system that are similar to those observed in other theropods (Hendrickx and Mateus 2014). The promaxillary recess and maxillary antrum are separated by a pronounced preantral strut that is parallel to the posterior boundary of the promaxillary fenestra. The promaxillary recess, however, is quite elongate as this recess occupies all the dorsomedial surface of the anterior ramus. This is clearly observed in *Saurornitholestes langstoni* as well (Figs. 2.6C, 2.7B) (Currie and Varricchio 2004). The elongation of the promaxillary recess in *Acheroraptor temertyorum* reflects the elongation of the anterior ramus. Because of this, the maxillary antrum is anteroposteriorly short compared to the promaxillary recess. The dorsomedial surface of the ascending ramus has a smooth sutural facet for contact with the nasal that is present over the distal half of this ramus (Figs. 2.4C-D). The shape of this facet in *Acheroraptor temertyorum* is ovate with tapering anterior and posterior ends demarcating the transition between forms of nasal contact-contact and the terminus of the ascending ramus, respectively. In medial view, the palatal shelf is roughly straight (Fig. 2.4B-C) as observed in *Saurornitholestes langstoni* (Fig. 2.7B) (Currie and Varricchio 2004) but unlike the sinusoidal shape observed in other theropods like tyrannosaurids (Hendrickx and Mateus 2014).

The dorsal surface of the maxilla of ROM 63777 is dorsally convex from the anterodorsal corner of the anterior ramus to about halfway along the ramus (Figs. 2.2B, 2.4E). The transverse width of the dorsolateral edge of the maxilla tapers posteriorly. This is like other eudromaeosaurian maxillae and likely represents the sutural contact surface for the maxillary process of the premaxilla. This feature was not noted in the initial description, in which the length of the maxillary process of the premaxilla was depicted as relatively short (Evans et al. 2013). Reanalysis suggests that the maxillary process of the premaxilla of *Acheroraptor*

temertyorum was longer than previously hypothesized, extending well posterior to the nares. This condition is shared with most eudromaeosaurians apart from *Atrociraptor marshalli* (Figs. 2.9-2.12), *Saurornitholestes langstoni* (Fig. 2.7D), and *Tsaagan mangas* (Currie and Varricchio 2004, Norell et al. 2006, Currie and Evans 2019). However, the length of sutural-contact surface for the maxillary process of the premaxilla relative to the length of the anterior ramus observed for *Acheroraptor temertyorum* is similar to *Atrociraptor marshalli* and *Saurornitholestes langstoni* but shorter than what is observed in *Linheraptor exquisitus* and *Velociraptor mongoliensis* (Barsbold and Osmólska 1999, Xu et al. 2015). The dorsolateral surface of the maxilla changes from dorsally convex to concave at the terminus of the sutural surface for the maxillary process of the premaxilla (Figs. 2.2B, 2.3A, 2.4E). This trough-like surface extends for approximately one third of the anteroposterior length of the maxilla, then switches to a sharp ridge for the remainder of the length of the ascending ramus. This region of the dorsolateral edge is where contact with the nasal occurs. The switch between the trough-like contact and the sharp ridge is visible in lateral view and is demarcated by the posterodorsal extent of the antorbital fossa visible on the maxilla (Figs. 2.2C-E, 2.3A, 2.4E). In dorsal view the palatal shelf of the maxilla is widest in the regions that include the anteromedial process and the medial wall of the maxillary antrum (Figs. 2.3A, 2.4E).

2.4.2 TMP 1995.166.0001-*Atrociraptor marshalli*

. At the time of the description of *Atrociraptor marshalli* (Currie and Varricchio 2004), the lateral surface of the maxilla was not completely prepared, and the dorsal half could not be described. The dorsal portion is largely composed of the ascending ramus (Figs. 2.9, 2.10). The medial side of this specimen has not been prepared due to the fragile nature of the bone and the hardness of the rock. It is here described from the computed tomography scans.

The length to height ratio of the anterior ramus for *Atrociraptor marshalli* is 0.75 (Table 2.1). The anterior ramus contributes to 32% of total maxillary length. The anterior edge of the anterior ramus is not straight in lateral view as in other saurornitholestines and possesses an accessory anterior process (Figs. 1.1A, 2.9-2.11). Other dromaeosaurids such as *Tsaagan mangas* and *Velociraptor mongoliensis* have a small accessory anterior process of the maxilla that has a rounded to triangular shape and is more tab-like than in *Atrociraptor marshalli*. A complementary notch along the posterior margin of the main body of right premaxilla of *Atrociraptor marshalli* is inferred by the orientation of the ventral edge anterior to the broken edge of the maxillary process (Fig. 2.11A). This inference is supported by the dorsoventral thickness at the base of the maxillary process of the left premaxilla (Fig. 2.11B). The development of a dorsoventrally tall and squared accessory anterior process observed in *Atrociraptor marshalli* is distinct and currently sets this taxon apart from all other members of the group. The ascending ramus is anteroposteriorly narrow at the level of the maxillary fenestra and projects posterodorsally (Figs. 2.9, 2.10), like *Acheroraptor temertyorum* (Figs. 2.2A, 2.4A-B). The junction between the process and the main body of the maxilla is demarcated by a notch located posteriorly on the dorsal margin of the anterior ramus, and is similar to concavities observed in *Acheroraptor temertyorum* (Fig. 2.4A-B), *Bambiraptor feinbergi* (Burnham et al. 2000), *Linheraptor exquisitus* (Xu et al. 2015), *Saurornitholestes langstoni* (Fig. 2.7A) (Currie and Varricchio 2004, Currie and Evans 2019), and some specimens of *Velociraptor mongoliensis* (Currie and Varricchio 2004, Godefroit et al. 2008) (MPC-D 100/25 and MPC-D 100/54). The angle of the distal end of the ascending ramus to the alveolar margin in *Atrociraptor marshalli* is the steepest observed in Eudromaeosauria (Table 2.1, Figs. 2.9A, 2.10A-B), projecting at an angle of 49.3° from the alveolar margin. *Achillobator* (44.7°), *Bambiraptor* (37.9°-42.9°), and

Deinonychus (37.8°) approach this angle more than other eudromaeosaurians. The broad range for *Bambiraptor feinbergi* is reflective of an ontogenetic shift from steeply inclined ascending ramus in the juvenile (AMNH FARB 30556) to the shallower condition observed in the adult (MOR 553S – 7.30.91.274) (Table 2.1). The distal portions of the ascending ramus are missing in both *Achillobator giganticus* and both specimens of *Bambiraptor feinbergi*, which may also inflate the angle. The anterodorsal margin of the antorbital fossa of *Atrociraptor marshalli* extends more than halfway up the ascending ramus, reaching the dorsolateral edge of the ramus at a position directly dorsal to the posterior extent of the maxillary fenestra (Fig. 2.9A). This condition is like that observed in *Linheraptor exquisitus* and *Tsaagan mangas* (Fig. 2.8A). However, it is more like the condition of this feature in *Acheroraptor temertyorum* (Fig. 2.4A-B). In cross section, the distal ascending ramus, anterior to the lacrimal contact, has a medially swooped tear drop shape (Fig. 2.9B-C). The sutural surface for the lacrimal is bifurcated into transversely narrow dorsolateral and ventromedial prongs (Fig. 2.9B) as observed in *Acheroraptor temertyorum* (Fig. 2.4A, C) and *Saurornitholestes langstoni* (Fig. 2.7A-C) (Currie and Varricchio 2004, Evans et al. 2013).

The maxillary fenestra of *Atrociraptor* is sub-circular as in the holotype of *Velociraptor mongoliensis* (Osborn 1924, Turner et al. 2012) (Fig. 2.9A). However, it is much larger relative to the antorbital fossa and located on the ascending ramus rather than having a central location in the antorbital fossa as observed in *Velociraptor mongoliensis*. The posterior placement of the maxillary fenestrae in *Atrociraptor marshalli* is more like what is observed for *Bambiraptor feinbergi* (Burnham et al. 2000, Currie and Varricchio 2004), *Deinonychus antirrhopus* (Fig. 2.14A) (Ostrom 1969), and *Saurornitholestes langstoni* (Fig. 2.7A) (Currie and Varricchio 2004, Currie and Evans 2019) (Fig. 1.2). The maxillary fenestra sits in an accessory antorbital fossa (or

maxillary fossa) like those of *Acheroraptor temertyorum* (Figs. 2.2-2.5), *Bambiraptor feinbergi*, and *Saurornitholestes langstoni* (Figs. 2.6A, 2.7A) (Currie and Varricchio 2004). The maxillary fenestra of *Atrociraptor marshalli* opens predominantly medially into the maxillary antrum as opposed to ventromedially as in the three previously mentioned dromaeosaurids. The maxillary fossa is oriented posterodorsally in lateral view, with the maxillary fenestra at the anteroventral end (Fig. 2.10) and a pneumatic excavation *sensu* (Hendrickx and Mateus 2014) in the posterodorsal end. A pronounced strut oriented posteroventrally to anterodorsally is observed between these two structures. The pneumatic excavation is apparent in the preserved specimen (Figs. 2.9A, 2.10A), although the delicate nature of the bone in this region and the low resolution of the scans could not recover the base of the excavation by means of thresholding (Fig. 2.10A-B). The maxillary fossa is comparatively shallow around the maxillary fenestra and appears primarily in the anteromedial sloping of the pila interfenestralis, deepening posterodorsally towards the pneumatic excavation (Fig. 2.10). The structure of the maxillary fenestra observed for *Atrociraptor marshalli* is most like that observed in *Bambiraptor feinbergi* but like *Saurornitholestes langstoni* (Figs. 2.7A, 2.10A-B). The pneumatic excavation appears as a fenestra in *Bambiraptor feinbergi* (Burnham et al. 2000, Currie and Varricchio 2004), but this could be due to the delicate nature of the described specimens of *Bambiraptor feinbergi*. In dorsal view it can be observed that the promaxillary fenestra is split by a small transverse strut (Fig. 2.10E). This is a morphology not commonly observed in eudromaeosaurians, although one specimen of *Velociraptor mongoliensis* (MPC-D 100/54) has a similar promaxillary fenestra morphology, and it may be a developmental anomaly. In Figure 2.9E, however, the promaxillary fenestra appears slit-like as in *Acheroraptor temertyorum* and *Saurornitholestes langstoni* (Figs.

2.2, 2.6). Therefore, the rendered model in Figure 2.10E may alternatively be displaying an artefact of poor scan resolution.

The medial surface of the maxilla shows a great deal of dorsolateral distortion (Figs. 2.9B-F, 2.10C-D). The palatal shelf is deflected dorsolaterally which can be seen through the antorbital fenestra in lateral view (Figs 2.10A, 2.11A). Following the series of interdental gaps along the ventral border of the palatal shelf, it can be ascertained that the shelf slopes posteroventrally. This observation is corroborated by the dorsoventral tapering of the medial alveolar wall posteriorly, and a depression on the medial side of the premaxilla that would receive the anteromedial process in contact (Fig. 2.11B'). The anteromedial process projects medially in other dromaeosaurids, further supporting the dorsolateral distortion interpretation. In dorsal view, the anteromedial process projects slightly medially with a convex medial edge, likely for contact with the anteromedial process of the other maxilla and vomers in life (Figs. 2.10D, 2.11C). The preantral strut is visible in medial view (Fig. 2.10C) but unlike in *Saurornitholestes langstoni*, is anterior to the antorbital fossa. The preantral strut is angled posterodorsally as in *Acheroraptor temertyorum* and *Saurornitholestes langstoni*, but the posterior extent is aligned with the anterior extent of the antorbital fossa in all three taxa. The promaxillary recess observed in *Atrociraptor marshalli* fills the anterodorsal space of the maxilla, as in *Acheroraptor temertyorum* (Fig. 2.3D) and *Saurornitholestes langstoni* (Fig. 2.7) (Currie and Varricchio 2004). The maxillary antrum is closed off posteriorly by the postantral strut (Fig. 2.10B, E). Although damaged and incomplete, this strut would have likely completely separated the maxillary antrum from the antorbital cavity as in *Saurornitholestes langstoni* (Fig. 2.7D).

In dorsal view the anterior ramus dorsally convex surface until approximately halfway posteriorly along the anterior ramus where it transitions to a trough-like morphology as in *Acheroraptor temertyorum* (Figs. 2.4E, 2.10D). The trough deepens along the dorsolateral surface of the anterior ramus and the base of the ascending ramus, and the medial side of this surface becomes more dorsoventrally tall posteriorly until terminating in a simple ridge morphology. The morphology of the nasal suture in *Atrociraptor marshalli* is like that observed for both *Acheroraptor temertyorum* and *Saurornitholestes langstoni* (Figs. 2.4E, 2.7D, 2.9, 2.10A-C).

2.4.3 YPM 5232 (557)-*Deinonychus antirrhopus*

YPM 5232 is comprised of the right maxilla, the right lacrimal, parts of both nasals that are still partially in contact with each other, the nasal process of the left premaxilla, the paired vomers on the medial surface of the maxilla, and a taphonomically distorted right premaxilla in contact at the anterior end of the maxilla (Figs. 2.12-2.13). In the initial description (Ostrom 1969), the right premaxilla was considered to be the most anterior portion of the maxilla and the lacrimal was considered the most posterodorsal extent of the ascending ramus. CT scans reveal that the anterior fragment is the right premaxilla as the maxillary process of the premaxilla can be seen, extending nearly to a point dorsal to the anterior border of the antorbital fossa. The promaxillary recess of the maxillary sinus system terminates posterior to the main body of the premaxilla (Figs. 2.12K, 2.14B). A clear separation between these bones can be followed and the anteromedial process of the maxilla is observed in contact with the premaxilla throughout its entirety (Fig. 2.13D). The anteromedial process becomes confluent with the medial wall of the maxilla above the junction between the first and second maxillary alveoli, as in other dromaeosaurids (Figs. 2.4B, 2.7B, 2.8C, 2.10B, 2.16F). The maxillary tooth count was

previously overestimated due to the inclusion of the partial premaxilla at 15 (Ostrom 1969).. There are, however, only 13 maxillary alveoli, following the removal of the two previously included premaxillary alveoli (Table 2.1). The maxilla process of the lacrimal slots between two processes of the distal end of the ascending ramus of the maxilla, and also contacts a ventral projection of the nasal along the distal portions of the maxilla process (Fig. 2.12E-G). These observations and new interpretations of the maxillary boundaries greatly change the proportions of the maxilla and how it contributes to the shape of the skull (Fig. 2.15).

The maxilla of *Deinonychus antirrhopus* is dorsoventrally tall compared to its anteroposterior length, with a length to height ratio of 1.70. Based on the former description of this specimen (Ostrom 1969) the length to height ratio would have been 1.93. The anterior ramus is shorter than it is tall (length to height ratio = 0.68). Previous interpretations would have put it at 1.13 (Table 2.1), however, this new measurement is more comparable to *Atrociraptor marshalli* (0.75) and *Bambiraptor feinbergi* (0.70). The anterior ramus contributes 22% of the total maxillary length based on new interpretations, whereas before it constituted 32% of the total maxillary length (Table 2.1). The ascending ramus ends in a forked morphology in lateral view (Fig. 2.14C-D). The prongs of this fork surround the anterior tip of the lacrimal, concealing it in lateral view (Figs 2.12E-G, 2.13A-B). The prongs are dorsoventrally tall and narrowly separated from each other as in *Acheroraptor temertyorum* (Fig. 2.4A, C) (Evans et al. 2013), *Atrociraptor marshalli* (Fig. 2.10E) and *Sauornitholestes langstoni* (Fig. 2.7A) (Currie and Varricchio 2004). The maxillary fenestra is broken along the anteroventral edge of the fenestra. However, based on the rest of the border of the maxillary fenestra, it would have been slightly elongated with a semi-circular ventral border (Fig. 2.14A). The entrance to the fenestra is oriented medioventrally as observed by the sloping condition of the bone along the top of the

fenestra (Figs. 2.13A-B, 2.14A). The shape and orientation of the maxillary fossa in *Deinonychus antirrhopus* is similar to *Acheroraptor temertyorum* (Fig. 2.4B), *Atrociraptor marshalli* (Fig. 2.9), *Bambiraptor feinbergi* (Burnham et al. 2000, Currie and Varricchio 2004), and *Saurornitholestes langstoni* (Currie and Evans 2019) (Fig. 2.6A), but lacks the posterodorsal pneumatic excavation observed in these taxa. The structure of the maxillary fenestra in *Deinonychus antirrhopus* is like those observed in *Linheraptor exquisitus*, *Tsaagan mangas* (Fig. 2.8A), select specimens of *Velociraptor mongoliensis* (MPC-D 100/54), and *Velociraptor osmolskae*, but contrasts with the simple perforation of troodontids (Currie 1985, Xu et al. 2002, Senter et al. 2010). Another difference between the maxillary fossa in *Deinonychus antirrhopus* and the Asian velociraptorines is that in *Deinonychus antirrhopus* the maxillary fossa is completely within the antorbital fossa rather than opening posteriorly into the antorbital fenestra (Figs. 2.8, 2.13, 2.16).

The medial surface of the maxilla demonstrates morphology similar to that of other dromaeosaurids (Ostrom 1969, Witmer 1997, Barsbold and Osmólska 1999, Currie and Varricchio 2004). The upper extremities of the alveoli are demarcated by the palatal shelf (Fig. 2.13B). The palatal shelf becomes confluent with the postantral strut just posterior to the maxillary fenestra and roughly level with the anterior edge of the antorbital fenestra. Ventral to the palatal shelf, the alveolar wall is tall, extending dorsally beyond the ventral border of the antorbital fossa. The palatal shelf is confluent with the anteromedial process that extends from the medial wall between the first and second alveoli towards the premaxilla and terminates in a pointed attachment to the premaxilla. The anteromedial process is long and roughly triangular in dorsal view (Fig. 2.14C). This morphology is markedly like the condition in *Atrociraptor marshalli* (Fig. 2.10D). The anteromedial process in both these taxa are transversely broad with

slight lateral curves along the medial edge but it is unclear if this morphology is characteristic or due to plastic deformation in both specimens. The postantral region of the palatal shelf is well preserved in YPM 5232 (557) but most of this wall is lost at the maxillary antrum due to crushing (Fig. 2.14C-D). The postantral strut is incomplete in posterior view (Fig. 2.14D); however, it would have likely separated the maxillary antrum from the rest of the antorbital fenestra as observed in TMP 1994.012.0844 (Fig. 2.7C) and other theropods (Witmer 1997, Witmer and Ridgely 2008, Hendrickx and Mateus 2014). Like TMP 1994.012.0844, this wall would have likely extended anteromedially to encapsulate the maxillary antrum and promaxillary recess in a maxillary bulla. However, due to the fragile nature of these bones, they are not completely preserved in any of the specimens examined in this study apart from ROM 63777 (Fig. 2.4C). As in *Acheroraptor temertyorum*, *Atrociraptor marshalli* and *Saurornitholestes langstoni*, a preantral strut demarcates the maxillary antrum from the promaxillary recess and is parallel to the posterior margin of the promaxillary fenestra (Fig. 2.14B). In *Deinonychus antirrhopus*, the promaxillary fenestra extends posteriorly beyond the anterior border of the antorbital fossa in lateral view (Fig. 2.14A-B). The roof of the maxillary antrum is squared off mostly by a relatively thin wall of bone (Fig. 2.14B-C). The roof becomes more rounded anteriorly until the termination of the promaxillary recess at the most anterior extent of the maxilla.

The dorsal surface of the maxilla changes from a convex dorsolateral edge anteriorly to a trough-like morphology in the middle region, to a simple sharp ridge in the posterior extent (Figs. 2.12H-K, 2.14C). Based on the relative length and orientation of the maxillary process of the premaxilla (YPM 5232 [237]), the convex dorsolateral edge seems to correlate with the sutural contact surface for the maxillary process of the premaxilla. The length of the sutural

surface for the maxillary process of the premaxilla is roughly half the length of the anterior ramus in lateral view and is followed posteriorly by a relatively anteroposteriorly restricted trough-like sutural surface for the nasal before transitioning into the sharp ridge morphology (Fig. 2.14C). The extent of the ridge morphology for contact with the nasal is more extensive than in *Acheroraptor temertyorum*, and *Atrociraptor marshalli*, but is similar in proportions to *Saurornitholestes langstoni* (Fig. 2.7D).

2.4.4 Comparative description

Maxilla – The maxillae of *Atrociraptor marshalli* and *Deinonychus antirrhopus* have the lowest length to height ratios of eudromaeosaurians measured in this study (length to height ratio = 1.70). These two taxa are closest in their maxillary dimensions to *Bambiraptor feinbergi* (1.76-2.01) and *Saurornitholestes langstoni* (1.87-2.02). All North American species measured in this study show ratios below species found in Campanian aged rocks of Mongolia with a range of 1.70-2.36 for North American representatives to a range of 2.42-3.44 for Asian specimens (Table 2.1). The only Asian specimen to show dimensions within the North American eudromaeosaurian range is *Achillobator giganticus* (2.22), known from Cenomanian-Santonian rocks of Mongolia (Perle et al. 1999). The length to height ratio for the maxilla of *Achillobator giganticus* is likely inflated, as the maxilla of this taxon is missing a portion of the ascending ramus.

Anterior ramus – The anterior rami of eudromaeosaurians are generally featureless with the only surficial feature being neurovascular foramina (Currie and Varricchio 2004, Norell et al. 2006, Godefroit et al. 2008, Evans et al. 2013). Because neurovascular foramina were not altered by deformation, only ratios of the anterior rami across specimens are reported. The adult specimen of *Bambiraptor feinbergi* (MOR 553S-7.30.91.274) has the lowest anterior ramus

length to height ratio (0.60), closest to *Deinonychus antirrhopus* (0.68), then *Atrociraptor marshalli* (0.75) and the juvenile specimen of *Bambiraptor feinbergi* (AMNH FARB 30556; 0.70) (Table 2.1). Collectively, these three taxa are closest in anterior rami dimensions to *Achillobator giganticus* (0.87) and *Saurornitholestes langstoni* (0.81-0.91), all of which have ratios below 1.00 and could be classified as short. *Acheroraptor temertyorum* has an anterior ramus length to height ratio of 1.09, which would be classified as elongate much like other taxa such as *Linheraptor exquisitus* (1.51), *Tsaagan mangas* (1.30), and *Velociraptor* spp. (1.40-1.75). However, the value of *Acheroraptor temertyorum* is closer in an absolute sense to the upper range of *Saurornitholestes langstoni* (0.91) than to the Campanian aged Asian taxa. In relation to maxillary length, the anterior ramus of *Deinonychus antirrhopus* is the shortest observed (0.22) (Table 2.1). *Deinonychus antirrhopus* overlaps the low end of the range observed in *Bambiraptor feinbergi* (0.22-0.23), followed by a specimen of *Velociraptor* (MPC-D 100/982) (0.27). *Atrociraptor marshalli* and *Acheroraptor temertyorum* have comparable anterior rami lengths comprising 0.32 and 0.31 of maxillary length, respectively. The proportion of maxillary length made up by the anterior ramus in these two taxa is within the range of *Velociraptor mongoliensis* (0.31-0.33) and are at the upper range of this ratio observed in *Saurornitholestes langstoni* (0.28-0.31). Furthermore, they are above the ratio observed for *Achillobator giganticus* (0.29), and below *Linheraptor exquisitus* (0.46) and *Tsaagan mangas* (0.38). These two ratios are characterized in the character-taxon matrix from Currie and Evans (2019), characters 28 and 29. Character 28 is based on the ratio of anterior ramus to maxillary length, and if the proportion of maxillary length made up by the anterior ramus is 0.25 or greater, than the state is considered elongate [0]. Based on the coding of Currie and Evans (2019) from previous interpretations, *Deinonychus antirrhopus* would be changed from the elongate state [0]

to the short condition [1]. Character 29 also deals with the elongation of the anterior ramus; however, it deals with only the dimensions of anterior ramus (length to height ratio) and the feature is considered elongate if it has a ratio greater than 1. Based on the reinterpretation of the specimens in this study, *Deinonychus antirrhopus* would again be changed from the elongate state [0] to the short condition [1]. *Acheroraptor temertyorum* would not change in its coding from Currie and Evans (2019).

The length and height of the anterior ramus of eudromaeosaurians are correlated to the length and height of their respective maxillae (Fig. 2.17). The length of the anterior ramus relative to the maxillary length is much more variable ($r^2=0.571$; Fig. 2.17B) compared to the height of the anterior ramus relative to maxillary height ($r^2=0.934$; Fig. 2.17A). The 95% confidence intervals for each slope encompass 1 but the confidence interval for anterior ramus height relative to maxillary height is much narrower (0.87, 1.23; Fig. 2.17A) compared to anterior ramus length relative to maxillary length (0.29, 1.50; Fig. 2.17B).

Ascending ramus – The ascending rami of *Atrociraptor marshalli* and *Saurornitholestes langstoni* are bowed dorsally throughout (Figs. 2.6A, 2.9A). There is a slight bend in the distal portion of the ascending ramus observed in *Acheroraptor temertyorum*, but its ascending ramus is straighter and is like the conditions observed in other eudromaeosaurians in this study (Fig. 2.4B). The angle of the ascending ramus from the tooth row is greatest in *Atrociraptor marshalli* (49.3°) and least in *Velociraptor* sp. (MPC-D 100/982) (20.15°), showing a range in maxillary angles of nearly 30° throughout Eudromaeosauria (Table 2.1). The antorbital fossa is abbreviated anteroposteriorly in *Atrociraptor marshalli* and *Acheroraptor temertyorum* contributing to relatively narrow bases to the ascending rami for these taxa (Figs. 2.4B, 2.10A-B). Although the antorbital fossae of *Linheraptor exquisitus* and *Tsaagan mangas* are also abbreviated, the low

angle of the ascending rami in these taxa produce broader bases of the ascending rami (Xu et al. 2015) (Fig. 2.8A). The ascending ramus of *Deinonychus antirrhopus* is also narrow with sub-parallel anterodorsal and posteroventral borders for most of its extent in lateral view, only tapering slightly toward the lacrimal contact, most like *Acheroraptor temertyorum* (Figs. 2.4, 2.14A). The anterior border of the antorbital fossa, terminates along the dorsal margin of the maxilla, anterior to the maxillary fenestra in *Bambiraptor feinbergi*, *Deinonychus antirrhopus*, *Saurornitholestes langstoni*, and *Velociraptor* sp. (Figs. 2.7A, 2.14A, 2.16B) as opposed to posterior to, or dorsal to, the posterior margin of the maxillary fenestra as observed in *Acheroraptor temertyorum*, *Atrociraptor marshalli*, *Linheraptor exquisitus*, and *Tsaagan mangas* (Figs. 2.4B, 2.8A, 2.10A). In the latter two taxa, the maxillary fenestra is at the anterior margin of the antorbital fossa, whereas *Acheroraptor temertyorum* and *Atrociraptor marshalli* each maintains a broad pila promaxillaris (Figs. 2.4A-B, 2.10A-B). Pneumatic recesses are present on the nasals of both *Deinonychus antirrhopus* and *Saurornitholestes langstoni* and they are positioned at the dorsal edge of the antorbital fossa, however, the antorbital fossa has greater lateral exposure on the nasals in *Deinonychus antirrhopus* than in *Saurornitholestes langstoni* (Fig. 2.15) (Ostrom 1969, Currie and Evans 2019). The pneumatic recesses of the nasal in *Saurornitholestes langstoni* alternatively are tucked discretely below the protruding lateral edge that demarcates the dorsal extent of the antorbital fossa.

Nasal/Lacrimal contact – The dorsolateral surfaces of the maxillae of *Acheroraptor temertyorum*, *Atrociraptor marshalli*, and *Deinonychus antirrhopus* share a similar morphology, transitioning from a dorsally convex anterior portion for contact with the maxillary process of the premaxilla (Figs. 2.3, 2.9, 2.12) to a dorsally concave, trough-like morphology to receive the nasal throughout the mid-region of the maxilla, and finally transitioning to a simple dorsal ridge

leading to the forked lacrimal contact. This morphology is shared with *Saurornitholestes langstoni* (Fig. 2.7D) but differs from *Tsaagan mangas* and *Velociraptor* (Figs. 2.8, 2.16). The sutural surface for the nasal in *Tsaagan mangas* differs from other taxa in this study in showing an abrupt change in the dorsal margin of the maxilla in the form of a dorsal step just posterior to the sutural surface for the maxillary process of the premaxilla (Fig. 2.8A, C). The nasal suture of the maxilla in *Tsaagan mangas* is simple and transversely narrow throughout the preserved maxillary length without distinct regions as in the North American taxa previously described (Fig. 2.8J-G). *Velociraptor* sp. differs from *Tsaagan mangas* and the other observed taxa in having a transverse expansion of the nasal suture above the maxillary fenestra (Fig. 2.16G). In *Deinonychus antirrhopus* and *Velociraptor* sp. (MPC-D 100/982), the simple dorsal ridge topology of the distal half of the ascending ramus is abutted medially by a ventrolateral process of the nasal throughout most of this length and continues onto the lacrimonasal suture (Figs. 2.12E-G, 2.16I-K). While no nasal is known for *Acheroraptor temertyorum*, ROM 63777 possesses a smooth facet along the dorsomedial surface of the distal ascending ramus indicative of a similar contact arrangement (Fig. 2.4A-D). The distal tip of the ascending ramus is not preserved in *Tsaagan mangas*, although it shows a morphology unlike the other dromaeosaurids observed in that the posterodorsal edge of the ascending ramus is deflected medially near the posterior extent of the preserved ascending ramus (Fig. 2.8G-H).

The contact with the lacrimal at the junction between the maxilla, lacrimal and nasal is conservative amongst all specimens where it can be observed. In *Deinonychus antirrhopus* and *Velociraptor* sp., the maxillary process of the lacrimal fits between two prongs of the ascending ramus, abutting against the ventrolateral process of the nasal for a short distance (Figs. 2.12E-G, 2.16I-K) The arrangement and morphology of the prongs is similar to those of *Acheroraptor*

temertyorum (Evans et al. 2013) and *Saurornitholestes langstoni* (Fig. 2.7) (Currie and Varricchio 2004). *Acheroraptor temertyorum*, *Atrociraptor marshalli*, *Deinonychus antirrhopus* and *Saurornitholestes langstoni* are alike in having a narrow mediolateral spread of the maxillary prongs at the distal end of the ascending ramus whereas *Velociraptor* sp. differs in having a broad mediolateral spread of the same prongs (Fig. 2.16I). While the sutural surface for the lacrimal is not preserved in *Tsaagan mangas*, it may have been similar to all other eudromaeosaurians in general configuration, but possibly more like the condition observed in *Velociraptor* sp. in having more mediolaterally flared prongs for receiving the lacrimal.

Maxillary fenestra - *Acheroraptor temertyorum* possesses a maxillary fenestra deeply embedded in a maxillary fossa that extends posterodorsal from the maxillary fenestra. This is like what has been observed in other dromaeosaurids such as *Atrociraptor marshalli*, *Bambiraptor feinbergi*, and *Saurornitholestes langstoni* (Figs. 2.2D-E, 2.6B, E-F, 2.9, 2.10A). In the dorsoposterior ends of the maxillary fossae observed in these specimens, there is a pneumatic excavation *sensu* (Hendrickx and Mateus 2014). This arrangement of maxillary fenestra, accessory struts, and excavations is unique among dromaeosaurids to these eudromaeosaurians. The one possible exception is *Shanag ashile* Turner et al., 2007, which has a maxillary fenestra that appears deeply embedded in a maxillary fossa. However, the exposed wall in the maxillary fenestra of *Shanag ashile* could be the exposure of the postantral strut, a condition observable in *Linheraptor exquisitus* (Xu et al. 2015) and some articulated specimens of *Velociraptor mongoliensis*. This would mean the fenestra of *Shanag ashile* is a simple perforation that is not embedded within a maxillary fossa. Of the eudromaeosaurians with the previously described condition, the fossae are also much deeper and better defined in *Acheroraptor temertyorum* and *Saurornitholestes langstoni* than observed in *Atrociraptor marshalli* and *Bambiraptor feinbergi*.

A narrow, laterally open, diverticulum is observed in the posterodorsal pneumatic excavation within the maxillary fossa of *Acheroraptor temertyorum* (Fig. 2.3B-D). It continues anteriorly partway along the anterior ramus to open ventrolaterally into the promaxillary recess (Fig. 2.3C). A small canal within the pneumatic excavation connects this diverticulum to a pneumatic canal traveling through the ascending ramus (Figs. 2.2E, 2.3B). This feature is not observed in *Atrociraptor marshalli* or *Saurornitholestes langstoni*, even though these two taxa possess pneumatic recesses posterodorsally (Figs. 2.6D-E, 2.9C). A pneumatic system through the ascending ramus is also observed in *Deinonychus antirrhopus*, which shows a small canal opening medially for a short distance (Fig. 2.12C, H). This seems to contrast with Asian eudromaeosaurians, which show much less development of these pneumatic structures (Figs. 2.8G-I, 2.16I-K). The maxillary fenestra of other eudromaeosaurians are also coded as being within a fossa and being positioned posterodorsal to the promaxillary fenestra (Currie and Evans 2019). This study reveals that this distinction is far more complicated than that. The maxillary fossae of North American taxa observed in this study and *Achillobator giganticus* are completely within the antorbital fossae and have an posterodorsal orientation (Figs. 2.4B, D, 2.7A, 2.9A, 2.13A) whereas the Campanian velociraptorines of Asia have maxillary fossae oriented more posteriorly and opening broadly into the antorbital cavity (Figs. 2.8A, C, 2.16A). In all conditions the maxillary fenestra occupies the most anterior-anteroventral extent of the accessory antorbital fossa. *Velociraptor* sp. (MPC-D 100/982) has a unique condition in having a maxillary fenestra within a broad, shallow maxillary fossa that extends anterior to the anterior extent of the maxillary fenestra (Fig. 2.16B). The position of the maxillary fenestra relative to the promaxillary fenestra is also variable within Eudromaeosauria. The maxillary fenestrae are posterodorsal relative to the promaxillary fenestrae in *Acheroraptor temertyorum*, *Atrociraptor*

marshalli, *Bambiraptor feinbergi*, *Deinonychus antirrhopus*, *Saurornitholestes langstoni*, *Velociraptor osmolskae*, and most *Velociraptor mongoliensis* specimens. However, the maxillary fenestra is more dorsal in *Atrociraptor marshalli* than in the other previously mentioned taxa. The maxillary fenestrae are posterior to the promaxillary fenestrae in *Achillobator giganticus*, and a few specimens of *Velociraptor* spp. (AMNH 6515 and MPC-D 100/982) (Figs. 2.3C, 2.16B-D) (Perle et al. 1999). *Acheroraptor temertyorum* has a more posteriorly positioned maxillary fenestra than other North American taxa but remains more posterodorsal to the promaxillary fenestra than observed in *Achillobator giganticus* and some *Velociraptor* spp. The maxillary fenestrae are dorsal to the promaxillary fenestrae in *Linheraptor exquisitus* and *Tsaagan mangas* (Fig. 2.8E-F) (Xu et al. 2015).

The maxillary fenestra of *Saurornitholestes langstoni* has been described as oval (Currie and Varricchio 2004). Generally, this is true although it is anteroposteriorly longer at the anteroventral end and constricts slightly posterodorsally to give a slight tear drop shape. This is similar to *Acheroraptor temertyorum*, *Deinonychus antirrhopus*, *Linheraptor exquisitus*, *Velociraptor osmolskae*, and some specimens of *Velociraptor mongoliensis* (MPC-D 100/25 and MPC-d 100/54) (Figs. 2.4B, 2.14A) (Godefroit et al. 2008, Xu et al. 2015). However, it differs from the round maxillary fenestrae observed in *Atrociraptor marshalli*, *Bambiraptor feinbergi*, *Tsaagan mangas*, and several specimens of *Velociraptor* spp. (AMNH 6515 and MPC-D 100/982) (Figs. 2.8, 2.16) (Burnham et al. 2000). *Acheroraptor temertyorum* has an elongate maxillary fenestra that extends posterodorsally along the ascending ramus like *Deinonychus antirrhopus* and *Saurornitholestes langstoni*, both of which all have relatively thin pila interfenestralis. However, the most ventral point and anteroposteriorly widest opening of the maxillary fenestra of *Acheroraptor temertyorum* is located more centrally on the maxilla. The

position of the maxillary fenestra relative to the anterior border of the antorbital fossa in both *Acheroraptor temertyorum*, and *Deinonychus antirrhopus* is more like those of *Bambiraptor feinbergi*, *Saurornitholestes langstoni*, and *Velociraptor* spp. in that there are anteroposteriorly broad pilae promaxillaris (Figs. 2.4, 2.6A, 2.16B). Due to the abbreviated antorbital fossa of *Atrociraptor marshalli*, and the more dorsal position of the maxillary fenestra relative to the promaxillary fenestra, the pila promaxillaris is dorsoventrally broad and anteroposteriorly narrow (Fig. 2.10A-B). In *Linheraptor exquisitus* and *Tsaagan mangas* the maxillary fenestra is positioned dorsal to the promaxillary fenestra and the pila promaxillaris is dorsoventrally narrow and oriented anteroposteriorly as opposed to dorsoventrally as in the other taxa (Fig. 2.8). The relative position of the maxillary fenestra to the ventral margin of the antorbital fossa is related to the ventral extent of the antorbital fossa. *Atrociraptor marshalli*, *Bambiraptor feinbergi*, *Deinonychus antirrhopus*, *Saurornitholestes langstoni*, and *Velociraptor* spp. all possess antorbital fossae that expand ventrally towards the posterior extents of the jugal margins, restricting the exposed ventral laminae (Figs. 2.7, 2.10A-B, 2.13A-B, 2.16B). The degree to which the antorbital fossa expands may vary between these taxa but appears morphologically similar. In contrast, the ventral boundaries of the antorbital fossae in *Acheroraptor temertyorum*, *Achillobator giganticus*, *Linheraptor exquisitus*, and *Tsaagan mangas* are clearly defined from the lateral walls or ventral laminae of the maxillae (Figs. 2.4A-B, 2.8A). The first two of these four taxa possess sloped lateral walls ventral to the ventral boundary of the antorbital fossa that expand ventrally towards the backs of the jugal rami. The relative position of the maxillary fenestra in all taxa compared was consistently in the upper half of the maxilla as viewed laterally. This can be ascertained by using the point of inflection along the most anterior border

of the antorbital fenestra for reference; all maxillary fenestra can be observed at or dorsal to this point.

Maxillary sinus – The maxillary sinus systems in eudromaeosaurians generally adhere to the previously described arrangements (Witmer 1997, Barsbold and Osmólska 1999, Currie and Varricchio 2004, Hendrickx and Mateus 2014). A maxillary antrum is medial to the maxillary fenestra, posterior to the promaxillary recess that is demarcated by a preantral strut on the medial surface near the promaxillary fenestra. The maxillary antrum is closed off from the cavity for the antorbital fenestra by a postantral strut (Figs. 2.3C, 2.6C, 2.12D). The only notable difference in arrangement is in *Tsaagan mangas*. Given the dorsal position and proximity of the maxillary fenestra to the promaxillary fenestra in *Tsaagan mangas*, it looks as if this specimen effectively has one sinus chamber in medial view (Fig. 2.8). The preantral strut is visible but is greatly reduced compared to the other taxa in this study, is oriented anterodorsally rather than posterodorsally, and is only as long as the anteroventral border of the maxillary fenestra (Fig. 2.8E). The sinus system in *Tsaagan mangas* and all other taxa observed in this study is dorsolateral to the palatal shelf. The floor of the sinus system is at the same level as the dorsal extent of the alveoli. The condition described for *Saurornitholestes langstoni* (Currie and Varricchio 2004) is similar to those of *Acheroraptor temertyorum* and *Deinonychus antirrhopus*, and is somewhat similar to *Atrociraptor marshalli*, all of which adhere to previous descriptions of theropod maxillary sinus systems (Witmer 1997, Witmer and Ridgely 2008, Hendrickx and Mateus 2014). In *Atrociraptor marshalli*, the preantral strut is slightly less well defined, is twisted anteriorly so that the medial edge of the strut is directed anteromedially and is positioned anterior to the promaxillary fenestra (Fig. 2.9E, 2.10C). In both *Acheroraptor temertyorum* and *Atrociraptor marshalli*, the maxillary antrum is short due to the abbreviation of the antorbital

fossa. However, the maxillary antrum of *Acheroraptor temertyorum* is shorter only relative to the proportionately longer promaxillary recess. In *Acheroraptor temertyorum*, the maxillary antrum and promaxillary recess are well developed and distinctly divided by a preantral strut like *Saurornitholestes langstoni* (Fig. 2.3C). The condition is unlike that in *Tsaagan mangas* (Fig. 2.8E), even though each has an elongate anterior ramus (Evans et al. 2013). The promaxillary recess mirrors the elongation of the anterior ramus but the morphology of the maxillary sinus system remains consistent with most other eudromaeosaurians. The condition of the sinus system in *Velociraptor* sp. is like those in *Acheroraptor temertyorum* and *Deinonychus antirrhopus* in having two chambers divided by a preantral strut. However, it differs in having dorsoventrally shallow maxillary sinus chambers that are constricted by the dorsally expanded maxillary alveoli (Fig. 2.16D-E). The preantral strut in MPC-D 100/982 is oriented posterodorsally as in all other eudromaeosaurians examined apart from *Tsaagan mangas*. However, the strut has shifted medially along its extent because an alveolus projects posterodorsally anterolateral to the strut (Fig. 2.16D-E).

Palatal shelf – The palatal shelf extends medially from the body of the maxilla and is generally located dorsomedial to the alveoli. However, in the case of MPC-D 100/982 the dorsal limits of the alveoli extend higher than the palatal shelf (Fig. 2.16D, F). MPC-D 100/982 also differs from all other specimens in this study in that the palatal shelf appears sinuous in medial view rather than straight. The palatal shelf in *Velociraptor osmolskae* also appears to be slightly sinuous in medial view (Godefroit et al. 2008), although the illustration of this specimen does not depict it as such. Whereas the sinuous palatal shelf was not observed in other specimens in this study, this condition does appear to be shared with *Achillobator giganticus* (Perle et al. 1999). The palatal shelf in *Deinonychus antirrhopus* has a slight dorsal arching in medial view rather

than being straight or sinuous (Fig. 2.13C-D). Whether sinuous or straight, the shelf tends to angle posteroventrally.

The width of the palatal shelf varies, the shelf being broadly expanded medially in *Acheroraptor temertyorum*, *Atrociraptor marshalli*, and likely *Deinonychus antirrhopus* – based on the medial projection of the anteromedial process – although the shelf posterior to this process is badly crushed laterally (Figs. 2.4E, 2.7D, 2.11B, 2.14). Conversely the palatal shelves are transversely narrow in MPC-D 100/982 and *Tsaagan mangas* (Figs. 2.8, 2.16). *Saurornitholestes langstoni* shows an intermediate condition possessing a broad palatal shelf relative to MPC-D 100/982 and *Tsaagan mangas* but noticeably narrow relative to other North American taxa (Fig. 2.7C). The anteromedial process extends from the medial wall of the maxilla at approximately the level of the second maxillary tooth position, or between the first and second in each dromaeosaurid examined. The anterior projection is well anterior to the anterior border of the anterior ramus in *Atrociraptor marshalli*, *Deinonychus antirrhopus*, and *Saurornitholestes langstoni* (Figs. 2.7, 2.8, 2.14) but distinctly less so in MPC-D 100/982 and *Tsaagan mangas* (Figs. 2.8, 2.16). The anterior portion of the anteromedial process is missing for the specimen of *Acheroraptor temertyorum* and its full anterior extent is unknown (Evans et al. 2013). The anteromedial processes of *Acheroraptor temertyorum*, *Saurornitholestes langstoni*, *Tsaagan mangas*, and *Velociraptor* sp. are mediolaterally narrow compared to those of *Atrociraptor marshalli* and *Deinonychus antirrhopus*, and do not show the triangular shape that these two taxa exhibit (Figs. 2.11B, 2.14D).

The medial wall of the palatal shelf expands to form the postantral strut posterior to, or at the position of the maxillary fenestra. The palatal shelf posterior to the postantral strut is visible in lateral view in each of *Atrociraptor marshalli*, and *Tsaagan mangas* (Figs. 2.8A, 2.9A).

However, the palatal shelf of *Atrociraptor marshalli* has been deflected dorsolaterally by compression and may not have been observable in lateral view when undistorted. *Tsaagan mangas* does not show a great deal of lateral compression and the palatal shelf and postantral strut are visible in lateral view as noted by Norell et al. (2006). The palatal shelves are parallel to the most ventral extent of the ventral margins of the antorbital fossae in *Acheroraptor temertyorum*, *Atrociraptor marshalli*, and *Tsaagan mangas* (Figs. 2.4D, 2.8C, 2.10A-C).

Dentition—The medial walls of the maxillae below the palatal shelves are higher towards the front of the maxillae in *Atrociraptor marshalli*, *Deinonychus antirrhopus*, *Tsaagan mangas*, and *Velociraptor* sp. (Figs. 2.8C, 2.10C, 2.13C-D). The dorsoventral height of the medial wall of the first alveolus in *Acheroraptor temertyorum* and *Saurornitholestes langstoni*, however, is noticeably shorter than the second alveolus (Figs. 2.4C-D, 2.7B). The most anterior alveolus in each specimen is angled posterodorsally, although to a lesser degree in *Deinonychus antirrhopus* and *Saurornitholestes langstoni*. The number of anterior maxillary alveoli that are posterodorsally angled varies between the eudromaeosaurians examined. Generally, the alveoli of *Deinonychus antirrhopus* and *Saurornitholestes langstoni* are straight with only the first alveolus being angled, whereas angling includes the first three in *Atrociraptor marshalli*, four in *Tsaagan mangas*, five in *Velociraptor* sp., and six or seven in *Acheroraptor temertyorum* (Fig. 2.18). The preantral strut is angled with the alveoli in all specimens and lines up between the third and fourth alveoli in all specimens except for *Tsaagan mangas* in which the preantral strut is dorsal to the fourth alveolus and the strut is not parallel to alveoli (Figs. 2.3C, 2.6, 2.8, 2.10C, 2.12, 2.16). Given the morphology of the palatal shelf, and the depth of the medial alveolar wall observed in MPC-D 100/982, *Velociraptor osmolskae* may have shared this condition and it may have also been found in other *Velociraptor* specimens. In all cases where the resolution of the

CT data is high, it is observed that the outer boundaries of the functional teeth do not contact the alveolar walls (Fig. 2.18A, C). This is consistent with the hypothesized tooth attachment in theropod dinosaurs, and other dinosaurs alike (Fong et al. 2016, LeBlanc et al. 2017).

Tooth replacement across specimens cannot be compared to the same degree. ROM 63777 and MPC-D 100/982 have the most complete series of maxillary teeth with observed replacement patterns (Fig. 2.18A, C). Tooth replacement in both *Acheroraptor temertyorum* and *Velociraptor* sp. appear to follow the same pattern observed in other theropod dinosaurs (Fong et al. 2016, LeBlanc et al. 2017, Hanai and Tsuihiji 2019). The teeth alternate between stages of development with earlier stage teeth surrounded by adjacent teeth at later stages of development in a pattern described as waves of development (Edmund 1960). Longevity of teeth before they are shed can offset the pattern and manifests in a series of large erupted teeth with variable levels of resorption for the developing teeth, as observed in ROM 63777 (Fig. 2.18A). Due to the offset in development of replacement teeth relative to erupted, functional teeth, multiple teeth can exist in a single tooth family (Edmund 1960, Fong et al. 2016, LeBlanc et al. 2017). While this can lead to situations with greater than two teeth per tooth family (LeBlanc et al. 2017, Hanai and Tsuihiji 2019), no more than two teeth per tooth family are observed across the specimens in this study (Fig. 2.18). In the fourth alveolus of ROM 63777 some remnants of the former erupted tooth remain in the alveolus (Fig. 2.18A). This is not abnormal and this type of material is often incorporated into the alveolar bone between alveoli (LeBlanc et al. 2017). In the case of TMP 1994.012.0844 a clear replacement pattern cannot be discerned from the three preserved alveoli with teeth. Each maxillary tooth preserved in TMP 1994.012.0844 has a replacement tooth developing anteromedially within its alveolus (Fig. 2.18B).

2.5 Discussion

2.5.1 Snout morphology interpretations

The maxillae of *Atrociraptor marshalli* (TMP 1995.166.0001) and *Deinonychus antirrhopus* (YPM 5232 [557]) did not suffer much post-mortem distortion relative to *Acheroraptor temertyorum* (ROM 63777). Post-mortem damage to the first two specimens is restricted largely to the medial surfaces that are crushed laterally against the main bodies of the maxillae. The additional difficulties with YPM 5232 (557) arose from discerning contacts with surrounding bones, and identifying which bones were in contact. The morphological interpretation of *Atrociraptor marshalli* has not changed drastically but instead has been confirmed in a few ways by understanding the anatomy more completely.

The maxilla of *Atrociraptor marshalli* is tall and anteroposteriorly short as expected, and it shares numerous morphological features with *Bambiraptor feinbergi* and *Saurornitholestes langstoni*, which have been previously proposed to be close relatives (Currie and Varricchio 2004, Currie and Evans 2019). What is revealed is the medial expansion of the anteromedial process which affirms the previous interpretation of a broad snout overall, that was based on the transverse breadth of the premaxillae (Currie and Varricchio 2004). Interestingly, *Deinonychus antirrhopus* shares a tall maxilla and a laterally expanded anteromedial process with *Atrociraptor marshalli*, although the anteromedial process is more robust in *D. antirrhopus* (Table 2.1). These two taxa exemplify the opposite condition to elongate snouts of Asian forms like *Tsaagan mangas* and *Velociraptor* sp. (Figs. 2.8, 2.16). Ostrom (1969) pointed out that the angle of lateral deflection of the maxilla from the contact with the nasal was steeper than in larger theropods like allosaurids and would have led to a relatively narrower snout. The snout of *Deinonychus antirrhopus* may be narrow relative to larger theropods, but the development of the anteromedial process of the maxilla and the lateral expansion of the nasals posteriorly clearly demonstrate

there was a broad snout relative to other dromaeosaurids (Fig. 2.13C-D). The nasals are unknown for *Atrociraptor marshalli* but based on all the other proportions, this taxon appears to have converged on the short snout morphology of *Deinonychus antirrhopus*. This pronounced stoutness of the snouts in these taxa may reflect an ecomorphological adaptation for specialization on larger prey (Slater et al. 2009).

Additionally, these two taxa share dentitions of posteriorly angled ('raked') maxillary teeth (Character 83, Currie and Evans 2019). The re-curvature of teeth have been shown to increase posteriorly along the tooth row in theropods (D'Amore 2009). In the case of a short maxilla, it is possible that the 'raking' (inclination towards the throat) of the maxillary teeth relates to the line of action required for teeth during biting. The juvenile specimen of *Bambiraptor feinbergi* (AMNH FARB 30556) also has raked maxillary teeth and shares similar maxillary proportions to *Atrociraptor marshalli* and *Deinonychus antirrhopus* (Table 2.1). The condition is well contrasted by the tooth orientation in the relatively long snouted eudromaeosaurians *Tsaagan mangas* and *Velociraptor* sp., which have teeth that are oriented more perpendicular to the maxilla, although the most anterior teeth have slight anterior orientations. Contrasting tooth orientation supports the possibility that the abbreviation of the snout anteroposteriorly in *Atrociraptor marshalli* and *Deinonychus antirrhopus* serves a functional purpose for prey capture and handling. These two dromaeosaurids were separated by a large amount of time but converged on morphologies shown to be conducive to handling larger prey for modern carnivores (Slater et al. 2009).

2.5.2 The effects of taphonomic processes on ratio-based characters

The effects of post-mortem deformation on the interpretations of morphology can be quite extensive as exemplified by the maxillae of *Acheroraptor temertyorum* and *Deinonychus*

antirrhopus. The initial interpretation of the latter has led to drastically different interpretations of the skull shape (Ostrom 1969) that can have serious implications for understanding the ecology and phylogeny of the animal. The interpretation put forth in this study presents a reconstruction of *Deinonychus antirrhopus* that is much more similar to the general morphologies of other dromaeosaurids (Fig. 2.15) (Currie 1995, Burnham et al. 2000, Norell et al. 2006, Xu et al. 2010a, Currie and Evans 2019). It also reveals features of the maxilla not previously described, such as the anteromedial process, which was initially described as a premaxillary process of the nasal (Ostrom 1969). With the re-examination of YPM 5253 (557) it has also been shown that the anterior ramus is not elongate compared to the maxilla (Character 28, Currie and Evans 2019), nor does it possess an elongate shape (length to height ratio of 1 or greater) as in other eudromaeosaurians, even though it has been coded as such in recent phylogenetic analyses (Longrich and Currie 2009, Evans et al. 2013, Currie and Evans 2019). This removes some support for the close relationship of *Deinonychus antirrhopus* to velociraptorines and demonstrates that *Deinonychus antirrhopus* was more like North American forms like *Atrociraptor marshalli*, *Bambiraptor feinbergi*, *Saurornitholestes langstoni*. However, it is most similar to the Early Cretaceous *Achillobator giganticus* regarding the shape and length of the anterior ramus.

Due to the retention of an elongate anterior ramus in Late Cretaceous eudromaeosaurians from Asia, this characteristic has been suggested to define velociraptorines and originated in Asia. The elongate anterior ramus of the North American taxon, *Acheroraptor temertyorum* was thus used as evidence for an Asian migration during the latest Cretaceous (Evans et al. 2013). The importance of having accurate measurements of specimens becomes clear when one looks at the subsequent levels of inference made after morphological description. Inferences covering

phylogenetic relationships, ecological significance, and species dispersal events have been drawn from this single element predominantly using the anterior ramus as the distinct feature. While the coding of *Acheroraptor temertyorum* for two characters pertaining to anterior ramus length and elongation as coded in Currie and Evans (2019) did not change, the ratio of elongation did change, 1.22 before retro-deformation to 1.09 after retro-deformation (Table 2.1). This still meets the criteria of the elongate condition [0] for character 29 (Currie and Evans 2019) by having a length to height ratio of greater than 1. However, the close proximity of this value to the proposed threshold of 1 compared to the previously compared taxa – *Linheraptor exquisitus* (1.51) and *Tsaagan mangas* (1.30) – is a point of concern when one considers the nature of continuous data (Simões et al. 2016). Ratio-based characters can vary intraspecifically owing to ontogeny, sexual dimorphism, or individual variation (Ibiricu et al. 2013, Schott and Evans 2017, Holmes et al. 2020), or as in the case of this study, through post-mortem distortion. These problems of interpretation can make it difficult to use these features in a phylogenetic framework. In the case of the anterior ramus elongation, it has not been demonstrated that the cut-off for length to height ratios of the anterior rami of eudromaeosaurians should be 1.0 given the spread of data. With the maxilla of *Acheroraptor temertyorum* falling closer to the threshold than to other taxa with this feature it is unclear whether the anterior ramus of *Acheroraptor temertyorum* was being reduced in length from an Asian dromaeosaurid ancestor, or if it was elongating through time relative to a North American ancestor that possessed the short trait. Elongation of a tooth bearing element in particular can also serve a functional purpose in prey acquisition and preference (van Cakenberghe et al. 2002, Slater et al. 2009, Whitlock 2011). This makes characterizing elongation of maxillae, premaxillae, and dentaries as homologous features difficult given the potential for convergence due to niche overlap. Traits of elongation or

stoutness may become fixed in a population, leading to speciation, if there is geographic separation, variability in ecological niche, or both (Slater et al. 2009, Ferreira-Cardoso et al. 2019). Only when the suite of maxillary characters is considered can the rationale behind character construction be gauged, and a different relationship of similarity is observed.

It is also noted in this study that the length to height ratio (elongation) of the anterior ramus (Character 29) is dependent on the height of the maxilla (Fig. 2.17A), and the proportion of maxillary length that is composed of the anterior ramus (Character 28). An anterior ramus can be as long relative to maxillary length as that of another specimen but the feature itself can be less elongate, as observed for *Acheroraptor temertyorum* and *Atrociraptor marshalli* (Table 2.1). This occurs when there is a tall maxilla (length to height ratio ≤ 2.5 as a rough estimation) as in *Atrociraptor marshalli* and *Saurornitholestes langstoni*. In these animals, large proportions of their maxillary lengths are made up by the anterior rami, but the feature itself is not elongate because the height of the anterior ramus increases with the height of the maxilla (Fig. 2.17). Another contributing factor may be the angle of the ascending ramus relative to the tooth row. A high angle causes the anterior ramus to deepen dorsoventrally to a greater extent posteriorly along the maxilla. Maxillae with acutely angled ascending rami tend to possess more elongate anterior rami and maxillae than those with larger ascending ramus angles (Table 2.1). Use of both character 28 and 29 from Currie and Evans (2019) should be cautioned against based on the dependency of character 29 on other aspects of maxillary proportions such as maxillary height (Fig. 2.17A), and angle of the ascending ramus. Furthermore, the junction between the anterior ramus and antorbital fossa delineates the extent of both of these features, ambiguity exists as to which feature is really changing in its proportion to maxillary length (i.e., the anterior ramus gets longer and the antorbital fossa gets shorter, or vice versa).

2.5.3 Maxillary sinus system and character construction

The maxillary sinus system in eudromaeosaurians is generally consistent in the arrangement of its features and is like most theropods (Witmer 1997, Witmer and Ridgely 2008, Hendrickx and Mateus 2014). The condition does change, however, when the maxillary fenestra is positioned more dorsally than posterodorsally to the promaxillary fenestra as observed in *Tsaagan mangas* (Fig. 2.8E) because the preantral strut becomes more horizontally oriented. Proximity of the maxillary and promaxillary fenestra also affects the chamber morphology as in *Tsaagan mangas*; the preantral strut is reduced to an anteroposteriorly short strut that is horizontally oriented and serves only to divide the two fenestrae. In contrast, there is the comparatively large dorsal displacement of the maxillary fenestra from the promaxillary fenestra in *Atrociraptor marshalli* and the retention of a dorsoventrally extensive preantral strut (Fig. 2.10C). The result of the condition in *Tsaagan mangas* is that the maxillary sinus system is composed of effectively one chamber. Character 14 in Currie and Evans (2019) describes the anteroposterior position of the maxillary fenestra relative to the anterior border of the antorbital fossa. The condition of an anteriorly placed maxillary fenestra is also observed in *Stenonychosaurus inequalis* Sternberg, 1932 (Currie 1985), which is similar to *Tsaagan mangas* in that there is only one chamber for the maxillary sinus.

What this character does not capture is the variation of the sinus system when the maxillary fenestra is positioned dorsally to the promaxillary fenestra as in *Atrociraptor marshalli*, in which a well developed preantral strut is retained. It also potentially misses the effect on the maxillary sinus system when there is variable promaxillary fenestra morphology. *Geminiraptor suarezarum* Senter et al., 2010, has an anteriorly positioned maxillary fenestra, but retains a distinct, dorsoventrally tall, slit-like promaxillary fenestra anterolateral to the maxillary

fenestra. Although the preantral strut cannot be observed in *Geminiraptor suarezarum*, the promaxillary fenestra of *Acheroraptor temertyorum* is similar in its morphology. Furthermore, medially adjacent to the promaxillary fenestra of *Acheroraptor temertyorum* is a well developed preantral strut. Therefore, the condition observed in *Tsaagan mangas* relates to several factors; the maxillary fenestra is positioned very near/within the anterior border of the antorbital fossa, the maxillary fenestra is dorsal to the promaxillary fenestra, and the promaxillary fenestra is small and subcircular. The dorsal position of the maxillary fenestra relative to the promaxillary fenestra is coded in a combined character state with being nested within a distinct fossa (character 10; Currie and Evans 2019). However, this is not sufficient for the range of eudromaeosaurians observed in this study and the dependency of maxillary fenestra development and relative position is here challenged.

Character 10 from Currie and Evans (2019) describes the development of the maxillary fenestra as either being a simple perforation or within a secondary antorbital fossa. It has also combined the position of the maxillary fenestra relative to the promaxillary fenestra into the character description, stating that all maxillary fenestrae within a secondary antorbital fossa are positioned posterodorsal to the promaxillary fenestra. Within the eudromaeosaurian taxa examined in this study alone it is observed that these criteria are violated. The positions of the maxillary fenestrae in *Acheroraptor temertyorum* and *Velociraptor* spp. (AMNH 6515 and MPC-D 100/982) are posterior – but not dorsal – to the promaxillary fenestrae (Figs. 2.4A-B, 2.16B). The variation of fossae in which the maxillary fenestra sits is also not captured by the current wording of this feature and it seems to have been used to simply separate dromaeosaurids from troodontids. The maxillary fossae of *Acheroraptor temertyorum*, *Atrociraptor marshalli*, *Bambiraptor feinbergi*, and *Saurornitholestes langstoni* are distinct from all other taxa in being

well-defined and each has a posterodorsal pneumatic excavation separated from the fenestra by a distinct anterodorsally oriented strut. The fossae are deep in *Acheroraptor temertyorum* and *Saurornitholestes langstoni* compared to the other two taxa but share the arrangement and general placement of features. These two taxa also share a strong resemblance in the morphology of their respective maxillary sinus systems demonstrating the connection of these features. The shared condition of the maxillary fenestra and fossa in *Acheroraptor temertyorum* went overlooked due to post-mortem distortion of the original specimen. The maxillary fossa of *Tsaagan mangas* is markedly different from those previously described in being comparatively shallow, being bordered dorsally by the dorsal border of the antorbital fossa, and in that the ventral border of maxillary fossa opens broadly posteriorly (Fig. 2.8A). This maxillary fossa morphology is observed in *Linheraptor exquisitus*, and *Velociraptor* spp. but the depth of the fossa varies among specimens (Fig. 2.16B) The condition in *Deinonychus antirrhopus* is different from the previously mentioned taxa in having the maxillary fossa completely enclosed within the antorbital fossa and oriented posterodorsally, more like those of *Acheroraptor temertyorum* and *Saurornitholestes langstoni*. Its condition is unlike the posteriorly oriented maxillary fossa of *Tsaagan mangas* and other derived Asian taxa in which the maxillary fossa opens into the antorbital fenestra. The *Velociraptor* sp. specimen (MPC-D 100/982) shows another condition, in that the maxillary fenestra is situated within a maxillary fossa sharing only a small portion of the anteroventral border (Fig. 2.16B). Some representatives of *Velociraptor mongoliensis* have maxillary fenestrae that are within very shallow maxillary fossae and appear like simple perforations (MPC-D 100/25). The range of variation of features pertaining to the maxillary fenestra in eudromaeosaurians is not currently reflected by current character construction as it has been simplified by combining several states into one. Combining character

states implies a dependency of those character states (Simões et al. 2016) and in this case, misses variation vital for higher precision characterization of morphological variation within Eudromaeosauria. Position of the maxillary fenestra relative to the promaxillary fenestra should be distinct from the maxillary fenestra being positioned within a fossa as species like *Acheroraptor temertyorum*, *Tsaagan mangas* and *Velociraptor mongoliensis* violate this assumption of dependency. Furthermore, the states of the maxillary fossae should be divided into separate states rather than being treated as equivalents. Saurornitholestines and *Acheroraptor temertyorum* possess a maxillary fenestra morphology distinct enough from other eudromaeosaurians to warrant their own state whereas velociraptorines of Asia possess a maxillary fenestra morphology that generally matches the current state describing a secondary fossa. *Deinonychus antirrhopus* possesses another distinct state in having a similar position and orientation to saurornitholestines but lacking a pneumatic excavation in the posterodorsal corner of the maxillary fossa.

The characterization of the promaxillary fenestra (Character 9) by Currie and Evans (2019) also combines states in coding that a slit-like condition is only present when hidden in the anteroventral border of the antorbital fossa (as opposed to being subcircular and exposed broadly in lateral view). This character should be broken into two characters based on specimens like *Deinonychus antirrhopus* or *Saurornitholestes langstoni* which possess promaxillary fenestrae tucked in the anterior border of the antorbital fossa but vary between subcircular and slit like, respectively (Figs. 2.7A, 2.13A). It is challenged again by *Velociraptor mongoliensis*, which possesses a slit-like promaxillary fenestra concealed by the anterior or anterodorsal border of the antorbital fossa; this condition is also observable in MPC-D 100/982 (Fig. 2.16B). In this specimen of *Velociraptor* sp., the promaxillary fenestra is slit-like, exposed in lateral view and positioned

along the anterodorsal border of the antorbital fossa. The promaxillary fenestra is weathered and extends farther posteriorly than would be natural, exposing the preantral strut in lateral view (Fig. 2.16B). CT scans show that the promaxillary fenestra would have continued in an elongate opening as opposed to a simple subcircular fenestra; it would not have been exposed in lateral view if not for weathering. These issues require the division of the character to capture the variability and compare eudromaeosaurians more thoroughly and more accurately.

The shape of the maxillary fenestra is also variable beyond what is characterized in Currie and Evans (2019) in their Character 11, which describes three conditions of maxillary fenestra shape: small and subcircular, large and subcircular, and anteroposteriorly elongate. The coding for this character puts most dromaeosaurids as the same state, subcircular and small, whereas troodontids and unenlagiines are characterized by the anteroposteriorly elongate maxillary fenestra. Only *Archaeopteryx lithographica* Meyer, 1861, is characterized by a large subcircular maxillary fenestra. Under this coding system a variety of shapes and variations in relative size of the maxillary fenestrae are missed. This character could be divided into two characters, one defining size of the fenestra and the other describing the shape of the fenestra. Elongation of a fenestra is more related to shape, implying a longer axis in one direction than another, which would deviate from the subcircular shape. For example, the maxillary fenestra of *Atrociraptor marshalli* would be considered subcircular and large relative to the maxilla when compared to other eudromaeosaurians (Fig. 2.10A-B). Conversely the maxillary fenestra of *Deinonychus antirrhopus* would be small relative to the maxilla and posterodorsally elongate (Fig. 2.14A). Distinguishing large from small fenestra should be further quantified to justify state parameters. Relative size of the maxillary fenestra compared to a maxillary measurement relating to overall size would be the best approach to quantifying distinct states. Software such as ImageJ

allows for the measurements of area and could be used to compare maxillary fenestra size to overall size of the maxilla. A character describing the size of the maxillary fenestra could be multistate to accommodate extreme enlargement of maxillary fenestra in troodontid outgroups, and still be able to distinguish relative size variations within dromaeosaurids. Dividing this character up gives more options in terms of coding and avoids the compounding of states unjustifiably.

The position of the maxillary fenestra relative to the ventral margin of the antorbital fossa is characterized by character 12 in Currie and Evans (2019) and has three states; maxillary fenestra is at the level of the ventral margin of the antorbital fossa, low but not touching the ventral margin, and in the upper half of the antorbital fossa. This character has several issues. First, the maxillary fenestra is here shown to be limited in its ventral placement by the dorsal extent of the maxillary alveoli (Figs. 2.2-2.4, 2.6-2.9, 2.12, 2.16). Except for the condition observed in MPC-D 100/982, the dorsal extent of the maxillary alveoli is approximately parallel to the point of attachment for the palatal shelf making these features natural limits to the ventral position of the maxillary fenestra. In some cases, the antorbital fossa is restricted ventrally and is roughly parallel to the upper limit of the maxillary alveoli and palatal shelf (Figs. 2.4B, D, 2.8, 2.9-2.10). However, in taxa like *Deinonychus antirrhopus*, *Saurornitholestes langstoni* and *Velociraptor* sp., the antorbital fossa extends ventrally below the dorsal extent of the maxillary alveoli (Figs. 2.7, 2.14, 2.16). Therefore, it is implausible for the maxillary fenestra to be positioned low in the antorbital fossa while the fossa is expanded ventrally. Due to the independent variability of the dorsoventral position of the maxillary fenestra and the ventral expansion of the antorbital fossa, the ventral margin of the antorbital fossa does not represent a good landmark for characterizing the position of the maxillary fenestra. The ventral border of the

antorbital fossa is limited in its dorsal extent by the same structures that limit the ventral placement of the maxillary fenestra. However, each can vary in their position relative to the dorsal limit of the maxillary alveoli independently. Therefore, alternative landmarks should be used to characterize the dorsoventral position of the maxillary fenestra. With the use of CT this can be solved relatively easily by comparing the relative position of the maxillary fenestra and/or the position of the ventral border of the antorbital fossa to the palatal shelf or the ventral extent of the maxillary antrum. This character should be reworked to demonstrate relative position of the maxillary fenestra to a dependent landmark such as the alveolar depth or a complementary structure on the lateral surface to reflect structural relationships between the maxillary fenestra and its dorsoventral position.

Another character used in the Currie and Evans (2019) analysis to describe the dorsoventral position of the maxillary fenestra is Character 13, which compares the dorsal extent of the maxillary fenestra to the height of the largest maxillary tooth. The significant variant is whether the maxillary fenestra is dorsally displaced from the maxillary tooth row by 2x or more the height of the largest maxillary tooth. This character requires the “largest” tooth to be present and fully erupted to confidently code a single specimen. Tooth size can be quite different among taxa when tooth counts are highly variable such as in troodontids (Norell et al. 2009) and unenlagiines (Makovicky et al. 2005, Novas et al. 2009), which possess many but individually smaller maxillary teeth relative to the maxilla than in eudromaeosaurians and other dromaeosaurids. Position of the largest tooth can vary taxonomically and generally occurs anterior to the maxillary fenestra along the tooth row. Partial extrusion of maxillary teeth may cause the maxillary tooth to be measured as larger than it really is potentially leading to incorrectly coding this character for a given specimen. Measuring the length of the posterior

carina could solve this problem and should be included in the character description for consistency and repeatability. This character could measure the distance of the maxillary fenestra from the top of the deepest alveolus, however, this would require CT data and is quite irregular when you consider the condition of MPC-D 100/982 (Fig. 2.16D) compared to other eudromaeosaurians. Because tooth size and count can both be quite taxonomically variable, and the position of the maxillary fenestra is not limited by the antorbital fossa but the maxillary antrum it feeds into, this character should be further examined across Dromaeosauridae using the aid of CT and reworked based on correlated features. The ventral extent of the maxillary sinus system is limited by the depth of maxillary alveoli. Due to the angle of the palatal shelf and the larger, more deeply rooted teeth anterior to the maxillary fenestra (Figs. 2.3, 2.6, 2.8, 2.9, 2.12), the largest tooth does not directly relate to the dorsoventral position of the maxilla. Therefore, character 13 could work if both the tooth chosen was ventral to the maxillary fenestra, and if the root and tooth crown were sub-equal in dorsoventral length. As is, character 13 from Currie and Evans (2019) may add extra weight to characters describing tooth size (i.e. Characters 82, 89, 90) and other characters describing the dorsoventral position of the maxillary fenestra (i.e. Character 12).

The antorbital fossa has two characters utilized in Currie and Evans (2019) to describe the condition of ventral extent relative to the jugal ramus; Character 7, which characterizes the ventral extent of the antorbital fossa and its lateral exposure on the jugal ramus, and character 32, describes the height of the jugal ramus below the antorbital fossa as either being “low” or “dorsoventrally tall”. While the first describes the condition observed in *Atrociraptor marshalli*, *Deinonychus antirrhopus*, *Saurornitholestes langstoni*, and *Velociraptor mongoliensis*, the second character describes the amount of the fossa exposed on the jugal ramus. While one could

divide the condition of *Atrociraptor marshalli* as having a tall jugal ramus ventral to the antorbital fossa and *Velociraptor mongoliensis* as having the short condition, taxa like *Linheraptor exquisitus* and *Tsaagan mangas* would be double weighted in having a restricted antorbital fossa. Furthermore, the cut-off of tall vs short for character 32 is completely subjective. It is not defined as to when to pick one over the other outside the obvious tall condition in *Linheraptor exquisitus* and *Tsaagan mangas* that do not have laterally exposed antorbital fossae on the jugal rami. Of the two, character 32 should be reworked or avoided. No alternative is here proposed so the use of this character is cautioned against until a consistent delineation criterion can be produced. Character 7 should contain a third state to accommodate taxa like *Acheroraptor temertyorum* and *Achillobator giganticus* that possess restricted antorbital fossae. However, each also possesses a laterally sloped surface ventral to the ventral border of the antorbital fossa that is distinct from the more vertical lateral wall of the maxilla observed in *Linheraptor exquisitus* and *Tsaagan mangas*.

The palatal shelf and postantral strut become confluent at or near the posterior end of the anterior border of the antorbital fenestra, posterior to the maxillary fenestra. There is a character for the exposure of each of these structures in lateral view (Characters 27 and 26 from Currie and Evans 2019). The justification for the separation of these characters is unclear with the specimens observed in this study. However, it is implied by the coding of taxa within Currie and Evans (2019) where *Atrociraptor marshalli* and *Saurornitholestes langstoni* are coded as having a palatal shelf exposed in lateral view, whereas the postantral strut is not exposed. This interpretation is challenged in this study by the compressed nature of *Atrociraptor marshalli* and *Saurornitholestes langstoni* (UALVP 55700, Currie and Evans 2019), which would deflect the palatal shelf dorsolaterally, revealing it in lateral view through the antorbital fenestra. TMP

1994.012.0844, which is exceptionally well preserved in three dimensions, shows minimal exposure of the palatal shelf through the antorbital fenestra, no more than observed in *Velociraptor* sp. (MPC-D 100/982) (Figs. 2.6A, 2.17B), which Currie and Evans (2019) coded as being concealed in lateral view. Interestingly, *Linheraptor exquisitus* and *Tsaagan mangas* were coded as having a revealed postantral strut but not a palatal shelf, despite the confluence of these features and the continuous border observed in lateral view for these taxa along the dorsal border of the jugal ramus (Fig. 2.8A, Xu et al. 2015). Two options could be to keep these two characters but re-evaluate the distribution throughout the data set and include taxa like *Velociraptor mongoliensis* as having a revealed palatal shelf, like *Atrociraptor marshalli* and *Saurornitholestes langstoni*. Alternatively, one could code all these taxa as not having a revealed palatal shelf in lateral view due to the subjective nature of identifying it and the potential influence of post-mortem distortion on this character. The latter then creates a potential artificial weight to the revealed postantral strut as it becomes confluent with the palatal shelf posteriorly and is visible in lateral view in the two eudromaeosaurians where it is observable.

The antorbital fossa has been coded for an additional character in Currie and Evans (2019) for a character relating its anterior extent to maxillary tooth positions (Character 6). This character has three states based on the anterior margin of the antorbital fossa being in line dorsally with maxillary alveoli three, four, and five or more. A few logical and wording problems exist with this character. First, it is unclear if the anterior margin being in line with tooth alveolus means the central alveolus, anterior end of the alveolus, or posterior end of the alveolus. Nowhere does it specify how much overlap is acceptable between states either. In the study by Currie and Evans (2019) *Acheroraptor temertyorum* is united with *Deinonychus antirrhopus* and Late Cretaceous Asian eudromaeosaurians in having the anterior margin of the

antorbital fenestra in line with the fifth alveolus (or further posterior). However, the anterior margin of the antorbital fossa is between the fourth and fifth alveolus in *Acheroraptor temertyorum*, like in *Velociraptor mongoliensis* (AMNH 6515, MPC-D 100/25 and MPC-D 100/54) but different from *Tsaagan mangas*, in which the junction is dorsal to the centre of the fifth alveolus. *Deinonychus antirrhopus* was coded as level with the fifth due to the inclusion of the right premaxilla, so its coding should be corrected based on the reinterpretation here in which it would share the state of MPC-D 100/982 in having the anterior margin of the antorbital fossa dorsal to the middle point between the third and fourth alveoli (Fig. 2.14A). *Atrociraptor marshalli* was coded as having the anterior margin dorsal to the fourth alveolus, however, its position is between alveolus 4 and 5, like in most specimens of *Velociraptor mongoliensis*. This indicates no clear way of coding this and needs rewording and reworking. The most consistent way to reword this character would be to consider the anterior margin of the antorbital fossa as in line with a tooth position when it is above the tooth distinctly or just posterior to it. This change would require that *Acheroraptor temertyorum* and *Velociraptor mongoliensis* be recoded as being above the fourth alveolus like *Atrociraptor marshalli* and *Saurornitholestes langstoni*, and *Deinonychus antirrhopus* be recoded as above or just behind the third alveolus, like *Achillobator giganticus*. The last issue with this character is in the assumptions. It assumes that the anterior margin of the antorbital fossa is homologous among eudromaeosaurians and that all the structures around it will alter in their shape from this central position. This cannot be clearly demonstrated in this study, nor has it been in previous studies. However, in this study it is observed that the preantral strut lines up between the third and fourth maxillary alveoli in all taxa except for *Tsaagan mangas*. The preantral strut is also quite modified in *Tsaagan mangas* compared to the other eudromaeosaurians in this study and may not be directly comparable.

Describing this character based on the preantral strut seems more consistent but is not observable from the lateral surface due to the anterior angles of the anterior maxillary alveoli. Additionally, the tooth counts of eudromaeosaurians vary between nine (*Dromaeosaurus albertensis*) and 13 (*Deinonychus antirrhopus*) meaning that tooth position relative to the antorbital fossa and anterior ramus may vary just depending on tooth count. This character seems to serve to enhance the already heavily weighted anterior ramus feature. The anterior ramus may elongate relative to the maxilla, but there is also a notable anteroposterior constriction of the antorbital fossa where this trait is observed in eudromaeosaurians (*Acheroraptor temertyorum*, *Linheraptor exquisitus*, and *Tsaagan mangas*) (Figs. 2.4A-B, 2.8A, Xu et al. 2015). Unenlagiines and troodontids share the character state of the anterior border of the antorbital fossa being above or posterior to the fifth maxillary alveolus with eudromaeosaurians possessing an elongate anterior ramus due to greater tooth counts and elongate anterior rami observed in these outgroups (Norell et al. 2009, Novas et al. 2009). This makes the character homoplastic within the dataset and may cause noise in a phylogenetic analysis in the data set if material is limited. The use of this character is here cautioned as it primarily serves to enhance the character weight of the anterior ramus as it is logically dependent on that feature. Inconsistent maxillary tooth counts across the taxonomic sample also make this character homoplastic, therefore problematic for phylogenetic resolution. Use of this character in tandem with others defining the anterior ramus may overshadow more homologous characteristics reflective of the maxillary sinus system which shows more consistency across eudromaeosaurians.

2.5.4 Nasal and lacrimal contacts

The morphology of the contact surface between the lacrimal, nasal and premaxilla along the dorsolateral surface of the maxilla is markedly similar between all North American taxa

observed in this thesis. The trough like morphology along the anterior ramus of the maxilla and anterodorsal portion of the ascending ramus is still observed in the Asian taxa examined in this thesis. However, it is divided along the dorsal margin of the ascending ramus in *Velociraptor* sp., where it expands into a transversely wide trough above the maxillary fenestra (Fig. 2.16G). This transverse expansion of the dorsal margin above the maxillary fenestra is not observed in any capacity in the other dromaeosaurids in my study but is visible in lateral view on other *Velociraptor mongoliensis* specimens (Norell et al. 2006). This feature of *Velociraptor* spp. could be related to the dorsoposterior position of the maxillary fenestra, which puts it into proximity with the maxillonasal contact. This is different from *Deinonychus antirrhopus* and *Saurornitholestes langstoni* in which the maxillary fenestrae are located farther below the dorsal margins of the maxillae. The mediolaterally broadened dorsal surface of the maxilla could be important for structural integrity around the border of the maxillary fenestra. In *Deinonychus antirrhopus* and *Saurornitholestes langstoni*, the lack of a transverse expansion of the dorsal margin of the maxilla is possibly due to the more ventral placement of the maxillary fenestra and anterior termination of the border of the antorbital fossa relative to other taxa. The maxillary fenestra is structurally supported in these taxa by a well developed postantral strut that extends medially to form the dorsal wall of the maxillary antrum (Figs. 2.7C, 2.14C). The transverse expansion in *Velociraptor* spp. serves this same function as it contributes to the dorsolateral ceiling to the antrum. The contact with the nasal along the dorsal margin of the maxilla is conserved in all eudromaeosaurians observed in this study. Major deviations may relate to strengthening the dorsal border of the maxillary fenestra via transverse expansion of the nasal contact above the maxillary fenestra or the lateral bulging of the dorsal border of the ascending ramus in *Tsaagan mangas* (Fig. 2.8G).

Tsaagan mangas differs from these previous taxa in possessing a dorsomedially curved dorsal margin of the ascending ramus, rather than a relatively straight, thin ridge. This causes the maxillary nasal suture to remain less complex than in the other taxa in that the maxilla slots dorsolaterally into the nasal rather than fitting into a forked slot on the ventrolateral side of the nasal. While this differs from the condition observed in *Velociraptor* sp., the general shape (anteroposteriorly short and dorsoventrally shallow) of the ascending ramus is similar. Therefore, it is likely that the ascending ramus of *Tsaagan mangas* would terminate in the same morphology of contact with the lacrimal as observed in *Velociraptor* sp. The similarity shared by *Tsaagan mangas* and *Velociraptor* sp. is suggestive of a shared developmental pattern. Given the shallow but long maxillae of Asian taxa, except for *Achillobator giganticus*, the transverse widening of the ascending ramus may serve to strengthen the contact with the nasals and lacrimals and in effect the junction between snout and temporal region. The arrangement of the lacrimal-maxilla contact is conserved in eudromaeosaurians despite some proportionate differences. These proportionate variations do, however, serve to distinguish the interconnection of the lacrimal, maxilla and nasals of the elongate maxillae of Asian forms from the snout, from the stocky maxillae observed in North American taxa. *Acheroraptor temertyorum* does present an interesting case in which the maxilla has become more elongate relative to other North American forms, however, the maxilla-lacrimal, and maxilla-nasal contact remains similar to those observed in typical North American taxa, which is suggestive of a close relationship to them.

Character 34 (Currie and Evans 2019) describes the condition of the nasal possessing pneumatopores and participating in the margin of the antorbital fossa – Nasal participation in margin of antorbital fossa: and has pneumatopores: 0, no; 1, yes, and has pneumatopores. This is

a compound character (Simões et al. 2016), combining two states into one, and serves to characterize the condition in *Deinonychus antirrhopus* and *Saurornitholestes langstoni*. However, differences of this condition in the two taxa are apparent in that the antorbital fossa extends onto and is exposed on the lateral surface of the nasals in *Deinonychus antirrhopus* while the ventrolateral shelf of *Saurornitholestes langstoni* demarcates the upper extent of the fossa in this specimen. This character should be split to characterize the presence of pneumatopores on the nasals, and the extent of the antorbital fossa observed on the nasals separately. This would still characterize *Deinonychus antirrhopus* and *Saurornitholestes langstoni*, which would still share the character of pneumatopores on the nasals at the upper extent of the antorbital fossa and capture the difference in nasal morphology between these taxa.

2.5.5 Tooth characters

Tooth characters make up a large portion of the characters in Currie and Evans (2019) comprising 10% of the total dataset of 180 characters. Teeth are difficult to characterize as they show serial homologous trends showing slight variation along a tooth row (D'Amore 2009). They are difficult to identify down to species level based on their morphology (Larson and Currie 2013). Use of isolated teeth to distinguish species has been done in previous analyses (Sankey 2001, Larson and Currie 2013). However, the results of Larson and Currie (2013) could not distinguish teeth to lower taxonomic clades and were restricted to larger groups of closely related genera or families. Teeth and their morphology can also be related to functional purposes and associated niches (Henderson 1998, Torices et al. 2018). Feeding characteristics frequently converge due to functional relationships (Zanno and Makovicky 2011). Therefore, phylogenetic characters constructed on tooth morphology need to consider possible functional applications as well as phylogenetic characters of the tooth bearing element itself. While this study focuses on

the maxilla, many of the tooth characters pertain exclusively or in part to the maxillary teeth and deserve comment.

Character 81 separates taxa with tooth counts fewer than 20 or numbering at least 20. What this cut-off serves to do is unclear. Based on the taxa used it only serves to isolate unenlagiines without lumping them with troodontids. Troodontids show consistently higher tooth counts than dromaeosaurids other than unenlagiines. While the troodontids used in the study by Currie and Evans (2019) have more than 20 maxillary teeth, other derived taxa such as *Saurornithoides mongoliensis* Osborn, 1924, and *Zanabazar* (Norell et al., 2009) have less than 20 maxillary teeth and would share coding with most dromaeosaurids. A formal analysis on varying tooth counts should be formed prior to making such delineations but seems worth the effort to capture the variation among different subfamilies. This character is like character 89 that is coded for maxillary and dentary teeth large, or small and greater than 25 in number. This character is not only redundant with character 81, it is compounding tooth count with size without justification and comparing two non-comparable units. Character state 1 has no mention of tooth count and should not be compared as such. Large-small comparisons are also ambiguous and require context (Simões et al. 2016).

Character 82 describes the condition of large fang-like teeth posterior in the maxillary tooth row as opposed to subequal tooth sizes. This condition is largely relating to Microraptorinae Senter et al, 2004, which possess enlarged teeth anteroventral to the maxillary fenestra. While this is interesting for this clade it has been shown here that large “fang-like” teeth also exist in *Velociraptor* sp. (MPC-D 100/982). However, they are not as extreme as observed in microraptorines and are found in the anterior half of the maxillary tooth row and get smaller posteriorly. Characterization of fang-like teeth in dromaeosaurids requires more consideration to

the range in morphology observable and should be reworked with the range of variation in mind. It may be possible to expand this character into more states that include anteriorly enlarged teeth or alter it to explicitly distinguish microraptorines.

Character 87 and 88 (Currie and Evans 2019) characterize shapes and orientations of denticles respectively. Both characters mention an apical orientation of sorts; character 87 refers to a hook shape pointed towards the apex of the tooth crown while 88 describes a condition in which the denticles themselves are oriented towards the apex of the tooth crown. The apical hook shape is easy to observe in groups like troodontids (Zanno and Makovicky 2011, Larson and Currie 2013) and is well documented in a number of eudromaeosaurians (Currie and Varricchio 2004) whereas the orientation of the denticles to the carinae is less convincing. The condition of *Acheroraptor temertyorum* described in Evans et al. (2013) is suggestive of a slight apical hook shape rather than the denticle being oriented apically. These characters are difficult to distinguish in this case as they both address apical orientation of some kind. The wording of character 87 should reflect that it only pertains to the shape of the cutting edge of the denticle and not the whole body. It should also be made clear that this shape is separate from the orientation of the denticle relative to the main body of the tooth crown so as not to confuse these characters. Additionally, both characters, as well as characters 85 and 92, each have a state delineating the absence of denticles. This may be unavoidable with the dataset that describes multiple character states of the denticles, but it should be noted that doing this artificially weights the character state of absent denticles, which may lead to incorrect phylogenetic hypotheses.

Character 90 describes maxillary and dentary teeth either being subequal in number and size, or the dentary teeth being more numerous and smaller than maxillary teeth. This character serves to polarize the dromaeosaurids in having relatively small dentary teeth compared to

maxillary teeth and the dentary teeth being more numerous than those in the maxilla (Currie and Evans 2019). Problems with this character are in regard to its compound nature, referring to size and number of teeth treating them as unified (Simões et al. 2016). Sub-equal numbers of teeth mean that the dentary teeth could be greater or less in number than the maxillary teeth.

Therefore, conditions in which both criteria could be met is possible if the dentary teeth are slightly fewer in number than the maxillary teeth but of equal size. This redundancy enforces the need for this character to be reworded or split to characterize size and tooth number separately.

Tooth characters used in Currie and Evans (2019) are useful for polarizing the larger subclades such as families and subfamilies, however, the excessive use of characters of tooth morphologies may cause recovery of artificially monophyletic clades united by synapomorphies of tooth characteristics that are converged upon due to function.

2.5.6 Tooth replacement

Tooth replacement in eudromaeosaurian maxillae is best visualized in *Acheroraptor temertyorum*, where clear alternating patterns were observed. The replacement of teeth in the maxilla of MPC-D 100/982 follows a similar pattern to what is observed in *Acheroraptor temertyorum* (Fig. 2.18). However, during development the tooth roots grow dorsally from the interdental gaps to a much greater extent in *Velociraptor* sp. (MPC-D 100/982) than in *Acheroraptor temertyorum*. Based on this observation, extensive expansion of the tooth root during replacement may occur in other taxa where the rooting extends dorsal to the palatal shelf such as in *Shanag ashile* (Turner et al. 2007a). Alternating waves of tooth replacement are observed going posterior along the tooth row as described for lower vertebrates by Edmund (1960) and reflected by the tyrannosaur *Tarbosaurus bataar* (Hanai and Tsuihiji 2019). Unlike *Tarbosaurus bataar*, dromaeosaurids in this study do not have any third-generation replacement

teeth. This could be due to longevity of the functional teeth being greater in tyrannosaurids (Erickson 1996), which would allow for more time to develop new, overlapping generations of teeth. The lack of a third developing tooth in any of the tooth families observed for the eudromaeosaurians in this study could also be due to their maturity and replacement may have slowed to some degree during ontogeny. Alternatively, the relatively small sizes of dromaeosaurids may not have allowed space for the greater number of tooth generations observed in larger taxa. Although the replacement waves cannot be clearly observed in *Atrociraptor marshalli*, *Saurornitholestes langstoni* or *Tsaagan mangas*, replacement arrangement is consistent across a broad range of taxa with polyphyodonty and it is unlikely to vary much (Edmund 1960, Fong et al. 2016, LeBlanc et al. 2017, Chen et al. 2018, Hanai and Tsuihiji 2019). The patterns of replacement are here only reported on and an in-depth study examining the tooth ages and replacement rates in more detail could shed light on the more subtle intricacies of these patterns within Eudromaeosauria.

2.6 Conclusions

Post-mortem distortion was shown to have a major effect on our interpretations of maxillary features causing misinterpretations of morphology in two key taxa in understanding the evolution of Eudromaeosauria. CT data was instrumental in gaining more information to rectify ambiguity in morphological interpretations and relationships with other bones, as well as allowing detailed description and comparison of the previously partially described *Atrociraptor marshalli*. It was observed that *Atrociraptor marshalli*, once thought to be unique in its maxillary proportions among dromaeosaurids, shares a great deal in common with *Bambiraptor feinbergi*, and *Deinonychus antirrhopus*. All these animals have comparably stout maxillae regarding their dimensions and posteriorly angled teeth, providing evidence for functional drivers of these

convergent morphologies. *Acheroraptor temertyorum* was conversely found to possess a more elongate maxilla than previously described. However, the length of the anterior ramus, which has been paramount in its proposed relationship to Asian eudromaeosaurians was found to be less elongate after retro-deformation.

Ratio-based characters used in previous analyses of eudromaeosaurian phylogenetics have been treated as more informative for species level variation within the clade whereas characters pertaining to typological morphology were restricted to polarizing the in-group Eudromaeosauria from outgroups such as Microraptorinae, Troodontidae Gilmore, 1924, and Unenlagiinae Bonaparte, 1999. When these characters were assessed for their merit across the observable morphological variation within representatives of Eudromaeosauria, it was revealed that many characters pertaining to the maxilla, the crux of many species diagnoses within the group, were either problematic in wording, or did not capture the relationships of homologous structures within the group. Once these features were compared across the clade it was shown that despite elongation of the anterior ramus and maxilla of *Acheroraptor temertyorum*, it shares more characters with North American taxa of the Late Cretaceous. The complex type of maxillary fenestra – in which the fenestra is deeply embedded within a posterodorsally oriented maxillary fossa and has a pneumatic excavation posterodorsal the fenestra proper – is exclusive to *Acheroraptor temertyorum* and saurornitholestines. These Late Cretaceous, North American taxa share this feature (among others), which relates to maxillary nasal sutures and maxillary sinus features. Features suggesting a closer relationship between *Acheroraptor temertyorum* and Asian taxa are ratio-based characters. Ratio-based characters can be affected by ontogeny as in the case of *Bambiraptor feinbergi*, or ecomorphological change as a potential cause for the extreme variation between taxa like *Atrociraptor marshalli* and *Velociraptor* spp. Therefore,

they should not be weighed more heavily than consistent homologous structures to support potentially monophyletic clades. For greater taxonomic resolution in phylogenetic analysis, characterization of the variation of the in-group is important. Ratio-based characters in combination with non-informative characters for the in-group can tell a very specific story of evolution that, in this case is explained through homoplasy rather than homology. Improvements of maxillary characters presented in this study aim to improve the phylogenetic resolution within Eudromaeosauria and maximize our utilization of the limited material available for the group.

2.7 Literature Cited

- Arbour, V.M., and Currie, P.J. 2012. Analyzing taphonomic deformation of ankylosaur skulls using retrodeformation and finite element analysis. *PLoS ONE*, **7**: 1–13.
doi:10.1371/journal.pone.0039323.
- Baert, M., Burns, M.E., and Currie, P.J. 2014. Quantitative diagenetic analyses of *Edmontosaurus regalis* (Dinosauria: Hadrosauridae) postcranial elements from the Danek Bonebed, Upper Cretaceous Horseshoe Canyon Formation, Edmonton, Alberta, Canada: Implications for allometric studies of fossil. *Canadian Journal of Earth Sciences*, **51**: 1007–1016. doi:10.1139/cjes-2014-0060.
- Barsbold, R., and Osmólska, H. 1999. The skull of *Velociraptor* (Theropoda) from the Late Cretaceous of Mongolia. *Acta Palaeontologica Polonica*, **44**: 189–219.
- Bonaparte, J. 1999. Tetrapod faunas from South America and India: A palaeobiogeographic interpretation. *PINSA*, **65**: 427–437.
- Burnham, D.A., Derstler, K.L., Currie, P.J., Bakker, R.T., Zhou, Z., and Ostrom, J.H. 2000. Remarkable new birdlike dinosaur (Theropoda: Maniraptora) from the Upper Cretaceous of Montana. *The University of Kansas Paleontological Contributions*, **13**: 14.
- Brown, C.M., Evans, D.C., Campione, N.E., O'Brien, L.J., and Eberth, D.A. 2013. Evidence for taphonomic size bias in the Dinosaur Park Formation (Campanian, Alberta), a model Mesozoic terrestrial alluvial-paralic system. *Palaeogeography, Palaeoclimatology, Palaeoecology*, **372**: 108–122. Elsevier B.V. doi:10.1016/j.palaeo.2012.06.027.
- van Cakenberghe, V., Herrel, A., and Aguirre, L.F. 2002. Evolutionary relationships between cranial shape and diet in bats (Mammalia : Chiroptera). *In* *Topics in Functional and*

- Ecological Vertebrate Morphology. *Edited by* P. Aerts, K. D'Aour, A. Herrel, and R. Van Damme. Staker Publishing. pp. 205–236.
- Chen, J., Leblanc, A.R.H., Jin, L., Huang, T., and Reisz, R.R. 2018. Tooth development, histology, and enamel microstructure in *Changchunsaurus parvus*: Implications for dental evolution in ornithomimid dinosaurs. PLoS ONE, **13**: 1–18.
doi:10.1371/journal.pone.0205206.
- Currie, P., and Varricchio, D.J. 2004. A new dromaeosaurid from the Horseshoe Canyon Formation (Upper Cretaceous) of Alberta, Canada. *In* Feathered Dragons. *Edited by* P.J. Currie, E.B. Koppelhus, M.A. Shugar, and J.L. Wright. Indiana University Press, Bloomington and Indianapolis. pp. 112–132.
- Currie, P.J. 1985. Cranial anatomy of *Stenonychosaurus inequalis* (Saurischia, Theropoda) and its bearing on the origin of birds. Canadian Journal of Earth Sciences, **22**: 1643–1658.
doi:10.1139/e85-173.
- Currie, P.J. 1995. New information on the anatomy and relationships of *Dromaeosaurus albertensis* (Dinosauria: Theropoda). Journal of Vertebrate Paleontology, **15**: 576–591.
doi:10.1080/02724634.1995.10011250.
- Currie, P.J., and Evans, D.C. 2019. Cranial anatomy of new specimens of *Saurornitholestes langstoni* (Dinosauria, Theropoda, Dromaeosauridae) from the Dinosaur Park Formation (Campanian) of Alberta. The Anatomical Record, **04715**: 1–25. doi:10.1002/ar.24241.
- D'Amore, D.C. 2009. A functional explanation for denticulation in theropod dinosaur teeth. Anatomical Record, **292**: 1297–1314. doi:10.1002/ar.20977.

- Edmund, G. 1960. Tooth replacement phenomena in the lower vertebrates. Royal Ontario Museum, Life Sciences Division, Contributions, **52**: 1–190.
- Erickson, G.M. 1996. Incremental lines of von Ebner in dinosaurs and the assessment of tooth replacement rates using growth line counts. Proceedings of the National Academy of Sciences of the United States of America, **93**: 14623–14627. doi:10.1073/pnas.93.25.14623.
- Evans, D.C., Larson, D.W., and Currie, P.J. 2013. A new dromaeosaurid (Dinosauria: Theropoda) with Asian affinities from the latest Cretaceous of North America. Naturwissenschaften, **100**: 1041–1049. doi:10.1007/s00114-013-1107-5.
- Ferreira-Cardoso, S., Billet, G., Gaubert, P., Delsuc, F., and Hautier, L. 2019. Skull shape variation in extant pangolins (Pholidota: Manidae): Allometric patterns and systematic implications. Zoological Journal of the Linnean Society, : 255–275. doi:10.1093/zoolinnean/zlz096.
- Fong, R.K.M., LeBlanc, A.R.H., Berman, D.S., and Reisz, R.R. 2016. Dental histology of *Coelophysis bauri* and the evolution of tooth attachment tissues in early dinosaurs. Journal of morphology, **277**: 916–924. doi:10.1002/jmor.20545.
- Gauthier, J. 1986. Saurischian monophyly and the origin of birds. Memoirs of the California Academy of sciences, **8**: 55.
- Gilmore, C.W. 1924. On *Troodon validus*, an orthopodus dinosaur from the Belly River Cretaceous of Alberta, Canada. University of Alberta Bulletin, **1**: 43.
- Godefroit, P., Currie, P.J., Hong, L., Shang, C.Y., and Dong, Z.M. 2008. A new species of *Velociraptor* (Dinosauria: Dromaeosauridae) from the Upper Cretaceous of northern China.

- Journal of Vertebrate Paleontology, **28**: 432–438. doi:10.1671/0272-4634(2008)28[432:ANSOVD]2.0.CO;2.
- Hanai, T., and Tsuihiji, T. 2019. Description of tooth ontogeny and replacement patterns in a juvenile *Tarbosaurus bataar* (Dinosauria: Theropoda) using CT-scan data. *Anatomical Record*, **302**: 1210–1225. doi:10.1002/ar.24014.
- Henderson, D.M. 1998. Skull and tooth morphology as indicators of niche partitioning in sympatric Morrison Formation theropods. *Gaia*, **226**: 219–226.
- Hendrickx, C., and Mateus, O. 2014. *Torvosaurus gurneyi* n. sp., the largest terrestrial predator from Europe, and a proposed terminology of the maxilla anatomy in nonavian theropods. *PLoS ONE*, **9**. doi:10.1371/journal.pone.0088905.
- Holmes, R.B., Persons, W.S., Rupal, B.S., Qureshi, A.J., and Currie, P.J. 2020. Morphological variation and asymmetrical development in the skull of *Styracosaurus albertensis*. *Cretaceous Research*, **107**: 104308. Elsevier Ltd. doi:10.1016/j.cretres.2019.104308.
- Ibiricu, L.M., Martínez, R.D., Casal, G.A., and Cerda, I.A. 2013. The behavioral implications of a multi-individual bonebed of a small theropod dinosaur. *PLoS ONE*, **8**: 1–11.
- Larson, D.W., and Currie, P.J. 2013. Multivariate analyses of small theropod dinosaur teeth and implications for paleoecological turnover through time. *PLoS ONE*, **8**. doi:10.1371/journal.pone.0054329.
- LeBlanc, A.R.H., Brink, K.S., Cullen, T.M., Reisz, R.R., Leblanc, A.R.H., Brink, K.S., Cullen, T.M., and Reisz, R.R. 2017. Evolutionary implications of tooth attachment versus tooth implantation : A case study using dinosaur , crocodylian , and mammal teeth. *Journal of*

- Vertebrate Paleontology, **37**. doi:10.1080/02724634.2017.1354006.
- Longrich, N.R., and Currie, P.J. 2009. A microraptorine (Dinosauria-Dromaeosauridae) from the Late Cretaceous of North America. *Proceedings of the National Academy of Sciences of the United States of America*, **106**: 5002–5007. doi:10.1073/pnas.0811664106.
- Makovicky, P.J., Apesteguía, S., and Agnolín, F.L. 2005. The earliest dromaeosaurid theropod from South America. *Nature*, **437**: 1007–1011. doi:10.1038/nature03996.
- Matthew, W.D., and Brown, B. 1922. The family Deinodontidae, with notice of a new genus from the Cretaceous of Alberta. *Bulletin of the American Museum of Natural History*, **46**: 367–385.
- Meyer, H. von. 1861. *Archaeopteryx lithographica* (Vogel-Feder) und *Pterodactylus* von Solnhofen. *Neues Jahrbuch für Mineralogie, Geognosie, Geologie und Petrefakten-Kunde*, **1861**: 678–679.
- Norell, M.A., Clark, J.M., Turner, A.H., Makovicky, P.J., Barsbold, R., and Rowe, T. 2006. A new dromaeosaurid theropod from Ukhaa Tolgod (Ömnögov, Mongolia). *American Museum Novitates*, **3545**: 51. doi:10.1206/0003-0082(2006)3545[1:andtfu]2.0.co;2.
- Norell, M.A., Makovicky, P.J., Bever, G.S., Balanoff, A.M., Clark, J.M., Barsbold, R., and Rowe, T. 2009. A review of the Mongolian Cretaceous dinosaur *Saurornithoides* (Troodontidae: Theropoda). *American Museum Novitates*, **3654**: 1–63. doi:10.1206/648.1.
- Novas, F.E., Pol, D., Canale, J.I., Porfiri, J.D., and Calvo, J.O. 2009. A bizarre Cretaceous theropod dinosaur from Patagonia and the evolution of Gondwanan dromaeosaurids. *Proceedings of the Royal Society B: Biological Sciences*, **276**: 1101–1107.

doi:10.1098/rspb.2008.1554.

Osborn, H.F. 1924. Three new Theropoda, *Protoceratops* Zone, central Mongolia. American Museum Novitates,; 1–12.

Ostrom, J.H. 1969. Osteology of *Deinonychus antirrhopus*, an unusual theropod from the Lower Cretaceous of Montana. Peabody Museum of Natural History, **30**: 1–165.

Perle, A., Norell, M.A., and Clark, J.M. 1999. A new maniraptoran theropod - *Achillobator giganticus* (Dromaeosauridae)- from the Upper Cretaceous of Burkhan, Mongolia. National University of Mongolia,; 102.

Sankey, J.T. 2001. Late Campanian southern dinosaurs, Aguja Formation, Big Bend, Texas. Journal of Paleontology, **75**: 208–215. doi:10.1017/S0022336000031991.

Schott, R.K., and Evans, D.C. 2017. Cranial variation and systematics of *Foraminacephale brevis* gen. nov. and the diversity of pachycephalosaurid dinosaurs (Ornithischia: Cerapoda) in the Belly River Group of Alberta, Canada. Zoological Journal of the Linnean Society, **179**. doi:10.1111/zoj.12465.

Senter, P., Barsbold, R., Britt, B.B., and Burnham, D.A. 2004. Systematics and evolution of Dromaeosauridae (Dinosauria, Theropoda). Bulletin of Gunma Museum of Natural History, **8**: 1–20.

Senter, P., Kirkland, J.I., Bird, J., and Bartlett, J.A. 2010. A new troodontid theropod dinosaur from the lower cretaceous of Utah. PLoS ONE, **5**: 1–5. doi:10.1371/journal.pone.0014329.

Simões, T.R., Caldwell, M.W., Palci, A., and Nydam, R.L. 2016. Giant taxon-character matrices: Quality of character constructions remains critical regardless of size. Cladistics,; 1–22.

- Slater, G.J., Dumont, E.R., and Van Valkenburgh, B. 2009. Implications of predatory specialization for cranial form and function in canids. *Journal of Zoology*, **278**: 181–188. doi:10.1111/j.1469-7998.2009.00567.x.
- Sternberg, C.M. 1932. Two new theropod dinosaurs from the Belly River Formation of Alberta. *Canadian Field-Naturalist*, **46**: 99–105.
- Sues, H.-D. 1976. A new small theropod dinosaur from the Judith River Formation (Campanian) of Alberta. *Zoological Journal of the Linnean Society*, **62**: 381–400.
- Torices, A., Wilkinson, R., Arbour, V.M., Ruiz-Omeñaca, J.I., and Currie, P.J. 2018. Puncture-and-pull biomechanics in the teeth of predatory coelurosaurian dinosaurs. *Current Biology*, **28**: 1467-1474.e2. doi:10.1016/j.cub.2018.03.042.
- Turner, A.H., Hwang, S.H., and Norell, M.A. 2007a. A small derived theropod from Öösh, Early Cretaceous, Baykhangor Mongolia. *American Museum Novitates*, **3557**: 27. doi:10.1206/0003-0082(2007)3557[1:asdtfs]2.0.co;2.
- Turner, A.H., Makovicky, P.J., and Norell, M.A. 2012. A review of dromaeosaurid systematics and paravian phylogeny. *Bulletin of the American Museum of Natural History*, **371**: 1–206. doi:10.1206/748.1.
- Whitlock, J.A. 2011. Inferences of diplodocoid (Sauropoda: Dinosauria) feeding behavior from snout shape and microwear analyses. *PLoS ONE*, **6**. doi:10.1371/journal.pone.0018304.
- Witmer, L.M. 1997. The evolution of the antorbital cavity of archosaurs: A study in soft-tissue reconstruction in the fossil record with an analysis of the function of Pneumaticity. *Journal of Vertebrate Paleontology*, **17**: 1–76. doi:10.1080/02724634.1997.10011027.

- Witmer, L.M., and Ridgely, R.C. 2008. The paranasal air sinuses of predatory and armored dinosaurs (Archosauria: Theropoda and Ankylosauria) and their contribution to cephalic structure. *Anatomical Record*, **291**: 1362–1388. doi:10.1002/ar.20794.
- Xu, X., Choiniere, J.N., Pittman, M., Tan, Q., Xiao, D., Li, Z., Tan, L., Clark, J.M., Norell, M.A., Hone, D.W.E., and Sullivan, C. 2010a. A new dromaeosaurid (Dinosauria: Theropoda) from the Upper Cretaceous Wulansuhai Formation of Inner Mongolia, China. *Zootaxa*, **9**: 1–9.
- Xu, X., Norell, M.A., Wang, X.L., Makovicky, P.J., and Wu, X.C. 2002. A basal troodontid from the Early Cretaceous of China. *Nature*, **415**: 780–784. doi:10.1038/415780a.
- Xu, X., Pittman, M., Sullivan, C., Choiniere, J.N., Tan, Q.-W., Clark, J.M., Norell, M. a., and Wang, S. 2015. The taxonomic status of the Late Cretaceous dromaeosaurid *Linheraptor exquisitus* and its implications for dromaeosaurid systematics. *Vertebrata Palasiatica*, **53**: 29–62.
- Zanno, L.E., and Makovicky, P.J. 2011. Herbivorous ecomorphology and specialization patterns in theropod dinosaur evolution. *Proceedings of the National Academy of Sciences of the United States of America*, **108**: 232–237. doi:10.1073/pnas.1011924108.

2.8 Tables and Figures

Table 2.1. Maxillary ratios, proportions, posterodorsal inclination, and tooth counts of eudromaeosaurian dromaeosaurids.

Taxon	Specimen	Maxilla L/H ratio	Anterior Ramus L/H Ratio	Anterior ramus/Maxilla Length	Angle Ascending ramus/maxillary tooth row	Maxillary tooth count
<i>Acheroraptor temertyorum</i>	ROM 63777	2.18*	1.22	0.34*	34.5°	9+
	Post retro-deformation	2.36*	1.09	0.31*	32.0°	
<i>Achillobator giganticus</i>	MNUFR 15	2.22	0.87	0.29	44.7°	11
<i>Atrociraptor marshalli</i>	TMP 1995.166.0001	1.70	0.75	0.32	49.3°	11
<i>Bambiraptor feinbergi</i>	AMNH FARB 30556	2.02	0.70	0.23	42.9°	12
<i>Deinonychus antirrhopus</i>	MOR 553S – 7.30.91.274	1.76	0.60	0.22	37.9°	11
	YPM 5232 (557) – This study	1.70	0.68	0.22	37.8°	13
	Based on interpretation by Ostrom 1969	1.93	1.13	0.32	29.7°	15
<i>Linheraptor exquisitus</i>	IVPP V16923	2.42	1.51	0.46	30.3°	11
<i>Saurornitholestes langstoni</i>	TMP 1994.012.0844	1.87	0.91	0.31	34.6°	12
	UALVP 55700	2.01	0.81	0.28	31.3°	12
<i>Tsaagan mangas</i>	MPC-D 100/1015	2.70	1.30	0.38	30.6°	12
<i>Velociraptor</i> sp.	MPC-D 100/982	3.44	1.40	0.27	20.2°	12
<i>Velociraptor mongoliensis</i>	AMNH FARB 6515	3.08	1.75	0.31	22.6°	10

	MPC-D 100/25	2.81	1.40	0.33	28.9°	11
	MPC-D 100/54	2.98	1.42	0.33	25.7°	11
<i>Velociraptor osmolskae</i>	IMM99NM- BYM-3/3A	3.08*	1.41	0.31*	26.8°	10+

Measurements were taken using calipers or ImageJ. All angles were taken with ImageJ, and tooth counts were either observed in person or taken from Currie and Evans (2019). The distal ascending ramus is missing for *Achillobator* and *Bambiraptor* specimens, and the angle for these specimens may be a slight underestimate. An Asterix (*) beside a ratio indicates it was made using an estimated measurement.



Figure 2.1. Angle of ascending ramus. The angle of the ascending ramus is measured between a straight line across the maxillary tooth margin to the anteroventral point of the maxilla and another straight line to the most posterodorsal extent of the ascending ramus. TMP 1994.012.0844 is used as reference. Scale bar = 5 cm.

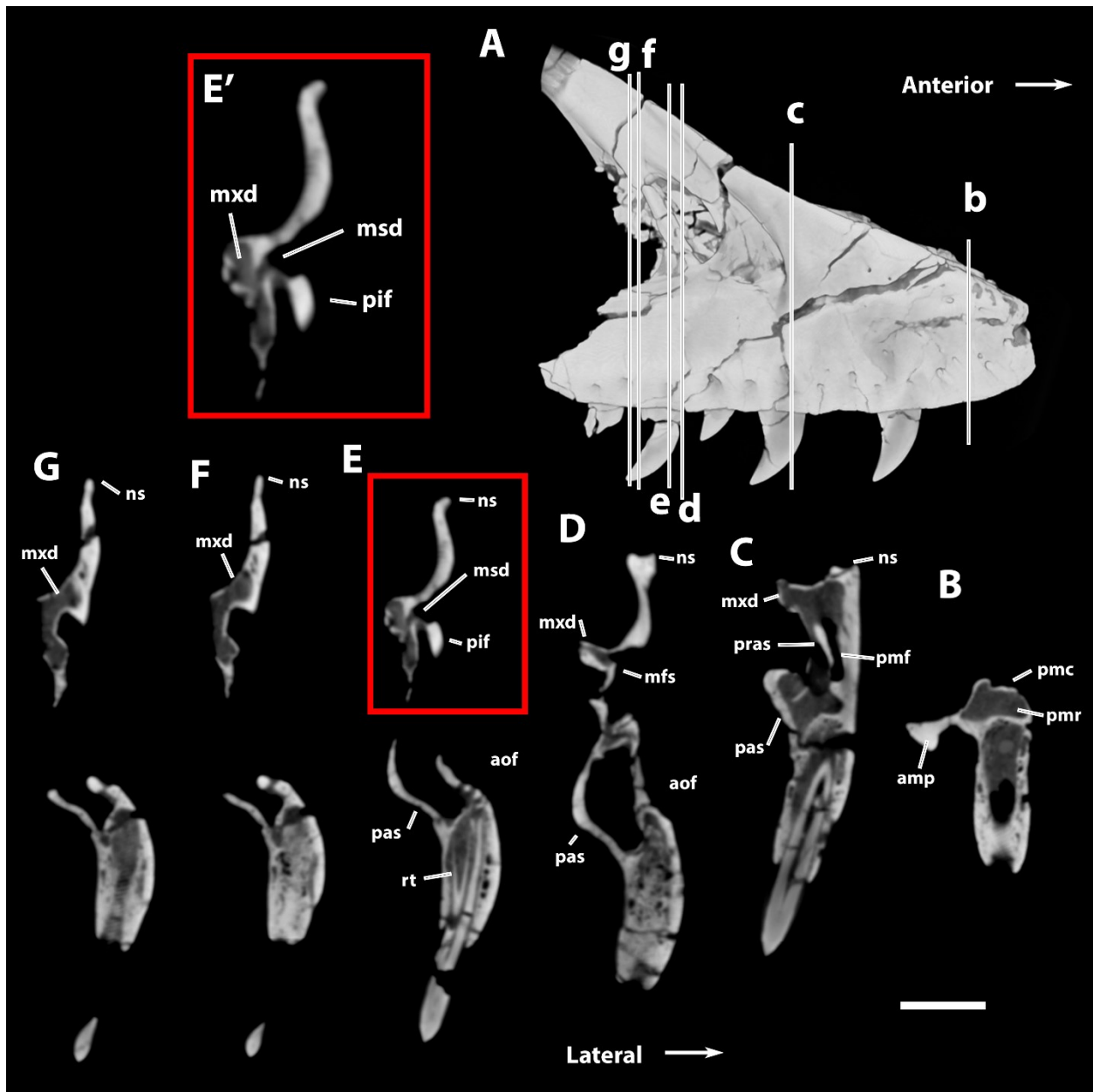


Figure 2.2. Maxillary fenestra and sinus system of *Acheroraptor temertyorum*. A) 3D rendered dataset of ROM 63777 in lateral view. B) coronal section of anterior ramus; C) coronal section at junction between anterior ramus and antorbital fossa; D) coronal section through maxillary fenestra; E) coronal section through pneumatic recess of maxillary fenestra structure, E' is a close up of the maxillary diverticulum; F and G) coronal sections through ascending ramus showing posterodorsal continuation of the maxillary diverticulum. Scale bar = 1 cm and is

for the serial sections only. 3D rendering and zoomed image (E') are not to scale. Lower case letters indicate the area of the slice corresponding to the coronal section. Abbreviations: **amp**, anteromedial process; **aof**, antorbital fossa; **mfo**, maxillary fossa; **mfs**, maxillary fenestra strut; **msd**, maxillary sub-diverticulum; **mxd**, maxillary diverticulum; **ns**, nasal suture; **pas**, palatal shelf; **pif**, pila interfenestralis; **pmc**, premaxilla contact; **pmf**, promaxillary fenestra; **pmr**, promaxillary recess; **pne**, pneumatic excavation; **pras**, preantral strut; **rt**, replacement tooth.

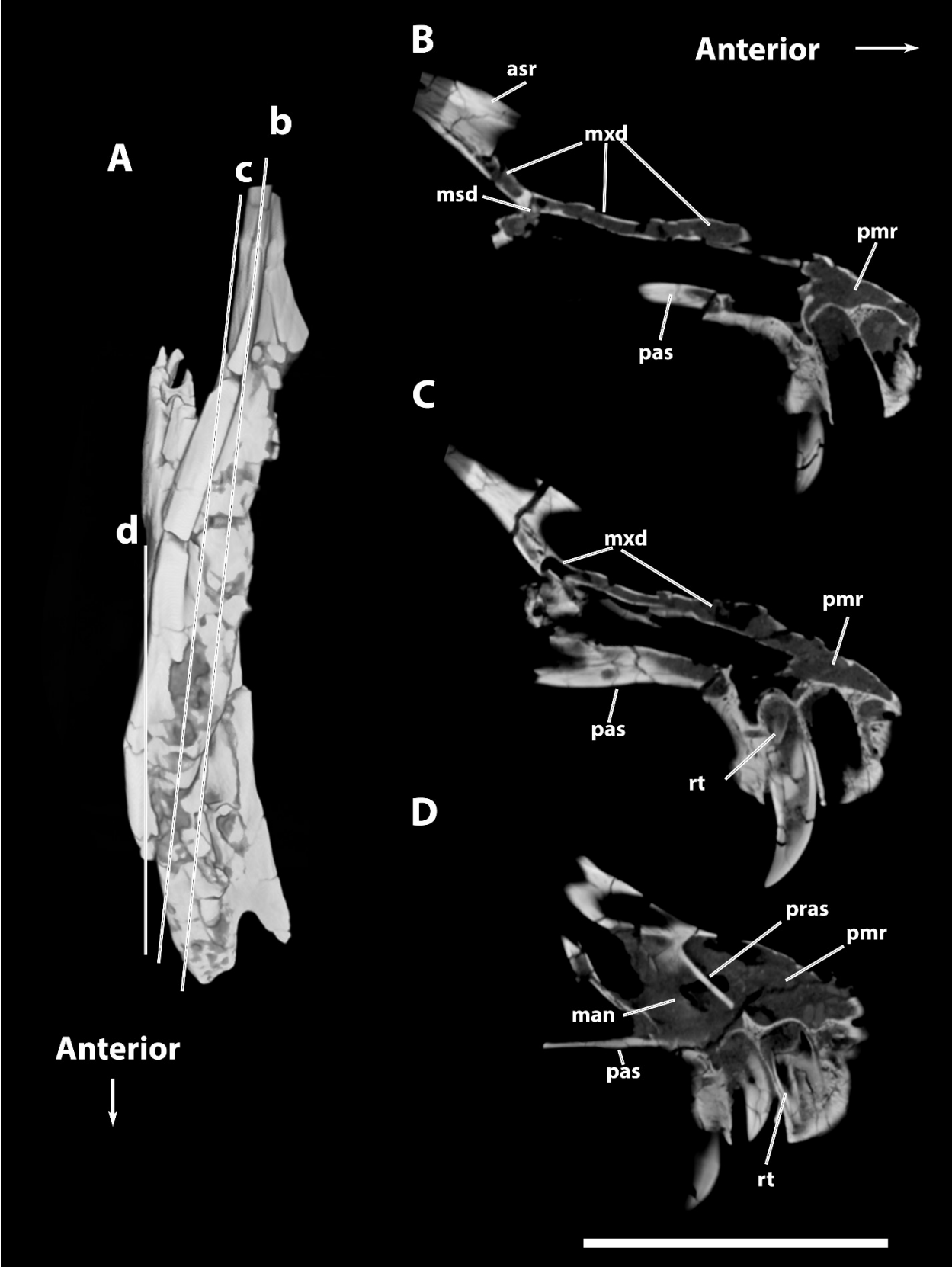


Figure 2.3. Parasagittal sections of ROM 63777 showing internal maxilla structures. A) dorsal view of 3D rendered data file of ROM 63777; B) parasagittal section of maxillary diverticulum extending through the upper maxillary fenestra; C) parasagittal section of maxillary diverticulum opening into promaxillary recess; D) parasagittal section of the preantral strut, maxillary antrum, and promaxillary recess. Lower case letters correspond to upper case letter parasagittal sections. Scale bar = 5 cm for parasagittal sections. 3D rendered ROM 63777 is not to scale. Abbreviations: **asr**, ascending ramus; **man**, maxillary antrum; **msd**, maxillary sub-diverticulum; **mxd**, maxillary diverticulum; **pas**, palatal shelf; **pmr**, promaxillary recess; **pras**, preantral strut; **rt**, replacement tooth.

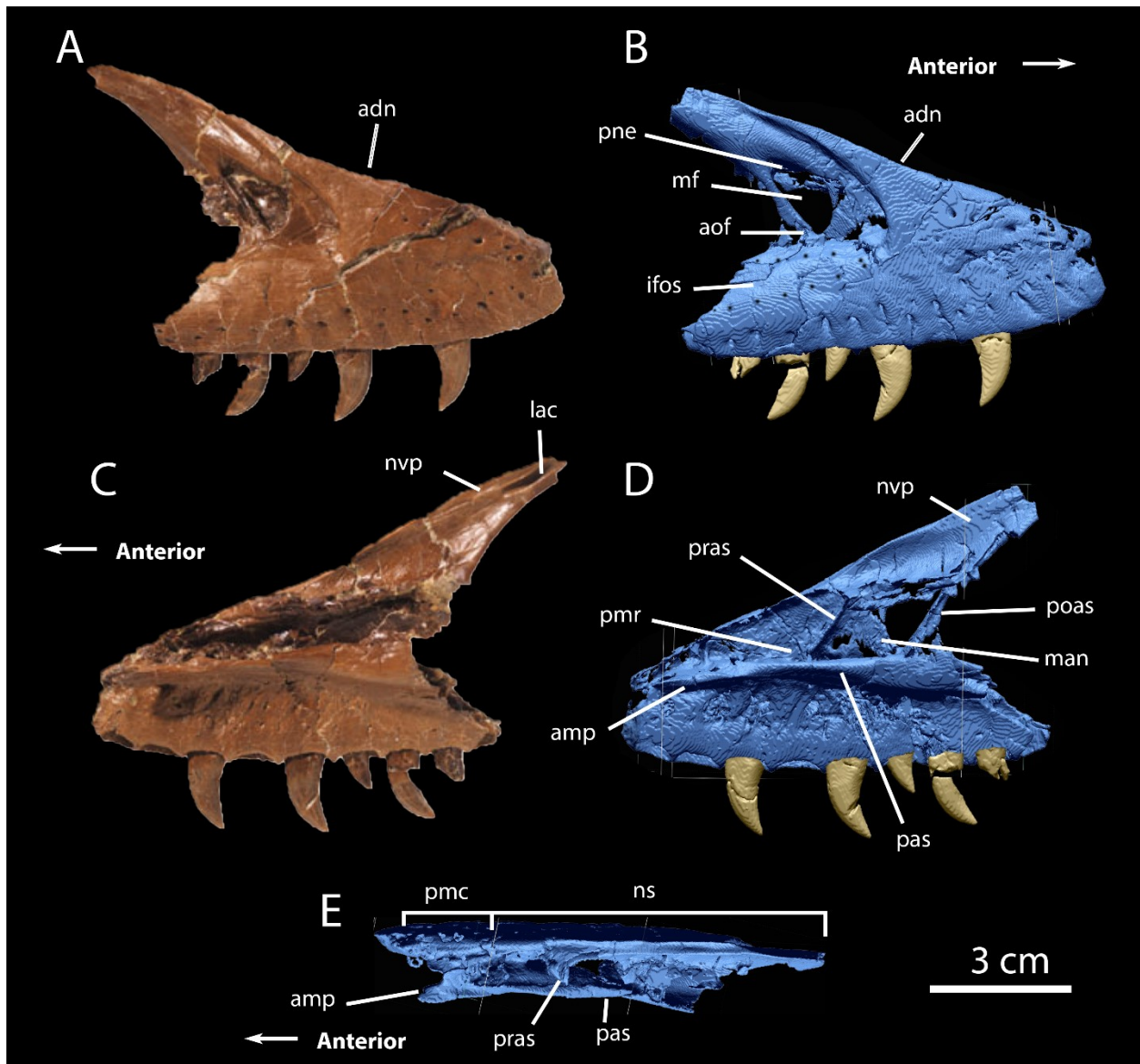


Figure 2.4. Retro-deformed right maxilla of *Acheroraptor temertyorum*. ROM 63777 in lateral (A) and medial view (C) adapted from Evans et al. (2013) Fig. 1, compared to the retro-deformed specimen in lateral (B), medial (D), and dorsal view (E). The crushed medial wall was not rendered in B, D, and E to observe the anatomical details of the maxillary sinus system. Abbreviations: **adh, anterodorsal notch; **amp**, anteromedial process; **aof**, antorbital fossa; **ifos**, inferior antorbital fossa slope; **lac**, sutural facet for the lacrimal contact; **man**, maxillary antrum; **ns**, sutural surface for nasal; **nvp**, facet for ventrolateral process of the nasal; **pas**, palatal shelf;**

pmc, sutural surface for the maxillary process of the premaxilla; **pmr**, promaxillary recess; **pne**, pneumatic excavation; **poas**, postantral strut; **pras**, preantral strut.

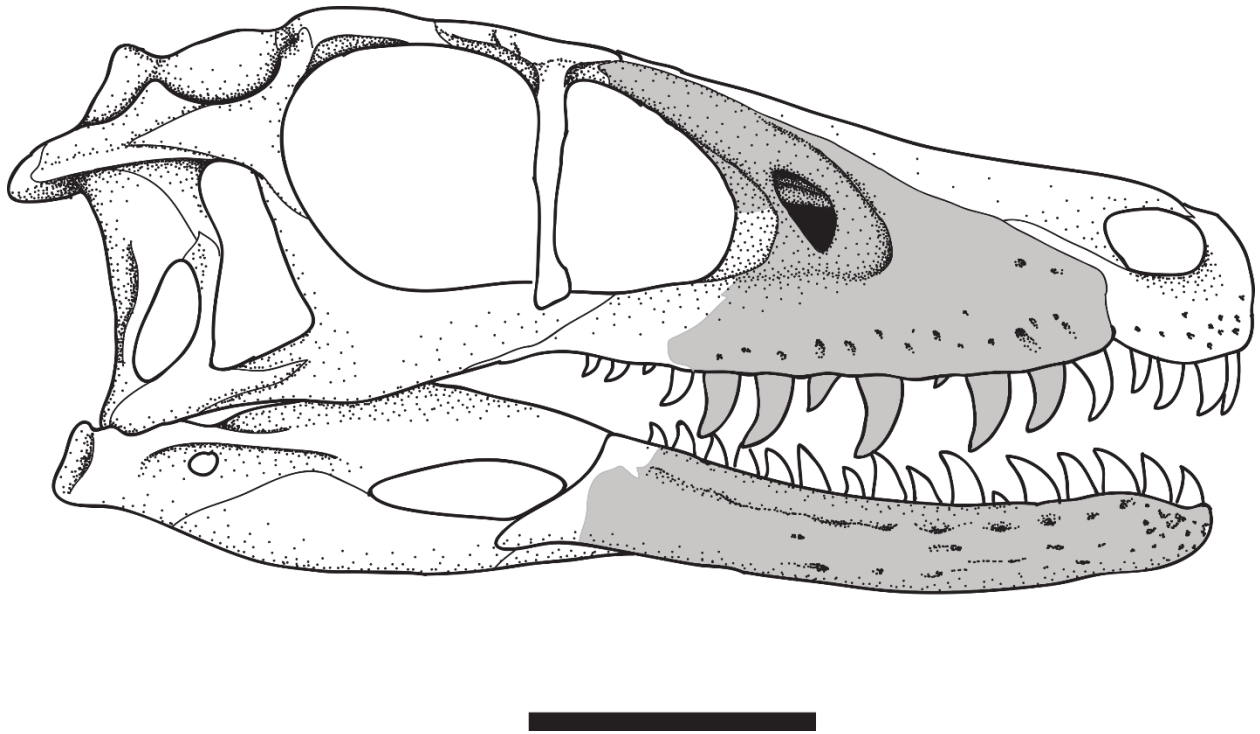


Figure 2.5. Skull reconstruction of *Acheroraptor temertyorum*. The skull was reconstructed using the reconstructed maxilla of ROM 63777. The greyed areas were illustrated using the reconstructed maxilla and the associated dentary, ROM 63778. Areas that are not greyed in were reconstructed using the reconstruction of Evans et al., 2013 but modified to reflect possible close relationship with North American dromaeosaurids. Scale bar = 5 cm.

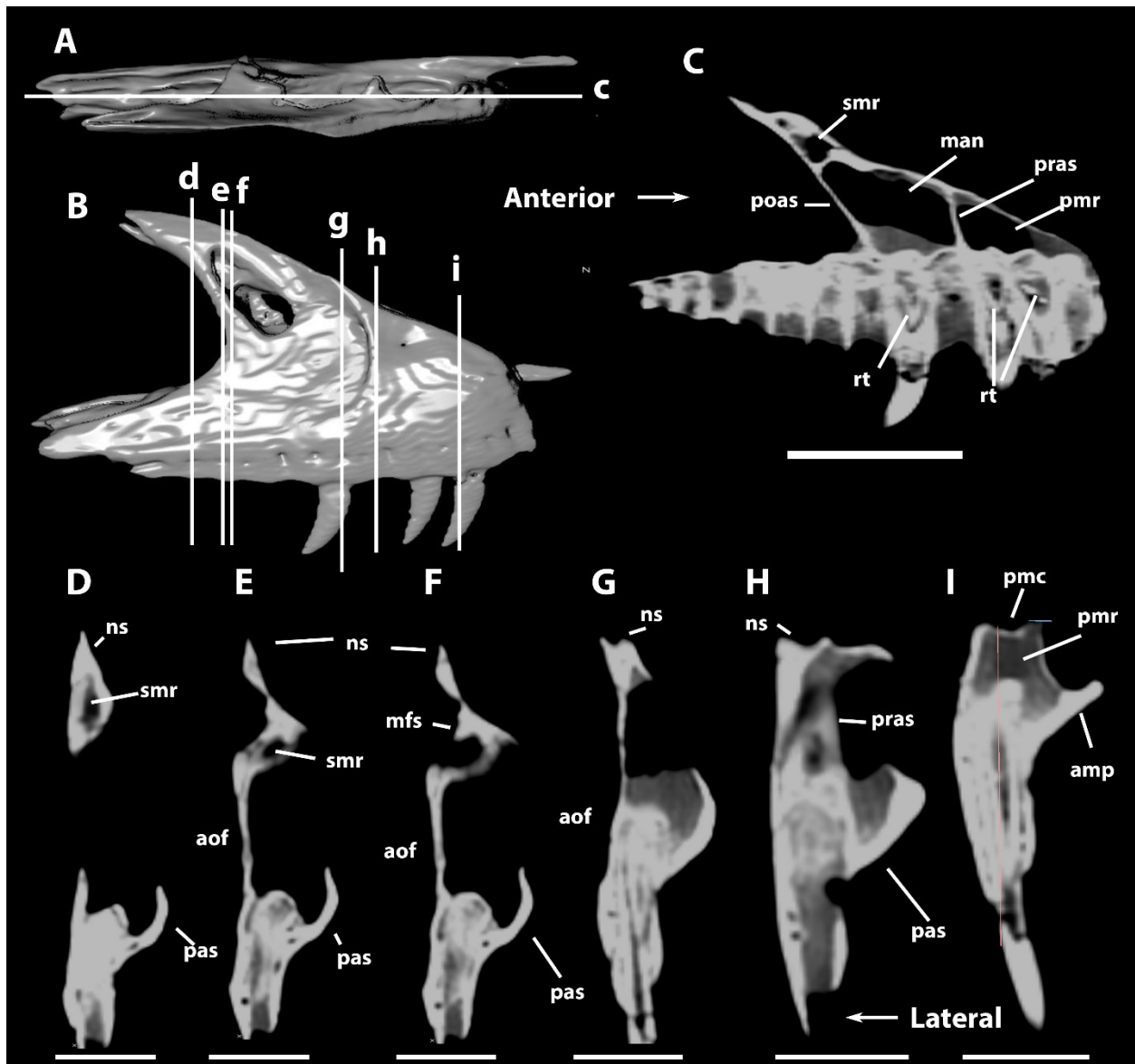


Figure 2.6. Coronal and parasagittal sections of TMP 1994.012.0844, *Saurornitholestes langstoni* CT data. A and B) dorsal and right lateral views of 3D mesh generated from CT data for TMP 1994.012.0844. C) parasagittal section through the maxillary sinus system; D-I) series of coronal sections through TMP 1994.012.0844 from posterior to anterior, lower case letters indicate the section that corresponds to the coronal section with the matching uppercase letter. Scale bars for coronal sections = 1 cm, scale bar for parasagittal section and 3D renderings = 3 cm. Abbreviations: **amp**, anteromedial process; **aof**, antorbital fossa; **man**, maxillary antrum;

mfs, maxillary fenestra strut; **ns**, nasal suture; **pas**, palatal shelf; **pmc**, premaxilla contact surface; **pmf**, promaxillary fenestra; **pmr**, promaxillary recess; **pne**, pneumatic excavation; **poas**, postantral strut; **pras**, preantral strut; **prb**, preantorbital bar; **rt**, replacement tooth; **smr**, supramaxillary recess.

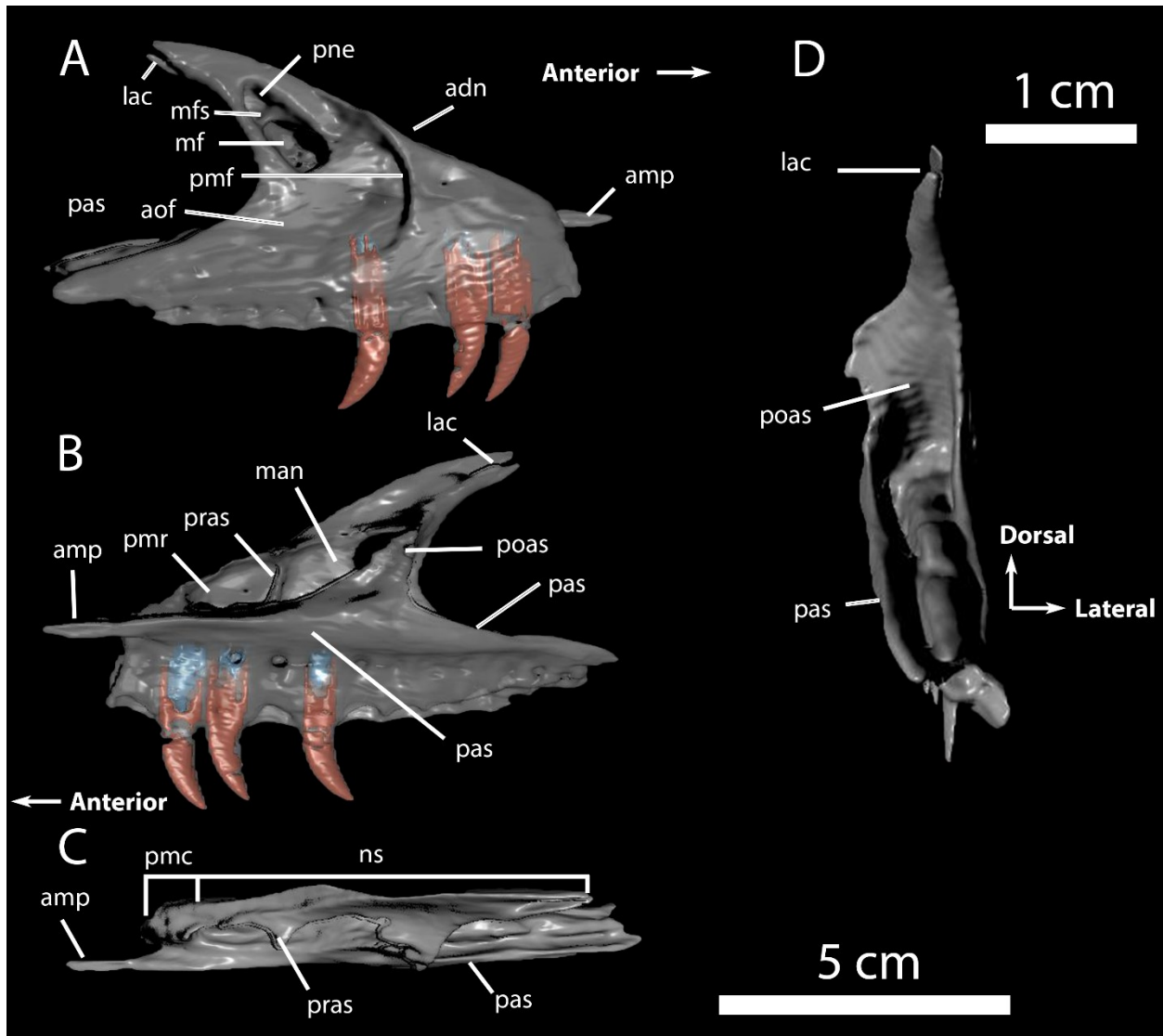


Figure 2.7. 3D rendering of *Saurornitholestes langstoni* (TMP 1994.012.0844) and maxillary teeth. A) lateral view, B) medial view, C) dorsal view, D) posterior view. The maxilla is slightly transparent to observe the maxillary teeth (red) and the replacement teeth (blue) sharing those alveoli. 5 cm scale bar for A-C, 1 cm scale bar for D. Abbreviations: **adn**, anterodorsal notch; **amp**, anteromedial process; **aof**, antorbital fossa; **lac**, facet for the lacrimal contact; **man**, maxillary antrum; **mf**, maxillary fenestra; **mfs**, maxillary fenestral strut; **ns**, sutural surface for nasal; **pas**, palatal shelf; **pmc**, contact surface for the maxillary process of the premaxilla; **pmf**,

promaxillary fenestra; **pmr**, promaxillary recess; **pne**, pneumatic excavation; **poas**, postantral strut; **pras**, preantral strut.

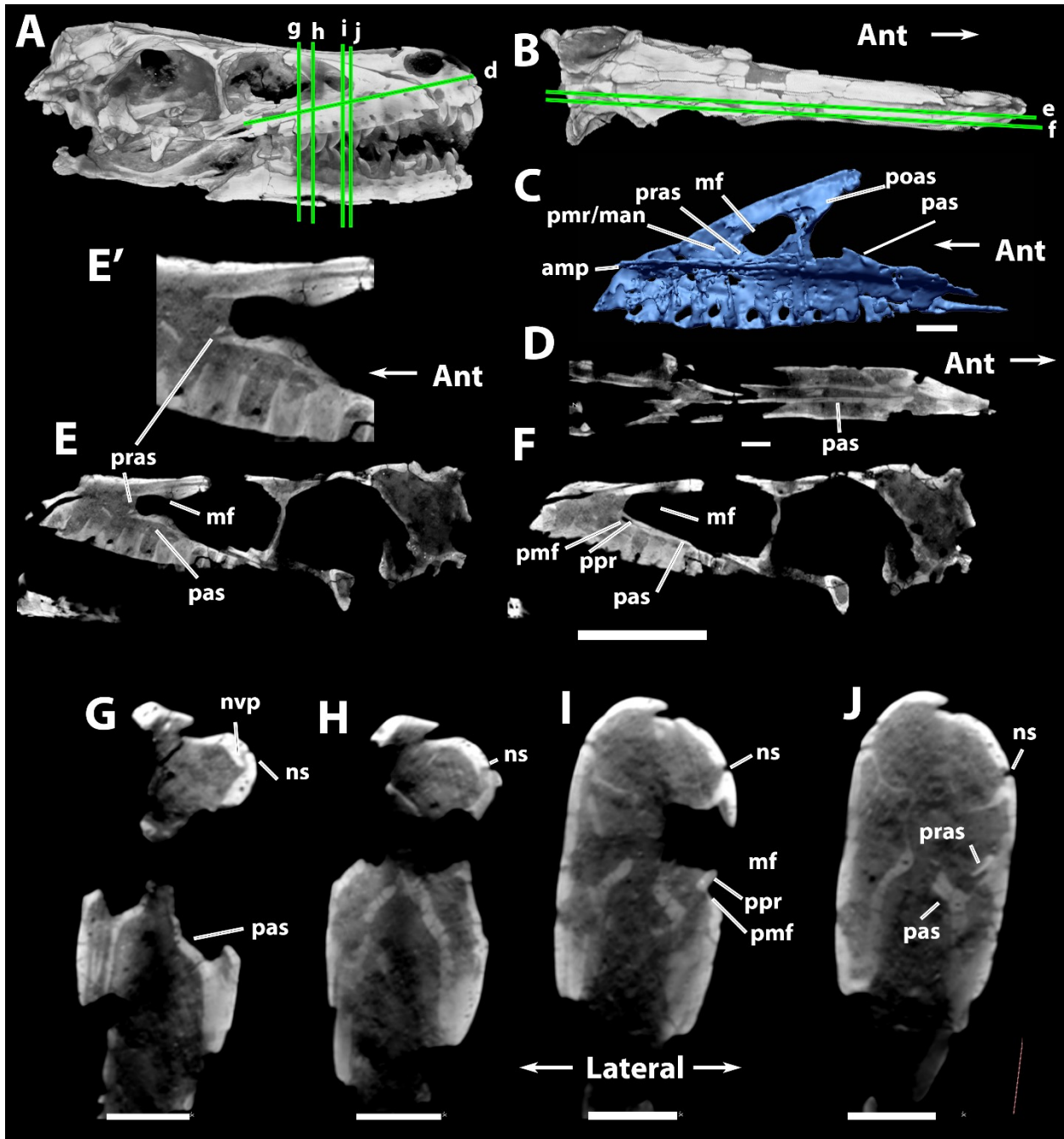


Figure 2.8. CT data of *Tsaagan mangas* maxilla with 3D rendering of the right maxilla. A) rendered CT data in lateral and (B) dorsal view. C) a mesh of the right maxilla in medial view (scale bar = 1 cm); D) transverse section of the palatal shelf (scale bar = 1 cm); E and F) parasagittal sections of the pila promaxillaris and preantral strut, E' is a close up of the preantral strut; G-J) coronal sections across the maxilla, lowercase letters by lines through the skull

correspond to the respective section. Scale bars for G-J = 1 cm, scale bar for A, B, E and F is 5 cm. Abbreviations: **amp**, anteromedial process; **Ant**, Anterior; **man**, maxillary antrum; **mf**, maxillary fenestra; **ns**, nasal suture; **nvp**, nasal ventral process; **pas**, palatal shelf; **pmf**, promaxillary fenestra; **pmr**, promaxillary recess; **poas**, postantral strut; **ppr**, pila promaxilaris; **pras**, preantral strut.

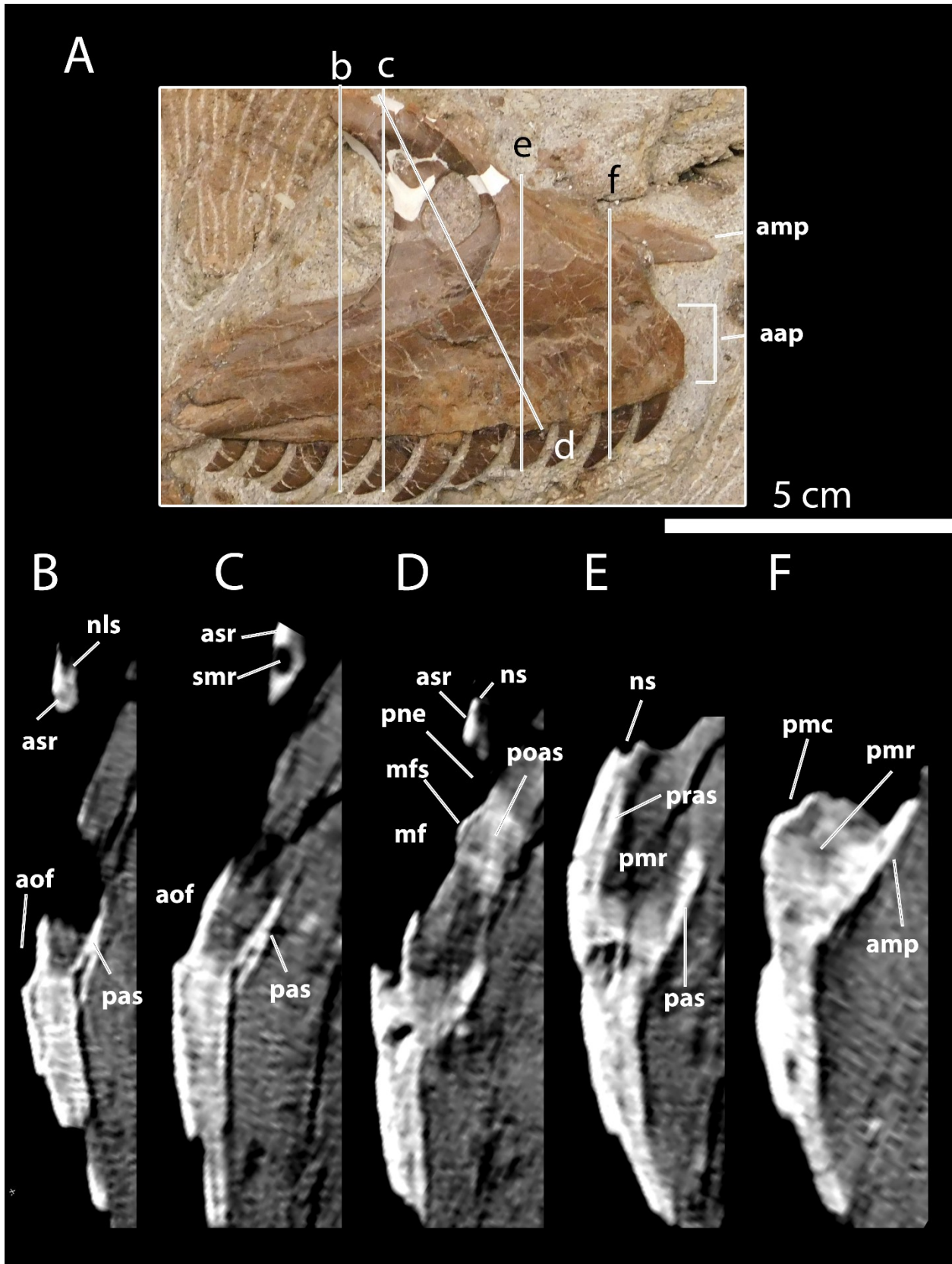


Figure 2.9. Right lateral view of the holotype of *Atrociraptor marshalli* with coronal CT sections. A) right lateral view of TMP 1995.166.0001 completely prepared; B-F) coronal sections moving posteriorly through the maxilla. Lowercase letters by straight lines over the maxilla indicate the location of the coronal sections. Sections are not to scale, however, the extent displayed is proportionate to the lines through the maxilla in A. Abbreviations: **aap**, accessory anterior process; **amp**, anteromedial process; **aof**, antorbital fossa; **asr**, ascending ramus; **mf**, maxillary fenestra; **mfs**, maxillary fenestra strut; **nls**, nasolacrimal suture; **ns**, nasal suture surface; **pas**, palatal shelf; **pmc**, premaxillary contact surface; **pmf**, promaxillary fenestra; **pmr**, promaxillary recess; **pne**, pneumatic excavation; **poas**, postantral strut; **pras**, preantral strut; **smr**, supramaxillary recess.

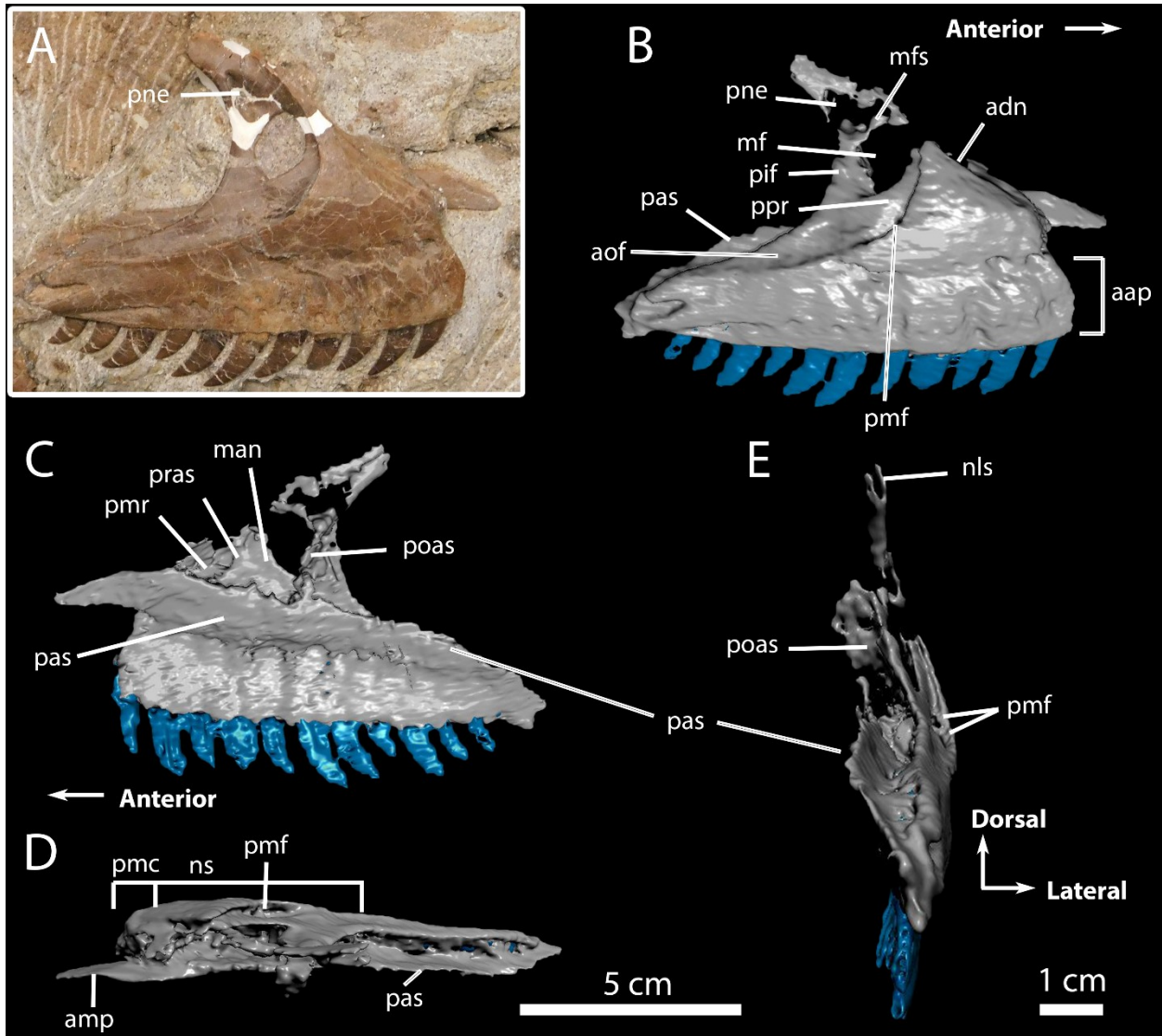


Figure 2.10. 3D rendering of the maxilla of *Atrociraptor marshalli*. A) photograph of TMP 1995.166.0001 in right lateral view; B-E) 3D mesh of TMP 1995.166.0001 in (B) lateral, (C) medial, (D) dorsal view, and (E) posterior view. Abbreviations: **aap**, accessory anterior process; **amp**, anteromedial process; **aof**, antorbital fossa; **asr**, ascending ramus; **man**, maxillary antrum; **mf**, maxillary fenestra; **mfs**, maxillary fenestra strut; **nls**, nasolacrimal suture; **ns**, nasal suture surface; **pas**, palatal shelf; **pmc**, premaxillary contact surface; **pmf**, promaxillary fenestra; **pmr**, promaxillary recess; **pne**, pneumatic excavation; **poas**, postantral strut; **pras**, preantral strut; **smr**, supramaxillary recess.

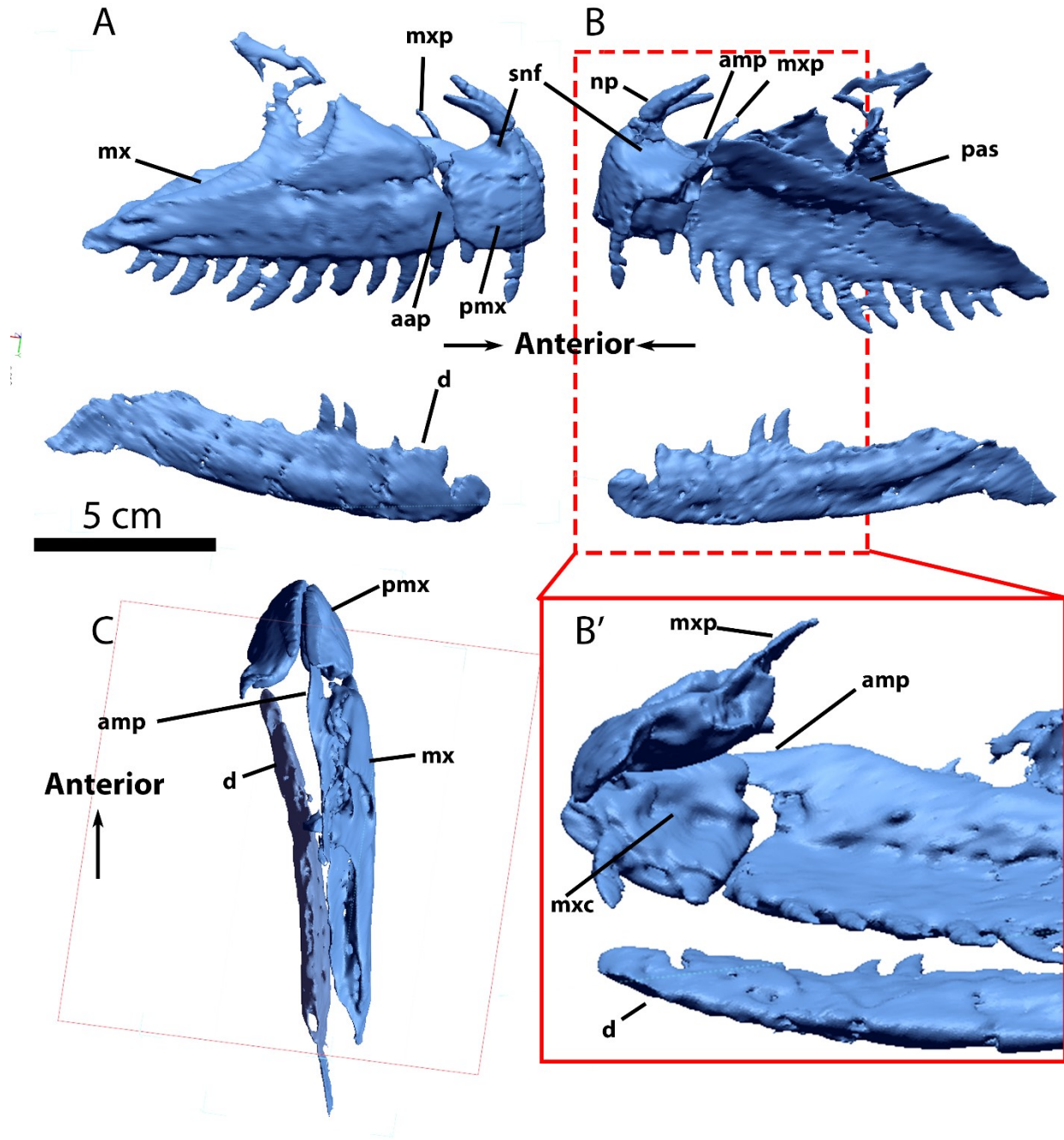


Figure 2.11. Articulated 3D models of TMP 1995.166.0001. A) right lateral view of 3D meshes of the holotype material for *Atrociraptor marshalli* placed in anatomical position; B) medial view, B' is this section rotated laterally to expose the ventral surface at an oblique angle and zoomed in. No scale bar; C) dorsal view. Abbreviations: **aap**, accessory anterior process; **amp**, anteromedial process; **amc**, contact surface for the anteromedial process; **d**, dentary; **mx**,

maxilla; **mxp**, maxillary process of the premaxilla; **np**, nasal process of the premaxilla; **pas**, palatal shelf; **pmx**, premaxilla; **snf**, subnarial fossa.

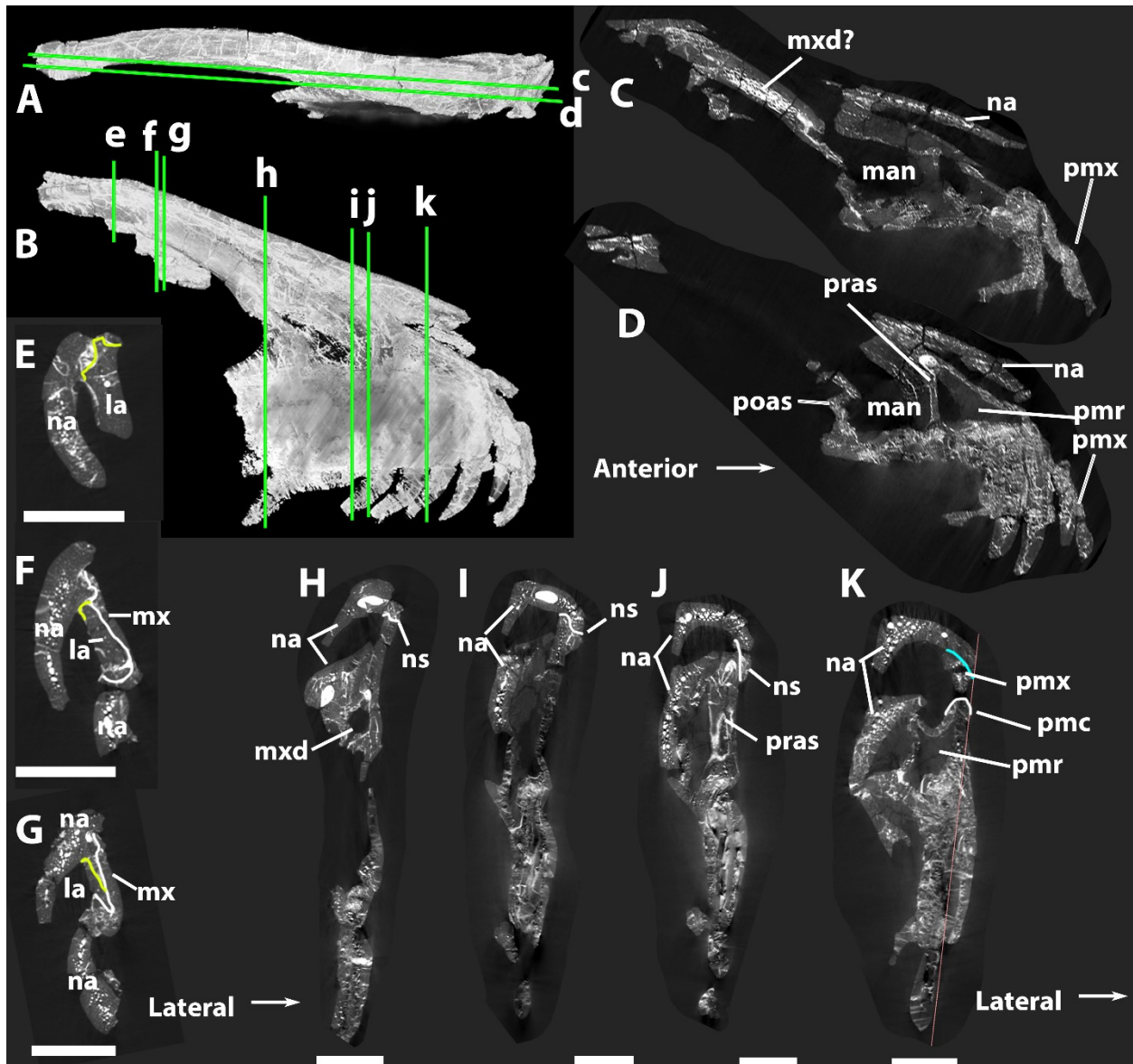


Figure 2.12. CT data of YPM 5232 (557) *Deinonychus antirrhopus*. A) dorsal and (B) right lateral view of rendered data for YPM 5232 (557); C and D) parasagittal sections of the specimen examining the pneumatic systems; E-G) nasolacrimal contacts with maxilla and transition from maxillonasal contact to nasolacrimal contact; H-K) coronal sections moving from posterior to anterior, lowercase letters next to green lines correspond to the respective section. White lines are used to outline the sutures with the maxilla, yellow for nasal and lacrimal, and blue for nasal and premaxilla. Scale bars=1 cm, A-D have no scale bar but are scaled to each

other. Abbreviations: **la**, lacrimal; **man**, maxillary antrum; **mf**, maxillary fenestra; **mx**, maxilla; **mxd**, maxillary diverticulum; **na**, nasal; **ns**, nasal suture; **pas**, palatal shelf; **pmc**, premaxilla contact surface; **pmr**, promaxillary recess; **pmx**, premaxilla; **poas**, postantral strut; **pras**, preantral strut.

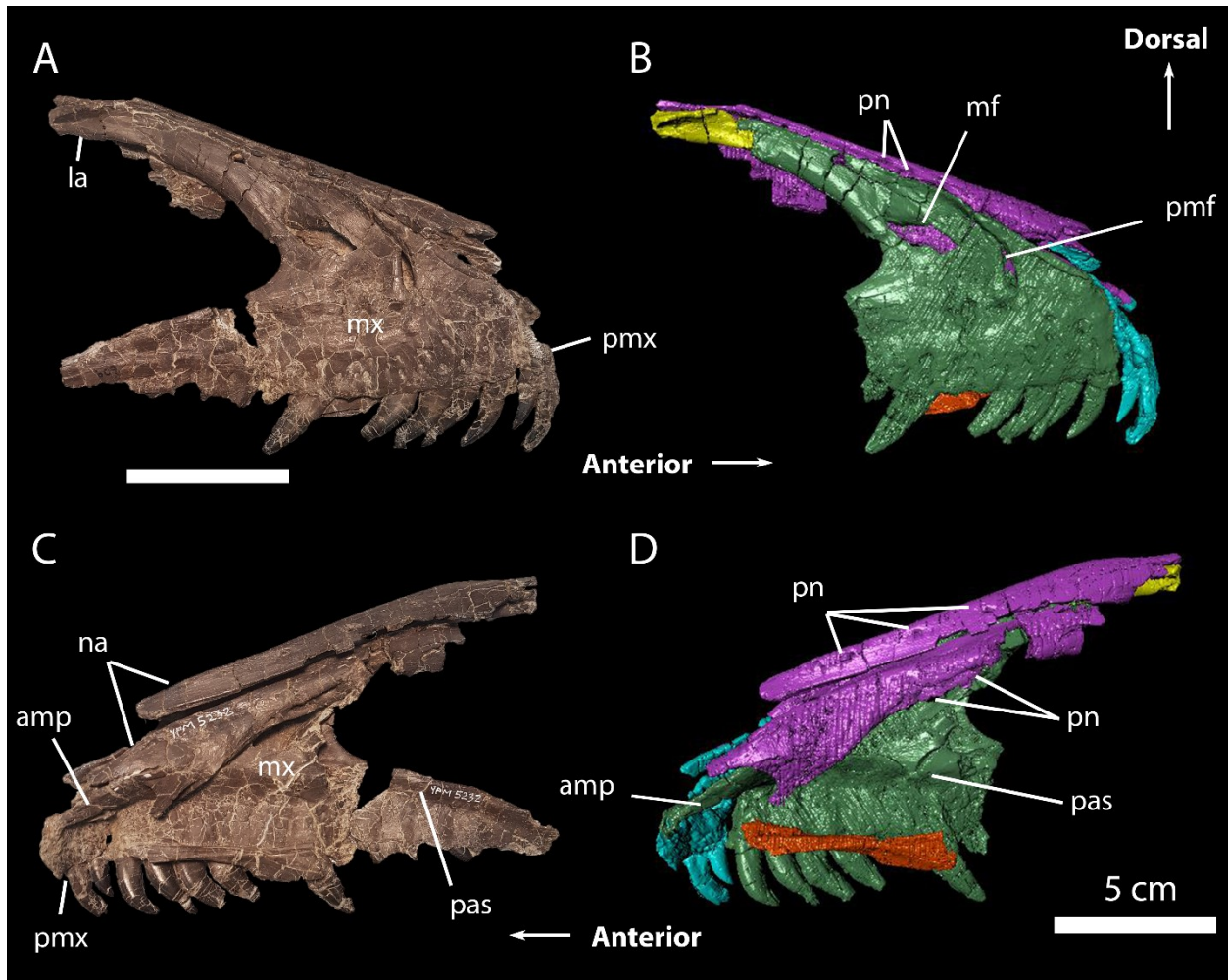


Figure 2.13. Segmentation of the maxilla of *Deinonychus antirrhopus* (YPM 5232 [557]).

YPM 5232 (557) figured in lateral view (A) and medial view (C) compared to the same specimen with all bones segmented (B and D). Segmentation: **premaxilla**, blue; **maxilla**, green; **nasals**, purple; **lacrimal**, yellow; **vomers**, orange. Abbreviations: **amp**, anteromedial process; **la**, lacrimal; **mf**, maxillary fenestra; **mx**, maxilla; **na**, nasal; **pas**, palatal shelf; **pmf**, promaxillary fenestra; **pmx**, premaxilla; **pn**, pneumatopore. Both scale bars = 5 cm.

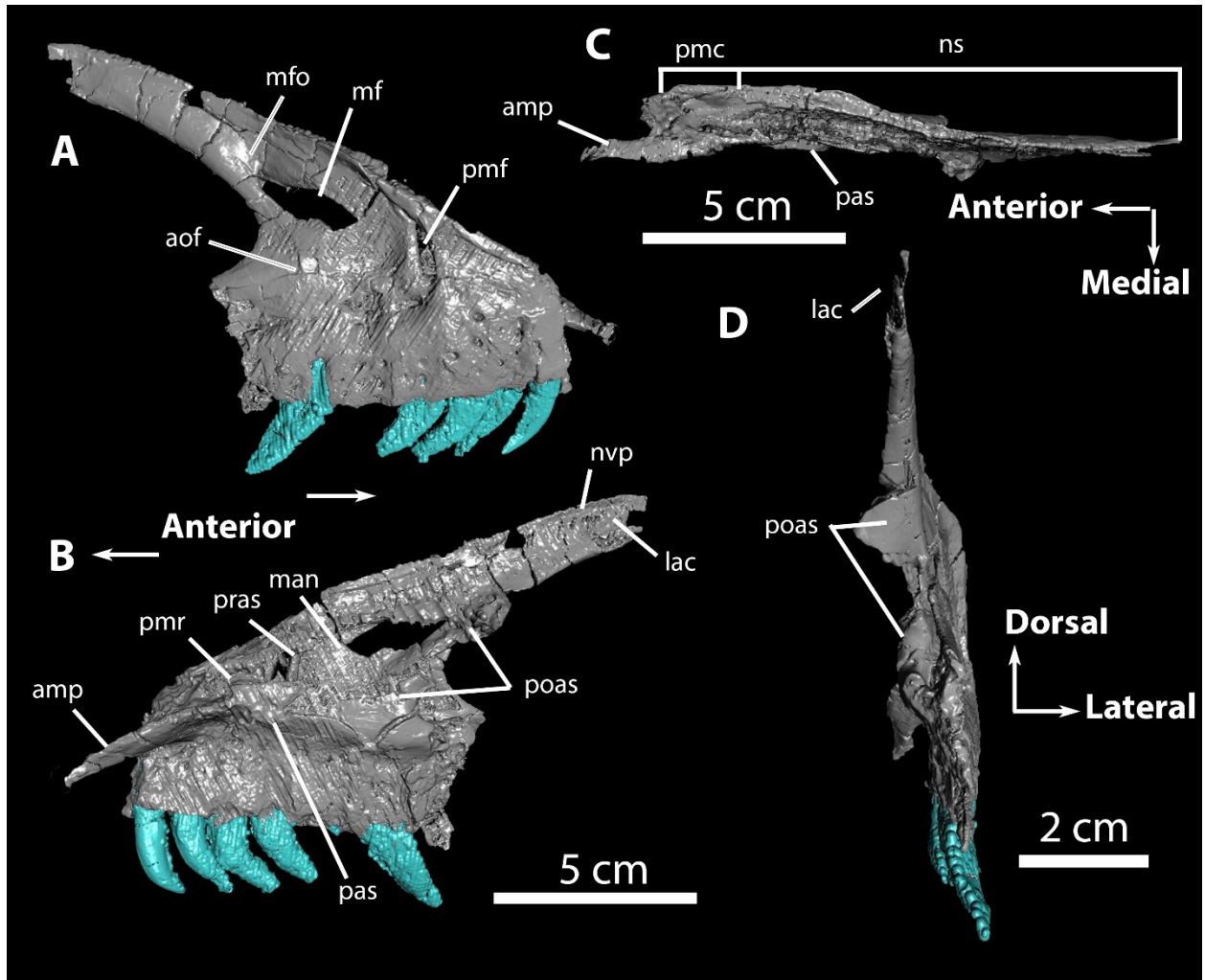


Figure 2.14. 3D mesh of the maxilla of YPM 5232 (557) *Deinonychus antirrhopus*. A) right lateral, (B) medial, (C) dorsal, and (D) posterior view. Abbreviations: **amp**, anteromedial process; **aof**, antorbital fossa; **lac**, facet for lacrimal contact; **man**, maxillary antrum; **mf**, maxillary fenestra; **mfo**, maxillary fossa; **ns**, nasal suture; **nvp**, facet for the ventral process of the nasal; **pas**, palatal shelf; **pmc**, premaxilla contact surface; **pmf**, promaxillary fenestra; **pmr**, promaxillary recess; **poas**, postantral strut; **pras**, preantral strut;

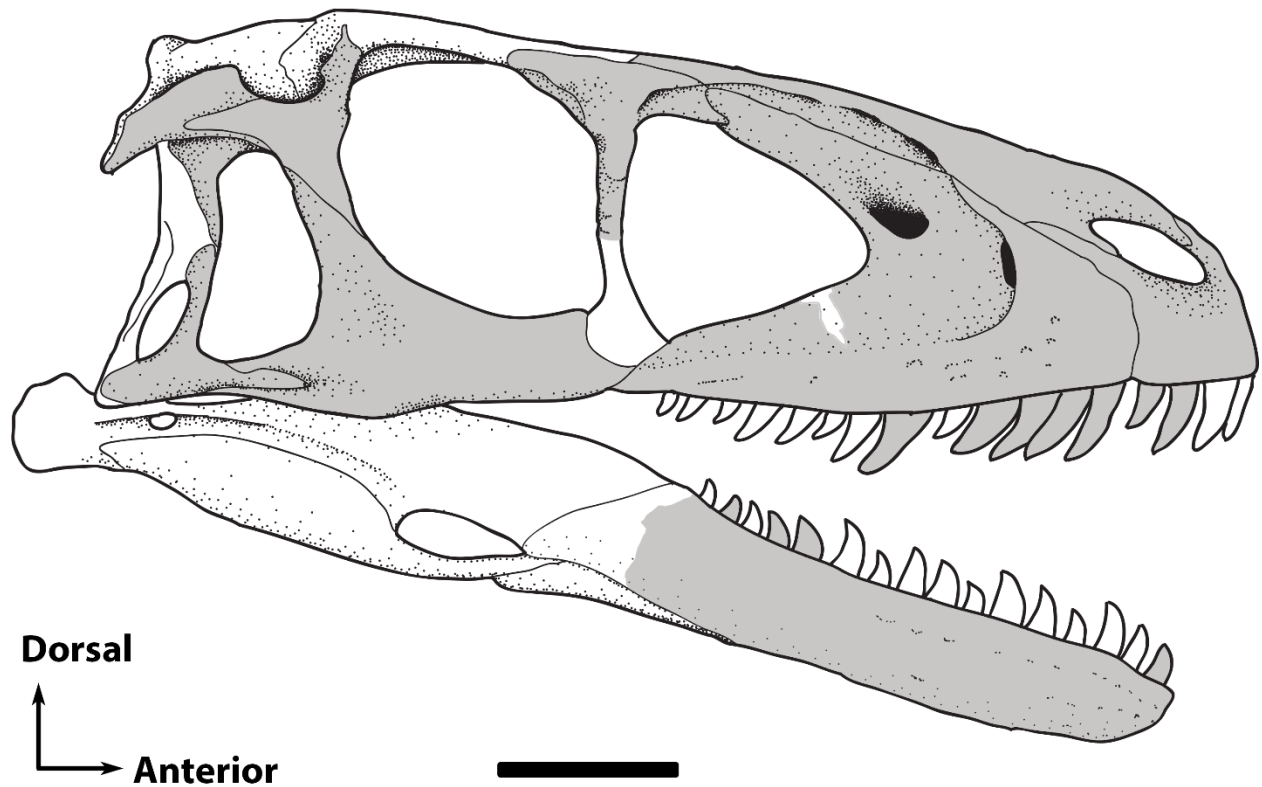


Figure 2.15. Skull reconstruction of *Deinonychus antirrhopus*. The skull was reconstructed using specimens described from Ostrom 1969 and were all photographed by the author (greyed in). The maxilla and nasal were illustrated based on the CT data and photographs of the specimen YPM 5232 (557). Surrounding greyed elements include: YPM 5232 (237), right premaxilla; YPM 5232 (613) right lacrimal; YPM 5210 (458), left jugal; YPM 5210, right postorbital; YPM 5210, right squamosal; YPM 5210 (268), left quadratojugal; YPM 5232 (66-11), left dentary. All specimens were scaled to the maxilla if needed. Non-greyed elements were illustrated using *Dromaeosaurus albertensis* (AMNH FARB 5356) and *Velociraptor mongoliensis* (MPC-D 100/25) for reference. Scale bar = 5 cm.

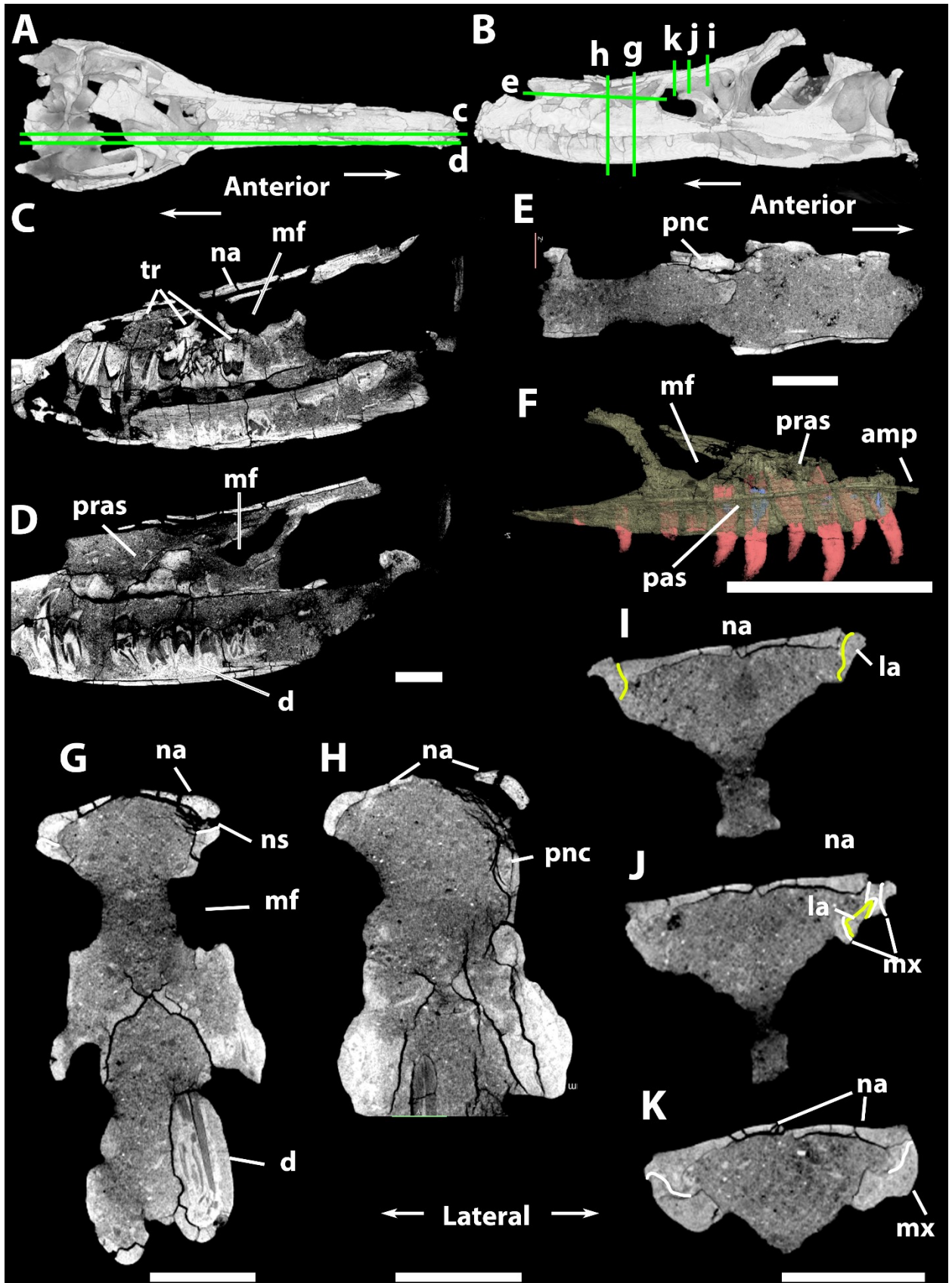


Figure 2.16. CT data of the skull of a *Velociraptor* sp. specimen (MPC-D 100/982). A) dorsal and (B) left lateral view of rendered CT data for MPC-D 100/982; C and D) parasagittal sections through the maxilla showing depth of maxillary tooth roots (C) and preantral strut (D); E) transverse section through a pneumatic excavation anterior to secondary antorbital fossa; F) semi transparent mesh of the left maxilla of MPC-D 100/982 to show maxillary teeth and roots; G and H) coronal sections through the skull of MPC-D 100/982 showing the maxillonasal suture and the pneumatic recess in coronal section; I-K) coronal sections of the transition between maxilla-nasal contact to nasolacrimal contact. White lines indicate maxilla-nasal contacts while yellow lines indicate lacrimal-nasal contacts. C-E, G-K) lower case letters by green lines correspond to the location where the sections were taken from. Scale bars C-E, G-K = 1 cm. Scale bar F = 5 cm. No scale bar for A and B, however, they are scaled to each other. Abbreviations: **amp**, anteromedial process; **d**, dentary; **la**, lacrimal; **mf**, maxillary fenestra; **mx**, maxilla; **na**, nasal; **ns**, nasal suture; **pas**, palatal shelf; **pnc**, pneumatic cavity; **pras**, preantral strut; **tr**, tooth root.

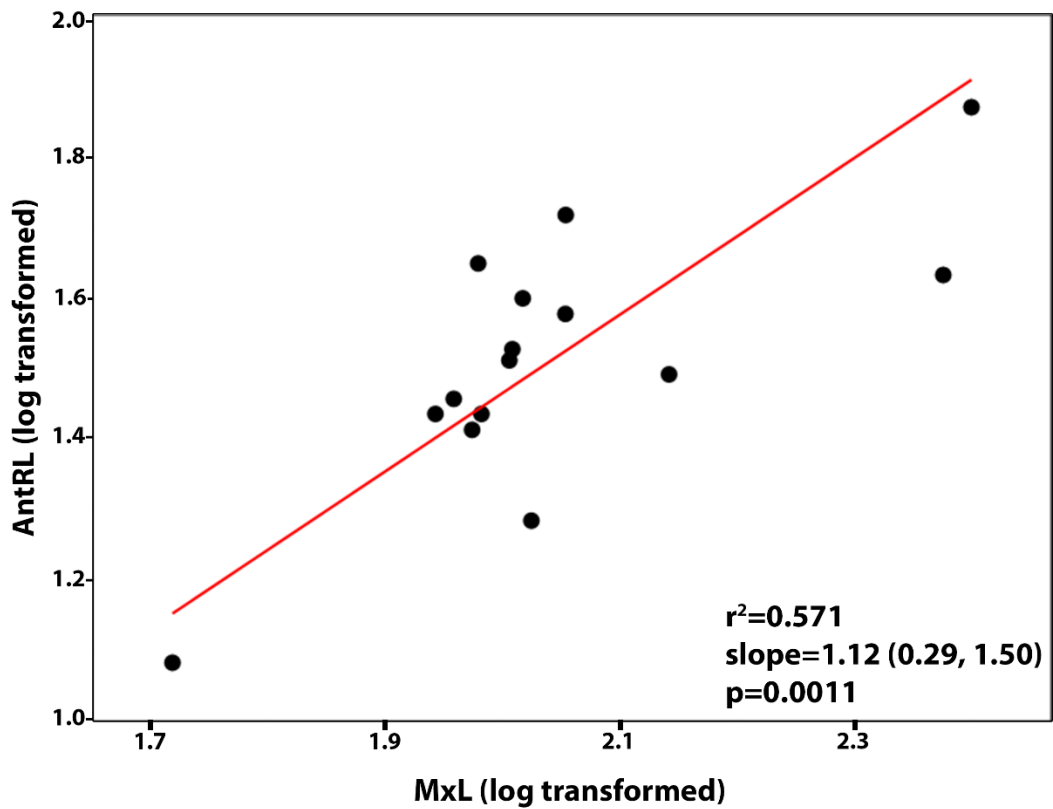
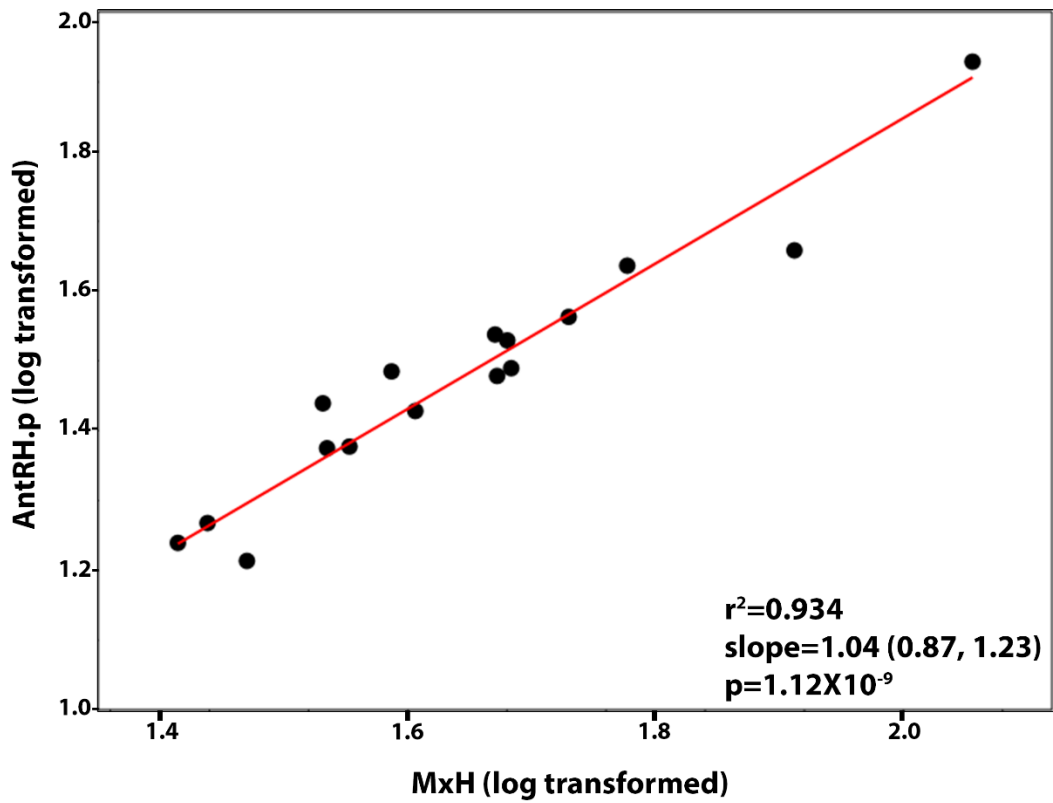


Figure 2.17. Reduced Major Axis regression analysis of eudromaeosaurian anterior ramus and maxillary dimensions. A) Regression analysis of anterior ramus and maxillary height; B) regression analysis of anterior ramus and maxillary length. Trendlines are plotted as a red line and correlation coefficient (r^2), slope with 95% confidence intervals, and p-values are reported in the lower right corner of each analysis.

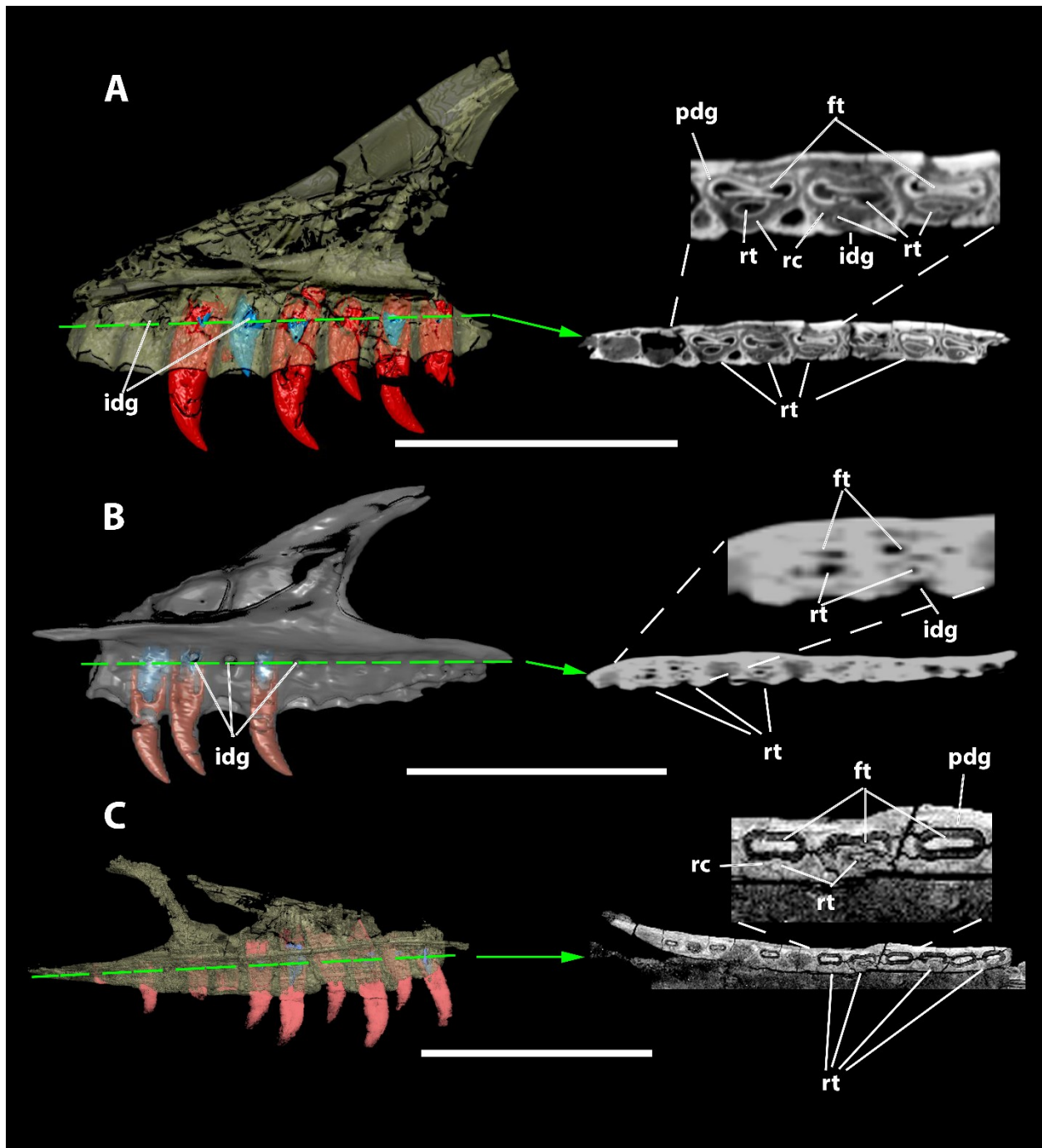


Figure 2.18. Tooth replacement in eudromaeosaurians. A) medial view of a mesh of ROM 63777, *Acheroraptor temertyorum* with CT transverse slice through the maxillary tooth row; B) medial view of a mesh of TMP 1994.012.0844, *Saurornitholestes langstoni* with corresponding transverse CT section of the maxillary tooth row; C) medial view of a mesh of the left maxilla of

MPC-D 100/982, *Velociraptor* sp. with corresponding CT transverse section of the maxillary tooth row. Green dashed lines indicate the location of the slice. Sections of the tooth row are blown up to show greater alveolar detail and are not to scale. Erupted teeth on the meshes and those without sign of replacement are coloured red, while replacement teeth are coloured blue. Scale bars = 5 cm. Abbreviations: **ft**, functional tooth; **idg**, interdental gap; **pdg**, periodontal gap; **rc**, replacement crypt; **rt**, replacement tooth.

**Chapter 3. Re-examining ratio based premaxillary and maxillary characters in
Eudromaeosauria (Dinosauria: Theropoda): divergent trends in snout morphology
between Asian and North American taxa**

3.1. Introduction

Eudromaeosauria Longrich and Currie, 2019, is a group of dromaeosaurids that diversified during the Late Cretaceous across Laurasia (Longrich and Currie 2009, Turner et al. 2012). This clade is distinct in its adaptations for terrestrial carnivory and would have filled the small to medium sized predator niche in their respective ecosystems. Most Asian representatives possess long narrow snouts compared to contemporaneous North American taxa that are typified by shorter, broader muzzles (Barsbold and Osmólska 1999, Currie and Varricchio 2004, Evans et al. 2013). The Campanian rocks – from which the majority of eudromaeosaurians have been found – represent a wide variety of habitats. The depositional environments described for these rocks were arid to semi-arid in Asia (Dashzeveg et al. 2005, Dingus et al. 2008) and temperate to subtropical in North America (Eberth and Brinkman 1997, Eberth and Braman 2012). Geographic separation and niche partitioning are two factors in variation of snout morphology observed for modern carnivorans (Slater et al. 2009, Ferreira-Cardoso et al. 2019). Although ecomorphological adaptations are highly convergent (Zanno and Makovicky 2011), the morphological and subsequent phylogenetic framework of eudromaeosaurians has focused heavily on the elongation of the snout (Barsbold and Osmólska 1999, Currie and Varricchio 2004, Longrich and Currie 2009, Evans et al. 2013, Currie and Evans 2019).

Characterization of skeletal elements that describe elongation are often presented as ratios (i.e., longer than tall, X% the length of X element). Characters described this way are problematic as they represent a continuum of data that has been treated as discrete (Simões et al.

2016). This can work but it requires justification in the form of natural disjunct in the data pertaining to the character. Many morphological datasets use ratio-based characters but provide little, if any, justification for the state delineation (Longrich and Currie 2009, Carr et al. 2017, Cau et al. 2017). In the case of eudromaeosaurians many of these characters focus around skull elements, especially characters pertaining to the snout (Fig. 1.1) (Longrich and Currie 2009). This is largely due to the limited material for many eudromaeosaurian taxa. The maxilla has been considered to be diagnostic due to its complex structure (Fig. 1.1B-C) and variation within Dromaeosauridae Matthew and Brown, 1922, and Troodontidae Gilmore, 1924, (Currie and Varricchio 2004, Senter et al. 2010, Evans et al. 2013). Because the comparative framework for eudromaeosaurians has focused on the elongation of the snout following the work of Barsbold and Osmólska (1999), this has been applied to the maxilla itself (Evans et al. 2013). In the description of the North American taxon *Acheroraptor temertyorum* Evans et al, 2013, the authors focused on the elongation of the anterior ramus of the maxilla suggesting Asian affinity. Despite the maxilla of *Acheroraptor temertyorum* being incomplete, the authors extrapolated an elongate maxilla based on the condition of the anterior ramus. The relationship between the anterior ramus and the maxilla dimensions in eudromaeosaurians was not demonstrated by Evans et al., (2013) nor was the relationship of the maxilla to snout dimensions. Elongation of the snout carries ecological implications for a predatory animal (Biknevicius and Ruff 1992, Slater et al. 2009, Sakamoto 2010) and thus may represent homoplastic characteristics (Zanno and Makovicky 2011). The elongation of maxillae and the features thereon in eudromaeosaurians have been treated as homologous traits within Velociraptorinae Barsbold 1983, despite being shared by other dromaeosaurid groups and troodontids (Currie and Evans 2019). Due to the observed convergence of these features and potential ecomorphological relationship of snout

elongation, the proportions of maxillae and their features should be examined for natural breaks, and characters based on corresponding ratios should be revised if necessary.

Alternatively, continuous data can be used for multivariate ordinations (Larson and Currie 2013, Evans et al. 2017, Schott and Evans 2017). Multivariate analyses, such as Principal Component Analyses (PCA) (Pearson 1901), have been used by some authors to identify morphometrically distinct sets of specimens that might be taxonomically separable (Larson and Currie 2013, Evans et al. 2017). Evans et al. (2017) performed such analyses on troodontid frontals from North America, successfully identifying a new species using landmarks and linear measurements. Most dromaeosaurid taxa that have been named from isolated elements, however, have been established based on maxillae rather than frontals (Currie and Varricchio 2004, Godefroit et al. 2008, Evans et al. 2013). No multivariate analysis has so far been performed on dromaeosaurid maxillae, but it has been suggested that the multivariate approach could be used to search for taxonomic variation within potentially over-lumped dromaeosaurid taxa such as *Velociraptor* Osborn, 1924, (Xu et al. 2015). While Xu et al. (2015) suggested no specific skeletal element, the dromaeosaurid maxilla would make an excellent test case for the utility of multivariate methods in delineating taxa. Additionally, PCA can be used to identify features that exhibit a high degree of variance and may prove to be phylogenetically informative upon further examination.

Availability of specimens is typically a limiting factor in vertebrate palaeontological research. It is therefore important to test what information can be obtained from a single element and determine the degree of inference that can be appropriately drawn. Here, the morphologies of eudromaeosaurian maxillae are examined from this perspective using bivariate and multivariate methods. Specific goals of this chapter are to test if the maxilla can serve as a good

proxy for overall snout dimensions; test previously proposed proportion-based maxillary characters for distinct breaks in the continuous data; test the effect of revised character state delineation on tree topology, and; analyse linear measurements of dromaeosaurid maxillae to determine if their clustering patterns reflect established phylogenetic hypotheses, or in other words if closely related dromaeosaurids tend to have similarly proportioned maxillae. Asian and North American eudromaeosaurians are also compared throughout, to test if their respective ranges of morphological variation differ in any significant way that might indicate adaptation to disparate Cretaceous ecosystems.

3.2 Materials and Methods

For this study, I measured 28 premaxillae and 36 maxillae representing a total of 20 taxa, in addition to a cast of a complete skull belonging to an undescribed eudromaeosaurian (Table 3.1). Left and right sides of specimens were both measured when possible and averaged for use in the analyses. The cast, UALVP 49389, is of a specimen in private collections and has no available locality data. The likeness of this specimen is akin to that of an Asian dromaeosaurid, and has been frequently labeled as *Velociraptor*. However, its morphology is quite different from other specimens referred to this genus (Fig. 1.2J-M). Because the location of the original specimen is unknown, this maxilla cannot be used as the holotype of a new species. However, its peculiar morphology provides an excellent data point for my study of variation among dromaeosaurids. The unenlagiine *Austroraptor cabazai* Novas et al., 2009, (MML 195), the microraptorine *Sinornithosaurus millenii* Xu et al., 1999, the microraptorine or stem-eudromaeosaurian *Shanag ashile* Turner et al., 2007, and the troodontids *Geminiraptor suarezarum* Senter et al., 2010, (CEUM 73719), *Gobivenator mongoliensis* Tsuihiji et al., 2014 (MPC-D 100/86), *Saurornithoides mongoliensis*, Osborn, 1924 (Norell et al. 2009), *Sinovenator*

changii Xu et al., 2002, and *Zanabazar junior* (Norell et al. 2009) were used for outgroup comparison.

Linear measurements of maxillae were taken using 150 mm Mastercraft digital callipers, 152 cm measuring tape, and the calibrated Line tool in ImageJ. Specimens to which we did not have physical access were measured exclusively with ImageJ (Table 3.1). ImageJ was tested for accuracy by remeasuring MPC-D 100/982 completely using the software. This validated the use of ImageJ to capture data from specimens that could not be physically measured. A further justification of the use of ImageJ is that the tests in this study focus on proportion-based variables, which are meaningful when calculated from measurements taken at a consistent scale even if the scale is slightly inaccurate. Two premaxillary and 16 maxillary measurements (Fig. 3.1) were taken for each side of each specimen when possible (Table 3.2). However, portions of some specimens were missing. When the missing portions were minimal or restricted to terminal parts of structures, measurements were estimated as needed. All relevant recorded measurements are available in the appendix (A 2.1). Bivariate plots and statistical tests were done using PAST 3 (Hammer et al. 2001), which was also used for visualizing direct comparisons of premaxillary and maxillary length to height ratios. All figures were produced in PAST 3 and exported as PNG files. Photoshop CS6 was used to create the figures and enhance features such as labels and scales. Illustrator CS6 was used to make line drawings from photos taken by the authors, or from published images for specimens to which I did not have access.

3.2.1 Regression analysis

To test the power of maxillary measurements to predict the shape of the lateral profile of the snout, I examined the relationship between the length-to-height ratio of the premaxilla and that of the maxilla in eudromaeosaurians. These two elements were chosen for evaluation due to

their large contributions to the lateral surface of the snout (Fig. 1.1). The nasal was not included because this bone is nearly hidden in a lateral view of a dromaeosaurid skull (Ostrom 1969, Barsbold and Osmólska 1999, Norell et al. 2006, Xu et al. 2010a), and 3-dimensional analysis of snout shape was beyond the scope of this study. I performed a least squares linear regression of the length-to-height ratio of the premaxilla on that of the maxilla. A strong relationship (high R^2 value) between the two ratios would indicate that the premaxilla tended to be similar in overall shape to the maxilla, allowing the lateral profile of the snout as a whole to be reconstructed with relatively high confidence from measurements of the maxilla alone. PAST 3 was used to carry out the regression analysis and plot a line of best fit. The *Deinonychus antirrhopus* Ostrom, 1969, premaxilla used in this analysis (YPM 5232 [237]) does not belong to the individual represented by the maxilla (YPM 5232 [557]), but the two bones were collected from the same quarry, are both from the right side, and appear to be from individuals of similar size. Therefore, the two *Deinonychus* elements were treated as being from a single skull in the regression analysis. All specimens in the study appeared to be mature, except for *Bambiraptor feinbergi* Burnham et al., 2000 (AMNH FARB 30556). To prevent ontogenetic signals from clouding our results, the premaxilla and maxilla of AMNH FARB 30556 were excluded from the regression.

3.2.2 Principal component analysis (PCA) and cluster analysis

PCA was used to assess taxonomic variation in the morphology of the maxilla among eudromaeosaurians and their close outgroups. Use of colour on the PCA plots to distinguish between Asian and North American taxa allowed the plots to provide a visual test of the possibility that eudromaeosaurians from the two continents tend to differ in snout shape. The full PCA data set used in this study consisted of the widest suite of maxillary measurements available, across the widest range of taxa. Not all specimens could be used in the PCA and

cluster analysis, as some were highly incomplete. Measurements were scaled by dividing by either the length of the maxilla or the total length of the first 9 maxillary alveoli (A 2.3). Four variants of the analysis, characterized by different choices of scaling factor and/or taxonomic scope, were performed. The four variants were as follows: (1) all taxa, with measurements scaled to maxillary length; (2) eudromaeosaurian taxa only, with measurements scaled to maxillary length; (3) eudromaeosaurian taxa only, with measurements scaled to the length of the first nine maxillary alveoli; (4) eudromaeosaurian taxa only, with AMNH FARB 30556 (the holotype of *Bambiraptor feinbergi*) excluded and measurements scaled to the length of the first nine maxillary alveoli (A 2.4). Comparing results from the second and third variants made it possible to determine whether the choice of maxilla length or length of first nine maxillary alveoli as a scaling variable had any major effect on the analysis. The third variant, however, was the main analysis in this study of morphological variation within Eudromaeosauria and the possible dichotomy in snout proportions between Asian and North American eudromaeosaurians. Scaling by the length of the first nine alveoli allowed for the greatest number of eudromaeosaurian maxillae to be compared, as those of *Acheroraptor temertyorum*, *Velociraptor osmolskae* Godefroit et al., 2008, and a specimen of *Saurornitholestes langstoni* Sues, 1976 (TMP 1994.012.0844) were too incomplete for their lengths to be determined. The fourth variant was intended to examine the effect of the known juvenile specimen AMNH FARB 30556 (Burnham et al. 2000) on the PCA results. The PCAs were performed in PAST 3 using the multivariate PCA function, which provided summary of eigenvalues, PC loadings and scatter plots. The broken stick method was used to determine the number of principal components to examine (Jackson 1993).

Scaling the linear measurements according to the length of the first nine maxillary alveoli could be not readily applied across the full range of taxa included in the PCA because of variation in maxillary tooth count. The maxillary tooth count for eudromaeosaurian taxa is usually between 9-15 (Godefroit et al. 2008, Currie and Evans 2019). However, in Chapter 2 *Deinonychus antirrhopus* was observed as having 13 maxillary teeth based on CT data. Due to the incompleteness of all known material of *Dromaeosaurus albertensis* Matthew and Brown, 1922, which has nine maxillary teeth, this species could not be included in this analysis. Therefore, the eudromaeosaurian taxa included in the PCA have 10-13 maxillary teeth. The troodontids and the single unenlagiine specimen, *Austroraptor cabazai* (MML 195), have much higher maxillary tooth counts (19-25) (Norell et al. 2009, Novas et al. 2009, Senter et al. 2010, Tsuihiji et al. 2014). The large number of maxillary teeth in *Austroraptor cabazai* and troodontids suggests that each tooth occupies a smaller portion of the alveolar margin than in eudromaeosaurians, and accordingly that the total length of the first nine maxillary alveoli cannot be used as a meaningful, consistent measure of size in an analysis including eudromaeosaurians alongside troodontids and/or *Austroraptor cabazai*. It is for this reason that maxillary length was used as a scaling factor in the first variant of the PCA, which included all taxa, whereas the length of the first nine maxillary alveoli was used in two of the variants (the third and fourth) that included only eudromaeosaurians.

A classic cluster analysis was used to carry out phenetic pairing of specimens based on the PCA results, in order to determine whether specimens that were conspecific or belonged to closely related species would prove to be highly similar in their maxillary proportions. This procedure was performed for the full range of taxa in this study, using the same data that went into the first variant of the PCA, and again using the eudromaeosaurian-only data from the third

PCA variant. Classic cluster analysis was chosen over neighbour joining because the former method produces a dendrogram with a simple branching and node system visually comparable with a phylogenetic tree. A positive result would be the recovery of successively nested clusters that paralleled proposed monophyletic groups (Longrich and Currie 2009, Evans et al. 2013, Currie and Evans 2019). The classic cluster analysis was run through PAST 3 using the UPGMA clustering algorithm and Euclidean distance measure.

3.2.3 Character assessment

Characters 8, 20, 22, 28 and 29 from the phylogenetic data matrix of Currie and Evans (2019) were tested in the present study to examine, and if necessary, revise the character state definitions prior to carrying out an analysis of the modified matrix. This data matrix was chosen due to its comprehensive character set and its focus on dromaeosaurids, which make it a useful framework for evaluating the potential for inferences regarding dromaeosaurid phylogeny to be drawn from premaxillary and maxillary elements. Because the data matrix is taxonomically restricted compared to those used in larger analyses including, for example, all theropods (Turner et al. 2012), numerical distributions of quantitative characters such as ratios should be more likely to contain discernible gaps (Bull et al. 1993). Currie and Evans (2019) is essentially the latest version of an earlier matrix that has been used in various forms in numerous previous studies of dromaeosaurid systematics (Longrich and Currie 2009, Turner et al. 2012, Evans et al. 2013).

All five characters chosen for character state assessment are binary in their original form and pertain to ratios between measurements of the premaxilla or maxilla. For each character, some threshold value of the ratio defines the boundary between the two character-states given in Currie and Evans (2019). To test the appropriateness of these thresholds, the distributions of ratio

data for all dromaeosaurid and available outgroups in the study were plotted as histograms using PAST 3. Fifteen bins were used for each histogram. Kernel density curves were also plotted, to represent the data in a continuous fashion and reveal any subtle group distinctions not clearly visible from the discrete bins used in the histograms. A Jenks Natural Breaks Optimization function was used in Microsoft Excel with the XRealStats package to analyze the distributions for natural breaks. Each set of data was initially tested for the presence of two groups separated by such a break ($k=2$), to reflect the binary coding method used by Currie and Evans (2019). Each test was performed with 1000 iterations, and a goodness of variance fit (GVF) of 0.7 or more was considered acceptable as values in this range were reliably associated with gaps that remained stable or nearly so, over the full set of iterations. If the GVF was below 0.7, the analysis was rerun to test for the possible presence of three groups separated by two natural breaks ($k=3$). If this produced a GVF of 0.7 or more, the character would be reformulated as having three discrete states. Lists of ratio values for each character in the taxa considered in the present study can be found in the supplementary information (A 2.5). The ratio values for each character were tested with an unequal variance t-test in PAST 3 to determine whether a significant difference existed between Asian and North American taxa. Box plots were generated in PAST 3 to visualize the distribution of values for each of these biogeographic groups.

The method outlined was also used to define states for two new proportionate characters: maxilla length/height ratio, and antorbital fossa length/height ratio. The data pertaining to each of these characters were analysed for any significant difference between Asian and North American taxa via an unequal variance t-test in PAST 3.

3.2.4 Phylogenetic analysis

Using results from the character assessments, character state scorings for the five re-evaluated characters from Currie and Evans (2019) were altered as needed, and scorings for the two new characters were compiled (Table 3.3). A modified taxon-character matrix incorporating the new scorings was assembled in Mesquite V3.2 (Maddison and Maddison 2017). The new matrix consists of 37 taxa and 182 characters as opposed to the 180 characters from Currie and Evans (2019). The original matrix (taxa=37; characters=180) from Currie and Evans (2019), another version in which the tested characters (8, 20, 22, 28, and 29) were removed for all taxa (taxa=37; characters=175), and finally the modified matrix from this study, were all analyzed with TNT V1.5 (Goloboff and Mattoni 2006). All matrices were analysed with a New Technology search parsimony analysis, using 10 000 replicates with 10 rounds of ratcheting, 5 rounds of tree fusing, and 5 rounds of drifting. Each new replicate commenced after the shortest tree length had been found once in the previous replicate. *Archaeopteryx lithographica* Meyer, 1861, was set as the outgroup for all analyses, in line with the approach proposed by Currie and Evans (2019). A 50% majority rule consensus tree was made from the most parsimonious trees produced by each of the three data matrices. The new and tested characters were then mapped onto each majority rule tree, and the three majority rule trees were compared topologically. Finally, the fit (i.e. CI value) of each new or tested character on the majority rule consensus tree generated in the analysis from which the tested characters had been removed was computed. CI on this tree was also computed for the original versions of the tested characters from Currie and Evans (2019), making it possible to determine which version of each character had a better fit with the rest of the data. This process was done in Mesquite V3.2 (Maddison and Maddison, 2017) after majority rule consensus trees had been constructed in TNT V1.5 (Goloboff and Mattoni, 2006).

3.3 Results

3.3.1 Regression analysis

The length-to-height ratio of the maxilla is predictive of that of the premaxilla and by extension of the overall profile of the snout in lateral view, as indicated by the r^2 of 0.848 (p-value=0.0005) from the regression analysis (Fig. 3.2). This demonstrates that there is relatively little scatter around the trend line. The line of best fit is positive and described by the equation $y=0.516x+0.128$ (Fig. 3.2). The fact that the slope is less than one indicates that the maxilla, as expected, consistently has a greater length-to-height ratio than the premaxilla in eudromaeosaurians. Raw PAST 3 outputs are available in the appendix (A 2.2).

3.3.2 Principal component analysis (PCA) and cluster analysis

In the principal component analysis containing all taxa (i.e. variant 1 of the PCA), three components contributed significantly to explaining the variation in the data (A 2.3). With the exclusion of the troodontids and non-eudromaeosaurian dromaeosaurids (i.e. in variants 2-4 of the PCA), however, only two components were significant. Component loadings were closely similar between variants 2, 3 and 4 of the PCA. Variants 2 and 3 of the PCA were corrected to different size related measurements (maxillary length and length of the first nine maxillary alveoli respectively) and showed nearly identical loadings and percent variance values for the two significant PCs. Variants 3 and 4 of the PCA differed only in exclusion of *Bambiraptor feinbergi* from the latter (A 2.4). Accordingly, the presence of the juvenile specimen representing this species had a minimal effect on the analysis of eudromaeosaurian taxa, so variant 4 of the analysis is not considered further. Results for the other three variants are shown in Figure 3.3.

In the PCA including all taxa, the variables with the highest loadings across all significant PCs were antorbital fossa length (AntFH) and maxilla height (MxH) (A 2.3), while the next highest loadings were associated with antorbital fossa length anterior to the maxillary fenestra (AntAF-MxFen), height related variables (AntFenH, AntFH, AntRH.p), length of the first nine maxillary alveoli (L9Alv), and distance from the antorbital fenestra to the 9th alveolus (AntFen.9Alv). In the analyses including eudromaeosaurian taxa only (i.e. variants 2 and 3), the variables with the highest loadings were length of anterior ramus (AntRL), height variables (predominantly the heights of the maxilla (MxH), antorbital fenestra (AntFenH) and fossa (AntFH), and proximal anterior ramus (AntRH.p)), length of antorbital fossa (AntFL), and distance between maxillary fenestra and anterior border of antorbital fossa (AntAF-MxFen) (A 2.4). Maxilla height and length of antorbital fossa anterior to maxillary fenestra (AntAF-MxFen) had much greater loadings in the analyses including only eudromaeosaurians than in the one performed with all taxa. In the PCA including all taxa, dromaeosaurids and troodontids were clearly separated along PC 1, although the unenlagiine *Austroraptor cabazai* was considerably closer to the troodontids than was any other dromaeosaurid (Fig. 3.3 A-B). Taxonomic separation along PC 1 was probably due mainly to a difference between dromaeosaurids and troodontids in the length of the first 9 maxillary alveoli (L9Alv), the variable with the greatest loading on this component. Troodontids seemed to cluster closely along PC 3 and to some extent PC 2. However, *Sinovenator* was an outlier relative to other troodontids on PC 3 (Fig. 3.3A, B), on which maxillary height (MxH) and antorbital fossa length (AntFL) had the greatest loadings.

Eudromaeosaurians clustered in distinct Asian and North American groups on the plot of PC 3 vs. PC 1 (Fig. 3.3B) in the complete analysis, and on the plot of PC 2 vs. PC 1 in both eudromaeosaurian-specific versions (i.e. variants 2 and 3) of the analysis (Fig. 3.3C, D). This

separation was also observed to some extent on the plot of PC 2 vs. PC 1 for the complete analysis (Fig. 3.3A). On this plot, however, *Achillobator giganticus* Perle et al., 1999, *Linheraptor exquisitus* Xu et al., 2010, *Tsaagan mangas* Norell et al., 2006, and UALVP 49389 overlapped with North American eudromaeosaurians on the positive part of PC 2, on which the variable with the greatest loading was the height of the anterior ramus proximally (AntRH.p). The other eudromaeosaurians plotted on the negative part of this component, due to having greater values of antorbital fossa length (AntFL) and distance from the anterior margin of the antorbital fenestra to the maxillary fenestra (AntAF-MxFen).

Specimens belonging to the same genus plotted closer to each other than to other taxa in all analyses (Figs. 3.3, 3.4). The specimen representing *Bambiraptor feinbergi* (AMNH FARB 30556) plotted closer to UALVP 55700 than any other eudromaeosaurian in nearly all ordinations (Fig. 3.3B-D). Cluster analyses, however, placed UALVP 55700 closest to the other maxilla identified as *Saurornitholestes langstoni*, with *Bambiraptor feinbergi* falling closest to this pairing (Fig. 3.4). Specimens identified as *Velociraptor* plotted close together along PC 1 but varied more in their positions along PC 2 and PC 3 (Fig. 3.3), a pattern obtained in all analyses. The cluster analysis corroborated the PCA in placing all specimens within this genus in an exclusive cluster (Fig. 3.4). The specimen representing *Velociraptor osmolskae* (IMM99NM-BYM-3/3A) plotted close to specimens identified as *Velociraptor mongoliensis* Osborn, 1924 (Figs. 3.3C, D, 3.4B). However, MPC-D 100/982 plotted far away from all other specimens referred to the genus *Velociraptor*, the separation being greater than that seen among many specimens representing different species. The closest other *Velociraptor* specimen to MPC-D 100/982, in all plots except that of PC 3 vs. PC 1 in the complete analysis (Fig. 3.3B), was AMNH FARB 6515. The cluster analysis placed *V. osmolskae* somewhat closer to the cluster of

V. mongoliensis specimens (distance ≈ 0.19) than MPC-D 100/982 (distance ≈ 0.24) (Fig. 3.4B), but in the eudromaeosaurian-specific PCA *V. osmolskae* and MPC-D 100/982 were the most widely separated specimens in the *Velociraptor* grouping with respect to PC 2 (Fig. 3.3D). *Achillobator giganticus* (MNUFR 15) plotted closer to North American dromaeosaurids than any other Asian taxon (Figs. 3.3B-D), with the exceptions of *Linheraptor*, *Tsaagan*, and UALVP 49389 in the plot of PC 2 vs. PC 1 for the complete analysis (Fig. 3.3A). In the eudromaeosaurian-specific analysis ROM 63777 plotted closest to MNUFR 15 (Fig. 3.3D), a relationship largely based on height variables as well as anterior ramus length (AntRL) (A 2.4). The cluster analysis corroborated the similarity between these specimens (distance ≈ 0.23) (Fig. 3.4B).

The cluster analysis of the dataset including all taxa recovered troodontids and dromaeosaurids as separate clusters (Fig. 3.4A). Within the dromaeosaurid cluster, the microraptorine *Sinornithosaurus millenii* and possible microraptorine *Shanag ashile* formed a pair separate from a large cluster including all the eudromaeosaurians in the analysis as well as the unenlagiine *Austroraptor cabazai* (Fig. 3.4A), which was placed adjacent to the cluster containing specimens of *Velociraptor*. *Linheraptor* and *Tsaagan* fell closest to each other in nearly all the PC plots (Fig. 3.3). This relationship was corroborated in the cluster analyses, as the two specimens were found to be most like one another (Fig. 3.4). In the cluster analysis UALVP 49389 was found to be most like these two specimens (Fig. 3.4) and often plotted close to them but toward the extreme of variation along each PC (Fig. 3.3). Within the grouping of Asian dromaeosaurids, UALVP 49389 plotted at or near the opposite extreme from the cluster of *Velociraptor* specimens on PC 2 in all variants of the PCA analysis, and also on PC 3 in the complete analysis (Fig. 3.3). Similarly, the complete cluster analysis positioned UALVP 49389

farthest from the *Velociraptor* cluster within the large cluster containing Asian eudromaeosaurians and *Austroraptor cabazai* (Fig. 3.4). North American eudromaeosaurian taxa were grouped together, albeit in a cluster that also included *Achillobator giganticus*, in both versions of the cluster analysis (Fig. 3.4). In the complete cluster analysis, the specimens representing *Atrociraptor marshalli* Currie and Varricchio, 2004, and *Deinonychus antirrhopus* were found to be most dissimilar from all other North American eudromaeosaurian specimens (distance ≈ 0.29 and 0.31 respectively) (Fig. 3.4A). In the eudromaeosaurian-specific analysis, they formed a widely spaced pair (distance ≈ 0.38) that fell closest to the cluster of North American specimens and *Achillobator giganticus* (distance ≈ 0.06) (Fig. 3.4B).

3.3.3 Character assessment

Character 8 “Antorbital fenestra; 0, longer than tall; 1, subequal or taller than long” (Currie and Evans 2019) is problematic as worded. Several specimens included in this study fall on or around the threshold of 1.00 for the length-to-height ratio used by Currie and Evans (2019) (Fig. 3.5A). The data points can be divided based on Jenks Optimization into two distinct classes, with a goodness of variance fit (GVF) of 0.73. One class includes specimens with values ranging from 0.94 to 1.18, while the other includes specimens with values of 1.47 to 2.45, for a gap size of 0.29 between the classes. The threshold between character states is most appropriately positioned at the midpoint of this gap, or ≈ 1.33 . Revised character definitions for this character and others examined in the present section can be found in the appendix (A 2.5).

An unequal variance t-test of variation in this character between Asian and North American eudromaeosaurian taxa returns a p-value of 0.0022, indicating a significant difference in the proportions of the antorbital fenestra between these biogeographic groups (Fig. 3.5B). North American specimens are restricted to a small range of values (0.94, *Saurornitholestes*

langstoni - 1.11, *Deinonychus antirrhopus*), which does not overlap the range for Asian specimens. The closest Asian taxon to this range is *Linheraptor exquisitus* (1.12), whereas the Asian specimen with the highest value is UALVP 49389 (2.13) (A 2.5).

Character 20 “Premaxilla shape: 0, elongate; 1, body of premaxilla short, no more than 15% length of maxilla” (Currie and Evans, 2019) is uninformative for dromaeosaurid taxa examined in this study. All dromaeosaurid specimens fall above the premaxilla/maxilla length ratio threshold of 0.15, while troodontid specimens fall below (Fig. 3.5C). Jenks Optimization found two distinct classes, with a GVF of 0.87. Values for the first class range from 0.07 to 0.10, while values for the second class range from 0.19 to 0.29 (Fig. 3.5C).

No significant difference in values between Asian and North American eudromaeosaurians was found for this character by an unequal variance t-test ($p=0.106$) (Fig. 3.5D). The ranges of variation of the two groups overlap extensively, though North American representatives show larger ratios (0.22, *Saurornitholestes langstoni* - 0.29, *Dromaeosaurus albertensis*) overall than their Asian relatives (0.19, *Tsaagan mangas* - 0.26, *Velociraptor* sp.) (A 2.5). In addition to *Dromaeosaurus albertensis*, *Deinonychus antirrhopus* (0.29) falls above the range of variation observed in Asian eudromaeosaurians and *Bambiraptor feinbergi* (0.26) overlaps with the upper range of the Asian representatives.

Character 22 “Premaxilla, main body below naris: 0, longer than tall; 1, at least as tall as long” (Currie and Evans, 2019) is a Type II-B problematic character *sensu* Simões et al. (2016). Jenks Optimization with $k=2$ finds two distinct groups, with a GVF of 0.71 (Fig. 3.5E), when the extreme outlier *Sinornithosaurus millenii* (premaxilla length-to-height = 3.83) is excluded from the analysis. Premaxilla length-to-height ratios for the first class range from 0.62-1.28, while values for the second class range from 1.42-2.00. A new threshold value of 1.35 is suggested, to

minimize the proximity of data points to the threshold. A Jenks Optimization test for the presence of three classes ($k=3$) with *Sinornithosaurus millenii* included results in an even higher GVF (0.91), but *Sinornithosaurus millenii* is then the only occupant of the class with the highest value range. Accordingly, it is more appropriate to accept the two character-states indicated by the $k=2$ optimization and assign the second character state to *Sinornithosaurus millenii*.

Value ranges for character 22 in Asian and North American eudromaeosaurians were compared via an unequal variance t-test and found to be distinct (p -value = 0.0049) (Fig. 3.5F). The distribution of values for Asian taxa is somewhat normal, whereas that for North American taxa is skewed toward the lower part of the range. Curiously, the two specimens of *Utahraptor ostrommaysi* Kirkland et al., 1993, in this study account for the high and low extremes in the range of variation observed in North American taxa (CEUM 01430 = 0.94, and BYUVP 14585 F#1984 = 1.28). Most North American specimens, however, fall between 0.94 (CEUM 01430) and 1.12 (*Dromaeosaurus albertensis*), with only *Deinonychus antirrhopus* and BYUVP 14585 F#1984 reaching 1.28. The only Asian taxon with a value overlapping the North American range is *Linheraptor exquisitus* (1.22), and the Asian specimen with the highest value is *Velociraptor* sp., MPC-D 100/982 (2.0) (A 2.5).

Character 28 “Maxilla, anterior ramus: 0, elongate, 25% or more of the length of maxilla; 1, short, less than 25% length” (Currie and Evans 2019). Values for this character are found by Jenks Optimization to be separable into three distinct classes, with a GVF of 0.87 (Fig. 3.5G). When we test for two distinct groups the GVF is 0.68, and the gap between classes is only 0.011 (A 2.5), so division into three classes is preferred. Values for the first class range from 0.15-0.25, while those for the second range from 0.27-0.36 and those for the third range from 0.38-0.47 (Fig. 3.5G). Placement of thresholds separating character states at the midpoints of the small

gaps between classes results in a threshold value of 0.37 between states [0] and [2], and a threshold of 0.26 between states [1] and [0]. The threshold between states [1] and [0] is close to the single threshold given in Currie and Evans (2019) but does fit the data better, albeit marginally. Taxa that are assigned state [2] based on our proposed thresholds include *Austroraptor cabazai*, *Linheraptor exquisitus*, *Tsaagan mangas*, and the cast UALVP 49389.

The range of variation for Asian eudromaeosaurians (0.27 – 0.47) is distinct from that for North American ones (0.18 – 0.32) (p-value = 0.0075) (Fig. 3.5H). However, the two ranges overlap between 0.27 (*Velociraptor* sp.) and 0.32 (*Atrociraptor marshalli*) (A 2.5). Specimens that fall within the zone of overlap are *Achillobator giganticus* (0.29), two specimens of *Saurornitholestes langstoni* (0.28, UALVP 55700; 0.31, TMP 1994.012.0844), and *Velociraptor mongoliensis* (0.31, AMNH FARB 6515).

Character 29 “Maxilla, anterior ramus: 0, longer than tall; 1, short, at least as tall as long” (Currie and Evans 2019). Values for this character are found to be separable by Jenks Optimization into three distinct classes, with a GVF of 0.90 (Fig. 3.5I). Testing for potential separation into two classes produces a less optimal result, with a GVF of only 0.62 (A 2.5). Values for the first class range from 0.68-1.02, while those for the second range from 1.22-1.75 and those for the third range from 2.15-2.4 (Fig. 3.5I). Proposed thresholds between character states are 1.11 ([1] to [0]) and 1.95 ([0] to [2]). Only *Austroraptor cabazai* and *Shanag ashile* are assigned character state [2] based on these thresholds.

The range of variation in this character for Asian eudromaeosaurian specimens (0.87, *Achillobator giganticus* – 1.75, *Velociraptor mongoliensis*) is distinct from that for North American specimens (0.68, *Deinonychus antirrhopus* – 1.22, *Acheroraptor temertyorum*) (p-value=0.0004) (Fig. 3.5J). Among Asian eudromaeosaurians, only *Achillobator giganticus* has a

value overlapping with the North American range (A 2.5), while *Acheroraptor temertyorum* and *Saurornitholestes langstoni* (0.91, TMP 1994.012.0844) are the only North American eudromaeosaurians whose values overlap with the Asian range.

New Character #1 (181)–Maxilla shape: elongate [0], maxilla at least 2.62 times as long anteroposteriorly as tall dorsoventrally; short [1], less than 2.62 times as long as tall (Fig. 3.6A). The states presented for this character are supported by the observed distribution of ratio data, tested with Jenks Natural Breaks Optimization (k=2; GVF=0.74). Values for the first class range from 1.70-2.54, while those for the second class range from 2.70-3.53. The proposed threshold between the character states is the midpoint between the highest value in class 1 and the lowest value in class 2.

There is no overlap between the ranges for Asian (2.22-3.44) and North American (1.7-2.02) eudromaeosaurian specimens (Fig. 3.6B). A significant difference exists between the two distributions (p-value=9.36x10⁻⁵), as expected given their visible separation. All North American taxa fall into the range for character state [1], and all Asian specimens except for *Achillobator giganticus* and *Linheraptor exquisitus* fall into that for character state [0] (A 2.5).

New Character #2 (182)–Antorbital fossa shape: elongate [0], distance from anterior margin to most anterior part of posterior margin at least 1.13 times dorsoventral height exposed on maxilla; short [1] less than 1.13 times height exposed on maxilla (Fig. 3.6C). The states presented for this character are supported by the observed distribution of data, tested with Jenks Natural Breaks Optimization (k=2; GVF=0.75). Values for the first class range from 0.19-1.08, while those for the second class range from 1.17-1.88. The proposed threshold between the character states is the midpoint between the highest value in class 1 and the lowest value in class 2.

The range of variation observed for this character in North American eudromaeosaurians (0.41-0.74) falls completely within the range for Asian ones (0.19-1.17) (Fig. 3.6D). Among Asian taxa, however, only *Achillobator giganticus* (0.59) and *Tsaagan mangas* (0.64) fall within the range of North American specimens, overlapping with *Deinonychus antirrhopus* (0.60) and *Saurornitholestes langstoni* (0.60, TMP 1994.012.0844) (A 2.5).

3.3.4 Phylogenetic analysis

Character statements and character state definitions were modified as needed to reflect the analysis of ratio data presented in this study (A 2.6). Because all modifications to character state thresholds were increases (Fig. 3.5), and an above-threshold value of the ratio on which the character was based always implied being scored as [0] rather than [1], specimens coded as state [0] in Currie and Evans (2019) for modified characters were changed to [?] for all taxa for which we were unable to take measurements or obtain a reasonable estimate of the ratio in question. For characters that remained binary, this was due to uncertainty regarding whether the taxa in question should be reassigned state [1] because they fell just below the new threshold, or should retain state [0] because they fell within the new range for that state. For characters that were reformulated as multivariate, the same possibilities existed alongside a third, namely that the ratio value was high enough to result in the taxon being coded as state [2]. Relative to the original taxon-character matrix, 32 codings (0.48%) were changed in total

The phylogenetic analysis of the modified matrix recovered 205 most parsimonious trees, each with a length of 426 steps. A 50% majority rule consensus tree was constructed from the 205 MPTs, producing a tree with a length of 439 steps, a retention index (RI) of 0.61 and a consistency index (CI) of 0.45 (Fig. 3.7A). The analysis using the original taxon-character matrix from Currie and Evans (2019) recovered 22 most parsimonious trees, each with a length of 412

steps. Perhaps because the parameters of the analysis were slightly different, this result differs from the 48 MPTs with lengths of 400 reported by Currie and Evans (2019). The 22 MPTs recovered in this analysis were used to construct a 50% majority rule consensus tree with a length of 416 steps, an RI of 0.64 and a CI of 0.47 (Fig. 3.7B).

The topologies of the consensus trees produced from the modified matrix and the original matrix (Currie and Evans 2019) are similar in recovering the family and subfamily clades Dromaeosaurinae Matthew and Brown, 1922, Microraptorinae Senter et al., 2004, Saurornitholestinae Longrich and Currie, 2009, Troodontidae, Unenlagiinae Bonaparte, 1999, and Velociraptorinae. Eudromaeosauria is recovered as sister to *Bambiraptor feinbergi* (Fig. 3.7). By contrast, the two consensus trees differ in that the tree from the new analysis includes more polytomies and fails to recover a monophyletic Halszkaraptorinae Cau et al., 2017. The new analysis does, however, recover Troodontidae as sister to Dromaeosauridae, while the analysis of the original dataset posits Troodontidae as sister to a clade of taxa typically considered unenlagiines (Fig. 3.7B). The new analysis recovers *Achillobator giganticus* and *Utahraptor ostrommaysi* as members of Dromaeosaurinae, as in some previous studies (Longrich and Currie 2009, Turner et al. 2012, Evans et al. 2013), in contrast to their recovery as velociraptorines by Currie and Evans (2019). The new analysis agrees with that of the original dataset in recovering a paraphyletic *Velociraptor* but differs in placing *Adasaurus mongoliensis* Barsbold 1983, in a polytomy with *Velociraptor osmolskae* and the clade containing *Linheraptor exquisitus* and *Tsaagan mangas* (Fig. 3.7A).

Adjustments to character state thresholds in the modified taxon-character matrix have caused the reconstructed ancestral states for characters 8 and 29 to change from [0] in the original analysis by Currie and Evans (2019) to [1] in this analysis following character state re-

evaluation (Fig. 3.7A). Partly as a result, a total of 18 state changes from the ancestral states occur across the tree for all tested characters, rather than only 10 changes as implied by analysis of the original matrix (Fig. 3.7). CI values for characters analysed or added in this study are given in Table 3.4. Those for characters 8 and 22 are lower in the new analysis (0.25 for both) than in the analysis of the original matrix (0.33 and 0.50, respectively), whereas those for characters 28 and 29 are higher (0.29 and 0.40, respectively, compared to 0.25 and 0.33). The new characters proposed in this study have CI values of 0.33 (181) and 1 (182).

3.4 Discussion

3.4.1 Maxilla length/height ratio as a proxy for snout shape

The proportions of the premaxilla can be predicted from those of the maxilla for specimens within Eudromaeosauria (Fig. 3.2), suggesting that the maxilla could be used to infer the overall profile of the snout in lateral view. The slope of the line of best fit is less than one, indicating that the maxilla is longer in proportion to its height than the premaxilla. This is also indicated by the fact that dromaeosaurids have generally lower premaxillary length-to-height values (Fig. 3.5F) than maxillary length-to-height values (Fig. 3.6B). Overlap between Asian and North American taxa is minimal with respect to premaxillary proportions, and nonexistent with respect to maxillary ones. However, there is no significant difference in the ratio of premaxilla length to maxilla length between Asian and North American taxa (Fig. 3.5D), an unsurprising result given that the sizes of these elements must be correlated. The premaxilla-to-maxilla length ratio is nevertheless higher on average in North American taxa than in Asian ones (Fig. 3.5D), a difference that probably results primarily from the tendency of the maxilla to be relatively short in North American eudromaeosaurians. Inferring some aspects of snout morphology from the maxilla alone (Evans et al. 2013) seems reliable given the evidence that maxillary shape is a

good predictor of premaxillary shape within Eudromaeosauria (Fig. 3.2). From the regression results and observed distributions of values for premaxillary and maxillary ratio-based characters, it can be inferred that the snout varies in shape between eudromaeosaurian taxa as a modular unit. Modular variation in snout shape has also been observed in modern carnivorans (Slater et al. 2009, Ferreira-Cardoso et al. 2019). Modular variation, the result of modular evolution, often involves suites of anatomical features that are related to a specific function, such as flight in pterosaurs (Lü et al. 2010) or skull shape in canids (Slater et al. 2009). Within the maxilla, the length of the anterior ramus has been used as a proxy for elongation of the entire element (Evans et al. 2013). However, it is shown here that the length-to-height ratio of the anterior ramus shows less continuous variation than the ratio between the length of the anterior process and that of the whole maxilla (Fig. 3.5G-J). This difference demonstrates some level of independence between the two ratios, so using the proportions of the anterior ramus to infer maxillary length is cautioned against.

3.4.2 Maxillary shape variation and clustering

The PCA recovers groups of specimens that cluster together based on various combinations of taxonomic affinity and geographic range (Fig. 3.3). Within Eudromaeosauria, maxillae do cluster in ways reflective of tree topologies obtained in previous phylogenetic analyses (Longrich and Currie 2009, Evans et al. 2013, Currie and Evans 2019). Asian taxa other than *Achillobator giganticus* cluster together (Fig. 3.4), but *Austroraptor cabazai* falls close to the cluster containing *Velociraptor* specimens in the total cluster analysis (Fig. 3.4A). *Achillobator giganticus* shows a great deal of similarity to North American taxa, plotting close to eudromaeosaurians from this continent (Fig. 3.3) and clustering with them rather than with other Asian taxa (Fig. 3.4). *Achillobator giganticus* is known from the lower Upper Cretaceous of

Mongolia (Perle et al., 1999), making it much older than the derived Asian dromaeosaurids occupying the negative extreme of PC 1 (Fig. 3.3C, D). In variants 2 and 3 of the PCA, *Deinonychus antirrhopus* plots on the extreme positive end of the range of North American dromaeosaurids along PC 1, and the extreme negative end for PC 2 (Fig. 3.3C, D). This species is known from the Albian of Montana (Ostrom, 1969) and like *Achillobator giganticus* has a much more stoutly built maxilla, with a relatively low length-to-height ratio, than the Campanian-Maastrichtian dromaeosaurids in the analysis. *Atrociraptor marshalli* represents a major outlier to inferred general trends in having independently acquired a stout maxillary morphology during the Late Cretaceous, in contrast to the elongation seen in many coeval species (Figs. 3.3, 3.4, 3.7). The stout maxilla of this taxon is peculiar and, along with the hyper-elongate maxilla of *Austroraptor cabazai*, demonstrates the disparity in form of dromaeosaurid snouts.

Bambiraptor feinbergi was consistently recovered close to the *Saurornitholestes langstoni* cluster (Figs. 3.3, 3.4). A close relationship between *Bambiraptor feinbergi* and *Saurornitholestes langstoni* has been suggested numerous times, some authors having hypothesized that the former represents a juvenile of the latter (Burnham et al. 2000, Currie and Varricchio 2004, Turner et al. 2012). The consistent placement of *Bambiraptor* near *Saurornitholestes*, and the minimal effect on PCA loadings of removing *Bambiraptor feinbergi* from the analysis further supports a close relationship and has implications for dromaeosaurid ontogeny. If *Bambiraptor* is a junior synonym of *Saurornitholestes*, then growth of the maxilla in this taxon appears to be approximately isometric, in contrast to the tendency of the maxilla to undergo many proportional changes during ontogeny in other theropods such as tyrannosaurids (Currie 2003b, 2003a). Due to the small sample size available for *Bambiraptor* and

Saurornitholestes, neither the possible synonymy of these taxa nor their ontogenetic patterns can be readily analysed further. It is noteworthy, however, that our results are consistent with previous suggestions that *Bambiraptor* might be a junior synonym of *Saurornitholestes*.

Linheraptor exquisitus and *Tsaagan mangas* plotted close to each other in each PCA (Fig. 3.3) and were recovered in the cluster analysis as most similar to each other (Fig. 3.4), mirroring the sister relationship between these species posited by the phylogenetic analysis (Fig. 3.7). This close phenetic similarity and phylogenetic proximity is of interest, as the two species have been proposed to be synonymous (Turner et al. 2012). However, Xu et al. (2015) argued that enough discrete differences existed between the holotypes of *Linheraptor exquisitus* and *Tsaagan mangas* to justify their taxonomic separation, especially in the absence of a larger sample that might provide more insight into intraspecific variation. When only eudromaeosaurian maxillae are considered, the two specimens are almost indistinguishable (Fig. 3.3D), but with the addition of outgroups they plot further apart (Fig. 3.3A, B). The degree of separation between them in the total analysis is no greater than that between some pairs of congeneric specimens, however, suggesting that the holotype maxillae of *Linheraptor exquisitus* and *Tsaagan mangas* are at least as similar as some specimens that are assigned to a single genus. Given the similarity between these specimens and their close phylogenetic relationship (Fig. 3.7), this analysis supports the interpretation that these species could reasonably be classified in the same genus. Despite their morphological similarity, however, the two species are distinguished by some character states, a point reinforced by the fact that they are coded differently for characters 8 and 22 based on the revised thresholds proposed in this study (Table 3.3 and Fig. 3.7).

Another finding of note is that the *Velociraptor* specimens in the analysis form a cluster (Figs. 3.3, 3.4). *Velociraptor osmolskae* clusters within the range of variation of *V. mongoliensis* specimens provided MPC-D 100/982, a partially described specimen that plots as the farthest outlier in the *Velociraptor* cluster, is accepted as a member of *V. mongoliensis*. MPC-D 100/982 is displaced negatively along PC 2 (Fig. 3.3A, C, D), largely because of its elongate antorbital fossa. It differs in this respect from all other *Velociraptor* specimens but plots closest in the PCA ordinations to AMNH FARB 6515, the holotype of *V. mongoliensis* (Figs. 3.3A, C, D, 3.4A). MPC-D 100/982 is coded [0] for character 182, while all other *Velociraptor* specimens are coded [1] (A 2.5). The range for undoubted *V. mongoliensis* specimens with respect to the ratio that provides the basis for this character is 0.78-0.85, while *V. osmolskae* has a ratio of 1.07, the highest observed value for a specimen with state [1] (Fig. 3.6C). MPC-D 100/982 has a ratio of 1.17, which is the lowest observed value for a specimen having state [0] but is nevertheless 139% greater than any specimen referred to *Velociraptor mongoliensis*. A description of this specimen and review of variation within the genus *Velociraptor* is reported in Chapter 4. The PCA performed here highlights the large variation that exists with respect to the proportions of the antorbital fossa, supporting the use of this feature as a phylogenetic character.

3.4.3 Character assessment

The characters used previously by Currie and Evans (2019) that are tested here were all based on continuous data, but coded in terms of discrete states (Simões et al. 2016), raising the possibility that specimens falling on or near the threshold between states might be coded differently by different researchers. This creates a fundamental problem with repeatability and produces ambiguity for specimens coded according to character state delineations imposed on continuous data without adequate statistical testing. This study attempted to minimize these

difficulties by examining the distribution of the continuous data for each character, to identify natural breaks where character state thresholds could be placed.

Character 8 not only deals with proportions but is also problematic in pertaining to the shape of a fenestra, which is determined by the morphologies of all the surrounding bones (in this case the maxilla, lacrimal, nasal and jugal). For this study only the maxillary portions of the antorbital fenestra and fossa were measured. As a result, the measurements taken here differ from those in previous studies. However, they remain useful in partially capturing the shapes of the antorbital fossa and fenestra (Fig. 3.5A), especially given that the maxilla surrounds most of the fenestra and bears most of the fossa. The CI for character 8, however, dropped from a value of 0.33 based on analysis of the original data matrix of Currie and Evans (2019) to a value of 0.25 based on the revised data matrix presented in this study (Table 3.4). It is possible that the CI could be improved by the addition of another state, as was the case for characters 28 and 29, if the ratio were calculated from measurements taken in the same way. Ideally, however, any increase in the number of character states would be justified by Jenks Optimization analysis. We propose using the measurement method outlined in this study rather than measuring the proportions of the entire fenestra, in order to keep the character rooted in the morphology of a single skeletal element and avoid creating redundant shape characters by simultaneously coding the fenestra and all surrounding bones (Simões et al. 2016).

When the ratio of premaxilla length to maxilla length (character 20) was tested for natural breaks in the continuum of data, all dromaeosaurids measured for this state were found to form a class that could confidently be taken to correspond to state [0] (Fig. 3.5C). The troodontid outgroups used in this study formed a separate class and accordingly were all coded [1], consistent with the coding of Currie and Evans (2019). Character state [0] for this character is

found in this study to be a synapomorphy of Dromaeosauridae (Fig. 3.7). In the context of this study and others that focus on Eudromaeosauria, however, this character is uninformative with regard to phylogenetic interrelationships and also, based on the range of variation within the clade (Fig. 3.5D), not particularly effective for delineating species. This character also suffers from having been defined in terms of a ratio between measurements of two elements, the premaxilla and maxilla, in the absence of prior testing to determine if the shapes of these elements were correlated. This character accordingly pertains to a feature that does not exist in the same way as a structure that might be coded present or absent, and resembles a character describing the shape of an orbit or fenestra in that it is affected by multiple locators (Caldwell 2012, Simões et al. 2016). State changes for characters that pertain to the shapes of features like fenestrae result from an accumulation of changes in the proportions and/or contact relationships of the surrounding bones, and therefore are dependent on multiple skeletal elements. This type of character was identified as problematic by Wilkinson (1995) and classified by Simões et al. (2016) as a Type I A.7 problematic character, suffering from “Unjustified composite locator coding”. However, this study has demonstrated that premaxilla shape can be predicted from maxilla shape within Eudromaeosauria, so characters based on comparisons between their proportions are therefore justified. This only applies, however, if the same pattern of correlation occurs in all taxonomic groups for which the characters in question are being coded in each analysis.

Premaxillary length-to-height ratios (character 22) were found to be widely variable and nearly continuous in their distribution (Fig. 3.5E). The threshold of “at least as tall as long” (Currie and Evans 2019) is subjective, albeit easy to express. The problem, however, is that continuous data are rarely distributed in ways that are maximally convenient. Examining the

range of variation across eudromaeosaurian taxa indicates that character 22, as worded, is a Type II-B problematic character – a continuous character unjustifiably treated as discrete (Simões et al. 2016). Following Jenks Natural Breaks Optimization, a value of 1.35 for the length-to-height ratio is proposed as the threshold between states of this character, replacing the threshold value of one implied by the original wording. The new threshold is appropriate given the data utilized in this study and is subject to change in future analyses that include a different range of taxa. The fit of this character with the reduced matrix tree topology is lower for the analysis of the revised data matrix in this study than the analysis using the matrix from Currie and Evans (2019) (Table 3.4), but it is notable that the codings for several eudromaeosaurians given in previous studies could not be replicated. Based on the previously stated threshold of 1.0, *Bambiraptor feinbergi* (1.57), *Deinonychus antirrhopus* (1.28), *Dromaeosaurus albertensis* (1.12) and *Saurornitholestes langstoni* (1.02) should have been assigned state [0], whereas *Utahraptor ostrommaysi* (0.94 and 1.28), should have been coded as polymorphic and the troodontid *Sinovenator changii* (1.0) should have been assigned state [1]. However, these taxa were all previously coded as the opposite state or as non-polymorphic (in the case of *Utahraptor ostrommaysi*). No complete premaxilla is known for *Dromaeosaurus albertensis*, but even a conservative estimate implies that the length of the premaxillary body in this taxon would have been greater than the premaxilla's subnarial height (A 2.5). Situations such as this emphasize the need for rigorous examination of characters and their states before they are used in a phylogenetic analysis.

The contrasting distributions of the premaxillary length-to-height ratio in Asian and North American eudromaeosaurians, with higher values typically occurring in Asian members of the group, support the concept of a morphological dichotomy between taxa from the two

continents (Fig. 3.5F). However, neither Asian nor North American taxa occur exclusively on one side of the threshold between character states. *Bambiraptor feinbergi* falls above the threshold (premaxilla length-to-height of 1.57) while *Linheraptor exquisitus* falls below (1.22). The threshold cleanly separates observed values into two ranges defining character states within Eudromaeosauria but could cause problems like those resulting from the original character formulation if more taxa were added to the analysis.

Both Characters 20 and 22 relate to elongation of the premaxilla. While character 22 is based on a single element's proportions and thus avoids unjustifiably coding multiple locators into a single character (Wilkinson 1995, Caldwell 2012, Simões et al. 2016), character 20 does exhibit this deficiency. Character 22 also directly captures elongation of the element, while character 20 focuses on the length of the premaxilla only in relation to that of the maxilla. The former addresses the shape of the premaxilla while the latter considers only one measurement of size. Of the two characters, character 22 is clearly worth keeping provided that the threshold value between character states is chosen with careful consideration for observable thresholds. Character 20 serves the purpose of distinguishing dromaeosaurids from outgroup clades (Fig. 3.7) but is potentially redundant with character 22. The inclusion of character 20 is justified here, even though the character combines information from the premaxilla and maxilla, based on the evidence that the proportions of the latter element can predict those of the former within the study clade (Fig. 3.2).

Character 28 concerns the ratio of anterior ramus length to total length of the maxilla. The threshold value between states [0] and [1] used here for this character (0.26) is similar to that used in previous studies (0.25) (Longrich and Currie 2009, Evans et al. 2013, Currie and Evans 2019). However, the GVF and CI values for this character were improved by adding a third state

[2] (Fig. 3.5G). Based on the observed distribution of the data, a value of 0.36 is proposed as the threshold between states [0] and [2] of this character. Like character 20, this character deals with the ratio of two anteroposterior length measurements on a single element. The wording of the character has been modified to better reflect its nature, and “elongation” has been removed from the character description (A 2.5). While Asian and North American eudromaeosaurian specimens seem to show distinct distributions of the ratio described by this character (Fig. 3.5H), with Asian taxa having higher values, the North American taxa once again fall across the character threshold, and the extreme upper end of their range of variation overlaps with the lower end of the range for Asian taxa (Fig. 3.5H). The clade Saurornitholestinae is distinct from other North American eudromaeosaurians in having long anterior rami more like those of Asian taxa (Fig. 3.7A). Addition of a third state improves the fit of this character on the tree generated from the matrix with all tested characters removed (CI: 0.25-0.29, relative to the results from analysis of the Currie and Evans (2019) matrix (Table 3.4). This character is a good representation of the proportional length of the anterior ramus and is worth keeping subject to future modification as needed.

Character 29 describes the elongation of the anterior ramus of the maxilla and has been reworded in terms of the length-to-height ratio of this feature (A 2.5). Although the character refers to the elongation of a feature on the maxilla, it has been suggested that the length-to-height ratio of the anterior ramus correlates with that of the maxilla as well (Evans et al. 2013). As the previous character shows, however, the relationship between anterior ramus length and maxillary length may vary (Fig. 3.5G-H). The distribution of the length-to-height ratio of the anterior ramus in dromaeosaurids shows two gaps: 1.02-1.22, and 1.75-2.15. While both these gaps are larger than those for character 28 (0.25-0.27, and 0.36-0.38), the separation between state [1] and

state [0] is still rather limited. However, the previously proposed criterion of “as long as tall” (Currie and Evans 2019) does seem to require only a slight adjustment to serve as a maximally informative threshold between two character-states, given our data. A threshold positioned at 1.12 times as long as tall is separated by about 0.1 from the nearest data point either above or below the threshold (Fig. 3.5I). The only Asian eudromaeosaurian to be coded [1] is *Achillobator giganticus*, and all other Asian taxa are coded as elongate [0] or hyper-elongate [2] (A 2.5). North American eudromaeosaurians all have a short anterior ramus, apart from *Acheroraptor temertyorum* (1.22), which has the lowest ratio value for any taxon with an elongate ramus in the dataset. This is a strong character for distinguishing derived Asian dromaeosaurids from North American ones (Fig. 3.7) and supports the hypothesis of Evans et al. (2013) that *Acheroraptor temertyorum* has Asian affinities. The elongate anterior ramus condition is independently acquired by several taxa, but this trait unites the velociraptorines other than *Deinonychus antirrhopus* (Fig. 3.7). The fit of the revised character is an improvement from Currie and Evans (2019), going from a CI of 0.33 in their study to 0.40 with its revised state delineations in this study (Table 3.4). Characters 28 and 29 both describe the length of the anterior ramus, albeit relative to different measurements. The distributions of ratio values for the two characters also appear similar. To avoid redundancy in phylogenetic data matrices, it may be appropriate to remove one of these characters. Based on their respective fits (i.e. CI and GVF values), character 29 is preferred for analysis of eudromaeosaurian phylogeny, although both characters were retained in this study.

The first new character proposed here (181) was investigated after carrying out a regression of premaxillary length-to-height ratio on maxillary length-to-height ratio within Eudromaeosauria (Fig. 3.2). The ranges of variation found in Asian and North American

dromaeosaurids are distinct from one another and the gap between these groups is rather close to the threshold for the character state delineation, as found by the Jenks Optimization. The results indicate that the maxilla tends to be relatively elongate in Asian eudromaeosaurians (Fig. 3.6A, B). A distinct threshold is found at a maxilla length-to-height ratio of 2.62 (Fig. 3.6A). A gap of at least 0.08 separates this threshold from the nearest data point on either side. Given that all North American dromaeosaurids fall well below the threshold, elongation of the entire maxilla is clearly sometimes more pronounced than the elongation of the anterior ramus (Figs. 3.5G-J, 3.6A). This character has a CI of 0.33, equal to the value for characters 8 and 29 in the original taxon-character matrix of Currie and Evans (2019) (Table 3.4), although this might change if further characters or taxa are added to the matrix in the future.

The second new character, 182, was suggested by the results of the PCA, which found that antorbital fossa length and height consistently explained a large amount of variation along most axes, regardless of taxonomic sampling (Fig. 3.3, A 2.4). This character has a CI of 1 given the data in our analysis, largely because the elongate state [0] occurs almost exclusively in derived troodontids such as *Saurornithoides mongoliensis* and *Zanabazar junior* (which could not be coded into the matrix), and in the microraptorine *Sinornithosaurus millenii* and possible microraptorine *Shanag ashile*. This character would be worth examining over a broader range of taxa, but in this study a short antorbital fossa (≤ 1.07) is inferred to represent the ancestral condition, with elongation potentially having taken place in microraptorine taxa (Fig. 3.7A). Elongation may also have occurred in derived troodontids, but the antorbital fossa appears short throughout Eudromaeosauria except in the single *Velociraptor* specimen MPC-D 100/982. The elongate condition of the antorbital fossa in this specimen may prove to represent an apomorphy

of a new species within *Velociraptor*, assuming further investigation confirms that the shape of the fossa falls outside the range of variation seen in *V. mongoliensis*.

3.4.4 Phylogenetic analysis

The main phylogenetic analysis carried out in this study recovers a topology more like those found in previous analyses (Longrich and Currie 2009, Turner et al. 2012) than the tree presented by Currie and Evans (2019), or that recovered from analysis of their dataset in this study (Fig. 3.7). The most important differences concern relationships within Eudromaeosauria, in that analysis of the Currie and Evans (2019) dataset recovers *Achillobator giganticus* and *Utahraptor ostrommaysi* as velociraptorines (Fig. 3.7B), while my analysis recovers them as part of a polytomy within Dromaeosaurinae (Fig. 3.7A). In my analysis I was able to code more characters for *Utahraptor ostrommaysi* than in previous studies, and to revise some codings for *Achillobator giganticus* and *Dromaeosaurus albertensis* to better reflect the available data. While it cannot be said for certain which of multiple conflicting topologies best captures the true phylogeny, the amount of topological variation that resulted from small modifications to the matrix suggests that either the characters in question are important for stabilizing the tree topology, or the whole matrix needs to be reworked to better reflect the data. Reworking, if indeed necessary, could focus particularly on proportionate characters, either clearly defined ratios or vaguer statements about the dimensions or positions of specific features, and on anything else that could be quantified to some extent (Simões et al. 2016). Repeatability is vital for producing consistent trees and, using the methods outlined in this study, continuous data can be assessed prior to character construction in order to determine if the quantitative character can be discretized or if the character should be left continuous (Goloboff and Mattoni 2006).

3.4.5 Evolutionary trends

The PCA shows an overall negative shift along PC 1 of the Late Cretaceous dromaeosaurids relative to *Deinonychus antirrhopus* and *Achillobator giganticus*, which are respectively Early Cretaceous and early Late Cretaceous in age (Fig. 3.3C, D). *Achillobator giganticus* and *Deinonychus antirrhopus* are taxa from their respective geographic regions with the most positive scores on PC 1, but Asian taxa all have more negative scores on PC 1 than their North American counterparts. This shift is indicative of elongation of the anterior ramus and dorsoventral shallowing of the maxilla, as implied by the significant height variable loadings on PC 1. *Achillobator giganticus* retains a stout maxilla bearing less resemblance to those of other Asian taxa than to those of *Acheroraptor temertyorum* (Fig. 3.3D) and *Saurornitholestes langstoni*, the North American forms with the lowest scores on PC 1 (Fig. 3.3C, D). The phylogenetic analysis performed with the new dataset shows a corresponding trend in that the more derived taxa have character states for characters #22, #29, and #181 that are reflective of elongation (state [0], or in some cases state [2] for character 181), while *Deinonychus antirrhopus* is coded as short (state [1]) for the same ratio-based characters (Table 3.3 and Fig. 3.7). The phylogeny suggests a distinct shift to elongate forms in the Late Cretaceous of Asia, which did not occur to the same extent in North America. The discrepancy may be due to faunal variation (Dashzeveg et al. 1995) between the two continents (Brinkman 1990, Eberth and Brinkman 1997), or abiotic environmental differences (Dashzeveg et al. 2005, Dingus et al. 2008, Eberth and Braman 2012)

Faunal variation between Asia and North America could have driven the dichotomy in snout shape, in that a differing range of available prey items could have resulted in the emergence of distinct prey acquisition strategies in dromaeosaurids (Therrien et al. 2005, Walmsley et al. 2013). The relatively long jaws of Asian taxa would have been effective at

quickly snapping at and grabbing small prey items, while the shorter and dorsoventrally deeper jaws of North American taxa would have been better suited to grabbing and holding larger prey. In modern ecosystems, a similar relationship between jaw proportions and the mode of prey acquisition exists among canids (Slater et al. 2009). While a Beam Theory (Biknevicius and Ruff 1992) analysis found little functional variation among available dromaeosaurid mandibles (Therrien et al. 2005), this previous study was limited to just a handful of dromaeosaurid specimens and the authors did postulate a likely difference in feeding mode between *Dromaeosaurus albertensis* and more *Velociraptor*-like forms. While the mandible may have performed similar functions during feeding in all or most eudromaeosaurians, it is possible that the morphology of the cranium reflects different adaptations to handle the forces involved (Rayfield et al. 2001, Sakamoto 2010).

A potentially useful living analogue is provided by canids, which are not phylogenetically close to eudromaeosaurians but do resemble them ecologically in occupying a small-medium carnivore niche. Slater et al. (2009) were able to assess functional models of a variety of canid taxa with varying snout morphologies and correlate them with observed prey preferences. They tested the effects of “intrinsic” forces exerted by the jaw musculature and “extrinsic” forces exerted by struggling prey on finite element models of canid crania and examined the relationship between jaw proportions and preferred prey size. Long-snouted canids (e.g. *Canis simensis*, Ethiopian wolf) were found to specialize on small prey, which could be captured most effectively with rapid jaw movements, while short-snouted canids (e.g. *Lycaon pictus*, African wild dog) specialized on large prey that could only be overcome with powerful bites. Slater et al. (2009) also found that canids with intermediate jaw proportions (e.g. *Canis mesomelas*, black-backed jackal) tended to have a more generalist diet.

Analyses of snout shape and prey acquisition in modern predators have found that the mandible showed relatively little variation compared to the rostrum of the skull (van Cakenberghe et al. 2002, Slater et al. 2009). Indeed, more morphological characters used in phylogenetic analyses have been derived from the rostrum rather than from the mandible (Evans et al. 2013, 2017, Currie and Evans 2019), corroborating the higher variability of the former. In the PCA results for eudromaeosaurians (Fig. 3.3C-D), elongation of the maxilla is captured to a large extent by PC 1. Taxa scoring high on this axis (*Atrociraptor marshalli* and *Deinonychus antirrhopus*) likely had short, deep snouts and resembled the short-snouted canids in the analysis of Slater et al. (2009) in specializing on larger prey. Taxa with moderate PC 1 scores (*Acheroraptor temertyorum*, *Achillobator giganticus*, and *Saurornitholestes langstoni*) were potentially intermediate in snout shape and more generalist in feeding habits, while those with low PC 1 scores (all Asian taxa observed in this study except for *Achillobator giganticus*) probably had elongate snouts and specialized on small quick prey. Circumstantial evidence in support of this interpretation comes from the initial discovery of *Deinonychus antirrhopus*, which involved three individuals positioned around a specimen of the much larger herbivorous dinosaur *Tenontosaurus tilleti* Ostrom, 1970. The group of *Deinonychus antirrhopus* may have been acting analogously to African wild dogs in attacking a large prey animal, although it is also possible that they were engaged in scavenging. Gregarious behaviour in theropods is still poorly understood but a number of sites have yielded multiple theropod individuals that may have been together in life (Currie and Eberth 2010). Currie and Eberth (2010) outlined several possible degrees of gregariousness, ranging from coordinated pack hunting to mutual tolerance while independently taking advantage of abundant food resources in a particular location. Whether the three co-occurring *Deinonychus antirrhopus* worked as a team to bring down the *Tenontosaurus*

tilleti (Ostrom 1969) or simply happened to be feeding on the same carcass, perhaps with some degree of agonistic behaviour towards one another (Roach and Brinkman 2007), their manner of occurrence in the fossil record implies they were likely together at the time of death (Currie and Eberth 2010).

There is also some fossil evidence against the possibility that a discrepancy in prey choice drove differentiation in snout morphology between Asian and North American eudromaeosaurians, as both *Saurornitholestes* and *Velociraptor* have been reported to have fed, at least occasionally, on pterosaurs (Currie and Jacobsen 1995, Hone et al. 2012). The evidence of pterosaur consumption by *Saurornitholestes* is from a tooth-marked partial azhdarchid skeleton that appears to have been scavenged (Currie and Jacobsen 1995), while one known *Velociraptor* specimen has a broken pterosaur long bone preserved as stomach contents (Hone et al. 2012). *Velociraptor* also preyed on *Protoceratops*, as in the case of the famous “fighting dinosaurs” specimen, MPC-D 100/25 (Kielan-Jaworowska and Barsbold 1971). Tooth-marked bone fragments from the Upper Cretaceous of Inner Mongolia, China provide additional evidence for this trophic relationship, or at least for feeding on basal neoceratopsians by velociraptorines (Hone et al. 2010). A recent analysis of cranial shape variation across pangolin species also showed that snout shape can vary geographically and contribute to taxonomic variation, without any corresponding difference in prey selection (Ferreira-Cardoso et al. 2019). Pangolins, however, are specialized insectivores analogous to anteaters, and may not represent an informative point of comparison to predatory animals such as canids or dromaeosaurids regarding snout variation and prey specialization.

Another possibility is that the elongation of the maxilla was to accommodate expansion of the pneumatic sinuses (Witmer 1997). The lengths of the anterior ramus and antorbital fossa

have large loadings in the ordinations, explaining most of the variation along PCs 1, 2 and 3. The exact function of the sinuses within the antorbital fossa region and the anterior ramus is poorly understood, although numerous hypotheses have been proposed. Most notably, the sinuses may have contributed to thermoregulation, an interpretation supported by the association of the sinuses with both jaw adductor muscles and extensive vasculature in modern birds (Witmer 1997, Witmer and Ridgely 2008). In modern birds, alternating contraction, and relaxation of the adductor musculature in the orbital region of the skull appears to actively pump air through the sinuses, permitting exchange of heat with the blood in the surrounding vessels. A similar mechanism may have operated in non-avian theropods, including dromaeosaurids. Actively ventilated sinuses could presumably also have been a site for exchange of moisture, which may have been physiologically important in long-snouted dromaeosaurids given their association with predominantly arid environments (Norell and Makovicky 1997, 1999, Dashzeveg et al. 2005, Norell et al. 2006, Dingus et al. 2008, Xu et al. 2010a).

The ancestral states inferred in this study for characters pertaining to maxillary proportions suggest the antorbital fossa was ancestrally short in dromaeosaurids, while the anterior ramus was ancestrally elongate (Fig. 3.7). The transition to anteroposteriorly short maxillae, and short anterior rami, occurred near the base of Eudromaeosauria. Elongation of the antorbital fossa was acquired early in dromaeosaurids and troodontids but lost in various eudromaeosaurian taxa. Previous studies have inferred homology of the elongate anterior ramus between Asian eudromaeosaurians and the Late Cretaceous North American taxon, *Acheroraptor temertyorum* (Evans et al. 2013). The results in this study imply numerous acquisitions of elongate anterior rami throughout dromaeosaurid evolution, but also show frequent elongation of the anterior ramus within Asian eudromaeosaurians (Fig. 3.7).

A faunal dispersal is hypothesized to have occurred both from North America to Asia during the Albian-Aptian (Russell 1993) and from Asia to North America during the Late Cretaceous (Evans et al. 2013), and this remains possible. The stout maxillae of *Achillobator giganticus* and *Deinonychus antirrhopus* compared to Late Cretaceous species from their respective continents, is suggestive of a possible dispersal of an ancestral eudromaeosaurian with an ancestrally stout snout morphology during the Early Cretaceous. However, despite circumstantial evidence suggesting Campanian-Maastrichtian faunal dispersal from Asia (Russell 1993), the possible dispersal of eudromaeosaurian taxa seems to have been restricted to the Maastrichtian, given that *Acheroraptor temertyorum* is the only known North American taxon with Asian affinities and the only other Maastrichtian eudromaeosaurian, *Atrociraptor marshalli*, has the extreme opposite maxillary proportions. Faunal dispersals from Asia to North America are inferred for clades of large-bodied animals such as hadrosaurids (Evans 2010), tyrannosaurids (Brusatte et al. 2010, 2016) and ceratopsians (Xu et al. 2010b), and for some medium-sized clades such as oviraptorosaurs (Funston and Currie 2016). While *Acheroraptor temertyorum* does share some characteristics with Asian eudromaeosaurians from the Late Cretaceous, they mostly concern elongation of the anterior ramus. This analysis shows that such features were repeatedly acquired by various non-eudromaeosaurian taxa (Fig. 3.7), most notably in the case of the extremely long-snouted *Austroraptor cabazai*. *Acheroraptor temertyorum* also shares features with *Atrociraptor marshalli*, including a short antorbital fossa, a maxillary fenestra approaching but not touching the anterior margin of the antorbital fossa, and lack of contact between the maxillary fenestra and the ventral margin of the antorbital fossa, as observed in UALVP 49389. Among eudromaeosaurians, the homologies of proportionate characters are much more difficult to track than those of discrete/presence absence characters, partly because

proportionate features show both wide variation and considerable overlap between taxa (Simões et al. 2016). The range of variation for ratio-based characters within a species can also be difficult to ascertain due to the poor preservation potential of small-medium sized eudromaeosaurians (Turner et al. 2012, Brown et al. 2013). Until more specimens can be added to the analysis and our understanding of intraspecific variation improves, it will remain generally preferable to rely on characters that are not based on simple ratios. Although *Acheroraptor temertyorum* may share morphological affinities with Asian taxa that indicate common ancestry, it is equally possible that the shared features were acquired convergently.

3.5 Conclusions

Maxillae of eudromaeosaurians are informative regarding both overall snout morphology and phylogenetic relationships. Phenetic clustering of maxillae replicates some pairwise relationships observed in phylogenetic analysis but cannot provide information on patterns of ancestral character change. Previously constructed proportionate characters required minor revisions to thresholds delineating character states, except in the case of a character (character 22) based on the premaxillary length to height ratio. Characters such as this emphasize the difficulty of producing good discrete characters from continuous data. Analysing the distributions of such data for the presence of gaps is necessary to justify the use of discrete states to code variables that are continuous in nature. Performing such quick optimization tests improves repeatability of coding for phylogenetic analysis and is encouraged as a preliminary step before coding begins. Elongation of skeletal features may be biologically meaningful, but an intuitive character state threshold such as “longer than tall” will be suboptimal if many observed values of the ratio used to capture elongation in fact fall on or near the threshold. Partitioning of continuous data into discrete character states should only be done with great care and should be

justified by analysis of empirical data. If no distinct break in the data distribution can be observed, then the data should be left as continuous. Discrete characters generated from continuous data are best used for restricted taxonomic groups that have relatively small ranges of variation and are less likely to lack gaps in the distribution of values of any given quantitative character.

Based on proportionate data collected from linear measurements of maxillae across Eudromaeosauria and several outgroup taxa, a distinct difference exists in snout proportions between Asian and North American eudromaeosaurians. These results corroborate previous hypotheses that long snouts are characteristic of Asian taxa whereas tall, anteroposteriorly short snouts are characteristic of North American taxa. PCA suggests potentially useful ratio-based characters by identifying features with high degrees of variation. Leading up to the end of the Cretaceous, a morphological shift toward elongate snout morphology occurred across Eudromaeosauria. It is unclear what drove this transition, but differences in snout proportions between Asian and North American faunal assemblages are suggestive of variation in feeding behaviour, regarding both prey selection and jaw mechanics.

3.6 Literature Cited

- Barsbold, R. 1983. Carnivorous dinosaurs from the Cretaceous of Mongolia. The Joint Soviet-Mongolian Palaeontological Expedition, **19**: 117.
- Barsbold, R., and Osmólska, H. 1999. The skull of *Velociraptor* (Theropoda) from the Late Cretaceous of Mongolia. *Acta Palaeontologica Polonica*, **44**: 189–219.
- Biknevicius, A.R., and Ruff, C.B. 1992. The structure of the mandibular corpus and its relationship to feeding behaviours in extant carnivorans. *Journal of Zoology*, **228**: 479–507. doi:10.1111/j.1469-7998.1992.tb04450.x.
- Bonaparte, J. 1999. Tetrapod faunas from South America and India: A palaeobiogeographic interpretation. *PINSA*, **65**: 427–437.
- Brinkman, D.B. 1990. Paleocology of the Judith River Formation (Campanian) of Dinosaur Provincial Park, Alberta, Canada: Evidence from vertebrate microfossil localities. *Palaeogeography, Palaeoclimatology, Palaeoecology*,: 18.
- Brown, C.M., Evans, D.C., Campione, N.E., O'Brien, L.J., and Eberth, D.A. 2013. Evidence for taphonomic size bias in the Dinosaur Park Formation (Campanian, Alberta), a model Mesozoic terrestrial alluvial-paralic system. *Palaeogeography, Palaeoclimatology, Palaeoecology*, **372**: 108–122. Elsevier B.V. doi:10.1016/j.palaeo.2012.06.027.
- Brusatte, S.L., Averianov, A., Sues, H.-D., Muir, A., and Butler, I.B. 2016. New tyrannosaur from the mid-Cretaceous of Uzbekistan clarifies evolution of giant body sizes and advanced senses in tyrant dinosaurs. *Proceedings of the National Academy of Sciences*,: 201600140. doi:10.1073/pnas.1600140113.
- Brusatte, S.L., Norell, M. a, Carr, T.D., Erickson, G.M., Hutchinson, J.R., Balanoff, A.M.,

- Bever, G.S., Choiniere, J.N., Makovicky, P.J., and Xu, X. 2010. Tyrannosaur paleobiology: new research on ancient exemplar organisms. *Science*, **329**: 1481–1485.
doi:10.1126/science.1193304.
- Bull, A.J.J., Huelsenbeck, J.P., Cunningham, C.W., Swofford, D.L., and Waddell, P.J. 1993. Partitioning and combining data in phylogenetic analysis. *Society of Systematic Biologists*, **42**: 384–397.
- Burnham, D.A., Derstler, K.L., Currie, P.J., Bakker, R.T., Zhou, Z., and Ostrom, J.H. 2000. Remarkable new birdlike dinosaur (Theropoda: Maniraptora) from the Upper Cretaceous of Montana. *The University of Kansas Paleontological Contributions*, **13**: 14.
- van Cakenberghe, V., Herrel, A., and Aguirre, L.F. 2002. Evolutionary relationships between cranial shape and diet in bats (Mammalia : Chiroptera). *In* *Topics in Functional and Ecological Vertebrate Morphology*. Edited by P. Aerts, K. D’Aour, A. Herrel, and R. Van Damme. Staker Publishing. pp. 205–236.
- Caldwell, M.W. 2012. A challenge to categories: “What, if anything, is a mosasaur?” *Bulletin de la Société Géologique de France*, **183**: 7–34. doi:10.2113/gssgfbull.183.1.7.
- Carr, T.D., Varricchio, D.J., Sedlmayr, J.C., Roberts, E.M., and Moore, J.R. 2017. A new tyrannosaur with evidence for anagenesis and crocodile-like facial sensory system. *Scientific Reports*, **7**: 1–11. doi:10.1038/srep44942.
- Cau, A., Beyrand, V., Voeten, D.F.A.E., Fernandez, V., Tafforeau, P., Stein, K., Barsbold, R., Tsogtbaatar, K., Currie, P.J., and Godefroit, P. 2017. Synchrotron scanning reveals amphibious ecomorphology in a new clade of bird-like dinosaurs. *Nature*, **552**: 395–399. Nature Publishing Group. doi:10.1038/nature24679.

- Currie, P., and Varricchio, D.J. 2004. A new dromaeosaurid from the Horseshoe Canyon Formation (Upper Cretaceous) of Alberta, Canada. *In Feathered Dragons. Edited by P.J. Currie, E.B. Koppelhus, M.A. Shugar, and J.L. Wright.* Indiana University Press, Bloomington and Indianapolis. pp. 112–132.
- Currie, P.J. 1995. New information on the anatomy and relationships of *Dromaeosaurus albertensis* (Dinosauria: Theropoda). *Journal of Vertebrate Paleontology*, **15**: 576–591. doi:10.1080/02724634.1995.10011250.
- Currie, P.J. 2003a. Cranial anatomy of tyrannosaurid dinosaurs from the Late Cretaceous of Alberta, Canada. *Acta Palaeontologica Polonica*, **48**: 191–226.
- Currie, P.J. 2003b. Allometric growth in tyrannosaurids (Dinosauria: Theropoda) from the Upper Cretaceous of North America and Asia. *Canadian Journal of Earth Sciences*, **40**: 651–665. doi:10.1139/e02-083.
- Currie, P.J., and Eberth, D.A. 2010. On gregarious behavior in *Albertosaurus*. *Canadian Journal of Earth Sciences*, **47**: 1277–1289. doi:10.1139/E10-072.
- Currie, P.J., and Evans, D.C. 2019. Cranial anatomy of new specimens of *Saurornitholestes langstoni* (Dinosauria , Theropoda , Dromaeosauridae) from the Dinosaur Park Formation (Campanian) of Alberta. *The Anatomical Record*, **04715**: 1–25. doi:10.1002/ar.24241.
- Currie, P.J., and Jacobsen, A.R. 1995. An azhdarchid pterosaur eaten by a velociraptorine theropod. *Canadian Journal of Earth Sciences*, **32**: 922–925. doi:10.1139/e95-077.
- Dashzeveg, D., Dingus, L., Loope, D.B., Swisher, C.C., Dulam, T., and Sweeney, M.R. 2005. New stratigraphic subdivision, depositional environment, and age estimate for the Upper

- Cretaceous Djadokhta Formation, southern Ulan Nur Basin, Mongolia. American Museum Novitates, **3498**: 31. doi:10.1206/0003-0082(2005)498[0001:nssdea]2.0.co;2.
- Dashzeveg, D., Novacek, M.J., Norell, M.A., Clark, J.M., Chiappe, L.M., Davidson, A., McKenna, M.C., Dingus, L., Swisher, C.C., and Altangerel, P. 1995. Extraordinary preservation in a new vertebrate assemblage from the Late Cretaceous of Mongolia. *Nature*, **374**: 446–449.
- Dingus, L., Loope, D.B., Dashzeveg, D., Swisher, C.C., Minjin, C., Novacek, M.J., and Norell, M.A. 2008. The geology of Ukhaa Tolgod (Djadokhta Formation, Upper Cretaceous, Nemegt Basin, Mongolia). American Museum Novitates, **3616**: 1. doi:10.1206/442.1.
- Eberth, D.A., and Braman, D.R. 2012. A revised stratigraphy and depositional history for the Horseshoe Canyon Formation (Upper Cretaceous), southern Alberta plains. *Canadian Journal of Earth Sciences*, **49**: 1053–1086. doi:10.1139/E2012-035.
- Eberth, D.A., and Brinkman, D.B. 1997. Paleocology of an estuarine, incised-valley fill in the Dinosaur Park Formation (Judith River Group, Upper Cretaceous) of southern Alberta, Canada. *Palaios*, **12**: 43. doi:10.2307/3515293.
- Elzanowski, A., and Wellnhofer, P. 1996. Cranial morphology of *Archaeopteryx*: Evidence from the seventh skeleton. *Journal of Vertebrate Paleontology*, **16**: 81–94. doi:10.1080/02724634.1996.10011286.
- Evans, D.C. 2010. Cranial anatomy and systematics of *Hypacrosaurus altispinus*, and a comparative analysis of skull growth in lambeosaurine hadrosaurids (Dinosauria: Ornithischia). *Zoological Journal of the Linnean Society*, **159**: 398–434. doi:10.1111/j.1096-3642.2009.00611.x.

- Evans, D.C., Cullen, T.M., Larson, D.W., and Rego, A. 2017. A new species of troodontid theropod (Dinosauria: Maniraptora) from the Horseshoe Canyon Formation (Maastrichtian) of Alberta, Canada. *Canadian Journal of Earth Sciences*, **54**: 813–826. doi:10.1139/cjes-2017-0034.
- Evans, D.C., Larson, D.W., and Currie, P.J. 2013. A new dromaeosaurid (Dinosauria: Theropoda) with Asian affinities from the latest Cretaceous of North America. *Naturwissenschaften*, **100**: 1041–1049. doi:10.1007/s00114-013-1107-5.
- Ferreira-Cardoso, S., Billet, G., Gaubert, P., Delsuc, F., and Hautier, L. 2019. Skull shape variation in extant pangolins (Pholidota: Manidae): Allometric patterns and systematic implications. *Zoological Journal of the Linnean Society*,: 255–275. doi:10.1093/zoolinnean/zlz096.
- Funston, G.F., and Currie, P.J. 2016. A new caenagnathid (Dinosauria: Oviraptorosauria) from the Horseshoe Canyon Formation of Alberta, Canada, and a reevaluation of the relationships of Caenagnathidae. *Journal of Vertebrate Paleontology*, **36**. doi:10.1080/02724634.2016.1160910.
- Gilmore, C.W. 1924. On *Troodon validus*, an orthopodus dinosaur from the Belly River Cretaceous of Alberta, Canada. *University of Alberta Bulletin*, **1**: 43.
- Godefroit, P., Currie, P.J., Hong, L., Shang, C.Y., and Dong, Z.M. 2008. A new species of *Velociraptor* (Dinosauria: Dromaeosauridae) from the Upper Cretaceous of northern China. *Journal of Vertebrate Paleontology*, **28**: 432–438. doi:10.1671/0272-4634(2008)28[432:ANSOVD]2.0.CO;2.
- Goloboff, P.A., and Mattoni, C.I. 2006. Continuous characters analyzed as such. *Cladistics*, **22**:

589–601.

Hammer, Ø., Harper, D.A.T., and Ryan, P.D. 2001. PAST: Paleontological statistics software package for education and data analysis. *Palaeontologia Electronica*, **4**: 9.

Hone, D., Choiniere, J., Sullivan, C., Xu, X., Pittman, M., and Tan, Q. 2010. New evidence for a trophic relationship between the dinosaurs *Velociraptor* and *Protoceratops*.

Palaeogeography, Palaeoclimatology, Palaeoecology, **291**: 488–492.

doi:10.1016/j.palaeo.2010.03.028.

Hone, D., Tsuihiji, T., Watabe, M., and Tsogtbaatr, K. 2012. Pterosaurs as a food source for small dromaeosaurs. *Palaeogeography, Palaeoclimatology, Palaeoecology*, **331–332**: 27–30.

doi:10.1016/j.palaeo.2012.02.021.

Jackson, D.A. 1993. Stopping rules in principal components analysis : A comparison of heuristical and statistical approaches. *Ecology*, **74**: 2204–2214.

Kielan-Jaworowska, Z., and Barsbold, R. 1971. Narrative of the Polish-Mongolian expeditions 1967-1971. *Palaeontologia Polonica*, **27**: 13.

Kirkland, J.I., Burge, D., and Gaston, R. 1993. A large dromaeosaur (Theropoda) from the Lower Cretaceous of eastern Utah. *Hunteria*, **2**: 1–16.

Larson, D.W., and Currie, P.J. 2013. Multivariate analyses of small theropod dinosaur teeth and implications for paleoecological turnover through time. *PLoS ONE*, **8**.

doi:10.1371/journal.pone.0054329.

Longrich, N.R., and Currie, P.J. 2009. A microraptorine (Dinosauria-Dromaeosauridae) from the Late Cretaceous of North America. *Proceedings of the National Academy of Sciences of the*

- United States of America, **106**: 5002–5007. doi:10.1073/pnas.0811664106.
- Lü, J., Unwin, D.M., Jin, X., Liu, Y., and Ji, Q. 2010. Evidence for modular evolution in a long-tailed pterosaur with a pterodactyloid skull. *Proceedings of the Royal Society B: Biological Sciences*, **277**: 383–389. doi:10.1098/rspb.2009.1603.
- Maddison, W., and Maddison, D. 2017. Mesquite.
- Matthew, W.D., and Brown, B. 1922. The family Deinodontidae, with notice of a new genus from the Cretaceous of Alberta. *Bulletin of the American Museum of Natural History*, **46**: 367–385.
- Meyer, H. von. 1861. *Archaeopteryx lithographica* (Vogel-Feder) und *Pterodactylus* von Solnhofen. *Neues Jahrbuch für Mineralogie, Geognosie, Geologie und Petrefakten-Kunde*, **1861**: 678–679.
- Norell, M.A., Clark, J.M., Turner, A.H., Makovicky, P.J., Barsbold, R., and Rowe, T. 2006. A new dromaeosaurid theropod from Ukhaa Tolgod (Ömnögov, Mongolia). *American Museum Novitates*, **3545**: 51. doi:10.1206/0003-0082(2006)3545[1:andtfu]2.0.co;2.
- Norell, M.A., and Makovicky, P.J. 1997. Important features of the dromaeosaur skeleton: information from a new specimen. *American Museum Novitates*, **3215**: 1–28.
- Norell, M.A., and Makovicky, P.J. 1999. Important features of the dromaeosaurid skeleton II: Information from newly collected specimens of *Velociraptor mongoliensis*. *American Museum Novitates*, **3282**: 1–45.
- Norell, M.A., Makovicky, P.J., Bever, G.S., Balanoff, A.M., Clark, J.M., Barsbold, R., and Rowe, T. 2009. A review of the Mongolian Cretaceous dinosaur *Saurornithoides*

- (Troodontidae: Theropoda). American Museum Novitates, **3654**: 1–63. doi:10.1206/648.1.
- Novas, F.E., Pol, D., Canale, J.I., Porfiri, J.D., and Calvo, J.O. 2009. A bizarre Cretaceous theropod dinosaur from Patagonia and the evolution of Gondwanan dromaeosaurids. Proceedings of the Royal Society B: Biological Sciences, **276**: 1101–1107. doi:10.1098/rspb.2008.1554.
- Osborn, H.F. 1924. Three new Theropoda, *Protoceratops* Zone, central Mongolia. American Museum Novitates,; 1–12.
- Ostrom, J.A. 1970. Stratigraphy and paleontology of the Cloverly Formation (Lower Cretaceous) of the Bighorn Basin area, Wyoming and Montana. Bulletin of the Peabody Museum of Natural History, **35**: 1–250. Peabody Museum of Natural History, Yale University, New Haven CT. doi:10.1086/407120.
- Ostrom, J.H. 1969. Osteology of *Deinonychus antirrhopus*, an unusual theropod from the Lower Cretaceous of Montana. Peabody Museum of Natural History, **30**: 1–165.
- Pearson, K. 1901. LIII. On lines and planes of closest fit to systems of points in space . The London, Edinburgh, and Dublin Philosophical Magazine and Journal of Science, **2**: 559–572. doi:10.1080/14786440109462720.
- Perle, A., Norell, M.A., and Clark, J.M. 1999. A new maniraptoran theropod - *Achillobator giganticus* (Dromaeosauridae)- from the Upper Cretaceous of Burkhan, Mongolia. National University of Mongolia,; 102.
- Rayfield, E.J., Norman, D.B., Horner, C.C., Horner, J.R., Smith, P.M., Thomason, J.J., and Upchurch, P. 2001. Cranial design and function in a large theropod dinosaur. Nature, **409**:

1033–1037. doi:10.1038/35059070.

- Roach, B.T., and Brinkman, D.L. 2007. A reevaluation of cooperative pack hunting and gregariousness in *Deinonychus antirrhopus* and other nonavian theropod dinosaurs. *Bulletin of the Peabody Museum of Natural History*, **48**: 103–138. doi:10.3374/0079-032x(2007)48[103:arocph]2.0.co;2.
- Russell, D.A. 1993. The role of Central Asia in dinosaurian biogeography. *Canadian Journal of Earth Sciences*, **30**: 2002–2012. doi:10.1139/e93-176.
- Sakamoto, M. 2010. Jaw biomechanics and the evolution of biting performance in theropod dinosaurs. *Proceedings of the Royal Society B: Biological Sciences*, **277**: 3327–3333.
- Schott, R.K., and Evans, D.C. 2017. Cranial variation and systematics of *Foraminacephale brevis* gen. nov. and the diversity of pachycephalosaurid dinosaurs (Ornithischia: Cerapoda) in the Belly River Group of Alberta, Canada. *Zoological Journal of the Linnean Society*, **179**. doi:10.1111/zoj.12465.
- Senter, P., Barsbold, R., Britt, B.B., and Burnham, D.A. 2004. Systematics and evolution of Dromaeosauridae (Dinosauria, Theropoda). *Bulletin of Gunma Museum of Natural History*, **8**: 1–20.
- Senter, P., Kirkland, J.I., Bird, J., and Bartlett, J.A. 2010. A new troodontid theropod dinosaur from the lower cretaceous of Utah. *PLoS ONE*, **5**: 1–5. doi:10.1371/journal.pone.0014329.
- Simões, T.R., Caldwell, M.W., Palci, A., and Nydam, R.L. 2016. Giant taxon-character matrices: Quality of character constructions remains critical regardless of size. *Cladistics*,: 1–22.
- Slater, G.J., Dumont, E.R., and Van Valkenburgh, B. 2009. Implications of predatory

- specialization for cranial form and function in canids. *Journal of Zoology*, **278**: 181–188.
doi:10.1111/j.1469-7998.2009.00567.x.
- Sues, H.-D. 1976. A new small theropod dinosaur from the Judith River Formation (Campanian) of Alberta. *Zoological Journal of the Linnean Society*, **62**: 381–400.
- Therrien, F., Henderson, D.M., and Ruff, C.B. 2005. Bite me. Biomechanical models of theropod mandibles and implications for feeding behavior. *In The Carnivorous Dinosaurs. Edited by K. Carpenter.* Indiana University Press, Bloomington. pp. 179–237.
- Tsuihiji, T., Barsbold, R., Watabe, M., Tsogtbaatar, K., Chinzorig, T., Fujiyama, Y., and Suzuki, S. 2014. An exquisitely preserved troodontid theropod with new information on the palatal structure from the Upper Cretaceous of Mongolia. *Naturwissenschaften*, **101**: 131–142.
doi:10.1007/s00114-014-1143-9.
- Turner, A.H., Hwang, S.H., and Norell, M.A. 2007a. A small derived theropod from Öösh, Early Cretaceous, Baykhangor Mongolia. *American Museum Novitates*, **3557**: 27.
doi:10.1206/0003-0082(2007)3557[1:asdtfs]2.0.co;2.
- Turner, A.H., Makovicky, P.J., and Norell, M.A. 2012. A review of dromaeosaurid systematics and paravian phylogeny. *Bulletin of the American Museum of Natural History*, **371**: 1–206.
doi:10.1206/748.1.
- Walmsley, C.W., Smits, P.D., Quayle, M.R., McCurry, M.R., Richards, H.S., Oldfield, C.C., Wroe, S., Clausen, P.D., and McHenry, C.R. 2013. Why the long face? The mechanics of mandibular symphysis proportions in crocodiles. *PLoS ONE*, **8**: 34.
doi:10.1371/journal.pone.0053873.

- Wilkinson, M. 1995. A comparison of two methods of character construction. *Cladistics*,: 297–308.
- Witmer, L.M. 1997. The evolution of the antorbital cavity of archosaurs: A study in soft-tissue reconstruction in the fossil record with an analysis of the function of Pneumaticity. *Journal of Vertebrate Paleontology*, **17**: 1–76. doi:10.1080/02724634.1997.10011027.
- Witmer, L.M., and Ridgely, R.C. 2008. The paranasal air sinuses of predatory and armored dinosaurs (Archosauria: Theropoda and Ankylosauria) and their contribution to cephalic structure. *Anatomical Record*, **291**: 1362–1388. doi:10.1002/ar.20794.
- Xu, X., Choiniere, J.N., Pittman, M., Tan, Q., Xiao, D., Li, Z., Tan, L., Clark, J.M., Norell, M.A., Hone, D.W.E., and Sullivan, C. 2010a. A new dromaeosaurid (Dinosauria: Theropoda) from the Upper Cretaceous Wulansuhai Formation of Inner Mongolia, China. *Zootaxa*, **9**: 1–9.
- Xu, X., Norell, M.A., Wang, X.L., Makovicky, P.J., and Wu, X.C. 2002. A basal troodontid from the Early Cretaceous of China. *Nature*, **415**: 780–784. doi:10.1038/415780a.
- Xu, X., Pittman, M., Sullivan, C., Choiniere, J.N., Tan, Q.-W., Clark, J.M., Norell, M. a., and Wang, S. 2015. The taxonomic status of the Late Cretaceous dromaeosaurid *Linheraptor exquisitus* and its implications for dromaeosaurid systematics. *Vertebrata Palasiatica*, **53**: 29–62.
- Xu, X., Wang, K., Zhao, X., Sullivan, C., and Chen, S. 2010b. A new leptoceratopsid (Ornithischia: Ceratopsia) from the Upper Cretaceous of Shandong, China and its implications for neoceratopsian evolution. *PLoS ONE*, **5**. doi:10.1371/journal.pone.0013835.

- Xu, X., Wang, X.L., and Wu, X.C. 1999. A dromaeosaurid dinosaur with a filamentous integument from the Yixian Formation of China. *Nature*, **401**: 262–266. doi:10.1038/45769.
- Zanno, L.E., and Makovicky, P.J. 2011. Herbivorous ecomorphology and specialization patterns in theropod dinosaur evolution. *Proceedings of the National Academy of Sciences of the United States of America*, **108**: 232–237. doi:10.1073/pnas.1011924108.

3.7 Tables and Figures

Table 3.1. Specimens and measurement methods for morphometric analysis.

Specimen #	Taxon	Specimen Condition	Measured	Measured with
AMNH FARB 5356	<i>Dromaeosaurus albertensis</i>	Partial cranium and associated postcrania	Both maxillae; partial right premaxilla	Mastercraft digital callipers (150 mm); ImageJ
AMNH FARB 6515	<i>Velociraptor mongoliensis</i>	Nearly complete skull with some postcrania	Left maxilla; right premaxilla	Mastercraft digital callipers (150 mm); ImageJ
AMNH FARB 6516	<i>Saurornithoides mongoliensis</i>	Nearly complete skull with some postcrania	Both maxillae and premaxillae	ImageJ (Norell et al. 2009; Fig. 3)
AMNH FARB 30556	<i>Bambiraptor feinbergi</i>	Nearly complete associated skeleton	Left maxilla and premaxilla	Mastercraft digital callipers (150 mm); ImageJ
BYUVP 14585 F#1984	<i>Utahraptor ostrommaysi</i>	Isolated premaxilla	Left premaxilla	Mastercraft digital callipers (150 mm)
BYUVP 19965 F# 4252	<i>Utahraptor ostrommaysi</i>	Isolated partial right maxilla	Right maxilla	ImageJ; 152 cm measuring tape
CEUM 01430	<i>Utahraptor ostrommaysi</i>	Isolated premaxilla	Left premaxilla	152 cm measuring tape
CEUM 73719	<i>Geminiraptor suarezarum</i>	Isolated partial maxilla	Left maxilla	152 cm measuring tape; ImageJ
IMM99NM-BYM-3/3A	<i>Velociraptor osmolskae</i>	Partial maxillae; left lacrimal	Left maxilla	ImageJ (Godefroit et al. 2008; Fig. 2A)
IVPP V12615	<i>Sinovenator changii</i>	Partial skull and associated postcrania	Left maxilla and premaxilla	ImageJ (Xu et al. 2002; Fig. 1A)
IVPP V12811	<i>Sinornithosaurus millenii</i>	Crushed articulated skeleton	Left maxilla and premaxillae	ImageJ (Xu et al. 1999; Fig. 3)
IVPP V16923	<i>Linheraptor exquisitus</i>	Most of an articulated skeleton	Left and Right maxillae; left and right premaxillae	ImageJ (Xu et al. 2015; Fig. 1A&C)

MML 195	<i>Austroraptor cabazai</i>	Most of an associated skull; associated partial postcrania	Left maxilla	ImageJ (Novas et al. 2009; Fig. 1B)
MNUFR 15	<i>Achillobator giganticus</i>	Associated partial skull	Left maxilla	Image J (pictures taken by Currie P.J.)
MPC-D 100/1	<i>Zanabazar junior</i>	Articulated cranium with partial mandible and postcrania	Both maxillae and premaxillae	Image J (Norell et al. 2009; Fig. 22)
MPC-D 100/25	<i>Velociraptor mongoliensis</i>	Most of an articulated skeleton	Right maxilla and premaxilla	ImageJ (pictures taken by Funston G.F.)
MPC-D 100/54	<i>Velociraptor mongoliensis</i>	Nearly complete, articulated skeleton	Left maxilla and premaxilla	ImageJ (pictures taken by Funston G.F.)
MPC-D 100/86	<i>Gobivenator mongoliensis</i>	Nearly complete, articulated skeleton	Left maxilla	ImageJ (Tsuihiji et al. 2014; Fig. 3A)
MPC-D 100/982	<i>Velociraptor</i> sp.	Nearly complete and articulated skeleton	Left maxilla; right premaxilla	Mastercraft digital callipers (150 mm); ImageJ
MPC-D 100/1015	<i>Tsaagan mangas</i>	Articulated skull and cervical vertebrae	Right maxilla and premaxilla	Mastercraft digital callipers (150 mm); ImageJ
MPC-D 100/1119	<i>Shanag ashile</i>	Right maxilla and dentary	Right maxilla	ImageJ (Turner et al. 2007; Fig. 2)
ROM 63777	<i>Acheroraptor termeryorum</i>	Left maxilla	Left maxilla	Mastercraft digital callipers (150 mm); ImageJ
TMP 1994.012.0844	<i>Saurornitholestes langstoni</i>	Isolated right maxilla	Right maxilla	Mastercraft digital callipers (150 mm); ImageJ
TMP 1995.166.0001	<i>Atrociraptor marshalli</i>	Associated cranial elements	Right maxilla and premaxilla	Mastercraft digital callipers (150 mm); ImageJ
UALVP 49389	<i>Velociraptor</i> sp.	Cast of articulated skull and foot	Right and left maxillae; right and left premaxillae	Mastercraft digital callipers (150 mm); ImageJ

UALVP 55700	<i>Saurornitholestes langstoni</i>	Nearly complete, articulated skeleton	Right and left maxillae; right and left premaxillae	Mastercraft digital callipers (150 mm); ImageJ
YPM 5232 (237)	<i>Deinonychus antirrhopus</i>	Associated elements of skull and skeleton	Right premaxilla	Mastercraft digital callipers (150 mm)
YPM 5232 (557)	<i>Deinonychus antirrhopus</i>	Associated elements of skull and skeleton	Right maxilla	Mastercraft digital callipers (150 mm); 152 cm measuring tape; ImageJ

Elements measured are listed together with the tools or software they were measured with. Unless specified, all specimens were observed and

photographed by the author.

Table 3.2. Linear measurements of maxillae and premaxillae in lateral aspect.

Measurement and abbreviation	From	To
Maxilla length (MxL)	Anteroventral corner	Posteroventral corner or posterodorsal corner, whichever gives the greater distance
Maxilla height (MxH)	Ventral extent of alveolar margin	Dorsal extent of ascending ramus
Anterior ramus length (AntRL)	Anteroventral corner of maxilla	Most anterior edge of antorbital fossa
Anterior ramus height distal (AntRH.d)	Anteroventral corner of maxilla	Dorsal corner of anterior edge of maxilla (adjacent to the maxillary process of the premaxilla meets the premaxillary body)
Anterior ramus height proximal (AntRH.p)	Alveolar margin ventral to anterior edge of antorbital fossa	Point on dorsal margin of maxilla directly above anterior edge of antorbital fossa
Antorbital fenestra height (AntFenH)	Ventral extent of antorbital fenestra	Posteroventral corner of ascending ramus
Antorbital fossa length (AntFL)	Most anterior extent of antorbital fossa	Most anterior extent of antorbital fenestra
Antorbital fossa height (AntFH)	Most posterior point, anterior to jugal contact facet, on ventral margin of antorbital fossa	Posterodorsal extent of ascending ramus
Anterior margin of antorbital fossa to maxillary fenestra (AntAF-MxFen)	Most anterior extent of maxillary fenestra	Most anterior extent of antorbital fossa
Pila interfenestralis width (PIW)	Most posterior extent of maxillary fenestra	Most anterior extent of antorbital fenestra
Maxillary fenestra long axis (MxFen.L)	One end of long axis of maxillary fenestra	Opposite end of long axis of maxillary fenestra
Maxillary fenestra short axis (MxFen.S)	One end of short axis of maxillary fenestra	Opposite end of short axis of maxillary fenestra
Ventral margin height anterior (VentMH.ant)	Point along alveolar margin ventral to point of inflection of ventral border of antorbital fossa	Point of inflection of ventral border of antorbital fossa

Ventral margin height posterior (VentMH.post)	Point along alveolar margin just anterior to jugal contact facet	Point on ventral border of antorbital fossa just anterior to jugal contact facet
Length of the first 9 alveoli (L9Alv)	Anteroventral corner of maxilla	Most posterior extent of 9 th alveolus
Distance from 9 th alveolus to antorbital fenestra (AntFen.9Alv.L)	Most posterior extent of 9 th alveolus	Most anterior extent of antorbital fenestra
Premaxilla main body length (PmxL.bdy)	Anteroventral corner of premaxilla	Most posterior point of premaxilla along alveolar margin
Premaxilla main body height (PmxH.bdy)	Ventral extent of alveolar margin	Ventral extent of external naris

Measurements were taken as straight lines either from point to point, or along vertical or horizontal axes between points defined by how far

particular features extended in the specified directions.

Table 3.3. Character state changes and additions to Currie and Evans (2019) data matrix.

Character	Taxon	Character state (Currie and Evans 2019)	Character state post-assessment
8	<i>Achillobator</i>	?	1
	<i>Dromaeosaurus</i>	1	?
	<i>Deinonychus</i>	0	1
	<i>Linheraptor</i>	0	1
	<i>Sinornithosaurus</i>	1	0
	<i>Sinovenator</i>	0	1
20	<i>Dromaeosaurus</i>	?	0
22	<i>Bambiraptor</i>	1	0
	<i>Linheraptor</i>	0	1
	<i>Sinovenator</i>	0	1
28	<i>Austroraptor</i>	0	2
	<i>Deinonychus</i>	0	1
	<i>Linheraptor</i>	0	2
	<i>Sinovenator</i>	0	1
	<i>Tsaagan</i>	0	2
	<i>Utahraptor</i>	?	1
29	<i>Austroraptor</i>	0	2
	<i>Shanag</i>	0	2
	<i>Sinornithosaurus</i>	?	0
	<i>Sinovenator</i>	0	1
New Character 1	<i>Achillobator</i>	-	1

	<i>Atrociraptor</i>	-	1
	<i>Austroraptor</i>	-	0
	<i>Bambiraptor</i>	-	1
	<i>Deinonychus</i>	-	1
	<i>Linheraptor</i>	-	0
	<i>Saurornitholestes</i>	-	1
	<i>Shanag</i>	-	1
	<i>Sinornithosaurus</i>	-	1
	<i>Sinovenator</i>	-	1
	<i>Tsaagan</i>	-	0
	<i>V. mongoliensis</i>	-	0
New Character 2	<i>Acheroraptor</i>	-	1
	<i>Achillobator</i>	-	1
	<i>Atrociraptor</i>	-	1
	<i>Bambiraptor</i>	-	1
	<i>Deinonychus</i>	-	1
	<i>Linheraptor</i>	-	1
	<i>Saurornitholestes</i>	-	1
	<i>Shanag</i>	-	0
	<i>Sinornithosaurus</i>	-	0
	<i>Sinovenator</i>	-	1
	<i>Tsaagan</i>	-	1
	<i>V. mongoliensis</i>	-	1
	<i>V. osmolskae</i>	-	1

Characters that could not be measured in this study for a given taxon were scored as [?], unless they were originally scored as [1] by Currie and Evans (2019). The modified data matrix is available in the Appendix (A 2.6).

Table 3.4. Character consistency index values for characters added or analysed in this study, for analysis of the new dataset and from Currie and Evans (2019) where applicable.

Character	CI (Currie and Evans 2019)	CI (New data matrix)
8	0.33	0.25
20	1	1
22	0.5	0.25
28	0.25	0.29
29	0.33	0.4
181	-	0.33
182	-	1

Consistency index for each character were calculated by testing their fit with a 50% majority rules consensus tree topology obtained by analysis

of a version of the dataset from which the examined characters had been removed.

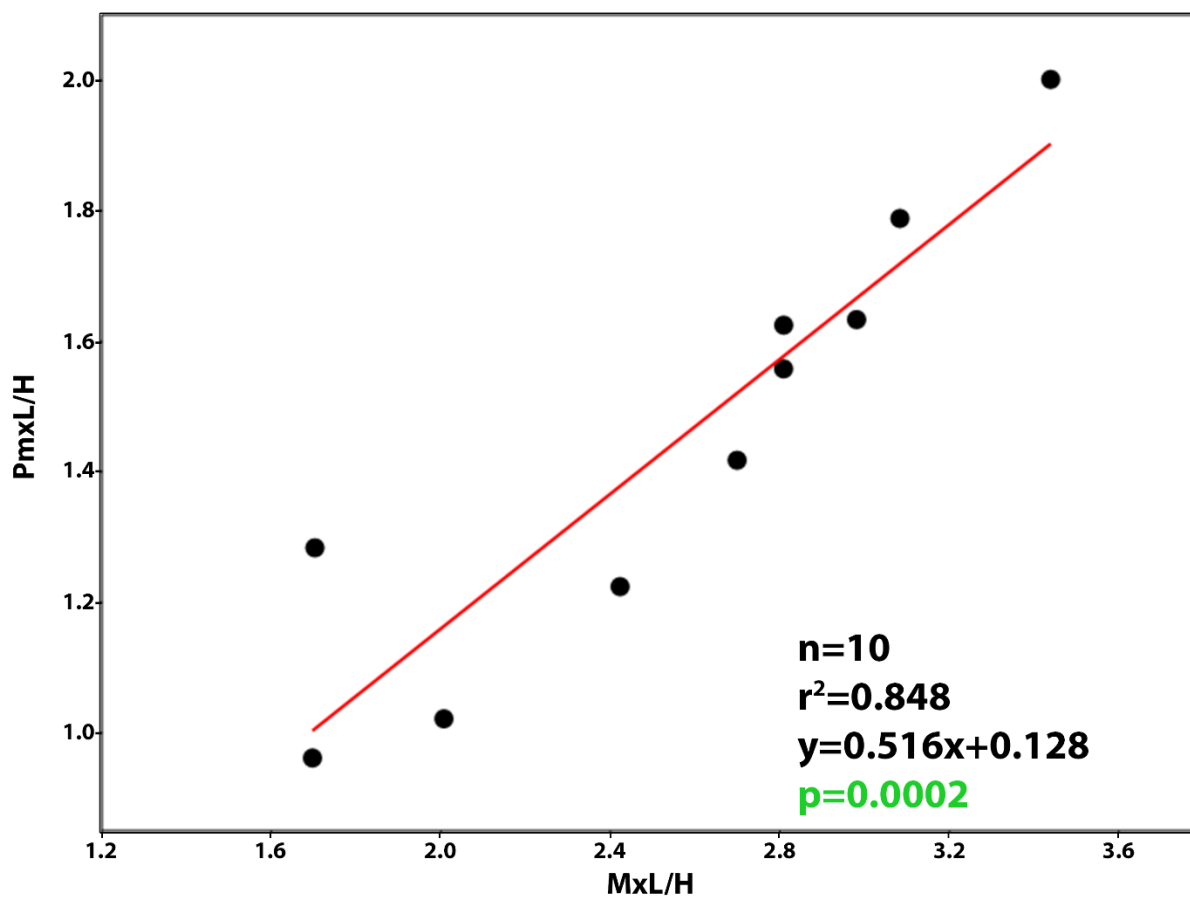


Figure 3.2. Simple linear regression of premaxillary length-to-height ratio on maxillary length-to-height ratio in eudromaeosaurian specimens.

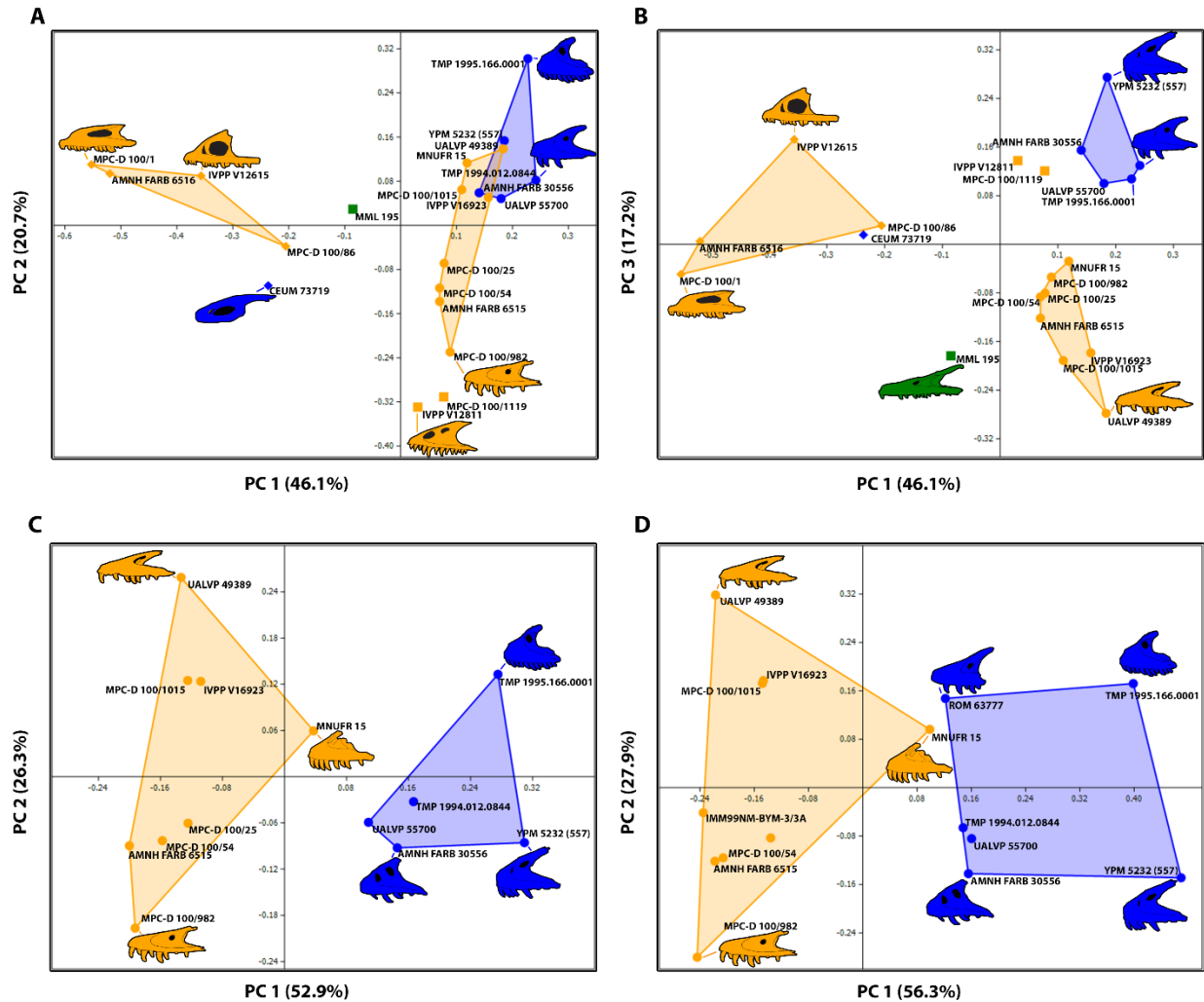


Figure 3.3. Results from linear measurement principal component analyses of the maxillae of eudromaeosaurian taxa and closely related outgroups. A, B) analysis including eudromaeosaurian and outgroup specimens, measurements scaled to maxillary length (MxL); C) eudromaeosaurian specimens only, measurements scaled to MxL; D) eudromaeosaurian specimens only, measurements corrected to length of the first nine maxillary alveoli (L9Alv). Shapes represent larger taxonomic groupings: diamonds, troodontids; circles, eudromaeosaurians; squares, non-eudromaeosaurian dromaeosaurids. Colours represent geographic provenance: blue, North America; green, South America; orange, Asia. Line

drawings are shown for some specimens at extreme positions along PC axes and/or within taxonomically and geographically defined groupings.

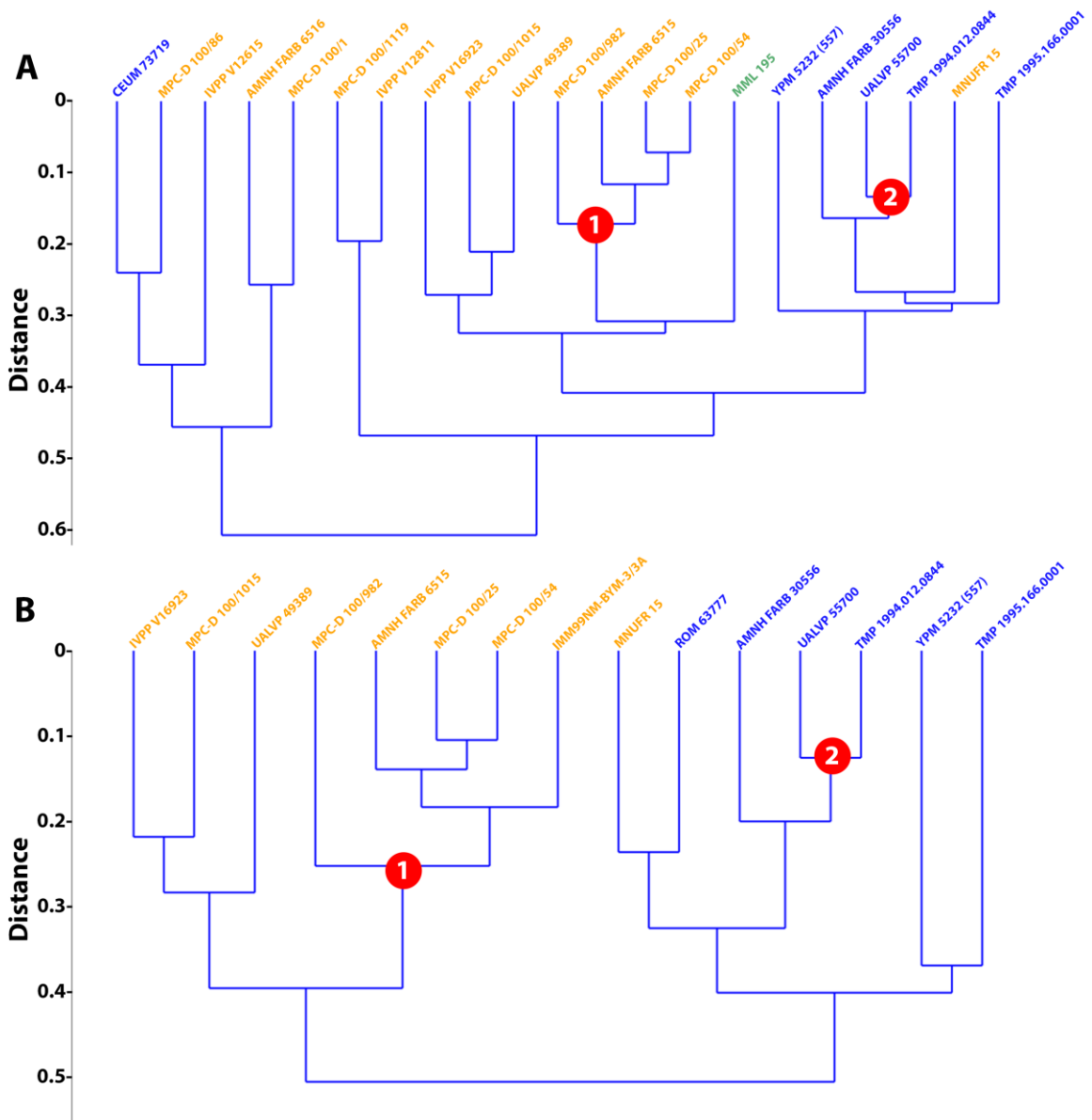


Figure 3.4. Classic cluster analysis using UPGMA pairing algorithm and Euclidean similarity index. A) results from cluster analysis of linear measurements scaled to maxillary length for all taxa (corresponding to PCA variant 1); B) results from cluster analysis of linear measurements scaled to length of first nine maxillary alveoli for eudromaeosaurian taxa (corresponding to PCA variant 3). Specimen numbers are placed at the corresponding termini and font colours reflect geographic provenance: blue, North America; green, South America;

orange, Asia. Distances are indicated along the y-axis. Two nodes exclusively containing specimens assigned to a single genus have been highlighted with circled numbers: 1)

Saurornitholestes; 2) *Velociraptor*.

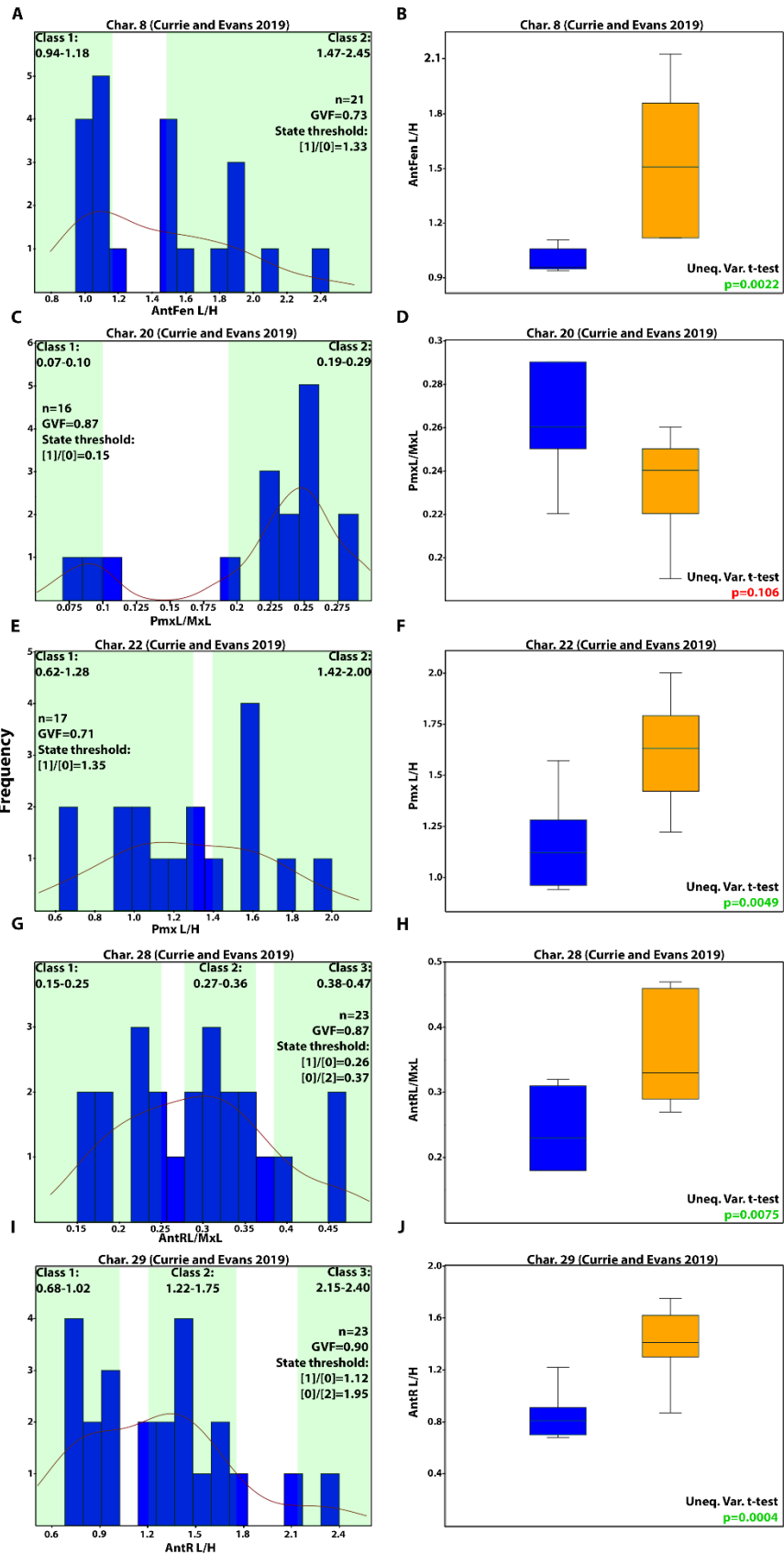


Figure 3.5. Ratio-based character distributions with Jenks Natural Breaks Optimization results for all dromaeosaurid and troodontid taxa, and variation in each character between Asian and North American eudromaeosaurians. Histograms showing the distribution of values in our data set for each character are accompanied by kernel density curves, and distinct classes of values are highlighted in green and separated by white gaps (A, C, E, G, I); number of specimens (n), goodness of variance fit (GVF), value ranges for classes, and proposed thresholds between character states are included on each graph. Box plots of values for Asian (orange) and North American (blue) eudromaeosaurians are given for each character (B, D, F, H, J); p-values from unequal variance t-tests of variation between specimens from the two continents are included on each plot.

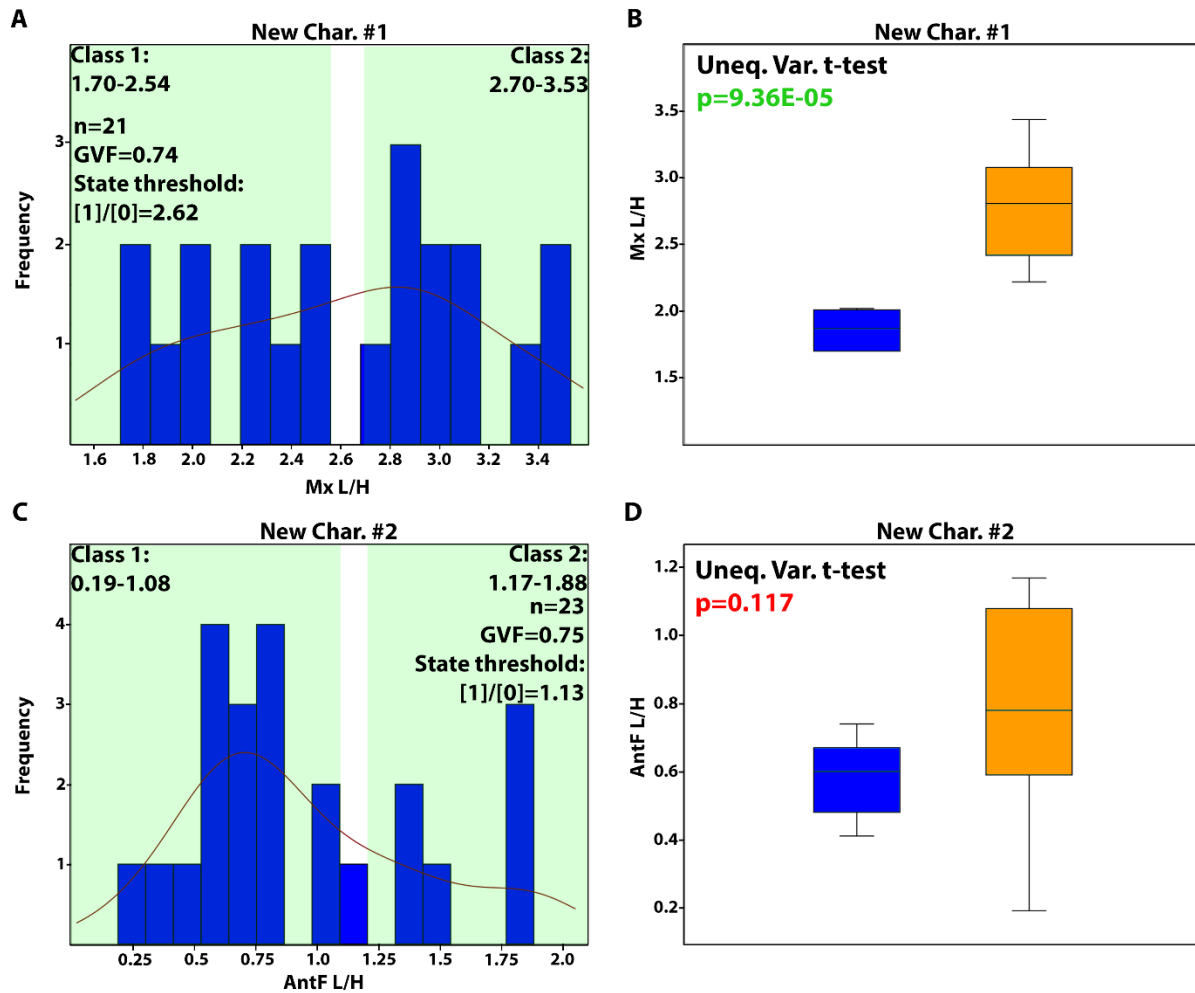


Figure 3.6. Character distributions for new ratio-based characters in dromaeosaurids, with corresponding box plots and unequal variance t-test results to assess variation between Asian and North American eudromaeosaurian taxa. Histograms showing the distribution of values in our data set for each character are accompanied by kernel density curves, and distinct classes are highlighted in green and separated by white gaps (A, C); number of specimens (n), goodness of variance fit (GVF), value ranges for classes, and proposed thresholds between character states are included on each graph. Box plots of values for Asian (orange) and North American (blue) eudromaeosaurians are given for each character (B, D).

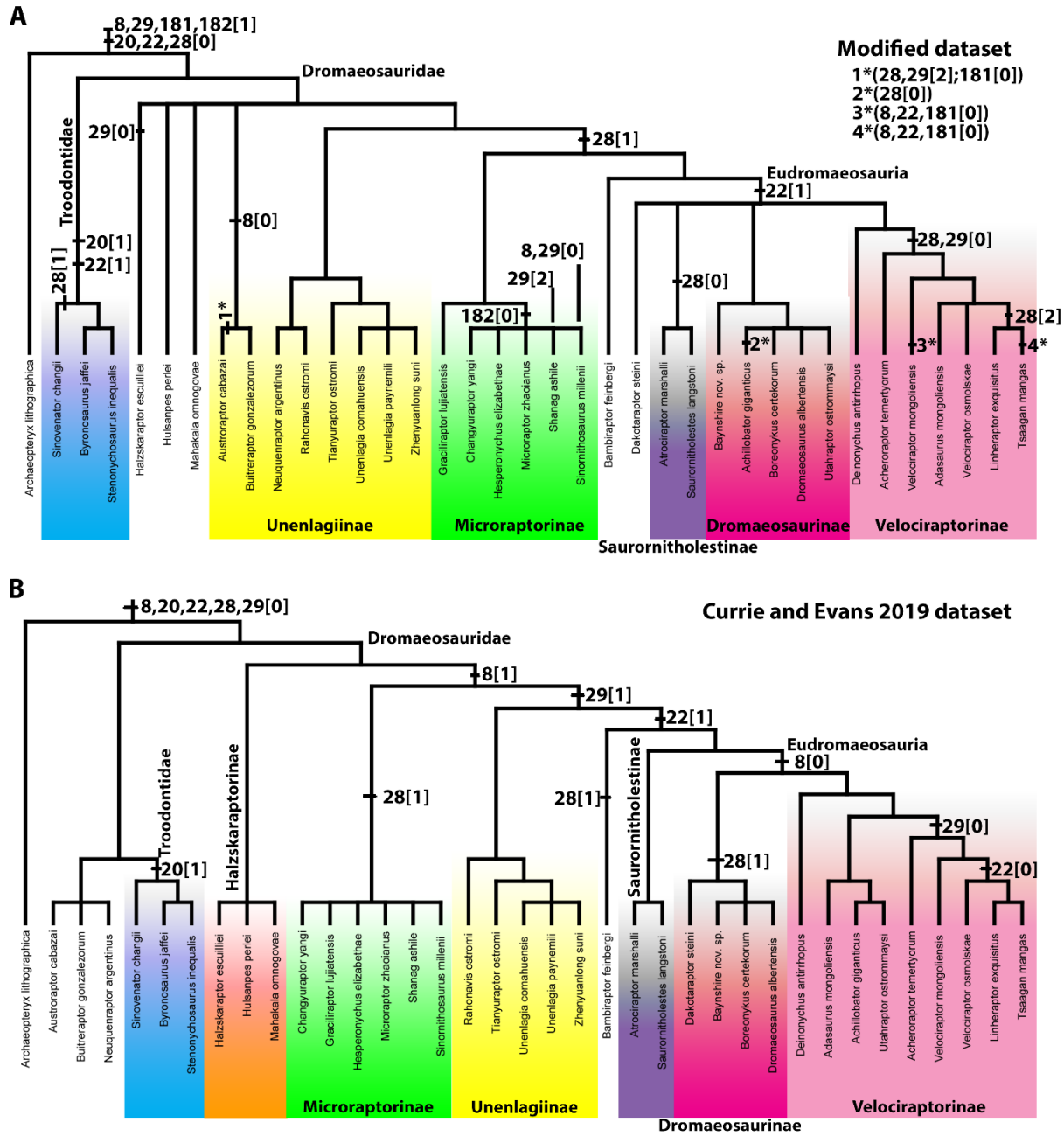


Figure 3.7. 50% majority rule consensus trees generated from a modified taxon-character matrix (A) and the original matrix (B) from Currie and Evans (2019). Higher order taxonomic groups are labeled at the appropriate nodes and family/subfamily groups are labeled and highlighted. States of characters analysed or added in this study are mapped using parsimony

ancestral states character trace in Mesquite V3.2. Where needed for space and clarity, symbols (#*) are used to mark terminal branches on which character state changes occur.

Chapter 4. Description of a new species of *Velociraptor* and new insights into intrageneric variation

4.1 Introduction

Dromaeosaurids were a diverse group of small to medium sized theropod dinosaurs that inhabited nearly every continent during the Late Cretaceous (Turner et al. 2012). Although there are a few dozen species described today, relatively few are well represented in terms of skeletal completeness (Ostrom 1969, Burnham et al. 2000, Xu et al. 2000, 2010a, Zheng et al. 2010, Lü and Brusatte 2015, Cau et al. 2017, Currie and Evans 2019). Much of the diversity comes from geographically and geologically isolated specimens with relatively little in the way of overlapping material (Currie 1995, Perle et al. 1999, Currie and Varricchio 2004, Godefroit et al. 2008, Novas et al. 2009, Turner et al. 2012, Evans et al. 2013). Among the taxa described from limited material, eudromaeosaurians have largely been described based on maxillae (Perle et al. 1999, Currie and Varricchio 2004, Godefroit et al. 2008, Evans et al. 2013). It has been suggested that the maxillae of deinonychosaurian theropods, among other theropod groups, show a high amount of taxonomic variation (Currie and Varricchio 2004, Godefroit et al. 2008, Senter et al. 2010, Evans et al. 2013). Because of this, there is a lot of emphasis placed on this element for phylogenetic and ecological inferences with little attempt having been made to assess the validity of its phylogenetic usefulness. A challenge facing the use of a single element for phylogenetic reconstruction is quantifying the level of intraspecific variation that is present in the element in question.

While dromaeosaurid material is typically quite rare compared to material of other theropod clades such as ornithomimids and tyrannosaurids (Brown et al. 2013), numerous specimens have been referred to the species *Velociraptor mongoliensis* Osborn, 1924, a medium

sized dromaeosaurid from the Gobi Desert of Mongolia (Kielan-Jaworowska and Barsbold 1971, Norell and Makovicky 1997, 1999, Barsbold and Osmólska 1999, Norell et al. 2004, Hone et al. 2012). Many specimens collected from the localities of Bayn Dzag (Flaming Cliffs), Tögrögiin Shiree, and other sites in the region have been referred to *V. mongoliensis* without looking at the range of variation for outliers. The assumption that all specimens belong to the single species *V. mongoliensis* potentially limits our understanding of the diversity of eudromaeosaurians in Asia during the Late Cretaceous. A similar issue has occurred in recent years with regard to two Asian dromaeosaurids closely related to *V. mongoliensis*; *Linheraptor exquisitus* Xu et al., 2010, and *Tsaagan mangas* Norell et al., 2006. Turner et al. (2012) proposed that the two taxa were synonymous suggesting that *Linheraptor exquisitus* was the junior synonym of *Tsaagan mangas*. Xu et al. (2015) defended the validity of *Linheraptor exquisitus* as distinct from *Tsaagan mangas* based on a plethora of discrete, but subtle characteristics. Xu et al. (2015) also mentioned that the currently observed variation in specimens referred to *V. mongoliensis* may in fact represent several distinct taxa.

Evans et al. (2017) demonstrated that multivariate and bivariate methods can be used to determine distinct morphological species from multiple specimens. The authors used the frontal – a frequently collected element of troodontids – to perform shape and regression analyses. They wanted to determine the fit of one specimen, found in the Horseshoe Canyon Formation of Alberta, Canada, within the range of variation observed for a known species, *Stenonychosaurus inequalis* Sternberg, 1932, found at a different stratigraphic level (the Dinosaur Park Formation) in Alberta. They established that the new specimen fell outside the range of variation for *S. inequalis* and was an outlier to expected trends for the species. Thus, Evans et al. (2017) erected a new genus and species, *Albertavenator curriei* Evans et al., 2017, based on the thorough

investigation of the overall morphology of a geographically and stratigraphically separated specimen. The maxillae of eudromaeosaurians seem a fitting element to examine in the same way, given the importance the bone holds to phylogenetic inference for the group, the availability of specimens, and taxonomic clustering during PCA analysis (Fig. 3.3).

The taxonomic variation of the maxilla has been examined within Eudromaeosauria Longrich and Currie, 2009, and closely related outgroups. The maxilla has been found to have a high amount of morphological variation due to the anatomical complexity of the element (Fig. 1.1B-C) and varies a great deal among species that are not proposed to be closely related. Maxillae show tight clustering with members of the same species, or closely related species (Chapter 3). One specimen previously referred to *V. mongoliensis* (MPC-D 100/982) demonstrates a maxillary morphology distinct from other eudromaeosaurians. The specimen was collected in 1995 and has been awaiting formal description since. Despite its clearly unusual maxillary morphology, the skull has been figured several times and declared to represent normal variation within *V. mongoliensis* (Norell et al. 2006, Turner et al. 2012). In this chapter, MPC-D 100/982 is described in detail using morphological characters and computed tomography data to describe details not previously observed. Using multivariate and bivariate analyses, the maxilla of this specimen is compared to the range of variation of specimens referred to *V. mongoliensis*, and *Velociraptor osmolskae* Godefroit et al., 2008.

4.2 Materials and Methods

4.2.1 Principal component analyses

To examine range of variation within the species of *Velociraptor mongoliensis*, linear measurement principal component analysis was used to analyse specimens of *Velociraptor* spp.

and the close Asian relatives *Linheraptor exquisitus* and *Tsaagan mangas* from which all measurements could be acquired. For use in PCA analysis, 16 maxillary measurements (Table 3.2) were taken from eight specimens (Table 4.1; all but MPC-D 100/24) and run through the principal component analysis tool using PAST 3 (Hammer et al. 2001). Raw data for PCA analysis can be found in A 3.1. Two iterations were performed, one using the raw data and all 16 measurements, and the other using log transformed data using 15 measurements. For the log transformed data, the distance from the anterior margin of the antorbital fenestra to the posterior edge of the ninth maxillary alveolus was removed because of the effect “0” values had on ordination with log transformed data. The first iteration was performed as all the specimens are of similar size and it was unnecessary to transform the data to a size related measurement. Use of raw data is warranted as it follows the procedures used for linear measurement morphometrics performed on troodontid frontals of similar size by Evans et al. (2017). The second iteration was performed to examine if there was any major effect on the ordination.

A third PCA was performed following the methods outlined for the eudromaeosaurian specific analysis outlined in Chapter 3 (3.2). Measurements were corrected to length of the first nine maxillary alveoli (L9Alv) to include the broadest range of taxa. One additional specimen was added to the dataset from Chapter 3, MOR 553S-7.30.91.274. This specimen is a maxilla that has been identified as belonging to an adult individual of *Bambiraptor feinbergi* (Currie and Varricchio 2004). This PCA was performed to compare ontogenetic trends between *Bambiraptor feinbergi* and *Velociraptor mongoliensis*. Measurements of maxillae used in Chapter 3 can be found in A 2.4 and PCA values for MOR 553S-7.30.91.274 can be found in A 3.1.

4.2.2 Regression analyses

A simple least squares regression was performed on the PC1 scores for each taxon from the raw data linear measurement PCA and plotted against the log transformed maxillary length measurement. Multiple regression analyses were performed in PAST 3 on all the log transformed measurements used for the PCA outlined previously. Several multiple regression analyses were performed to examine trends of maxillary proportions within *V. mongoliensis* (n=4) and the effect of adding additional specimens proposed to belong to different species within *Velociraptor* (MPC-D 100/982, *Velociraptor* sp.; IMM99NM-BYM-3/3A, *V. osmolskae*). An additional multiple regression including specimens of *V. mongoliensis*, *Linheraptor exquisitus* and *Tsaagan mangas* was used as a control for demonstrating the effect of adding different species to the regression. Log transformed length measurements were used as the independent variable for all the regressions. The length measurement was chosen as a proxy for the overall size of the maxilla and allows for the comparison of various maxillary features against the size of the individual.

For measurements that were greatly affected by the addition of MPC-D 100/982, a separate reduced major axis regression was run using PAST 3. When MPC-D 100/24 was applicable for bivariate analysis, it was included. These included regressions examining antorbital fossa length and anterior ramus length relative to maxillary length. Reduced major axis regression was chosen as it is standard among biological analyses of allometry (Evans et al. 2017, Schott and Evans 2017). An additional reduced major axis regression was performed in PAST 3 on the log transformed data of the height of the maxilla against quadrate height. Quadrate height was selected as a measurement that is independent of maxillary portions but could provide a useful indicator of snout depth compared to temporal depth. It was also selected as a metric due to its presence and resistance to post-mortem distortion in the available

specimens. Trends of regressions were considered isometric if the confidence interval of the slope captured 1.0. If the slope was significantly greater than 1.0 but captured 1.0 in the confidence interval it was considered a probable positive allometric trend. If both the slope and the confidence was above 1.0 then the trend was considered positively allometric. If the confidence interval for slopes was broad (i.e. greater than three), no trend of allometry was reported. Graphs for all regression analyses were produced using PAST 3, then formatted into figures using Photoshop CS6.

4.2.3 Phylogeny

MPC-D 100/982 was coded for a data matrix modified from Currie and Evans (2019) after examination of the specimen in comparison to other specimens. Comparisons were largely focused on similarities with eudromaeosaurians as MPC-D 100/982 has clear affinity to the highly derived eudromaeosaurian species *Velociraptor mongoliensis*, being referred to this taxon in previous publications (Norell and Makovicky 1999, Norell et al. 2006, Turner et al. 2012).

Both parsimony and Bayesian analyses were performed on two character-taxon data matrices. The first includes revised characters from Currie and Evans (2019) using a reduced number of taxa. This character-taxon matrix includes 177 characters and 33 taxa, and was formatted using Mesquite V3.6 (Maddison and Maddison 2017). The second dataset was a matrix with a reduced number of taxa, limited to one or two representatives of the outgroup clades to Eudromaeosauria and was also formatted with Mesquite. This matrix consisted of the same 177 characters, but the number of taxa was reduced to 22. Outgroup taxa removed were those that had a greater degree of missing data (i.e. coded as “?”). Bootstrap analysis was performed on the parsimony consensus trees at 1000 replicates in TNT and values over 50 were

reported. The character list and character-taxon data matrix can be found in the appendix (A 3.2, A 3.3).

Specific to the Bayesian analyses, character-taxon matrices were exported using Mesquite V3.6 to Mr. Bayes format. The nexus files were adjusted afterward to perform 5000000 replicates, temp was set to 0.01, *Archaeopteryx lithographica* Meyer, 1861, is the outgroup, and the command “contype=allcompat” was used in order to produce a fully resolved tree. This was chosen to examine probabilistic groupings based on the data with the understanding that support for individual nodes will be less than those with numerous congruent characters.

The parsimony analysis was performed in TNT V1.5 (Goloboff and Mattoni 2006) using the New Technology Search feature. The parameters for both datasets were 10000 replicates, each finding the shortest tree once. Trees were replaced as shorter ones were found. For each replicate there were ten rounds of ratcheting, five rounds of drifting and five rounds of tree fusing. Once all the shortest trees were acquired a strict, and a 50% majority rules consensus tree were calculated. Synapomorphies were mapped for the consensus tree using the TNT software and were placed on the tree topology afterward using Photoshop CS6. The tree was examined in Mesquite V3.6 to record tree and character values, and to trace character histories using the parsimony model.

Bayesian analyses were performed using Mr. Bayes (3.2.7a) on XSEDE using CIPRES Science Gateway. The parameters were as follows; nchains=4; nruns=2; run version 7; maximum runtime=168 hours. The consensus tree generated from the analysis was examined in Mesquite V3.6 to acquire tree values, character values, and track character history using the parsimony and likelihood models.

Maxillary characters modified in this thesis (and two premaxillary characters; characters 6-15, 21, 23, 27-29, and 32) were compared for their consistency indices within the dataset using Mesquite V3.6. Characters with indices of 0.5 or above were mapped onto the ingroup tree topologies.

4.3 Systematic Palaeontology

Theropoda, Marsh 1881

Dromaeosauridae, Matthew and Brown 1922

Eudromaeosauria, Longrich and Currie 2009

Velociraptor, Osborn 1924

Velociraptor vadarostrum, sp. nov.

Holotype

MPC-D 100/982, consists of a nearly complete skeleton missing the skull roof and the majority of the caudal vertebrae. The specimen has little 3-dimensional post-mortem distortion. However, the ends of a number of appendicular elements are lost due to insect damage (Norell and Makovicky 1997, 1999) and much of the axial skeleton is obscured by matrix. The specimen is permanently curated by the Paleontological and Geological Center of the Mongolian Academy of Sciences, Ulaan Baatar, Mongolia and is currently on loan to the American Museum of Natural History in New York City, New York, USA. The holotype has been partially described in several papers (Norell and Makovicky 1999, Norell et al. 2004, 2006, Turner et al. 2012).

Type Locality

MPC-D 100/982 was collected from the Flaming Cliffs (Bayan Zag) near the Volcano sub-locality in 1995 (Norell and Makovicky 1999).

Etymology

Specific epithet is derived from Latin, ‘vada’, or ‘vadum’ meaning ‘shallow’ and ‘rostrum’ meaning snout. This name was chosen due to the restricted dorsoventral depth of the snout relative to skull depth, compared to other dromaeosaurids including the closely related species *Velociraptor mongoliensis*.

Diagnosis

A medium sized dromaeosaurid that is differentiated from all other eudromaeosaurian dromaeosaurids by the following autapomorphies: an elongate skull relative to body size (skull is 129% femur length, which is greater than observed in *Velociraptor mongoliensis* (117-126%) (Currie and Evans 2019); an elongate antorbital fossa (L/H ratio=1.17) compared to other eudromaeosaurians (0.19-1.08) (A 2.5); there is limited lateral exposure of the splenial; a relatively straight supraorbital rim of the frontal; a sharply constricted anterior cerebral cavity preceded by a long olfactory canal; a radius shaft diameter that is less than 0.5 that of the ulna; presence of an anterodorsally oriented vertical crest on the ilium. *Velociraptor vadarostrum* can be identified as a species of *Velociraptor* by the following synapomorphies; an antorbital skull length that is 60% or greater than the femur length (this character is ambiguous for more derived Asian eudromaeosaurians due to a lack in all specimens of both skulls and femora); a promaxillary fenestra positioned anterior to anterodorsally within the anterior border of the antorbital fossa; a broad pila promaxillaris relative to the pila interfenestralis; an anteriorly bowed ascending process of the quadratojugal; the presence of ovoid depressions on the

posterior surface of the basioccipital tubera; possession of deep lateral ligament pits of pedal phalanx II-2.

Velociraptor vadarostrum is differentiated from *V. mongoliensis* and *V. osmolskae* by the following features; the anterior border of the antorbital fossa is above the third maxillary alveolus instead of the fourth; the maxillary fenestra lies within an accessory fossa that shares a limited border with the anterior border of the maxillary fenestra whereas the two structures share an anterior border in *V. mongoliensis* and *V. osmolskae*; the maxilla has a nearly horizontal dorsal border whereas in *V. mongoliensis* and *V. osmolskae* the dorsal border is posterodorsally angled; the dorsoventral height of the maxilla is less than the height of the quadrate whereas the maxilla is subequal or greater in height than the quadrate in *V. mongoliensis*; the quadratojugal has a long, ventrally bowed jugal process whereas the jugal process in *V. mongoliensis* is straighter and less elongate; five sacral vertebrae are present, rather than six as in *V. mongoliensis*; and the humerus is elongate, being over 75% the length of the femur whereas the humerus is less than 75% of the femur length in *V. mongoliensis*.

4.4 Description

4.4.1 Cranium

The snout of MPC-D 100/982 is notably shallow compared to other *Velociraptor* specimens. The snout length relative to skull length (Snout Length/Skull length = 0.61; Table 4.2) is comparable to specimens of *Velociraptor mongoliensis* (0.58-0.65) but the snout depth at the lacrimomaxilla contact to snout length ratio is markedly lower (0.23 – *V. vadarostrum*; 0.27-0.31 – *V. mongoliensis*) (Fig. 4.1). This, coupled with the missing skull roof, gives the profile of the snout of *V. vadarostrum* a distinct appearance that seems relatively long and flat compared to

other *Velociraptor* specimens that possess an anteroventrally sloped snout. A strongly anteroventrally angled lacrimal in *V. vadarostrum*, however, shows that the temporal region would have been much deeper than the snout. This is like *V. mongoliensis* but differs in having a greater disparity in dorsoventral depth between the antorbital and temporal regions.

The disparity between antorbital and temporal regions is demonstrated by the difference in maxillary depth and the depth of the quadrate. In *V. vadarostrum*, the ratio of maxillary height to quadrate height is 0.84 compared to a range of 1.00-1.09 for *V. mongoliensis* (A 3.1). A further distinction between these species regarding the disparity of the antorbital and temporal regions is that *V. vadarostrum* has an anteroposteriorly expanded postorbital region. The postorbital region is here defined as the anteroposterior length from the anteroventral part of the jugal-postorbital contact to the most posterior extent of the quadrate. The postorbital region makes up 21% of the total skull length in *V. vadarostrum* (Table 2.1) as opposed to the 17-18% observed in *V. mongoliensis*. The snout length of *V. vadarostrum* compared to its postorbital length is 2.97 times as long, compared to specimens of *V. mongoliensis*, which have proportionately longer snouts compared with the postorbital length (3.41-3.88). The temporal region between the heads of the quadrate of *V. vadarostrum* is also transversely expanded relative to the mid snout width in comparison to the well preserved MPC-D 100/25 (3.19 and 2.73, respectively) (Fig. 4.2).

Premaxilla

The main body of the premaxilla is long and shallow with a length to subnarial height ratio of 2.00 (Fig. 4.3). This ratio is higher than the observed range for *V. mongoliensis* (1.56-1.79) (Fig. 4.1). The premaxilla houses four premaxillary alveoli like other dromaeosaurids and the second premaxillary tooth is notably larger than the third or fourth. The cross section of the

second premaxillary tooth shares a flat lingual surface like *Saurornitholestes langstoni* Sues, 1976 (Currie and Evans 2019).

The subnarial fossa ends anteriorly above the third premaxillary alveolus, like the condition in *V. mongoliensis* (Figs. 4.1, 4.2). The subnarial fossa is most deeply depressed just posterior to the base of the nasal process. Both premaxillae are missing most of the nasal process. The posterior ends of these processes are retained in contact with the nasals (Fig. 4.2). The nasal processes of the premaxillae are connected at the most anterior points of the nasals and diverge posterolaterally at a shallow angle from each other as observed in *V. mongoliensis*. The maxillary processes are broken on both premaxillae. However, grooves for the maxillary process are present and show a long sutural surface extending posteriorly beyond the fifth maxillary tooth position. It is lost, however, due to post-mortem damage (either insects or erosion) so its terminus is not visible (Fig. 4.3). The maxillary processes are triangular in cross section with a near right angle formed by the medial and ventral surfaces.

Maxilla

The maxilla is anteroposteriorly long, and forms most of the snout (0.80). It is nearly half the length of the skull (0.49) (Table 4.2, Fig. 4.3). The maxilla is more elongate (L/H ratio = 3.44) than in any other *Velociraptor* specimen (2.81-3.08) (Char. 32, A 3.2). The maxilla is shallow relative to total muzzle height being little over twice the height of the dentaries (2.10) compared to *V. mongoliensis* (2.23-2.47) (Fig. 4.1). In lateral view, the maxilla appears more like a deep sideways “U” than the acute triangular shape as observed in *V. mongoliensis*. The dorsal border of the maxilla of *V. vadarostrum* forms a continuous line as in *Tsaagan mangas* (Norell et al. 2006), *V. osmolskae*, and the holotype of *V. mongoliensis*; it lacks a notched dorsal surface near the junction of the anterior ramus and antorbital fossa as observed in *Linheraptor exquisitus*

(Xu et al. 2015) and all other specimens of *V. mongoliensis* (Fig. 4.1). The alveolar margin of the maxilla is bowed ventrally, paralleling the curvature of the dentary, and reflecting the overall curvature of the snout. The maxilla of *V. vadarostrum* houses 12 alveoli, a number greater than any known *V. mongoliensis* specimen (10-11) (Table 2.1). The teeth are deeply rooted and the first five maxillary teeth angle anteroventrally towards the anterior end of the tooth row (Fig. 2.18C). The alveoli of the first three maxillary teeth share the same anteroventral angles as the tooth crowns. While some angulation is observed in specimens of *V. mongoliensis* it is restricted to the most anterior tooth or two as in MPC-D 100/24. This specimen of *V. mongoliensis*, however, is badly deformed, especially around the anterior ramus, and the true tooth angle is uncertain. Maxillary tooth angulation in *V. mongoliensis* is otherwise perpendicular to the alveolar margin.

The anterior edge of the anterior ramus is missing on both maxillae, However, the anteroventral corner of the right maxilla is present, and has a small protuberance extending anteriorly as in the holotype of *V. mongoliensis* (Figs. 4.1, 4.3). Given the rounded space for contact with the premaxillae, the anterior edge of the anterior rami would likely also be rounded. This is also observed in other specimens of *V. mongoliensis* and the closely related taxa *Linheraptor exquisitus* and *Tsaagan mangas*. The anterior ramus makes up less than 1/3 of the overall length (0.27), which is lower than all *V. mongoliensis* specimens (0.31-0.33), lower than *Achillobator giganticus* Perle et al., 1999 (0.29), *Atrociraptor marshalli* Currie and Varricchio, 2004 (0.32), *Saurornitholestes langstoni* (0.28-0.31), and much lower than compared to those observed in *Linheraptor exquisitus* (0.46) and *Tsaagan mangas* (0.38). The length to height ratio of the anterior ramus in *V. vadarostrum* (1.40) is within the range observed for *V. mongoliensis*

(1.40-1.75) but is on the low end, likely due to the shallow maxilla and relatively short anterior ramus (Fig. 2.17).

The anterior border of the antorbital fossa is rounded and appears like a sideways “U” in lateral view, reflective of the overall maxilla shape. The most anterior extent is just posterior to the third maxillary alveolus to slightly above the most anterior part of the fourth alveolus. In *V. mongoliensis*, the transition between anterior ramus and antorbital fossa is just posterior to the fourth maxillary alveolus, with little observed variation (Fig. 4.1). The length of the antorbital fossa relative to the maxillary length is high in *V. vadarostrum* (0.34) compared to the closely related *V. mongoliensis* (0.25-0.29), and *V. osmolskae* (0.26 based on estimated maxilla length). The antorbital fossa expands ventrally posteriorly and is broadly exposed on the jugal ramus in lateral view. This is like the condition observed in *Atrociraptor marshalli*, *Deinonychus antirrhopus* Ostrom, 1969, *Saurornitholestes langstoni*, and *V. mongoliensis*. This feature differs, however, from some specimens of *V. mongoliensis* (MPC-D 100/25, and MPC-D 100/54) or *V. osmolskae* in which the ventral border of the antorbital fossa does not extend as ventrally. The ventral extent of the antorbital fossa in *V. vadarostrum* is markedly different from the condition in *Acheroraptor temertyorum* Evans et al., 2013, *Achillobator giganticus*, *Linheraptor exquisitus*, or *Tsaagan mangas* where the antorbital fossa is not exposed laterally along the jugal ramus. The antorbital fossa itself, however, is medially shallow like the latter two taxa and *V. mongoliensis*. The jugal ramus deflects laterally posterior to the 12th maxillary alveolus, toward the contact with the jugal (Fig. 2.18C). Throughout the length of the maxilla, there is little to no evidence of mediolateral deformation suggesting that this deflection is not exaggerated.

Dorsal to the tooth margin, there is a series of neurovascular foramina that run parallel to the tooth margin that are just ventral to a distinct lateral ridge, a trait shared with *V. mongoliensis*

(Barsbold and Osmólska 1999) (Fig. 4.1). The anterior foramina are oriented anteroventrally and shift to a posteroventral orientation posteriorly. The foramina are spaced evenly with the visible teeth on the left maxilla like in the holotype of *V. mongoliensis* (AMNH FARB 6515). However, the spacing of these neurovascular foramina in AMNH FARB 6515 is tighter, and more foramina are present. Both *V. vadarostrum* and AMNH FARB 6515 share a slit-like foramen originating between the eighth and ninth alveoli and extend posteriorly, terminating dorsal to the 10th alveolus. The position of this elongate neurovascular foramen is variable in other eudromaeosaurian taxa; however, it is in the same area in all observed maxillae (between the eighth and 11th alveoli).

The maxillary fenestra is positioned posteriorly within the antorbital fossa compared to *V. mongoliensis*, closer to the anterior edge of the antorbital fenestra than the anterior border of the antorbital fossa (Fig. 4.3). As in AMNH FARB 6515, the maxillary fenestra of *V. vadarostrum* is resting within a maxillary fossa; however, the anterior margin of the maxillary fenestra in AMNH FARB 6515 shares the anterior border of the maxillary fossa whereas the maxillary fenestra of *V. vadarostrum* only shares the anteroventral portion of its border with the maxillary fossa (Fig. 4.1). Whereas the development of the maxillary fossa is variable in *V. mongoliensis*, the position of the maxillary fenestra within the fossa is consistent. Only *V. vadarostrum* shows the condition of possessing a maxillary fenestra positioned posteriorly to the anterior border of the maxillary fossa. There is breakage obscuring the right maxillary fenestra (Fig. 4.3C). However, the left retains the dorsal and ventral borders. Given the shape of the retained borders, the shape of the maxillary fenestra appears to have been rounded with a slight posterodorsal extension. This morphology most closely resembles the shape of the maxillary fenestra observed in *V. mongoliensis* although it is a little more subcircular than elongate.

The promaxillary fenestra is positioned medially to the anterior border of the antorbital fossa as in all dromaeosaurids. In *V. vadarostrum*, it is located posterodorsal to the most anterior point of the antorbital fossa and directly anterior in relation to the maxillary fenestra. This is true for AMNH FARB 6515 but is variable among other specimens (Fig. 4.1). *Velociraptor osmolskae*, however, has large maxillary and promaxillary fenestrae and the centroid of the maxillary fenestra is positioned posterodorsal to the promaxillary fenestra (Godefroit et al. 2008), like some other specimens of *V. mongoliensis* (MPC-D 100/25 and MPC-D 100/54) (Fig. 4.1). The promaxillary fenestra of *V. vadarostrum* is expanded posteriorly due to erosion, like in MPC-D 100/54. In both *V. vadarostrum* and MPC-D 100/54, pillars of bone are observed within the eroded promaxillary fenestrae. In the case of *V. vadarostrum* this structure was confirmed to be the preantral strut (Fig. 2.16). If this feature is the same in MPC-D 100/54, the position of the preantral strut is more anterior in *V. vadarostrum*, positioned between the deeply rooted third and fourth maxillary teeth. This would put the position of the preantral strut in MPC-D 100/54 between the fourth and fifth alveolus. In both, however, the preantral strut is positioned well posterior to the anterior margin of the antorbital fossa, unlike the directly posterior position observed in other eudromaeosaurians (Chapter 2).

The promaxillary recess is distinguished from the maxillary antrum by the preantral strut as in other eudromaeosaurians. However, due to the deeply rooted teeth, this chamber is greatly reduced in its capacity (Fig. 2.16). Whereas this has not been observed in specimens of *V. mongoliensis* based on the position of the promaxillary fenestra it can be inferred that the depths of the maxillary tooth roots are relatively less in *V. mongoliensis* than *V. vadarostrum*. AMNH FARB 6515 also has a dorsally positioned promaxillary fenestra and a shallower maxilla than

larger specimens of *V. mongoliensis*, so the depth of maxillary tooth roots may be relative to maxillary depth.

The maxillary antrum is well defined, expanding dorsoventrally posteriorly as tooth root depths decrease (Fig. 2.16C). The first five maxillary alveoli are deep, extending dorsally to meet the ventral extent of the maxillary fenestra. The alveoli also angle posterodorsally from the fifth alveoli and increases in intensity in each alveolus anteriorly. Unlike in other observed eudromaeosaurians, the palatal shelf does not delineate the upper extent of the tooth roots, or the floor to the maxillary sinus system. It has not been observed in *V. mongoliensis* but *Tsaagan mangas* follows this general trend and possesses a straight but anteriorly inclined palatal shelf (Fig. 2.8C). It is possible that *V. mongoliensis*, like *V. vadarostrum* possesses deeply rooted teeth and a sinuous palatal shelf (Fig. 2.16). The latter is observed in *V. osmolskae* (Godefroit et al. 2008) and therefore could be a generic trait for *Velociraptor*. The low position of the interdental gaps observed in *V. osmolskae* do not necessarily define the depth of the tooth rooting as demonstrated in *V. vadarostrum* (Chapter 2). Extensive expansion of maxillary tooth roots during tooth development may represent another generic trait for *Velociraptor*.

Nasal

The nasal is mediolaterally narrow for the posterior 2/3 of its length (Fig. 4.2). In lateral view it appears like a flat, thin bone running along the dorsal surface of the maxilla for most of its extent (Fig. 4.3). It expands ventrally at the junction between it and the dorsal most extent of the antorbital fossa of the maxilla. It is at this point the cross section of the nasal becomes L-shaped as in *V. mongoliensis* (Barsbold and Osmólska 1999). This change in shape is dorsal to the ventral most extent of the bowed dentaries giving the entire snout a slightly bowed morphology (Fig. 4.3). The dorsal edge of the nasal in *V. vadarostrum* is not as concave in lateral

view as in *V. mongoliensis* (Barsbold and Osmólska 1999, Norell et al. 2006). This is because in *V. mongoliensis* the nasal is more strongly angled anteroventrally over the posterior 2/3 of its length (Fig. 4.1). The lateral exposure of the nasal in *V. vadarostrum* is much less than is observed for *Linheraptor exquisitus* (Xu et al. 2015), *Tsaagan mangas*, and *V. mongoliensis*, and is also less exposed laterally when compared to North American taxa such as *Bambiraptor feinbergi* (Burnham et al. 2000), *Deinonychus antirrhopus* (Fig. 2.15), and *Saurornitholestes langstoni* (Currie and Evans 2019). The most anterior and most posterior portions of the nasals are missing on in MPC-D 100/982. However, the distal extent of the nasal processes of the premaxillae are present, contacting the most anterior preserved portion of the nasals. The maxillary process of the right nasal of *V. vadarostrum* is preserved and reveals the posterior border of the external naris was semicircular and positioned above the second maxillary tooth at its most posterior extent. The maxillary process is short and abruptly ends in a sharp point. The contact of the nasals with the maxilla appear like those of other eudromaeosaurians with the exception of a mediolaterally expanded sutural surface for the nasal dorsal to the maxillary fenestra, a trait shared with *V. mongoliensis*.

Lacrimal

The lacrimal is triradiate and in lateral view would have been “T” shaped and slanted anteroventrally along the anterior process like other dromaeosaurids (Figs. 4.3, 4.4). The anterior process of *V. vadarostrum* is longer than the ventral ramus rather than sub-equal as in *V. mongoliensis* or distinctly shorter as in *Linheraptor exquisitus* (Xu et al. 2015), *Saurornitholestes langstoni* (Currie and Evans 2019), or *Tsaagan mangas* (Norell et al. 2006). The anterior ramus of the lacrimal is much longer than the posterior process like *V. mongoliensis* but differing from the other mentioned taxa where the anterior and posterior rami of the lacrimal are sub-equal in

length. The maxilla-nasal process of the lacrimal can be observed most clearly in dorsal view of the segmented model (Fig. 4.4D). This process extends anteromedially from the anterior ramus and is confluent with a medial ridge that continues to the central body of the lacrimal where it originates. The medial flange is similar to that of *Saurornitholestes langstoni* (Currie and Evans 2019) but the maxilla-nasal process differs in *V. vadarostrum* due to its predominantly medial orientation. In *Saurornitholestes langstoni*, the maxilla-nasal process curves medially and the terminus is anteriorly oriented. The maxilla-nasal process of *V. vadarostrum* also differs from *Saurornitholestes langstoni* in being mediolaterally broad relative to its dorsoventral depth. The anterior ramus has a distinct dorsolateral ridge which defines the dorsal margin of the antorbital fossa like *V. mongoliensis* and other eudromaeosaurians (Fig. 4.4B). The lacrimal duct is observed medial to the concave ventrolateral surface of the anterior ramus. Lateral to this is another pneumatic recess that may house the diverticulum for the nasal gland observed in other theropods (Fig. 4.4C) (Witmer 1997).

Ventral from the duct, the anterior surface of the ventral ramus is concave throughout its length and convex along the posterior surface (Fig. 4.4C). This is like *V. mongoliensis* and other eudromaeosaurians. However, the mediolateral width of the ventral ramus is broader than in North American dromaeosaurids and more like *V. mongoliensis* and other Asian taxa. The ventral ramus of *V. vadarostrum* is bowed medially as in other dromaeosaurids and terminates in a double notched contact with the jugal and palatine (Fig. 4.4C, E). Because most *V. mongoliensis* specimens have complete skulls, the sutural surfaces for the jugal and palatine cannot be directly observed. The contact surfaces for the jugal and palatine for *V. vadarostrum* is in line with the condition proposed by Barsbold and Osmólska (1999) for *V. mongoliensis*. The ventral ramus of the lacrimal in *V. vadarostrum* is inclined posteriorly as in *Adasaurus*

mongoliensis Barsbold, 1983, albeit to a lesser extent (Figs. 4.3, 4.4A-B). A similar condition has been described for *V. osmolskae*, although the lacrimal for this specimen is incomplete and the morphology of the central body is quite variable from *V. vadarostrum*. Like in *V. mongoliensis* the proximal most part of the ventral ramus remains anteroposteriorly thin, only expanding at the lacrimal crest and immediately into the anterior and posterior processes of the lacrimal (Fig. 4.4B). This condition differs from *V. osmolskae* and other close relatives like *Linheraptor exquisitus* and *Tsaagan mangas*, all of which have anteroposteriorly expanding ventral rami beginning approximately at mid-shaft and expanding into blunt triangular central bodies.

The lacrimal crest is not as pointed laterally as in some specimens of *V. mongoliensis* (MPC-D 100/25 and MPC-D 100/54) (Fig. 4.2) and is most similar in appearance to the lacrimals of AMNH FARB 6515 and *Saurornitholestes langstoni* (Currie and Evans 2019). The lacrimal crest of *V. vadarostrum* is restricted laterally to an extent even greater than AMNH FARB 6515 or *Saurornitholestes langstoni*, and does not extend laterally beyond the lateral extent of the ventral ramus as is observed in the other two taxa (Fig. 4.4E). This can be variable on a single specimen, and as is observed for *Linheraptor exquisitus* (Xu et al. 2015), which has a blunt lacrimal crest on the right side and a pointed crest on the left. *Velociraptor vadarostrum* potentially shows a similar asymmetry. However, the right lacrimal is broken and the fragments thereof are displaced. Therefore, the pointed right lacrimal crest may be an artefact (Fig. 4.2). In lateral view the crest expands posteroventrally into a protuberance joining with a small lateral protuberance on the ventral ramus (Fig. 4.4B). This is like *V. mongoliensis* and *Saurornitholestes langstoni*. However, this condition is variable in the former as MPC-100/25 and MPC-D 100/54

have relatively small posteroventral protuberances compared with AMNH FARB 6515 (Fig. 4.1).

The posterior ramus of the right lacrimal is visible in dorsal view (Fig. 4.2). It has a similar morphology to *V. mongoliensis* specimens in that the medial edge extends medially from the central body to overlap the anterolateral corner of the dorsal surface of the frontal. The lateral edge is parallel with the medial border for much of the distance before tapering out in a blunt posterior terminus. The morphology of the posterior ramus is markedly different from those observed in *Bambiraptor feinbergi* Burnham et al., 2000 and *Saurornitholestes langstoni*, which have notched posterolateral edges, and spade shaped posterior termini.

Frontal

The frontal of *V. vadarostrum* is relatively narrow along the orbital margin as in *V. mongoliensis* (Fig. 4.5) and transitions into the postorbital process via a curved rim. This is different from *V. mongoliensis*, however, which possess a more subtle transition that in dorsal view appears as an oblique angle between the supraorbital and postorbital regions of the orbital rim. *Tsaagan mangas* shares the same morphology of the orbital rim of the frontal as *V. mongoliensis*. However, it appears less anteromedially angled along the orbital margin and is more like the condition in *V. vadarostrum*. The condition observed for *Linheraptor exquisitus* (Xu et al. 2015) is similar to *Tsaagan mangas* and *V. mongoliensis*. However, the orbital rim is slightly curved throughout. This condition also contrasts that observed for *V. vadarostrum* in not having a distinct inflection between the postorbital and supraorbital regions of the orbital rim observed at the base of the postorbital process. The distal half of the postorbital process and posterior extent of the frontal are missing in the holotype of *V. vadarostrum* (Fig. 4.5B, D). The nasal and lacrimal contacts are similar to those of *V. mongoliensis* in their positions. The frontal-

nasal contact is straight mediolaterally as in *V. mongoliensis* and *Tsaagan mangas* but different from the anteromedially angled contact observed in *Linheraptor exquisitus*. The suture patterns of *V. vadarostrum* differ from *V. mongoliensis* in that they are dorsoventrally shallow and highly striated as opposed to the deep interfingering suture observed in *V. mongoliensis*.

The ventral surface of the frontal of *V. vadarostrum* is further differentiated from *V. mongoliensis* in having an anteroposteriorly restricted depression for the cerebrum (Fig. 4.5D, F). The lateral extent of the cavity for the cerebrum constricts abruptly adjacent to the postorbital process in *V. vadarostrum* similar to *Dromaeosaurus albertensis* Matthew and Brown, 1922 (Currie 1995) and *Saurornitholestes langstoni* (Sues 1976), whereas the cavity constricts more gradually anteriorly in *V. mongoliensis*, and the lateral extent of the cavity parallels the orbital rim, a condition shared with troodontids (Currie 1985, Evans et al. 2017). The channel between the olfactory and cerebral cavities in *V. vadarostrum* is anteroposteriorly long relative to that observed in other eudromaeosaurians and even troodontids, but the mediolateral constriction is similar in the latter. The mediolateral breadth of the olfactory cavity is similar in *V. vadarostrum* to *V. mongoliensis* both of which have olfactory cavities that are relatively narrow compared to *Dromaeosaurus albertensis* and *Saurornitholestes langstoni*.

The shelf of the supraorbital fossa is incomplete in *V. vadarostrum* (Fig. 4.5B-C). However, the dorsoventral depth is like what is observed in *V. mongoliensis*. The dorsomedial margin of the supraorbital fossa (Fig. 4.5B) is also like *V. mongoliensis* in the “S-shaped” morphology described by Barsbold and Osmólska (1999). Based on this similarity it is likely that relatively little of the posterior portion of the frontal is missing in *V. vadarostrum*.

Jugal

The jugal is roughly triangular in lateral view with a shallowly concave orbital margin (Fig. 4.3). The ventral margin is weathered, and its full extent cannot be ascertained but the ventral margin expands laterally and posteroventrally. It would have likely had a similar ventral protuberance as those observed in *V. mongoliensis* and other Asian eudromaeosaurians. In dorsal view (Fig. 4.2A, B), the suborbital ramus of the jugal curves anteromedially to a degree unobserved in *V. mongoliensis*. Whereas this may seem unique to this species it is difficult to assess the true extent of the bowing in specimens of *V. mongoliensis* due to post-mortem distortion. Therefore, this lateral bowing may be a generic feature of *Velociraptor*, at least for individuals of a certain size. The suborbital ramus is distinctly concave on its lateral surface from the contact with the maxilla until flattening out at a position perpendicular to the contact with the ectopterygoid (Fig. 4.2).

The posterior edge of the postorbital process of the jugal is convex in lateral view as in most dromaeosaurids. However, the angle between the postorbital process and the quadratojugal process is more acute than in most specimens of *V. mongoliensis* apart from MPC-D 100/25 (Fig. 4.1D). Therefore, the lateral temporal fenestra has a broader opening anteroposteriorly in *V. vadarostrum* than in its close relatives. Because of this difference, the lateral temporal fenestra in *V. vadarostrum* appears more pear shaped (Fig. 4.1). The inflexion between the postorbital and quadratojugal processes is more ventral as in *Adasaurus mongoliensis* and *V. mongoliensis* than in *Linheraptor exquisitus* and *Tsaagan mangas*. This is also like what is observed in North American species such as *Bambiraptor feinbergi*, *Deinonychus antirrhopus*, *Dromaeosaurus albertensis*, and *Saurornitholestes langstoni*. However, the angle between the postorbital and quadratojugal processes in *V. vadarostrum* is not as acute as in North American taxa, which possesses a more L-shaped postorbital and quadratojugal process junction.

The postorbital process of the jugal is broad at the base and tapers towards the distal extent (Figs. 4.1, 4.3). In MPC-D 100/982 the most distal ends of the postorbital processes are missing on both the left and right jugals. The shape of the postorbital process is within the range of variation of *V. mongoliensis*, which suggests that it probably would not have extended much further dorsally.

The quadratojugal process of the jugal is bifurcated as in other dromaeosaurids and has a narrow slot to receive the jugal process of the quadratojugal (Fig. 4.3). The dorsal prong of the quadratojugal process is shorter than the ventral one, which extends posteriorly to terminate just anterior to the center of the quadratojugal.

Postorbital

MPC-D 100/982 is missing the right postorbital and most of the left (Figs 4.2, 4.3). The jugal ramus of the left postorbital tapers anteroventrally to a thin point (Fig. 4.3). The overlap with the jugal is extensive and it would have extended over half the length of the preserved ventral border of the postorbital. The contact with the jugal is similar to that of *V. mongoliensis* but differs from the conditions in *Linheraptor exquisitus* (Xu et al. 2015) and *Tsaagan mangas* (Norell et al. 2006) in that the postorbital would still have contributed partially to the border of the lateral temporal fenestra. The postorbital also differs from the condition in *Tsaagan mangas* in having a straight posteroventral border rather than possessing a distinct bulge as observed in lateral view for *Tsaagan mangas*. The squamosal process of the postorbital is largely missing and does not preserve the sutural region. Given the close similarity of this taxon to *V. mongoliensis*, it likely would be very similar in appearance. The differences in the orbital margins of the frontals of *V. vadarostrum* and *V. mongoliensis* suggest there were differences in the contacts between the postorbitals and frontals between these taxa. However, the contacts of

the frontals and postorbitals in other eudromaeosaurians such as *Linheraptor exquisitus*, *Saurornitholestes langstoni* (Currie and Evans 2019) and *Tsaagan mangas* are fairly conservative in their morphology. Therefore, any differences in the frontal processes of *V. vadarostrum* and *V. mongoliensis* would likely be minute.

In dorsal view (Fig. 4.2), a medial process that contacts the laterosphenoid buttress is observed near the anterior margin of the preserved part of the postorbital. This feature is typically concealed in articulated specimens of *V. mongoliensis*, but is visible on the right side of the holotype of *Tsaagan mangas* (Norell et al. 2006).

Quadratojugal

The quadratojugal of *V. vadarostrum* is triradiate like those of most other eudromaeosaurians (Fig. 4.3). The squamosal process bows anteriorly to a lesser extent than observed in North American eudromaeosaurians and some specimens of *V. mongoliensis*. The quadratojugal of *V. vadarostrum* differs from the observed range of variation in *V. mongoliensis* in that the jugal process is subequal in length to the squamosal process of the quadratojugal rather than distinctly shorter. The jugal process is also bowed ventrally along its length, a morphology like the North American eudromaeosaurians. The angle between the squamosal process and jugal process is more obtuse than in the North American eudromaeosaurians and is more like *V. mongoliensis* and other Asian eudromaeosaurians in this way. The long jugal process of *V. vadarostrum* contributes to the more pear-shaped lateral temporal fenestra.

The squamosal process curves posterodorsally as in most eudromaeosaurians (Fig. 4.3). A sharp ridge on the anterolateral edge of the squamosal process slopes into a trough-like depression along the posterior surface. This differs slightly from *V. mongoliensis* in which it is

flatter. Anterior to this ridge is a noticeable flange projecting into the lateral temporal fenestra. This differs from *V. mongoliensis* where the anterolateral edge is the most posterior edge of the squamosal process.

The quadrate process is squared-off posteriorly at its contact with the quadrate. This region is variably square-edged or rounded in *V. mongoliensis*, and rounded in *Tsaagan mangas* (Norell et al. 2006). The length of this process is somewhat variable within *V. mongoliensis* but is anteroposteriorly long in *V. vadarostrum*. It is also relatively longer than is observed in the quadratojugals of North American dromaeosaurids.

Squamosal

Only the ventral process of the right squamosal is preserved in MPC-D 100/982 (Fig. 4.3). The ventral process is triangular and abuts posteroventrally along the anterodorsal border of the squamosal process of the quadratojugal and the anterodorsal border of the blade of the quadrate. This condition is typical in theropods. As in *V. mongoliensis* (Fig. 4.1) the anteroventral process of the squamosal does not contact the postorbital process of the jugal. MPC-D 100/54 shows the condition most clearly (Fig. 4.1C) whereas in MPC-D 100/982 the postorbital process of the jugal is incomplete (Fig. 4.1A) and appears most like MPC-D 100/25 (Fig. 4.1D). This condition differs from *Linheraptor exquisitus* (Xu et al. 2015) and *Tsaagan mangas* (Norell et al. 2006), in which the postorbital is excluded from the border of the lateral temporal fenestra by the squamosal-jugal contact.

Quadrate

The left quadrate of MPC-D 100/982 is complete and well preserved whereas the right quadrate is plastically deformed medially (Fig. 4.3). The quadrate morphology is like that of *V.*

mongoliensis (Fig. 4.1) and has a nearly straight shaft in lateral view but bows slightly medially in posterior view (Fig. 4.6). The shaft twists anterolaterally dorsally and terminates in a well-defined head as in other dromaeosaurids. The lateral face expands anteriorly into a triangular flange that contacts the posteroventral edge of the squamosal and the ventral edge of the squamosal process of the quadratojugal, as in other dromaeosaurids (Fig. 4.3). Ventral to this flange, the quadratic fenestra is broadly exposed in lateral and posterior views as in *V. mongoliensis* and other eudromaeosaurians. The posterior surface of the quadrate shaft is concave from the articular condyles until about halfway up the shaft (Figs. 4.3, 4.6). There the shaft twists anterolaterally as in *V. mongoliensis* (Fig. 4.1) and other dromaeosaurids, but to a greater extent than observed in *Saurornitholestes langstoni* (Currie and Evans 2019). The quadrate differs from *Tsaagan mangas* (Norell et al. 2006) in that the quadrate shaft is not perforated visibly in posterior view, and is similar to *V. mongoliensis* and *Linheraptor exquisitus* (Xu et al. 2015) in this way.

The pterygoid flange is clearly observed in dorsal view (Fig. 4.2), and diverges from the anterolateral flange at a more acute angle than in *Saurornitholestes langstoni*, at a slightly less acute angle than observed for *Tsaagan mangas*, and about the same angle as in *V. mongoliensis*.

Braincase

The braincase of MPC-D 100/982 was described in detail by Norell et al. (2004) and compared to another isolated *Velociraptor* braincase. Differences between these braincases were described as intraspecific variation within *V. mongoliensis* because MPC-D 100/982 was referred to this species at the time. The authors noted some variation in the spacing between the basioccipital tubera. Those of MPC-D 100/25 and MPC-D 100/54 are less mediolaterally separated in comparison with MPC-D 100/982 (Figs. 4.6, 4.7C-D). MPC-D 100/982 also has a

thin wall of bone connecting the basioccipital tubera, a feature also observed in MPC-D 100/54, a specimen of *V. mongoliensis* (Fig. 4.7D). The basioccipital recess observed in MPC-D 100/982 is like the condition observed in *V. mongoliensis* but some features are difficult to compare because they are more obscured in MPC-D 100/54 (Fig. 4.7B-C). The basipterygoid processes of *V. vadarostrum* are widely spaced as in MPC-D 100/54 but the lateral walls of the basisphenoid gradually converge towards the basioccipital tubera. This differs from MPC-D 100/54, in which the walls converge abruptly posterior to the basipterygoid processes then expand laterally towards the basioccipital tubera. The condition in MPC-D 100/54 is more similar to what is seen in both *Linheraptor exquisitus* and *Tsaagan mangas* (Xu et al. 2015).

Palate

The pterygoids of *V. vadarostrum* are largely weathered away. The palatal wing of each pterygoid is a relatively thin sheet of bone that is mostly covered by other bones but the contact with the palatine can be seen. It is slender and sub-rectangular in cross section (Fig. 4.7A). The contacts with the basipterygoid processes are well preserved (Figs. 4.2, 4.6). The contact is mediolaterally narrow and cups the basipterygoid process ventrally with a short hook-like process, and dorsally in a broad dorsomedially expanded process. The hook-like process of the pterygoid wraps around the basipterygoid process and ends in a tapering, triangular point directed posterolaterally. The angle of contact of the pterygoid to the basipterygoid process of *V. vadarostrum* appears similar to the condition in *Tsaagan mangas* and *V. mongoliensis*, although the distal ends of the hook-like processes for the pterygoids in these taxa are eroded or obscured. The quadrate process of the pterygoid extends posterolaterally to meet the pterygoid wing of the quadrate (Fig. 4.2A-B). In dorsal view it is observed near the anteromedial process of the right quadrate.

The lateral process of the right ectopterygoid can be seen in contact with the jugal (Figs. 4.2, 4.7). The lateral process and a small portion of the central body of the left ectopterygoid is still in contact with the left pterygoid. Of the portion of the central body of ectopterygoid that is preserved, not enough of the dorsal surface is present to determine if the ectopterygoid possesses a dorsal recess. However, in ventral view (Fig. 4.7A), there are anterior and posterior recesses in relation to a central ridge associated with the lateral process. The morphology of the ectopterygoid seems like what has been described in *V. mongoliensis*.

The palatines are both preserved but the left one is more complete (Fig. 4.3). The choanal process is strongly arched dorsally as observed in *V. mongoliensis* (Figs. 4.1, 4.3) and contributes to a dorsally restricted choanal fenestra. The lacrimal process is visible in contact with the lacrimal in left lateral view (Fig. 4.3A-B) and is posterolateral to the pneumatic recess of the palatine as in *V. mongoliensis* (Barsbold and Osmólska 1999). The maxillary process is missing on the left side but is mostly preserved on the right and is positioned anterolateral to the pneumatic recess of the palatine (Fig. 4.3C). The palatine of *V. vadarostrum* is quite like the morphology of *V. mongoliensis* and in both cases the choanal process arches dorsally until it is level with the maxillary fenestrae. Because of this, the palatine of *V. vadarostrum* appears larger in comparison to the maxillary fenestra than that of *V. mongoliensis*. However, the difference may simply be an artefact of the shallow snout of *V. vadarostrum*.

4.4.2 Mandible

Dentary

The dentaries of MPC-D 100/982 are long, shallow and bowed ventrally as in *Acheroraptor temertyorum* (Evans et al. 2013), *Linheraptor exquisitus* (Xu et al. 2015), *Tsaagan*

mangas (Norell et al. 2006), and *V. mongoliensis* (Figs. 4.1, 4.3). The dentaries of *V. vadarostrum* are also mediolaterally thin as in *V. mongoliensis* and other dromaeosaurids (Fig. 4.7A-B). However, the dentaries of *Dromaeosaurus albertensis* appear markedly thicker mediolaterally than is the norm for eudromaeosaurian taxa. In ventral view, the dentary is straight throughout most of its anteroposterior length, although there is a slight lateral deflection at the anterior contact with the splenial. A similar lateral deflection is noticed in *V. mongoliensis* (MPC-D 100/25), but it is not as abrupt as in *V. vadarostrum*. This could, however, be due to medial deformation of MPC-D 100/25, particularly in the mandibles. The dentary houses 15 to 16 alveoli depending on how much is obscured anteriorly. *V. mongoliensis* varies between 14 and 15 dentary tooth positions, but has an equal number of dentary teeth compared to the upper jaws of any given specimen (Currie and Evans 2019). This pattern is also shared with the North American taxon *Atrociraptor marshalli*. *V. vadarostrum* likely shares this pattern. The L/H ratio of the left dentary of *V. vadarostrum* is 7.90, which is like the holotype of *V. mongoliensis* (8.05) but is slightly lower than the range in variation observed for *V. mongoliensis* (7.95-8.54). This ratio is higher in *Velociraptor* than in any other eudromaeosaurian genus. The dentary of *Acheroraptor temertyorum* is incomplete but has a L/H ratio of 7.05, although it may have been similarly proportioned to *Tsaagan mangas* (7.54) when complete. The dorsal and ventral borders of the dentaries in MPC-D 100/982 appear parallel throughout their lengths (Fig. 4.3) like other dromaeosaurids other than *Linheraptor exquisitus* and *Tsaagan mangas*. These taxa possess upper and lower margins that diverge posteriorly. The anterior end of each dentary of MPC-D 100/982 cannot be seen, so it is unclear if this specimen has the ventral deflection of the most anterior alveolus that is observed in most other dromaeosaurids. However, the limited anterior portion of the dentary does seem to be deflected downwards towards the front.

The dentaries of *V. vadarostrum* have two parallel rows of neurovascular foramina like *V. mongoliensis*. However, the ventrally positioned neurovascular foramina in *V. vadarostrum* are more ventrally positioned than in *V. mongoliensis* and have limited exposure in lateral view when they are near the ventral border (Figs. 4.3, 4.7). Like *V. mongoliensis* and other dromaeosaurids, the dorsal row of neurovascular foramina is set in a shallow groove and are more closely spaced anteriorly. Anteroposteriorly longer foramina are found towards the back in both species.

The posterior end of the dentary covers most of the splenial in lateral view (Fig. 4.3), although the most posterior ends of both dentaries are missing. The condition observed in *V. vadarostrum* seems to be different from *V. mongoliensis* and other eudromaeosaurians, all of which have more broadly exposed splenials in lateral view.

Splenial

The splenial of *V. vadarostrum* is mostly covered in lateral view but can be observed ventrally and somewhat medially (Figs. 4.3, 4.7). In ventral view, the splenial narrows anteriorly to a thin plate on the inner surface of the dentary, and expands posteriorly to terminate in a blunt, cupping structure to receive the angular (Fig. 4.7A). In lateral view, the splenial likely had a similarly triangular shape to other dromaeosaurids.

Angular

The angulars of *V. vadarostrum* are missing parts of the posterior blades on both sides (Fig. 4.3). The anterior portion of the bone curves anterodorsally as in other dromaeosaurids. The dorsal border is concave in lateral view from the anterior apex until it contacts the surangular. This dorsal border makes up the ventral boundary of the external mandibular fenestra that is

anteroposteriorly elongate and dorsoventrally shallow as in *V. mongoliensis* (Figs. 4.1, 4.3). The anteroventral tip of the angular is cradled by the posterior end of the splenial and would have been covered laterally by the posterior tip of the dentary as is observed in other dromaeosaurids. Behind the sliding contact with the splenial, the ventral margin of the angular forms a gentle convexity in lateral view. Along the anterior portion of the angular, the ventral border wraps around to the medial surface of the mandible similarly to other dromaeosaurids (Fig. 4.7A). The sutural facet for the prearticular is observable on the left mandible and extends posteriorly to a point ventral to the posterior surangular fenestra, like the condition in *V. mongoliensis*.

Surangular

The surangular of *V. vadarostrum* makes up most of the posterior half of the mandible in lateral view as in most theropods (Fig. 4.3). The surangular is anteroposteriorly elongate as in other dromaeosaurids but is shallower dorsoventrally than it is in *Dromaeosaurus albertensis*. A prominent prearticular shelf extends anterior to the jaw joint. Its anterior extent is concealed by the jugal in lateral view, but it is oriented parallel to the mandible as in *V. mongoliensis* (Figs. 4.1, 4.3). This condition differs from that of *Linheraptor exquisitus* and *Tsaagan mangas*, which both have anterodorsally angled prearticular shelves (Norell et al. 2006, Xu et al. 2015). Below the shelf on the left surangular, there is a sub-circular posterior surangular fenestra as observed in other dromaeosaurids (Fig. 4.3). Some of the border is missing due to breakage. However, the shape can be ascertained from the preserved anterior and posterior borders.

The surangular tapers posteriorly in lateral view (Fig. 4.3) but extends medially underneath the mediolaterally broad articular surface of the quadrate, a condition shared among theropods. In *V. vadarostrum*, the area of the surangular that contacts the articular is dorsoventrally low and the posterior edge is angled posteromedially, matching the angle of the

articular condyles of the quadrate (Fig. 4.6). In lateral view (Fig. 4.3), the morphology is similar to *Saurornitholestes langstoni* and *V. mongoliensis* in being dorsoventrally shallow, angled horizontally so as to be parallel to the axis of the mandible and there is no posterior extension beyond the articular quadrate joint.

Articular

The right articular of MPC-D 100/982 is missing and only the surangular remains in articulation with the lateral condyle of the quadrate (Fig. 4.6A-B). The left articular is preserved in articulation with the quadrate, but a small portion of the lateral half may be missing. At the posterior end of the articular is what appears to be a well developed retroarticular process (Figs. 4.3, 4.6). In ventral view it is part of the articular and has a medial deflection (Fig. 4.7). In posterior view it is observed to have a brief posteroventrally sloped surface directly following the contact with the quadrate as has been described for *V. mongoliensis* (Barsbold and Osmólska 1999). A well developed process on the retroarticular process is known for *Deinonychus antirrhopus* (Ostrom 1969), *Tsaagan mangas* (Norell et al. 2006) and all other dromaeosaurids where this part of the bone is well preserved. The presence of an anteroposteriorly long retroarticular process with a posterodorsally cupped surface is present for strong abductor muscle attachment as in other dromaeosaurids.

4.4.3 Axial skeleton

Cervical vertebrae

Five or six cervical vertebrae are preserved in articulation and folded over the dorsal region. The ventral surfaces of the anterior three preserved cervicals are broadly exposed (Figs. 4.8, 4.9). The atlas-axis complex, and several of the anterior cervicals were not preserved in this

specimen and are not in articulation. Much of the axial series is, however, obscured by matrix or damaged from scavenging (Norell and Makovicky 1999).

The preserved anterior cervical vertebrae are similar in morphology to those of *V. mongoliensis* and *Tsaagan mangas* in having transversely expanded zygapophyses and low neural arches with dorsoventrally shallow neural spines. The cervical centra are mediolaterally wide at their anterior intervertebral surfaces but constrict transversely abruptly behind the articulation. They remain relatively narrow posteriorly for most of their length. Anteroposteriorly elongate and flat cervical ribs attach to the parapophyses and extend posteriorly parallel to the longitudinal axes of the centra. On the second anterior cervical, there is a deep pneumatic fossa on the lateral surface of the centrum (Fig. 4.9). Whereas the centra cannot be examined thoroughly in this specimen, there are several additional pneumatic structures. For example, the second last cervical vertebra has rotated to expose complex pneumatic networks inside the broken neural arch (Figs. 4.8, 4.10A).

The elongate, blade-like cervical ribs are similar in morphology to those observed in other Asian dromaeosaurids (Fig. 4.10A). The articular processes (capitula) of the cervical ribs are largely missing due to damage or because they are covered by matrix.

The most posterior preserved cervical (Fig. 4.8) appears transitional in morphology to a more dorsal-like form similar to what is observed in *Linheraptor exquisitus* (Xu et al. 2010a). The centrum is not constricted posterior to the anterior intervertebral articulation like those at the front of the cervical series, and the centrum is not as elongate as those of anterior cervicals. A small pneumatopore is ventral to the base of the right prezygapophysis.

Dorsal vertebrae

The dorsal vertebrae are largely covered by matrix and ribs (Figs. 4.8-4.10). There is a small pneumatopore in the first dorsal vertebra (Fig. 4.10). Four dorsal vertebrae are partially exposed anterior to and partially overlapped by the pectoral girdle. Two dorsals can be seen anterior to the sacrum (Fig. 4.11). The first definitive dorsal vertebra is positioned just anterior to the pectoral girdle and is identified as such by its articulation with a well developed, two headed rib (Fig. 4.10B). The ventral surface of the first dorsal vertebra has a broad, midline keel that tapers posteriorly to end in the midsection. The hypapophysis expands laterally to connect with the broad parapophyses. A small circular pneumatopore is on each side of the centrum near the base of the parapophysis.

The centra of the dorsal vertebrae are anteroposteriorly short relative to those of the cervical vertebrae (Figs. 4.8, 4.10). The posterodorsally directed neural spines of the dorsal vertebrae are more dorsoventrally tall than those of the cervical vertebrae. The apices of the neural spines expand transversely into mediolaterally expanded tables as observed in *Linheraptor exquisitus* and *V. mongoliensis*. The transverse processes of the dorsal vertebrae are best exposed near the pelvic girdle and are dorsolaterally oriented and anteroposteriorly broad (Fig. 4.11A). A small pneumatopore is observed on the second last centrum exposed anterior to the sacrum. The pneumatopore is ventral to the transverse process. Norell and Makovicky (1999) noticed a large pneumatopore on the last dorsal centrum in *V. mongoliensis* below the transverse process. Unfortunately, pneumatic features tend to be quite variable.

The dorsal ribs are two-headed and thin in cross section (Fig. 4.8). The tuberculum articulates with the transverse process of its corresponding dorsal vertebra and the capitulum attaches to the parapophysis. The shaft of a dorsal rib is bowed laterally and has a groove extending down the anterior surface. The groove begins lateral to the centrum and likely

continues along most if not all the shaft. No distal ends remain in position, but the grooves extend to the distal ends in other theropods, including *V. mongoliensis* (Norell and Makovicky 1999).

Sacrum

The sacrum consists of five sacral vertebrae, all of which are fused together. Fusion of the last two sacral centra is observed (Figs. 4.8, 4.9, 4.11A)) and so is the fusion of the neural spines of five sacral vertebrae into a continuous lamina as has been described for *V. mongoliensis* (Fig. 4.9) (Norell and Makovicky 1999). The first caudal vertebra (caudosacral) of MPC-D 100/982 is unfused and distinct from the sacral vertebra. This is a trait suggested by Norell and Makovicky (1999) to be an indication of a pre-adult ontogenetic stage within *V. mongoliensis*. This might be a difference between *V. mongoliensis* and *V. vadarostrum* given the more mature nature of *V. vadarostrum* based on cranial fusion (Norell et al. 2004). It is also possible that the caudal centrum never fused into the sacrum. The sacral ribs of the sacral vertebrae extend posterolaterally from the centra and expand anteroposteriorly near their contacts with the medial surface of the ilia. In *V. mongoliensis*, the caudosacral vertebra has broad transverse processes that extent anterolateral to contact the postacetabular blade (Norell and Makovicky 1997). It seems that this caudosacral was in the process of being integrated into the sacrum in *V. mongoliensis*, but only one specimen shows fusion of the sixth sacral centrum into the sacrum (MPC-D 100/986; Norell and Makovicky, 1999). Both the posterior extent of the iliac blades and the transverse processes of the caudosacral vertebra are missing in MPC-D 100/982 so it is unclear if the caudosacral participated in the sacrum this way. Eudromaeosaurians from the Late Cretaceous of North America typically have six fused sacral centra.

Caudal vertebrae

Most of the caudal series is missing and only the first six caudal vertebrae are preserved (Figs. 4.8, 4.9, 4.11A-B). The caudosacral vertebra is anteroposteriorly short compared to the following caudal centra. The outlines of the ventral surfaces of the first five caudal vertebrae are rectangular and have parallel ventrolateral ridges. This feature is least pronounced on the first caudal, which is closer to a square because of its anteroposterior shortness. The sixth caudal centrum is rounded at the base and lacks the ventrolateral ridges of the anterior caudal vertebrae. The second to sixth caudal vertebrae are constricted ventrally at their anteroposterior midpoints, and the ventral surface of each is dorsally arched in lateral view. The posteroventral corners of each caudal centrum have two ventrolateral posterior facets for articulation with the haemal arches. A complementary pair of facets are present on the anterolateral corners of the centrum of the second caudal vertebra (and subsequent caudal centra). These anteroventral facets also articulate with the haemal arches, although they are much smaller than the posterolateral facets.

The neural arches are variably preserved on the anterior caudals of *V. vadarostrum*. The prezygopophyses are well developed, arched dorsally, and extended anterodorsally to meet the postzygopophyses of the preceding vertebra (Figs. 4.8, 4.9). Postzygopophyses are positioned near the base of the neural arch and are angled ventromedially to complement the dorsolateral orientation of the prezygopophyses. The neural spine of the first caudal is oriented dorsally, but the angle of the neural spine shifts progressively to a more posterodorsal orientation on more posterior caudals. The transverse processes of the first caudal are missing and those of the second are short relative to the more posterior caudals. The transverse processes of the caudal vertebrae posterior to the first, are oriented posterolaterally. Posterior to the second caudal, the transverse processes are elongate and project quite far laterally. The neural arches of the caudal vertebrae in *V. vadarostrum* are quite like those of *V. mongoliensis*. The only apparent difference is that the

prezygopophyses of the caudal vertebrae in *V. vadarostrum* are slightly curved as opposed to them being straight in *V. mongoliensis*. This slight curvature might possibly be variable within species of *Velociraptor*.

The haemal arches are angled posteroventrally from the vertebral column and are long and flat when observable (Figs. 4.8, 4.9, 4.11). The first haemal arch is more gracile in lateral view than the more posterior five caudals. The first haemal arch is angled more posteriorly than the other arches a trait observed in other theropods. By the fifth haemal arch, the spine becomes anteroposteriorly broader in lateral view towards the distal end. The arrangement of haemal arches and the shape of the anterior six caudal vertebrae in *V. vadarostrum* are similar to what is described for *V. mongoliensis* (Norell and Makovicky 1997, 1999).

4.4.4 Appendicular skeleton

Pectoral girdle

The pectoral girdle of MPC-D 100/982 is nearly complete with both scapulae, a large portion of the left coracoid, half of the furcula, and large portions of the highly fragmented sternal plates (Figs. 4.8-4.10, 4.12). Several features of the pectoral girdle were described in Norell and Makovicky (1999). Therefore, only areas not addressed will be discussed here, or points of comparison where the specimen varies from what is observed in specimens of *V. mongoliensis*.

Scapulocoracoid

The scapula is long and strap-like with an anterior expansion where it meets the coracoid (Fig. 4.10). A small fossa on the ventrolateral surface is observed in *V. vadarostrum* distal to the laterally oriented glenoid fossa. This surface is convex in specimens of *V. mongoliensis*

previously described. The dorsal and ventral borders of the scapular blade are roughly parallel throughout its length, and there is a slight dorsoventral expansion towards the distal end.

The coracoids are badly damaged and their morphology difficult to ascertain. The posterior edge of the right coracoid ventral to the glenoid is rugose in texture and has a prominent coracoid tuber (Figs. 4.10, 4.12). A relatively steep sub-glenoid fossa is present posterior to the coracoid tuber. The tuber appears more prominent and is surrounded by a greater area of rugose texture than what has been described for *V. mongoliensis*.

The furcula of *V. mongoliensis* was described by Norell and Makovicky (1999) and included mention of the furcula of MPC-D 100/982. The furcula is a chevron shaped element with dorsolateral processes extending on either side from a ventral zone of fusion on the midline. In both MPC-D 100/982 and MPC-D 100/976, only the right half of the furcula is preserved. An apical ridge is oriented ventrolaterally to the left side in MPC-D 100/976 but the zone of fusion where the apical ridge is observed is completely missing in MPC-D 100/982.

The sternal plates are badly damaged and only commented on by Norell and Makovicky (1999). Whereas not much more can be said here, the general shape of the sternal plates can be inferred based on what is preserved and comparisons with other specimens (Fig. 4.12). The posterior border of the right sternal plate can be discerned by the presence of gastralium in association with this edge. Anterolateral to the first gastralium is a preserved natural edge of the sternal plate. This corner was not preserved in MPC-D 100/985 (Norell and Makovicky 1997) but the borders leading into this corner suggest it would be comparable. It is also observed on MPC-D 100/985 that the sternal plates can be asymmetrical in their shapes. Regardless, by following the lateral edge of the sternal plate that is preserved, it can be observed that the general shape is retained. The right sternal plate has an hourglass shape, its lateral border curves

medially to a constricted mid region in ventral view, then expands again posteriorly to meet the coracoid. The left sternal plate is much less complete but the parts that are present reflect a similar shape, suggesting this is a reasonable interpretation. It is also consistent with the outline of the sternum in other dromaeosaurid taxa (Godfrey and Currie 2004). The sternal plate does not preserve the contact with the coracoids, so its anterolateral edge is unknown.

There are many anteroventral striations present on the posterior region of the ventral surface of the sternal plate (Fig. 4.12). The striations are not regular or parallel, and a few of them meet. This texture is not observed in *V. mongoliensis* but does not appear to be caused by preparation or weathering.

Forelimb

The humerus of *V. vadarostrum* is described in Norell and Makovicky (1999) and shares similar morphology with *V. mongoliensis*. The relative length of the humerus in *V. vadarostrum* is 75% the length of the femur, which is longer than observed in *V. mongoliensis* (Table 4.2, Figs. 4.8, 4.10A). The humeral heads of *V. vadarostrum* and *V. mongoliensis* are strongly deflected posteriorly compared to the weakly deflected humeral heads of *Deinonychus antirrhopus* or *Saurornitholestes langstoni*. This causes the deltopectoral crests of the Asian taxa to be directed more anterodorsally than those of North American taxa. The humerus is also robust compared to *Saurornitholestes langstoni* with a mid-shaft diameter 0.10 the length of the humerus for *V. vadarostrum* whereas the width to length ratio of the humerus is 0.080 for *Saurornitholestes langstoni* (TMP 1989.121.0039). The diameter to length ratio is like that of *V. mongoliensis* (0.097-0.11). The deltopectoral crest is largely missing. However, the distal limits of the crests along both humeri can be identified by the anterolateral expansions of the shafts. Based on the proximal position and the estimated proximal extent of the humerus, it is hypothesized that the

deltpectoral crest would occupy approximately 0.33 of the length of the humerus. This is greater than observed for *Saurornitholestes langstoni* (0.29) and is at the upper range for *V. mongoliensis* (0.25-0.32).

The ulnae are distinctly bowed posteriorly and much thicker than the radii. The proximal end of the ulnae expands dorsoventrally and would likely terminate in an olecranon process (Figs. 4.8, 4.10A). From the proximal end throughout most of the length of the ulna, the shaft is triangular in cross section. In right lateral view, however, a small portion of the cupped articular surface for the humerus remains. The distal end of the left ulna, however, expands mediolaterally where it would articulate with the carpals. The proximal and distal ends of the ulnae are either obscured by matrix or damaged.

The radii are relatively straight compared to the ulnae and much thinner at mid shaft (Figs. 4.8, 4.10A). The radii are triangular in cross section throughout most of their shaft lengths but become circular towards the proximal and distal ends. The distal and proximal ends are either obscured by matrix or are largely missing due to weathering or insect damage. However, they are shorter in proximodistal length than the ulnae.

The manus was described in detail by Norell and Makovicky (1999) and has served as a reference for *Velociraptor* manual morphology and comparison amongst dromaeosaurids. When examining the manus of *V. vadarostrum*, it differs from *V. mongoliensis* in the proportions of the digits. In specimens of *V. mongoliensis*, digit I is more robust and longer in relation to digit II than what is observed *V. vadarostrum*, which has a relatively short digit I that is of subequal thickness to digit II. The ratio of the combined lengths of metacarpal I and phalanx I-1 to metacarpal II in *V. mongoliensis* is 1.22-1.29 compared to 1.16 in *V. vadarostrum*, which is a proportion more similar to *Deinonychus antirrhopus* (Ostrom 1969).

Pelvic girdle

The ilia of *V. vadarostrum* were described by Norell and Makovicky (1999), who considered them to fall within the range of variation of *V. mongoliensis*. These authors did note a vertical crest dorsal to the acetabulum on the left ilium (Figs. 4.9, 4.11B) not noticed on other specimens of *V. mongoliensis*. They suggested it was a variant morphology. The ilia of *V. vadarostrum* have suffered some transverse post-mortem distortion in a manner similar to specimens of *V. mongoliensis* but no other specimen has shown anything that looks like the vertical crest even with deformation taken into account. Furthermore, a ridge is present on the right ilium in the same location although it is a little less obvious because of the horizontal deformation. Vertical crests are a defining characteristic of many theropods but probably arose independently several times, including in other groups such as Aves (Hutchinson 2001). The vertical crest of *V. vadarostrum* differs from those described in tyrannosauroids in being anterodorsally oriented as opposed to dorsoventrally oriented in the latter (Carrano and Hutchinson 2002, Brusatte and Carr 2016).

The ilium is rounded anteriorly rather than notched as in other eudromaeosaurians such as *Achillobator giganticus*, *Bambiraptor feinbergi*, *Deinonychus antirrhopus* and *Saurornitholestes langstoni* (Figs. 4.8, 4.11B). *V. mongoliensis* has been coded as having a notched anterior margin of the iliac blade in recent analyses (Evans et al. 2013, Currie and Evans 2019). This has largely been based on early described specimens of *V. mongoliensis* that lost anterior portions of the iliac blade to post-mortem damage (Norell and Makovicky 1997, 1999). However, observations of well-preserved specimens such as MPC-D 100/25 demonstrate that the anterior margin of the ilium in *V. mongoliensis* is also rounded. This makes this characteristic

synapomorphic for *Velociraptor* and open for reinterpretation of species such as *Adasaurus mongoliensis*, which is also supposed to have the “notched” condition (Barsbold 1983).

The pubes are preserved in contact with each other but are dislocated from the pelvic girdle and displaced anteroventrally relative to the sacrum (Figs. 4.8, 4.11A). The pubes are proximodistally long and anteroventrally narrow. Based on the edge of the pubis displaced from the ilium, the pubes would have been retroverted naturally as is observed throughout Dromaeosauridae. Most of the pubes are obscured by other bones of the articulated specimen, and by matrix. Proximally there is a pubic tubercle near the iliac peduncle as in *V. mongoliensis* (Fig. 4.11). The pubic apron has limited exposure in posterior view, but the pair undergo mediolateral tapering towards the distal end, which is broken (Fig. 4.11A, C). In *V. mongoliensis*, there is a subtle lateral ridge on the pubic shaft distal to where the pubic apron originates (Fig. 4.11C) (Norell and Makovicky 1997, 1999). There is no observable pubic boot on this specimen but broken edges on the posterodistal edges of the pubes suggest there was a posterior pubic boot as in other eudromaeosaurians (Fig. 4.11A).

The ischium is almost completely weathered away (Figs. 4.8, 4.11A). All that remains is a small triangular bit that likely represents the posterodorsal region of the ischium. The iliac peduncle of the ilium is missing on both sides, and the puboischiatic peduncle is obscured by the femora. Therefore, the orientation of the ischium is uncertain. Based on close relatives such as *V. mongoliensis*, the ischium should be elongate proximodistally, with a squared-off distal end in lateral view.

Hindlimb

The femora of *V. vadarostrum* are nearly complete, although there was some lost bone surface from the left femoral shaft (Figs. 4.9, 4.11B), and the ends of both femora have suffered some damage (Fig. 4.8, 4.9, 4.11A-B). The femora are proximodistally shorter than the tibiae (Table 4.2) and approximately twice the length of the metatarsals. The femora are bowed anteriorly and of subequal circumference throughout their proximodistal lengths. The greater and lesser trochanter are missing from the right femur and only the lesser trochanter is preserved on the left femur (Fig. 4.11B). The lesser trochanter is well developed with a rugose anterolateral surface as in *V. mongoliensis* (Norell and Makovicky 1999). A proximal lateral ridge and posteriorly adjacent posterior trochanter are also preserved on the left femur, which is like *V. mongoliensis*. A fourth trochanter was also described for *V. mongoliensis* (MPC-D 100/986) on the posteromedial edge of the femur, medial to a proximally opening nutrient foramen. In MPC-D 100/982, a thin broken edge is observed medial to a proximally opening foramen on the right femur. This is likely the location of the broken fourth trochanter. Comparatively, the fourth trochanter of *V. vadarostrum* seems to be more mediolaterally narrow than what was described for *V. mongoliensis* but extends proximodistally to a similar extent.

The heads are largely missing from both femora. However, the medioventral surfaces of the shafts are retained in both femora, and have the dorsomedial angle leading to the head that is typical in dromaeosaurids (Figs. 4.8, 4.9, 4.11A-B). The femora are slightly laterally bowed as in *V. mongoliensis*. The distal condyles are largely lost; however, a posterolateral ridge is observed on the right femur, and about 2/3 of the way from the proximal end of the bone there is a shallow intercondylar fossa delineating its extent (Fig. 4.11A). This ridge extends down to the lateral condyle. The intercondylar fossa is not observed in MPC D 100/986 but may be variable as the left femur of *V. vadarostrum* lacks a discernable fossa anterolateral to the posterolateral ridge.

The tibiae of *V. vadarostrum* resemble those described for *V. mongoliensis* in being long, laterally bowed, anteroposteriorly thin and mediolaterally wide. The cnemial crest of the right tibia is missing, but it is partially preserved on the left tibia (Fig. 4.8). The cnemial crest projects anteriorly as a triangular process that is slightly deflected laterally. It has a rugose texture around the apex of the crest as in *V. mongoliensis*. The proximal condyles are missing from both tibiae, and the distal end of the right tibia is missing. The distal end of the left tibia is preserved with the astragalus and calcaneum in articulation (Figs. 4.9, 4.13A). The calcaneum is in contact with the astragalus as well as with the distal end of the fibula. The arrangement of these elements matches what has been described for *V. mongoliensis*. The condition of MPC-D 100/982 does show that the calcaneum and astragalus have shifted slightly anteriorly and are slightly separated from the tibia.

A tarsal is preserved in association with the proximal ends of the fourth and fifth metatarsals (Fig. 4.13A). Based on the position and comparison with specimens of *V. mongoliensis* this tarsal is probably the fourth distal tarsal rather than the third as was suggested by Norell and Makovicky (1999). The fifth metatarsal is positioned at the posterolateral edge of the metatarsus and is thin throughout its length like observed in *V. mongoliensis* (Norell and Makovicky 1997) and just about every other theropod. The fifth metatarsal originates slightly dorsal to the rest of the metatarsals and bows posteriorly along its proximodistal length. Although it is broken distally, the fifth metatarsal would not likely have extended more than halfway distally along the fourth metatarsus.

The arrangements and morphologies of the metatarsals of *V. vadarostrum* are like those described for *V. mongoliensis* (Norell and Makovicky 1997; 1999). However, there is a pathology of the right metatarsal II just proximal to the articulation for metatarsal I (Fig. 4.13B).

This pathology has a rugose surface and is exposed medially as two distinct bulges. The proximal growth is split into two rounded protuberances that appear almost as a condylar surface. Distal to this growth is a trough followed by the second growth that overlaps with the proximal tip of the first metatarsal.

4.5 Results

4.5.1 Principal component analysis

PCA analysis of *Velociraptor* specimens, *Linheraptor exquisitus*, and *Tsaagan mangas* using untransformed linear measurements shows that most of the variation is contributed by PC 1 (72.6%) with PC 2 comprising 14.8% of the variation (Fig. 4.14). Measurements that loaded positively in PC 1 are maxillary length, height of the maxilla, length of the anterior ramus, and proximal height of the anterior ramus (Table 4.4). Length of the first nine maxillary alveoli was equally loaded with maxillary length in PC 1; however, these two variables are highly correlated (Table 4.7) and are most likely compounding one another. Negative placement of specimens along PC 1 is primarily from the measurement of the distance between the maxillary fenestra and the anterior border of the antorbital fossa. Along PC 1, there is extensive overlap of taxa; *Tsaagan mangas*, *V. osmolskae*, and *V. vadarostrum* fall within the range of variation of *V. mongoliensis* along this axis (Fig. 4.10A). Measurements with the most positive loadings in PC 2 are maxillary length, length of the antorbital fossa, and the space between the anterior border of the antorbital fossa and the maxillary fenestra (Table 4.4). Negative displacement is influenced by length of the anterior ramus, and the height of the ventral lamina below the antorbital fossa along the length of the maxilla. Positive positions of specimens along both axes is mostly influenced by maxillary length.

The cluster of *V. mongoliensis* spreads positively along both PC 1 and PC 2, suggesting they are following a trend in maxillary size (Fig. 4.10A). Although spaced distantly, *Linheraptor exquisitus* and *Tsaagan mangas* are along the same orientation as the *V. mongoliensis* cluster. However, both are more negatively placed along PC 2 than the cluster of *V. mongoliensis* specimens. The extreme negative position of *Tsaagan mangas* along PC 2 is indicative of a long anterior ramus, tall ventral lamina of the maxilla, and a maxillary fenestra positioned against the anterior border of the antorbital fossa. These features are all shared with *Linheraptor exquisitus*. Conversely, *V. vadarostrum* is positioned positively on PC 2 due to a long antorbital fossa, dorsoventrally shallow ventral margin below the antorbital fossa, and a relatively large space between the maxillary fenestra and anterior boundary of the antorbital fossa. *V. osmolskae* is positioned close to the cluster of *V. mongoliensis* but has a relatively negative position along PC 2. *V. osmolskae* has a dorsoventrally deeper ventral margin than *V. mongoliensis* and a more anteriorly positioned maxillary fenestra, approaching the conditions of *Linheraptor exquisitus* and *Tsaagan mangas*. The position of *V. osmolskae* in relation to the *V. mongoliensis* cluster is much closer than with the position of the *V. mongoliensis* cluster to *V. vadarostrum*. *Velociraptor vadarostrum* demonstrates an extreme morphology to *Linheraptor exquisitus* and *Tsaagan mangas*.

The principal component analysis of the log transformed data is quite different but does recover the same distinct groupings as the previous analysis, primarily along the PC 1 axis (Fig. 4.14B). Similar arrangements occur as *V. mongoliensis* forms a cluster with a large spread across PC 2 but is restricted in spread along PC 1. *Velociraptor vadarostrum* and *V. osmolskae* are spaced away from the *V. mongoliensis* cluster along PC 1. *Velociraptor vadarostrum* is placed at the extreme negative end of PC 1 whereas *Linheraptor exquisitus* plots on the extreme positive

end of PC 1. *Linheraptor exquisitus* is positively placed along PC 2 compared to *Tsaagan mangas* in an arrangement parallel to the linear spread of the *V. mongoliensis* cluster. PC 1 constitutes 79.8% of the variations, and the loadings are predominantly influenced positively by the depth of the ventral margin and the length of the long axis of the maxillary fenestra. On the other hand, negative loadings are dominated by the distance between the maxillary fenestra and anterior margin of the antorbital fossa and to a much lesser degree by the length of the antorbital fossa (Table 4.4). PC 2 comprises 10% of the variation and is loaded most positively for the distance between the maxillary fenestra and the anterior border of the antorbital fossa, the length of the long axis of the maxillary fenestra, and the anteroposterior length of the preantorbital bar (Table 4.4).

Loadings for the PCA including all taxa including MOR 553S-7.30.91.274 (Fig. 4.15) did not change significantly from the analysis in Chapter 3 (A 2.4; Fig. 3.3D). MOR 553S-7.30.91.274 plotted more positively along PC 1 than the juvenile specimen of *Bambiraptor feinbergi* (AMNH FARB 30556) but plotted in roughly the same position along the axis for PC 2. *Velociraptor mongoliensis* specimens plotted in a straight line primarily along the axis of PC 1 with only a slight positive shift along PC 2 for larger specimens such as MPC-D 100/25.

4.5.2 Regression analyses

Simple least squares regressions of *Velociraptor* specimens for the PC 1 scores (Table 4.3) and the log transformed maxillary length shows a strong correlation coefficient ($r^2=0.92$; $p=0.0024$) (Fig. 4.16A). *Velociraptor osmolskae* plots within the 95% confidence range of potential slopes whereas *V. vadarostrum* falls outside of this interval. Specimens of *V. mongoliensis* fit tightly to the trendline whereas specimens of other species of *Velociraptor* plot lower than the expected trend.

Multiple regression analysis between *V. mongoliensis* specimens and multiple regressions including different species show highly variable results (Table 4.5). The correlation coefficient of the multiple regression analysis for *V. mongoliensis* ($R^2=0.747$) is quite high with low error (MSE=0.00355) compared to when *V. osmolskae* ($R^2=0.294$; MSE=0.168) or *V. vadarostrum* ($R^2=0.362$; MSE=0.0164) are added into the analysis. The results of the multiple regression are similarly affected by the addition of *Linheraptor exquisitus* and *Tsaagan mangas* to the analysis ($R^2=0.237$; MSE=0.0422).

The individual regressions of the multiple regression analyses that are affected by the addition of *V. osmolskae* or *V. vadarostrum* do not show much overlap (Table 4.6). Adding *V. osmolskae* to the *V. mongoliensis* group for regression analyses causes the degradation of the regressions of the distal anterior ramus height ($r=0.608 - r=0.310$), antorbital fossa ($r=0.978$, $p=0.022 - r=0.873$, $p=0.058$) and antorbital fenestra height ($r=0.721 - r=0.423$), distance between the maxillary fenestra and anterior margin of the antorbital fossa ($r=0.829 - r=0.337$), and the distance between the anterior margin of the antorbital fenestra from the ninth maxillary alveolus ($r=0.875 - r=0.005$). Interestingly addition of *V. osmolskae* to the regression analysis improves the regression of the long axis length of the maxillary fenestra ($r=0.852$, $p=0.148 - r=0.876$, $p=0.052$). Addition of *V. vadarostrum* to the multiple regression causes the degradation of the individual regressions for maxillary height ($r=0.967$, $p=0.033 - r=0.865$, $p=0.059$), length of the anterior ramus ($r=0.997$, $p=0.003 - r=0.799$, $p=0.105$), antorbital fossa length ($r=0.914 - r=0.666$), distance between the maxillary fenestra and the anterior border of the antorbital fossa ($r=0.829 - r=0.140$), the height of the ventral margin anteriorly ($r=0.987$, $p=0.013 - r=0.865$, $p=0.58$), width of the preantorbital bar ($r=0.893 - r=0.589$), and the distance between the anterior margin of the antorbital fenestra and the ninth maxillary alveolus ($r=0.875 - r=0.505$). The

addition of both *V. osmolskae* and *V. vadarostrum* destabilize the regression for maxillary fenestra position in relation to the anterior margin of the antorbital fossa, and the distance between the anterior margin of the antorbital fenestra and the ninth maxillary alveolus. In the former measurement, they are disparate from the *V. mongoliensis* trend in opposite ways (Fig. 4.16E). Of the measurements affected, the addition of *V. vadarostrum* caused three measurements to lose significant correlations: maxillary height, length of the anterior ramus, and the height of the ventral margin anteriorly (Table 4.6). Comparatively, the addition of *V. osmolskae* only caused the loss of one significant correlation: height of the antorbital fenestra.

Reduced major axis regression (RMA) was used to examine the variables where the addition of *V. vadarostrum* to the *V. mongoliensis* dataset had a great effect on the slope, correlation coefficient or significance of the correlation. The RMA for the height measurement showed a similar degradation as in the multiple regression analysis losing significance ($p=0.027 - 0.071$) and producing a looser trend ($r^2=0.946 - r^2=0.716$) (Table 4.7). The slope had a broad confidence interval before the addition of *V. vadarostrum* (0.61, 2.69) but did broaden with its addition (-0.034, 2.81). *Velociraptor vadarostrum* plots below expected trends for this measurement (Fig. 4.16B). Addition of MPC-D 100/24 to *V. mongoliensis* in the RMA of antorbital fossa length to maxillary length, caused the group to show significantly correlated results ($r^2=0.824$, $p=0.033$) with a narrow slope confidence interval (0.48, 1.99) but when *V. vadarostrum* was added to the regression the trend destabilized ($r^2=0.480$, $p=0.127$) broadening the confidence interval for slope (-0.87, 3.92). *Velociraptor vadarostrum* plots higher than expected for the trend of this character (Fig. 4.11D). MPC-D 100/24 was also added to the RMA of anterior process length to maxillary length and resulted in comparable stats to the previous regression ($r^2=0.991$, $p=0.00035$). The slope for this regression was also narrow, capturing the

value of 1 (0.99, 1.34) Addition of *V. vadarostrum* this time did not cause the loss of significant correlation ($p=0.034$) but did cause a large decline in correlation coefficient ($r^2=0.626$) and also broadened the slope confidence interval (0.43, 2.17). *Velociraptor vadarostrum* plots low compared to the trend for this measurement but retains correlation with the trend (Fig. 4.16C). RMA of the distance between the maxillary fenestra and anterior border of the antorbital fossa showed no significant correlation ($p=0.171$) and low fit of the trend ($r^2=0.688$). However, addition of *V. vadarostrum* caused these values to drastically change ($p=0.822$, $r^2=0.020$). Whereas the slope confidence interval without *V. vadarostrum* was already broad (-1.48, 2.51), it broadened to a great extent positively (-1.50, 16.46). *Velociraptor vadarostrum* plots higher than expected of the trend for this character (Fig. 4.16E). The height of the ventral margin of the antorbital fossa anteriorly shows a strong correlated trend ($r^2=0.974$, $p=0.013$) with a positive slope confidence interval greater than 1 (1.73, 3.21). Addition of *V. vadarostrum* causes the trend to lose significance ($p=0.058$), have a poorer fit ($r^2=0.749$) and broaden the slope confidence interval negatively (-1.87, 4.45). *Velociraptor vadarostrum* plots lower than is expected of the trend for this measurement (Fig. 4.16F). The anteroposterior length of the preantorbital bar shows insignificant correlation ($p=0.107$) but a good trend ($r^2=0.798$) with a broad confidence interval (0.39, 6.53). Adding *V. vadarostrum* causes destabilization the trend ($r^2=0.347$) and broadens the confidence interval of the slope (-1.63, 14.52). *Velociraptor vadarostrum* plots high compared to the trend for this measurement (Fig. 4.16G). The last RMA compared quadrate height to height of the maxilla and its variation within *V. mongoliensis* and the effect of adding *V. vadarostrum*. The RMA shows a strong correlation between these two variables ($r^2=0.951$, $p=0.025$) with a restricted slope confidence interval capturing 1 (0.66, 1.35). The addition of *V. vadarostrum* causes the loss of correlation ($r^2=0.492$, $p=0.187$) and a broadening of the slope

confidence interval (-0.17, 5.34). *Velociraptor vadarostrum* plots lower than expected given the trend (Fig. 4.16H).

4.5.3 Phylogeny

Parsimony analysis of the complete dataset recovers several unenlagiine taxa nested within Troodontidae Gilmore, 1924, and two other, proposed unenlagiines, as sister to Eudromaeosauria in a clade with *Tianyuraptor ostromi* Zheng et al., 2010 (Fig. 4.17A). Halszkaraptorinae Cau et al., 2017, is paraphyletic, *Mahakala omnogavae* Turner et al., 2007, being sister to a clade containing *Halszkaraptor escuilliei* Cau et al., 2017, and *Tsaagan mangas*. Microraptorinae Senter et al., 2004, is recovered as monophyletic and is sister to a clade containing *Rahonavis ostromi* (Forster et al., 1998), and *Tsaagan mangas*; however, all the microraptorine species are recovered in a single large polytomy. The Bayesian analysis recovered more traditional outgroups including a monophyletic Troodontidae sister to Dromaeosauridae, defined as a clade containing *Buitreraptor gonzalezorum* Makovicky et al., 2005, and *Tsaagan mangas* (Fig. 4.17B). Unenlagiinae Bonaparte, 1999, is recovered as polyphyletic and includes a paraphyletic clade containing *Buitreraptor gonzalezorum* and *Rahonavis ostromi* as the most basal taxa within Dromaeosauridae, and *Neuquenraptor argentinus* Novas and Pol, 2005, is recovered as a terminal taxon between a monophyletic Halszkaraptorinae (more basal) and Microraptorinae (more derived) (Fig. 4.17B). Microraptorinae is recovered as sister to Eudromaeosauria in the Bayesian analysis and *Tianyuraptor ostromi* and *Zhenyuanlong suni* Lu and Brusatte, 2015, are recovered within Eudromaeosauria.

Parsimony analysis of the whole dataset recovers an almost completely resolved, monophyletic Eudromaeosauria (Fig. 4.17A). The taxon *Zhenyuanlong suni* was recovered

within a monophyletic Eudromaeosauria in both parsimony and Bayesian analysis (Fig. 4.17). In the parsimony analysis *Zhenyuanlong suni* is recovered as sister to taxon to *Deinonychus antirrhopus*. In the Bayesian analysis of the complete dataset, *Deinonychus antirrhopus* is recovered as sister to a clade containing *Zhenyuanlong suni* as the most basal member showing an alternative close relationship between these taxa. The parsimony analysis of the whole matrix recovers a monophyletic Saurornitholestinae Longrich and Currie, 2009, supported by seven synapomorphies (5[1], 48[1], 77[1], 84[1], 101[1], 104[0], 153[1]), as the basal clade within Eudromaeosauria (Fig. 4.17A). This is like the topology recovered by Currie and Evans (2019). However, here *Bambiraptor feinbergi* is recovered as a member of Saurornitholestinae. The Bayesian analysis recovers a paraphyletic Saurornitholestinae but the position of the taxa making up this clade is basal within Eudromaeosauria as in the parsimony analysis (Fig. 4.17). The parsimony analysis of total data recovers a paraphyletic Dromaeosaurinae basal to the terminal cluster of Asian taxa that often comprise the Velociraptorinae Barsbold, 1983. *Deinonychus antirrhopus* and *Zhenyuanlong suni* form the most basal clade of the non-saurornitholestine eudromaeosaurians (Fig. 4.17A). Similarly, the Bayesian analysis of the total data matrix recovers *Deinonychus antirrhopus* as basal but not in Velociraptorinae as it has been recovered previously (Currie and Evans 2019). The Bayesian analysis recovers *Deinonychus antirrhopus* as the basal member of a monophyletic Dromaeosaurinae supported by seven synapomorphies (5[0], 11[2], 28[1], 33[1], 48[0], 66[0], 77[0]). A distinct monophyletic Velociraptorinae is recovered in the Bayesian analysis but is nested within Dromaeosaurinae in the parsimony analysis (Fig. 4.10). Velociraptorinae is represented by a clade containing *Acheroraptor temertyorum* and *Tsaagan mangas* (Fig. 4.17B) and is supported by three synapomorphies (65[1], 66[1], 67[1]).

Both parsimony and Bayesian ingroup analyses recover a monophyletic Eudromaeosauria that excludes *Tianyuraptor ostromi* and *Zhenyuanlong suni* (Fig. 4.18). Eudromaeosauria is supported by the following synapomorphies; 39[1], 103[1], 115[1], 122[1], 125[0], 155[1], 175[0]. The parsimony analysis recovers a monophyletic Saurornitholestinae that includes *Deinonychus antirrhopus* as a basal member (Fig. 4.18A). Dromaeosaurinae is not recovered, and instead there is a polytomy of all other eudromaeosaurians and a monophyletic Velociraptorinae that excludes *Acheroraptor temertyorum*. Bayesian analysis of the ingroup alternatively recovers a monophyletic Dromaeosaurinae (a clade containing *Deinonychus antirrhopus* and *Dromaeosaurus albertensis*), a monophyletic Saurornitholestinae (*Saurornitholestes langstoni* and *Bambiraptor feinbergi*), and a monophyletic Velociraptorinae (*Acheroraptor temertyorum* and *Tsaagan mangas*) (Fig. 4.18B).

The taxon *V. vadarostrum* is recovered as sister taxon to *V. mongoliensis* in all analyses (Figs. 4.17, 4.18). The genus *Velociraptor* is paraphyletic in both parsimony analyses as *V. osmolskae* places as sister to the clade containing *Linheraptor exquisitus* and *Tsaagan mangas* in the ingroup analysis. It is part of a polytomy with this clade and *Adasaurus mongoliensis* in the parsimony analysis with the complete dataset. Both Bayesian analyses recover a polyphyletic *Velociraptor* with *V. osmolskae* placing sister to the *Linheraptor exquisitus* and *Tsaagan mangas* clade, which together with these two taxa forms a clade sister to *Adasaurus mongoliensis* (Figs. 4.17, 4.18). The clade *Velociraptor* (*V. mongoliensis* + *V. vadarostrum*) is supported by three synapomorphies that distinguish them from other velociraptorines: 10[1], a promaxillary fenestra positioned in the anterodorsal portion of the antorbital fossa anterior margin; 48[1], an anteriorly bowed squamosal process of the quadratojugal; 57[1], basioccipital tubera with ovoid depressions. Bootstrap values for the total data parsimony analysis show greatest support for the

clades containing *Stenonychosaurus inequalis* and *Byronosaurus jaffei* Norell et al., 2000 (61), *V. mongoliensis* and *V. vadarostrum* (50), and *Linheraptor exquisitus* and *Tsaagan mangas* (58). Similarly, the latter two clades show bootstrap values of 60 and 62 respectively in the ingroup parsimony analysis. The troodontid clade containing *Sinovenator changii* Xu et al., 2002, and *Stenonychosaurus inequalis* also has a bootstrap support of 50 in the ingroup parsimony analysis.

Of the 17 premaxillary and maxillary characters examined for their consistency indices, only six were found to have CI values of 0.5 or higher (Table 4.9). Of those characters, one was only at 0.5 in the parsimony analysis of the complete dataset (Character 12) and only two were ratio-based characters (Characters 21 and 29). Ingroup analyses improved the CI for several characters compared to the total data analyses (Characters 6, 7 and 28) and parsimony analysis showed better CI for character 8 (A 3.2).

4.6 Discussion.

4.6.1 Variation in *Velociraptor*

Velociraptor vadarostrum differs from other eudromaeosaurians in its maxilla morphology more obviously than any other cranial element (Figs. 3.3, 4.14-4.16). This is in part due to the morphological complexity of the maxilla, which has many variable anatomical features. Using linear measurements associated with maxillary features and their proportions, *V. vadarostrum* is shown to have more separation from *V. mongoliensis* than *V. osmolskae* (Fig. 4.14A), a species accepted as distinct (Turner et al. 2012). When PC 1 scores (which were largely influenced by length and height measurements) were plotted against the size standard measurement of maxillary length, *V. vadarostrum* fell out of the confidence interval of the regression (Fig. 4.16A) suggesting it is the most unlike all other *Velociraptor* specimens

examined with these comparative methods. Within the genus *Velociraptor*, the maxilla of *V. vadarostrum* is approximately the same length as the “Moscow” specimen of *V. mongoliensis* (98 mm and 99 mm respectively). However, it is greatly disparate from this specimen in its placement in PCA (Figs. 4.14, 4.16) and numerous regression analyses (Fig. 4.16). In the multiple regression analyses *V. vadarostrum* destabilized *V. mongoliensis* trends of more variables than did *V. osmolskae* (7 and 5 respectively; Table 4.6), although *V. osmolskae* had an overall greater effect on the multiple regression results (Table 4.5). The effects on regression analyses that these two specimens have when added to the *V. mongoliensis* dataset has a similar effect as when more distantly related taxa like *Linheraptor exquisitus* and *Tsaagan mangas* are added to the regressions (Table 4.5). These results support the taxonomic distinction of these two species from *V. mongoliensis* based on similar results obtained for frontals in troodontids (Evans et al. 2017) and the clustering of maxillae taxonomically shown in this thesis (Fig. 3.3C-D).

If the maxillae of *V. osmolskae* and *V. vadarostrum* were part of the variation within *V. mongoliensis*, it would be expected that the element would not show such strong correlations in its proportions across the range in size presented in this study. However, PCA analysis shows a positive linear trend across both principal components in the raw measurement analysis (Fig. 4.14A) and a positive linear trend along PC 2 in the log transformed data (Fig. 4.14B). In the analysis of all eudromaeosaurians (Fig. 4.15) a similar linear trend is observed for *Bambiraptor feinbergi* and *V. mongoliensis* but is along the axis of PC 1 rather than PC 2. This trend seems related to size as larger specimens place more positively in all cases. These trends are reminiscent of allometric trends reported for other theropods such as tyrannosaurids (Currie 2003b). These results are corroborated by regression analyses of *V. mongoliensis* specific tests for various maxillary proportions that are tightly correlated (maxillary height, anterior ramus

length and proximal height, and the height of the maxilla ventral to the anterior edge of the antorbital fossa; Table 4.7). Of these measurements *V. mongoliensis* shows isometric growth in regard to maxillary height, albeit with a much broader positively skewed slope (CI = 0.61, 2.69; Table 4.7), anterior ramus length (slope CI = 0.99, 1.34) and antorbital fossa length (CI = 0.48, 1.99). The latter two measurements are linked to some extent as one changes in proportion, so should the other. The anterior ramus length just captures 1.0 in its confidence interval and may actually show subtle positive allometry. The junction between the antorbital fossa and anterior ramus in *V. vadarostrum* is anteriorly placed relative to *V. mongoliensis*, being just posterior to the third maxillary alveolus whereas the placement of this junction in *V. mongoliensis* is posterior to the fourth maxillary alveolus. Therefore, it could be argued that the elongation of the antorbital fossa may be a result of the shortening of the anterior ramus. In either case *V. vadarostrum* does not fit the allometric trends observed for these features in *V. mongoliensis* (Fig. 4.16). The elongate antorbital fossa in *V. vadarostrum* is separate from the abbreviation of the anterior ramus for two reasons regarding the maxillary tooth row. The anterior border of the antorbital fenestra (posterior extent of the measured antorbital fossa for this study) is above the posterior edge of the ninth maxillary alveolus in *V. vadarostrum* whereas this landmark is between the seventh and eighth in *V. mongoliensis*. Together this puts six maxillary teeth along the anteroposterior length of the antorbital fossa in *V. vadarostrum* compared to three or four in *V. mongoliensis*. This reveals another interesting difference between *V. vadarostrum* and *V. mongoliensis* – the depth of the maxilla ventral to the anteroventral margin of the antorbital fossa (Fig. 4.1).

The height of the maxilla ventral to the anteroventral margin of the antorbital fossa changes with positive allometry in *V. mongoliensis* (slope CI = 1.73, 3.21), increasing in depth as

the size of the maxilla increases. The length of the maxilla of *V. vadarostrum* is comparable in size to the “Moscow” specimen of *V. mongoliensis* but has a ventral margin height less than that of the smaller maxilla of AMNH FARB 6515 (*V. mongoliensis* holotype) (A 3.1). These combined features demonstrate that the expansion of the antorbital fossa in *V. vadarostrum* is not a consequence of changing proportions in other maxillary features but rather the expansion of the antorbital fossa results in disparate proportions in other regards. The relative size of the maxillary fenestra also is suggestive of this morphological development as this feature did not expand with the antorbital fossa. *Velociraptor vadarostrum* is positioned well above the trendline for regressions comparing the distance between the anterior border of the antorbital fossa to the maxillary fenestra, and the length of the preantorbital bar (Fig. 4.16E, G). The expansion of the antorbital fossa to the extent observed in *V. vadarostrum* is interesting given its large, deeply rooted maxillary teeth (Chapter 2). The thin bone wall around the rooted teeth would seem to have functional limitations. However, *V. vadarostrum* is similar to *Deinonychus antirrhopus* and *Shanag ashile* in this regard, which both possess large, deeply rooted teeth medial to thinly walled, expanded antorbital fossae (Turner et al. 2007a) (Chapter 2). Other dromaeosaurids have shown modifications to the maxilla to either increase the robustness around the maxillary alveoli by reducing the ventral extent of the antorbital fossa (*Acheroraptor temertyorum*, *Achillobator giganticus*), reduce tooth size relative to maxillary depth (*Atrociraptor marshalli*, *Saurornitholestes langstoni*), or both (*Linheraptor exquisitus*, *Tsaagan mangas*) (Perle et al. 1999, Norell et al. 2006, Xu et al. 2010a, Evans et al. 2013, Currie and Evans 2019). *V. osmolskae* shows a morphology of the antorbital fossa that approaches the condition in *Linheraptor exquisitus* and *Tsaagan mangas* in the restriction of its ventral extent relative to *V. mongoliensis* (Figs. 4.14A, 4.16F, Table 4.4). Whereas PCA analyses of specimens throughout

Eudromaeosauria found the greatest variables being the length of the antorbital fossa and anterior ramus (Figs. 3.3, 4.15, Appendix 2.1), PCA analyses of derived Asian taxa reveals more subtle variations of the antorbital fossa with greater loadings on the ventral extent. It produces a PC 1 axis, not emphasized by elongation of the maxilla (Figs. 3.3C-D, 4.15) but the area of the antorbital fossa and the placement of the maxillary fenestra within (Fig. 4.14A, Table 4.4). Based on currently available data, *V. vadarostrum* represents one extreme end of a spectrum of variation in maxilla morphology, distinguishing it among Asian velociraptorines.

Among eudromaeosaurians, *V. vadarostrum* is most like *V. mongoliensis* in many cranial and postcranial features. Both have long skulls relative to body size, *V. mongoliensis* having a range of skull to femur ratios from 1.17 to 1.26 (Currie and Evans 2019) and *V. vadarostrum* having a ratio of 1.29. The proportionate lengths of the snouts within these taxa are also comparable, making up 60% or more of the total skull length, a trait shared with other derived Asian eudromaeosaurians *Linheraptor exquisitus* and *Tsaagan mangas*. Areas in which *V. vadarostrum* differs from *V. mongoliensis* are predominantly with the cranial elements relating to the rostrum and jaw musculature. The snout is nearly straight in profile, which differs from all specimens referred to *V. mongoliensis* that show an anteroventral angle of their proximal snout with a distinct dorsal deflection near the external nares (Fig. 4.1). This gives the dorsal margin of the rostrum in *V. mongoliensis* a distinct inflection along the dorsal surface that it shares with other Asian taxa like *Linheraptor exquisitus* and *Tsaagan mangas* (Norell et al. 2006, Xu et al. 2015). The parallel borders of the snout in *V. vadarostrum* also distinguish this species from other eudromaeosaurians from North America, which have an anteroventral inclination of the dorsal margin of the snout anteriorly (Ostrom 1969, Currie and Evans 2019). The shallow snout of *V. vadarostrum* is emphasized by the relatively tall and wide temporal region (Fig. 4.2). The

width between quadrate heads for *V. vadarostrum* compared with mid snout width was notably wider than in an exceptionally preserved *V. mongoliensis* specimen (MPC-D 100/25) showing that the temporal region was transversely expanded relative to the snout. The dorsoventral depth of the quadrate is greater than that of the maxilla in *V. vadarostrum* whereas the depth of the maxilla is sub-equal or greater to quadrate depth in *V. mongoliensis* (A 3.1), emphasizing the low height of the rostrum. Within *V. mongoliensis*, the heights of the maxilla and quadrate are correlated ($r^2=0.95$, $p=0.025$) and grow isometrically (slope CI = 0.66, 1.36) (Schott and Evans 2017). Lastly the anteroposterior expansion of the temporal region in *V. vadarostrum* is distinct from specimens referred to *V. mongoliensis*. Whereas the temporal arcade is incomplete in the holotype of *V. vadarostrum*, the proportions of the temporal region relative to the snout dimensions suggest well developed muscle groups associated with jaw adduction and strong neck musculature at the occiput (Snively and Russell 2007, Sakamoto 2010). If the muscle arrangement was more robust than *V. mongoliensis* is uncertain but it was likely comparable given the data available. The emphasis toward development of the snout in *V. vadarostrum* is not the only area of variation where it deviates from *V. mongoliensis*.

The anterior process of the lacrimal is angled anteroventrally strongly and the ventral ramus is inclined posterodorsally giving the junction between the snout and temporal region a distinctly sloped appearance in lateral view. The illustration that Turner et al. (2012) made for *V. mongoliensis* was largely based off the holotype for *V. vadarostrum* and captures the described snout to dorsal morphology quite well. It is possible that the stark transition between the snout and temporal region of the skull would cause a great deal of variation in temporal elements as well. The long olfactory canal could be related to the abrupt posterodorsal slope of the temporal region, but it is difficult to tell because of the absence of the skull roof. Either way, it is a distinct

morphology that is not observed in *V. mongoliensis* or other eudromaeosaurians. The cerebellar cavity constricts abruptly behind the postorbital process as in *Saurornitholestes langstoni* (Sues 1976) and troodontids (Currie 1985). Frontals have been considered informative for both dromaeosaurids and troodontids with endocast morphologies being emphasized and used for evolutionary interpretations (Sues 1976, Currie 1985, 1995, Norell et al. 2009). Therefore, variation in endocast morphology is of interest and not something expected to be highly variable within a species even if the morphology of the braincase is (Piechowski et al. 2019). Therefore, differences in the braincase observed for *V. vadarostrum* (Figs. 4.5, 4.7C-D) could be susceptible to high degrees of intraspecific variation and may not be reliable in how future specimens are referred. Deviations from the norm for *V. mongoliensis* go beyond proportionate snout characteristics, and cranial morphology, although they may be functionally tied.

Velociraptor vadarostrum has a humerus that is a little more than 75% the length of the femur and a comparatively reduced manual digit 1 in both length (Table 4.2) and robustness. Longer arms coupled with a slightly reduced manus is less useful in terms of prey handling. However, it may allow for more precise movements of the forelimb. Whereas the differences from *V. mongoliensis* are perhaps subtle, looking at the whole picture, it may make sense for an organism investing in its snout to reduce emphasis on other aspects of its anatomy. This can also be addressed with the reduced development of a fourth trochanter. Whereas it cannot be observed in the figure (Fig. 4.7B) a slight protuberance along the posterior edge of the proximal end of the femur is evidence of its existence. The trochanter observed on *V. vadarostrum*, is diminutive compared to a specimen of *V. mongoliensis* with a fourth trochanter that is remarkably pronounced for a dromaeosaurid (Norell and Makovicky 1999). Presence of fourth trochanters in both *V. vadarostrum* and *V. mongoliensis* suggests they retained some level of tail

driven locomotion (Gatesy 1991, Persons and Currie 2016). Each of these two species also share a long, widely flared postacetabular blade (Fig. 4.7), which supports the assessment of present tail driven locomotion (Farlow et al. 2000, Hutchinson 2001, Carrano and Hutchinson 2002). *Velociraptor vadarostrum* is distinguished from *V. mongoliensis*, however, by the possession of an anterodorsally oriented vertical crest (Figs. 4.9, 4.11B), a feature similar to what is in ornithomimids, tyrannosaurids and groups of modern birds (Hutchinson 2001, Carrano and Hutchinson 2002). The homology of the ridge is shown to be problematic and thus its interaction with pelvic musculature, uncertain. Regardless, the development of the femur and pelvis in *Velociraptor* shows a greater dependence on traditional dinosaurian modes of locomotion than North American eudromaeosaurians which have greatly reduced their postacetabular blades (Ostrom 1969, 1976, Burnham et al. 2000, Currie and Evans 2019). It is possible, however, that the North American clades may be moving towards knee driven (rather than tail driven) locomotion and potentially reduced locomotion capabilities (Hutchinson 2001). Given the environment that both *V. mongoliensis* and *V. vadarostrum* lived in during the Late Cretaceous, well developed hindlimbs would have been a great asset in traversing expanses of an arid ecosystem (Dashzeveg et al. 2005). The possibility that *V. vadarostrum* represents an outlier in the range of variation within *V. mongoliensis* is a possibility that will need to be tested with each new specimen collected. However, based on the current evidence and the tests of variation performed here, it is more parsimonious to accept *V. vadarostrum* as a distinct taxon.

Variation observed for *V. mongoliensis* in this thesis fits into predominantly isometric ontogenetic sequences with subtle positively allometric trends (Fig. 4.15). The general shifts in maxillary proportions within this taxon are a reduction in elongation and lengthening of the anterior ramus (Figs. 4.14, 4.16). Similar regressions were observed in tyrannosaurids by Currie

(2003b) who demonstrated ontogenetic shifts towards more stout maxillae and snouts within various tyrannosaur species. PCA analyses capture ontogenetic sequences along axes loaded with size related measurements (Figs. 4.14, 4.15). This is corroborated by the positive shift along PC 1 for *Bambiraptor feinbergi* (Fig. 4.15), which is represented in this study by a juvenile and adult specimen. The PC 1 axis for the PCA including all eudromaeosaurians represents a gradient of elongation (greater elongation plotting negatively) (Chapter 3 Discussion). The positive placement of larger specimens in various species within Eudromaeosauria suggests that the snout becomes less elongate as an individual grows within this clade. Decreasing snout elongation through ontogeny in eudromaeosaurians observed in this thesis corroborates recent isotope analyses of *Deinonychus antirrhopus* teeth that indicate niche partitioning between juveniles and adults (Frederickson et al. 2020). Slater et al. (2009) found that snout shape in canids is correlated to dietary preference. The findings of Frederickson et al. (2020) further support the use of canids as a modern analog to eudromaeosaurians presented in this thesis.

4.6.2 Evolution and ecology

The phylogenetic placement of *V. vadarostrum* is well supported, this species being recovered as sister to *V. mongoliensis* in all iterations of the phylogenetic analysis (Figs. 4.17, 4.18). There was less bootstrap support for the clade containing *V. mongoliensis* and *V. vadarostrum* than the sister relationship between *Linheraptor exquisitus* and *Tsaagan mangas* (Figs 4.17A, 4.18A). Whereas the latter two species have been debated in terms of their synonymy (Turner et al. 2012, Xu et al. 2015), they show disparate placement along PC 2 of the PCA (Fig. 4.14). This could be a similar relationship to that observed in *V. mongoliensis*. As specimens of *V. mongoliensis* plot in a linear fashion relating to size, so may *Linheraptor exquisitus* and *Tsaagan mangas* be plotting based on maxillary morphology. Discovery of more

specimens would be the only way to assess if their differences are a matter of ontogeny or taxonomy.

Regarding maxillary morphology, *Velociraptor vadarostrum* shows more size independent variation from *V. mongoliensis* than *Linheraptor exquisitus* and *Tsaagan mangas* do from each other, and yet these two *Velociraptor* species are recovered as sister taxa. *Velociraptor osmolskae* shows less morphological disparity from *V. mongoliensis* but is recovered in a separate clade from the other *Velociraptor* species, showing that *Velociraptor* paraphyletic (Figs. 4.17, 4.18). *Velociraptor osmolskae* is consistently recovered as closely related to the clade containing *Linheraptor exquisitus* and *Tsaagan mangas* (Figs. 4.17, 4.18), a result supported by morphometric analyses that demonstrate a shift toward the morphology of these two species (Fig. 4.14). The consistent phylogenetic placement of *V. osmolskae* closer to *Linheraptor exquisitus* and *Tsaagan mangas*, along with the morphometric trends, suggest that this taxon may be distinct from the genus *Velociraptor*. The clade containing *Velociraptor mongoliensis* and *Tsaagan mangas* are united by the elongation of the anterior ramus, anteriorly positioned maxillary fenestrae, and maxillary fenestrae that are in posteriorly oriented accessory fossae that open broadly (Fig. 4.18).

Although proportional maxillary characters are acquired independently in various outgroups, within Eudromaeosauria the elongation of the maxilla (most significantly the anterior ramus) distinguishes the Late Cretaceous Asian taxa from the remaining (predominantly North American) taxa. This is due to the closest outgroups and basal eudromaeosaurians possessing short anterior rami and generally having tall maxillae (Fig. 4.18). A shift to elongate maxillae is observed throughout Eudromaeosauria (Chapter 3). However, the Late Cretaceous dromaeosaurids of North America fall in a “mid-range” category of maxilla proportions (Fig.

3.3C-D). It is only the Asian forms which seem to emphasize the elongation of the maxilla, with the currently single exception being the North American taxon *Acheroraptor temertyorum*. Whereas it does show elongation approaching what is observed in Asian eudromaeosaurians, it also shares multiple characters with North American taxa belonging to Saurornitholestinae (Chapter 2; Fig. 4.18B), the most intriguing of which is the complex maxillary fenestra arrangement.

The maxillary fenestra and its morphology are also informative within Eudromaeosauria. The complex morphology of the maxillary fenestra described for Saurornitholestinae and *Acheroraptor temertyorum* (Chapter 2) has not been observed in Early Cretaceous dromaeosaurids and is unlikely to represent an ancestral state. In previous analyses, Saurornitholestinae has been recovered as the basal clade within Eudromaeosauria (Longrich and Currie 2009, Evans et al. 2013, Currie and Evans 2019). However, the Bayesian analysis performed here with reformed maxillary characters recovers Saurornitholestinae as sister to Velociraptorinae. The contentious *Acheroraptor temertyorum* could be classified in either of these two subfamilies. The elongation of the maxilla in *Acheroraptor temertyorum* is not to the same degree as that of Velociraptorinae, and elongation as a homologous characteristic has its shortcomings.

Snout shape can be highly variable in closely related species in modern ecosystems (Slater et al. 2009, Ferreira-Cardoso et al. 2019) and in the case of competing predators, pressures can drive similar morphological changes between more distantly related species that undergo similar ecological pressures. This is observed readily in modern mammalian carnivores such as canids (Slater et al. 2009). Slater et al. (2009) found that phylogenetically distant species, such as members of the genus *Vulpes*, converged on cranial proportions of members of *Canis*

distinguished by genetic analysis and/or discrete morphological diagnostic traits. They also demonstrated that cranial proportions were closely tied to diet, with long snouted individuals specializing in small prey acquisition and short snouted species specializing in larger prey. Dietary preference and snout shape have been shown in numerous other studies ranging from dinosaurs (Carrano et al. 1999, Whitlock 2011) to crocodylians (Walmsley et al. 2013) to bats (van Cakenberghe et al. 2002) and whereas these features can become fixed in a population, becoming taxonomically significant, they should be examined after phylogenetic analyses of datasets that avoid using ecomorphological characters as primary homologues (Patterson 1982). In the case of *Acheroraptor temertyorum*, elongation of the maxilla does not represent grounds for inferring homology. *Acheroraptor temertyorum* does share several characteristics of the dentary with velociraptorines, which include a dentary curved in lateral view, and a ventral deflection of the anterior dentary. Whereas this is not directly a proportional character, it is only observed in taxa with elongate maxillae and snouts. Also, the concave anterior margin of the dentary is shared with members of Saurornitholestinae, with which *Acheroraptor temertyorum* shares even more discrete characteristics in addition to the maxillary fenestra morphology. These include the morphology of the nasal suture, a well developed two-chamber maxillary sinus system, a vertically oriented sutural facet for the lacrimal, and a long, narrow ascending ramus (Chapter 2). Although the difference between *Acheroraptor temertyorum* and members of Saurornitholestinae might be convincing as clear separation between these two taxa, it is worth noting that within Saurornitholestinae, *Atrociraptor marshalli* is often recovered as sister to *Saurornitholestes langstoni* and the proportions of these taxa are drastically different (Fig. 3.3). *Acheroraptor temertyorum* shows less morphological disparity from *Saurornitholestes langstoni* than *Atrociraptor marshalli* does (Fig. 3.3). All these taxa are distinct from each other and their

snout proportions reflect evolutionary relationships. However, closely related species may vary considerably in ecomorphological features such as snouts, especially in predatory animals.

The suite of shared maxillary characteristics that define Velociraptorinae revolve largely around elongation of the snout and rearrangement of the dental arcade as exemplified by the clade containing *Linheraptor exquisitus* and *Tsaagan mangas* (Fig. 4.18). This clade is distinguished by elongate snouts with extremely long anterior rami relative to other eudromaeosaurians and a ventrally restricted antorbital fossa with a sharp delineation between the fossa and lateral margin. The shallow, snout of *V. vadarostrum* and its broadly developed antorbital fossa contrasts the trend of evolutionary change in Velociraptorinae (Figs. 4.1, 4.14), yet it possesses the most elongate snout amongst its close relatives. The snout of *V. vadarostrum* is no longer relative to skull length compared to other Asian eudromaeosaurians but instead is long compared to its depth demonstrating a maxillary length to height ratio (3.44) in the range of derived troodontids (Norell et al. 2009) (Character 32, A 3.2). This deviation from the range observed for *V. mongoliensis* (2.81-3.08) could be reflective of the evolutionary trends underway in Asia during the Late Cretaceous with *V. vadarostrum* representing an earlier morphology which underwent selective pressures.

The holotype of *V. vadarostrum* was found in the Flaming Cliffs (Bayan Zag) locality where the holotypes of *V. mongoliensis* and *Saurornithoides mongoliensis* Osborn, 1924, were found. The majority of *V. mongoliensis* specimens, however, were collected from Tögrögiin Shiree to the west of the Flaming Cliffs (Barsbold and Osmólska 1999, Norell and Makovicky 1999). Stratigraphic data is intermittent at these localities and exact dates are not known but it has been shown that there is a succession of rocks between the Flaming Cliffs and Tögrögiin Shiree (Dashzeveg et al. 2005). This puts the holotype for *V. mongoliensis* and *V. vadarostrum*

as older than the specimens from the Tögrögiin Shiree and with no dromaeosaurid fossil record leading up to these species. It cannot be said that *V. vadarostrum* and *V. mongoliensis* were coeval or if there was a speciation event with replacement of *V. vadarostrum*, but it does offer insights into the evolution trends of Asian eudromaeosaurians.

The shallowness of the snout of *V. vadarostrum* is independent of size (Fig. 4.16) showing a morphology not found in other *Velociraptor* specimens (Fig. 4.1). There is a more positively skewed trend in relation to the maxilla height and its length with the smallest *V. mongoliensis* specimen (AMNH FARB 6515, maxillary length = 91 mm) having the highest length to height ratio of the maxilla (3.08) and the largest *V. mongoliensis* specimen (MPC-D 100/25, mx length = 113 mm) having the lowest length to height ratio (2.81). This relationship can be observed with the skulls of *V. mongoliensis* lined up and size scaled (Fig. 4.1); as the skull grows, the maxillary height grows and subsequently the angle of the dorsal margin of the snout changes. If *V. vadarostrum* were an ontogenetic stage within *V. mongoliensis* it should have a maxillary length to height ratio equal to or less than AMNH FARB 6515. In *V. mongoliensis*, the dorsal margin of the maxilla shows a more prominent inflection above the junction with the anterior ramus and antorbital fossa that becomes more distinct with increases in size (Fig. 4.1B-D). The distinction between the species is supported by the strong correlation between proximal anterior ramus height (ventral to the inflection point) and maxillary length between all *Velociraptor* specimens (Table 4.6). Within *V. mongoliensis* the increasing height of the maxilla is predominantly the result of the increasing angle of the ascending ramus throughout growth (Table 2.1). Of the various *V. mongoliensis* specimens, the morphology of the largest specimen (MPC-D 100/25) also plots closest to the morphology of *V. osmolskae*, which shows morphology approaching the conditions of *Linheraptor exquisitus* and *Tsaagan mangas* (Figs.

3.3, 4.14). Ontogeny in *V. mongoliensis* has not been examined to any great effect before but the data presented in this study gives us the first indication of some of the ontogenetic trends. As the individual grows the maxilla decreases in elongation while the anterior ramus becomes relatively longer, and the ventral lamina increases in dorsoventral height. The ontogenetic trends in *V. mongoliensis* reflect the evolutionary shifts occurring within Velociraptorinae except for the anterior migration of the maxillary fenestra (Figs. 4.14-4.16).

The persistence of long snouts within Velociraptorinae may be reflective of their environments. The conditions of what is now Mongolia during the Late Cretaceous was arid with seasonal fluvial influences (Dashzeveg et al. 2005, Dingus et al. 2008). This differs markedly from the temperate to sub-tropical climate of the Late Cretaceous North America (Eberth and Braman 2012), where there are dromaeosaurids with generally stouter snouts (Fig. 3.3). Different abiotic environmental factors such as local climate support different faunal assemblages, which may lead to different ecological relationships within respective ecosystems. The arid environment of the Djadokhta Formation had a predominance of smaller vertebrates like mammals, lizards, and small dinosaurs (Dashzeveg et al. 1995, 2005, Dingus et al. 2008) whereas the more temperate environments (Dinosaur Park Formation, Horseshoe Canyon Formation) had a higher abundance of larger animals and more morphologically diverse dinosaur assemblages (Brinkman 1990, Peng et al. 2001, Eberth and Braman 2012, Brown et al. 2013). There is no direct analog of eudromaeosaurian predators today and the use of phylogenetic bracketing for inferring behaviour or ecological niche does not seem sufficient to examine trends in functional morphology (Roach and Brinkman 2007). The comparison of small to medium sized mammalian predatory animals to dromaeosaurids of the Late Cretaceous has been brought up numerous times in this thesis. The logic is based on the size and niche they both fill in their

respective, terrestrial, ecosystems. The analogy is further reflected by the frequent acquisition of long snouts in canid species that live in arid environments such as the Ethiopian wolf (*Canis simensis*), or the Tibetan sand fox (*Vulpes ferrilata*) which have the longest snouts relative to width of any of their close relatives (Slater et al. 2009). These species specialize in the capture of small, infrequent prey that exist in these environments. Development of a long snout helps in acquisition of these prey items but at the cost of bite force. The relatively longer jaws in velociraptorines would have been well adapted to rapid biting (Biknevicius and Ruff 1992, Sakamoto 2010). The anterior teeth are perpendicular to the alveolar margin, to slightly angled anteriorly in *V. vadarostrum* and a lesser extent in *V. mongoliensis*, would have been effective at puncturing and holding small, potentially fast-moving prey. It has also been noted that the shallowness of the muzzle can help with extrinsic forces as observed in crocodylians (Walmsley et al. 2013). This would have made *V. vadarostrum* exceptional at using its jaws to apprehend and handle small prey items. Whereas the other velociraptorines retained the long narrow snout morphology, the trend over the Late Cretaceous was towards a deeper, more angled snout (Fig. 4.10) with teeth relatively smaller compared to the maxillary body. This suggests that there were potentially directional shifts towards structural integrity (Rayfield et al. 2001, Slater et al. 2009, Walmsley et al. 2013) for diversifying diets.

4.7 Conclusions

The maxilla morphology within velociraptorines shows a great deal of variation with a general trend towards deeper, more triangular snout profiles with greater definition of a restricted antorbital fossa. The range of variation of the maxilla within the species *V. mongoliensis* is indicative of a tight ontogenetic trend with little individual variation. Distinct species such as *V. osmolskae* and *V. vadarostrum*, show variations in maxilla morphology distinct in different

ways. The maxilla of *V. osmolskae* shows a transitional morphology between *V. mongoliensis* and more derived Asian dromaeosaurids like *Linheraptor exquisitus* and *Tsaagan mangas*. *Velociraptor vadarostrum* possesses an extreme maxillary morphology more disparate from derived velociraptorines. The morphological trends are corroborated by phylogenetic placement of taxa within Velociraptorinae, *V. vadarostrum* being sister to *V. mongoliensis*, together representing the basal velociraptorines whereas *V. osmolskae* shows a strong phylogenetic pull to the derived velociraptorines making *Velociraptor* paraphyletic.

The first report of proportionate change through ontogeny is demonstrated for *V. mongoliensis*. Throughout the growth of *V. mongoliensis* the maxilla is demonstrated as having a potentially positive allometric shift of maxillary height, anterior ramus length, and a well supported positively allometric shift in the height of the lateral lamina ventral to the anteroventral edge of antorbital fossa. This lends to an overall shift in maxillary proportions through ontogeny toward less elongate dimensions. This observation is supported by a similar shift observed for *Bambiraptor feinbergi* and is like what has been documented for other theropods such as tyrannosaurids. *Velociraptor vadarostrum* falls well out of the range of variation for maxilla morphology in *V. mongoliensis* and has a shallow snout with extensive development of the antorbital fossa, which is conservative in *V. mongoliensis*.

The retention of long narrow snouts within Velociraptorinae is likely driven by consistent environmental and ecological pressures from the arid environment they inhabited. Development of long snouts for small prey acquisition is well demonstrated in modern small-bodied terrestrial carnivorans and makes these features susceptible to convergence via changes in predator-prey interactions through time. The contentious placement of the long-snouted eudromaeosaurian *Acheroraptor temertyorum* in or near Velociraptorinae, is challenged by shared discrete

characters with members of Saurornitholestinae. Use of ratio-based characters for assessment of homology is cautioned against due to the relationship of structure and function within elements of the skeleton that are intimately tied to necessary functions.

4.8 Literature Cited

- Barsbold, R. 1983. Carnivorous dinosaurs from the Cretaceous of Mongolia. The Joint Soviet-Mongolian Palaeontological Expedition, **19**: 117.
- Barsbold, R., and Osmólska, H. 1999. The skull of *Velociraptor* (Theropoda) from the Late Cretaceous of Mongolia. *Acta Palaeontologica Polonica*, **44**: 189–219.
- Biknevicius, A.R., and Ruff, C.B. 1992. The structure of the mandibular corpus and its relationship to feeding behaviours in extant carnivorans. *Journal of Zoology*, **228**: 479–507. doi:10.1111/j.1469-7998.1992.tb04450.x.
- Bonaparte, J. 1999. Tetrapod faunas from South America and India: A palaeobiogeographic interpretation. *PINSA*, **65**: 427–437.
- Brinkman, D.B. 1990. Paleocology of the Judith River Formation (Campanian) of Dinosaur Provincial Park, Alberta, Canada: Evidence from vertebrate microfossil localities. *Palaeogeography, Palaeoclimatology, Palaeoecology*,: 18.
- Brown, C.M., Evans, D.C., Campione, N.E., O'Brien, L.J., and Eberth, D.A. 2013. Evidence for taphonomic size bias in the Dinosaur Park Formation (Campanian, Alberta), a model Mesozoic terrestrial alluvial-paralic system. *Palaeogeography, Palaeoclimatology, Palaeoecology*, **372**: 108–122. Elsevier B.V. doi:10.1016/j.palaeo.2012.06.027.
- Brusatte, S.L., and Carr, T.D. 2016. The phylogeny and evolutionary history of tyrannosaurid dinosaurs. *Scientific Reports*, **6**: 1–8. Nature Publishing Group. doi:10.1038/srep20252.
- Burnham, D.A., Derstler, K.L., Currie, P.J., Bakker, R.T., Zhou, Z., and Ostrom, J.H. 2000. Remarkable new birdlike dinosaur (Theropoda: Maniraptora) from the Upper Cretaceous of Montana. *The University of Kansas Paleontological Contributions*, **13**: 14.

- van Cakenberghe, V., Herrel, A., and Aguirre, L.F. 2002. Evolutionary relationships between cranial shape and diet in bats (Mammalia : Chiroptera). *In Topics in Functional and Ecological Vertebrate Morphology. Edited by P. Aerts, K. D'Aour, A. Herrel, and R. Van Damme. Staker Publishing. pp. 205–236.*
- Carrano, M.T., and Hutchinson, J.R. 2002. Pelvic and hindlimb musculature of *Tyrannosaurus rex* (Dinosauria: Theropoda). *Journal of Morphology*, **253**: 207–228.
doi:10.1002/jmor.10018.
- Carrano, M.T., Janis, C.M., and Sepkoski, J.J. 1999. Hadrosaurs as ungulate parallels: Lost lifestyles and deficient data. *Acta Palaeontologica Polonica*, **44**: 237–261.
- Cau, A., Beyrand, V., Voeten, D.F.A.E., Fernandez, V., Tafforeau, P., Stein, K., Barsbold, R., Tsogtbaatar, K., Currie, P.J., and Godefroit, P. 2017. Synchrotron scanning reveals amphibious ecomorphology in a new clade of bird-like dinosaurs. *Nature*, **552**: 395–399.
Nature Publishing Group. doi:10.1038/nature24679.
- Currie, P., and Varricchio, D.J. 2004. A new dromaeosaurid from the Horseshoe Canyon Formation (Upper Cretaceous) of Alberta, Canada. *In Feathered Dragons. Edited by P.J. Currie, E.B. Koppelhus, M.A. Shugar, and J.L. Wright. Indiana University Press, Bloomington and Indianapolis. pp. 112–132.*
- Currie, P.J. 1985. Cranial anatomy of *Stenonychosaurus inequalis* (Saurischia, Theropoda) and its bearing on the origin of birds. *Canadian Journal of Earth Sciences*, **22**: 1643–1658.
doi:10.1139/e85-173.
- Currie, P.J. 1995. New information on the anatomy and relationships of *Dromaeosaurus albertensis* (Dinosauria: Theropoda). *Journal of Vertebrate Paleontology*, **15**: 576–591.

- Currie, P.J. 2003b. Allometric growth in tyrannosaurids (Dinosauria: Theropoda) from the Upper Cretaceous of North America and Asia. *Canadian Journal of Earth Sciences*, **40**: 651–665. doi:10.1139/e02-083.
- Currie, P.J., and Evans, D.C. 2019. Cranial anatomy of new specimens of *Saurornitholestes langstoni* (Dinosauria , Theropoda , Dromaeosauridae) from the Dinosaur Park Formation (Campanian) of Alberta. *The Anatomical Record*, **04715**: 1–25. doi:10.1002/ar.24241.
- Dashzeveg, D., Dingus, L., Loope, D.B., Swisher, C.C., Dulam, T., and Sweeney, M.R. 2005. New stratigraphic subdivision, depositional environment, and age estimate for the Upper Cretaceous Djadokhta Formation, southern Ulan Nur Basin, Mongolia. *American Museum Novitates*, **3498**: 31. doi:10.1206/0003-0082(2005)498[0001:nssdea]2.0.co;2.
- Dashzeveg, D., Novacek, M.J., Norell, M.A., Clark, J.M., Chiappe, L.M., Davidson, A., McKenna, M.C., Dingus, L., Swisher, C.C., and Altangerel, P. 1995. Extraordinary preservation in a new vertebrate assemblage from the Late Cretaceous of Mongolia. *Nature*, **374**: 446–449.
- Dingus, L., Loope, D.B., Dashzeveg, D., Swisher, C.C., Minjin, C., Novacek, M.J., and Norell, M.A. 2008. The geology of Ukhaa Tolgod (Djadokhta Formation, Upper Cretaceous, Nemegt Basin, Mongolia). *American Museum Novitates*, **3616**: 1. doi:10.1206/442.1.
- Eberth, D.A., and Braman, D.R. 2012. A revised stratigraphy and depositional history for the Horseshoe Canyon Formation (Upper Cretaceous), southern Alberta plains. *Canadian Journal of Earth Sciences*, **49**: 1053–1086. doi:10.1139/E2012-035.
- Evans, D.C., Cullen, T.M., Larson, D.W., and Rego, A. 2017. A new species of troodontid theropod (Dinosauria: Maniraptora) from the Horseshoe Canyon Formation (Maastrichtian)

- of Alberta, Canada. *Canadian Journal of Earth Sciences*, **54**: 813–826. doi:10.1139/cjes-2017-0034.
- Evans, D.C., Larson, D.W., and Currie, P.J. 2013. A new dromaeosaurid (Dinosauria: Theropoda) with Asian affinities from the latest Cretaceous of North America. *Naturwissenschaften*, **100**: 1041–1049. doi:10.1007/s00114-013-1107-5.
- Farlow, J.O., Gatesy, S.M., Holtz, T.R., Hutchinson, J.R., and Robinson, J.M. 2000. Theropod locomotion. *American Zoologist*, **40**: 640–663. doi:10.1093/icb/40.4.640.
- Ferreira-Cardoso, S., Billet, G., Gaubert, P., Delsuc, F., and Hautier, L. 2019. Skull shape variation in extant pangolins (Pholidota: Manidae): Allometric patterns and systematic implications. *Zoological Journal of the Linnean Society*,: 255–275. doi:10.1093/zoolinnea/zlz096.
- Forster, C.A., Sampson, S.D., Chiappe, L.M., and Krause, D.W. 1998. The theropod ancestry of birds: New evidence from the Late Cretaceous of Madagascar. *Science*, **279**: 1915–1919. doi:10.1126/science.279.5358.1915.
- Frederickson, J.A., Engel, M.H., and Cifelli, R.L. 2020. Ontogenetic dietary shifts in *Deinonychus antirrhopus* (Theropoda ; Dromaeosauridae): Insights into the ecology and social behavior of raptorial dinosaurs through stable isotope analysis. *Palaeogeography, Palaeoclimatology, Palaeoecology*, **552**: 109780. doi:10.1016/j.palaeo.2020.109780.
- Gatesy, S.M. 1991. Hind limb scaling in birds and other theropods: Implications for differences in terrestrial locomotion. *Journal of Morphology*, **209**: 83–96.
- Gilmore, C.W. 1924. On *Troodon validus*, an orthopodus dinosaur from the Belly River

- Cretaceous of Alberta, Canada. *University of Alberta Bulletin*, **1**: 43.
- Godefroit, P., Currie, P.J., Hong, L., Shang, C.Y., and Dong, Z.M. 2008. A new species of *Velociraptor* (Dinosauria: Dromaeosauridae) from the Upper Cretaceous of northern China. *Journal of Vertebrate Paleontology*, **28**: 432–438. doi:10.1671/0272-4634(2008)28[432:ANSOVD]2.0.CO;2.
- Godfrey, S.J., and Currie, P.J. 2004. A theropod (dromaeosauridae, dinosauria) sternal plate from the Dinosaur Park Formation (Campanian, Upper Cretaceous) of Alberta, Canada. *In* Feathered Dragons. *Edited by* P.J. Currie, E.B. Koppelhus, M.A. Shugar, and J.L. Wright. Indiana University Press, Bloomington and Indianapolis. pp. 144–149.
- Goloboff, P.A., and Mattoni, C.I. 2006. Continuous characters analyzed as such. *Cladistics*, **22**: 589–601.
- Hammer, Ø., Harper, D.A.T., and Ryan, P.D. 2001. PAST: Paleontological statistics software package for education and data analysis. *Palaeontologia Electronica*, **4**: 9.
- Hone, D., Tsuihiji, T., Watabe, M., and Tsogtbaatr, K. 2012. Pterosaurs as a food source for small dromaeosaurs. *Palaeogeography, Palaeoclimatology, Palaeoecology*, **331–332**: 27–30. doi:10.1016/j.palaeo.2012.02.021.
- Hutchinson, J.R. 2001. The evolution of pelvic osteology and soft tissues on the line to extant birds (Neornithes). *Zoological Journal of the Linnean Society*, **131**: 123–168. doi:10.1006/zjls.2000.0254.
- Kielan-Jaworowska, Z., and Barsbold, R. 1971. Narrative of the Polish-Mongolian expeditions 1967-1971. *Palaeontologia Polonica*, **27**: 13.

- Longrich, N.R., and Currie, P.J. 2009. A microraptorine (Dinosauria-Dromaeosauridae) from the Late Cretaceous of North America. *Proceedings of the National Academy of Sciences of the United States of America*, **106**: 5002–5007. doi:10.1073/pnas.0811664106.
- Lü, J., and Brusatte, S.L. 2015. A large, short-armed, winged dromaeosaurid (Dinosauria : Theropoda) from the Early Cretaceous of China and its implications for feather evolution. *Scientific Reports*,: 1–11. doi:10.1038/srep11775.
- Maddison, W., and Maddison, D. 2017. Mesquite.
- Makovicky, P.J., Apesteguía, S., and Agnolín, F.L. 2005. The earliest dromaeosaurid theropod from South America. *Nature*, **437**: 1007–1011. doi:10.1038/nature03996.
- Matthew, W.D., and Brown, B. 1922. The family Deinodontidae, with notice of a new genus from the Cretaceous of Alberta. *Bulletin of the American Museum of Natural History*, **46**: 367–385.
- Meyer, H. von. 1861. *Archaeopteryx lithographica* (Vogel-Feder) und *Pterodactylus* von Solnhofen. *Neues Jahrbuch für Mineralogie, Geognosie, Geologie und Petrefakten-Kunde*, **1861**: 678–679.
- Norell, M.A., Clark, J.M., Turner, A.H., Makovicky, P.J., Barsbold, R., and Rowe, T. 2006. A new dromaeosaurid theropod from Ukhaa Tolgod (Ömnögov, Mongolia). *American Museum Novitates*, **3545**: 51. doi:10.1206/0003-0082(2006)3545[1:andtfu]2.0.co;2.
- Norell, M.A., and Makovicky, P.J. 1997. Important features of the dromaeosaur skeleton: information from a new specimen. *American Museum Novitates*, **3215**: 1–28.
- Norell, M.A., and Makovicky, P.J. 1999. Important features of the dromaeosaurid skeleton II:

- Information from newly collected specimens of *Velociraptor mongoliensis*. *American Museum Novitates*, **3282**: 1–45.
- Norell, M.A., Makovicky, P.J., Bever, G.S., Balanoff, A.M., Clark, J.M., Barsbold, R., and Rowe, T. 2009. A review of the Mongolian Cretaceous dinosaur *Saurornithoides* (Troodontidae: Theropoda). *American Museum Novitates*, **3654**: 1–63. doi:10.1206/648.1.
- Norell, M.A., Makovicky, P.J., and Clark, J.M. 2000. A new troodontid theropod from Ukhaa Tolgod, Mongolia. *Journal of Vertebrate Paleontology*, **20**: 7–11.
- Norell, M.A., Makovicky, P.J., and Clark, J.M. 2004. The braincase of *Velociraptor*. In *Feathered Dragons*. Edited by P.J. Currie, E.B. Koppelhus, M.A. Shugar, and J.L. Wright. Indiana University Press, Bloomington and Indianapolis. pp. 133–143.
- Novas, F.E., and Pol, D. 2005. New evidence on deinonychosaurian dinosaurs of the Late Cretaceous of Patagonia. *Nature*, **433**: 858–861.
- Novas, F.E., Pol, D., Canale, J.I., Porfiri, J.D., and Calvo, J.O. 2009. A bizarre Cretaceous theropod dinosaur from Patagonia and the evolution of Gondwanan dromaeosaurids. *Proceedings of the Royal Society B: Biological Sciences*, **276**: 1101–1107. doi:10.1098/rspb.2008.1554.
- Osborn, H.F. 1924. Three new Theropoda, *Protoceratops* Zone, central Mongolia. *American Museum Novitates*,: 1–12.
- Ostrom, J.H. 1969. Osteology of *Deinonychus antirrhopus*, an unusual theropod from the Lower Cretaceous of Montana. *Peabody Museum of Natural History*, **30**: 1–165.
- Ostrom, J.H. 1976. On a new specimen of the Lower Cretaceous theropod dinosaur *Deinonychus*

antirrhopus. *Breviora*, **439**: 1–21.

- Patterson, C. 1982. Morphological characters and homology. *In* Problems of Phylogenetic Reconstruction. *Edited by* K.A. Joysey and A.E. Friday. Academic Press, London and New York. pp. 21–74.
- Peng, J., Brinkman, D., and Russell, A.P. 2001. Vertebrate microsite assemblages (exclusive of mammals) from the Foremost and Oldman formations of the Judith River group (Campanian) of southeastern Alberta : An illustrated guide. Provincial Museum of Alberta Natural History Occasional Paper,: 54. doi:10.5962/bhl.title.115853.
- Perle, A., Norell, M.A., and Clark, J.M. 1999. A new maniraptoran theropod - *Achillobator giganticus* (Dromaeosauridae)- from the Upper Cretaceous of Burkhan, Mongolia. National University of Mongolia,: 102.
- Persons, W.S., and Currie, P.J. 2016. An approach to scoring cursorial limb proportions in carnivorous dinosaurs and an attempt to account for allometry. *Scientific Reports*, **6**: 21–24. doi:10.1038/srep19828.
- Piechowski, R., Niedźwiedzki, G., and Tałanda, M. 2019. Unexpected bird-like features and high intraspecific variation in the braincase of the Triassic relative of dinosaurs. *Historical Biology*, **31**: 1065–1081. Taylor & Francis. doi:10.1080/08912963.2017.1418339.
- Rayfield, E.J., Norman, D.B., Horner, C.C., Horner, J.R., Smith, P.M., Thomason, J.J., and Upchurch, P. 2001. Cranial design and function in a large theropod dinosaur. *Nature*, **409**: 1033–1037. doi:10.1038/35059070.
- Roach, B.T., and Brinkman, D.L. 2007. A reevaluation of cooperative pack hunting and

- gregariousness in *Deinonychus antirrhopus* and other nonavian theropod dinosaurs. *Bulletin of the Peabody Museum of Natural History*, **48**: 103–138. doi:10.3374/0079-032x(2007)48[103:arocph]2.0.co;2.
- Sakamoto, M. 2010. Jaw biomechanics and the evolution of biting performance in theropod dinosaurs. *Proceedings of the Royal Society B: Biological Sciences*, **277**: 3327–3333. doi:10.1098/rspb.2010.0794.
- Schott, R.K., and Evans, D.C. 2017. Cranial variation and systematics of *Foraminacephale brevis* gen. nov. and the diversity of pachycephalosaurid dinosaurs (Ornithischia: Cerapoda) in the Belly River Group of Alberta, Canada. *Zoological Journal of the Linnean Society*, **179**. doi:10.1111/zoj.12465.
- Senter, P., Barsbold, R., Britt, B.B., and Burnham, D.A. 2004. Systematics and evolution of Dromaeosauridae (Dinosauria, Theropoda). *Bulletin of Gunma Museum of Natural History*, **8**: 1–20.
- Senter, P., Kirkland, J.I., Bird, J., and Bartlett, J.A. 2010. A new troodontid theropod dinosaur from the lower cretaceous of Utah. *PLoS ONE*, **5**: 1–5. doi:10.1371/journal.pone.0014329.
- Slater, G.J., Dumont, E.R., and Van Valkenburgh, B. 2009. Implications of predatory specialization for cranial form and function in canids. *Journal of Zoology*, **278**: 181–188. doi:10.1111/j.1469-7998.2009.00567.x.
- Snively, E., and Russell, A.P. 2007. Functional variation of neck muscles and their relation to feeding style in Tyrannosauridae and other large theropod dinosaurs. *Anatomical Record*, **290**: 934–957. doi:10.1002/ar.20563.

- Sternberg, C.M. 1932. Two new theropod dinosaurs from the Belly River Formation of Alberta. *Canadian Field-Naturalist*, **46**: 99–105.
- Sues, H.-D. 1976. A new small theropod dinosaur from the Judith River Formation (Campanian) of Alberta. *Zoological Journal of the Linnean Society*, **62**: 381–400.
- Turner, A.H., Hwang, S.H., and Norell, M.A. 2007a. A small derived theropod from Öösh, Early Cretaceous, Baykhangor Mongolia. *American Museum Novitates*, **3557**: 27.
doi:10.1206/0003-0082(2007)3557[1:asdfs]2.0.co;2.
- Turner, A.H., Makovicky, P.J., and Norell, M.A. 2012. A review of dromaeosaurid systematics and paravian phylogeny. *Bulletin of the American Museum of Natural History*, **371**: 1–206.
doi:10.1206/748.1.
- Turner, A.H., Pol, D., Clarke, J.A., Erickson, G.M., and Norell, M.A. 2007c. A basal dromaeosaurid and size evolution preceding avian flight. *Science*, **317**: 1378–1381.
doi:10.1126/science.1144066.
- Walmsley, C.W., Smits, P.D., Quayle, M.R., McCurry, M.R., Richards, H.S., Oldfield, C.C., Wroe, S., Clausen, P.D., and McHenry, C.R. 2013. Why the long face? The mechanics of mandibular symphysis proportions in crocodiles. *PLoS ONE*, **8**: 34.
doi:10.1371/journal.pone.0053873.
- Whitlock, J.A. 2011. Inferences of diplodocoid (Sauropoda: Dinosauria) feeding behavior from snout shape and microwear analyses. *PLoS ONE*, **6**. doi:10.1371/journal.pone.0018304.
- Witmer, L.M. 1997. The evolution of the antorbital cavity of archosaurs: A study in soft-tissue reconstruction in the fossil record with an analysis of the function of Pneumaticity. *Journal*

of Vertebrate Paleontology, **17**: 1–76. doi:10.1080/02724634.1997.10011027.

Xu, X., Choiniere, J.N., Pittman, M., Tan, Q., Xiao, D., Li, Z., Tan, L., Clark, J.M., Norell, M.A., Hone, D.W.E., and Sullivan, C. 2010a. A new dromaeosaurid (Dinosauria: Theropoda) from the Upper Cretaceous Wulansuhai Formation of Inner Mongolia, China. *Zootaxa*, **9**: 1–9.

Xu, X., Norell, M.A., Wang, X.L., Makovicky, P.J., and Wu, X.C. 2002. A basal troodontid from the Early Cretaceous of China. *Nature*, **415**: 780–784. doi:10.1038/415780a.

Xu, X., Pittman, M., Sullivan, C., Choiniere, J.N., Tan, Q.-W., Clark, J.M., Norell, M. a., and Wang, S. 2015. The taxonomic status of the Late Cretaceous dromaeosaurid *Linheraptor exquisitus* and its implications for dromaeosaurid systematics. *Vertebrata Palasiatica*, **53**: 29–62.

Zheng, X., Xu, X., You, H., Zhao, Q., and Dong, Z. 2010. A short-armed dromaeosaurid from the Jehol group of China with implications for early dromaeosaurid evolution. *Proceedings of the Royal Society B: Biological Sciences*, **277**: 211–217. doi:10.1098/rspb.2009.1178.

4.9 Tables and Figures

Table 4.1. List of specimens used for metric comparison with *V. vadarostrum* n. sp.

Taxon	Specimen #	Condition	Measurement method
<i>Linheraptor exquisitus</i>	IVPP V16923	Articulated nearly complete skeleton	ImageJ software (Xu et al. 2010a, 2015)
<i>Tsaagan mangas</i>	MPC-D 100/1015	Articulated skull and cervical series	Digital calipers, fabric measuring tape, ImageJ personal photos
<i>V. mongoliensis</i>	AMNH FARB 6515	Nearly complete skull with partial first digit	Digital calipers, fabric measuring tape, ImageJ personal photos
<i>V. mongoliensis</i>	MPC-D 100/24	Articulated skull Damaged.	ImageJ photos by Dr. Currie
<i>V. mongoliensis</i>	MPC-D 100/25	Articulated skeleton, nearly complete.	ImageJ photos by Dr. Currie
<i>V. mongoliensis</i>	MPC-D 100/54	Nearly complete articulated skeleton	ImageJ photos by Dr. Currie
<i>V. mongoliensis</i>	“Moscow” specimen	Nearly complete articulated skull	ImageJ photos by Dr. Currie, digital calipers from cast in UALVP collections.
<i>V. osmolskae</i>	IMM99NM-BYM-3/3A	Nearly complete left maxilla and partial right maxilla and lacrimal.	ImageJ (Godefroit et al. 2008)
<i>V. vadarostrum</i> n. sp.	MPC-D 100/982	Articulated skeleton missing skull roof, anterior cervicals and distal caudals	Digital calipers, fabric measuring tape, ImageJ personal photos, CT data.

Table 4.2. Size measurements of *V. vadarostrum* n. sp.

Element	Measurement (mm)
Skull Length	200
Snout Length	122
Snout depth (maxillolacrimal contact)	46
Snout depth (cranium only)	29
Snout width (mid)	17
Temporal length	78
Temporal width (quadrate to quadrate)	53
Length of the postorbital region	41
Mandible length	190
Dentary length	114
Dentary height mid	14.5
Humerus length	119
Deltopectoral crest length	39
Metacarpal I + Phalanx I-1 length	60
Metacarpal II length	50
Ilium length	129
Femur length	155
Femur circumference	54
Tibia length	182
MT III length	89

Measurements were averaged between sides if two were available and were rounded to the nearest millimetre unless it was near the middle between values like the dentary height.

Table 4.3. List of PCA scores for raw linear measurements and log transformed data.

Dataset	Specimen	Principal component						
		PC 1	PC 2	PC 3	PC 4	PC 5	PC 6	PC 7
Raw data PCA	MPC-D 100/982	-19.29	7.44	-5.57	0.24	3.86	0.09	0.53
	AMNH 6515	-21.58	-8.57	-1.35	4.36	-2.15	-2.42	-0.28
	Moscow	-10.32	-2.73	2.73	0.76	-0.35	3.85	-2.02
	MPC-D 100/25	10.18	10.29	7.33	2.57	0.73	-1.92	-1.11
	MPC-D 100/54	-2.56	5.09	2.38	-0.20	-2.57	1.34	3.16
	IMM99NM- BYM-3/3A	1.65	2.52	-2.79	-8.64	-1.98	-1.09	-1.16
	MPC-D 100/1015	10.02	-12.92	3.91	-2.97	2.95	-0.42	1.07
	IVPP V16923	31.91	-1.12	-6.63	3.88	-0.50	0.57	-0.19
log transformed data	MPC-D 100/982	-0.60	0.02	0.06	-0.22	-0.04	0.04	0.01
	AMNH 6515	-0.47	-0.41	0.05	0.11	0.00	0.00	0.03
	Moscow	-0.26	-0.02	-0.02	-0.06	0.03	-0.11	-0.03
	MPC-D 100/25	-0.22	0.21	0.11	0.05	0.13	0.03	0.00
	MPC-D 100/54	-0.30	0.10	0.03	0.13	-0.08	0.03	-0.05
	IMM99NM- BYM-3/3A	-0.03	0.21	-0.30	0.04	-0.03	-0.01	0.03
	MPC-D 100/1015	0.89	-0.22	-0.16	-0.06	0.04	0.04	-0.03
	IVPP V16923	0.99	0.09	0.23	0.00	-0.05	-0.02	0.02

Table 4.4. List of PC loadings for raw data linear measurement PCA and log transformed data PCA.

Dataset	Measurement	Principal Component						
		PC 1	PC 2	PC 3	PC 4	PC 5	PC 6	PC 7
Raw data								
PCA	Length	0.38	0.42	0.17	-0.42	-0.07	-0.13	-0.37
	Height	0.36	0.00	0.11	0.14	-0.16	-0.27	-0.26
	Anterior Process Length	0.44	-0.17	-0.19	0.29	-0.18	0.14	0.09
	Ant. Proc. Height Distal	0.14	0.03	-0.11	0.41	0.37	0.28	-0.61
	Ant. Proc. Height Proximal	0.34	-0.08	0.04	-0.06	0.35	0.05	0.43
	Antorbital Fen. Height	0.18	0.18	0.02	0.17	0.41	-0.14	0.34
	Antorbital fossa Length - ant. Fen	-0.02	0.55	-0.21	-0.02	-0.19	0.22	0.17
	Antorbital F. Height	0.13	0.13	0.14	0.43	-0.09	-0.55	0.10
	Mx. Fen. To ant edge of fossa	-0.27	0.55	0.02	0.03	0.12	-0.03	0.06
	Mx. Fen. Long axis	0.23	0.01	-0.19	-0.04	-0.46	0.39	0.10
	Mx. Fen. Short axis	0.08	-0.04	-0.13	0.06	-0.08	-0.04	0.19
	Ventral Margin height ant.	0.20	-0.12	-0.05	-0.22	0.01	-0.05	0.06
	Ventral Margin Height Post.	0.13	-0.19	-0.05	-0.50	0.33	-0.06	-0.06
	Length first 9 alveoli	0.39	0.24	0.11	-0.06	0.03	0.07	0.10
	Width Preantorbital bar	0.05	0.14	-0.18	0.10	0.34	0.33	0.02
	Dist. Ant marg ant fen to 9th alveolus	0.00	-0.04	0.86	0.10	-0.05	0.41	0.09
log transformed data	Length	0.03	0.12	0.01	0.04	0.09	0.08	0.04
	Height	0.10	0.15	0.09	0.21	0.29	0.04	0.13
	Anterior Process Length	0.14	0.12	0.14	0.21	0.08	-0.08	0.08
	Ant. Proc. Height Distal	0.10	0.11	0.43	-0.25	0.52	-0.47	0.33
	Ant. Proc. Height Proximal	0.16	0.21	0.06	0.09	0.20	0.31	-0.43
	Antorbital Fen. Height	0.06	0.19	0.18	-0.04	0.17	0.50	-0.14
	Antorbital fossa Length - ant. Fen	-0.07	0.28	0.14	-0.04	-0.30	0.10	0.34
	Antorbital F. Height	0.03	0.06	0.19	0.16	0.24	0.28	0.15
	Mx. Fen. To ant edge of fossa	-0.83	0.46	-0.16	0.10	0.13	-0.03	0.06
	Mx. Fen. Long axis	0.20	0.41	0.07	0.45	-0.31	-0.49	-0.29
	Mx. Fen. Short axis	0.13	0.06	0.16	0.19	-0.41	0.26	0.58
	Ventral Margin height ant.	0.23	0.25	-0.14	0.30	0.14	0.07	0.06

Ventral Margin Height							
Post.	0.35	0.37	-0.69	-0.35	0.10	-0.02	0.22
Length first 9 alveoli	0.05	0.14	0.05	0.06	0.10	0.10	-0.06
Width Preantorbital bar	0.05	0.41	0.37	-0.58	-0.31	0.04	-0.23

High positive values were indicated with green highlights whereas high negative values were indicated with yellow. Length and length of the first nine alveoli were not highlighted because they are used as a metric of size and are tightly correlated.

Table 4.5. Results of multiple regression analysis of Asian eudromaeosaurian maxillary comparative analyses.

Group analysed	R²	MSE (mean standard error)
<i>Velociraptor mongoliensis</i> (n=4)	0.747	0.00355
<i>V. mongoliensis</i> + <i>V. vadarostrum</i> n. sp. (n=5)	0.362	0.0164
<i>V. mongoliensis</i> + <i>V. osmolskae</i> (n=5)	0.294	0.0168
<i>Velociraptor</i> (n=6)	0.224	0.0216
<i>V. mongoliensis</i> + <i>Linheraptor exquisitus</i> and <i>Tsaagan mangas</i> (n=6)	0.237	0.0422

Table 4.6. Results of multiple regression analysis of maxillary measurements comparison across *Velociraptor*.

Variable	<i>Velociraptor mongoliensis</i>			<i>V. mongoliensis</i> + <i>V. vadarostrum</i> n. sp.			<i>V. mongoliensis</i> + <i>V. osmolskae</i>		
	Slope	r	p	Slope	r	p	Slope	r	p
Height	1.497	0.967	0.033	1.664	0.865	0.059	1.369	0.945	0.015
Anterior Process Length	1.162	0.997	0.003	1.353	0.799	0.105	1.058	0.971	0.006
Ant. Proc. Height Distal	1.442	0.608	0.392	1.376	0.590	0.295	0.767	0.310	0.611
Ant. Proc. Height Proximal	2.302	0.993	0.007	2.372	0.982	0.003	2.164	0.983	0.003
Antorbital Fen. Height	2.016	0.978	0.022	1.907	0.936	0.019	1.659	0.873	0.054
Antorbital fossa Length - ant. Fen	1.384	0.914	0.086	1.166	0.666	0.219	1.312	0.912	0.031
Antorbital F. Height	0.930	0.721	0.279	0.999	0.725	0.166	0.559	0.423	0.478
Mx. Fen. To ant edge of fossa	0.967	0.829	0.171	0.421	0.140	0.822	0.470	0.337	0.579
Mx. Fen. Long axis	2.615	0.852	0.148	2.945	0.780	0.119	2.807	0.876	0.052
Mx. Fen. Short axis	0.374	0.319	0.681	0.449	0.360	0.552	0.494	0.421	0.480
Ventral Margin height ant.	2.221	0.987	0.013	2.483	0.865	0.058	2.674	0.923	0.025
Ventral Margin Height Post.	2.856	0.778	0.222	2.757	0.764	0.133	4.474	0.717	0.173
Length first 9 alveoli	1.193	0.998	0.002	1.211	0.995	0.000	1.107	0.982	0.003
Width	2.889	0.893	0.107	2.346	0.589	0.296	2.431	0.816	0.092
Preantorbital bar									
Dist. Ant marg ant fen to 9th alveolus	4.133	0.875	0.125	6.024	0.505	0.385	0.050	0.005	0.994

Bolded values indicate situations in which adding the specimen indicated in the column would destabilize the trend either by reducing the fit (r values) or by causing a loss in correlation significance (p value > 0.05).

Table 4.7. Reduced major axis regression analysis of *V. mongoliensis* with and without *V. vadarostrum* n. sp.

Variable	<i>V. mongoliensis</i>			<i>V. mongoliensis</i> + <i>V. vadarostrum</i> n. sp.		
	Slope CI 95%	r ²	p	Slope CI 95%	r ²	p
Height	(0.61, 2.69)	0.946	0.027	(-0.034, 2.81)	0.716	0.071
AntRL	(0.99, 1.34)	0.991	0.0003	(0.43, 2.17)	0.626	0.034
AntFL	(0.48, 1.99)	0.824	0.033	(-0.87, 3.92)	0.480	0.127
MxFen - AntF	(-1.48, 2.51)	0.688	0.171	(-1.50, 16.46)	0.020	0.822
VentMargin-Anterior	(1.73, 3.21)	0.974	0.013	(-1.87, 4.45)	0.749	0.058
Preantral bar	(0.39, 6.53)	0.798	0.107	(-1.63, 14.52)	0.347	0.296
QuH-MxH	(0.66, 1.35)	0.951	0.025	(-0.17, 5.34)	0.492	0.187

Table 4.8. Values for parsimony and Bayesian consensus trees.

Analysis	Consistency Index	Retention Index	Tree Length
Dromaeosaurid	0.45	0.61	425
Parsimony			
Dromaeosaurid	0.43	0.59	442
Bayesian			
Eudromaeosauria	0.49	0.54	371
Parsimony			
Eudromaeosauria	0.50	0.56	364
Bayesian			

Table 4.9. Comparison of premaxillary and maxillary character CI values among phylogenetic analyses.

Character	Parsimony all taxa	Parsimony ingroup	Bayesian all taxa	Bayesian ingroup
5	0.4	0.4	0.33	0.4
6	0.5	0.5	0.5	0.5
7	0.25	0.33	0.25	0.33
8	0.25	0.33	0.2	0.33
9	0.33	0.33	0.25	0.25
10	0.2	0.2	0.2	0.2
11	0.75	0.75	1	1
12	0.5	0.4	0.4	0.4
13	0.167	0.143	0.143	0.167
14	0.5	0.5	0.5	0.5
15	0.25	0.25	0.25	0.25
21	1	1	1	1
23	0.167	0.2	0.2	0.167
27	0.25	0.33	0.25	0.25
28	0.25	0.286	0.25	0.33
29	0.5	0.5	0.5	0.5
32	0.25	0.25	0.2	0.25

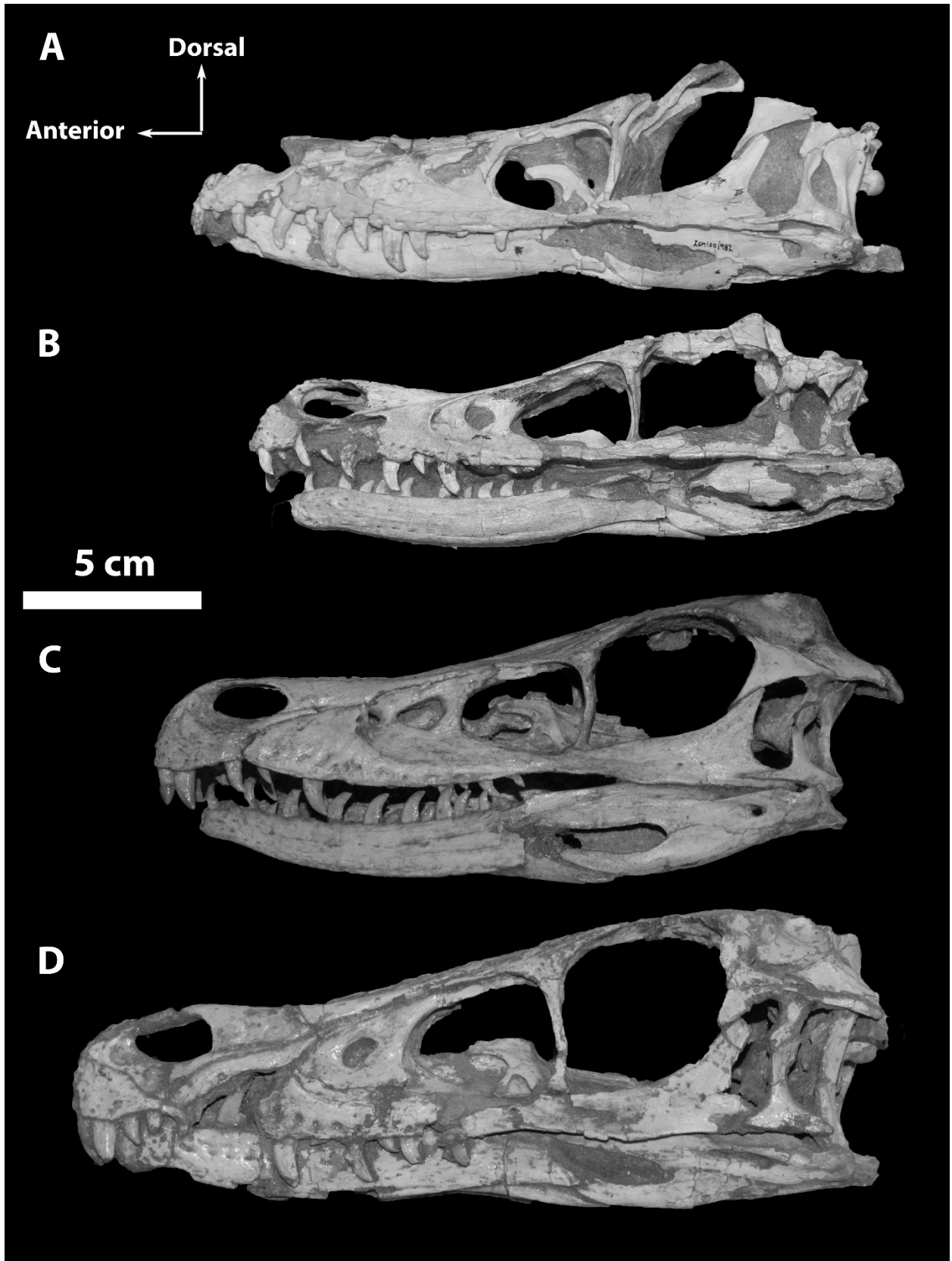


Figure 4.1. Comparison of *Velociraptor* skull profiles. A) Left lateral aspect of the holotype of *V. vadarostrum* n. sp. (MPC-D 100/982); B) Left lateral aspect of the holotype of *V. mongoliensis* (AMNH FARB 6515); C) Left lateral aspect of a specimen of *V. mongoliensis* (MPC-D 100/54); D) left lateral aspect of the ‘fighting dinosaurs’ *V. mongoliensis* specimen (MPC-D 100/25). Photos of C and D are credited to Dr. Currie. All skulls were scaled to reflect their relative size to one another.

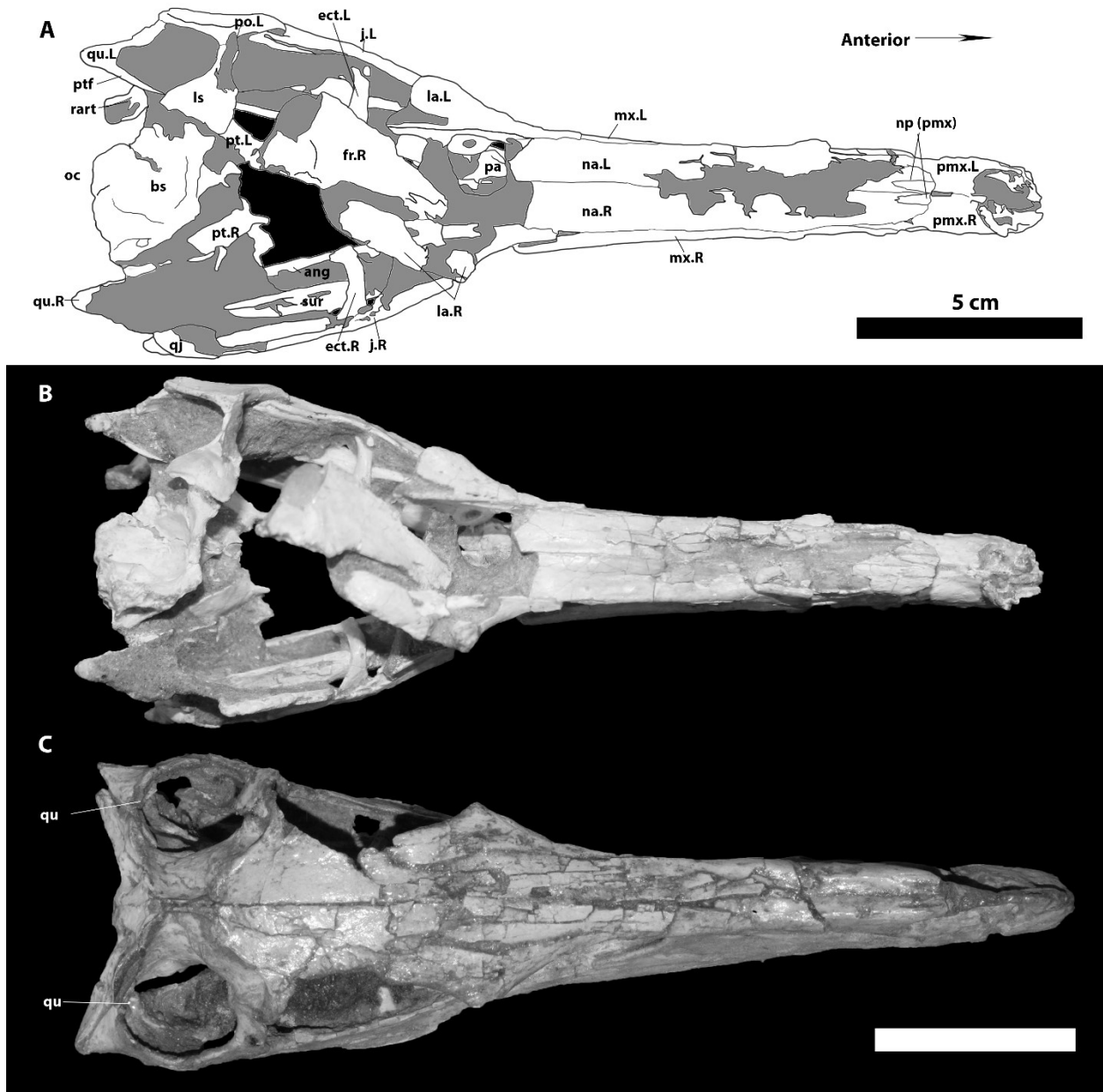


Figure 4.2. Dorsal aspect of the skull of *V. vadarostrum* n. sp. with comparison to *V. mongoliensis*. A) line drawing and label of elements the holotype of *V. vadarostrum* n. sp. in dorsal view; B) photograph of the skull of the holotype of *V. vadarostrum* n. sp. in dorsal view. Scale bar with label is for A and B; C) Photograph of the ‘fighting dinosaurs’ *V. mongoliensis* specimen in dorsal view (photo credit to Dr. Philip Currie). Scale bar for C = 5cm.

Abbreviations: **af**, antorbital fenestra; **ang**, angular; **aof**, antorbital fossa; **bs**, basisphenoid; **d**,

dentary; **ect**, ectopterygoid; **fr**, frontal; **j**, jugal; **la**, lacrimal; **ls**, laterosphenoid; **mx**, maxilla; **na**, nasal; **np**, nasal process of the premaxilla; **oc**, occipital condyle; **pa**, palatine; **pmx**, premaxilla; **po**, postorbital; **pt**, pterygoid; **ptf**, pterygoid flange of the quadrate; **qj**, quadratojugal; **qu**, quadrate; **rart**, retroarticular process; **sq**, squamosal; **sur**, surangular. Capital R or L refers to the side the element is from.

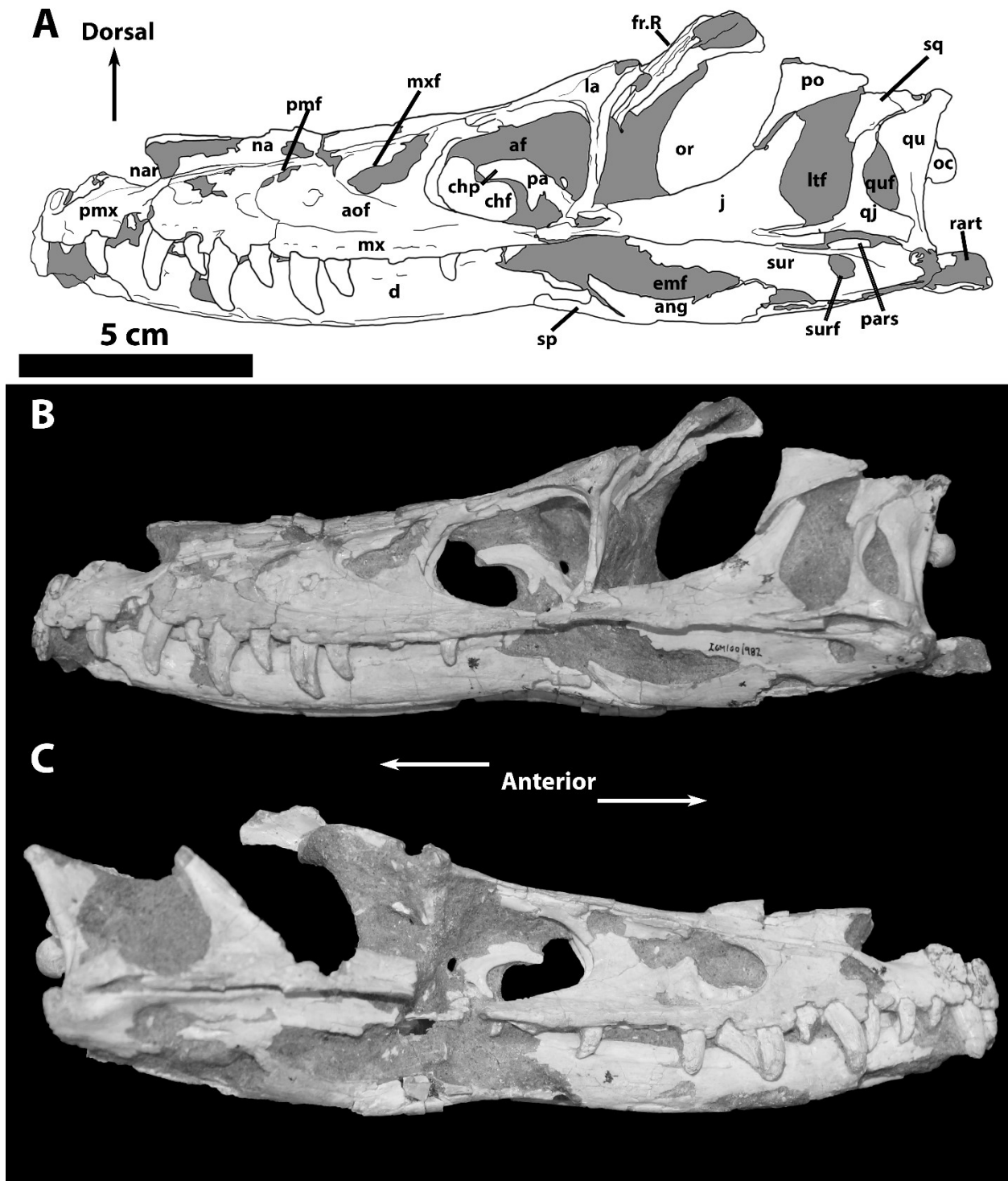


Figure 4.3. Lateral aspects of the skull of *V. vadarostrum* n. sp. A) a line drawing of the left side of the skull of the holotype of *V. vadarostrum* n. sp. with labels for skull elements and

fenestrae. B and C) photos of left lateral and right lateral view of the skull of *V. vadarostrum* n. sp. Abbreviations: **af**, antorbital fenestra; **ang**, angular; **aof**, antorbital fossa; **chf**, choanal fenestra; **chp**, choanal process; **d**, dentary; **emf**, external mandibular fenestra; **fr**, frontal; **j**, jugal; **la**, lacrimal; **ltf**, lateral temporal fenestra; **mx**, maxilla; **mxl**, maxillary fenestra; **na**, nasal; **nar**, external nares; **oc**, occipital condyle; **or**, orbit; **pa**, palatine; **pars**, prearticular shelf; **pmf**, promaxillary fenestra; **pmx**, premaxilla; **po**, postorbital; **qj**, quadratojugal; **qu**, quadrate; **quf**, quadrate fenestra; **rart**, retroarticular process; **sp**, splenial; **sq**, squamosal; **sur**, surangular; **surf**, surangular fenestra. Capital R or L refers to the side the element is from.

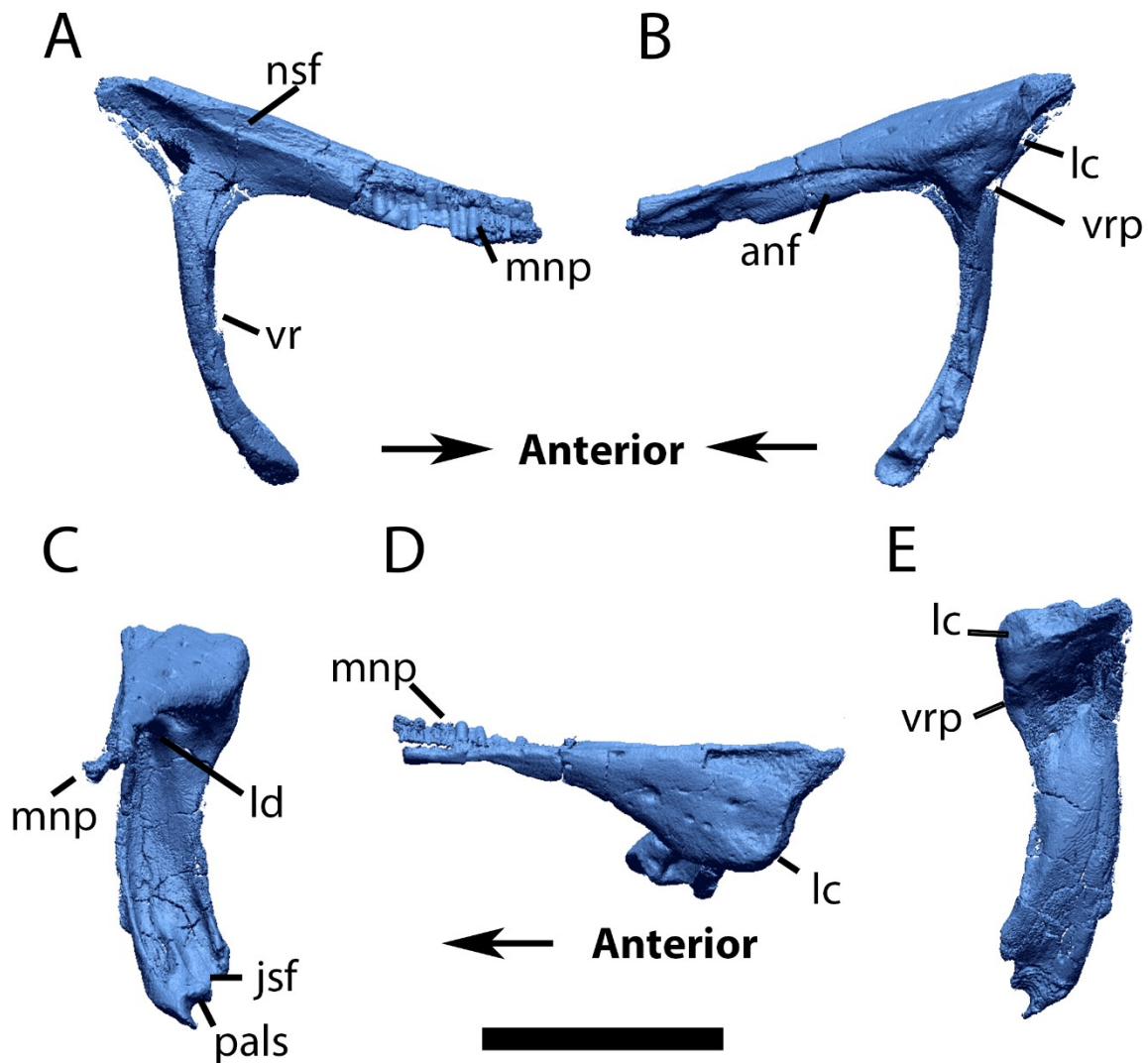


Figure 4.4. 3D rendering of the left lacrimal of *V. vadarostrum* n. sp. A) medial, B) lateral, C) anterior, D) dorsal, and E) posterior views. Scale bar = 2 cm. Abbreviations: **anf**, antorbital fossa; **jsf**, jugal sutural facet; **lc**, lacrimal crest; **ld**, lacrimal duct; **mnp**, maxilla-nasal process; **nsf**, nasal sutural facet; **pals**, palatine sutural facet; **vr**, ventral ramus; **vrp**, ventral ramus protuberance.

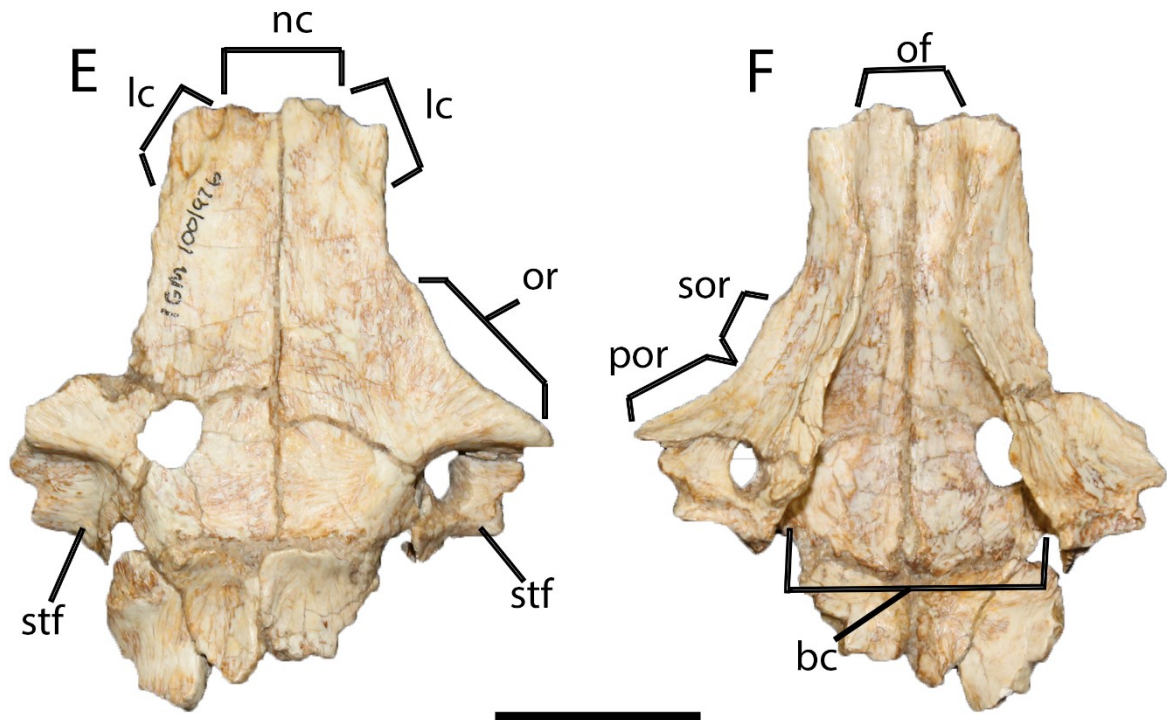
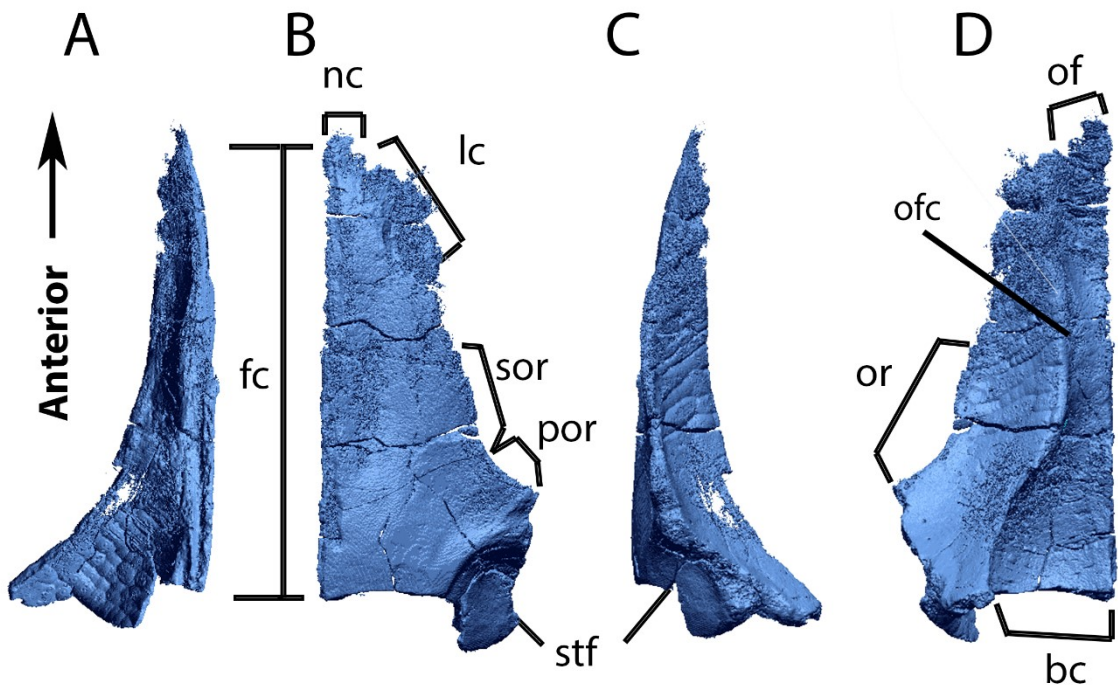


Figure 4.5. Frontal comparison between *V. vadarostrum* n. sp. and *V. mongoliensis*. A-D) 3D rendering of the frontal of the holotype of *V. vadarostrum* n. sp. in A) medial, B) dorsal, C) lateral, and D) ventral aspects. E-F) paired frontals of a specimen of *V. mongoliensis* (MPC-D 100/976) in A) dorsal and B) medial view. Scale bars = 2 cm. Abbreviations: **bc**, brain cavity (cerebellar); **fc**, frontal contact; **lc**, lacrimal contact; **nc**, nasal contact; **of**, olfactory recess; **ofc**, olfactory canal; **or**, orbital rim; **por**, postorbital region of orbital rim; **sor**, supraorbital region of the orbital rim; **stf**, supratemporal fossa.

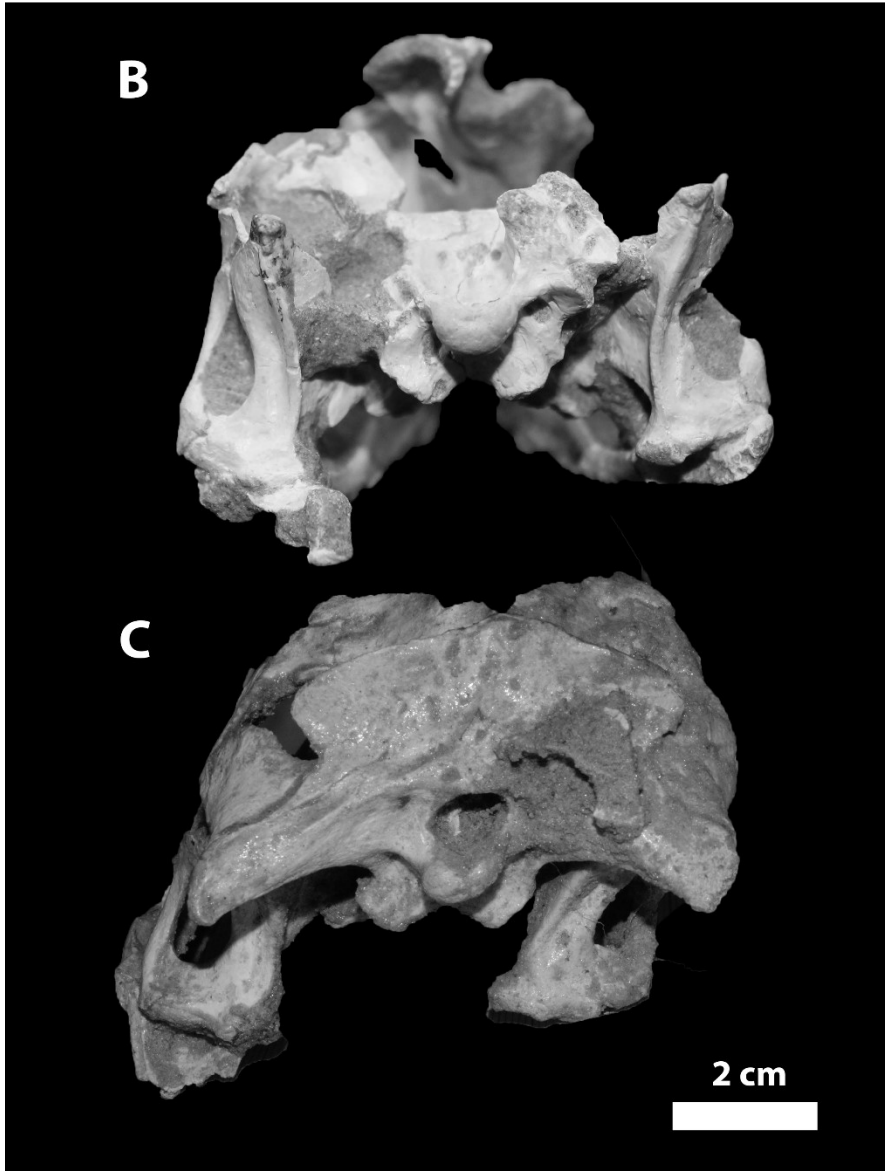
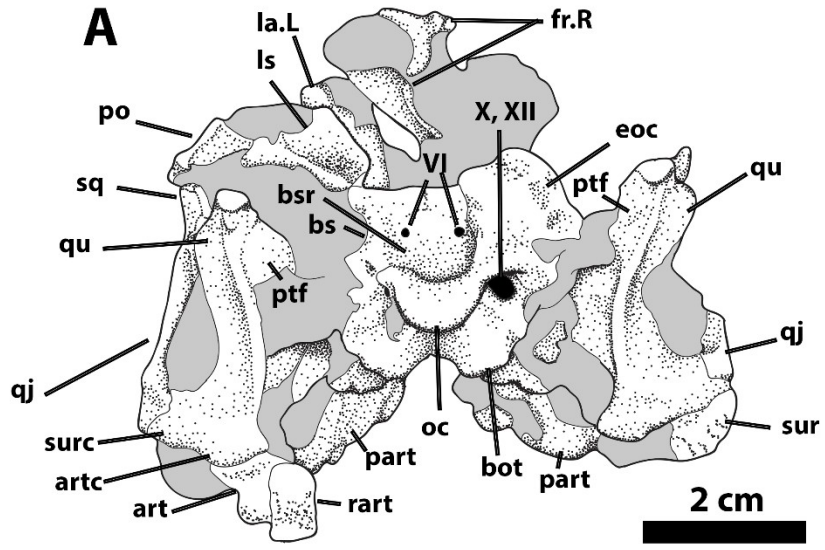


Figure 4.6. Skull of *V. vadarostrum* n. sp. in posterior view with comparison to *V. mongoliensis*. Illustration (A) and photograph (B) of MPC-D 100/982 in posterior view. C) photograph of a *V. mongoliensis* specimen (MPC-D 100/54) in posterior view (photo credit to Dr. Philip Currie). Grey regions indicate areas obscured by matrix. Abbreviations: **art**, articular; **artc**, articular condyle of the quadrate; **bot**, basioccipital tuber; **bs**, basisphenoid; **bsr**, basisphenoid recess; **eoc**, exoccipital; **fr**, frontal; **la**, lacrimal; **ls**, laterosphenoid; **oc**, occipital condyle; **part**, prearticular; **po**, postorbital; **ptf**, pterygoid flange of the quadrate; **qj**, quadratojugal; **qu**, quadrate; **rart**, retroarticular process; **sq**, squamosal; **sur**, surangular; **surc**, surangular condyle of the quadrate; **VI**, cranial nerve six; **X**, cranial nerve ten; **XII**, cranial nerve 12. Capital letters refer to the side of the skull in which the element belongs.

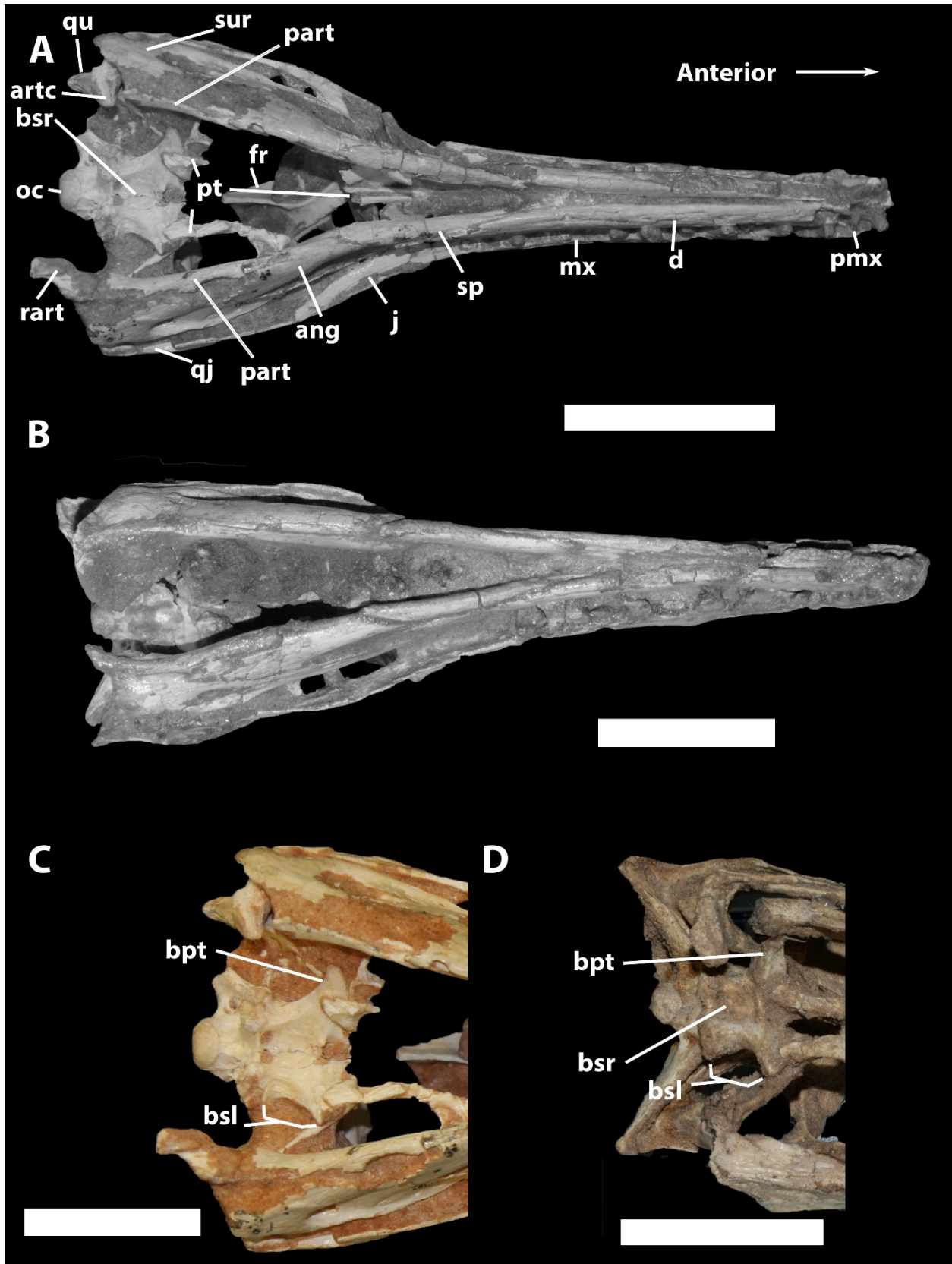


Figure 4.7. Ventral aspect of the skull of *V. vadarostrum* n. sp. with comparison to *V.*

***mongoliensis*.** A) photograph of the ventral aspect of the skull of the holotype of *V. vadarostrum* with labels of elements; B) photograph of the ventral aspect of the ‘fighting dinosaurs’ *V. mongoliensis* specimen (MPC-D 100/25, photo credit to Dr. Currie); C and D) ventral aspects of the braincase of both *V. vadarostrum* (C) and a specimen of *V. mongoliensis* (D, MPC-D 100/54). Scale bar for A and B = 5 cm; for C and D = 3 cm. Abbreviations: **ang**, angular; **artc**, articular condyle of the quadrate; **bpt**, basiptyergoid tuber; **bsl**, basisphenoid lateral wall; **bsr**, basisphenoid recess; **d**, dentary; **ect**, ectopterygoid; **fr**, frontal; **j**, jugal; **mx**, maxilla; **oc**, occipital condyle; **part**, prearticular; **pmx**, premaxilla; **pt**, pterygoid; **qj**, quadratojugal; **qu**, quadrate; **rart**, retroarticular process; **sp**, splenial; **sq**, squamosal; **su**, surangular. Capital R or L refers to the side the element is from.

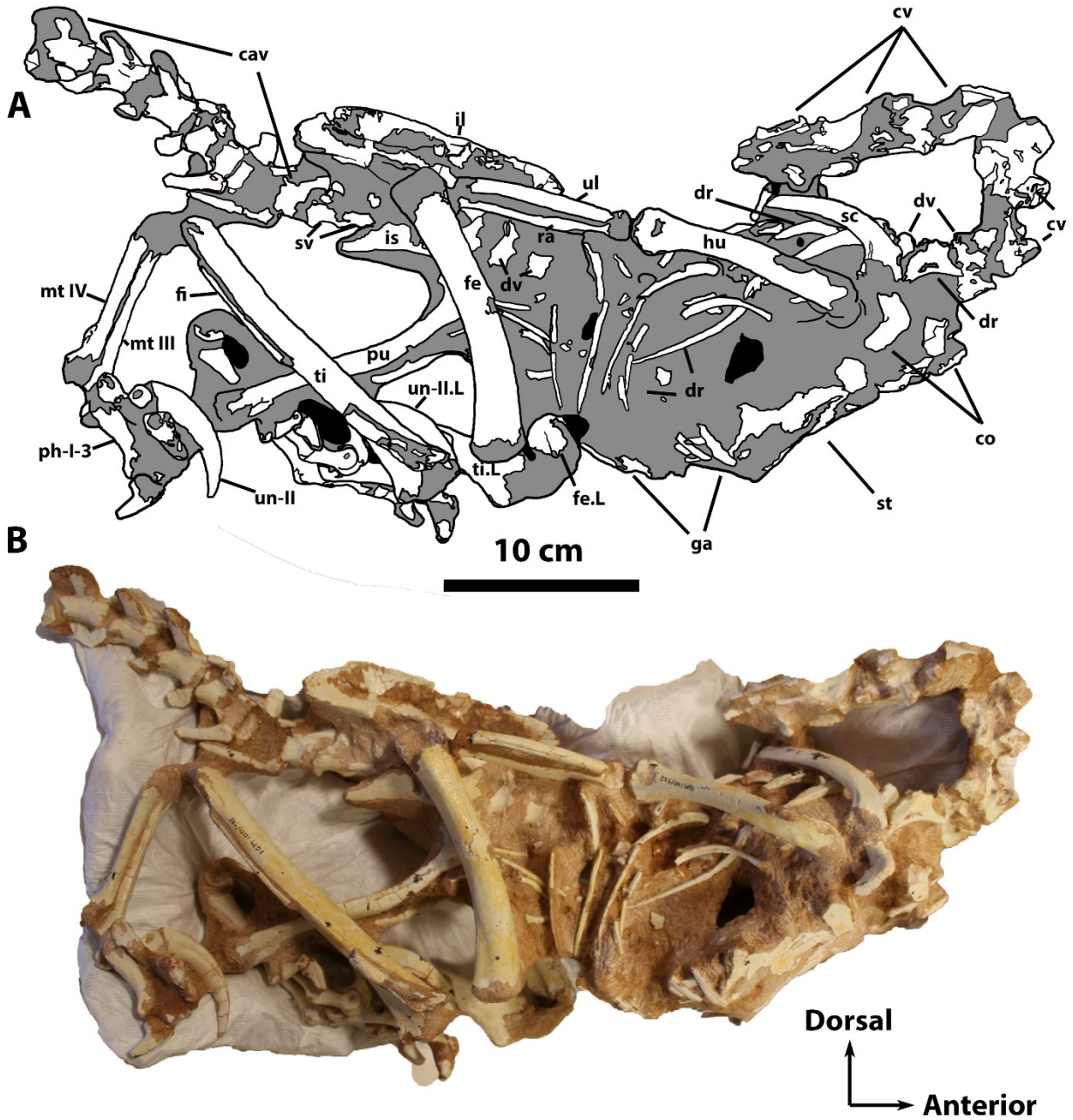
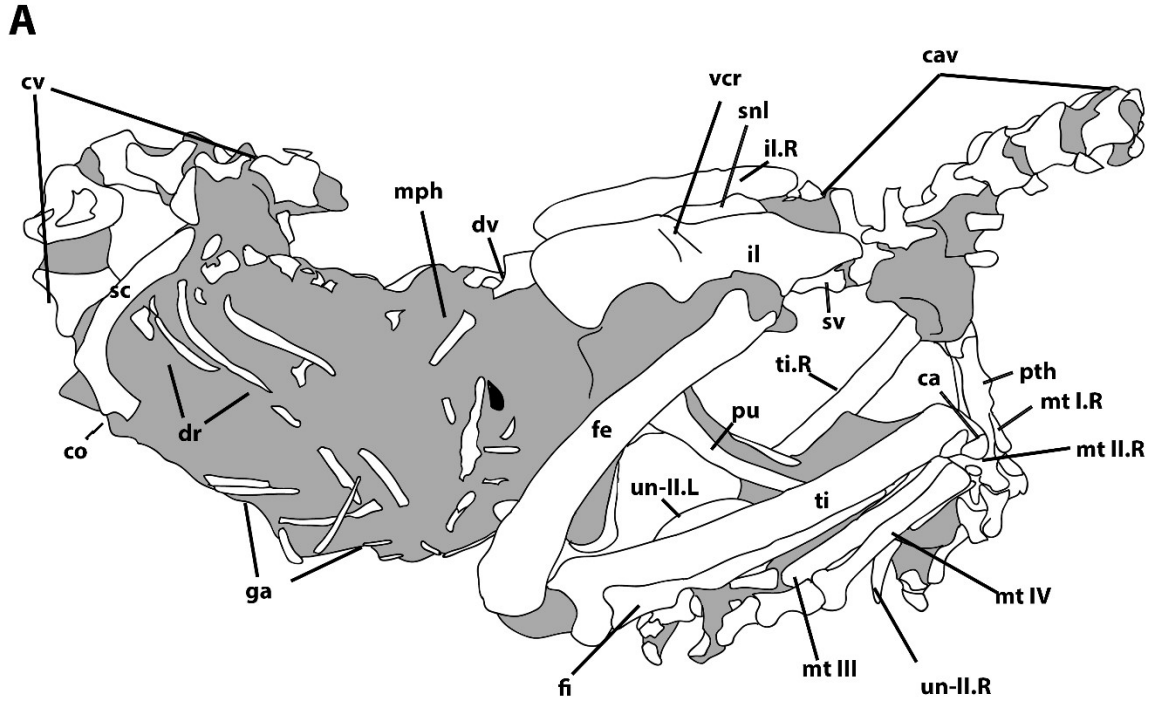


Figure 4.8. Articated skeleton of the holotype of *Velociraptor vadarostrum* n. sp. in right lateral view. A) line drawing and (B) photograph of the right aspect of MPC-D 100/982. Grey regions of the line drawing indicate matrix cover, and black areas are small canals through the specimen. Larger openings were left as white. Abbreviations: **cav**, caudal vertebra; **co**, coracoid; **cv**, cervical vertebra; **dr**, dorsal rib; **dv**, dorsal vertebra, **fe**, femur; **fi**, fibula; **ga**, gastralia; **hu**,

humerus; **il**, ilium; **is**, ischium; **mph**, manual phalanx; **mt**, metatarsal; **ph**, pedal phalanx; **pu**, pubis; **ra**, radius; **sc**, scapula; **st**, sternal plate; **sv**, sacral vertebra; **ul**, ulna; **un**, pedal ungual.

Capital letters (R and L) represent the side of the skeleton to which the labelled element belongs.



10 cm



B



Dorsal

Anterior



Figure 4.9. Articulated skeleton of *Velociraptor vadarostrum* n. sp. in left lateral aspect. A) line drawing and (B) photograph of the left aspect of MPC-D 100/982. Grey regions of the line drawing indicate matrix cover, and black areas are small canals through the specimen. Larger openings were left as white. Abbreviations: **cav**, caudal vertebra; **co**, coracoid; **cv**, cervical vertebra; **dr**, dorsal rib; **dv**, dorsal vertebra; **fe**, femur; **fi**, fibula; **ga**, gastralia; **hu**, humerus; **il**, ilium; **is**, ischium; **mph**, manual phalanx; **mt**, metatarsal; **ph**, pedal phalanx; **pth**, pathology; **pu**, pubis; **ra**, radius; **sc**, scapula; **snl**, sacral neural arch lamina; **st**, sternal plate; **sv**, sacral vertebra; **ul**, ulna; **un**, pedal ungual; **vcr**, vertical crest. Capital letters (R and L) represent the side of the skeleton to which the labelled element belongs.

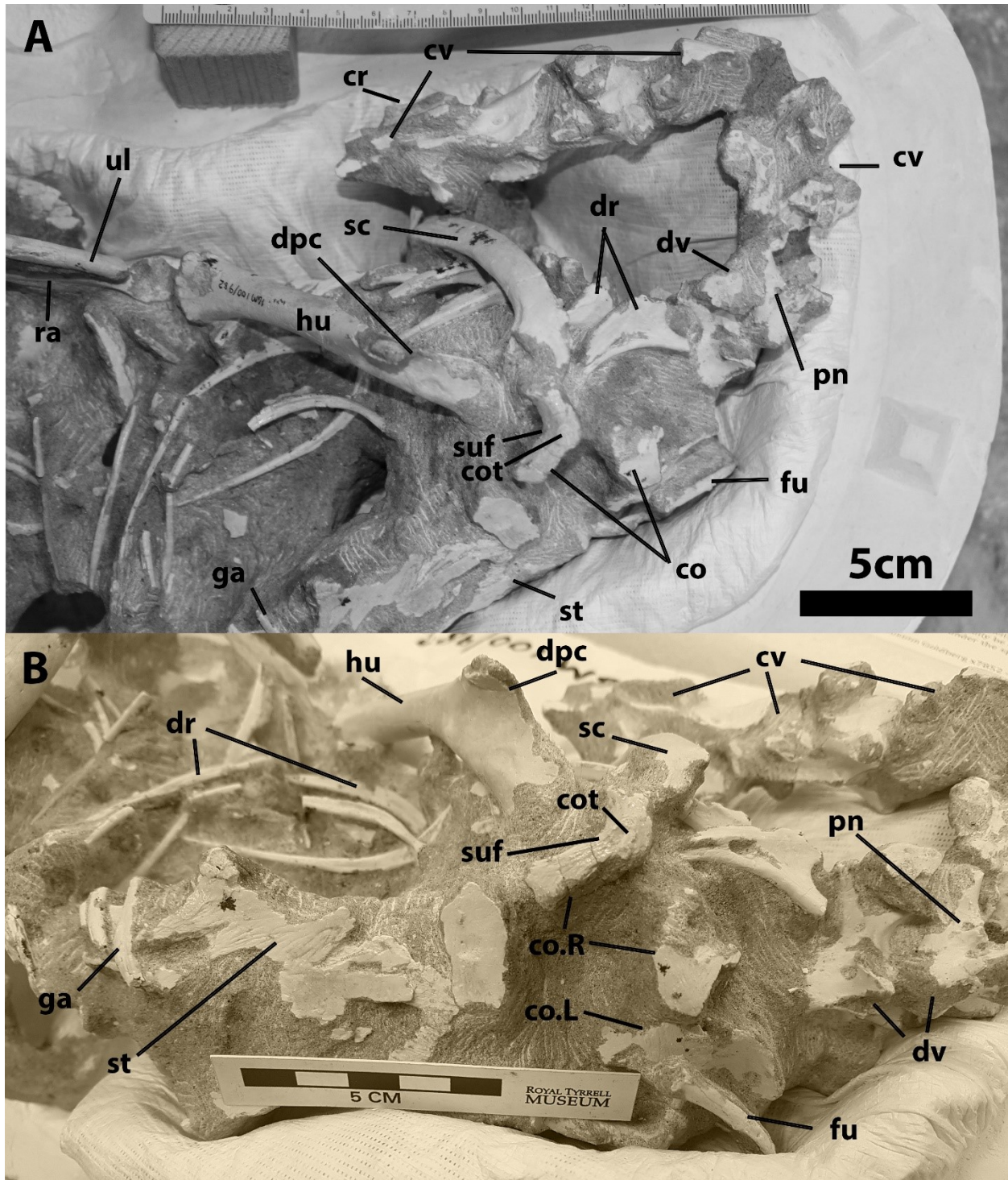


Figure 4.10. Pectoral girdle of *Velociraptor vadarostrum* n. sp. A) right lateral aspect and B) an oblique angle of the pectoral girdle of MPC-D 100/982. Abbreviations: **co**, coracoid; **cot**, coracoid tuber; **cr**, cervical rib; **cv**, cervical vertebra; **dpc**, deltapectoral crest; **dr**, dorsal rib; **dv**,

dorsal vertebra; **fu**, furcula; **ga**, gastralia; **hu**, humerus; **pn**, pneumatopore; **ra**, radius; **sc**, scapula; **st**, sternal plate; **suf**, sub-glenoid fossa; **ul**, ulna. Capital letters (R and L) represent the side of the skeleton to which the labelled element belongs.

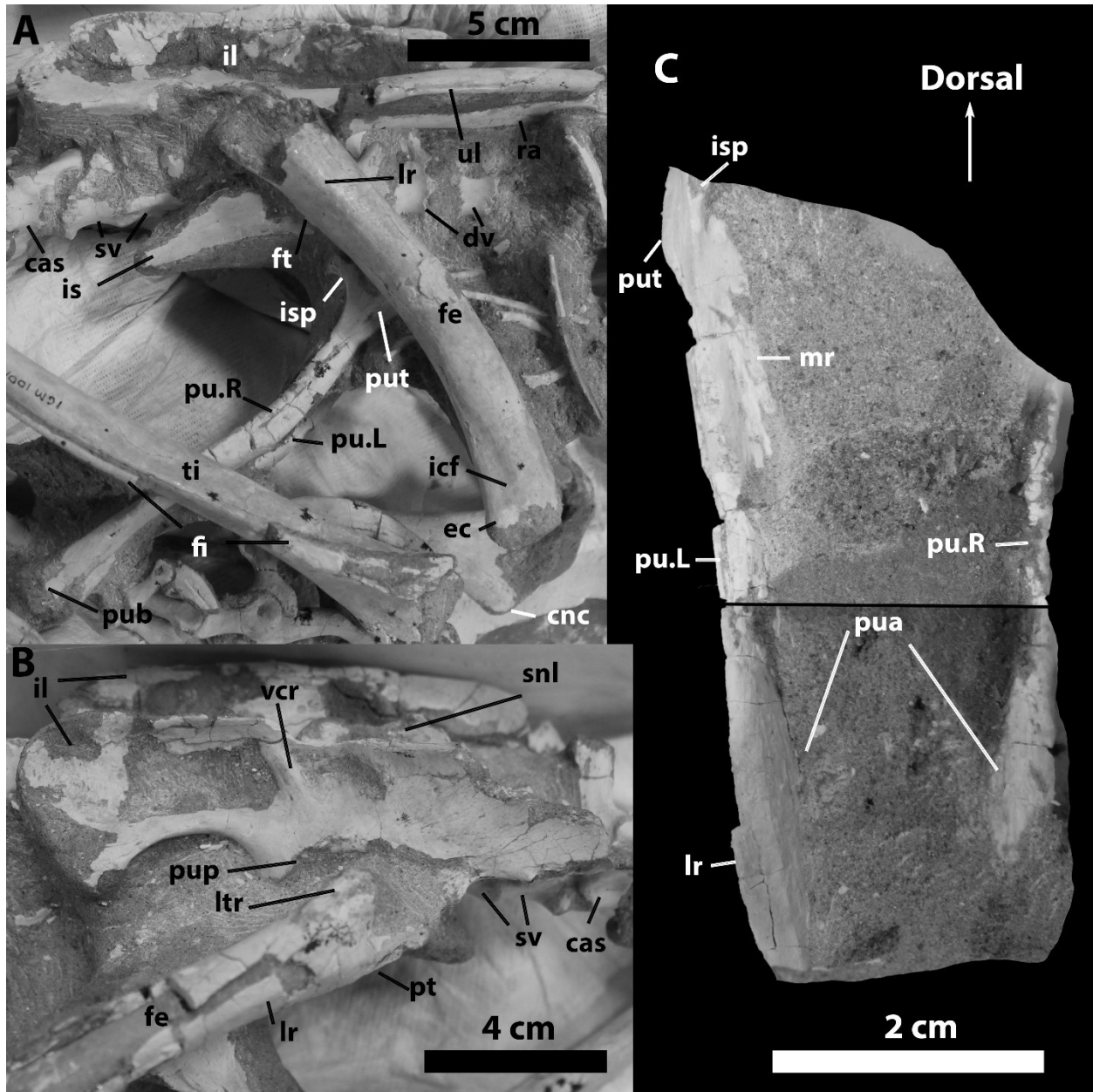


Figure 4.11. Pelvis and upper hindlimb of *Velociraptor vadarostrum* n. sp. A) right side of pelvis and upper hindlimb, and B) left side of pelvis and proximal femur in lateral aspect of MPC-D 100/982. C) partial pubes of MPC-D 100/982 in posterior view. The pubes figured are of two photos, matched at midshaft. Abbreviations: **cas**, caudosacral vertebra; **cnc**, cnemial crest; **dv**, dorsal vertebra; **ec**, ectocondyle; **fe**, femur; **fi**, fibula; **ft**, fourth trochanter of the femur; **icf**, intercondylar fossa; **il**, ilium; **is**, ischium; **isp**, ischial peduncle of the pubis; **lr**, lateral ridge

(pubis and femur); **lt**, lesser trochanter of the femur; **mr**, medial ridge of the pubis; **pt**, posterior tubercle; **pu**, pubis; **pua**, pubic apron; **pub**, pubic boot; **pup**, pubic peduncle of the ilium; **put**, pubic tubercle; **ra**, radius; **snl**, sacral neural arch lamina; **sv**, sacral vertebra; **ul**, ulna; **ver**, vertical crest. Capital letters (R and L) represent the side of the skeleton to which the labelled element belongs.

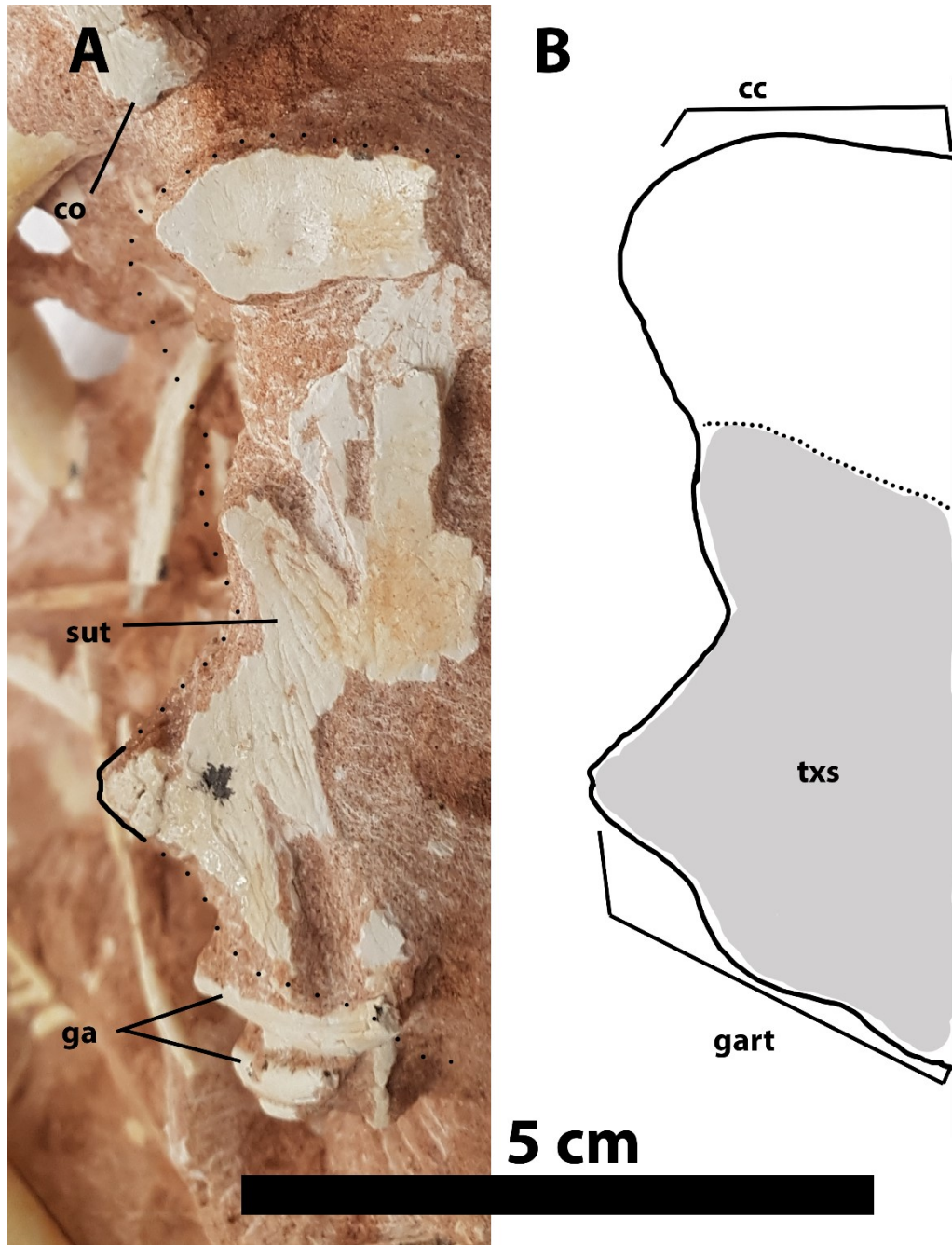


Figure 4.12. Interpretive line drawing of the sternal plate of *Velociraptor vadarostrum* n. sp.

A) closeup anterior view of the right sternal plate of *V. vadarostrum* n. sp. Dotted line is the interpreted boundary of the sternal plate and the solid black line indicates where a natural edge was preserved. B) reconstructed sternal plate based on interpreted border. Grey region indicates

proposed extent of the striated surface. Abbreviations: **cc**, coracoid contact; **co**, coracoid; **ga**, gastralia; **gart**, articulation for the gastralia; **sut**, surface texture; **txs**, textured surface.

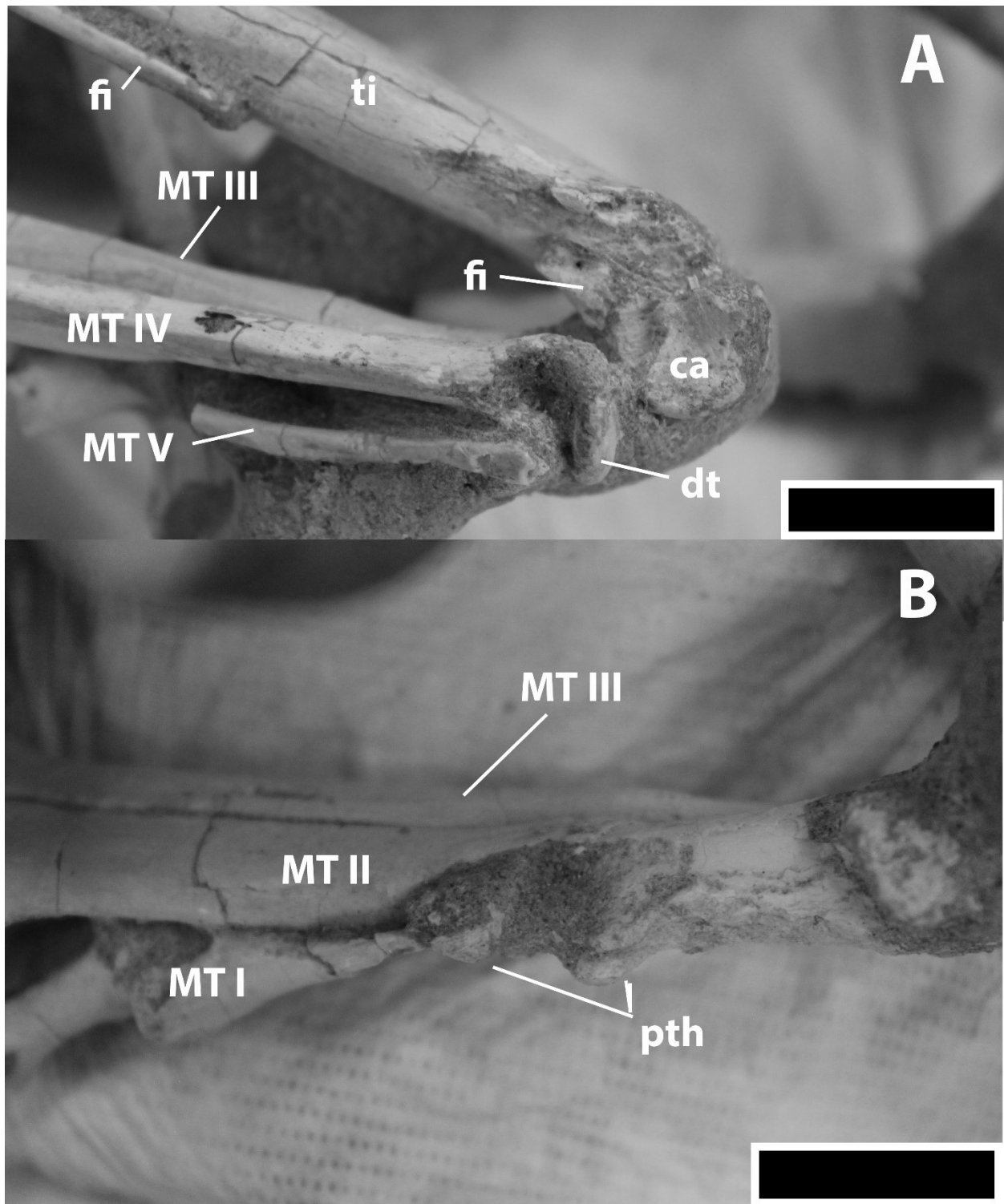


Figure 4.13. Left and right proximal metatarsus of *Velociraptor vadarostrum* n. sp. A) left metatarsus in lateral view showing ankle joint; B) right metatarsus in medial view showing

pathology of metatarsal II. Scale bars = 2 cm. Abbreviations: **ca**, calcaneum; **dt**, distal tarsal; **fi**, fibula; **MT**, metatarsal; **pth**, pathology; **ti**, tibia.

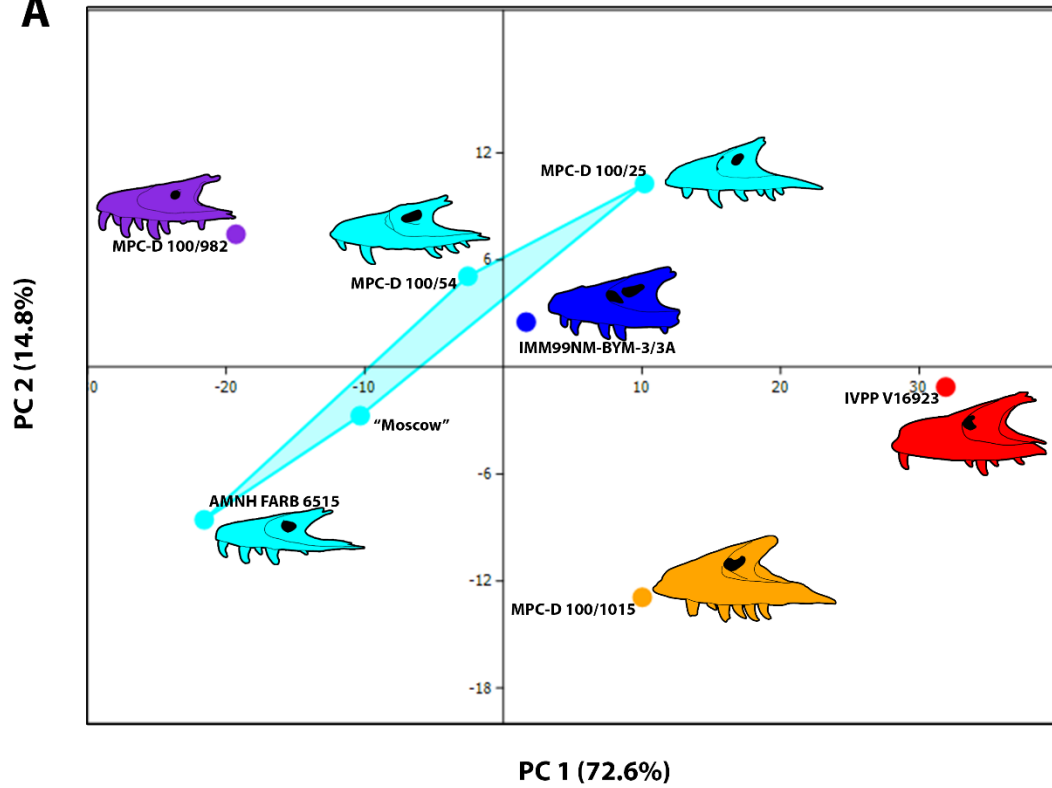
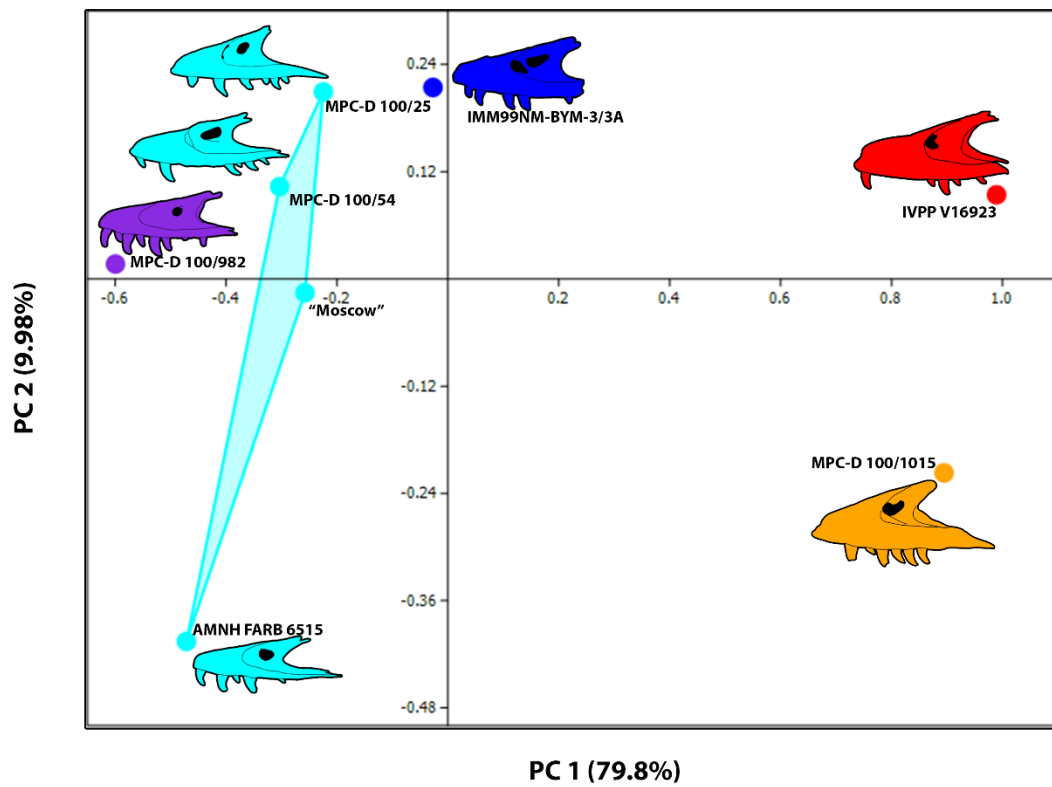
A**B**

Figure 4.14. PCA analysis of Asian eudromaeosaurians using both raw linear measurements and log transformed data. A) linear measurement PCA of *Velociraptor* specimens and close relatives. B) log transformed linear measurements PCA (-DistAntFen9Alv) of *Velociraptor* and close relatives. All illustrations were rotated to the same orientation. Purple = *V. vadarostrum* n. sp.; light blue = *V. mongoliensis*; dark blue = *V. osmolskae*; orange = *Tsaagan mangas*; red = *Linheraptor exquisitus*.

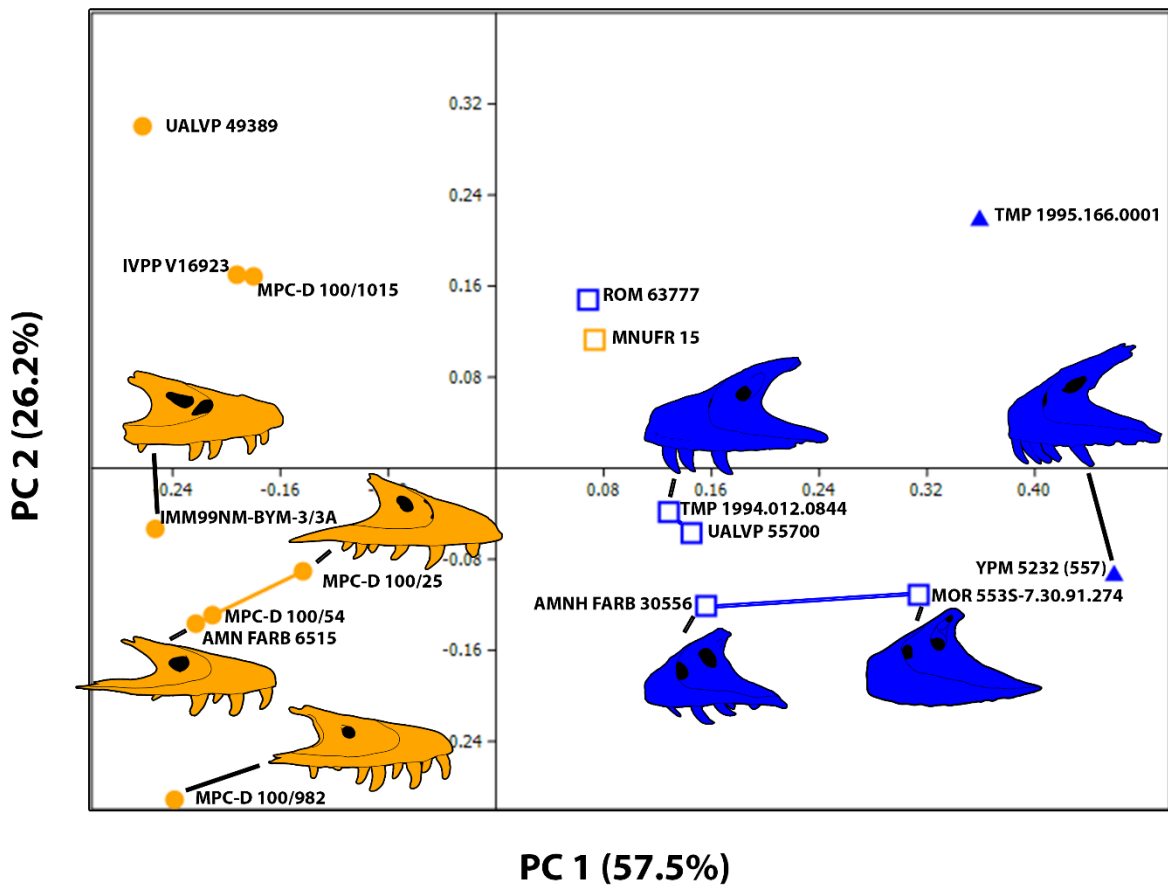


Figure 4.15. Linear measurement PCA analysis of eudromaeosaurian taxa. Measurements were divided by the length of the first nine maxillary alveoli (L9Alv). Shapes follow the clustering of taxa in Figs. 3.3 and 3.4; filled circles represent elongate specimens, filled triangles represent stout specimens, and squares are intermediates. Orange shapes represent Asian specimens whereas blue shapes represent North American taxa. Coloured lines connecting shapes indicate that the specimens they represent belong to a single taxon.

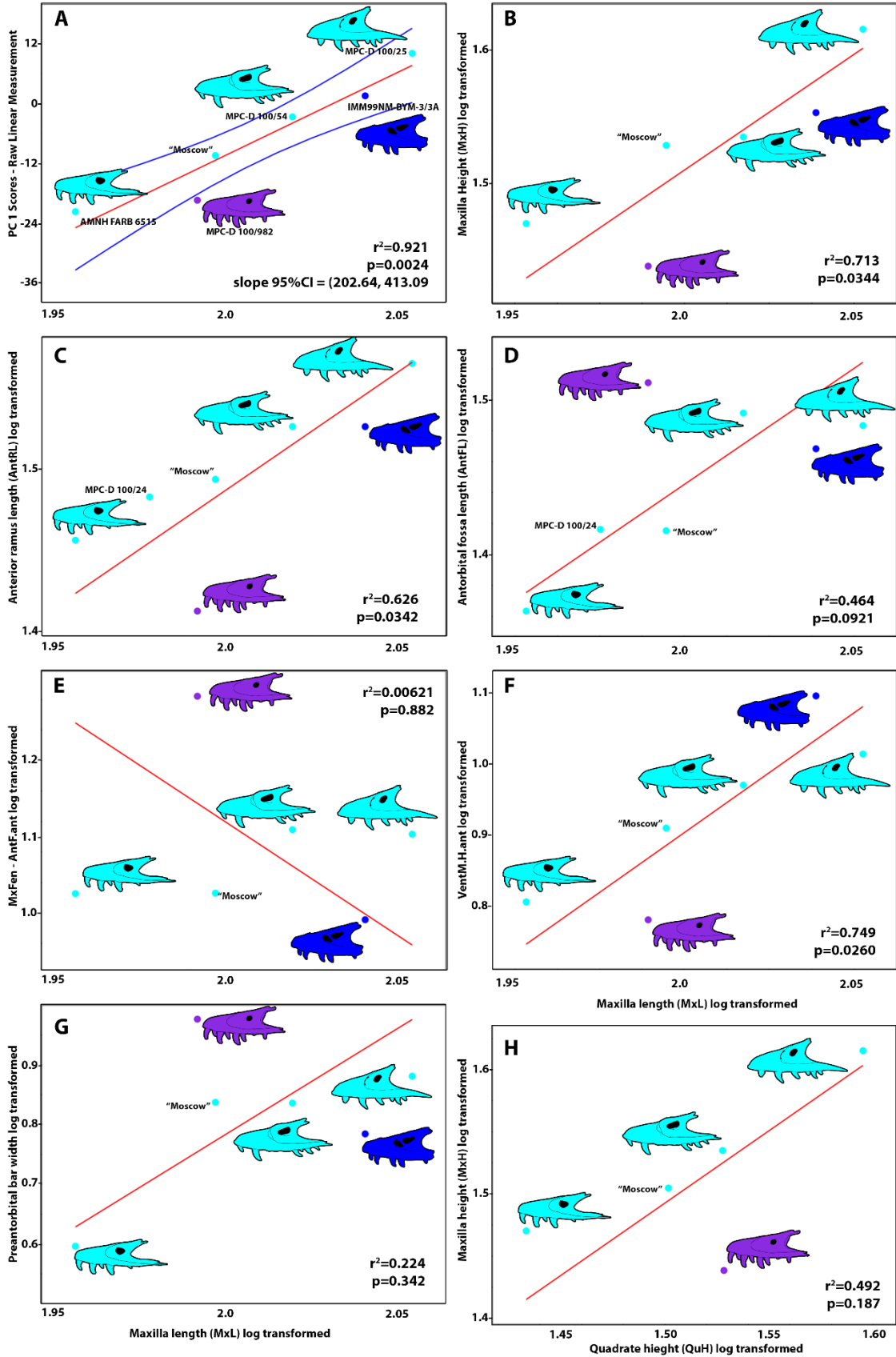
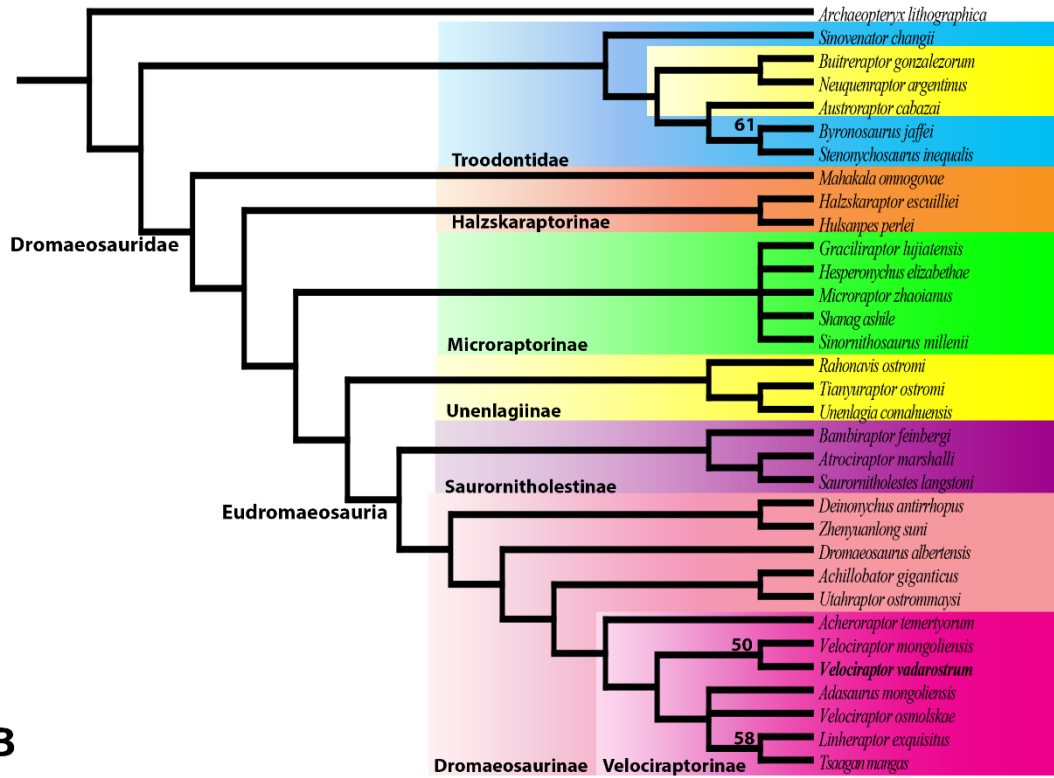


Figure 4.16. Ordinary least squares and reduced major axis regression analyses of *Velociraptor maxillae*. A) ordinary least squares analysis of PC 1 scores from Fig. 4.14A plotted against the size measurement, length (log transformed) Statistics appear in the bottom right corner. B-G) reduced major axis regression analysis of maxillae measurements which showed higher variation against length (log transformed). Measurements chosen are highlighted in Table 4.6 but excludes distance from antorbital fenestra to 9th alveolus due to its instability within *V. mongoliensis*. H) reduced major axis regression analysis of maxilla height plotted against quadrate height. All statistics for RMA analyses are plotted in the bottom right or top right of their respective plots. B-G show the statistics for all *Velociraptor* specimens whereas Table 4.6 has the stats for regressions without *V. osmolskae* and compared to those without *V. vadarostrum* n. sp. as well. All illustrations were rotated to the same orientation. Purple dot/maxilla = *V. vadarostrum* n. sp.; Light blue dots/maxillae = *V. mongoliensis*; dark blue dot/maxilla = *V. osmolskae*.

A



B

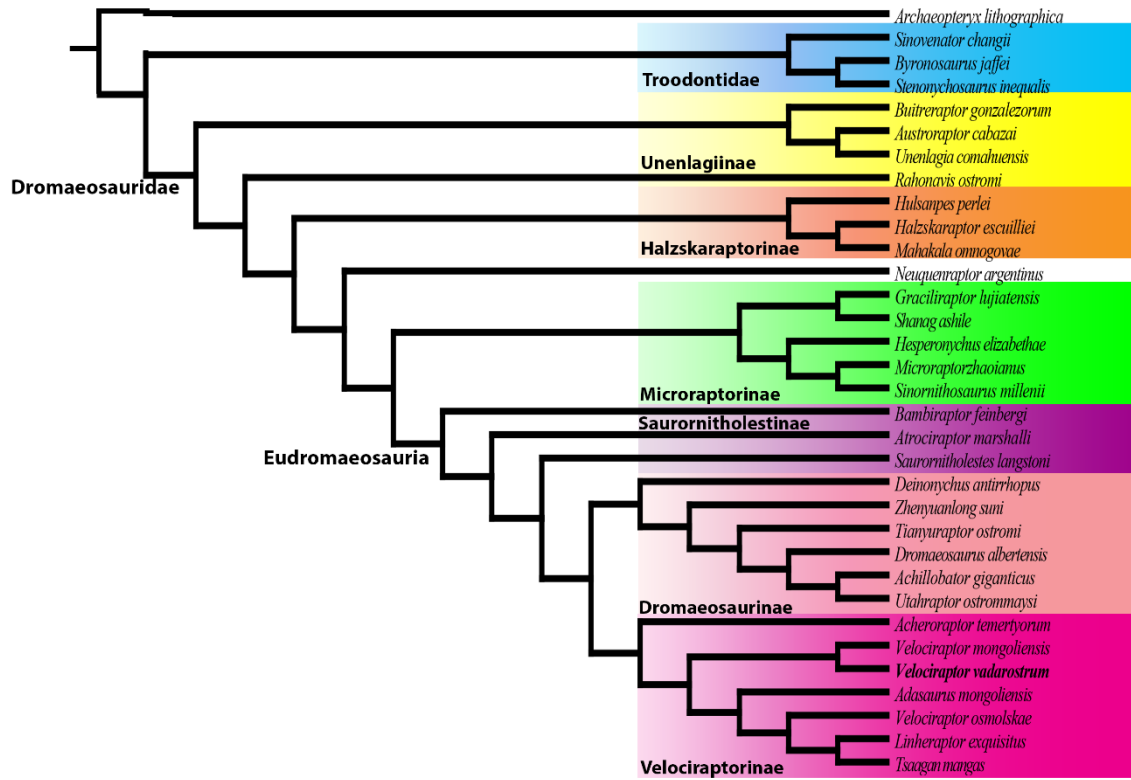


Figure 4.17. Consensus trees of parsimony and Bayesian analyses of Dromaeosauridae dataset including *Velociraptor vadarostrum* n. sp. A) 50% majority rules consensus tree generated from New Technology Search parsimony analysis. Boot strap values above 50 are reported above the nodes to which they apply. B) Bayesian inference resolved consensus tree recovered from a Mr.Bayes XSEDE analysis.

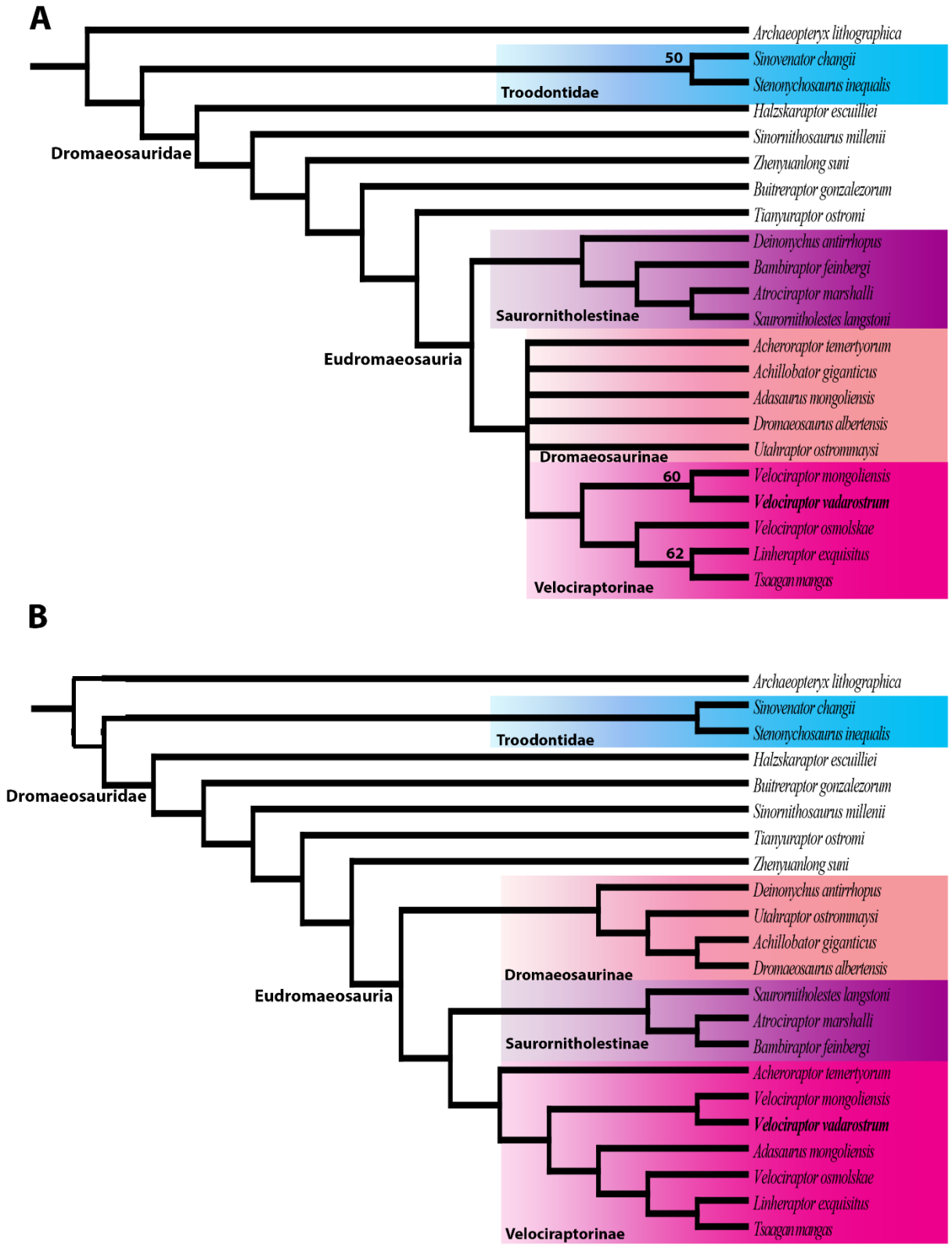


Figure 4.18. Consensus trees of parsimony and Bayesian analyses of Eudromaeosauria dataset including *Velociraptor vadarostrum* n. sp. A) 50% majority rules consensus tree generated from a New Technology Search parsimony analysis. Bootstrap values 50 or above are reported above the node to which they apply. B) Bayesian inference fully resolved consensus tree recovered from a Mr.Bayes XSEDE analysis. Character ancestral states are placed below the branch/node for which they apply.

Chapter 5. Conclusions

Examination of the maxillae of eudromaeosaurian taxa demonstrates that the element shows a great deal of variation indicative of taxonomic distinction. Defining characteristics of the maxilla show remarkable range of variation between species but remain conservative within a single species. The structure and placement of these features offers more information into the homology of this element. The sinus system along the medial surface shows large variation that can be traced with features on the lateral surface. A well developed two-chamber maxillary sinus system, dorsal to the alveoli and the palatal shelf is typical for theropod dinosaurs (Witmer 1997, Hendrickx and Mateus 2014) and is observed in non-velociraptorine eudromaeosaurians. Deviations from the normal maxillary sinus condition are observed in velociraptorine taxa such as *Tsaagan mangas* Norell et al., 2006, which possesses a single maxillary sinus chamber due to the extreme anterior placement of the maxillary fenestra. The promaxillary recess extends to the distal end of the maxilla in all eudromaeosaurians examined and mirrors the proportions of the anterior ramus. Examining the maxillary sinus chambers helps to distinguish the homology of maxillary features between species like *Acheroraptor temertyorum* Evans et al., 2013 and *Tsaagan mangas* which both have elongate anterior rami but differ markedly in the development of their maxillary sinus system.

A complex maxillary fenestra morphology is reported for members of Saurornitholestinae Longrich and Currie, 2009, and *Acheroraptor temertyorum*, which possess a maxillary fenestra with a deep pneumatic excavation posterodorsal to the fenestra proper. The position of the maxillary fenestra is also consistently close to the antorbital fenestra within these taxa whereas it has a more anterior placement within the antorbital fossa in Asian velociraptorines. A maxillary diverticulum is observed in *Acheroraptor temertyorum* extending through the ascending ramus

and opening into the pneumatic excavation of the maxillary fenestra, then continues along the dorsomedial edge of the maxilla before opening into the promaxillary recess. Whereas an extensive pneumatic system like this is not observed across members of Saurornitholestinae, a pneumatic recess is observed extending posterodorsal from the pneumatic excavation in members of this clade. The pneumatic recess in Saurornitholestines may connect with the maxillary diverticulum along the ascending ramus as in *Acheroraptor temertyorum*. However, higher resolution scans will be needed to assess this connection. The ascending ramus of velociraptorines is comparatively compact and the pneumatic systems of the maxilla is reduced in its complexity. Due to these large variations of complex structures the inclusion of *Acheroraptor temertyorum* in Velociraptorinae Barsbold, 1983, is challenged on the grounds of complex structures being more difficult to converge on than proportionate characters, the latter being more directly associated to jaw mechanics.

Velociraptor vadarostrum maintains a two-chamber maxillary sinus system but the chamber arrangement deviates from typical theropods by being well above the palatal shelf due to deeply rooted maxillary teeth. The replacement teeth originate below the palatal shelf where large interdental gaps feed into the pulp cavity of developing teeth. The preantral strut is reduced in *Velociraptor* Osborn, 1924, and may represent early onset of the chambers becoming confluent within velociraptorine eudromaeosaurians. The palatal shelf of *Velociraptor* is also sinuous in medial view which differs from all other eudromaeosaurians examined with the exception of *Achillobator giganticus* Perle et al., 1999. This structure is also observed in large theropods with powerful bites such as tyrannosaurids (Hendrickx and Mateus 2014) and coupled with large maxillary teeth may provide *Velociraptor* with greater structural integrity of the anterior jaws to handle biting and torsional loads from prey handling.

Maxillae were found to be good indicators of overall snout dimensions within Eudromaeosauria, following a correlated tight trend between the length to height ratios of the maxilla and premaxilla. Therefore, inferences on snout morphology can be ascertained to some level of confidence from just the maxilla or premaxilla. Morphometric analyses of maxillae throughout Eudromaeosauria demonstrate reliability in recovering clusters reflective of species distinction. Biogeographical and evolutionary trends toward more elongate forms in the Late Cretaceous were also observed. It reflects close phylogenetic relationships between sister taxa like *Linheraptor exquisitus* Xu et al., 2010, and *Tsaagan mangas* as well as the close relationship of *Bambiraptor feinbergi* Burnham et al., 2000 with *Saurornitholestes langstoni* Sues, 1976, which have been proposed as potential ontogenetic series. However, the synonymy of *Bambiraptor feinbergi* and *Saurornitholestes langstoni* is challenged in this thesis by observed ontogenetic trends in eudromaeosaurian taxa. *Saurornitholestes langstoni* maxillae are morphometrically similar to the juvenile *Bambiraptor feinbergi* specimen but quite disparate from the adult specimen of *B. feinbergi*. Outliers in PCA plots such as the Late Cretaceous *Atrociraptor marshalli* Currie and Varricchio, 2004, support an ecomorphological relationship for snout dimensions (van Cakenberghe et al. 2002, Slater et al. 2009, Sakamoto 2010, Whitlock 2011). Maxillary dimensions, and by extension snout dimensions, across Eudromaeosauria Longrich and Currie, 2009, split into three distinct groupings, like modern canids (Fig. 5.1). Slater et al. (2009) found a correlation between snout dimensions and preference of prey, canids with long narrow snouts preferentially going after small, fast prey whereas ones with short and wide snouts prefer large prey, and intermediate snout morphologies are associated with generalist diets. Variable large and small bodied prey items in North American ecosystems during the Late Cretaceous (Brinkman 1990, Eberth and Braman 2012, Brown et al. 2013, Eberth

et al. 2013) and the acquisition of intermediate and stout snouts in North American eudromaeosaurians (Fig. 5.1) support the comparative analog with modern canids. The harsher, more arid environment of Mongolia during the Late Cretaceous (Dashzeveg et al. 1995, 2005, Dingus et al. 2008) possessed an assemblage of small-bodied fauna and the persistence of long, narrow snouted eudromaeosaurians further supports the analog.

Within Asian velociraptorines, the most taxonomically variable feature of the maxilla was the position of the maxillary fenestra within the antorbital fossa. When a larger sample size was available, as in the case of *V. mongoliensis* Osborn, 1924, individual variation was noticeably low in maxillary dimensions. Two prominent structures of the maxilla, the anterior ramus and the antorbital fossa, were conservative, following slightly allometric and isometric trends, respectively. Intraspecific variations of the position of the maxillary fenestra within the maxilla relative to the anterior border of the antorbital fenestra seems high. However, the absolute distance between these features is stable within the species and the preantorbital bar shows a positive allometric trend. Whereas the preantorbital bar is not correlated with size in *V. mongoliensis*, there is a strong positive trend suggestive of positive allometry. Correlation of this feature may be hindered by the anterior border of the antorbital fenestra being variable in shape. The stable location of the maxillary fenestra anteriorly in the antorbital fossa is suggestive of taxonomic variation and clearly distinguishes *V. mongoliensis* from other *Velociraptor* species.

The distinction of *V. vadarostrum* from *V. mongoliensis* has been supported throughout this study as the holotype for this taxon shows distinct maxillary proportions not just from *V. mongoliensis* but from all other eudromaeosaurians. Snout dimensions in *V. vadarostrum* converge in a few ways with derived troodontids such as being extremely elongate and possessing an elongate antorbital fossa. When these features in *V. vadarostrum* were compared

with *V. mongoliensis* and *Velociraptor osmolskae* Godefroit et al., 2008, *V. vadarostrum* was a clear outlier and would often destabilize the trends observed for *V. mongoliensis*. *Velociraptor vadarostrum* is distinguished from *V. mongoliensis* by its maxillary and snout proportions, a cerebral endocast that rapidly constricts anteriorly followed by a long olfactory canal, a long humerus relative to femur size, and a vertical crest on the ilium. The variation between *V. vadarostrum* and *V. mongoliensis* could be related to niche partitioning or geographic separation with limited overlap. The extreme shallow snout of *V. vadarostrum* would be ideal for small prey acquisition whereas the snout of *V. mongoliensis* shows some shift towards a more generalist form. The location from which the holotypes for *V. mongoliensis* and *V. vadarostrum* were collected was an arid environment with seasonal fluvial influence and may have been more supportive of a range of organisms compared to peripheral environments that may have been more arid comparatively. Although it is currently not possible to know, the coexistence of two closely related *Velociraptor* species has implications for sympatric speciation and biogeography of Asian eudromaeosaurians. Coeval eudromaeosaurians is not unheard of and is already documented in the Dinosaur Park Formation of Alberta, Canada. *Dromaeosaurus albertensis* Matthew and Brown, 1922, and *Saurornitholestes langstoni* are coeval eudromaeosaurians with disparate snout dimensions and demonstrate that this relationship is possible. Like the relationship between *V. mongoliensis* and *V. vadarostrum*, the more generalist species – *Saurornitholestes langstoni* and *V. mongoliensis* – are more common than the more specialized species *Dromaeosaurus albertensis* (stout snouted) and *V. vadarostrum* (extreme elongation). In the case of the latter two taxa, their preservation in these environments may be rare due to it not being their home ranges and they were at the edges of their territories.

Overall, the maxilla is useful for phylogenetic and ecological inference within Eudromaeosauria due to the high level of variation. This element is complex not only within Eudromaeosauria, but across a broad range of vertebrates and the results here have implications for assessments of maxillary morphology regarding evolution and ecology across numerous groups. It is important to keep revisiting assessments with the addition of more data and to keep perspective on the scope of the inferences. This is especially important for discretization of continuous data such as ratio-based characteristics. The range of the data should always be examined before proposing thresholds for character state delineations and if no distinct groups exist, the data should be left as continuous. Ratio-based characters can be attractive but also misleading as relative proportions can be highly variable within a species and show extensive overlap between species. Homologous structures that are not described on the bases of proportionate measurements will be more reliable and provide a clearer comparison of evolutionary change through time.

Phylogenetic hypothesis of dromaeosaurid evolution have been constructed largely on a comparative framework around snout elongation over the past 20 years following the description of the skull of *Velociraptor mongoliensis* (Barsbold and Osmólska, 1999). The hypothesis built from this description and subsequent discoveries of new Asian taxa with elongate snouts is one in which elongate snouts of eudromaeosaurians originated in Asia. Description of the North American taxon *Acheroraptor temertyorum*, a eudromaeosaurian with an elongate anterior ramus, has been interpreted as supporting a dispersal of Asian eudromaeosaurians into North America during the latest Cretaceous. It has been shown in this thesis that the anterior ramus elongation is distinct from maxillary elongation (Fig. 2.17) and therefore snout elongation (Fig. 3.2). *Acheroraptor temertyorum* has an elongate anterior ramus but intermediate maxillary

dimensions more like saurornitholestines such as *Bambiraptor feinbergi* and *Saurornitholestes langstoni* (Fig. 5.1). The proportion of maxillary length made up by the anterior ramus in *Acheroraptor temertyorum* is like the stout snouted saurornitholestine, *Atrociraptor marshalli*. Maxillae, and by extension snouts, of eudromaeosaurian taxa fall into three distinct classes of maxillary dimensions like modern canids. The trends of snout dimensions in canids are largely ecomorphological, changing in proportions relating to prey acquisition (Slater et al. 2009). When snout dimensions of eudromaeosaurians are mapped onto a phylogeny, it is observed that they do not define any sub-clades. Sister relationships exist between taxa with distinctly different snout morphologies like between *Atrociraptor marshalli* and *Saurornitholestes langstoni* possessing a stout snout and intermediate snout morphology, respectively. The position of *Acheroraptor temertyorum* between Asian velociraptorines and Saurornitholestinae demonstrates the challenges of using snout dimensions for phylogenetic inference. Eudromaeosaurians were active predators of the Cretaceous living under the shadows of giants. To support the behemoths they lived with, ecosystems had to be abundant in diverse flora and fauna. Although tyrannosaurids dominated the large bodied predator role, there would have been an excess of resources for smaller bodied predators like eudromaeosaurians. This allowed them to capitalize on the small predator niche, experiment with specialization and utilize more restrictive environments that could not support large-bodied predators like tyrannosaurids.

The next steps that need to be done to follow up on this thesis would be to examine proportional characters throughout the dataset for disjunct separations in the continuous data, and allometry. Revising the character-taxon matrix via removing or modifying problematic characters could greatly change the current prevailing hypotheses on the evolution of Eudromaeosauria and Dromaeosauridae. Phylogenetic analysis is the test of congruence with the

intent of discovering synapomorphy from homologous structures (Patterson 1982). Homoplastic characters in the dataset should be examined then revised or removed depending on the level of problems they possess. Ecomorphological features that may be homoplastic throughout the taxa in the dataset should be identified and mapped on tree topologies to trace their history after the phylogenetic analysis rather than included within. Studying the functional relationship of various morphologies within dromaeosaurids would provide useful insights into evolutionary drivers.

The snout dimensions of eudromaeosaurian taxa do fall into three categories like modern canids but it would be useful to examine the skull morphologies through use of models just as Slater et al. (2009) did with canids. If canids really do represent a good analog for dromaeosaurids regarding snout dimensions, it would be expected that FEA models would corroborate each other as well. The raptorial claw in dromaeosaurids is another morphology worth looking into. This feature has been proposed by some authors to be the primary weapon of these animals, the muzzle being the secondary weapon. The results of this thesis would argue the opposite as the dimensions of snouts of eudromaeosaurians show similar disjunct separations as in modern canids, which do not have raptorial claws and rely almost exclusively on their snouts for handling prey. The raptorial claw of dromaeosaurids may have allowed them to acquire larger prey than would have been the norm in extreme situations such as with the ‘fighting dinosaurs’ specimen (Barsbold 2016). Or it may have provided a useful tool to hold or tear at incapacitated prey (Manning et al. 2009, Fowler et al. 2011). Morphometric analysis presented in this thesis and in other studies has offered a useful way to examine both taxonomic and functional morphologies. Carrying this research forward, I would examine a broader suite of skeletal elements in the same way. Elements such as the raptorial claw would be informative for function, whereas cranial elements such as the frontal would be interesting to look at given the

diagnostic potential of this element in other clades. FEA of snout morphologies would help to test the hypothesis of canids as ecological analogs to eudromaeosaurians presented in this thesis. This thesis and the research that follows offer great opportunities to parse out ecomorphological features from conservative homologous structures, which can be used to better inform on analyses in other clades. It exemplifies the importance of ecological factors in driving evolutionary trends and demonstrates the morphological disparity that can result from ecological drivers.

5.1 Literature Cited

- Barsbold, R. 1983. Carnivorous dinosaurs from the Cretaceous of Mongolia. The Joint Soviet-Mongolian Palaeontological Expedition, **19**: 117.
- Barsbold, R. 2016. “The Fighting Dinosaurs”: The position of their bodies before and after death. *Paleontological Journal*, **50**: 1412–1417. doi:10.1134/S0031030116120042.
- Barsbold, R., and Osmólska, H. 1999. The skull of *Velociraptor* (Theropoda) from the Late Cretaceous of Mongolia. *Acta Palaeontologica Polonica*, **44**: 189–219.
- Brinkman, D.B. 1990. Paleocology of the Judith River Formation (Campanian) of Dinosaur Provincial Park, Alberta, Canada: Evidence from vertebrate microfossil localities. *Palaeogeography, Palaeoclimatology, Palaeoecology*,: 18.
- Brown, C.M., Evans, D.C., Campione, N.E., O’Brien, L.J., and Eberth, D.A. 2013. Evidence for taphonomic size bias in the Dinosaur Park Formation (Campanian, Alberta), a model Mesozoic terrestrial alluvial-paralic system. *Palaeogeography, Palaeoclimatology, Palaeoecology*, **372**: 108–122. Elsevier B.V. doi:10.1016/j.palaeo.2012.06.027.
- Burnham, D.A., Derstler, K.L., Currie, P.J., Bakker, R.T., Zhou, Z., and Ostrom, J.H. 2000. Remarkable new birdlike dinosaur (Theropoda: Maniraptora) from the Upper Cretaceous of Montana. *The University of Kansas Paleontological Contributions*, **13**: 14.
- van Cakenberghe, V., Herrel, A., and Aguirre, L.F. 2002. Evolutionary relationships between cranial shape and diet in bats (Mammalia : Chiroptera). *In* *Topics in Functional and Ecological Vertebrate Morphology*. Edited by P. Aerts, K. D’Aour, A. Herrel, and R. Van Damme. Staker Publishing. pp. 205–236.
- Currie, P., and Varricchio, D.J. 2004. A new dromaeosaurid from the Horseshoe Canyon

- Formation (Upper Cretaceous) of Alberta, Canada. *In Feathered Dragons. Edited by P.J. Currie, E.B. Koppelhus, M.A. Shugar, and J.L. Wright.* Indiana University Press, Bloomington and Indianapolis. pp. 112–132.
- Dashzeveg, D., Dingus, L., Loope, D.B., Swisher, C.C., Dulam, T., and Sweeney, M.R. 2005. New stratigraphic subdivision, depositional environment, and age estimate for the Upper Cretaceous Djadokhta Formation, southern Ulan Nur Basin, Mongolia. *American Museum Novitates*, **3498**: 31. doi:10.1206/0003-0082(2005)498[0001:nssdea]2.0.co;2.
- Dashzeveg, D., Novacek, M.J., Norell, M.A., Clark, J.M., Chiappe, L.M., Davidson, A., McKenna, M.C., Dingus, L., Swisher, C.C., and Altangerel, P. 1995. Extraordinary preservation in a new vertebrate assemblage from the Late Cretaceous of Mongolia. *Nature*, **374**: 446–449.
- Dingus, L., Loope, D.B., Dashzeveg, D., Swisher, C.C., Minjin, C., Novacek, M.J., and Norell, M.A. 2008. The geology of Ukhaa Tolgod (Djadokhta Formation, Upper Cretaceous, Nemegt Basin, Mongolia). *American Museum Novitates*, **3616**: 1. doi:10.1206/442.1.
- Eberth, D.A., and Braman, D.R. 2012. A revised stratigraphy and depositional history for the Horseshoe Canyon Formation (Upper Cretaceous), southern Alberta plains. *Canadian Journal of Earth Sciences*, **49**: 1053–1086. doi:10.1139/E2012-035.
- Eberth, D.A., Evans, D.C., Brinkman, D.B., Therrien, F., Tanke, D.H., and Russell, L.S. 2013. Dinosaur biostratigraphy of the Edmonton group (Upper Cretaceous), Alberta, Canada: Evidence for climate influence. *Canadian Journal of Earth Sciences*, **50**: 701–726. doi:10.1139/cjes-2012-0185.
- Evans, D.C., Larson, D.W., and Currie, P.J. 2013. A new dromaeosaurid (Dinosauria:

- Theropoda) with Asian affinities from the latest Cretaceous of North America. *Naturwissenschaften*, **100**: 1041–1049. doi:10.1007/s00114-013-1107-5.
- Fowler, D.W., Freedman, E.A., Scannella, J.B., and Kambic, R.E. 2011. The predatory ecology of *Deinonychus* and the origin of flapping in birds. *PLoS ONE*, **6**. doi:10.1371/journal.pone.0028964.
- Godefroit, P., Currie, P.J., Hong, L., Shang, C.Y., and Dong, Z.M. 2008. A new species of *Velociraptor* (Dinosauria: Dromaeosauridae) from the Upper Cretaceous of northern China. *Journal of Vertebrate Paleontology*, **28**: 432–438. doi:10.1671/0272-4634(2008)28[432:ANSOVD]2.0.CO;2.
- Hendrickx, C., and Mateus, O. 2014. *Torvosaurus gurneyi* n. sp., the largest terrestrial predator from Europe, and a proposed terminology of the maxilla anatomy in nonavian theropods. *PLoS ONE*, **9**. doi:10.1371/journal.pone.0088905.
- Longrich, N.R., and Currie, P.J. 2009. A microraptorine (Dinosauria-Dromaeosauridae) from the Late Cretaceous of North America. *Proceedings of the National Academy of Sciences of the United States of America*, **106**: 5002–5007. doi:10.1073/pnas.0811664106.
- Manning, P.L., Margetts, L., Johnson, M.R., Withers, P.J., Sellers, W.I., Falkingham, P.L., Mummery, P.M., Barrett, P.M., and Raymont, D.R. 2009. Biomechanics of dromaeosaurid dinosaur claws: Application of X-ray microtomography, nanoindentation, and finite element analysis. *Anatomical Record*, **292**: 1397–1405. doi:10.1002/ar.20986.
- Matthew, W.D., and Brown, B. 1922. The family Deinodontidae, with notice of a new genus from the Cretaceous of Alberta. *Bulletin of the American Museum of Natural History*, **46**: 367–385.

- Norell, M.A., Clark, J.M., Turner, A.H., Makovicky, P.J., Barsbold, R., and Rowe, T. 2006. A new dromaeosaurid theropod from Ukhaa Tolgod (Ömnögov, Mongolia). *American Museum Novitates*, **3545**: 51. doi:10.1206/0003-0082(2006)3545[1:andtfu]2.0.co;2.
- Osborn, H.F. 1924. Three new Theropoda, *Protoceratops* Zone, central Mongolia. *American Museum Novitates*,: 1–12.
- Patterson, C. 1982. Morphological characters and homology. *In* Problems of Phylogenetic Reconstruction. *Edited by* K.A. Joysey and A.E. Friday. Academic Press, London and New York. pp. 21–74.
- Perle, A., Norell, M.A., and Clark, J.M. 1999. A new maniraptoran theropod - *Achillobator giganticus* (Dromaeosauridae)- from the Upper Cretaceous of Burkhan, Mongolia. National University of Mongolia,: 102.
- Sakamoto, M. 2010. Jaw biomechanics and the evolution of biting performance in theropod dinosaurs. *Proceedings of the Royal Society B: Biological Sciences*, **277**: 3327–3333. doi:10.1098/rspb.2010.0794.
- Slater, G.J., Dumont, E.R., and Van Valkenburgh, B. 2009. Implications of predatory specialization for cranial form and function in canids. *Journal of Zoology*, **278**: 181–188. doi:10.1111/j.1469-7998.2009.00567.x.
- Sues, H.-D. 1976. A new small theropod dinosaur from the Judith River Formation (Campanian) of Alberta. *Zoological Journal of the Linnean Society*, **62**: 381–400.
- Whitlock, J.A. 2011. Inferences of diplodocoid (Sauropoda: Dinosauria) feeding behavior from snout shape and microwear analyses. *PLoS ONE*, **6**. doi:10.1371/journal.pone.0018304.

Witmer, L.M. 1997. The evolution of the antorbital cavity of archosaurs: A study in soft-tissue reconstruction in the fossil record with an analysis of the function of Pneumaticity. *Journal of Vertebrate Paleontology*, **17**: 1–76. doi:10.1080/02724634.1997.10011027.

Xu, X., Choiniere, J.N., Pittman, M., Tan, Q., Xiao, D., Li, Z., Tan, L., Clark, J.M., Norell, M.A., Hone, D.W.E., and Sullivan, C. 2010a. A new dromaeosaurid (Dinosauria: Theropoda) from the Upper Cretaceous Wulansuhai Formation of Inner Mongolia, China. *Zootaxa*, **9**: 1–9.

5.2 Figures

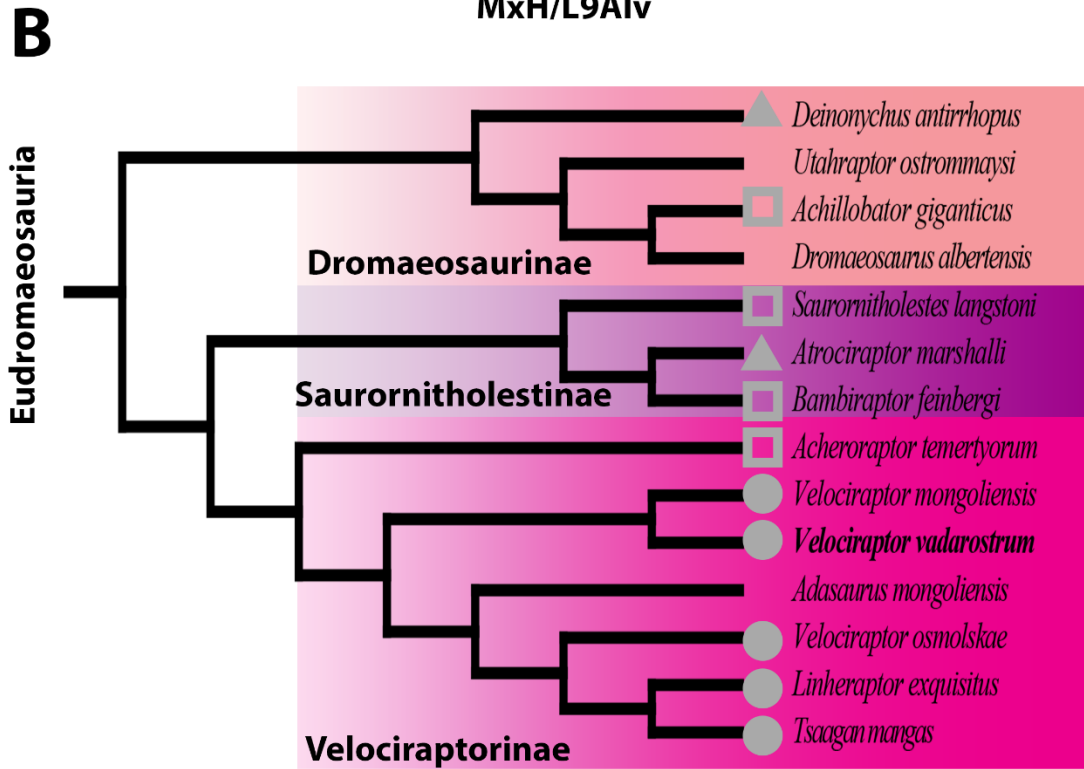
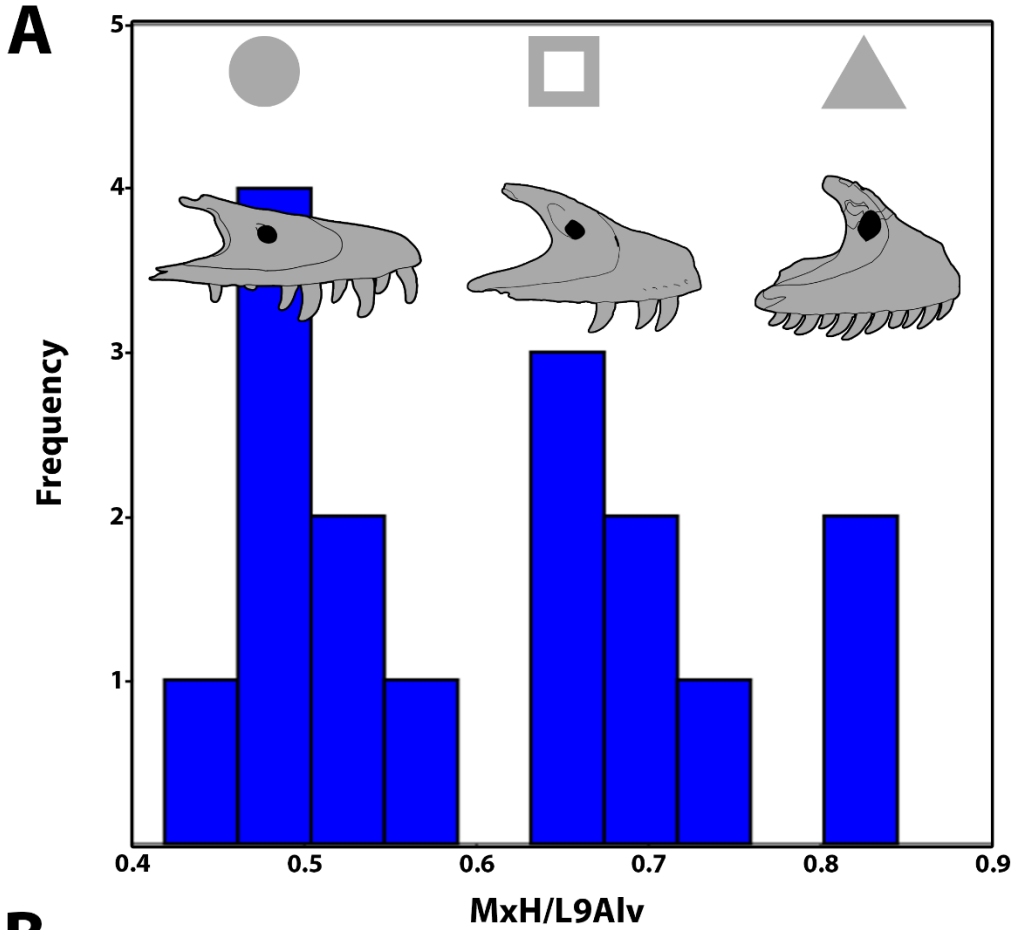


Figure 5.1. Eudromaeosauria snout dimensions mapped onto Bayesian phylogeny. A) histogram showing three classes of eudromaeosaurian maxillary dimensions with grey silhouettes of representatives of their respective classes (least stout=filled grey circle; intermediate=grey square; most stout=filled grey triangle). Shapes were adapted from Slater et al. (2009) following the hypothetical ecomorphological analog between canids and eudromaeosaurians. B) Bayesian phylogeny of Eudromaeosauria (=allcompat) with snout dimensions mapped onto taxa by corresponding shapes.

References

- Arbour, V.M., and Currie, P.J. 2012. Analyzing taphonomic deformation of ankylosaur skulls using retrodeformation and finite element analysis. *PLoS ONE*, **7**: 1–13. doi:10.1371/journal.pone.0039323.
- Baert, M., Burns, M.E., and Currie, P.J. 2014. Quantitative diagenetic analyses of *Edmontosaurus regalis* (Dinosauria: Hadrosauridae) postcranial elements from the Danek Bonebed, Upper Cretaceous Horseshoe Canyon Formation, Edmonton, Alberta, Canada: Implications for allometric studies of fossil. *Canadian Journal of Earth Sciences*, **51**: 1007–1016. doi:10.1139/cjes-2014-0060.
- Barsbold, R. 1974. Saurornithoididae, a new family of small theropod dinosaurs from Central Asia and North America. *Palaeontologia Polonica*, **30**: 5–52.
- Barsbold, R. 1983. Carnivorous dinosaurs from the Cretaceous of Mongolia. *The Joint Soviet-Mongolian Palaeontological Expedition*, **19**: 117.
- Barsbold, R. 2016. “The Fighting Dinosaurs”: The position of their bodies before and after death. *Paleontological Journal*, **50**: 1412–1417. doi:10.1134/S0031030116120042.
- Barsbold, R., and Osmólska, H. 1999. The skull of *Velociraptor* (Theropoda) from the Late Cretaceous of Mongolia. *Acta Palaeontologica Polonica*, **44**: 189–219.
- Barta, D.E., Nesbitt, S.J., and Norell, M.A. 2018. The evolution of the manus of early theropod dinosaurs is characterized by high inter- and intraspecific variation. *Journal of Anatomy*, **232**: 80–104. doi:10.1111/joa.12719.
- Biknevicius, A.R., and Ruff, C.B. 1992. The structure of the mandibular corpus and its relationship to feeding behaviours in extant carnivorans. *Journal of Zoology*, **228**: 479–507.

doi:10.1111/j.1469-7998.1992.tb04450.x.

- Bonaparte, J. 1999. Tetrapod faunas from South America and India: A palaeobiogeographic interpretation. *PINSA*, **65**: 427–437.
- Boyd, A.A., and Motani, R. 2008. Three-dimensional re-evaluation of the deformation removal technique based on “jigsaw puzzling.” *Palaeontologia Electronica*, **11**.
- Brinkman, D.B. 1990. Paleocology of the Judith River Formation (Campanian) of Dinosaur Provincial Park, Alberta, Canada: Evidence from vertebrate microfossil localities. *Palaeogeography, Palaeoclimatology, Palaeoecology*,: 18.
- Brown, C.M., Evans, D.C., Campione, N.E., O’Brien, L.J., and Eberth, D.A. 2013. Evidence for taphonomic size bias in the Dinosaur Park Formation (Campanian, Alberta), a model Mesozoic terrestrial alluvial-paralic system. *Palaeogeography, Palaeoclimatology, Palaeoecology*, **372**: 108–122. Elsevier B.V. doi:10.1016/j.palaeo.2012.06.027.
- Brusatte, S.L., Averianov, A., Sues, H.-D., Muir, A., and Butler, I.B. 2016. New tyrannosaur from the mid-Cretaceous of Uzbekistan clarifies evolution of giant body sizes and advanced senses in tyrant dinosaurs. *Proceedings of the National Academy of Sciences*,: 201600140. doi:10.1073/pnas.1600140113.
- Brusatte, S.L., and Carr, T.D. 2016. The phylogeny and evolutionary history of tyrannosaurid dinosaurs. *Scientific Reports*, **6**: 1–8. Nature Publishing Group. doi:10.1038/srep20252.
- Brusatte, S.L., Norell, M. a, Carr, T.D., Erickson, G.M., Hutchinson, J.R., Balanoff, A.M., Bever, G.S., Choiniere, J.N., Makovicky, P.J., and Xu, X. 2010. Tyrannosaur paleobiology: new research on ancient exemplar organisms. *Science*, **329**: 1481–1485.

doi:10.1126/science.1193304.

- Bull, A.J.J., Huelsenbeck, J.P., Cunningham, C.W., Swofford, D.L., and Waddell, P.J. 1993. Partitioning and combining data in phylogenetic analysis. *Society of Systematic Biologists*, **42**: 384–397.
- Burnham, D.A., Derstler, K.L., Currie, P.J., Bakker, R.T., Zhou, Z., and Ostrom, J.H. 2000. Remarkable new birdlike dinosaur (Theropoda: Maniraptora) from the Upper Cretaceous of Montana. *The University of Kansas Paleontological Contributions*, **13**: 14.
- Butler, M.A., and Losos, J.B. 2002. Multivariate sexual dimorphism, sexual selection, and adaptation in greater antillean anolis lizards. *Ecological Monographs*, **72**: 541–559. doi:10.1890/0012-9615(2002)072[0541:MSDSSA]2.0.CO;2.
- van Cakenberghe, V., Herrel, A., and Aguirre, L.F. 2002. Evolutionary relationships between cranial shape and diet in bats (Mammalia : Chiroptera). *In Topics in Functional and Ecological Vertebrate Morphology. Edited by P. Aerts, K. D'Aour, A. Herrel, and R. Van Damme. Staker Publishing. pp. 205–236.*
- Caldwell, M.W. 2012. A challenge to categories: “What, if anything, is a mosasaur?” *Bulletin de la Société Géologique de France*, **183**: 7–34. doi:10.2113/gssgfbull.183.1.7.
- Carr, T.D., Varricchio, D.J., Sedlmayr, J.C., Roberts, E.M., and Moore, J.R. 2017. A new tyrannosaur with evidence for anagenesis and crocodile-like facial sensory system. *Scientific Reports*, **7**: 1–11. doi:10.1038/srep44942.
- Carrano, M.T., and Hutchinson, J.R. 2002. Pelvic and hindlimb musculature of *Tyrannosaurus rex* (Dinosauria: Theropoda). *Journal of Morphology*, **253**: 207–228.

doi:10.1002/jmor.10018.

Carrano, M.T., Janis, C.M., and Sepkoski, J.J. 1999. Hadrosaurs as ungulate parallels: Lost lifestyles and deficient data. *Acta Palaeontologica Polonica*, **44**: 237–261.

Cau, A., Beyrand, V., Voeten, D.F.A.E., Fernandez, V., Tafforeau, P., Stein, K., Barsbold, R., Tsogtbaatar, K., Currie, P.J., and Godefroit, P. 2017. Synchrotron scanning reveals amphibious ecomorphology in a new clade of bird-like dinosaurs. *Nature*, **552**: 395–399. Nature Publishing Group. doi:10.1038/nature24679.

Chen, J., Leblanc, A.R.H., Jin, L., Huang, T., and Reisz, R.R. 2018. Tooth development, histology, and enamel microstructure in *Changchunsaurus parvus*: Implications for dental evolution in ornithomimid dinosaurs. *PLoS ONE*, **13**: 1–18. doi:10.1371/journal.pone.0205206.

Crichton, M. 1991. *Jurassic Park*. In 25th Anniv. Ballantine Books, New York.

Currie, P., and Varricchio, D.J. 2004. A new dromaeosaurid from the Horseshoe Canyon Formation (Upper Cretaceous) of Alberta, Canada. In *Feathered Dragons*. Edited by P.J. Currie, E.B. Koppelhus, M.A. Shugar, and J.L. Wright. Indiana University Press, Bloomington and Indianapolis. pp. 112–132.

Currie, P.J. 1985. Cranial anatomy of *Stenonychosaurus inequalis* (Saurischia, Theropoda) and its bearing on the origin of birds. *Canadian Journal of Earth Sciences*, **22**: 1643–1658. doi:10.1139/e85-173.

Currie, P.J. 1995. New information on the anatomy and relationships of *Dromaeosaurus albertensis* (Dinosauria: Theropoda). *Journal of Vertebrate Paleontology*, **15**: 576–591.

doi:10.1080/02724634.1995.10011250.

Currie, P.J. 2003a. Cranial anatomy of tyrannosaurid dinosaurs from the Late Cretaceous of Alberta, Canada. *Acta Palaeontologica Polonica*, **48**: 191–226.

Currie, P.J. 2003b. Allometric growth in tyrannosaurids (Dinosauria: Theropoda) from the Upper Cretaceous of North America and Asia. *Canadian Journal of Earth Sciences*, **40**: 651–665.
doi:10.1139/e02-083.

Currie, P.J., and Eberth, D.A. 2010. On gregarious behavior in *Albertosaurus*. *Canadian Journal of Earth Sciences*, **47**: 1277–1289. doi:10.1139/E10-072.

Currie, P.J., and Evans, D.C. 2019. Cranial anatomy of new specimens of *Saurornitholestes langstoni* (Dinosauria , Theropoda , Dromaeosauridae) from the Dinosaur Park Formation (Campanian) of Alberta. *The Anatomical Record*, **04715**: 1–25. doi:10.1002/ar.24241.

Currie, P.J., and Jacobsen, A.R. 1995. An azhdarchid pterosaur eaten by a velociraptorine theropod. *Canadian Journal of Earth Sciences*, **32**: 922–925. doi:10.1139/e95-077.

D'Amore, D.C. 2009. A functional explanation for denticulation in theropod dinosaur teeth. *Anatomical Record*, **292**: 1297–1314. doi:10.1002/ar.20977.

Dashzeveg, D., Dingus, L., Loope, D.B., Swisher, C.C., Dulam, T., and Sweeney, M.R. 2005. New stratigraphic subdivision, depositional environment, and age estimate for the Upper Cretaceous Djadokhta Formation, southern Ulan Nur Basin, Mongolia. *American Museum Novitates*, **3498**: 31. doi:10.1206/0003-0082(2005)498[0001:nssdea]2.0.co;2.

Dashzeveg, D., Novacek, M.J., Norell, M.A., Clark, J.M., Chiappe, L.M., Davidson, A., McKenna, M.C., Dingus, L., Swisher, C.C., and Altangerel, P. 1995. Extraordinary

- preservation in a new vertebrate assemblage from the Late Cretaceous of Mongolia. *Nature*, **374**: 446–449.
- Dingus, L., Loope, D.B., Dashzeveg, D., Swisher, C.C., Minjin, C., Novacek, M.J., and Norell, M.A. 2008. The geology of Ukhaa Tolgod (Djadokhta Formation, Upper Cretaceous, Nemegt Basin, Mongolia). *American Museum Novitates*, **3616**: 1. doi:10.1206/442.1.
- Eberth, D.A., and Braman, D.R. 2012. A revised stratigraphy and depositional history for the Horseshoe Canyon Formation (Upper Cretaceous), southern Alberta plains. *Canadian Journal of Earth Sciences*, **49**: 1053–1086. doi:10.1139/E2012-035.
- Eberth, D.A., and Brinkman, D.B. 1997. Paleocology of an estuarine, incised-valley fill in the Dinosaur Park Formation (Judith River Group, Upper Cretaceous) of southern Alberta, Canada. *Palaios*, **12**: 43. doi:10.2307/3515293.
- Eberth, D.A., Evans, D.C., Brinkman, D.B., Therrien, F., Tanke, D.H., and Russell, L.S. 2013. Dinosaur biostratigraphy of the Edmonton group (Upper Cretaceous), Alberta, Canada: Evidence for climate influence. *Canadian Journal of Earth Sciences*, **50**: 701–726. doi:10.1139/cjes-2012-0185.
- Edmund, G. 1960. Tooth replacement phenomena in the lower vertebrates. *Royal Ontario Museum, Life Sciences Division, Contributions*, **52**: 1–190.
- Elzanowski, A., and Wellnhofer, P. 1996. Cranial morphology of *Archaeopteryx*: Evidence from the seventh skeleton. *Journal of Vertebrate Paleontology*, **16**: 81–94. doi:10.1080/02724634.1996.10011286.
- Erickson, G.M. 1996. Incremental lines of von Ebner in dinosaurs and the assessment of tooth

- replacement rates using growth line counts. *Proceedings of the National Academy of Sciences of the United States of America*, **93**: 14623–14627. doi:10.1073/pnas.93.25.14623.
- Erickson, G.M., Rauhut, O.W.M., Zhou, Z., Turner, A.H., Inouye, B.D., Hu, D., and Norell, M.A. 2009. Was dinosaurian physiology inherited by birds? Reconciling slow growth in *Archaeopteryx*. *PLoS ONE*, **4**. doi:10.1371/journal.pone.0007390.
- Evans, D.C. 2010. Cranial anatomy and systematics of *Hypacrosaurus altispinus*, and a comparative analysis of skull growth in lambeosaurine hadrosaurids (Dinosauria: Ornithischia). *Zoological Journal of the Linnean Society*, **159**: 398–434. doi:10.1111/j.1096-3642.2009.00611.x.
- Evans, D.C., Cullen, T.M., Larson, D.W., and Rego, A. 2017. A new species of troodontid theropod (Dinosauria: Maniraptora) from the Horseshoe Canyon Formation (Maastrichtian) of Alberta, Canada. *Canadian Journal of Earth Sciences*, **54**: 813–826. doi:10.1139/cjes-2017-0034.
- Evans, D.C., Larson, D.W., and Currie, P.J. 2013. A new dromaeosaurid (Dinosauria: Theropoda) with Asian affinities from the latest Cretaceous of North America. *Naturwissenschaften*, **100**: 1041–1049. doi:10.1007/s00114-013-1107-5.
- Farlow, J.O., Gatesy, S.M., Holtz, T.R., Hutchinson, J.R., and Röbinson, J.M. 2000. Theropod locomotion. *American Zoologist*, **40**: 640–663. doi:10.1093/icb/40.4.640.
- Ferreira-Cardoso, S., Billet, G., Gaubert, P., Delsuc, F., and Hautier, L. 2019. Skull shape variation in extant pangolins (Pholidota: Manidae): Allometric patterns and systematic implications. *Zoological Journal of the Linnean Society*,: 255–275. doi:10.1093/zoolinnean/zlz096.

- Fong, R.K.M., LeBlanc, A.R.H., Berman, D.S., and Reisz, R.R. 2016. Dental histology of *Coelophysis bauri* and the evolution of tooth attachment tissues in early dinosaurs. *Journal of morphology*, **277**: 916–924. doi:10.1002/jmor.20545.
- Forster, C.A., Sampson, S.D., Chiappe, L.M., and Krause, D.W. 1998. The theropod ancestry of birds: New evidence from the Late Cretaceous of Madagascar. *Science*, **279**: 1915–1919. doi:10.1126/science.279.5358.1915.
- Fowler, D.W., Freedman, E.A., Scannella, J.B., and Kambic, R.E. 2011. The predatory ecology of *Deinonychus* and the origin of flapping in birds. *PLoS ONE*, **6**. doi:10.1371/journal.pone.0028964.
- Frederickson, J.A., Engel, M.H., and Cifelli, R.L. 2020. Ontogenetic dietary shifts in *Deinonychus antirrhopus* (Theropoda ; Dromaeosauridae): Insights into the ecology and social behavior of raptorial dinosaurs through stable isotope analysis. *Palaeogeography, Palaeoclimatology, Palaeoecology*, **552**: 109780. doi:10.1016/j.palaeo.2020.109780.
- Funston, G.F., and Currie, P.J. 2016. A new caenagnathid (Dinosauria: Oviraptorosauria) from the Horseshoe Canyon Formation of Alberta, Canada, and a reevaluation of the relationships of Caenagnathidae. *Journal of Vertebrate Paleontology*, **36**. doi:10.1080/02724634.2016.1160910.
- Funston, G.F., Currie, P.J., and Burns, M.E. 2016. New elmisaurine specimens from North America and their relationship to the Mongolian *Elmisaurus rarus*. *Acta Palaeontologica Polonica*, **61**: 159–173. doi:10.4202/app.00129.2014.
- Gatesy, S.M. 1991. Hind limb scaling in birds and other theropods: Implications for differences in terrestrial locomotion. *Journal of Morphology*, **209**: 83–96.

- Gatesy, S.M., and Middleton, K.M. 1997. Bipedalism, flight, and the evolution of theropod locomotor diversity. *Journal of Vertebrate Paleontology*, **17**: 308–329.
doi:10.1080/02724634.1997.10010977.
- Gauthier, J. 1986. Saurischian monophyly and the origin of birds. *Memoirs of the California Academy of sciences*, **8**: 55.
- Gilmore, C.W. 1924. On *Troodon validus*, an orthopodus dinosaur from the Belly River Cretaceous of Alberta, Canada. *University of Alberta Bulletin*, **1**: 43.
- Godefroit, P., Currie, P.J., Hong, L., Shang, C.Y., and Dong, Z.M. 2008. A new species of *Velociraptor* (Dinosauria: Dromaeosauridae) from the Upper Cretaceous of northern China. *Journal of Vertebrate Paleontology*, **28**: 432–438. doi:10.1671/0272-4634(2008)28[432:ANSOVD]2.0.CO;2.
- Godfrey, S.J., and Currie, P.J. 2004. A theropod (dromaeosauridae, dinosauria) sternal plate from the Dinosaur Park Formation (Campanian, Upper Cretaceous) of Alberta, Canada. *In* Feathered Dragons. *Edited by* P.J. Currie, E.B. Koppelhus, M.A. Shugar, and J.L. Wright. Indiana University Press, Bloomington and Indianapolis. pp. 144–149.
- Goloboff, P.A., and Mattoni, C.I. 2006. Continuous characters analyzed as such. *Cladistics*, **22**: 589–601.
- Hammer, Ø., Harper, D.A.T., and Ryan, P.D. 2001. PAST: Paleontological statistics software package for education and data analysis. *Palaeontologia Electronica*, **4**: 9.
- Hanai, T., and Tsuihiji, T. 2019. Description of tooth ontogeny and replacement patterns in a juvenile *Tarbosaurus bataar* (Dinosauria: Theropoda) using CT-scan data. *Anatomical*

- Record, **302**: 1210–1225. doi:10.1002/ar.24014.
- Henderson, D.M. 1998. Skull and tooth morphology as indicators of niche partitioning in sympatric Morrison Formation theropods. *Gaia*, **226**: 219–226.
- Hendrickx, C., and Mateus, O. 2014. *Torvosaurus gurneyi* n. sp., the largest terrestrial predator from Europe, and a proposed terminology of the maxilla anatomy in nonavian theropods. *PLoS ONE*, **9**. doi:10.1371/journal.pone.0088905.
- Holmes, R.B., Persons, W.S., Rupal, B.S., Qureshi, A.J., and Currie, P.J. 2020. Morphological variation and asymmetrical development in the skull of *Styracosaurus albertensis*. *Cretaceous Research*, **107**: 104308. Elsevier Ltd. doi:10.1016/j.cretres.2019.104308.
- Hone, D., Choiniere, J., Sullivan, C., Xu, X., Pittman, M., and Tan, Q. 2010. New evidence for a trophic relationship between the dinosaurs *Velociraptor* and *Protoceratops*. *Palaeogeography, Palaeoclimatology, Palaeoecology*, **291**: 488–492. doi:10.1016/j.palaeo.2010.03.028.
- Hone, D., Tsuihiji, T., Watabe, M., and Tsogtbaatr, K. 2012. Pterosaurs as a food source for small dromaeosaurs. *Palaeogeography, Palaeoclimatology, Palaeoecology*, **331–332**: 27–30. doi:10.1016/j.palaeo.2012.02.021.
- Hutchinson, J.R. 2001. The evolution of pelvic osteology and soft tissues on the line to extant birds (Neornithes). *Zoological Journal of the Linnean Society*, **131**: 123–168. doi:10.1006/zjls.2000.0254.
- Ibiricu, L.M., Martínez, R.D., Casal, G.A., and Cerda, I.A. 2013. The behavioral implications of a multi-individual bonebed of a small theropod dinosaur. *PLoS ONE*, **8**: 1–11.

doi:10.1371/journal.pone.0064253.

Jackson, D.A. 1993. Stopping rules in principal components analysis : A comparison of heuristical and statistical approaches. *Ecology*, **74**: 2204–2214.

Janis, C.M., and Ehrhardt, D. 1988. Correlation of relative muzzle width and relative incisor width with dietary preference in ungulates. *Zoological Journal of the Linnean Society*, **92**: 267–284. doi:10.1111/j.1096-3642.1988.tb01513.x.

Kielan-Jaworowska, Z., and Barsbold, R. 1971. Narrative of the Polish-Mongolian expeditions 1967-1971. *Palaeontologia Polonica*, **27**: 13.

Kirkland, J.I., Burge, D., and Gaston, R. 1993. A large dromaeosaur (Theropoda) from the Lower Cretaceous of eastern Utah. *Hunteria*, **2**: 1–16.

Larson, D.W., and Currie, P.J. 2013. Multivariate analyses of small theropod dinosaur teeth and implications for paleoecological turnover through time. *PLoS ONE*, **8**. doi:10.1371/journal.pone.0054329.

LeBlanc, A.R.H., Brink, K.S., Cullen, T.M., Reisz, R.R., Leblanc, A.R.H., Brink, K.S., Cullen, T.M., and Reisz, R.R. 2017. Evolutionary implications of tooth attachment versus tooth implantation : A case study using dinosaur , crocodylian , and mammal teeth. *Journal of Vertebrate Paleontology*, **37**. doi:10.1080/02724634.2017.1354006.

Longrich, N.R., and Currie, P.J. 2009. A microraptorine (Dinosauria-Dromaeosauridae) from the Late Cretaceous of North America. *Proceedings of the National Academy of Sciences of the United States of America*, **106**: 5002–5007. doi:10.1073/pnas.0811664106.

Lü, J., and Brusatte, S.L. 2015. A large, short-armed, winged dromaeosaurid (Dinosauria :

- Theropoda) from the Early Cretaceous of China and its implications for feather evolution. *Scientific Reports*,: 1–11. doi:10.1038/srep11775.
- Lü, J., Unwin, D.M., Jin, X., Liu, Y., and Ji, Q. 2010. Evidence for modular evolution in a long-tailed pterosaur with a pterodactyloid skull. *Proceedings of the Royal Society B: Biological Sciences*, **277**: 383–389. doi:10.1098/rspb.2009.1603.
- Maddison, W., and Maddison, D. 2017. Mesquite.
- Makovicky, P.J., Apesteguía, S., and Agnolín, F.L. 2005. The earliest dromaeosaurid theropod from South America. *Nature*, **437**: 1007–1011. doi:10.1038/nature03996.
- Manning, P.L., Margetts, L., Johnson, M.R., Withers, P.J., Sellers, W.I., Falkingham, P.L., Mummery, P.M., Barrett, P.M., and Raymont, D.R. 2009. Biomechanics of dromaeosaurid dinosaur claws: Application of X-ray microtomography, nanoindentation, and finite element analysis. *Anatomical Record*, **292**: 1397–1405. doi:10.1002/ar.20986.
- Manning, P.L., Payne, D., Pennicott, J., Barrett, P.M., and Ennos, R.A. 2006. Dinosaur killer claws or climbing crampons? *Biology Letters*, **2**: 110–112. doi:10.1098/rsbl.2005.0395.
- Matthew, W.D., and Brown, B. 1922. The family Deinodontidae, with notice of a new genus from the Cretaceous of Alberta. *Bulletin of the American Museum of Natural History*, **46**: 367–385.
- Meyer, H. von. 1861. *Archaeopteryx lithographica* (Vogel-Feder) und *Pterodactylus* von Solnhofen. *Neues Jahrbuch für Mineralogie, Geognosie, Geologie und Petrefakten-Kunde*, **1861**: 678–679.
- Norell, M.A., Clark, J.M., Turner, A.H., Makovicky, P.J., Barsbold, R., and Rowe, T. 2006. A

- new dromaeosaurid theropod from Ukhaa Tolgod (Ömnögov, Mongolia). *American Museum Novitates*, **3545**: 51. doi:10.1206/0003-0082(2006)3545[1:andtfu]2.0.co;2.
- Norell, M.A., and Makovicky, P.J. 1997. Important features of the dromaeosaur skeleton: information from a new specimen. *American Museum Novitates*, **3215**: 1–28.
- Norell, M.A., and Makovicky, P.J. 1999. Important features of the dromaeosaurid skeleton II: Information from newly collected specimens of *Velociraptor mongoliensis*. *American Museum Novitates*, **3282**: 1–45.
- Norell, M.A., Makovicky, P.J., Bever, G.S., Balanoff, A.M., Clark, J.M., Barsbold, R., and Rowe, T. 2009. A review of the Mongolian Cretaceous dinosaur *Saurornithoides* (Troodontidae: Theropoda). *American Museum Novitates*, **3654**: 1–63. doi:10.1206/648.1.
- Norell, M.A., Makovicky, P.J., and Clark, J.M. 2000. A new troodontid theropod from Ukhaa Tolgod, Mongolia. *Journal of Vertebrate Paleontology*, **20**: 7–11.
- Norell, M.A., Makovicky, P.J., and Clark, J.M. 2004. The braincase of *Velociraptor*. In *Feathered Dragons. Edited by P.J. Currie, E.B. Koppelhus, M.A. Shugar, and J.L. Wright*. Indiana University Press, Bloomington and Indianapolis. pp. 133–143.
- Novas, F.E., and Pol, D. 2005. New evidence on deinonychosaurian dinosaurs of the Late Cretaceous of Patagonia. *Nature*, **433**: 858–861.
- Novas, F.E., Pol, D., Canale, J.I., Porfiri, J.D., and Calvo, J.O. 2009. A bizarre Cretaceous theropod dinosaur from Patagonia and the evolution of Gondwanan dromaeosaurids. *Proceedings of the Royal Society B: Biological Sciences*, **276**: 1101–1107. doi:10.1098/rspb.2008.1554.

- Osborn, H.F. 1906. *Tyrannosaurus*, Upper Cretaceous carnivorous dinosaur. (second communication.). Bulletin of the American Museum of Natural History, **XXII**: 259–265.
- Osborn, H.F. 1924. Three new Theropoda, *Protoceratops* Zone, central Mongolia. American Museum Novitates, : 1–12.
- Ostrom, J.A. 1970. Stratigraphy and paleontology of the Cloverly Formation (Lower Cretaceous) of the Bighorn Basin area, Wyoming and Montana. Bulletin of the Peabody Museum of Natural History, **35**: 1–250. Peabody Museum of Natural History, Yale University, New Haven CT. doi:10.1086/407120.
- Ostrom, J.H. 1969. Osteology of *Deinonychus antirrhopus*, an unusual theropod from the Lower Cretaceous of Montana. Peabody Museum of Natural History, **30**: 1–165.
- Ostrom, J.H. 1976. On a new specimen of the Lower Cretaceous theropod dinosaur *Deinonychus antirrhopus*. Breviora, **439**: 1–21.
- Patterson, C. 1982. Morphological characters and homology. In Problems of Phylogenetic Reconstruction. Edited by K.A. Joysey and A.E. Friday. Academic Press, London and New York. pp. 21–74.
- Pearson, K. 1901. LIII. On lines and planes of closest fit to systems of points in space . The London, Edinburgh, and Dublin Philosophical Magazine and Journal of Science, **2**: 559–572. doi:10.1080/14786440109462720.
- Peng, J., Brinkman, D., and Russell, A.P. 2001. Vertebrate microsite assemblages (exclusive of mammals) from the Foremost and Oldman formations of the Judith River group (Campanian) of southeastern Alberta : An illustrated guide. Provincial Museum of Alberta

- Natural History Occasional Paper, : 54. doi:10.5962/bhl.title.115853.
- Perle, A., Norell, M.A., and Clark, J.M. 1999. A new maniraptoran theropod - *Achillobator giganticus* (Dromaeosauridae)- from the Upper Cretaceous of Burkhan, Mongolia. National University of Mongolia, : 102.
- Persons, W.S., and Currie, P.J. 2016. An approach to scoring cursorial limb proportions in carnivorous dinosaurs and an attempt to account for allometry. *Scientific Reports*, **6**: 21–24. doi:10.1038/srep19828.
- Piechowski, R., Niedźwiedzki, G., and Tałanda, M. 2019. Unexpected bird-like features and high intraspecific variation in the braincase of the Triassic relative of dinosaurs. *Historical Biology*, **31**: 1065–1081. Taylor & Francis. doi:10.1080/08912963.2017.1418339.
- Rayfield, E.J., Norman, D.B., Horner, C.C., Horner, J.R., Smith, P.M., Thomason, J.J., and Upchurch, P. 2001. Cranial design and function in a large theropod dinosaur. *Nature*, **409**: 1033–1037. doi:10.1038/35059070.
- Roach, B.T., and Brinkman, D.L. 2007. A reevaluation of cooperative pack hunting and gregariousness in *Deinonychus antirrhopus* and other nonavian theropod dinosaurs. *Bulletin of the Peabody Museum of Natural History*, **48**: 103–138. doi:10.3374/0079-032x(2007)48[103:arocph]2.0.co;2.
- Russell, D.A. 1993. The role of Central Asia in dinosaurian biogeography. *Canadian Journal of Earth Sciences*, **30**: 2002–2012. doi:10.1139/e93-176.
- Sakamoto, M. 2010. Jaw biomechanics and the evolution of biting performance in theropod dinosaurs. *Proceedings of the Royal Society B: Biological Sciences*, **277**: 3327–3333.

doi:10.1098/rspb.2010.0794.

- Sampson, S.D., Ryan, M.J., and Tanke, D.H. 1997. Craniofacial ontogeny in centrosaurine dinosaurs (Ornithischia: Ceratopsidae): Taxonomic and behavioral implications. *Zoological Journal of the Linnean Society*,: 293–337. doi:10.1111/j.1096-3642.1997.tb00340.x.
- Sankey, J.T. 2001. Late Campanian southern dinosaurs, Aguja Formation, Big Bend, Texas. *Journal of Paleontology*, **75**: 208–215. doi:10.1017/S0022336000031991.
- Schott, R.K., and Evans, D.C. 2017. Cranial variation and systematics of *Foraminacephale brevis* gen. nov. and the diversity of pachycephalosaurid dinosaurs (Ornithischia: Cerapoda) in the Belly River Group of Alberta, Canada. *Zoological Journal of the Linnean Society*, **179**. doi:10.1111/zoj.12465.
- Schott, R.K., Evans, D.C., Goodwin, M.B., Horner, J.R., Brown, C.M., and Longrich, N.R. 2011. Cranial ontogeny in *Stegoceras validum* (Dinosauria: Pachycephalosauria): A quantitative model of pachycephalosaur dome growth and variation. *PLoS ONE*, **6**. doi:10.1371/journal.pone.0021092.
- Senter, P., Barsbold, R., Britt, B.B., and Burnham, D.A. 2004. Systematics and evolution of Dromaeosauridae (Dinosauria, Theropoda). *Bulletin of Gunma Museum of Natural History*, **8**: 1–20.
- Senter, P., Kirkland, J.I., Bird, J., and Bartlett, J.A. 2010. A new troodontid theropod dinosaur from the lower cretaceous of Utah. *PLoS ONE*, **5**: 1–5. doi:10.1371/journal.pone.0014329.
- Simões, T.R., Caldwell, M.W., Palci, A., and Nydam, R.L. 2016. Giant taxon-character matrices: Quality of character constructions remains critical regardless of size. *Cladistics*,: 1–22.

- Slater, G.J., Dumont, E.R., and Van Valkenburgh, B. 2009. Implications of predatory specialization for cranial form and function in canids. *Journal of Zoology*, **278**: 181–188. doi:10.1111/j.1469-7998.2009.00567.x.
- Snively, E., and Russell, A.P. 2007. Functional variation of neck muscles and their relation to feeding style in Tyrannosauridae and other large theropod dinosaurs. *Anatomical Record*, **290**: 934–957. doi:10.1002/ar.20563.
- Sternberg, C.M. 1932. Two new theropod dinosaurs from the Belly River Formation of Alberta. *Canadian Field-Naturalist*, **46**: 99–105.
- Sues, H.-D. 1976. A new small theropod dinosaur from the Judith River Formation (Campanian) of Alberta. *Zoological Journal of the Linnean Society*, **62**: 381–400.
- Therrien, F., Henderson, D.M., and Ruff, C.B. 2005. Bite me. Biomechanical models of theropod mandibles and implications for feeding behavior. *In* *The Carnivorous Dinosaurs*. Edited by K. Carpenter. Indiana University Press, Bloomington. pp. 179–237.
- Torices, A., Wilkinson, R., Arbour, V.M., Ruiz-Omeñaca, J.I., and Currie, P.J. 2018. Puncture-and-pull biomechanics in the teeth of predatory coelurosaurian dinosaurs. *Current Biology*, **28**: 1467-1474.e2. doi:10.1016/j.cub.2018.03.042.
- Tsuihiji, T., Barsbold, R., Watabe, M., Tsogtbaatar, K., Chinzorig, T., Fujiyama, Y., and Suzuki, S. 2014. An exquisitely preserved troodontid theropod with new information on the palatal structure from the Upper Cretaceous of Mongolia. *Naturwissenschaften*, **101**: 131–142. doi:10.1007/s00114-014-1143-9.
- Turner, A.H., Hwang, S.H., and Norell, M.A. 2007a. A small derived theropod from Öösh, Early

- Cretaceous, Baykhangor Mongolia. American Museum Novitates, **3557**: 27.
doi:10.1206/0003-0082(2007)3557[1:asdtfs]2.0.co;2.
- Turner, A.H., Makovicky, P.J., and Norell, M.A. 2007b. Feather quill knobs in the dinosaur *Velociraptor*. Science, **317**. doi:10.1126/science.1145076.
- Turner, A.H., Makovicky, P.J., and Norell, M.A. 2012. A review of dromaeosaurid systematics and paravian phylogeny. Bulletin of the American Museum of Natural History, **371**: 1–206.
doi:10.1206/748.1.
- Turner, A.H., Pol, D., Clarke, J.A., Erickson, G.M., and Norell, M.A. 2007c. A basal dromaeosaurid and size evolution preceding avian flight. Science, **317**: 1378–1381.
doi:10.1126/science.1144066.
- Walmsley, C.W., Smits, P.D., Quayle, M.R., McCurry, M.R., Richards, H.S., Oldfield, C.C., Wroe, S., Clausen, P.D., and McHenry, C.R. 2013. Why the long face? The mechanics of mandibular symphysis proportions in crocodiles. PLoS ONE, **8**: 34.
doi:10.1371/journal.pone.0053873.
- White, T. 2003. Early hominids - diversity or distortion? Science, **299**: 1994–1995.
doi:10.1126/science.1078294.
- Whitlock, J.A. 2011. Inferences of diplodocoid (Sauropoda: Dinosauria) feeding behavior from snout shape and microwear analyses. PLoS ONE, **6**. doi:10.1371/journal.pone.0018304.
- Wilkinson, M. 1995. A comparison of two methods of character construction. Cladistics, : 297–308.
- Williamson, T.E., and Carr, T.D. 2003. A new genus of derived pachycephalosaurian from

- western North America. *Journal of Vertebrate Paleontology*, **22**: 779–801.
doi:10.1671/0272-4634(2002)022[0779:ANGODP]2.0.CO;2.
- Witmer, L.M. 1997. The evolution of the antorbital cavity of archosaurs: A study in soft-tissue reconstruction in the fossil record with an analysis of the function of Pneumaticity. *Journal of Vertebrate Paleontology*, **17**: 1–76. doi:10.1080/02724634.1997.10011027.
- Witmer, L.M., and Ridgely, R.C. 2008. The paranasal air sinuses of predatory and armored dinosaurs (Archosauria: Theropoda and Ankylosauria) and their contribution to cephalic structure. *Anatomical Record*, **291**: 1362–1388. doi:10.1002/ar.20794.
- Witmer, L.M., Ridgely, R.C., Dufeu, D.L., and Semones, M.C. 2008. Using CT to Peer into the Past : 3D Visualization of the Brain and Ear Regions of Birds , Crocodiles , and Nonavian Dinosaurs. *Anatomical Imaging*,: 33. doi:10.1007/978-4-431-76933-0.
- Xu, X., Choiniere, J.N., Pittman, M., Tan, Q., Xiao, D., Li, Z., Tan, L., Clark, J.M., Norell, M.A., Hone, D.W.E., and Sullivan, C. 2010a. A new dromaeosaurid (Dinosauria: Theropoda) from the Upper Cretaceous Wulansuhai Formation of Inner Mongolia, China. *Zootaxa*, **9**: 1–9.
- Xu, X., Norell, M.A., Wang, X.L., Makovicky, P.J., and Wu, X.C. 2002. A basal troodontid from the Early Cretaceous of China. *Nature*, **415**: 780–784. doi:10.1038/415780a.
- Xu, X., Pittman, M., Sullivan, C., Choiniere, J.N., Tan, Q.-W., Clark, J.M., Norell, M. a., and Wang, S. 2015. The taxonomic status of the Late Cretaceous dromaeosaurid *Linheraptor exquisitus* and its implications for dromaeosaurid systematics. *Vertebrata Palasiatica*, **53**: 29–62.

- Xu, X., Wang, K., Zhao, X., Sullivan, C., and Chen, S. 2010b. A new leptoceratopsid (Ornithischia: Ceratopsia) from the Upper Cretaceous of Shandong, China and its implications for neoceratopsian evolution. *PLoS ONE*, **5**. doi:10.1371/journal.pone.0013835.
- Xu, X., Wang, X.L., and Wu, X.C. 1999. A dromaeosaurid dinosaur with a filamentous integument from the Yixian Formation of China. *Nature*, **401**: 262–266. doi:10.1038/45769.
- Xu, X., Zhou, Z., and Wang, X. 2000. The smallest known non-avian theropod dinosaur. *Nature*, **408**: 705–708. doi:10.1038/35047056.
- Zanno, L.E., and Makovicky, P.J. 2011. Herbivorous ecomorphology and specialization patterns in theropod dinosaur evolution. *Proceedings of the National Academy of Sciences of the United States of America*, **108**: 232–237. doi:10.1073/pnas.1011924108.
- Zheng, X., Xu, X., You, H., Zhao, Q., and Dong, Z. 2010. A short-armed dromaeosaurid from the Jehol group of China with implications for early dromaeosaurid evolution. *Proceedings of the Royal Society B: Biological Sciences*, **277**: 211–217. doi:10.1098/rspb.2009.1178.

Appendix 1

A 1.1. Anterior ramus regression analyses data

Log transformed data for Reduced Major Axis regression analysis of eudromaeosaurian anterior rami and maxillary length and height dimensions.

Specimen	Taxon	MxL	AntRL	MxH	AntRH.p
ROM 63777	<i>Acheroraptor temertyorum</i>			1.729813	1.563244
TMP 1995.166.001	<i>Atrociraptor marshalli</i>	2.00668	1.511215	1.777064	1.636588
AMNH FARB 30556	<i>Bambiraptor feinbergi</i>	1.719	1.083144	1.414472	1.239299
MOR 553S - 7.30.91.274	<i>Bambiraptor feinbergi</i>			1.683407	1.489677
YPM 5232 (557)	<i>Deinonychus antirrhopus</i>	2.143015	1.491362	1.911956	1.658488
AMNH FARB 5356	<i>Dromaeosaurus albertensis</i>	2.02547	1.284205		
UALVP 55700	<i>Saurornitholestes langstoni</i>	1.982814	1.435367	1.68029	1.52943
TMP 1994.12.844	<i>Saurornitholestes langstoni</i>	1.943544	1.435367	1.672098	1.478566
MNUFR 15	<i>Achillobator giganticus</i>	2.401211	1.869584	2.055684	1.928959
IVPP V 16923	<i>Linheraptor exquisitus</i>	2.054766	1.717004	1.670478	1.537882
IGM 100/1015	<i>Tsaagan mangas</i>	2.018076	1.599009	1.586868	1.485011
BYUVP 19965 F# 4252	<i>Utahraptor ostrommaysi</i>	2.37716	1.632052		
MPC-D 100/982	<i>Velociraptor</i> sp.	1.974834	1.412796	1.438384	1.267758
AMNH FARB 6515	<i>Velociraptor mongoliensis</i>	1.959185	1.45667	1.47019	1.213518
MPC-D 100/25	<i>Velociraptor mongoliensis</i>	2.054536	1.576917	1.606059	1.428297
MPC-D 100/54	<i>Velociraptor mongoliensis</i>	2.009196	1.526985	1.534851	1.374932
UALVP 49389	<i>Velociraptor</i> sp. (Cast)	1.980003	1.64836	1.531479	1.439333
IMM99NM-BYM- 3/3A	<i>Velociraptor osmolskae</i>			1.552911	1.377306

A 1.2. Character revisions

List of maxillary characters additional to, and modified characters from Currie and Evans (2019).

Modifications are mentioned below each character with indication of how the taxa from Chapter

2 would be coded for the updated characters. Ratio-based characters. However, are assessed in Chapter 3 and the modified ratio-based characters are available in Appendix 2.

Characters recommended for removal from the data set, or tentative removal until justification is presented are quoted followed by reasoning for the suggested use of the character.

All characters are mentioned in the order in which they appear in the taxon-character matrix used in Currie and Evans (2019)

Character 6 – Antorbital fossa, anterior margin is level with or just posterior to: 0, 3rd maxillary alveolus; 1, 4th alveolus; 2, 5th or any alveolus posterior to the 5th. (This character was modified to specify the range of qualification for the character states so as not to unjustly code taxa differently as was done with *Atrociraptor marshalli* and *Velociraptor mongoliensis* which now both show state [1] along with *Saurornitholestes langstoni*. *Deinonychus antirrhopus* and MPC-D 100/982 are coded as state [0], and *Acheroraptor temertyorum* and *Tsaagan mangas* would be coded as [2].

Character 7 - Antorbital fossa, ventral margin: 0, extends onto posterior half of the maxilla (jugal ramus) and is visible in lateral view; 1, does not extend onto the jugal process, antorbital fossa restricted ventrally by a ventrolateral sloped surface; 2, does not extend onto the jugal process, antorbital fossa restricted ventrally by a sharp dorsoventral lamina. (This character was given the additional state [2] to differentiate variation in the condition of ventrally restricted antorbital fossa. *Acheroraptor temertyorum* and *Achillobator giganticus* have state [1] which is distinct from state [2] observed in unenlagiines, troodontids, and the eudromaeosaurians *Linheraptor exquisitus* and *Tsaagan mangas*.)

Character 9-1 – Promaxillary fenestra of maxillae shape: 0, subcircular; 1, slit-like (This character was split in order to remove the dependence of shape and position relative to the antorbital fossa which was shown not to be by the specimens in this study.

Acheroraptor temertyorum, *Saurornitholestes langstoni*, and *Velociraptor mongoliensis* are coded as [1] whereas *Atrociraptor marshalli*, *Deinonychus antirrhopus*, and *Tsaagan mangas* are coded as [0]. This character may be variable in *Velociraptor* based on available data.)

Character 9-2 – Promaxillary fenestra: ventral border of the promaxillary fenestra of the maxilla position: 0, tucked into or near the anteroventral border of the antorbital fossa; 1, tucked into or near the most anterior point or anterodorsal border of the antorbital fossa (This character was modified to encompass the condition of *Velociraptor mongoliensis* where the promaxillary fenestra is often slit like, exposed in lateral view but still partially tucked into the anterodorsal margin of the antorbital fossa. The more dorsal position in this taxon was shown to relate to deeply rooted teeth that elevate the maxillary sinus system as a whole. The reference point of the promaxillary fenestra is the ventral border, as the ventral extent of the promaxillary fenestra cannot extend ventral to floor of the maxillary sinus system. This is emphasized by *Acheroraptor temertyorum* which has a promaxillary fenestra that extends for most of the anterior border of the antorbital fenestra. Under the new wording, all taxa in this study other than *Velociraptor mongoliensis* would be coded as [0], whereas *Velociraptor mongoliensis* would be coded as [1].)

Character 10-1 – Maxillary fenestra: 0, appears as a simple perforation; 1, is positioned in a broad posteriorly oriented secondary fossa; 2, is positioned in a posterodorsally oriented

secondary fossa within the antorbital fossa, parallel to the posterodorsal boundary of the antorbital fossa; 3, is positioned in a posterodorsally oriented secondary fossa within the antorbital fossa, parallel to the posterodorsal boundary of the antorbital fossa with the development of a pneumatic excavation in the posterodorsal end of the secondary fossa separated from the fenestra by a distinct strut. (This character was expanded into four states to capture the diversity observed within Eudromaeosauria, the in-group of interest. The position of the maxillary fenestra relative to the promaxillary fenestra was removed from this character as dependency between position of the maxillary fenestra and its position in a secondary fossa are violated by the specimens within this study.

Acheroraptor temertyorum, and *Velociraptor mongoliensis* both possess maxillary fenestra, posterior to the promaxillary fenestra rather than posterodorsal but still have fenestra housed in secondary fossae. Additionally, *Tsaagan mangas* has a maxillary fenestra directly dorsal to the promaxillary fenestra. The generalization of maxilla position in a fossa and relative to the promaxillary fenestra was insufficient for in-group relationships. Based on the new character and states *Tsaagan mangas*, and *Velociraptor mongoliensis* would be coded as [1], *Deinonychus antirrhopus* would be coded as [2], and *Acheroraptor temertyorum*, *Atrociraptor marshalli*, and *Saurornitholestes langstoni* would be coded as [3].)

Character 10-2 – Maxillary fenestra position relative to the promaxillary fenestra: 0, posterior; 1, posterodorsal; 2, dorsal. (This character was split from character 10 Currie and Evans (2019) as it better captures the variation observed in Eudromaeosauria whereas not giving dependency to the position of the maxillary fenestra within a secondary fossa unjustly. Character state [1] and [2] are distinct based on dorsal displacement from the maxillary

fenestra from the promaxillary fenestra. *Atrociraptor marshalli*, *Deinonychus antirrhopus*, and *Saurornitholestes langstoni* would be coded as [1] whereas *Tsaagan mangas* would be coded as [2], and *Acheroraptor temertyorum*, and *Velociraptor mongoliensis* would be coded as [0].)

Character 11-1 – Maxillary fenestra shape: 0, subcircular with subequal long axes; 1, elongate along the axis of orientation. (This character was split from the original wording in Currie and Evans (2019) in which it combined the states of shape and size without capturing variation within the in-group Eudromaeosauria. Under the new character wording, *Atrociraptor marshalli*, *Tsaagan mangas*, as well as the holotype of *Velociraptor mongoliensis* and MPC-D 100/982 would be coded as [0]. All other taxa examined in this study as well as some specimens of *Velociraptor mongoliensis* (MPC-D 100/25 and MPC-D 100/54) would be coded as [1]. The polymorphism within *Velociraptor mongoliensis* could be due to intraspecific variation but requires more investigation.)

Character 11-2 – Maxillary fenestra size: 0, small making up much less than half of the antorbital fossa surface; 1, large making up close to half of the area of the antorbital fossa. (This character still serves to distinguish troodontids and unenlagiines from microraptorines and eudromaeosaurians. All specimens examined would be considered state [0]. However, a survey of the study groups analyzing proportionate area of the maxillary fenestra and the antorbital fossa may be able to break this up further based on natural clusters. Its separation as a distinct character does remove the unjustified dependency it previously had.)

Character 12 – “Maxillary fenestra position: 0, low in antorbital fossa with ventral margin at level of ventral margin of antorbital fossa; 1, low in fossa but above ventral margin; 2, in

upper half of antorbital fossa.” This character is recommended for removal due to the impossibility of having a state [0] for this character and state [0] for character 7 from Currie and Evans (2019). This character is better exemplified by character 10-2 above which relates the position of two fenestrae associated with the maxillary sinus system thus a justified dependency.

Character 13 – “Maxillary fenestra, ratio of distance between lower edge of fenestra and alveolar margin divided by length of tallest tooth: 0, less than 2.0; 1, greater than 2.0.” This character should be revised to describe the height of the maxillary fenestra relative to a biologically limiting feature such as alveolar depth below the maxilla. A correlation between maxillary tooth crown and root dorsoventral height was not performed in this study and therefore this character was excluded until such a study can be done to test the validity of this metric.

Character 14 – Maxilla pila promaxillaris: 0, narrow relative to the pila interfenestralis; 1, broad relative to the pila interfenestralis. (This character was changed from the original wording in order to accommodate circumstances of abbreviated antorbital fossae as observed in *Atrociraptor marshalli*. The condition in this taxon was coded as being the same as observed in *Tsaagan mangas*. However, is shown here to be artificial due to the abbreviated antorbital fossa. Based on the modified wording here *Tsaagan mangas* would be coded as state [0] whereas all other taxa in this study would be coded as [1].)

Character 26+27 – Maxilla; palatal shelf: 0, concealed in lateral; 1, dorsally exposed along the jugal ramus only in lateral view; 2, posteriorly exposed to the antorbital fossa as the postantral wall and dorsally along the jugal ramus in lateral view. (Characters 26 and 27 from Currie and Evans (2019) were combined due to the observation that the palatal shelf

and postantoral wall are confluent at or anteriorly approaching the posterior border of the antorbital fossa. The independence of these characters cannot be justified based on the observable data. The observation of state [1] is contentious due to the effects of taphonomy on the palatal shelf as observed in *Atrociraptor marshalli*. It has been accepted as distinct here but is open to revision. Based on the new character, *Deinonychus antirrhopus* would be coded as state [0], *Atrociraptor marshalli*, *Saurornitholestes langstoni*, and *Velociraptor mongoliensis* would be coded as [1], and *Acheroraptor temertyorum*, and *Tsaagan mangas* would be coded as [2].)

Character 32 – “Maxilla, jugal process ventral to the antorbital fossa: 0, dorsoventrally low; 1, dorsoventrally tall.” This character seems to be redundant with Character 7 as both seem to refer to the degree of ventral sloping of the ventral border of the antorbital fossa posteriorly. This character could be referring to the thickness of the jugal ramus itself. However, that is unclear. Of the two characters, character 7 is preferred because it is clearer as to what the states are and suffers from less ambiguity.

Character 34-1 – Nasal participation in the antorbital fossa: 0, none; 1, ventrolateral edge of the nasal makes up the dorsal margin of the antorbital fossa; 2, the lateral surface of the nasal makes up part of the antorbital fossa. (This character was split into two characters, one defining the contribution of the nasal in the antorbital fossa, the other (Character 34-2) characterizing the presence or absence of pneumatopores. The absence of nasal involvement [0] would characterize troodontids and other outgroups, whereas state [1] would be common among most dromaeosaurids and [2] would characterize *Deinonychus antirrhopus*. Specimens in this study other than *Deinonychus antirrhopus* would all be characterized as being state [1].)

Character 34-2 – Nasals with pneumatopores near contact with the maxilla: 0, no; 1, yes. (This character was split from Character 34-1 to remove the unjustified dependency between the possession of pneumatopores and the inclusion of the nasals in the dorsal margin of the antorbital fossa. The only two taxa in this study to be confirmed to have pneumatopores near the contact with the maxilla [1] are *Deinonychus antirrhopus* and *Saurornitholestes langstoni* (Currie and Evans 2019). All others would be characterized by state [0].)

Appendix 2

Supplementary data for Chapter 3. This includes tables of raw data for PCA, bivariate, and Jenks natural breaks optimization analyses with character reassessment.

A 2.1. Raw data. Includes all specimens and all measurements used for linear regression, PCA, and Jenks Optimization analyses. Purple text represents measurements done using ImageJ; red text represents incomplete measurements; green text represents estimates.

Specimen	Taxon	Maxilla																	Premaxilla					
		MvL	MvH	AntRL	AntRH.d	AntRH.p	AntFenL	AntFenH	AntFL	AntFLtl	AntFH	AntAF-Mx	PIW	MxFen.L	MxFen.S	entM.H	anentM.H	po	L9Alv	ntFen.SAlv	PmxL.bdy	PmxH.bdy		
ROM 63777	<i>Acheroraptor temertyorum</i>	79.66	57.60	43.02	15.67	35.37	NA	37.12	19.94	49.52	41.41	10.71	4.58	18.05	5.06	20.12	17.50	79.66	10.87	NA	NA			
TMP 1995.166.001	<i>Atrocaptor marshali</i>	101.55	59.85	32.45	26.37	43.31	40.98	43.32	19.17	63.68	46.31	3.45	5.37	13.87	9.98	22.70	13.99	72.77	14.19	25.00	26.00			
AMNH FARB 30556	<i>Bambiraptor feinbergi</i>	52.36	25.97	12.11	8.43	17.35	21.19	19.98	15.79	34.29	21.34	7.12	2.13	8.18	4.36	5.37	2.35	39.27	9.39	13.79	8.77			
YPM 5232 (557)	<i>Deinonychus antirrhopus</i>	139.00	81.65	31.00	27.19	45.55	71.58	64.71	41.72	108.15	69.80	24.70	6.29	15.98	7.03	22.83	20.60	96.69	24.17	NA	NA			
YPM 5232 (237)	<i>Deinonychus antirrhopus</i>	NA	NA	NA	NA	NA	NA	NA	NA	NA	NA	NA	NA	NA	NA	NA	NA	NA	NA	NA	38.82	31.02		
AMNH FARB 5356 (Left)	<i>Dromaeosaurus albertensis</i>	115.46	NA	NA	19.7	NA	NA	NA	NA	NA	NA	NA	NA	NA	NA	NA	33.82	NA	85.54	NA	30.69	27.29		
AMNH FARB 5356 (Right)	<i>Dromaeosaurus albertensis</i>	96.61	NA	19.24	NA	NA	13.27	NA	NA	NA	NA	NA	NA	NA	8.48	NA	24.72	NA	75.31	NA	NA	NA		
UALVP 55700 (Left)	<i>Saurornitholestes langstoni</i>	90.50	46.00	27.40	16.42	35.97	31.97	30.70	26.03	58.00	38.54	12.43	2.65	11.39	7.43	13.19	6.13	69.70	7.20	25.00	25.00			
UALVP 55700 (Right)	<i>Saurornitholestes langstoni</i>	101.73	49.79	27.10	16.01	31.71	32.05	35.68	28.62	60.67	42.75	16.14	1.84	15.66	6.29	14.89	5.11	68.38	6.99	22.00	21.00			
TMP 1994.12.844	<i>Saurornitholestes langstoni</i>	87.81	47.00	27.25	17.05	30.10	33.12	35.11	24.18	57.30	40.21	12.00	4.21	17.28	6.45	9.05	5.50	67.98	5.90	NA	NA			
MNUR 15	<i>Achillobator giganteus</i>	251.89	113.68	74.06	30.31	84.91	88.68	79.25	50.47	174.06	85.85	17.45	36.32	30.75	12.05	49.53	38.21	176.42	34.90	NA	NA			
IVPP V 16923 (Left)	<i>Linheraptor exsistens</i>	117.61	45.76	54.93	21.46	35.21	32.34	30.28	28.87	63.38	35.92	0.00	9.86	19.43	11.14	16.20	8.45	83.80	0.00	25.35	20.42			
IVPP V 16923 (Right)	<i>Linheraptor exsistens</i>	107.75	47.89	49.30	18.23	33.80	33.80	28.87	26.06	55.63	33.10	0.00	10.56	21.69	10.16	16.20	9.16	81.69	0.00	24.65	20.42			
IGM 100/1015 (Left)	<i>Tsaagan mangas</i>	105.15	40.10	39.21	12.24	31.19	45.89	20.94	20.05	66.83	28.07	0.00	NA	NA	NA	14.70	11.59	72.63	9.36	21.83	12.92			
IGM 100/1015 (Right)	<i>Tsaagan mangas</i>	103.34	37.15	40.22	12.92	29.91	41.98	28.03	17.42	59.40	30.07	0.00	5.70	11.76	7.50	14.26	12.66	73.75	7.60	18.48	15.51			
BYUVF 14585 F41584	<i>Utahraptor ostrommaysi</i>	NA	NA	NA	NA	NA	NA	NA	NA	NA	NA	NA	NA	NA	NA	NA	NA	NA	NA	NA	69.87	54.59		
BYUVF 19955 F4 4252	<i>Utahraptor ostrommaysi</i>	238.32	NA	42.86	52.04	NA	109.39	NA	90.07	199.73	NA	51.16	14.69	NA	NA	62.59	33.20	178.55	46.61	NA	NA			
CEUM 01430	<i>Utahraptor ostrommaysi</i>	NA	NA	NA	NA	NA	NA	NA	NA	NA	NA	NA	NA	NA	NA	NA	NA	NA	NA	NA	68.02	72.25		
MPC-D 100/982 (Left)	<i>Velociraptor sp.</i>	89.87	28.32	26.17	10.61	19.28	35.06	25.77	34.67	69.73	28.30	19.33	8.43	6.90	6.31	6.00	4.72	63.05	0.00	22.12	12.97			
MPC-D 100/982 (Right)	<i>Velociraptor sp.</i>	98.87	26.56	25.56	13.66	17.77	35.51	21.05	30.20	65.71	27.07	19.17	10.53	6.20	5.11	6.07	2.38	68.05	0.00	24.58	12.28			
MPC-D 100/982 (Image Left)	<i>Velociraptor sp.</i>	91.38	30.36	25.06	10.61	20.34	35.67	25.65	37.73	73.40	28.00	22.11	8.43	6.90	5.60	7.37	4.72	63.05	0.00	22.12	12.97			
AMNH FARB 6515 (Left)	<i>Velociraptor mongoliensis</i>	91.03	29.40	27.92	9.48	15.80	34.71	20.72	22.04	56.50	27.30	9.87	3.95	7.55	6.90	5.20	2.63	59.87	3.29	NA	NA			
AMNH FARB 6515 (Right)	<i>Velociraptor mongoliensis</i>	NA	29.65	29.31	10.74	16.90	34.14	16.21	24.14	58.62	31.72	11.34	NA	5.69	5.53	7.59	1.72	61.38	4.50	22.32	12.48			
MPC-D 100/25 (Left)	<i>Velociraptor mongoliensis</i>	111.95	41.03	35.87	15.68	26.63	43.61	27.58	30.16	72.82	36.82	13.45	7.20	11.44	6.15	10.26	4.19	77.58	10.60	26.09	17.39			
MPC-D 100/25 (Right)	<i>Velociraptor mongoliensis</i>	114.81	39.71	37.75	14.85	26.99	41.47	29.14	30.71	72.57	34.82	11.93	8.02	11.22	6.64	10.37	4.50	79.41	9.98	26.60	16.43			
MPC-D 100/54 (Left)	<i>Velociraptor mongoliensis</i>	96.35	33.58	33.58	9.96	22.99	35.77	20.80	27.37	64.23	28.10	10.58	4.75	13.99	8.59	8.76	3.65	71.17	10.22	25.18	14.60			
MPC-D 100/54 (Right)	<i>Velociraptor mongoliensis</i>	107.93	34.95	33.71	9.59	24.43	38.97	27.52	34.64	74.53	33.09	15.15	8.97	11.26	5.40	9.90	3.71	73.91	5.57	24.43	15.77			
CEUM 49389 (Left)	<i>Velociraptor sp. (Cast)</i>	98.00	32.00	45.00	14.00	28.00	50.00	24.00	5.50	55.50	28.00	0.00	1.63	16.00	3.50	17.00	8.00	69.57	4.35	24.00	13.00			
UALVP 49389 (Right)	<i>Velociraptor sp. (Cast)</i>	93.00	36.00	44.00	10.50	27.00	49.00	22.50	5.00	54.00	28.00	0.00	4.74	19.50	3.50	16.00	8.00	73.68	7.90	21.50	15.00			
IMPS/NM-BHM-3/3A	<i>Velociraptor osmolskiae</i>	NA	35.72	33.64	9.54	23.84	NA	21.99	29.40	NA	27.29	9.80	6.09	13.25	6.79	12.45	9.80	72.85	1.33	NA	NA			
MPC-D 100/1119	<i>Shanag oslike</i>	50.95	20.08	12.98	2.30	5.40	15.40	15.57	22.40	30.32	16.19	17.02	1.98	7.64	3.78	3.07	1.51	38.02	3.18	NA	NA			
IVPP V 12811	<i>Sinornithosaurus millenii</i>	69.07	28.16	11.74	4.09	9.50	24.50	16.62	34.17	57.38	23.53	18.41	6.90	7.33	3.98	3.14	1.17	45.77	1.57	18.02	4.70			
MML 195	<i>Austroraptor cabazai</i>	382.32	133.54	153.66	41.46	71.34	145.73	96.95	80.49	232.93	113.42	0.00	46.34	35.77	13.80	42.07	21.95	185.37	49.39	NA	NA			
CEUM 73719	<i>Gobienator saurezerum</i>	95.00	32.50	14.00	13.00	20.50	38.98	15.92	41.50	NA	22.45	4.69	9.96	27.50	11.00	8.50	6.00	44.33	14.70	NA	NA			
MPC-D 100/96	<i>Gobienator mongoliensis</i>	87.08	28.33	18.75	11.67	18.33	47.50	25.00	33.33	80.42	25.00	7.50	10.83	17.50	5.83	5.58	5.42	37.08	15.83	NA	NA			
AMNH FARB 6516 (Left)	<i>Saurornithoides mongoliensis</i>	72.13	25.96	30.85	11.59	24.68	31.58	NA	34.26	NA	NA	13.83	3.83	16.82	7.47	15.75	9.15	21.70	42.98	8.94	12.55			
AMNH FARB 6516 (Right)	<i>Saurornithoides mongoliensis</i>	86.60	25.53	30.43	9.86	23.40	NA	16.60	NA	55.75	18.30	NA	NA	NA	NA	15.75	7.87	22.34	NA	7.02	13.19			
IVPP V 12615	<i>Sinovenator changii</i>	38.28	16.72	9.02	3.54	8.93	14.43	12.21	14.84	29.18	14.67	3.44	1.39	10.08	6.97	3.36	1.72	11.97	14.02	3.69	3.69			
MPC-D 100/1 (Left)	<i>Zanabazar junior</i>	116.29	32.41	43.71	16.83	26.16	24.81	24.14	47.43	71.73	24.64	0.00	10.30	37.20	9.46	15.70	9.11	33.25	57.90	9.45	12.66			
MPC-D 100/1 (Right)	<i>Zanabazar junior</i>	115.95	33.42	41.01	12.77	26.58	27.85	25.82	47.85	73.92	26.08	0.00	8.35	33.94	11.40	14.18	7.85	31.39	57.98	7.60	12.41			

A 2.2. Linear regression analysis. Raw data and results from a simple linear regression using normal and log transformed data.

Correlations

Raw Data

Specimen	Taxon	PmxL/H	MxL/H	PmxL/H (log)	Mx L/H (log)
TMP 1995.166.001	<i>Atrociraptor marshalli</i>	0.96	1.70	-0.01703	0.229616
YPM 5232 (557+237)	<i>Deinonychus antirrhopus</i>	1.28	1.70	0.108459	0.231059
UALVP 55700	<i>Saurornitholestes langstoni</i>	1.02	2.01	0.00934	0.302501
IVPP V 16923	<i>Linheraptor exquisitus</i>	1.22	2.42	0.087884	0.384288
IGM 100/1015	<i>Tsaagan mangas</i>	1.42	2.70	0.151636	0.431187
MPC-D 100/982	<i>Velociraptor</i> sp.	2.00	3.44	0.301384	0.53645
AMNH FARB 6515	<i>Velociraptor mongoliensis</i>	1.79	3.08	0.25248	0.488995
MPC-D 100/25	<i>Velociraptor mongoliensis</i>	1.56	2.81	0.192555	0.448478
MPC-D 100/54	<i>Velociraptor mongoliensis</i>	1.63	2.98	0.213124	0.474345
UALVP 49389	<i>Velociraptor</i> sp. (Cast)	1.63	2.81	0.210853	0.448524

Ordinary Least Squares Regression:

	MxL/H-PmxL/H	log transformed
95% bootstrapped confidence intervals (N=1999):		
Slope a:	(0.29666, 0.69088)	(0.36439, 1.2161)
Intercept b:	(-0.35824, 0.76665)	(-0.34596, 0.038313)
Correlation:		
r:	0.92096	0.89287
r²:	0.84817	0.79722
t:	6.685	5.6082
p		
(uncorr.):	0.000155	0.000505
Permutation		
p:	0.0002	0.0004

A 2.3. Length corrected measurements for PCA. All measurements were averaged from left and right sides then those that were used were divided by the length of the respective maxilla to remove size as a factor.

PCA All (Length corrected)		MxH	AntRL	AntRH.d	AntRH.p	AntFenL	AntFenH	AntFL	AntFH	AntAF-Mx	PIW	MxFen.L	MxFen.S	entMH.anentMH.po	L9Alv	ntFen.9Alv	
Specimen	Taxon																
TMP 1995.166.001	<i>Atraciraptor marshalli</i>	0.589365	0.319547	0.259675	0.426489	0.403545	0.426588	0.188774	0.456032	0.033973	0.05288	0.136583	0.098277	0.223535	0.137765	0.716613	0.139734
AMNH FARB 30556	<i>Bambiraptor feinbergi</i>	0.495989	0.231283	0.161001	0.33136	0.404698	0.381589	0.301566	0.407563	0.135982	0.04068	0.156226	0.08327	0.102559	0.044882	0.75	0.179335
YPM 5232 (557)	<i>Deinonychus antirrhopus</i>	0.58741	0.223022	0.195612	0.327698	0.514964	0.46554	0.300144	0.502158	0.177698	0.045252	0.114964	0.050576	0.164245	0.148201	0.695612	0.173885
UALVP 55700	<i>Saurornitholestes langstoni</i>	0.498309	0.283515	0.168704	0.352078	0.333039	0.345316	0.284295	0.422879	0.148624	0.023357	0.140717	0.071373	0.146075	0.058472	0.718306	0.073818
TMP 1994.12.844	<i>Saurornitholestes langstoni</i>	0.535247	0.310329	0.194169	0.342786	0.377178	0.399841	0.275367	0.457921	0.136659	0.047944	0.196789	0.073454	0.103063	0.062635	0.774172	0.067191
MNUFR 15	<i>Achillobator gigantius</i>	0.451308	0.294017	0.12033	0.337092	0.352058	0.314621	0.200365	0.340823	0.069276	0.14419	0.122077	0.047838	0.196633	0.151693	0.700385	0.138553
IVPP V 16923	<i>Linheraptor exquissitus</i>	0.412773	0.459406	0.174938	0.30417	0.29152	0.260711	0.24211	0.304214	0	0.090004	0.181241	0.093882	0.142807	0.077618	0.729416	0
IGM 100/1015	<i>Tsaagan mangas</i>	0.370521	0.380978	0.120677	0.29306	0.421459	0.234879	0.179721	0.278862	0	0.054679	0.112811	0.071946	0.138904	0.116313	0.702096	0.081347
MPC-D 100/982	<i>Velociraptor sp.</i>	0.29077	0.274081	0.12859	0.196302	0.373901	0.248082	0.3437	0.293367	0.203984	0.100456	0.069408	0.060507	0.06395	0.037618	0.694606	0
AMNH FARB 6515	<i>Velociraptor mongoliensis</i>	0.324344	0.314347	0.111062	0.179611	0.378172	0.202867	0.253653	0.324179	0.1165	0.043392	0.072723	0.068274	0.070252	0.023893	0.665989	0.042788
MPC-D 100/25	<i>Velociraptor mongoliensis</i>	0.356059	0.32466	0.134636	0.236461	0.375198	0.250132	0.268434	0.315929	0.111925	0.067119	0.099929	0.056403	0.090977	0.038322	0.692318	0.090757
MPC-D 100/54	<i>Velociraptor mongoliensis</i>	0.335471	0.329401	0.095702	0.232132	0.36587	0.236538	0.303554	0.29955	0.125955	0.067163	0.123605	0.068484	0.091345	0.036029	0.710202	0.077296
UALVP 49389	<i>Velociraptor sp. (Cast)</i>	0.356021	0.465969	0.128272	0.287958	0.518325	0.243455	0.054974	0.293194	0	0.033351	0.185864	0.036649	0.172775	0.08377	0.75	0.064136
MPC-D 100/1119	<i>Shanag ashile</i>	0.394112	0.25476	0.045142	0.105986	0.302257	0.305594	0.439647	0.317763	0.334053	0.038862	0.149951	0.07419	0.060255	0.029637	0.746222	0.062414
IVPP V 12811	<i>Sinornithosaurus millenii</i>	0.407702	0.169972	0.059215	0.137542	0.354713	0.240625	0.494716	0.340669	0.266541	0.099899	0.106124	0.057623	0.045461	0.016939	0.662661	0.022731
MMIL 195	<i>Austroraptor cabozai</i>	0.349289	0.401915	0.108443	0.186598	0.381173	0.253583	0.21053	0.296662	0	0.121207	0.09356	0.036095	0.110039	0.057413	0.484856	0.129185
CEUM 73719	<i>Geminiraptor saurezarum</i>	0.342105	0.147368	0.136842	0.215789	0.410316	0.167558	0.436842	0.236305	0.049411	0.104842	0.289474	0.115789	0.089474	0.063158	0.466632	0.154737
MPC-D 100/86	<i>Gobivenator mongoliensis</i>	0.325333	0.215319	0.134015	0.210496	0.545475	0.287092	0.382751	0.287092	0.086128	0.124368	0.200965	0.06695	0.110014	0.062242	0.425815	0.181787
AMNH FARB 6516	<i>Saurornithoides mongoliensis</i>	0.297286	0.353811	0.123845	0.277598	0.364665	0.191686	0.395612	0.211316	0.1597	0.044226	0.194226	0.086259	0.181871	0.098268	0.254273	0.496305
IVPP V 12615	<i>Sinovenator changii</i>	0.436782	0.235632	0.092476	0.233281	0.376959	0.318966	0.38767	0.383229	0.089864	0.036311	0.263323	0.182079	0.087774	0.044932	0.312696	0.366249
MPC-D 100/1	<i>Zanabazar junior</i>	0.283457	0.364795	0.127454	0.227093	0.226748	0.215122	0.410265	0.218395	0	0.080305	0.306321	0.089821	0.12866	0.073028	0.278333	0.498967

Summary scores for length corrected linear measurement PCA iterations.

Summaries for length corrected PCA iterations

PC	All taxa - Length Corrected+Al:C13		Eudromaeosauria - Length corrected	
	Eigenvalue	% variance	Eigenvalue	% variance
1	0.055975	46.074	0.033014	52.933
2	0.025197	20.74	0.016401	26.296
3	0.020839	17.153	0.005614	9.001
4	0.006443	5.3034	0.003242	5.1974
5	0.004276	3.5194	0.001453	2.3294
6	0.002393	1.97	0.001063	1.704
7	0.002237	1.8413	0.000664	1.0654
8	0.001143	0.9406	0.000413	0.66162
9	0.001084	0.89254	0.000276	0.44182
10	0.000777	0.63949	0.000184	0.29582
11	0.000354	0.29152	3.64E-05	0.058332
12	0.000293	0.24084	9.87E-06	0.015818
13	0.000232	0.19116		
14	1.10E-04	0.090303		
15	8.26E-05	0.067951		
16	5.40E-05	0.044435		

PC loadings for length corrected linear measurement PCA analyses.

PC loadings for Length corrected PCA		PC 1	PC 2	PC 3	PC 4	PC 5	PC 6	PC 7	PC 8	PC 9	PC 10	PC 11	PC 12	PC 13	PC 14	PC 15	PC 16
Loadings All Taxa Length-Corrected																	
MxH		0.22633	0.27696	0.40916	0.064177	-0.14017	-0.17012	-0.07361	0.1874	-0.03442	-0.38952	-0.32685	-0.24732	0.17975	-0.31483	0.28842	-0.27547
AntRL		0.038303	0.22001	-0.44602	0.37745	0.24571	-0.26141	0.15097	0.16058	0.53653	-0.00908	-0.13508	0.048047	0.30114	0.10516	0.13215	0.061075
AntRH.d		0.069881	0.21628	0.063021	-0.02635	-0.16221	0.11477	-0.12152	-0.36669	0.44328	0.34565	-0.18678	0.00985	-0.52366	-0.10191	0.34317	-0.40429
AntRH.p		0.12204	0.42072	0.081072	0.081392	-0.12272	0.38912	-0.10294	-0.4318	0.092094	-0.02118	0.34958	-0.06259	0.46219	0.16752	-0.15564	-0.17443
AntFenL		0.07244	0.097092	0.024349	-0.81848	0.26577	0.11383	0.31977	0.018284	0.18581	0.020958	-0.13841	0.045525	0.23665	-0.0105	0.10573	0.071704
AntFenH		0.17384	0.23009	0.36855	0.006589	0.10784	-0.25231	-0.00683	0.32073	0.13823	0.39778	0.25258	0.39074	-0.04246	-0.20563	-0.3703	-0.16658
AntFL		-0.25127	-0.38377	0.40369	0.10547	-0.23894	0.17379	-0.09357	0.019885	0.35948	0.12914	-0.40024	0.091203	0.35029	0.066485	-0.19301	0.20066
AntFH		0.20963	0.16214	0.35266	-0.01647	0.031022	-0.43073	-0.00509	-0.1343	-0.06174	0.021807	0.039277	-0.2185	-0.05987	0.53312	0.014663	0.50891
AntAF-MxFen		0.054383	-0.37737	0.37451	0.17956	0.51487	0.18611	0.10155	-0.02202	0.27577	-0.22514	0.37758	-0.06914	-0.1216	0.045887	0.25733	-0.12005
PIW		-0.0249	-0.0458	-0.05862	-0.12759	-0.15589	0.075245	-0.47542	0.4015	-0.01524	0.26483	0.34081	-0.0189	0.24135	0.017979	0.53072	0.18238
MxFen.L		-0.18132	0.11532	0.066109	0.036109	-0.50344	0.14349	0.6057	0.35465	0.157	-0.03508	0.2637	-0.19949	-0.16083	0.13723	0.038995	-0.00417
MxFen.S		-0.06065	0.029949	0.075926	0.044257	-0.21551	-0.12207	0.1604	-0.2292	-0.07476	-0.33794	0.11881	0.75002	0.060499	-0.0809	0.30758	0.21646
VentMH.ant		0.017336	0.25934	-0.02814	0.019783	0.10498	0.31789	-0.18818	0.17077	0.15818	-0.33446	0.064426	-0.06724	-0.19458	-0.36667	-0.2664	0.6048
VentMH.post		0.01984	0.18979	0.011381	-0.05095	0.066556	0.29565	-0.24905	0.34266	0.007746	-0.24746	-0.24266	0.31534	-0.2411	0.59732	-0.03869	-0.23139
L9Alv		0.69467	-0.13402	-0.03879	0.23862	-0.01221	0.37773	0.27518	0.097842	-0.24125	0.24857	-0.19435	0.10108	0.060005	-0.01343	0.099264	0.17691
AntFen.9Alv.L		-0.51146	0.36773	0.20759	0.23028	0.36524	0.19712	0.18232	0.020146	-0.35985	0.28513	-0.1731	0.008043	0.054003	-0.03347	0.21274	0.10506
Loadings Eudromaeosauria Length-cor																	
MxH		0.55315	0.080684	0.15241	0.019993	0.02488	-0.10825	0.0466	-0.36682	-0.01248	-0.12509	-0.06491	-0.31708				
AntRL		-0.21158	0.44963	0.21666	0.28469	0.19605	0.081755	0.26502	-0.24913	0.089643	0.40413	-0.24475	0.35039				
AntRH.d		0.20303	0.062437	0.17336	0.11989	0.35268	-0.21468	0.15515	0.49818	-0.34086	0.22906	-0.21145	-0.11828				
AntRH.p		0.32011	0.23619	0.20905	-0.1213	-0.18719	0.035936	-0.19476	0.42004	0.42358	-0.1111	-0.27712	0.24774				
AntFenL		0.089652	0.11852	-0.74183	0.34177	0.17084	0.12233	0.28578	0.15774	0.12295	-0.04629	0.10445	0.002801				
AntFenH		0.46847	-0.05272	-0.00154	0.083501	0.079649	0.23508	0.16817	0.17406	-0.12364	0.04888	0.016219	-0.17187				
AntFL		0.046402	-0.54645	0.27224	-0.04225	0.04159	0.060894	0.58134	-0.04998	0.39279	0.14542	0.012923	0.03778				
AntFH		0.40347	-0.11271	0.009517	0.22194	0.17966	-0.15729	-0.22896	-0.36583	-0.21156	-0.01342	0.1297	0.53021				
AntAF-MxFen		0.073325	-0.50918	-0.11651	0.15141	0.11505	0.33318	-0.39609	0.054427	0.13955	0.28469	-0.09957	0.15073				
PIW		-0.0446	-0.00843	0.087785	-0.41393	0.081186	0.53411	0.10759	0.033674	-0.53628	0.056214	0.067493	0.14498				
MxFen.L		0.075712	0.17539	0.1931	0.34068	-0.34402	0.37863	0.049989	-0.193	0.006922	0.078984	0.22265	-0.30892				
MxFen.S		0.023559	0.001143	0.16674	0.000746	-0.01621	-0.25134	0.21509	0.21502	-0.01273	-0.14457	0.67872	0.29874				
VentMH.ant		0.15029	0.27239	-0.0358	-0.29538	0.17131	0.086249	-0.23596	0.042193	0.29484	0.53042	0.47151	-0.11375				
VentMH.post		0.14161	0.18263	-0.13263	-0.38874	0.30554	0.26397	0.18698	-0.19104	0.2211	-0.38157	-0.10537	0.16347				
L9Alv		0.055264	0.076518	0.11412	0.29243	-0.32059	0.34582	0.01107	0.23734	-0.05059	-0.213	0.062496	0.27558				
AntFen.9Alv.L		0.2319	-0.00107	-0.33659	-0.28362	-0.60668	-0.18979	0.23932	-0.07122	-0.14527	0.38303	-0.15552	0.21261				

A 2.4. Length of the first nine alveoli corrected data for eudromaeosaurian specific PCA.

Measurements were averaged between left and right sides then divided by the length of the first nine maxillary alveolus to remove size affected data.

PCA Eudromaeosauria (L9Alv corrected)		MxH	AntRL	AntRH.d	AntRH.p	AntFenH	AntFL	AntFH	AntAF-Mx	PIW	MxFen.L	MxFen.S	entMH.anentMH.pontFen.9Alv
Specimen	Taxon												
ROM 63777	<i>Acheroraptor temertyorum</i>	0.723073	0.540045	0.196711	0.444012	0.46593	0.250314	0.519834	0.134446	0.057494	0.226588	0.06352	0.252573 0.219684 0.136455
TMP 1995.166.001	<i>Atrociraptor marshalli</i>	0.822432	0.445913	0.362365	0.595146	0.595284	0.263425	0.636371	0.047408	0.073792	0.190595	0.137141	0.311933 0.192244 0.194993
AMNH FARB 30556	<i>Bambiraptor feinbergi</i>	0.661319	0.308378	0.214668	0.441813	0.508785	0.402088	0.543417	0.181309	0.05424	0.208302	0.111026	0.136746 0.059842 0.239114
YPM 5232 (557)	<i>Deinonychus antirrhopus</i>	0.844451	0.320612	0.281208	0.471093	0.669252	0.431482	0.721895	0.255456	0.065053	0.16527	0.072707	0.236115 0.213052 0.249974
UALVP 55700	<i>Saurornitholestes langstoni</i>	0.693728	0.394699	0.234864	0.490151	0.480736	0.395785	0.588717	0.206909	0.032517	0.195901	0.099363	0.20336 0.081402 0.102767
TMP 1994.12.844	<i>Saurornitholestes langstoni</i>	0.69138	0.400853	0.250809	0.442777	0.516475	0.355693	0.591497	0.176523	0.06193	0.254192	0.094881	0.133127 0.080906 0.08679
MNUFR 15	<i>Achillobator giganticus</i>	0.644371	0.419794	0.171806	0.481295	0.449212	0.286079	0.486623	0.098912	0.205872	0.1743	0.068303	0.28075 0.216585 0.197823
IVPP V 16923	<i>Linheraptor exquisitus</i>	0.565895	0.629827	0.239833	0.417004	0.357423	0.331923	0.417064	0	0.123391	0.248474	0.128709	0.195782 0.106411 0
IGM 100/1015	<i>Tsaagan mangas</i>	0.527736	0.542629	0.171881	0.417407	0.33454	0.255978	0.397185	0	0.077879	0.160678	0.102473	0.197841 0.165665 0.115863
MPC-D 100/982	<i>Velociraptor sp.</i>	0.418612	0.394584	0.185126	0.282609	0.357155	0.494813	0.422349	0.293669	0.144622	0.099924	0.087109	0.092067 0.054157 0
AMNH FARB 6515	<i>Velociraptor mongoliensis</i>	0.48701	0.472	0.166763	0.269691	0.30461	0.380866	0.486763	0.174928	0.065155	0.109196	0.102515	0.105485 0.035876 0.064247
MPC-D 100/25	<i>Velociraptor mongoliensis</i>	0.5143	0.468947	0.194471	0.34155	0.361297	0.387732	0.456335	0.161666	0.096949	0.14434	0.08147	0.13141 0.055354 0.131091
MPC-D 100/54	<i>Velociraptor mongoliensis</i>	0.47236	0.463813	0.134753	0.326854	0.333058	0.427419	0.421781	0.17735	0.094569	0.174042	0.09643	0.128619 0.050731 0.108837
UALVP 49389	<i>Velociraptor sp. (Cast)</i>	0.474695	0.621291	0.17103	0.383944	0.324607	0.073298	0.390925	0	0.044468	0.247818	0.048866	0.230366 0.111693 0.085515
IMM99NM-BYM-3/3A	<i>Velociraptor osmolskae</i>	0.490323	0.461771	0.130954	0.327248	0.301853	0.403569	0.374605	0.134523	0.083596	0.181881	0.093205	0.170899 0.134523 0.018257

Summary scores for L9Alv corrected linear measurement PCA iterations.

Summaries for L9Alv corrected PCA iterations

PC	Eudromaeosauria - L9Alv corrected		Eudromaeosauria - L9Alv corrected - <i>Bambiraptor</i>	
	Eigenvalue	% variance	Eigenvalue	% variance
1	0.056381	56.257	0.058888	57.427
2	0.028016	27.954	0.028517	27.809
3	0.004807	4.7965	0.005152	5.0237
4	0.003686	3.678	0.00357	3.481
5	0.00255	2.5441	0.002022	1.972
6	0.001545	1.5419	0.00139	1.3555
7	0.001252	1.2491	0.00104	1.0138
8	0.000848	0.84588	0.000875	0.85352
9	0.000472	0.4705	0.000461	0.44923
10	0.000375	0.3739	0.000371	0.36137
11	0.000157	0.15626	0.000167	0.16249
12	9.71E-05	0.0969	6.14E-05	0.059833
13	3.37E-05	0.03362	3.23E-05	0.031463
14	2.50E-06	0.00249		

PC loadings for L9Alv corrected linear measurement PCA analyses.

PC loadings L9Alv corrected PCA		PC 1	PC 2	PC 3	PC 4	PC 5	PC 6	PC 7	PC 8	PC 9	PC 10	PC 11	PC 12	PC 13	PC 14
Eudromaeosauria	MxH	0.55276	0.08685	0.13591	0.11491	0.15534	0.15625	0.34831	0.011182	0.13507	-0.29057	-0.27707	0.44637	-0.19135	-0.26447
	AntRL	-0.21458	0.42855	0.29726	0.16348	0.30014	-0.21874	0.27881	0.40851	0.32535	0.30555	-0.1661	-0.16524	0.13409	-0.02388
	AntRH.d	0.20379	0.040765	0.36265	0.13786	-0.18112	-0.42708	-0.25276	0.068199	-0.24006	0.29358	0.000905	0.33654	-0.35368	0.37468
	AntRH.p	0.31346	0.22158	0.047832	0.15277	-0.37309	0.21904	-0.21975	-0.3403	0.34233	0.17713	-0.38634	-0.40095	0.003642	0.13096
	AntFenH	0.46849	-0.06708	0.056427	-0.01375	0.045904	0.030279	-0.23361	0.30011	-0.38013	0.32799	0.075773	-0.23273	0.26845	-0.49086
	AntFL	0.002941	-0.57632	0.10314	0.51267	-0.2025	0.11226	0.43973	0.075255	0.077431	0.19679	0.1952	-0.19405	-0.14467	0.018331
	AntFH	0.40351	-0.13671	0.21502	-0.15374	0.19358	-0.33068	-0.00323	0.057992	0.20209	-0.45692	0.28525	-0.40597	0.10835	0.30148
	AntAF-MxFen	0.066167	-0.50612	-0.07086	-0.0757	0.50075	0.085032	-0.27735	-0.03672	0.31961	0.31469	-0.25338	0.22368	0.18518	0.20678
	PIW	-0.03953	-0.01259	-0.31885	0.45224	-0.17661	-0.03308	-0.42397	0.54718	0.20011	-0.3515	-0.07636	0.10056	0.033335	0.001365
	MxFen.L	0.049301	0.16484	0.26324	-0.12442	-0.00028	0.72977	-0.05401	0.31841	-0.03043	0.027242	0.30506	0.088892	0.020722	0.38169
	MxFen.S	0.011705	-0.01152	0.17268	0.13477	-0.30634	-0.09703	0.1544	-0.12742	-0.07127	-0.07026	-0.02786	0.31983	0.82129	0.14426
	VentMH.ant	0.16336	0.27537	-0.23296	0.24287	0.11616	-0.06062	-0.09846	-0.2874	0.34287	0.22826	0.66496	0.21203	0.032845	-0.12996
	VentMH.post	0.15706	0.20787	-0.4107	0.38297	0.37899	0.045364	0.17425	-0.09994	-0.46914	0.004036	-0.12238	-0.14994	0.064301	0.41114
	AntFen.9Alv.L	0.2578	0.007126	-0.52015	-0.42606	-0.31668	-0.13582	0.34254	0.32013	0.15459	0.26303	-0.01209	0.07091	-0.00239	0.21117
	Eudromaeosauria A60:P63- Bambrapt	MxH	0.55979	-0.04832	-0.12209	0.064339	0.28573	0.28885	-0.12505	0.059083	0.041754	-0.38959	-0.21097	-0.4265	-0.09755
		AntRL	-0.1773	-0.41301	-0.27142	0.033727	0.17225	0.42019	0.35949	0.27419	0.45809	0.1044	-0.17043	0.24466	0.052992
AntRH.d		0.20968	-0.02032	-0.35179	0.18788	-0.3559	-0.04853	0.4422	-0.15656	-0.01502	0.25688	0.030401	-0.46977	-0.19556	
AntRH.p		0.32239	-0.21015	-0.05014	0.30242	-0.13459	-0.36194	-0.3972	-0.1447	0.31889	0.11287	-0.43386	0.3051	-0.07019	
AntFenH		0.46314	0.092275	-0.05518	-0.02694	0.04846	-0.18711	0.3196	0.1496	-0.21295	0.45859	0.036607	0.29608	0.15955	
AntFL		-0.02548	0.58599	-0.06722	0.55913	0.10252	0.35358	-0.19945	0.1643	0.096061	0.22229	0.16185	0.12435	-0.18307	
AntFH		0.40199	0.17405	-0.21005	-0.25875	-0.16105	0.11769	0.10695	0.058255	-0.02866	-0.44058	0.25417	0.48666	-0.02533	
AntAF-MxFen		0.044331	0.52442	0.087607	-0.29665	0.33432	-0.21123	0.21613	-0.13483	0.49704	0.054325	-0.21311	-0.14535	0.24536	
PIW		-0.03448	0.0228	0.35039	0.44974	-0.08632	-0.35273	0.38991	0.45451	0.048046	-0.42004	-0.04756	-0.02652	0.032423	
MxFen.L		0.050836	-0.17819	-0.28323	-0.02886	0.46253	-0.32903	-0.25252	0.46721	-0.11371	0.14798	0.29371	-0.17097	0.11695	
MxFen.S		0.008006	0.006039	-0.17338	0.26282	-0.20286	0.14623	-0.10059	-0.10759	-0.06321	-0.08934	0.016054	-0.07927	0.8929	
VentMH.ant	0.18669	-0.24865	0.25813	0.14479	0.069636	-0.04192	0.008649	-0.30595	0.45679	0.014925	0.70001	-0.03782	0.015917		
VentMH.post	0.18014	-0.17361	0.45353	0.17288	0.4151	0.24437	0.1957	-0.25971	-0.36385	0.12618	-0.14257	0.10605	0.067683		
AntFen.9Alv.L	0.23968	-0.03211	0.46949	-0.27683	-0.39197	0.26947	-0.19354	0.45546	0.15419	0.2817	-0.02453	-0.1857	0.088628		

A 2.5 Ratio-based character analysis. Characters modified from Currie and Evans (2019) based on analysis of the range of variation for the described ratio-based characters.

Character 8: Antorbital fenestra: elongate [0], antorbital fenestra at least 1.33 times

anteroposteriorly long as dorsoventrally tall; or short [1], less than 1.33 times as long as tall. (The threshold value for this character was modified from a length-to-height ratio of 1 (Currie and Evans 2019) to based on the data distribution observed in this study.)

**Character 8 - Currie and Evans 2019
Raw Data**

Specimen	Taxon	AntFenL/ H	Location N. Americ	Character coding (k=2)
CEUM 73719	<i>Geminiraptor saurezarum</i>	2.45	a	0
UALVP 49389	<i>Velociraptor</i> sp. (Cast)	2.13	Asia	0
AMNH FARB 6516	<i>Saurornithoides mongoliensis</i>	1.90	Asia	0
MPC-D 100/86	<i>Gobivenator mongoliensis</i>	1.90	Asia	0
AMNH FARB 6515	<i>Velociraptor mongoliensis</i>	1.86	Asia	0
IGM 100/1015	<i>Tsaagan mangas</i>	1.79	Asia	0
MPC-D 100/54	<i>Velociraptor mongoliensis</i>	1.55	Asia	0
MPC-D 100/982	<i>Velociraptor</i> sp.	1.51	Asia	0
MML 195	<i>Austroraptor cabazai</i>	1.50	a	0
MPC-D 100/25	<i>Velociraptor mongoliensis</i>	1.50	Asia	0
IVPP V 12811	<i>Sinornithosaurus millenii</i>	1.47	Asia	0
IVPP V 12615	<i>Sinovenator changii</i>	1.18	Asia	1
MNUFR 15	<i>Achillobator giganticus</i>	1.12	Asia	1
IVPP V 16923	<i>Linheraptor exquisitus</i>	1.12	Asia	1

YPM 5232 (557)	<i>Deinonychus antirrhopus</i>	1.11	N. Americ a	1
AMNH FARB 30556	<i>Bambiraptor feinbergi</i>	1.06	N. Americ a	1
MPC-D 100/1	<i>Zanabazar junior</i>	1.05	Asia	1
MPC-D 100/1119	<i>Shanag ashile</i>	0.99	Asia	1
UALVP 55700	<i>Saurornitholestes langstoni</i>	0.96	N. Americ a	1
TMP 1995.166.001	<i>Atrociraptor marshalli</i>	0.95	N. Americ a	1
TMP 1994.012.0844	<i>Saurornitholestes langstoni</i>	0.94	N. Americ a	1

Results of Jenks optimization.

Jenks Results

Jenks Natural Breaks Optimization
1000

iterations	k=2		
<i>class</i>	<i>lower</i>	<i>upper</i>	<i>count</i>
1	0.943321	1.181818	10
2	1.474128	2.4488	11
GVF	1.046483	3.8442	0.727776

Character 20: Premaxilla: long [0], at least 15% length of maxilla; or short [1], no more than 15% length of maxilla. (The threshold between the states of this character is unmodified from Currie and Evans (2019), but the wording has changed slightly to clarify that the character does not actually pertain to the shape of the premaxilla.)

**Character 20 - Currie and
Evans 2019
Raw Data**

GVF	0.008911	0.070364354	0.87
-----	----------	-------------	------

Character 22: Premaxilla, main body below external naris: elongate [0], at least 1.35 times as anteroposteriorly long as dorsoventrally tall; or short [1], less than 1.35 times as long as tall. (The threshold was moved from a length to height ratio of 1 to 1.35 to reflect the data)

**Character 22 - Currie and Evans 2019
Raw Data**

Specimen	Taxon	PmxL/Pmx H	Location	Character coding (k=2)
IVPP V 12811	<i>Sinornithosaurus millenii</i>	3.83	Asia	0
MPC-D 100/982	<i>Velociraptor</i> sp.	2.00	Asia	0
AMNH FARB 6515	<i>Velociraptor mongoliensis</i>	1.79	Asia	0
MPC-D 100/54	<i>Velociraptor mongoliensis</i>	1.63	Asia	0
UALVP 49389	<i>Velociraptor</i> sp. (Cast)	1.63	Asia	0
AMNH FARB 30556	<i>Bambiraptor feinbergi</i>	1.57	N. America	0
MPC-D 100/25	<i>Velociraptor mongoliensis</i>	1.56	Asia	0
IGM 100/1015	<i>Tsaagan mangas</i>	1.42	Asia	0
YPM 5232 (237)	<i>Deinonychus antirrhopus</i>	1.28	N. America	1
BYUVP 14585 F#1984	<i>Utahraptor ostrommaysi</i>	1.28	Asia	1
IVPP V 16923	<i>Linheraptor exquisitus</i>	1.22	N. America	1
AMNH FARB 5356	<i>Dromaeosaurus albertensis</i>	1.12	N. America	1
UALVP 55700	<i>Saurornitholestes langstoni</i>	1.02	Asia	1
IVPP V 12615	<i>Sinovenator changii</i>	1.00	Asia	1

TMP 1995.166.001	<i>Atrociraptor marshalli</i>	0.96	N. Americ a	1
CEUM 01430	<i>Utahraptor ostrommaysi</i>	0.94	N. Americ a	1
MPC-D 100/1	<i>Zanabazar junior</i>	0.68	Asia	1
AMNH FARB 6516	<i>Sauornithoides mongoliensis</i>	0.62	Asia	1

Results of Jenks Optimization

Jenks Natural Breaks Optimization

1000 iterations		k=2 (without <i>Sinornithosaurus</i>)		
<i>class</i>	<i>lower</i>	<i>upper</i>	<i>count</i>	
1	0.62004662	1.283688	10	
2	1.417868449	2.001629	7	
GVF	0.686626062	2.388835	0.712569	

Character 28: Anterior ramus: intermediate [0], between 26% and 37% of the total length of the maxilla; short [1], less than 26% of the total length of the maxilla; or long [2], greater than 37% of the total length of the maxilla. (Character was modified to be multistate due to better goodness of variance fit. The threshold was moved from 0.25 to 0.26 and the threshold between [0] and [2] was placed as 0.37 based on the data.)

Character 28 - Currie and Evans 2019 Raw Data

Specimen	Taxon	AntRL/MxL	Location	Character coding (K=3)
UALVP 49389	<i>Velociraptor</i> sp. (Cast)	0.47	Asia	2
IVPP V 16923	<i>Linheraptor exquisitus</i>	0.46	Asia	2
MML 195	<i>Austroraptor cabazai</i>	0.40	S. America	2
IGM 100/1015	<i>Tsaagan mangas</i>	0.38	Asia	2

MPC-D 100/1	<i>Zanabazar junior</i>	0.36	Asia	0
	<i>Saurornithoides</i>			
AMNH FARB 6516	<i>mongoliensis</i>	0.35	Asia	0
MPC-D 100/25	<i>Velociraptor mongoliensis</i>	0.33	Asia	0
MPC-D 100/54	<i>Velociraptor mongoliensis</i>	0.33	Asia	0
			N.	
TMP 1995.166.001	<i>Atrociraptor marshalli</i>	0.32	America	0
AMNH FARB 6515	<i>Velociraptor mongoliensis</i>	0.31	Asia	0
			N.	
TMP 1994.12.844	<i>Saurornitholestes langstoni</i>	0.31	America	0
MNUFR 15	<i>Achillobator giganticus</i>	0.29	Asia	0
			N.	
UALVP 55700	<i>Saurornitholestes langstoni</i>	0.28	America	0
MPC-D 100/982	<i>Velociraptor sp.</i>	0.27	Asia	0
MPC-D 100/1119	<i>Shanag ashile</i>	0.25	Asia	1
IVPP V 12615	<i>Sinovenator changii</i>	0.24	Asia	1
			N.	
AMNH FARB 30556	<i>Bambiraptor feinbergi</i>	0.23	America	1
			N.	
YPM 5232 (557)	<i>Deinonychus antirrhopus</i>	0.22	America	1
MPC-D 100/86	<i>Gobivenator mongoliensis</i>	0.22	Asia	1
			N.	
AMNH FARB 5356	<i>Dromaeosaurus albertensis</i>	0.18	America	1
			N.	
BYUVP 19965 F# 4252	<i>Utahraptor ostrommaysi</i>	0.18	America	1
IVPP V 12811	<i>Sinornithosaurus millenii</i>	0.17	Asia	1
			N.	
CEUM 73719	<i>Geminiraptor suarezarum</i>	0.15	America	1

Results of Jenks optimization.

Jenks Results

Jenks Natural Breaks Optimization

1000

iterations k=2

<i>class</i>	<i>lower</i>	<i>upper</i>	<i>count</i>
1	0.147368421	0.28351454	11.00
2	0.29401723	0.465968586	12.00
GVF	0.054969285	0.17197069	0.68

1000

iterations k=3

<i>class</i>	<i>lower</i>	<i>upper</i>	<i>count</i>
--------------	--------------	--------------	--------------

1	0.147368421	0.254759568	9.00
2	0.274080746	0.36479504	10.00
3	0.380977505	0.465968586	4.00
GVF	0.023176393	0.17197069	0.87

Character 29: Anterior ramus shape: elongate [0], between 1.12 and 1.95 times as anteroposteriorly long as dorsoventrally tall; short [1], less than 1.12 times as long as tall; or hyperelongate [2], greater than 1.95 times as long as tall. (The threshold between [1] and [0] from 1 to 1.12 to reflect the data and an additional state was added due to better goodness of variance fit. The threshold between [0] and [2] was set as 1.95 based on the data).

**Character 29 - Currie and Evans 2019
Raw Data**

Specimen	Taxon	AntRL/AntRH .p	Location	Character coding (k=3)
MPC-D 100/1119	<i>Shanag ashile</i>	2.40	Asia	2
MML 195	<i>Austroraptor cabazai</i>	2.15	S. America	2
AMNH FARB 6515	<i>Velociraptor mongoliensis</i>	1.75	Asia	0
UALVP 49389	<i>Velociraptor</i> sp. (Cast)	1.62	Asia	0
MPC-D 100/1	<i>Zanabazar junior</i>	1.61	Asia	0
IVPP V 16923	<i>Linheraptor exquisitus</i>	1.51	Asia	0
MPC-D 100/54	<i>Velociraptor mongoliensis</i>	1.42	Asia	0
IMM99NM-BYM-3/3A	<i>Velociraptor osmolskae</i>	1.41	Asia	0
MPC-D 100/25	<i>Velociraptor mongoliensis</i>	1.40	Asia	0
MPC-D 100/982	<i>Velociraptor</i> sp.	1.40	Asia	0
IGM 100/1015	<i>Tsaagan mangas</i>	1.30	Asia	0
AMNH FARB 6516	<i>Saurornithoides mongoliensis</i>	1.27	Asia	0

IVPP V 12811	<i>Sinornithosaurus millenii</i>	1.24	Asia N.	0
ROM 63777	<i>Acheroraptor temertyorum</i>	1.22	Americ a	0
MPC-D 100/86	<i>Gobivenator mongoliensis</i>	1.02	Asia	1
IVPP V 12615	<i>Sinovenator changii</i>	1.01	Asia N.	1
TMP 1994.12.844	<i>Saurornitholestes langstoni</i>	0.91	Americ a	1
MNUFR 15	<i>Achillobator giganticus</i>	0.87	Asia N.	1
UALVP 55700	<i>Saurornitholestes langstoni</i>	0.81	Americ a N.	1
TMP 1995.166.001	<i>Atrociraptor marshalli</i>	0.75	Americ a N.	1
AMNH FARB 30556	<i>Bambiraptor feinbergi</i>	0.70	Americ a N.	1
CEUM 73719	<i>Geminiraptor suarezarum</i>	0.68	Americ a N.	1
YPM 5232 (557)	<i>Deinonychus antirrhopus</i>	0.68	Americ a	1

Results of Jenks Optimization.

Jenks Natural Breaks Optimization			
1000 iterations			
	<i>k=2</i>		
<i>class</i>	<i>lower</i>	<i>upper</i>	<i>count</i>
1.00	0.68	1.022913257	9
2.00	1.22	2.403703704	14
GVF	1.72	4.594791204	0.625693
1000 iterations			
	<i>k=3</i>		
<i>class</i>	<i>lower</i>	<i>upper</i>	<i>count</i>
1	0.680570801	1.022913257	9
2	1.216284987	1.750152905	12
3	2.153910849	2.403703704	2

GVF	0.48	4.594791204	0.89573
------------	-------------	--------------------	----------------

Character 181: Maxilla shape: elongate [0], maxilla at least 2.62 times as anteroposteriorly long as dorsoventrally tall; or short [1], less than 2.62 times as long as tall.

**New Character Max L/H Ratio
Raw Data**

Specimen	Taxon	MxL/Mx H	Location	Character coding (k=2)
MPC-D 100/1	<i>Zanabazar junior</i>	3.53	Asia	0
MPC-D 100/982	<i>Velociraptor</i> sp. <i>Sauornithoides</i>	3.44	Asia	0
AMNH FARB 6516	<i>mongoliensis</i> <i>Velociraptor</i>	3.36	Asia	0
AMNH FARB 6515	<i>mongoliensis</i> <i>Gobivenator</i>	3.08	Asia	0
MPC-D 100/86	<i>mongoliensis</i> <i>Velociraptor</i>	3.07	Asia	0
MPC-D 100/54	<i>mongoliensis</i>	2.98	Asia	0
CEUM 73719	<i>Geminiraptor</i> <i>suarezarum</i>	2.92	N. America	0
MML 195	<i>Austroraptor cabazai</i>	2.86	a	0
UALVP 49389	<i>Velociraptor</i> sp. (Cast) <i>Velociraptor</i>	2.81	Asia	0
MPC-D 100/25	<i>mongoliensis</i>	2.81	Asia	0
IGM 100/1015	<i>Tsaagan mangas</i>	2.70	Asia	0
MPC-D 100/1119	<i>Shanag ashile</i> <i>Sinornithosaurus</i>	2.54	Asia	1
IVPP V 12811	<i>millenii</i>	2.45	Asia	1
IVPP V 16923	<i>Linheraptor exquisitus</i>	2.42	Asia	1
IVPP V 12615	<i>Sinovenator changii</i>	2.29	Asia	1
MNUFR 15	<i>Achillobator giganteus</i>	2.22	Asia	1
AMNH FARB 30556	<i>Bambiraptor feinbergi</i>	2.02	N. America	1

UALVP 55700	<i>Saurornitholestes langstoni</i>	2.01	N. Americ a	1
TMP 1994.12.844	<i>Saurornitholestes langstoni</i>	1.87	N. Americ a	1
YPM 5232 (557)	<i>Deinonychus antirrhopus</i>	1.70	N. Americ a	1
TMP 1995.166.001	<i>Atrociraptor marshalli</i>	1.70	N. Americ a	1

Results of Jenks Optimization.

Jenks Results

Jenks Natural Breaks Optimization

1000 k=2

<i>class</i>	<i>lower</i>	<i>upper</i>	<i>count</i>
1	1.696742	2.54	10.00
2	2.6989	3.53	11.00
GVF	1.630377	6.17	0.74

Character 182: Antorbital fossa shape: elongate [0], distance from anterior margin to most anterior posterior margin at least 1.13 times dorsoventral height exposed on maxilla; short [1], distance less than 1.13 times height exposed on maxilla.

New Character Antorbital Fossa L/H Ratio

Raw Data

Specimen	Taxon	AntFL/H	Location	Character coding (k=2)
MPC-D 100/1	<i>Zanabazar junior</i>	1.88	Asia	0
AMNH FARB 6516	<i>Saurornithoides mongoliensis</i>	1.87	Asia	0
CEUM 73719	<i>Geminiraptor suarezarum</i>	1.85	N. America	0
IVPP V 12811	<i>Sinornithosaurus millenii</i>	1.45	Asia	0
MPC-D 100/1119	<i>Shanag ashile</i>	1.38	Asia	0

MPC-D 100/86	<i>Gobivenator mongoliensis</i>	1.33	Asia	0
MPC-D 100/982	<i>Velociraptor</i> sp.	1.17	Asia	0
IMM99NM-BYM-3/3A	<i>Velociraptor osmolskae</i>	1.08	Asia	1
IVPP V 12615	<i>Sinovenator changii</i>	1.01	Asia	1
MPC-D 100/25	<i>Velociraptor mongoliensis</i>	0.85	Asia	1
IVPP V 16923	<i>Linheraptor exquisitus</i>	0.80	Asia	1
AMNH FARB 6515	<i>Velociraptor mongoliensis</i>	0.78	Asia	1
MPC-D 100/54	<i>Velociraptor mongoliensis</i>	0.78	Asia	1
AMNH FARB 30556	<i>Bambiraptor feinbergi</i>	0.74	America S.	1
MML 195	<i>Austroraptor cabazai</i>	0.71	America N.	1
UALVP 55700	<i>Saurornitholestes langstoni</i>	0.67	America	1
IGM 100/1015	<i>Tsaagan mangas</i>	0.64	Asia N.	1
TMP 1994.12.844	<i>Saurornitholestes langstoni</i>	0.60	America N.	1
YPM 5232 (557)	<i>Deinonychus antirrhopus</i>	0.60	America	1
MNUFR 15	<i>Achillobator giganticus</i>	0.59	Asia N.	1
ROM 63777	<i>Acheroraptor temertyorum</i>	0.48	America N.	1
TMP 1995.166.001	<i>Atrociraptor marshalli</i>	0.41	America	1
UALVP 49389	<i>Velociraptor</i> sp. (Cast)	0.19	Asia	1

Results of Jenks Optimization.

Jenks Results

Jenks Natural Breaks Optimization

1000 k=2

<i>class</i>	<i>lower</i>	<i>upper</i>	<i>count</i>
1	0.192378	1.077318	16
2	1.171573	1.878549	7
GVF	1.232938	4.996524	0.753241

A 2.6 Character-taxon data matrix modified from Currie and Evans (2019) to reflect analysis of ratio-based characters outlined above.

Acheroraptor_temertyorum

????20?111100?????????01?00001????????????????????????????????1111?101??1???10000
?001002100??
????????????1

Achillobator_giganticus

?????001?????0??????1?????001001??1???1000?1
?0?0?20????0100111?1???1?01?????0????????????????11001120020011100012111100???10??0??
?????1?11????11

Adasaurus_mongoliensis

????????????????001????????????????????????1?1?11110?1?01??100??1????????????????????????
??????0??10011?1???0?11?1?10??01????????????????1100100002001211??1111001?111101001
101111?011?0????

Archaeopteryx_lithographica

01?012??000000100?000?000000?0000?000000??00?000?0?00??????0?1??000001010000000
0001202210020001?0?1000?00000000000?000000110001000000?00000000020001000000?01
0?01?000??0000?000110??

Atrociraptor_marshalli

???11111011211?????0110000101001????????????????????????????????????00000101??11?1100
101011002100??
?????????????11

Austroraptor_cabazai

1???0200002000??1???0??010220100?0?11????00?0????????????????????????0?1?110?????01100
12?22100200?11??11?01????????????11??
????1?00????01

Bambiraptor_feinbergi

0??01111011200111??01000000110000?010?00?000101111100????010?1???0?1101011?111?1
00101011?011001001?011111?011102?1101101001010100111?0000000000120011101100101
?0100000001010011011??11

Baynshire_nov._sp.

????11????2?0????011?10?011001?????????1????????????????????00??101011?11?11000
01101002000?????111110??1102?????0100??1010000????0000?????11111111001?1?01000
011010000?0100????

Boreonykus_certekorum

?????????????01?????????????????211???1??0??
????20?????????????????1?0??
??1??????

Buitreraptor_gonzalezorum

1???0????20?001?1???????10??00000?0001?0010??000?????????????0??00110??0??01??0
0222100200011??1100?00?00?011?010?011010?????????????011??1??1?010110000?100?1101?
00??0??????????????

Byronosaurus_jaffei

???120??02000?????10?111????0100?1?1?????????????????0?10?00?1?11?001110001?2?00011
002022110211??01?00?????0?1??
??????0???????

Changyuraptor_yangi

0?????????2??
?????????????????????2?????0?????1?????????????????1?????????????1????????????????
?????0??

Dakotaraptor_steini

??
0??21?????????1?????1??2????????00?0?????????????????????????????????????010?0???0??0??
????0?????

Deinonychus_antirrhopus

??00211011200??1?10110000011001110??1?1??1010110??01?01?????????1000001011111011
001010010021001001101110110?11021??11111000010100001100000002001?0110111110001
10100000101010011010??11

Dromaeosaurus_albertensis

???0100?0???0000111011??0?0110?1????2111?010???101010101?00000000000001011110011
00001101002000??10??
1?11?101?11??????

Graciliraptor_lujiatensis

??01???01??
?0?21?????????????0??0?02?????????0?001?1111????????????????????????????????1??1101?????00
00?00??????

Halzskaraptor_escuilliei

0101?2????1210100??00010?0?00?000?01?0110000100????????????????????0000010?????0?011
0002?2210020?00?00?100???1?????011???????0??111?011?0?0000?????????????????????00?110
?0??000101?0?0????

Hesperonychus_elizabethae

??
??
??????????

Hulsanpes_perlei

??
??00?1??00?000?0??
??????????

Linheraptor_exquisitus

00?00211011101?11??011110102001100011111?111111001?10???0110??1?1111010111?1?1
10000100000130010?1???1?????1?2?1????1????????????????????????????00?2????????????????
??????0??????????11

Mahakala_omnogovae

?????????????100????????????????????000?????????0?0001?????00?????????????????1???02
?22?02?0?????????????10?100?????????????0?????????0?0000?????????????????0?0?10?00?00
0??01001?????

Microraptor_zhaoianus

01?0100?0???0???001?00???1?1?0??00?01?????0?1?????????????????000101011??100(0
1)0100100?0?1300?01010100?000?00?211 {0
1}1??00011001011111?0?000?0111020001000000?01001111?00?11000?00?110??

Neuquenraptor_argentinus

??
??
?00??????

Rahonavis_ostromi

??
????????????????110000110001?????0?011?????001100011000010201?00?00011011001000
10010?001?????

Sauornitholestes_langstoni

000101010112100111101100001010010101011110101011111????1????????10011010111111
10000101100210010011011111011102111?11010000101010111000000020012001010110010
100100000001010011010??11

Shanag_ashile

??????11?112?0?????1???00012100?????????????????????????????????????000001?????01?100
100?011101??
??????????10

Sinornithosaurus_millenii

0??000?001111??11??010??0??101?00?000011????10?10?????????????1???000101011111?010
1001001002100??????0?0000??2?1??0001?110010111111?0?00??111020001000000??00?1
?11?00?10?00?00?1??10

Sinovenator_changii

?1?01201002000100??1010010011000??1?100??00?????1000010?00?0111?00110000??0?00
100?1?00?013?1?1??11000?0000????????11?????0??0?????0?0?0?00120001001??00010100
?1010001??0?000??11

Appendix 3

A 3.1. Raw data for PCA and quadrateH/maxillaH RMA

Raw data for PCA and quadrate measurements for regression analyses performed in Chapter 4.

PCA data.

Specimen	Taxon	Length	Height	Anterior F	Ant. Proc.	Ant. Proc.	Antorbital	Antorbital	Antorbital	Mx. Fen. T	Mx. Fen. L	Mx. Fen. S	Ventral M	Ventral M	Length fir	Width Pre	Dist. Ant n
MPC-D 10	<i>V. rostrav</i>	98.565	27.44	25.865	12.135	18.525	23.4115	32.435	27.685	19.25	6.55	5.71	6.035	3.55	65.55	9.48	0
AMNH 65	<i>V. mongo</i>	91.03	29.525	28.615	10.11	16.35	18.467	23.09	29.51	10.605	6.62	6.215	6.395	2.175	60.625	3.95	3.895
Moscow	<i>V. mongo</i>	99.73	31.965	31.21	13.48	20.31	20.33	26.025	26.95	10.62	10.06	5.39	8.12	4.54	67.35	6.88	9.1
MPC-D 10	<i>V. mongo</i>	113.38	41.225	36.81	15.265	26.81	28.36	30.435	35.82	12.69	11.33	6.395	10.315	4.345	78.495	7.61	10.29
MPC-D 10	<i>V. mongo</i>	104.87	34.265	33.645	9.775	23.71	24.16	31.005	30.596	12.865	12.625	6.995	9.33	3.68	72.54	6.86	7.895
IMM99NN	<i>V. osmolsi</i>	109.96	35.72	33.64	9.54	23.84	21.99	29.4	27.29	9.8	13.25	6.79	12.45	9.8	72.85	6.09	1.33
MPC-D 10	<i>T. mangas</i>	104.245	38.625	39.715	12.58	30.55	24.485	18.735	29.07	0	11.76	7.5	14.48	12.125	73.19	5.7	8.48
IVPP V169	<i>L. exquisit</i>	113.44	46.825	52.115	19.845	34.505	29.575	27.465	34.51	0	20.56	10.65	16.2	8.805	82.745	10.21	0

L9Alv corrected data for MOR 553S-7.30.91.274 used with eudromaeosaurian data from A 2.4.

Specimen	Taxon	MxH	AntRL	AntRH.d	AntRH.p	AntFenH	AntFL	AntFH	AntAF-Mx	PIW	MxFen.L	MxFen.S	VentMH.a	VentMH.p	AntFen.9A
MOR 553S	Bambirap	0.728921	0.279994	0.245845	0.466606	0.551073	0.377758	0.626624	0.208824	0.066636	0.125718	0.10683	0.244485	0.048957	0.342248

Quadrate measurements for RMA.

Specimen	Quadrate height
AMNH FARB 6515	27.12
IGM 100/982	33.75
GIN 100/25	39.36
MPC D 100/54	33.7
Moscow Specimen	35.24

A 3.2. Finalized character list including support for ratio-based characters

Character-taxon data matrix for analysis of Eudromaeosauria and the inclusion of the new taxon, *Velociraptor vadarostrum*. Most characters were derived from Currie and Evans (2019) and ones that have been modified are indicated in brackets following the character description. For Ratio-based characters of the maxilla, data has been provided below with Jenks Natural Breaks Optimization results indicating justification for cut-offs between character states. Characters that were removed from the data set used by Currie and Evans (2019) are listed following the list of characters below. Justification for removal of maxilla and tooth characters is presented in Chapter 2 of this thesis whereas other ones removed were due to redundancy.

1. Skull length: 0, less than 125% length of femur; 1, at least 125% length of femur (*Velociraptor vadarostrum* coded as [1] as opposed to [0] coded for *V. mongoliensis*).
2. Skull height ratio, mid-naris level compared with mid-orbital level: 0, more than half; 1, less than half
3. Antorbital skull length to femur length ratio: 0, less than 60%; 1, more than 60%.
4. Narial opening, posterior margin; 0, posterior to PM-Max suture on alveolar margin; 1, well posterior
5. Antorbital fossa, anterior margin is level with or just posterior to: 0, 3rd maxillary alveolus; 1, 4th alveolus; 2, 5th or any alveolus posterior to the 5th (Modified from Currie and Evans 2019).
6. Antorbital fossa, ventral margin: 0, extends onto posterior half of the maxilla (jugal ramus) and is visible in lateral view; 1, does not extend onto the jugal process, antorbital fossa restricted ventrally by a ventrolateral sloped surface; 2, does not extend onto the jugal process, antorbital

fossa restricted ventrally by a sharp dorsoventral lamina. (This character was modified from Currie and Evans 2019 to accommodate the distinction between *Acheroraptor temertyorum* and *Achillobator giganticus* [1] from *Linheraptor exquisitus*, *Tsaagan mangas*, and *Velociraptor osmolskae* [2]. Unenlagiines and troodontids were also coded as [2].)

7. Antorbital fossa shape: elongate [0], distance from anterior margin to most anterior posterior margin at least 1.13 times dorsoventral height exposed on maxilla; short [1], distance less than 1.13 times height exposed on maxilla. (New Character based on distribution of ratios for this character across the study group. *Byronosaurus jaffei* was excluded from the Jenks Optimization due to it being an outlier (2.53) from the rest of the data (0.19-1.88). Removal improved GVF and *Byronosaurus jaffei* was coded as [0]).

Specimen	Taxon	AntFL/H	k=2 - <i>Byronosaurus</i>
MPC-D 100/983	<i>Byronosaurus jaffei</i>	2.53	0
MPC-D 100/1	<i>Zanabazar junior</i>	1.88	0
	<i>Saurornithoides</i>		
AMNH FARB 6516	<i>mongoliensis</i>	1.87	0
CEUM 73719	<i>Geminiraptor suarezarum</i>	1.85	0
MPC-D 102/109	<i>Halszkaraptor escuilliei</i>	1.62	0
IVPP V 12811	<i>Sinornithosaurus millenii</i>	1.45	0
MPC-D 100/1119	<i>Shanag ashile</i>	1.38	0
MPC-D 100/86	<i>Gobivenator mongoliensis</i>	1.33	0
MPC-D 100/982	<i>Velociraptor vadarostrum</i>	1.17	0
IMM99NM-BYM-3/3A	<i>Velociraptor osmolskae</i>	1.08	1
STM1-3	<i>Tianyuraptor ostromi</i>	1.07	1
IVPP V 12615	<i>Sinovenator changii</i>	1.01	1
	<i>Archaeopteryx</i>		
5th Eichstatt skeleton	<i>lithographica</i>	0.88	1
MPC-D 100/25	<i>Velociraptor mongoliensis</i>	0.85	1
IVPP V 16923	<i>Linheraptor exquisitus</i>	0.80	1
AMNH FARB 6515	<i>Velociraptor mongoliensis</i>	0.78	1
MPC-D 100/54	<i>Velociraptor mongoliensis</i>	0.78	1
AMNH FARB 30556	<i>Bambiraptor feinbergi</i>	0.74	1
MML 195	<i>Austroraptor cabazai</i>	0.71	1
UALVP 55700	<i>Saurornitholestes langstoni</i>	0.67	1

JPM - 0008	<i>Zhenyuanlong suni</i>	0.67	1
IGM 100/1015	<i>Tsaagan mangas</i>	0.64	1
TMP 1994.12.844	<i>Saurornitholestes langstoni</i>	0.60	1
YPM 5232 (557)	<i>Deinonychus antirrhopus</i>	0.60	1
MNUFR 15	<i>Achillobator giganticus</i>	0.59	1
ROM 63777	<i>Acheroraptor temertyorum</i>	0.48	1
TMP 1995.166.001	<i>Atrociraptor marshalli</i>	0.41	1
UALVP 49389	<i>Velociraptor</i> sp. (Cast)	0.19	1

Jenks Natural Breaks Optimization

1000 iterations K=2			
<i>class</i>	<i>lower</i>	<i>upper</i>	<i>count</i>
1.00	0.19	1.08	19.00
2.00	1.17	1.88	8.00
GVF	1.41	5.54	0.75

8. Antorbital fenestra: elongate [0], antorbital fenestra at least 1.43 times anteroposteriorly long as dorsoventrally tall; or short [1], less than 1.43 times as long as tall. (Modified from Currie and Evans 2019 to reflect the range in data for this ratio-based character. The inclusion of *Archaeopteryx lithographica* (antorbital fenestra length-height ratio = 1.38) and *Halszkaraptor escuilliei* (1.27), moved the natural break to a ratio of 1.43 from 1.33 found in Powers et al. 2020).

Specimen	Taxon	AntFenL/H	k=2
CEUM 73719	<i>Geminiraptor suarezarum</i>	2.45	0
UALVP 49389	<i>Velociraptor</i> sp. (Cast)	2.13	0
AMNH FARB 6516	<i>Saurornithoides mongoliensis</i>	1.90	0
MPC-D 100/86	<i>Gobivenator mongoliensis</i>	1.90	0
AMNH FARB 6515	<i>Velociraptor mongoliensis</i>	1.86	0
IGM 100/1015	<i>Tsaagan mangas</i>	1.79	0
MPC-D 100/983	<i>Byronosaurus jaffei</i>	1.59	0
MPC-D 100/54	<i>Velociraptor mongoliensis</i>	1.55	0
MPC-D 100/982	<i>Velociraptor vadarostrum</i>	1.51	0
MML 195	<i>Austroraptor cabazai</i>	1.50	0
MPC-D 100/25	<i>Velociraptor mongoliensis</i>	1.50	0
IVPP V 12811	<i>Sinornithosaurus millenii</i>	1.47	0
5th Eichstatt skeleton	<i>Archaeopteryx lithographica</i>	1.38	1

MPC-D 102/109	<i>Halszkaraptor escuilliei</i>	1.27	1
IVPP V 12615	<i>Sinovenator changii</i>	1.18	1
MNUFR 15	<i>Achillobator giganticus</i>	1.12	1
IVPP V 16923	<i>Linheraptor exquisitus</i>	1.12	1
YPM 5232 (557)	<i>Deinonychus antirrhopus</i>	1.11	1
AMNH FARB 30556	<i>Bambiraptor feinbergi</i>	1.06	1
MPC-D 100/1	<i>Zanabazar junior</i>	1.05	1
JPM - 0008	<i>Zhenyuanlong suni</i>	1.01	1
MPC-D 100/1119	<i>Shanag ashile</i>	0.99	1
UALVP 55700	<i>Saurornitholestes langstoni</i>	0.96	1
TMP 1995.166.001	<i>Atrociraptor marshalli</i>	0.95	1
TMP 1994.012.0844	<i>Saurornitholestes langstoni</i>	0.94	1
STM1-3	<i>Tianyuraptor ostromi</i>	0.83	1

Jenks Natural Breaks Optimization

1000

iterations	k=2		
<i>class</i>	<i>lower</i>	<i>upper</i>	<i>count</i>
1	0.828151	1.384095	14
2	1.474128	2.4488	12
GVF	1.284525	4.393973	0.707662

9. Promaxillary fenestra of maxillae shape: 0, subcircular; 1, slit-like (Split from Character 9 Currie and Evans 2019. The distinction for this character is rather ambiguous. However, *Acheroraptor temertyorum* shows a very dorsoventrally long promaxillary fenestra compared to other dromaeosaurids and does possess a clear “slit-like” morphology. *Saurornitholestes langstoni* is also changed to [1] based on the dorsoventral elongation and irregular posterior border which make it distinctly, not sub-circular. *Velociraptor mongoliensis* is polymorphic for this character as this feature seems to be easily affected by taphonomy and hard to be certain of coding.)
10. Promaxillary fenestra: ventral border of the promaxillary fenestra of the maxilla position: 0, tucked into or near the anteroventral border of the antorbital fossa; 1, tucked into or near the most anterior point or anterodorsal border of the antorbital fossa (Split from Character 9 Currie and Evans 2019).

11. Maxillary fenestra: 0, appears as a simple perforation; 1, is positioned in a broad posteriorly oriented secondary fossa; 2, is positioned in a posterodorsally oriented secondary fossa distinctly bordered on all sides within the antorbital fossa; 3, is positioned in a posterodorsally oriented secondary fossa completely within the antorbital fossa with, with the development of a pneumatic excavation in the posterodorsal end of the secondary fossa separated from the fenestra by a distinct strut. (Split from Character 10 Currie and Evans 2019).
12. Maxillary fenestra position relative to the promaxillary fenestra: 0, posterior; 1, posterodorsal; 2, dorsal. (Split from Character 10 Currie and Evans 2019).
13. Maxillary fenestra shape: 0, subcircular with subequal axes; 1, elongate along the axis of orientation. (Split from Character 11 Currie and Evans 2019. The cut-off here used is long axis 1.5x short axis or greater = [1]. However, this could use more extensive quantification. Based on this criteria *Velociraptor mongoliensis* is also polymorphic for this trait based on comparisons of specimens).
14. Maxillary fenestra size: 0, small making up much less than half of the antorbital fossa surface; 1, large making up close to half of the area of the antorbital fossa. (Split from Character 11 (Currie and Evans 2019).
15. Maxilla pila promaxillaris: 0, narrow relative to the pila interfenestralis; 1, broad relative to the pila interfenestralis. (Changed from Character 14 Currie and Evans 2019 to better encapsulate variation of the ingroup. Polarity for this character is reversed).
16. Orbit, margin: 0, smooth; 1, with raised rim. (24. Currie and Varricchio, 2004; 61, Kubota 2015)
17. Supratemporal fossa, extension onto frontal: 0, anterior emargination of fossa straight or slightly curved; 1, sinusoidal and reaching onto the postorbital process, often with a deep pit.

18. Supratemporal fossa on frontal: 0, restricted to the lateral half of the frontal; 1, supratemporal fossa extends medially.
19. Quadratic foramen/fenestra between quadrate and quadratojugal: 0, small foramen; 1, large fenestra.
20. External mandibular fenestra, size; 0, small and slit-like; 1, large and rounded.
21. Premaxilla: long [0], at least 16% length of maxilla; or short [1], no more than 16% length of maxilla. (Modified from Character 20 Currie and Evans 2019 to reflect the data of the study group. *Byronosaurus jaffei* has a premaxilla which is 15% of the maxillary length. Its inclusion in the data set pushed the ratio from 15% to 16% in order to place the threshold in an observed natural break in data distribution).

Specimen	Taxon	PmxL/MxL	k=2
AMNH FARB 5356	<i>Dromaeosaurus albertensis</i>	0.29	0
YPM 5232 (237+557)	<i>Deinonychus antirrhopus</i>	0.29	0
AMNH FARB 30556	<i>Bambiraptor feinbergi</i>	0.26	0
IVPP V 12811	<i>Sinornithosaurus millenii</i>	0.26	0
MPC-D 100/982	<i>Velociraptor vadarostrum</i>	0.26	0
	<i>Archaeopteryx</i>		
5th Eichstatt skeleton	<i>lithographica</i>	0.26	0
MPC-D 102/109	<i>Halszkaraptor escuilliei</i>	0.26	0
TMP 1995.166.001	<i>Atrociraptor marshalli</i>	0.25	0
AMNH FARB 6515	<i>Velociraptor mongoliensis</i>	0.25	0
MPC-D 100/54	<i>Velociraptor mongoliensis</i>	0.24	0
UALVP 49389	<i>Velociraptor</i> sp. (Cast)	0.24	0
MPC-D 100/25	<i>Velociraptor mongoliensis</i>	0.23	0
IVPP V 16923	<i>Linheraptor exquisitus</i>	0.22	0
UALVP 55700	<i>Saurornitholestes langstoni</i>	0.22	0
JPM - 0008	<i>Zhenyuanlong suni</i>	0.21	0
IGM 100/1015	<i>Tsaagan mangas</i>	0.19	0
STM1-3	<i>Tianyuraptor ostromi</i>	0.18	0
MPC-D 100/983	<i>Byronosaurus jaffei</i>	0.15	1
IVPP V 12615	<i>Sinovenator changii</i>	0.10	1

AMNH FARB 6516	<i>Saurornithoides</i>	0.09	1
MPC-D 100/1	<i>mongoliensis</i>		
	<i>Zanabazar junior</i>	0.07	1

Jenks Natural Breaks Optimization

1000

iterations k=2

<i>class</i>	<i>lower</i>	<i>upper</i>	<i>count</i>
1	0.073415	0.152752461	4.00
2	0.179041	0.289432734	17.00
GVF	0.017666	0.079033468	0.78

22. Premaxilla, maxillary process: 0, short; 1, elongate process separating nasal and maxilla
23. Premaxilla, main body below external naris: elongate [0], at least 1.35 times as anteroposteriorly long as dorsoventrally tall; or short [1], less than 1.35 times as long as tall. (Modified from Character 22 Currie and Evans (2019) to reflect the range of data for this character.

Archaeopteryx lithographica, *Sinornithosaurus millenii*, and *Halszkaraptor escuilliei* were considered outliers and the character was left as two state, coding these taxa as [0]).

Specimen	Taxon	PmxL/PmxH	k=2
MPC-D 102/109	<i>Halszkaraptor escuilliei</i>	5.36	0
IVPP V 12811	<i>Sinornithosaurus millenii</i>	3.83	0
	<i>Archaeopteryx</i>		
5th Eichstatt skeleton	<i>lithographica</i>	3.64	0
MPC-D 100/983	<i>Byronosaurus jaffei</i>	2.45	0
MPC-D 100/982	<i>Velociraptor vadarostrum</i>	2.00	0
JPM - 0008	<i>Zhenyuanlong suni</i>	1.83	0
AMNH FARB 6515	<i>Velociraptor mongoliensis</i>	1.79	0
MPC-D 100/54	<i>Velociraptor mongoliensis</i>	1.63	0
UALVP 49389	<i>Velociraptor</i> sp. (Cast)	1.63	0
AMNH FARB 30556	<i>Bambiraptor feinbergi</i>	1.57	0
MPC-D 100/25	<i>Velociraptor mongoliensis</i>	1.56	0
IGM 100/1015	<i>Tsaagan mangas</i>	1.42	0
YPM 5232 (237)	<i>Deinonychus antirrhopus</i>	1.28	1
BYUVP 14585 F#1984	<i>Utahraptor ostrommaysi</i>	1.28	1
IVPP V 16923	<i>Linheraptor exquisitus</i>	1.22	1
STM1-3	<i>Tianyuraptor ostromi</i>	1.22	1

AMNH FARB 5356	<i>Dromaeosaurus albertensis</i>	1.12	1
UALVP 55700	<i>Saurornitholestes langstoni</i>	1.02	1
IVPP V 12615	<i>Sinovenator changii</i>	1.00	1
TMP 1995.166.001	<i>Atrociraptor marshalli</i>	0.96	1
CEUM 01430	<i>Utahraptor ostrommaysi</i>	0.94	1
MPC-D 100/1	<i>Zanabazar junior</i>	0.68	1
	<i>Saurornithoides</i>		
AMNH FARB 6516	<i>mongoliensis</i>	0.62	1

Jenks Natural Breaks

Optimization

1000 iterations

<i>class</i>	<i>lower</i>	<i>upper</i>	<i>count</i>
1.00	0.62	1.28	11.00
2.00	1.42	2.45	9.00
3.00	3.64	5.36	3.00
GVF	3.06	27.92	0.89

24. Premaxilla, nasal process: 0, projects posterodorsally; 1, projects posteriorly.
25. Premaxilla, narial fossa: 0, limited exposure on lateral surface; 1, prominent anteroventral extension of narial fossa onto lateral surface of premaxilla
26. Maxilla, contribution to border of naris: 0, excluded from border; 1, narial fossa extends onto anterior ramus of maxilla
27. Maxilla; palatal shelf: 0, concealed in lateral; 1, dorsally exposed along the jugal ramus only in lateral view; 2, posteriorly exposed to the antorbital fossa as the postantoral wall and dorsally along the jugal ramus in lateral view. (This character combines characters 26 and 27 from Currie and Evans 2019 as the features they referred to are observed to be confluent. Due to the observations of taphonomic distortion in *Atrociraptor marshalli* and the lack of this feature in the well preserved *Saurornitholestes langstoni* maxilla, TMP 1994.012.0844, these two taxa were coded as [0]).

28. Anterior ramus: intermediate [0], between 25% and 34% of the total length of the maxilla; short [1], less than 25% of the total length of the maxilla; or long [2], greater than 34% of the total length of the maxilla. (Modified from Currie and Evans Character 28 based on the distribution of the data for this character across the study group).

Specimen	Taxon	AntRL/MxL	K=3
UALVP 49389	<i>Velociraptor</i> sp. (Cast)	0.47	2
IVPP V 16923	<i>Linheraptor exquisitus</i>	0.46	2
MML 195	<i>Austroraptor cabazai</i>	0.40	2
IGM 100/1015	<i>Tsaagan mangas</i>	0.38	2
MPC-D 102/109	<i>Halszkaraptor escuilliei</i>	0.38	2
5th Eichstatt skeleton	<i>Archaeopteryx lithographica</i>	0.37	2
MPC-D 100/1	<i>Zanabazar junior</i>	0.36	2
	<i>Saurornithoides mongoliensis</i>	0.35	2
AMNH FARB 6516		0.35	2
MPC-D 100/25	<i>Velociraptor mongoliensis</i>	0.33	0
MPC-D 100/54	<i>Velociraptor mongoliensis</i>	0.33	0
TMP 1995.166.001	<i>Atrociraptor marshalli</i>	0.32	0
AMNH FARB 6515	<i>Velociraptor mongoliensis</i>	0.31	0
ROM 63777	<i>Acheroraptor temertyorum</i>	0.31	0
TMP 1994.12.844	<i>Saurornitholestes langstoni</i>	0.31	0
MNUFR 15	<i>Achillobator giganticus</i>	0.29	0
MPC-D 100/983	<i>Byronosaurus jaffei</i>	0.29	0
UALVP 55700	<i>Saurornitholestes langstoni</i>	0.28	0
MPC-D 100/982	<i>Velociraptor vadarostrum</i>	0.27	0
MPC-D 100/1119	<i>Shanag ashile</i>	0.25	0
IVPP V 12615	<i>Sinovenator changii</i>	0.24	1
AMNH FARB 30556	<i>Bambiraptor feinbergi</i>	0.23	1
YPM 5232 (557)	<i>Deinonychus antirrhopus</i>	0.22	1
MPC-D 100/86	<i>Gobivenator mongoliensis</i>	0.22	1
AMNH FARB 5356	<i>Dromaeosaurus albertensis</i>	0.18	1
STM1-3	<i>Tianyuraptor ostromi</i>	0.18	1
BYUVP 19965 F# 4252	<i>Utahraptor ostrommaysi</i>	0.18	1
IVPP V 12811	<i>Sinornithosaurus millenii</i>	0.17	1
CEUM 73719	<i>Geminiraptor suarezarum</i>	0.15	1
JPM - 0008	<i>Zhenyuanlong suni</i>	0.12	1

Jenks Natural Breaks Optimization

1000 iterations	k=3		
<i>class</i>	<i>lower</i>	<i>upper</i>	<i>count</i>

1.00	0.12	0.24	10.00
2.00	0.25	0.33	11.00
3.00	0.35	0.47	8.00
GVF	0.03	0.23	0.86

29. Anterior ramus shape: elongate [0], between 1.17 and 1.95 times as anteroposteriorly long as dorsoventrally tall; short [1], less than 1.17 times as long as tall; or hyperelongate [2], greater than 1.95 times as long as tall. (Modified from Character 29 Currie and Evans 2019 based on the distribution of data for this character across the study group. *Acheroraptor temertyorum* is coded as [1] after retro-deformation of the maxilla).

Specimen	Taxon	AntRL/AntRH.p	k=3
MPC-D 102/109	<i>Halszkaraptor escuilliei</i>	3.15	2
MPC-D 100/1119	<i>Shanag ashile</i>	2.40	2
5th Eichstatt skeleton	<i>Archaeopteryx lithographica</i>	2.39	2
MPC-D 100/983	<i>Byronosaurus jaffei</i>	2.37	2
MML 195	<i>Austroraptor cabazai</i>	2.15	2
AMNH FARB 6515	<i>Velociraptor mongoliensis</i>	1.75	0
UALVP 49389	<i>Velociraptor</i> sp. (Cast)	1.62	0
MPC-D 100/1	<i>Zanabazar junior</i>	1.61	0
IVPP V 16923	<i>Linheraptor exquisitus</i>	1.51	0
MPC-D 100/54	<i>Velociraptor mongoliensis</i>	1.42	0
IMM99NM-BYM-3/3A	<i>Velociraptor osmolskae</i>	1.41	0
MPC-D 100/25	<i>Velociraptor mongoliensis</i>	1.40	0
MPC-D 100/982	<i>Velociraptor vadarostrum</i>	1.40	0
IGM 100/1015	<i>Tsaagan mangas</i>	1.30	0
AMNH FARB 6516	<i>Saurornithoides mongoliensis</i>	1.27	0
IVPP V 12811	<i>Sinornithosaurus millenii</i>	1.24	0
ROM 63777	<i>Acheroraptor temertyorum</i>	1.09	1
MPC-D 100/86	<i>Gobivenator mongoliensis</i>	1.02	1
IVPP V 12615	<i>Sinovenator changii</i>	1.01	1
TMP 1994.12.844	<i>Saurornitholestes langstoni</i>	0.91	1
MNUFR 15	<i>Achillobator giganticus</i>	0.87	1
UALVP 55700	<i>Saurornitholestes langstoni</i>	0.81	1
STM1-3	<i>Tianyuraptor ostromi</i>	0.76	1
TMP 1995.166.001	<i>Atrociraptor marshalli</i>	0.75	1

AMNH FARB 30556	<i>Bambiraptor feinbergi</i>	0.70	1
CEUM 73719	<i>Geminiraptor suarezarum</i>	0.68	1
YPM 5232 (557)	<i>Deinonychus antirrhopus</i>	0.68	1
JPM - 0008	<i>Zhenyuanlong suni</i>	0.57	1

Jenks Natural Breaks Optimization

1000 iterations		k=3		
<i>class</i>	<i>lower</i>	<i>upper</i>	<i>count</i>	
1.00	0.57	1.09	12.00	
2.00	1.24	1.75	11.00	
3.00	2.15	3.15	5.00	
GVF	1.12	11.12	0.90	

30. Maxilla, lateral surface: 0, smooth; 1, maxilla with a distinct lip (ridge) bounding the ventral margin of the antorbital fossa.
31. Maxilla, interfenestral bar between maxillary and antorbital fenestrae: 0, narrow; 1, anteroposteriorly broad.
32. Maxilla shape: elongate [0], maxilla at least 2.62 times as anteroposteriorly long as dorsoventrally tall; or short [1], less than 2.62 times as long as tall. (New Character based on the data distribution for this character across the study group).

Specimen	Taxon	MxL/MxH	k=2
MPC-D 100/983	<i>Byronosaurus jaffei</i>	5.05	0
MPC-D 102/109	<i>Halszkaraptor escuilliei</i>	3.82	0
MPC-D 100/1	<i>Zanabazar junior</i>	3.53	0
MPC-D 100/982	<i>Velociraptor vadarostrum</i>	3.44	0
AMNH FARB 6516	<i>Saurornithoides mongoliensis</i>	3.36	0
AMNH FARB 6515	<i>Velociraptor mongoliensis</i>	3.08	0
MPC-D 100/86	<i>Gobivenator mongoliensis</i>	3.07	0
MPC-D 100/54	<i>Velociraptor mongoliensis</i>	2.98	0

	<i>Geminiraptor</i>		
CEUM 73719	<i>suarezarum</i>	2.92	0
MML 195	<i>Austroraptor cabazai</i>	2.86	1
UALVP 49389	<i>Velociraptor</i> sp. (Cast)	2.81	1
	<i>Velociraptor</i>		
MPC-D 100/25	<i>mongoliensis</i>	2.81	1
IGM 100/1015	<i>Tsaagan mangas</i>	2.70	1
MPC-D 100/1119	<i>Shanag ashile</i>	2.54	1
IVPP V 12811	<i>Sinornithosaurus millenii</i>	2.45	1
	<i>Archaeopteryx</i>		
5th Eichstatt skeleton	<i>lithographica</i>	2.45	1
IVPP V 16923	<i>Linheraptor exquisitus</i>	2.42	1
	<i>Acheroraptor</i>		
ROM 63777	<i>temertyorum</i>	2.36	1
JPM - 0008	<i>Zhenyuanlong suni</i>	2.34	1
IVPP V 12615	<i>Sinovenator changii</i>	2.29	1
STM1-3	<i>Tianyuraptor ostromi</i>	2.27	1
MNUFR 15	<i>Achillobator giganticus</i>	2.22	1
AMNH FARB 30556	<i>Bambiraptor feinbergi</i>	2.02	1
	<i>Saurornitholestes</i>		
UALVP 55700	<i>langstoni</i>	2.01	1
	<i>Saurornitholestes</i>		
TMP 1994.12.844	<i>langstoni</i>	1.87	1
YPM 5232 (557)	<i>Deinonychus antirrhopus</i>	1.70	1
TMP 1995.166.001	<i>Atrociraptor marshalli</i>	1.70	1

Jenks Natural Breaks Optimization

Iterations

1000

<i>class</i>	<i>lower</i>	<i>upper</i>	<i>count</i>
1	1.696742	2.54	14.00
2	2.6989	3.82	12.00
GVF	2.342504	7.90	0.70

33. Nasal, dorsal outline in lateral view: 0, concave; 1, straight to convex.
34. Nasal participation in the antorbital fossa: 0, none; 1, ventrolateral edge of the nasal makes up the dorsal margin of the antorbital fossa; 2, the lateral surface of the nasal makes up part of the antorbital fossa. (Split from Character 34 Currie and Evans 2019 to remove unjustified dependency).

35. Nasals with pneumatopores near contact with the maxilla: 0, no; 1, yes. (Split from Character 34 Currie and Evans 2019 to remove unjustified dependency).
36. Lacrimal shape: 0, T-shaped with subequal anterodorsal and posterodorsal processes; 1, T-shaped with anterodorsal process much longer than posterodorsal process.
37. Prefrontal; 0, present as separate bone; 1, lost as a separate bone.
38. Frontonasal suture: 0, transverse orientation; 1, frontal narrows anteriorly into a wedge between nasals; 2, complex W-shaped suture.
39. Frontal, orbital margin in dorsal view: 0, straight or smoothly concave; 1, postorbital process sharply offset, and orbital margin L-shaped in dorsal view
40. Frontal notched to receive lacrimal: 0, absent; 1, present. Frontal edge smooth in region of lacrimal suture; 1, notched
41. Jugal pneumatic: 0, no; 1, yes
42. Jugal, suborbital process. 0, dorsal and ventral borders subparallel; 1, distinctly deeper at the back of the orbit than front, triangular.
43. Jugal, postorbital process: 0, slender with notable anterior embayment along the posterior edge of the postorbital process; 1, postorbital process broad so the posterior edge is straight. (Wording adjusted from Currie and Evans 2019 to keep focus on the postorbital of the jugal rather than jugal shape).
44. Postorbital in lateral view: 0, has a straight anterior (frontal) process; 1, frontal process curves anterodorsally and dorsal border of temporal bar is dorsally concave.

45. Postorbital, contribution to lateral temporal fenestra: 0, contributes to the dorsolateral margin in lateral view; 1, does not contribute to lateral temporal fenestra, excluded by jugal-squamosal contact.
46. Squamosal, tab-like process invades posterolateral corner of upper temporal fenestra: 0, no; 1, yes.
47. Quadratojugal: 0, without horizontal process posterior to ascending process (reversed L-shape); 1, with process (inverted T- or Y-shape).
48. Quadratojugal, ascending (squamosal) ramus: 0, straight ascending ramus; 1, ascending ramus bowed anteriorly.
49. Quadrate shaft pierced by large, pneumatic foramen: 0, present; 1, absent.
50. Quadrate shaft in lateral view: 0, straight or weakly curved; 1, strongly bowed anteriorly.
51. Occipital condyle: 0, lacks constricted neck; 1, subspherical with constricted neck.
52. Exoccipital, posterior surface with a bowl-like depression containing the exits of cranial nerves X and XII: 0, absent; 1, present.
53. Exoccipital-opisthotic, paroccipital processes: 0, projects ventrolaterally; 1, projects laterally.
54. Exoccipital-opisthotic, paroccipital process: 0, elongate and slender, with dorsal and ventral edges nearly parallel; 1, short, deep with convex distal end.
55. Exoccipital-opisthotic, paroccipital processes, occipital surface of distal end: 0, oriented more posteriorly than dorsally; 1, conspicuous twist in the distal end orients distal surface more dorsally than proximal region.

56. Paroccipital process plus squamosal: 0, does not extend beyond level of intertemporal bar of postorbital and squamosal; 1, ventrolateral process of squamosal and lateral extension of paroccipital process beyond head of quadrate.
57. Basioccipital tubera, posterior surfaces: 0, flat or smoothly concave; 1, with distinct, ovoid depressions
58. Basioccipital tubera: 0, separated by weak notch; 1, separated by a deep, broad, U-shaped ventral notch.
59. Basisphenoid recess with paired openings: 0, absent; 1, present
60. Lateral depression of braincase bounded by otosphenoidal crest prominent: 0, absent; 1, present.
61. Parasphenoid recess (parabasisphenoidal recess): 0, posterior to cultriform process; 1, adjacent to base of cultriform process.
62. Accessory tympanic recess dorsal to crista interfenestralis: 0, absent; 1, small pocket present; 2, extensive with indirect pneumatization.
63. Foramen magnum: 0, subcircular; 1, distinctly taller than wide.
64. Ectopterygoid, dorsal recess: 0, absent; 1, present.
65. Dentary symphysis, ventral deflection with lateral parapet centered on third tooth: 0, present; 1, absent.
66. Dentary, shape of dorsal symphysial region anterior to the third dentary tooth: 0, dorsal margin at same level and continuous with alveolar ramus; 1, alveolar margin concave.

67. Dentary, shape of symphysis, ventral margin: 0, at same level and continuous with ventral ramus of the dentary; 1, symphyseal region extends ventrally below the level of the dentary margin forming a symphyseal 'chin'.
68. Dentary curvature in lateral view: 0, straight or weakly curved; 1, strongly bowed, with curved dorsal and ventral margins. (*Saurornitholestes langstoni* recoded as [0] as it could not be justified to consider it strongly curved in relation to other dromaeosaurids).
69. Dentary curvature in dorsal view: 0, straight; 1, curves medially towards symphysis
70. Dentary shape: 0, subtriangular, with dorsal and ventral margins diverging posteriorly; 1, dorsal and ventral margins subparallel. *Velociraptor mongoliensis* is considered to have subparallel dentary margins in lateral view.
71. Dentary with distinct mid-length constriction and terminal expansion: 0, absent; 1, present.
72. Dentary, nutrient foramina: 0, inset into prominent groove along length of the lateral surface; 1, lateral groove reduced anteriorly or absent.
73. Splenial: 0, limited or no exposure on lateral surface of mandible; 1, conspicuous triangular exposure between dentary and angular.
74. Articular with tall, columnar process on retroarticular process: 0, absent; 1, present.
75. Interdental plates on premaxilla, maxilla, and dentary: 0, distinct and separate; 1, fused to each other and jaw margin; 2, no interdental plates (labial wall of each tooth socket is significantly higher than the lingual one).
76. Teeth, premaxillary teeth; 0, 2–4 subequal in size; 1, second premaxillary tooth larger than third and fourth.

77. Teeth, cross-section at base of premaxillary tooth #2: 0, J-shaped in cross-section. 1) flattened lingual surface with longitudinal striations.
78. Teeth: 0, constricted between root and crown; 1, root and crown confluent.
79. Teeth, maxillary teeth: 0, subequal in length along the jaw; 1, maxillary teeth occupying the mid region of the maxillary alveolar margin are elongate and fanglike, approximately 200% the length of most anterior and posterior maxillary teeth. (Modified for from Character 82 Currie and Evans 2019 in order to clarify identifying the character. Previous wording stated that the fang-like teeth were the posterior maxillary teeth. However, review of the specimens coded for this character show that it is the maxillary teeth in the middle of the alveolar margin that are fang-like).
80. Teeth, maxillary: 0, more or less perpendicular to jaw margin; 1, strongly raked posteriorly.
81. Teeth, roots of maxillary and dentary teeth: 0, mediolaterally compressed; 1, circular in cross-section.
82. Teeth, denticles: 0, large; 1, small; 2, absent. Farlow et al. (1991) quantify this difference
83. Teeth, mesial carina on maxillary and dentary teeth is close to midline of tooth near tip but twists toward the lingual surface: 0, absent; 1, present.
84. Teeth, denticle shape: 0, convex; 1, pointed at tip and hooked apically (Modified from Currie and Evans 2019 to remove the absent state as it is repeated multiple times and over weights this characteristic.)
85. Teeth, denticle orientation: 0, perpendicular to carina. 1, orientated toward the tip of the crown;(Modified to remove the absent state as it was duplicated many times).

86. Teeth, maxillary: 0, teeth large, crowns more than half the height of the dentary ramus; 1, small, less than half the height of the dentary ramus. (Modified from Character 89 Currie and Evans 2019 to remove tooth count and size as being dependent. Tooth number is also highly variable and difficult in its use to characterize clades following the argument made by Norell et al., 2009).
87. Teeth, maxillary and dentary: 0, subequal size; 1, dentary teeth smaller than maxillary teeth. (Split from Character 90 Currie and Evans 2019 in order to remove dependence on size and tooth count between dentaries and maxillae).
88. Teeth maxillary and dentary: 0, subequal in number, may vary by 1-3; 1, dentary teeth much more numerous, more than 3 additional dentary teeth. (Modified from Character 90 Currie and Evans 2019 to remove dependence on tooth size and numbers between dentaries and maxillae).
89. Teeth, relative denticle size of mesial and distal carinae on maxillary and dentary teeth: 0, subequal; 1, distal denticles much larger than mesial ones; 2, mesial denticles absent. (Modified to remove the absent denticles character state as it was duplicated many times).
90. Teeth, dentary: 0, in separate alveoli; 1, set in open groove.
91. Teeth, dentary: 0, evenly spaced; 1, mesial dentary teeth smaller, more numerous, and more closely appressed than those in middle of tooth row.
92. Vertebrae, epiphyses on axis: 0, short; 1, elongate, project laterally beyond postzygapophyses.
93. Vertebrae, anterior cervical centra: 0, level with or shorter than posterior extent of neural arch; 1, extends beyond posterior extent of neural arch.
94. Vertebrae, carotid process on anteroventral margin of posterior cervical vertebrae: 0, absent; 1, present.

95. Vertebrae, cervical: 0, with low neural spines; 1, cervical neural spines at least as tall as long anteroposteriorly.
96. Vertebrae, cervical prezygapophysis: 0, unflexed; 1, flexed.
97. Vertebrae, transverse processes of anterior dorsal vertebrae: 0, long and thin; 1, short, wide, and only slightly inclined.
98. Vertebrae, dorsal: 0, parapophyses short; 1, parapophyses on elongate pedicels.
99. Vertebrae, dorsal: 0, no pneumatopores; 1, pneumatopores present on dorsal centra.
100. Vertebrae, dorsal, neural spine height: 0, low, height does not exceed anteroposterior length; 1, taller than long anteroposteriorly ($\geq x 1.5$ anteroposterior length).
101. Vertebrae, dorsal: 0, neural arch does not have prominent anterior fossae on either side of neural canal; 1, present.
102. Vertebrae, posterior dorsals: 0, centra elongate; 1, short and massive, length of centrum less than diameter.
103. Vertebrae, posterior dorsals: 0, no expansion of neural spines distally; 1, distal end of neural spines transversely expanded by at least 200% to form a distinct spine table
104. Vertebrae, sacral: 0, five vertebrae incorporated into sacrum; 1, sacrum incorporating at least 6 vertebrae.
105. Vertebrae, sacral: 0, lack pneumatopores; 1, pneumatopores present in one or more sacral vertebrae.

106. Vertebrae, caudal, distal caudal centra: 0, have prominent lateral depressions; 1, lateral surfaces of centra flat or convex.
107. Vertebrae, caudal, distal: 0, greatly elongated, more than 200% the length of proximal caudals; 1, moderately elongate, no more than 200% the length of the proximal caudals
108. Vertebrae, caudal, distal: 0, with a convex or flat dorsal surface; 1, with a prominent dorsal groove
109. Vertebrae, caudal: 0, prezygapophyses short; 1, elongate; 2, extended by ossified tendons of caudal epaxial muscles.
110. Cervical ribs, shafts: 0, slender and longer than vertebrae to which they articulate; 1, broad and shorter than vertebra.
111. Sternal plates: 0, unossified; 1, ossified.
112. Furcula: 0, interclavicular angle less than 90°; 1, at least 90°.
113. Scapula, acromion margin: 0, continuous with blade; 1, anterior edge laterally everted.
114. Coracoid: 0, highly flexed in lateral view, with dorsal and ventral rami of coracoid forming an angle of 90°–100°; 1, coracoids weakly flexed, forming an angle larger than 100°.
115. Coracoid: 0, elongate, taller than wide; 1, short, at least as wide as tall.
116. Humerus length: 0, elongate and at least 75% length of femur; 1, humerus less than 75% length of the femur.
117. Humerus, internal tuberosity: 0, proximodistally short; 1, proximodistally elongate, about 50% the length of deltopectoral crest.

118. Humerus, proximal shaft with prominent longitudinal ridge on posterior surface: 0, absent; 1, present.
119. Radius shaft diameter: 0, greater than; 1, less than or subequal to 0.5× ulna in diameter.
120. Ulna, length compared to scapular length: 0, shorter; 1, longer.
121. Ulnar/femoral length ratio: 0, significantly less than one; 1, equal or greater than one.
122. Metacarpal I length compared with Mtc II length: 0, no more than 33%; 1, more than a third.
123. Metacarpal II, length compared with Mc I plus manual phalanx 1-1: 0, shorter; 1, subequal to or longer.
124. Manual phalanx I-1: 0, strongly bowed in medial view; 1, weakly curved or straight.
125. Manual phalanx I-2 (ungual): 0, proximodorsal 'lip' absent; 1, present.
126. Manual phalanx II-1: 0, posterior flange absent; 1, present.
127. Manual phalanx III-1 length compared to length of manual phalanx III-2: 0, less than twice the length; 1, more than double the length.
128. Manual phalanx III-1: 0, short; 1, elongate, at least 75% length of III-3.
129. Ilium, anterior wing: 0, 200% length of posterior wing; 1, short, less than twice length of posterior blade.
130. Ilium, anterior end of anterior wing: 0, rounded or straight; 1, with notched anterior margin.
131. Ilium, cuppeditic ridge: 0, ends on pubic peduncle; 1, extends posteriorly to acetabulum.
132. Ilium, medial antiliac shelf: 0, short; 1, elongate, approaching length of posterior wing.

133. Ilium, posterior wing: 0, slender, shallower than anterior wing; 1, posterior wing as deep or deeper than anterior wing.
134. Ilium, posterior wing: 0, longer than tall; 1, at least as tall as long.
135. Ilium: 0, has acuminate posterior margin; 1, brevis shelf lobate and projects posteriorly beyond postacetabular lamina; 2, brevis shelf notched in lateral view.
136. Ilium, posterior wing: 0, with straight or convex dorsal margin; 1, concave dorsal margin
137. Ilium, pubic peduncle in lateral view: 0, anteroposteriorly narrow; 1, broad anteroposterior length, approximately 200% of height.
138. Pubis, distal end: 0, with prominent posterior expansion; 1, distal end spatulate, both anterior and posterior expansions absent; 2, with prominent anterior and posterior expansions.
139. Pubis, shaft: 0, straight or gently curved; 1, distal end strongly bent posteriorly.
140. Pubis, lateral surface of shaft: 0, smooth or bearing a ridge; 1, with enlarged tubercle or process.
141. Pubis, pubic apron: 0, extends less than 50% length of pubis; 1, extends at least 50% length of pubis.
142. Pubis orientation: 0, propubic; 1, vertical; 2, posteriorly oriented (opisthopubic).
143. Ischium length: 0, no more than 50% length of pubis; 1, elongate, more than 50% length of pubis.
144. Ischium, proximodorsal process: 0, present; 1, absent; 2, hypertrophied, hooked and separated from iliac peduncle of ischium by a notch
145. Ischium, lateral ridge on shaft: 0, absent; 1, present.

146. Posterior edge of ischium: 0, straight; 1, with median or distal posterior process, except for proximodorsal process.
147. Ischium, distal dorsal process: 0, prominent; 1, highly reduced or absent.
148. Ischium, obturator process position: 0, at distal end of shaft; 1, at midshaft; 2, proximal in position
149. Ischium, obturator process: 0, elongate and spur-like; 1, broad and flange-like.
150. Ischium, obturator process: 0, separated from ischial shaft by posterior notch; 1, confluent.
151. Ischium, distal end: 0, tapers to a narrow point; 1, broadly expanded, blunt or spatulate.
152. Ischium, shaft: 0, mediolaterally compressed; 1, subcircular in section.
153. Ischium, ridge on medial surface connecting proximodorsal process and iliac peduncle: 0, absent; 1, present.
154. Femur, angle of femoral head: 0, projecting dorsomedially or medially relative to shaft; 1, projects ventromedially.
155. Metatarsal II length compared to that of Mt IV: 0, subequal; 1, markedly shorter.
156. Metatarsal II tuber along anterior surface: 0, absent. 1, present.
157. Metatarsal II, proximal end size compared to proximal end of Mt III: 0, as deep as or deeper than; 1, shallower; 2, no exposure of metatarsal III.
158. Metatarsal II, distal end: 0, smooth; 1, with well-developed ginglymus
159. Metatarsal II, width of distal condyles: 0, broad, subequal to Mt III; 1, more narrow than Mt III.

160. Metatarsal II, distal end compared with width of distal end of Mt IV: 0, wider than or as wide as; 1, narrower.
161. Metatarsal III, plantar surface: 0, broadly exposed; 1, largely covered by Metatarsals III and IV.
162. Metatarsal III, anterodorsal surface of shaft: 0, flat or rounded; 1, has a prominent longitudinal sulcus.
163. Metatarsal IV, lateral flange on proximal end of shaft: 0, absent; 1, present.
164. Metatarsal IV, prominent flange on posterolateral surface of shaft: 0, present; 1, highly reduced or absent.
165. Metatarsal IV, ventral surface proximal to distal articular surface: 0, no tuber; 1, has a prominent tuber.
166. Metatarsal IV, distal condylar surface: 0, trochlear to planar; 1, strongly ball-shaped.
167. Foot symmetry: 0, symmetrical; 1, asymmetrical with slender metatarsal II and robust metatarsal IV, excluding flange.
168. Pedal phalanx II-1 length: 0, elongate; 1, short and robust, shaft length does not exceed 200% the diameter of the distal condyle.
169. Pedal phalanx II-2 length: 0, subequal to or longer than II-1; 1, significantly shorter than II-1.
170. Pedal phalanx II-2 shaft: 0, slender to moderately robust; 1, massive, shaft diameter at least 50% of shaft length.
171. Pedal phalanx II-2 proximoventral flexor heel: 0, short; 1, elongate posterior projection.
172. Pedal phalanx II-2, ventromedial keel ventral to flexor heel: 0, absent; 1, present

173. Pedal phalanx II-2, collateral ligament pits: 0, deep; 1, shallow.
174. Pedal phalanx II-3, lateral and medial vascular grooves: 0, at same level; 1, lateral groove more dorsal and medial groove more ventral.
175. Pedal phalanx IV-4: 0, shorter than or subequal to pedal phalanx IV-3; 1 longer than pedal phalanx IV-3.
176. Vaned feathers on forelimb: 0, symmetric; 1, asymmetric.
177. Vaned feathers on tarsus: 0, present; 1, absent.

Characters removed from the Currie and Evans (2019) character-taxon data matrix.

Character 5 – Redundant with Character 4, character 4 was selected because it does not depend on a variable character such as the antorbital fossa, anterior extent.

Character 12 – Explained in Chapter 2

Character 13 – Explained in Chapter 2

Character 26 – Removed due to the dependency on character 27 Currie and Evans 2019.

Character 32 – Removed due to redundancy with Character 7 Currie and Evans 2019.

Character 40 – removed because it may only characterize a juvenile characteristic.

Character 43 – Does not specify the region of the suborbital process and seems redundant to Character 42. This could be worked out later with quantitative analyses of proportions.

Character 79 – some redundancy with character 92. Does not appear to capture the full variation of premaxilla denticles as some troodontids have mesial and distal denticles.

Character 81 – redundant with 89 but also unjustified in its number.

Character 91 – redundant with character 92 which includes the presence or absence of denticles on the mesial carinae as well as the size relationship.

A 3.3. Character-taxon matrix

Character-taxon data matrix used for phylogenetic analysis in Chapter 4. Following the character definitions from A3.2.

Acheroraptor_temertyorum

????211?1030101????????0201001?1????????????????????????????11110101??1??1000?0
1000?100??
????????

Achillobator_giganticus

????01110120100?????1??0201001??1??100?1?0
?0??0??0100111?1??1?01??0?????????????????11001120020011100012111100??10??0???
??1?11???

Adasaurus_mongoliensis

?????????????001????????????????????1??1110?1?01??100??1????????????????????????
??0??10011?1??0?11?1?10??01?????????????1100100002001211??1111001?111101001101
111?011?0??

Archaeopteryx_lithographica

01?02?110000011100?000000002200101?00000?0?000?0?00?????0?1??0000010100000000
120??100?0001?0?1000?0000000000?000000110001000000?0000000020001000000?010?01
?000??0000?000110

Atrociraptor_marshalli

??110111031001?????011000001001?1????????????????????????????????01000101??11?10101
011000100??
?????????

Austroraptor_cabazai

1??2210000?100??1??0??02220100000?11??0?0????????????????????0??1?110?????10012?
??110?00?11??11??01?????????????11??
1?00???

Bambiraptor_feinbergi

0??010110031001111??01000001100101?010?0?00101111100???010?1???0?1101011?11110
1010110001001001?011111?011102?1101101001010100111?0000000000120011101100101?0
100000001010011011??

Buitreraptor_gonzalezorum

1??????????11101?1??????2?000010?000?010??000????????????0??00110??0??1?002?
?????0011??1100?00?00?011?010?011010????????????011??1??1?010110000?100?1101?00?
?0???????????

Byronosaurus_jaffei

???2200?00110????100111?020100001?1????????????0?10?00?1?11?001110001?2?00100
20??111?11??01?00?????0?1??
??0???????

Deinonychus_antirrhopus

??000110121101??1?10110000110011210??1??010110??01?01???????10000010111110101
010010001001001101110110?11021??11111000010100001100000002001?0110111110001101
00000101010011010??

Dromaeosaurus_albertensis

??001??00?1??00111011??00110?1????211?00??101010101?000000000000010111100100
01101000000??10??1?1
1?101?11????

Graciliraptor_lujiatensis

????????????????????????????????????1??1??01??0?
?1??????????0??0?02?????????0001?1111????????????????????????????????1??1101????0000?
00???

Halzskaraptor_escuilliei

01012?01??001100?00010??22?000?01?01000100????????????????????0000010??0?10002
??100?0?00?00?100??1????011??????0?111?011?0?0000????????????????00?110?0??
000101?0?0??

Sauornitholestes_langstoni

00011011113110101111011000001001011010111001011110????1???????1011001011111110
00101100010010011011111011102111?11010000101010111000000020012001010110010100
100000001010011010??

Shanag_ashile

????0001?01101?????1??0002101?1????????????????????????????????0?000001?????110010
0?010101??
????????

Sinornithosaurus_millenii

0??000000101101?11??010??0?101?101?00001???10?10?????????????1??000101011111?1100
1001010100??????0?000??2?1?0001?110010111111?0?00??111020001000000?00?1?11
?00?10?00?00?1??

Sinovenator_changii

?1?022110000011100??101001011001???1?100??0?????1000010?00?0111?00110000??0?000
?1?0010?2?1?1??11000?0000????????11?????0??0?????0?0?0?00120001001??00010100?10
10001??0?000???

Tianyuraptor_ostromi

00??0?1100?1000????0?1???11001?????0????????????????????????????????0??????0??01?0
?000?0?0????????00??01?1?0?011010000?1?1?0??00?01000?101???111000?0?????0????
0??????1??

Tsaagan_mangas

00?022100012000?11??01011022001001001111?111111000?10??0110??1?1111010111?1?10
00100000020010?1??
??????????????

Stenonychosaurus_inequalis

????22??1000110100??0??10??01????1?1 {0
1}0??1????0110010?0001001?00101000??2000000001111111?110110010?1101?111?????0
00????????????????2000??1001111000010?001100000101101001??

Unenlagia_comahuensis

??

?????????1111001??????0??111?????????001101111010110200?11?001?0?????????????
????0??

Utahraptor_ostrommaysi

????????????????????100??1????????????????????????????????????000????????101???1?01?
??0??00??11101???1?02????11?????????????????00?0200?????00?1211?100???10?00111?01?
????1???

Velociraptor_mongoliensis 00101010{0 1}11{0 1}{0

1}010111101011020001001001011110101111001101?11101001111101011?111100010010001
001001101{0
1}1?11111020111111000010100001000100002001211011110001111010011110100111010011010
??

Velociraptor_vadarostrum_sp._nov.

1010000001100010111101011020001001001011110?0?111001????111?1?0????101010011110
0010??000100?1??10?01?1100????0111?10101001010000100010000?00?2?????????0?011011
100111101011101???

Velociraptor_osmolskae

????221?0011100?????????0?00010??1??100010?
?0??10??
??????

Zhenyuanlong_suni

0000001100?11011????0100?0211?0111?01?????????1?????????????????0?0?0??1??????0??
??000?00?????????????1?????????????1??00?0??0????????????10?2?????????????0????????????
????????11